ANALYZING THE EFFECT OF MOVING RESONANCE ON SEISMIC RESPONSE OF STRUCTURES USING WAVELET TRANSFORMS

Pradeep Naga

Thesis submitted to the faculty of the

Virginia Polytechnic Institute and State University

in partial fulfillment of the requirements for the degree of

Master of Science

In

Civil Engineering

Matthew R. Eatherton, Chair

Finley A. Charney

Martin C. Chapman

August 05, 2011

Blacksburg, VA

Key Words: Response History Analysis, Record-to Record Variability, Wavelet Transforms, Moving resonance

ANALYZING THE EFFECT OF MOVING RESONANCE ON SEISMIC RESPONSE OF STRUCTURES USING WAVELET TRANSFORMS

Pradeep Naga

ABSTRACT

Nonlinear structures, when subjected to multiple ground motion records that are scaled to consistent ground motion intensity show significant variation in their response. This effect of ground motion randomness on the variation of structural response is defined as Record-to-Record (RTR) Variability. Ground motion characteristics that contribute to this variability in response includes the variation of signal composition (frequency content) with time (spectral nonstationarity).The phenomenon of moving resonance which occurs when the frequency content of the ground motion shifts in a similar manner as the natural frequencies of the structural response, is likely a contributor to variability. This brings the need to further understand the sources of variability due to moving resonance.

The present study was carried out to develop a method to analyze the time-frequency content of a ground motion to assess the occurrence of moving resonance and to quantify its potential in effecting the structural systems. Bilinear elastic and elastoplastic hysteretic behavior was considered. Detailed analysis is done to quantify the effect of moving resonance on structural systems due to 22 far field ground motion records.

The wavelet coefficient plots gave very good detail of the characteristics of the ground motions that were not clear from the acceleration time histories and response spectra plots. Instances of moving resonance were found out to be significant. Amplification due to moving resonance was found to be quite large. One instance studied in detail (accelerogram of Northridge earthquake at Beverly Hills) had peak displacement amplified by 6 times compared to the amount of peak displacement expected if the system did not exhibit moving resonance. Based on the analyses results, the characteristics of the ground motion records that don't cause significant moving resonance effect on structural systems were observed. Similarly, the characteristics of the ground motions that do cause moving resonance effect on structural systems were examined.

Acknowledgements

I would like to express my appreciation and deep sense of gratitude to the Virginia Tech faculty for the knowledge that they imparted to me during my stay here. I would like to express my sincere thanks to Dr. Matthew Eatherton for giving me this opportunity to do research and serving as my primary advisor and committee chair. His endless patience and faith in me made me complete this research work successfully. I am really very thankful to him for all I have learned from him as a Graduate Research Assistant. I would like to extend my sincere thanks to Dr. Finley Charney, Dr. Martin Chapman and Dr. Russell Green for their support and assistance on this project.

I would like to express my thanks to my fellow graduate students and friends at Virginia Tech for their assistance and encouragement along the way. Some of them are Jagadeeshwaran Deventhiran, Karthik Kumaresan, Prasanna Kumar Ragavan, Vinay Balachandran, Yash Gajbhiye, Harshil Patel, Li Ma, Kamalika Pal, Maninder Singh Bajwa, Adam Bowland, Chirag Kapadia, David Padilla, Amber Verma, Manasa Koppal, Jeena Jayamon, Krishnan Gopalan, Krishna Kumar, Arjun Thottipally, Satyavrata Samavedi and all innumerable good friends that I have not been able to mention.

I owe many thanks to Rani Infrastructure Development Ltd., in particular Mr. Gundaiah Galla and his family for their outstanding support to my family and for indirectly contributing in my this accomplishment.

More importantly, I would like to express a vast amount of appreciation to my family and relatives for their continuous support, direction and love throughout my life without which I would not have been able to accomplish the goals that I have. Special thanks are due to my parents, my brother and friends especially Praveena Chinnaganta, Harini Thondamanati, Kushwanth Rambe and Devesh Guha.

Finally, I want to thank God especially Sai Baba for always being present in my life.

Table of Contents

List of Figures

List of Tables

CHAPTER 1 : INTRODUCTION

1.1 Statement of the Problem

As part of the development of Performance-Based Earthquake Engineering (PBEE), nonlinear response history analysis of structures has become common. Nonlinear response history analysis is important in PBEE as it gives detailed information on displacements, drifts, and inelastic deformations of a structure that are vital for performance based design methods. It also gives the deflected shape and force state of the structure at each time increment during an earthquake. Since each earthquake record has different characteristics, the results (e.g. peak forces or peak displacements) obtained from response history analyses are only representative of the demands for that particular earthquake record. Therefore, when performing response history analysis to determine forces and displacements for use in design, it is necessary to run a suite of analyses, each using different ground motion records as input. Structures, when subjected to multiple ground motion records that are scaled to consistent ground motion intensity show significant variation in their response. This effect of ground motion randomness on the variation of structural response is defined as Record-to-Record (RTR) Variability in FEMA p695 (FEMA 2009).

RTR variability also has an impact on the predicted collapse capacity of a structure. The collapse capacity for SDOF systems can be expressed in terms of relative intensity measure, defined as the ratio of ground motion intensity (acceleration) to structure strength parameter (force) (Ibarra and Krawinkler, 2011). The variance of collapse capacity is an important constituent of probabilistic methodologies used to evaluate the probability of collapse of structures subjected to earthquake ground motions. The effect of RTR variability on the variance of collapse capacity can be directly obtained by performing dynamic analysis of hysteretic models for a set of representative ground motions.

Incremental dynamic analysis (IDA) is a parametric analysis method that has recently emerged to analyze structural performance under varying magnitude of seismic loads (Vamvatsikos and Cornell, 2002). It involves subjecting a structural model to one (or more) ground motion record(s), each scaled to multiple levels of intensity, thus producing one (or more) curve(s) of response parameterized against intensity level. The ground motion records selected for IDA can

be those available from the past earthquakes that match the site soil conditions, source characteristics, distance to fault, and earthquake magnitude as a specific site, or a preselected set such as those from FEMA p695 (FEMA 2009). IDA results reveal additional aspects of RTR variability when compared to other traditional earthquake measures. It is not uncommon that the peak displacements do not increase monotonically with ground motion intensity. Instead, the peak displacement for one intensity level is sometimes smaller than the peak displacement from a lower intensity level. This hints at the complex interaction between a nonlinear structure and the ground motion excitation.

Ground motions characteristics that contribute to RTR variability includes the variation of signal composition with time. The variation of the statistical properties of a signal over time is called nonstationarity and there are two main contributions to the nonstationarity of ground motion signals. The time dependent variation in a signal`s frequency content is known as spectral nonstationarity and the time dependent variation of a signal`s magnitude is known as amplitude (or temporal) nonstationarity.

For ground motion signals, the high frequency content, generally, arrives sooner leading to a tendency for the ground motion frequency content to shift to lower frequencies as time increases. These non-stationarities can be partly attributed to the arrival times of the different types of waves, P waves (primary), S waves (secondary), and surface waves (Rayleigh). In other cases, the effect of decreasing dominant frequencies in ground motions has been attributed to site resonance.

The traditional earthquake demand measures such as the response spectra and the Fourier amplitude spectra do not capture time dependent variability in the frequency content. Hence, the estimates of nonlinear system response based solely on these measures may misrepresent the nonlinear response of a structure.

Real structures that are subjected to design level earthquake events are expected to experience nonlinearity in their structural response leading to time-varying structural properties. The natural frequencies of the structure shift to lower frequencies due to inelasticity and the resulting nonlinearity in the structural response. Inelasticity creates an effective softening of the system whereby the secant stiffness is smaller than the initial stiffness causing elongation of the

structural period. When the frequency content of the ground motion shifts in a similar manner as the natural frequencies of the structural response, a phenomenon referred to as moving resonance occurs. Resonance is the tendency of a system to oscillate at greater amplitude at some frequencies than at others. These are known as system`s resonant frequencies. At these frequencies, even small periodic driving forces can produce large amplitude oscillations, increasing the systems response. This increase in systems response is significant for nonlinear systems and hence the moving resonance is considered important in the present research.

Although RTR variability is identified as important and the effects of RTR variability have been analyzed statistically by some researchers, there is a gap in the research in analyzing the sources of this variability (Ibarra and Krawinkler, 2011). Therefore, there is need to further understand the sources of variability in structural response due to phenomena like moving resonance. Lack of understanding could lead to the selection of ground motions that do not properly represent the potential for moving resonance at a site, or require a larger than necessary set of ground motions to appropriately capture the effect. It is also necessary to understand the effect of spectral nonstationarity on structural response for creating artificial ground motions. Using artificial ground motions that do not have appropriate spectral nonstationarity for structural design will lead to results inconsistent with real earthquakes. Finally, if the potential for moving resonance is understood, methods for mitigating the detrimental effects in selecting structural systems can be devised. There is a clear need to better understand the effect of spectral nonstationarity and moving resonance on structural response.

1.2 Objectives of the project

The primary objective of this project is to develop a method to analyze the time-frequency content of a ground motion to assess the occurrence of moving resonance and to quantify its potential in effecting the structural systems. The method of assessing the occurrence of moving resonance is intended to be performed by means of finding correlation between the time-frequency content of the ground motion and the structural response. The correlation is intended to be obtained by projecting the wavelet coefficients of ground motion acceleration onto the wavelet coefficients of structural velocity. The method of investigation involves the following approach:

- Investigate time-frequency content of the ground motion and structural response using wavelet transforms.
- Developing tools to assess and quantify moving resonance.
- Conduct a detailed study for a selected ground motion with varying structural system period, strength, and hysteretic behavior.
- Extending the analyses to a suite of ground motions (representing a range of source distance, magnitude, and soil type).
- Categorizing earthquake ground motions as to the effect of moving resonance causing on the structural response.

1.3 Thesis Organization

This document contains eight chapters and three appendices. Chapter 1 gives the introduction of the project which includes the statement of the problem, objectives of the project and the organization of the document. Chapter 2 explains the background of wavelet analysis and Chapter 3 presents the summary of related research done in the field of earthquake engineering using wavelet analysis, in particular on the effect of moving resonance and spectral nonstationarity on the structural response. Chapter 4 describes the wavelet analysis program that is written as part of this research for the calculation of wavelet coefficients. Chapter 5 discusses the refinement of the time-frequency representation of earthquake signals. Chapter 6 discusses the tools developed to assess the occurrence and quantification of moving resonance and shows a detailed parametric study on a particular ground motion and Chapter 7 extends the analyses to a suite of ground motion records. Chapter 8 provides the conclusions and recommendations from the research performed. Appendix A presents some of the properties of the wavelet functions and Appendix B shows the different matlab in-built functions that were used in the wavelet analysis program. Appendix C shows some additional refinement plots of time-frequency data.

CHAPTER 2 : BACKGROUND ON WAVELETS

2.1 Introduction

Wavelets were introduced in 1980's by Morlet for processing seismic signals (Gaupillaud et al. 1984, Grossmann and Morlet 1984). Wavelets are mathematical functions that identify different frequency components of a signal at discrete windows of time using a variable resolution matched to the frequency under consideration. They have advantages over the traditional Fourier methods in analyzing physical situations where the signal contains discontinuities and sharp spikes. Wavelets were developed independently in the fields of mathematics, quantum physics, electrical engineering, and seismic geology. Interchanges between these fields during the last ten years have led to many new wavelet applications such as image compression, turbulence, human vision and radar.

This chapter presents a nice discussion on advantages of wavelet transforms over different types of transformations, types and functions of two different wavelet transforms (namely continuous and discrete) and forms of wavelet families. This chapter also shows differences between different types of wavelet transforms by performing sample analyses on a signal and helps to choose the appropriate wavelet function for the rest of the project.

2.2 Different types of Transformations

The following section describes the functions, advantages and disadvantages of various types of transformations that are by far the most popular. Transformation of a signal is a procedure used to obtain change in its composition. As per definition, the transformations need not to be reversible.

Transformations are applied to signals to obtain further information that is not readily available in the raw time history signal. There are a number of transformations that can be applied, among which the Fourier transforms (FT), Short Time Fourier transform (STFT) and Wavelet Transforms (WT) are the most popular. The functions and limitations of each of these transformations are given below.

2.2.1 Fourier Transform

The Fourier transform is a technique which breaks down a signal into constituent sinusoids of different amplitudes and phase. In other words, Fourier analysis is a mathematical technique for transforming the signal from a time-based representation to a frequency-based one. Figure 2-1 shows the transformation of a signal from time-based to frequency-based. Each rectangular box in the result corresponds to the Fourier coefficient with its amplitude given along the x-axis.

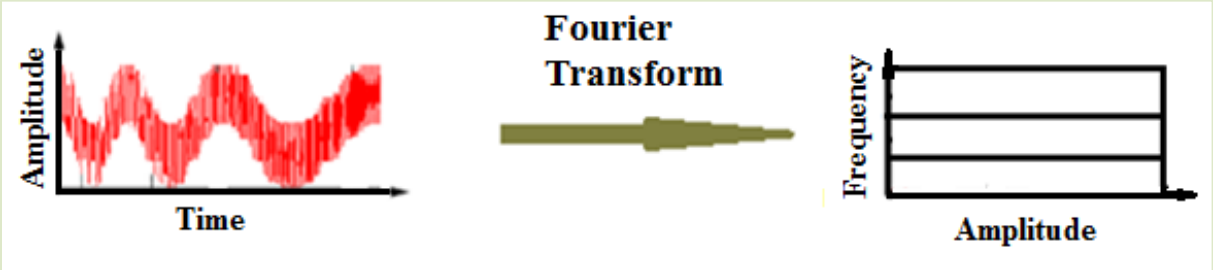

Figure 2-1 Graphical representation of Fourier Transform

The Fourier transform is a reversible transform. That is, it allows going back and forth between the raw signal and processed (transformed) representation. However, only time representation or frequency representation is available. That is, the variation in frequency information is not available in the time-domain which is clear from Figure 2-1.

The Fourier transform gives the frequency information of the signal, which means that it tells how much amplitude exists at each frequency, but it does not tell when in time these frequency components exist. That is because the fourier transform is only applicable to stationary signals (signals whose frequency content does not change in time). For stationary signals, it is not necessary to know at what times frequency components exist, since all frequency components exist at all times. In short, one of the primary limitations of Fourier analysis is that information about nonstationarity is lost. If a signal doesn't change much over time, that is, if it is a nearly stationary signal, this drawback isn't very important. However, earthquake ground motions and response signals contain numerous non-stationary or transitory characteristics. These characteristics are often an important part of the signal, and Fourier analysis is not suited in detecting them.

2.2.2 Short Time Fourier Transform (STFT)

In an effort to correct the deficiency involved in Fourier analysis, Gabor adapted the Short Time Fourier transform to analyze only a small section of the signal at a time - a technique called windowing the signal. For this purpose, a window function "w" is chosen. The width of this window must be equal to the segment of the signal where the assumption of stationarity is valid.

Figure 2-2 shows the graphical representation of Gabor's adaptation, called the Short-Time Fourier Transform (STFT), where the window is simply a square wave. The square wave window truncates the sine or cosine function to fit a window of a particular width. The result of the transformation is a 2D representation of time-frequency data as shown in Figure 2-2. Each square box in the result corresponds to a coefficient, the width along the x-axis represents its time resolution and the height along its y-axis represents its frequency resolution. Because a single fixed width window is used for all frequencies in the STFT, the resolution of the analysis is the same at all locations in the time-frequency plane.

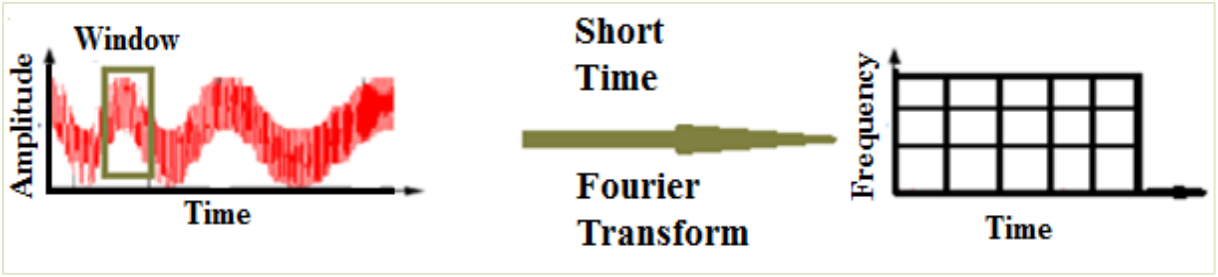

Figure 2-2 Graphical representation of Short Time Fourier Transform

This is of no good because windows meant for capturing high frequency content of the signal cannot capture low frequency content and vice-versa. Many signals can benefit from a more flexible approach, one where the window size can be varied to determine the amplitude at a given time and frequency with greater accuracy.

This is a problem of resolution, and it is the main reason why some researchers have switched to wavelet transforms from STFT. STFT gives a fixed resolution at all times, whereas wavelet transforms give a variable resolution.

The computer program for Nonlinear Dynamic Time History Analysis named NONLIN (2003) has an interactive tool to generate and display Fourier amplitude spectrum plots called Travelling FFT. It provides a space for determining the frequency content of segments of the ground motion consisting of 128,256 or 512 contiguous points in the motion. This is found similar to STFT and have the same limitations of STFT- fixed window size. The travelling FFT gives the frequency content of the current, previous and the next positions of the window as shown in Figure 2-3.

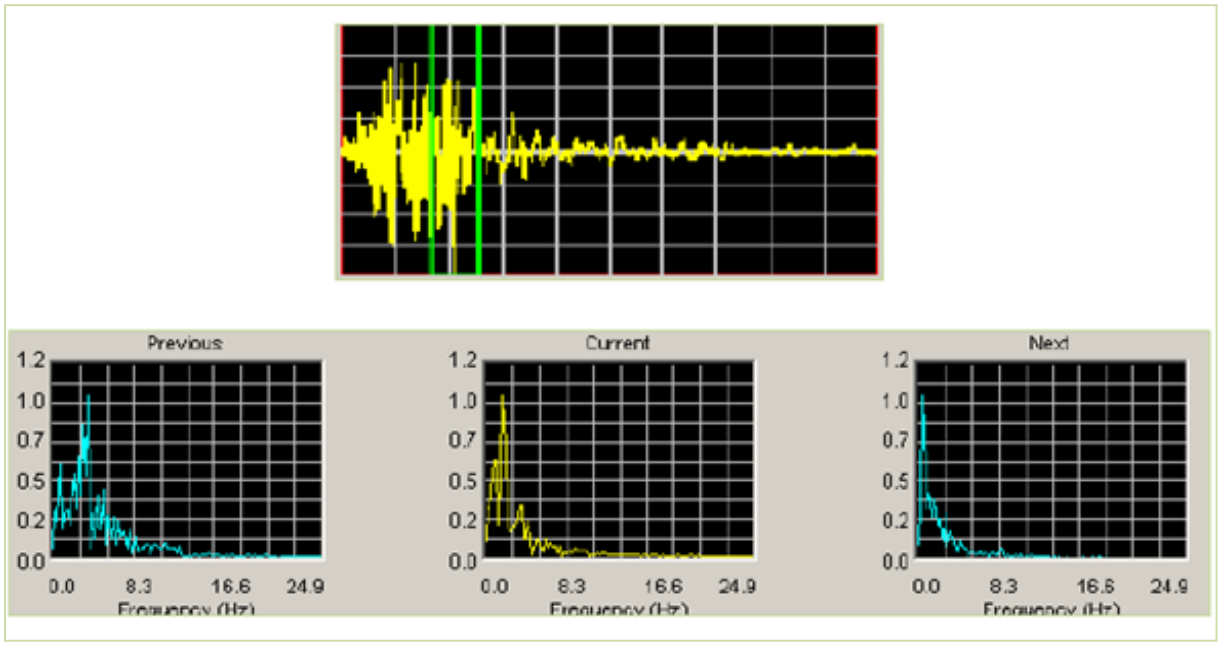

Figure 2-3 Snap shots of a Traveling FFT for Northridge earthquake

2.2.3 Wavelet Transform (WT)

Wavelet analysis represents a logical step forward: a transform technique with variable-sized windows called Wavelet Transform (WT). Wavelet analysis allows the use of long time windows where low frequency information is required, and shorter windows where high frequency information is required.

Figure 2-4 shows the graphical representation of Wavelet Transform (WT), where variable sized windows are used for analyzing the signal, allowing for the use of long time segments for capturing the low frequency contents, and narrow time segments for capturing high frequency contents. Although wavelet analysis is a time-scale analysis technique, relation to the time-frequency analysis can be made. Low scales correspond to compressed wavelets which are

capable of capturing rapidly changing features of the signal linked to higher frequencies. On the other hand, high scales correspond to dilated wavelets that are able to capture the slowly changing features of the signal linked to low frequencies. Hence, the term scale can be approximately taken as the inverse of frequency. The wavelet analysis plot for scale vs time as shown in Figure 2-4 can be interpreted as follows: Each rectangular box corresponds to a wavelet coefficient and the width of the box along x-axis represents its time resolution and the height along the y axis represents its frequency resolution.

Since, the amplitude at each frequency is calculated with different resolution; wavelet analysis is also called multiresolution analysis which is designed to give good time resolution at high frequencies and good frequency resolution at low frequencies. This concept of multiresolution analysis can be observed from Figure 2-4.The bottom row of the scale vs time plot as shown in Figure 2-4, which corresponds to higher frequencies, contains many rectangular boxes having small width along x (time) axis. This shows that there is more information in time and hence higher frequencies can be resolved better in time. The top row of the Figure 2-4, however, corresponds to lower frequencies, contains resolution boxes having small width along y (frequency) axis showing more information in frequency and hence lower frequencies are better resolved in frequency.

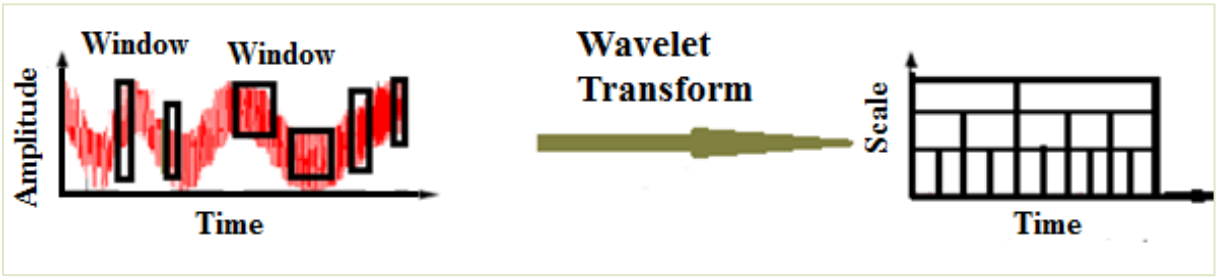

Figure 2-4 Graphical representation of Wavelet Transform

2.3 Definition of a Wavelet

A wavelet is a waveform of effectively limited duration that has an average value of zero. In other words, a wavelet is a wave-like oscillation with amplitude that starts out at zero, increases, and then decreases back to zero.

The wavelets are generated from a single basic wavelet$\Psi_{s,\tau}(x)$, called the mother wavelet, which is given by Equation 2-1 by means of scaling and shifting. The term mother implies that the functions with different region of support that are used in the transformation process are derived from the mother wavelet. In other words, the mother wavelet is a prototype for generating the other wavelet functions. The mother wavelet function varies depending on the type of wavelet used.

$$\Psi_{(s,\tau)}(x) = \frac{1}{\sqrt{s}}\Psi\left(\frac{x-\tau}{s}\right) \qquad \textbf{2-1}$$

The variables s and τ in Equation 2-1 corresponds to the scaling and shifting parameters respectively. The term $\frac{1}{\sqrt{s}}$ is the normalizing term and is used to maintain the same energy before and after the transformation process.

Scaling is a mathematical operation, which either dilates or compresses a signal. High scale values correspond to dilated (or stretched out) signals and low scales correspond to compressed signals which can be seen graphically from Figure 2-5. Low scales which correspond to compressed wavelets are capable of capturing rapidly changing features of the signal (higher frequencies). On the other hand, high scales which correspond to dilated wavelets can able to capture the slowly changing features of the signal (low frequencies). This way, the term scale and frequencies are related with each other.

Figure 2-5 Interpretation of Scaling term

Shifting a wavelet simply means delaying (or hastening) its onset. Mathematically, delaying a function $\Psi(x)$ by τ is represented by $\Psi(x-\tau)$. Figure 2-6 shows the representation of shifting a function.

Figure 2-6 Representation of shifting of a function

The term shifting (translation) corresponds to time information in the transform domain. It is used to describe the location of the window in time, as the window is shifted through the signal.

2.4 Comparison of Wavelets with Sine Wave

Wavelets are the basis of WT just as sine waves are the basis of FT. Figure 2-8 shows the comparison between sine wave and real part of complex morlet wavelet of band width 1 and center frequency 1.5. The mother wavelet function of the Complex Morlet wavelet is given by Equation 2-2.

$$\Psi(x) = \sqrt{\pi f_b}\, e^{2i\pi f_c x} e^{-x^2/f_b} \qquad \textbf{2-2}$$

Where

f_b is the bandwidth parameter

f_c is a wavelet center frequency

Bandwidth is the difference between upper and lower frequencies in a contiguous set of frequencies. It is typically measured in hertz. Wavelet center frequency is the number of oscillations the wavelet has in one sec. The real and imaginary part of the complex morlet wavelet of band width 1 and center frequency 1.5 is shown in Figure 2-7. From real part of the complex morlet wavelet shown in Figure 2-7, it is observed that it has 1.5 oscillations in 1 sec which corresponds to its center frequency and has a unit width between the upper and lower frequencies corresponding to its band width.

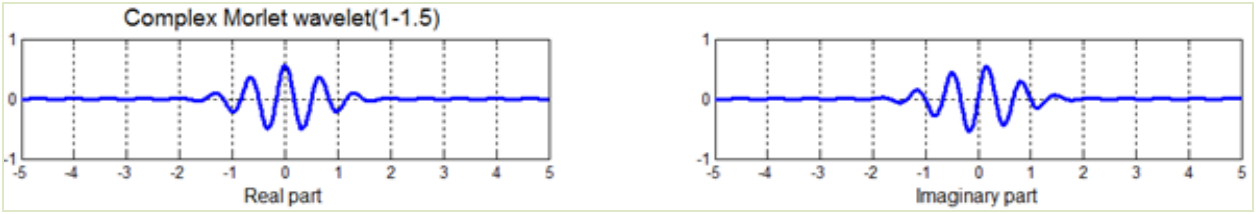

Figure 2-7 Real and Imaginary part of Complex Morlet Wavelet of bandwidth 1 and center frequency 1.5

Since the mother wavelet function of the complex morlet wavelet is complex as shown in Equation 2-2 (which contains both real and imaginary part), the real part is selected and compared with the sine wave as shown in Figure 2-8. It is observed that the sinusoids do not have limited duration — they extend from minus to plus infinity, whereas wavelets last for very limited duration. Also sinusoids are smooth and predictable, but wavelets can be irregular and asymmetric.

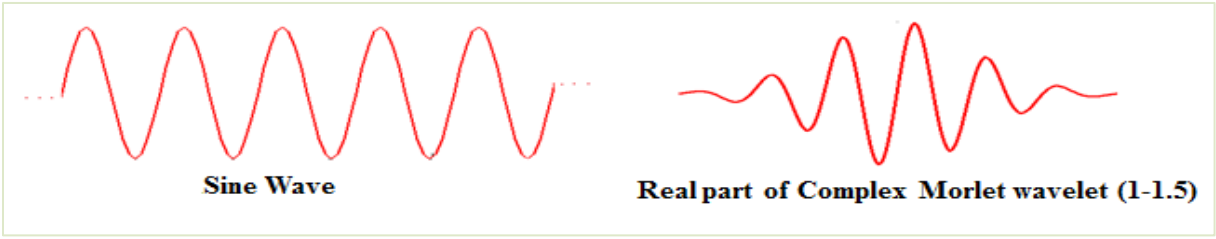

Figure 2-8 Comparison of sine wave with Wavelets

Fourier analysis is a method of breaking up a signal into sine waves of various frequencies. Similarly, wavelet analysis is the breaking up of a signal into shifted and scaled versions of the original (mother) wavelet.

2.5 Types of Wavelet Transforms

The wavelet transform is a recent solution to overcome the shortcomings of the other transform methods. In wavelet analysis, the use of a fully scalable modulated window (variable width windows) solves the fixed window problems of STFT described in the previous section. There are two types of wavelet transforms namely continuous wavelet transform (CWT) and discrete wavelet transform (DWT) based on the method followed for calculating wavelet coefficients and the main differences between two transformations are shown in Table 2-1.

Table 2-1 Differences between Continuous and Discrete wavelet transforms

Name of Wavelet Transformation	Continuous Wavelet Transform (CWT)	Discrete Wavelet Transform (DWT)
Basic functions	The Continuous wavelet transform was computed by changing the scale of the analysis window, shifting the window in time, multiplying by the signal, and integrating over all times.	In discrete case, filters of different cutoff frequencies are used to analyze the signal at different scales. The signal is passed through a series of high pass filters to analyze the high frequencies, and it is passed through a series of low pass filters to analyze the low frequencies.
Shifting of wavelet	Continuous in terms of shifting. Overlapping of wavelets takes place giving redundant information. Hence, CWT is NOT orthogonal	Wavelet translates along the time series in units-NO overlapping. Hence DWT is orthogonal.
Reconstruction of signal	Not possible because of highly redundant information	Possible

The resolution of the wavelet coefficients of both the transforms works on the principle of multiresolution analysis which is designed to give good time resolution at high frequencies and good frequency resolution at low frequencies. This concept of multiresolution analysis can be clearly explained with Figure 2-9.

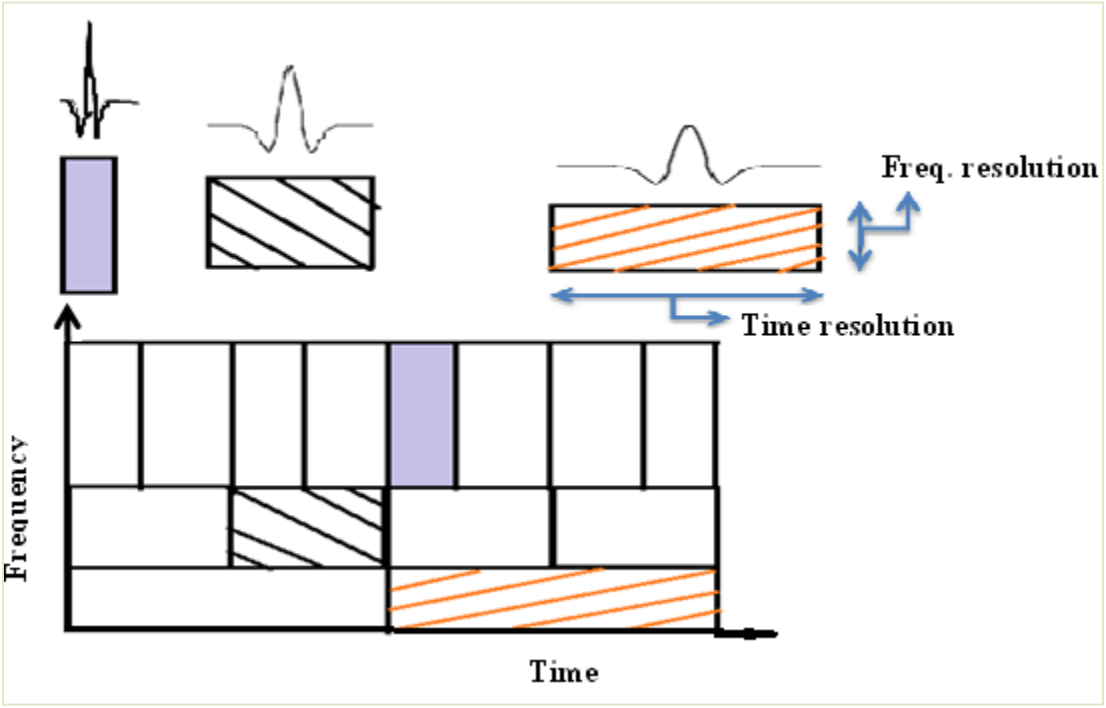

Figure 2-9 Resolution of wavelet coefficients

Figure 2-9 shown above gives the graphical representation of the wavelet transform explaining the time-frequency resolution. It can be interpreted as follows: Each rectangular box corresponds to a wavelet coefficient and the width of the box along x-axis represents its time resolution and the height along the y axis represents its frequency resolution. The top row of the Figure 2-9 contains many rectangular boxes having small width along x (time) axis and more width along the Y (frequency) axis. This shows that there is more information in time and hence higher frequencies can be resolved better in time. The bottom row of the Figure 2-9, however, corresponds to lower frequencies, contains resolution boxes having small width along y (frequency) axis showing more information in frequency and hence lower frequencies are better resolved in frequency.

2.6 Wavelet Families

The wavelet family comprises of two main types of wavelets namely continuous wavelets and discrete wavelets. Continuous wavelets are further classified into real and complex based on the type of wavelet function used. Following shown are some of the examples of different types of wavelets.

Discrete Wavelets

Some of the examples of discrete wavelets are:

- Daubechies wavelet of order (2, 4, 6, 8, 10, 12, 14, 16, 18, 20)
- Haar wavelet
- Meyer wavelet
- Coiflet of order (6, 12, 18, 24, 30)
- Symlet wavelet
- Daubechies biorthogonal wavelets

Continuous Wavelets

Some of the examples of real continuous wavelets are:

Real-Valued Continuous Wavelets

- Beta wavelet
- Meyer wavelet
- Hermitian hat wavelet
- Mexican hat wavelet

Complex Continuous Wavelets

Some of the examples of real continuous wavelets are: The mother wavelet functions of these wavelets are complex (containing both real and imaginary parts) in nature.

- Complex Guassian (Gabor) wavelet of varying orders (1,2,4,8)
- Complex Morlet wavelet of varying band widths and frequencies
- Shannon wavelet

The mother wavelet function and their graphical representation of some of the wavelets are shown below:

The mother wavelet function of the Mexican hat wavelet and Morlet wavelet which is given by Equation 2-3 and 2-4 respectively is shown graphically in Figure 2-10. These mother wavelets were plotted for their effective width along the x-axis and their amplitude along the y-axis. The effective width changes with every mother wavelet function.

$$\Psi(x) = \left(\frac{2}{\sqrt{3}}\pi^{-1/4}\right)(1-x^2)e^{-x^2/2} \qquad \textbf{2-3}$$

$$\Psi(x) = e^{-x^2/2}\cos(5x) \qquad \textbf{2-4}$$

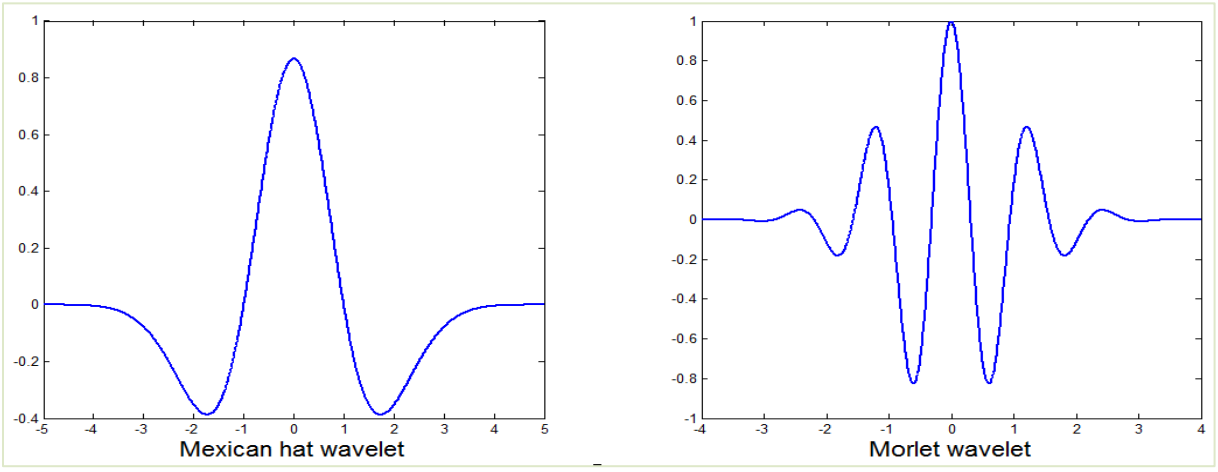

Figure 2-10 Mexican hat and Morlet wavelet

The mother wavelet function of the Complex Guassian wavelet which is given by Equation 2-5 is shown graphically in Figure 2-11.

$$\Psi(x,n) = C_n e^{-ix} e^{-x^2/2} \qquad \textbf{2-5}$$

The n in the Equation 2-5 is the parameter of the Complex Guassian family and corresponds to the order of the wavelet function. i.e. n=4 corresponds to the 4th derivative (order) of the original function $\Psi(x)$. C_n is such that the 2-norm of the nth derivative of $\Psi(x)$ is 1 which is mathematically by Equation 2-6.

$$\left|\Psi^{(n)}\right|^2 = 1 \qquad \textbf{2-6}$$

Where $\Psi^{(n)}$ is the n[th] derivative of $\Psi(x)$.

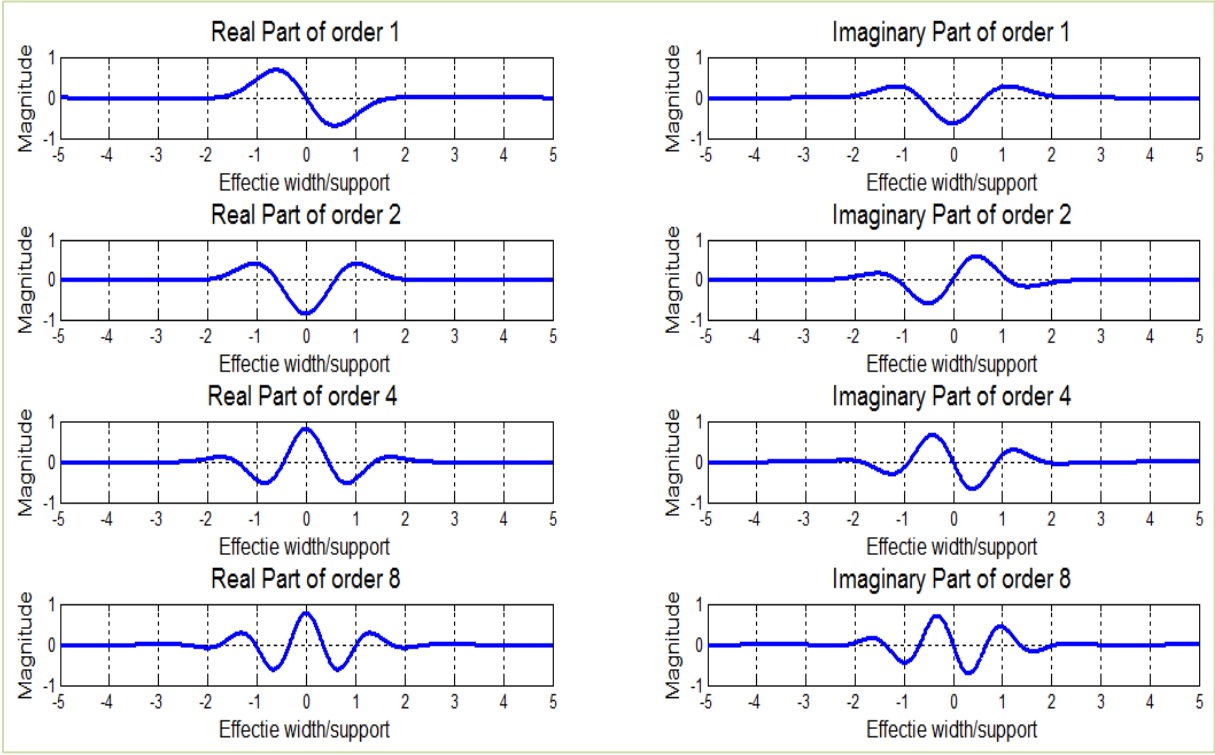

Figure 2-11 Real and imaginary parts of Complex Guassian wavelets of order 1, 2, 4 and 8

The mother wavelet function of the Complex Shannon wavelet of band width 0.5 and center frequency 1 which is given by Equation 2-7 is shown graphically in Figure 2-12.

$$\Psi(x) = \sqrt{f_b} sinc(f_b x) e^{2i\pi f_c x} \qquad \textbf{2-7}$$

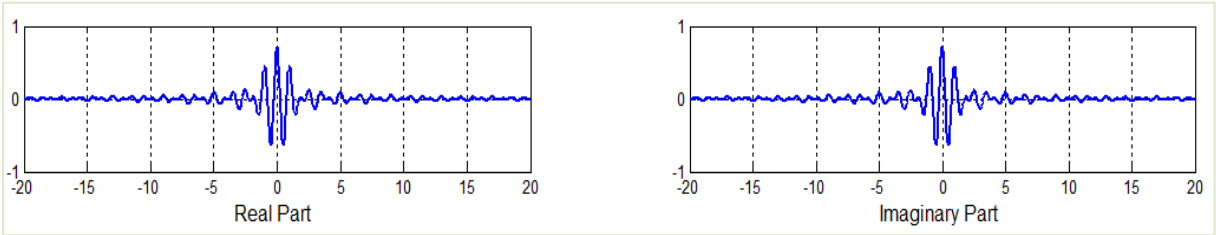

Figure 2-12 Real and imaginary parts of Complex Shannon wavelet of band width 0.5 and center frequency 1

2.7 Relationship between Scale in CWT and Period

Publications on wavelet analyses are typically presented in terms of scale instead of frequency or period. Scale can be taken as inversely proportional to frequency as discussed in section 2.3. The relationship between two is given by Equation 2-8. The scale refers to the width of the wavelet. As the scale increases and the wavelet gets wider, it includes more of the time series, and the resolution in time reduces, which was shown in Figure 2-9. For all wavelets, scale and period are proportional.

$$f_a = \frac{f_c}{S*\Delta T} \qquad \textbf{2-8}$$

where

- S is a scale.
- ΔT is the sampling period.
- f_c is the center frequency of a wavelet in Hz.
- f_a is the frequency corresponding to the scale S, in Hz.
- Period is inverse to frequency, period=1/f_a

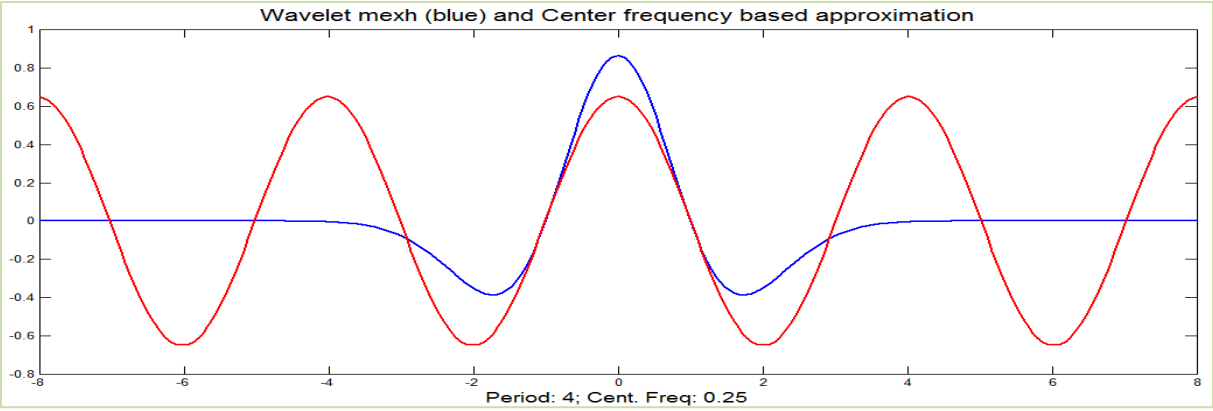

Figure 2-13 Wavelet mexh (blue) and center frequency based cosine wave

From the Figure 2-13, it is shown that the period for mexican hat wavelet is 4, and its corresponding frequency is fc=1/4=0.25.Using the formula given in Equation 2-8,the value of one variable (scale or freqency) can be calculated given the other.

2.8 Comparison of CWT, DWT and complex CWT, and Selection of Primary Tool for this Project

A sample analysis is done on a signal as shown in Figure 2-14 to compare the time-frequency representation of different types of wavelet transforms. The signal used for the analysis is the combination of two functions, the frequency content of one linearly increasing with time and the other decreasing with inverse of time as given by Equation 2-9.

$$f(t) = sin(0.15t^2) + sin\left(\frac{2000}{t+4}\right) \quad \text{2-9}$$

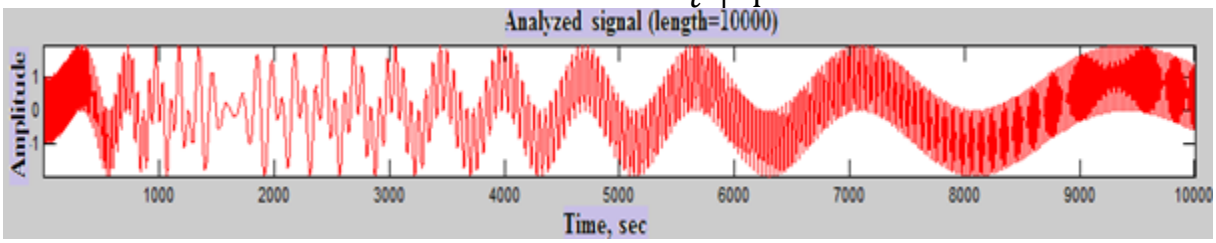

Figure 2-14 Sample signal used for the comparison of different types of wavelets

The signal is analyzed using Mexican Hat, Discrete Meyer and Complex Guassian of order 1 wavelets and the wavelet coefficients were plotted as shown in Figures 2-15, 2-16 and 2-17 respectively. These three wavelets chosen above represent the real continuous, discrete and complex continuous type of wavelets respectively. The wavelet coefficients of continuous wavelets (both real continuous and complex continuous) were plotted for time along horizontal axis and scale (inverse of frequency as discussed in previous sections) along vertical axis, whereas the wavelet coefficients of discrete wavelet are plotted for time along horizontal axis and level number along vertical axis. Each level number signifies a particular band of frequencies. Lower level number corresponds to higher frequency bands and higher level number corresponds to lower frequency bands. Since, the primary objective of this section is to compare the three wavelet coefficients plot, it is necessary to have the same vertical axis for all the plots. This leads to further investigate the significance of level number and its relation with scale (or frequency).

The following illustration will explain the significance of level number. Suppose there is a M-sample long signal sampled at N MHz (rate) and the problem is to obtain its DWT coefficients. Since the signal is sampled at N MHz, the highest frequency component that exists in the signal is N/2 MHz (Nyquists-Shannon sampling theorem) (Shannon 1949). At the first level, the signal is passed through the high pass and low pass filters. The output of the high pass filter which has

frequencies ranging between [N/4 N/2] corresponds to level 1 and similarly level 2 corresponds to a frequency band of [N/8 N/4],….so on and level P corresponds to a frequency band of $[(1/2)^{p+1} \quad (1/2)^{p}]$. This gives the relation between level number and frequency and since scale-frequency (refer to section 2.7) is already known, the vertical axis of all the plots is made consistent using these relations.

The sample signal analysed as shown in Figure 2-14 has a frequency of 1 Hz and as per Nyquists-Shannon sampling theorem, the highest frequency component that exists in the signal is ½. Using scale-frequency and level number-frequency relations, it is proved (Please refer to Appendix D) that the frequency content corresponding to a level number 9 of discrete meyer wavelet is equivalent to a scale of 125 for mexican hat wavelet (having center frequency f_c=0.25 and sampling period of 1) and a scale of 150 for complex guassian wavelet of order 1(having center frequency f_c=0.3 and sampling period of 1). The wavelet coefficient plots were plotted using these conversions along vertical axis and hence all plots are consistent for comparison.

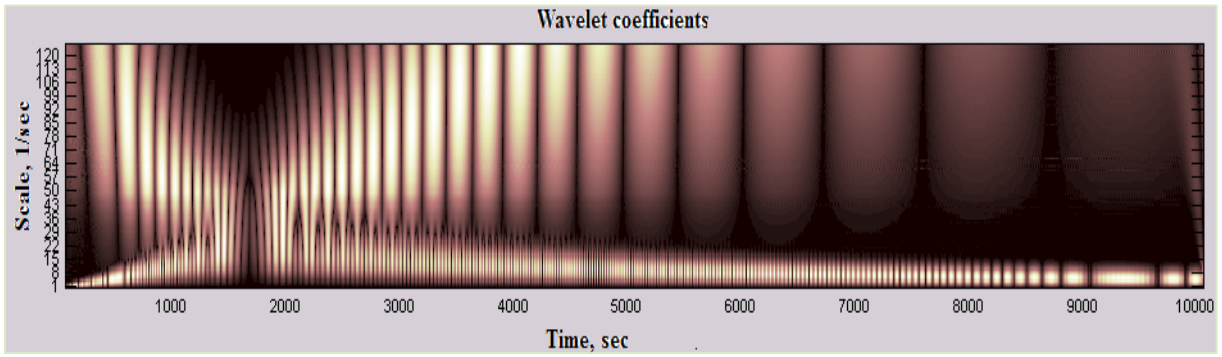

Figure 2-15 Wavelet coefficients plot of the sample signal using mexican hat wavelet

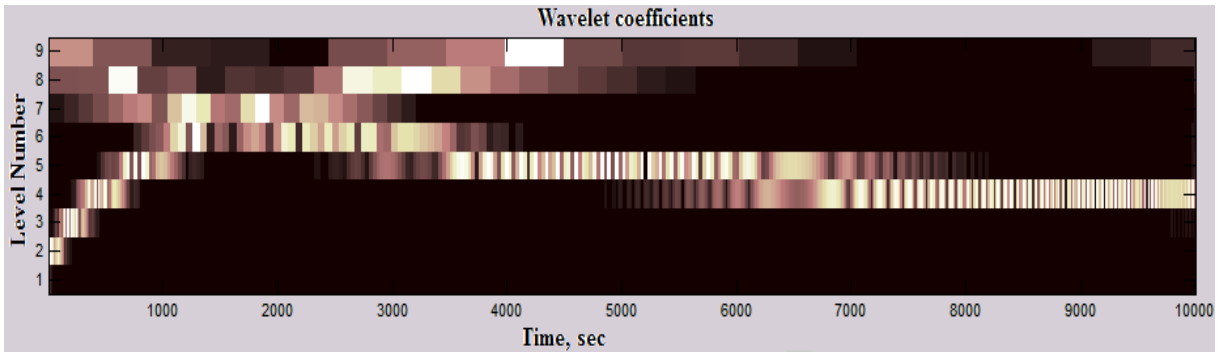

Figure 2-16 Wavelet coefficients plot of the sample signal using discrete meyer wavelet

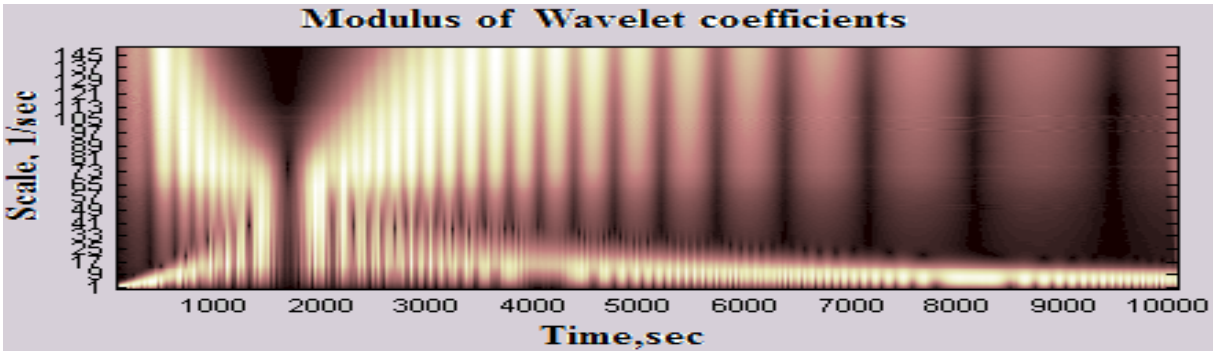

Figure 2-17 Wavelet coefficients plot of the sample signal using complex guassian wavelet of order 1

Figure 2-18 Color modulation of the magnitude of the coefficients

- Graphical representation shown in the Figure 2-18 gives the colour modulation for the wavelet coefficients from **minimum** (left) to **maximum** (right).
- Light colours represent larger magnitude coefficients (which imply the wavelet with that period and time closely matches with the signal) and darker shades represent the smaller coefficients.

For use in this project, continuous wavelet transforms are selected as the main tool for decomposing the frequency content of signals. The reasons for this selection include:

- The frequency content representation will be smooth and continuous because of overlapping of wavelets occurring in CWT.
- Unlike the DWT, the CWT can operate at any frequency, starting from minimum value to the maximum value. DWT is organized into frequency bands.
- The CWT is also continuous in terms of shifting. The analysing wavelet is shifted smoothly over the full domain of the signal.
- The frequency content can be better visualized because of more data in CWT unlike in DWT.

Since the objective of this project is to analyse the ground motion and structural response signals, more data will make analysis easier and this becomes the reason behind choosing CWT. The primary advantage of DWT is that the signal can be reconstructed using inverse wavelet transforms which is not required.

At this point, the use of continuous wavelet transforms for the rest of the project is decided, but in continuous there are again two types namely real continuous and complex continuous and to choose one among these needs further observation of the plots.

From the Figure 2-15, it is understood that wavelet coefficients exhibit interference bands when using the Mexican hat wavelet. These interference bands generally occur when the wavelet is out of phase with the signal. The Gabor (complex guassian) wavelet rectifies this problem because it includes a complex part (as shown in Equation 2-5).The magnitude of the resulting complex wavelet coefficients captures the frequency content in the signal regardless of phase as shown in Figure 2-17.

The complex continuous wavelets have the following additional advantages over real-valued continuous wavelets which are the reasons for selecting it as the main tool for decomposing the frequency content of signals.

- The continuous wavelet captures the frequency content irrespective of the signal being in phase or out of phase.
- The complex wavelet coefficient comprises two parts that provide information about phase as well as magnitude.

Also since the objective of the project is to find the correlation between the wavelet coefficient of ground motion and the wavelet coefficient of the structural response where phase plays a major role, the complex continuous wavelets is chosen for the rest of the project.

CHAPTER 3 : LITERATURE REVIEW

The previous chapter explained the background on wavelets and this chapter discusses the applications of wavelets in the field of earthquake engineering. Wavelet transforms have been used in different areas of earthquake engineering in the recent years. The literature review discussed herein is categorized based on its applications in those areas.

3.1 Time-Frequency Representations of Earthquake Ground Motions

Researchers have used wavelets to represent the time-frequency energy content of earthquake ground motions using a variety of approaches.

Chakraborty and Okaya (1995) compared short time Fourier Transform, continuous wavelet transform, and matching pursuit decomposition. Although the wavelet transform has better time-frequency resolution than an STFT, the resolution is not uniform across the entire time-frequency plane. The wavelet transform has good time resolution for high frequencies and good frequency resolution for low frequencies. To get good frequency resolution at intermediate to high frequencies, a wavelet transform alone is not sufficient. It was found that matching pursuit decomposition has the ability to improve the frequency resolution for intermediate to high frequency ranges. In the matching pursuit decomposition (MPD), a set of basis functions are generated by scaling, translating, and modulating a single window function similar to wavelet transform. But here, the basis functions are time-frequency atoms which have combinations of all possible time and frequency widths and as a result constitute a redundant set.

Kareem and Gurley (1999) presented example applications of wavelet transforms in ocean, wind and earthquake engineering. The analysis, identification, characterization and simulation of random processes utilizing both the continuous and discrete wavelet transform is addressed. The wavelet transform is used to decompose random processes into localized orthogonal basis functions, providing a convenient format for the modeling, analysis, and simulation of non-stationary processes. The time-frequency analysis made possible by the wavelet transform provides insight into the character of transient signals through time-frequency maps of the time variant spectral decomposition that traditional approaches lack.

Zhou and Adeli (2003) decomposed earthquake records using Mexican Hat wavelets. It was proposed that ground motions in earthquakes are postulated as a sequence of simple penny-shaped ruptures at different locations along a fault line and occurring at different times. The single point source displacement of ground motion is idealized by a Gaussian function. Interference bands were observed in the wavelet coefficients when using real valued wavelets and the investigation of these bands is given importance in the present study and more will be discussed in the later chapters.

3.2 Characterization of Ground Motions

Wavelet transforms have been used by Baker (2007) to identify near-field source pulses in ground motions. A Daubechies mother wavelet of order 4 was used to identify the largest pulse in the velocity response. The wavelet coefficients associated with the largest velocity pulse are compared to the largest wavelet coefficients after the velocity pulse is removed and therefore allows the quantification of whether the velocity pulse dominates the ground motion. This method allows the classification of the ground motion as pulse like. This approach is useful for a variety of seismology and engineering applications where pulse like ground motions are of interest, such as probabilistic seismic hazard analysis, ground motion prediction and nonlinear dynamic analysis of structures.

ElGawady et al. (2010) builds on Baker's method for extracting velocity pulses to examine structural response due to ordinary and forward-directivity ground motions. Three different generic multistory shear buildings were subjected to 54 near-fault set of ground motions including ordinary and forward-directivity pulses. It was found that the structural response was dominated by the pulses. A Gabor wavelet was used to simulate these pulse dominated ground motions. If the structure fundamental period was between 0.5 sec and 2.5 sec, the Gabor pulse could be used to reproduce the structural response due to the forward directivity ground motion, implying that the structural response is almost entirely dominated by the associated velocity pulse. Outside of this period range, it was found that higher frequency content of the ground motions played a significant role.

Mavroeidis et al. (2004) describes the requirements of the ground motion input in order to investigate the response of structures to near-fault seismic excitations. A parametric analysis of

the dynamic response of the SDOF system as a function of the input parameters of the mathematical model is performed to gain insight regarding the near-fault ground motion characteristics that significantly affect the elastic and inelastic structural performance. 'Pulse Duration' emerged as a key parameter of the problem under investigation and it was employed to normalize the elastic and inelastic response spectra of actual near-fault strong ground motion records.

Chanerley et al. (2010) used wavelet transforms to correct earthquake ground motions to eliminate the baseline shift. Shifts and offsets in the velocity and displacement time histories obtained from integrating the acceleration time history are identified as part of the low frequency content of the ground motion and eliminated. The high frequency noise is also eliminated using a soft threshold scheme where wavelet coefficients below a certain threshold are set to zero and smoothing out any resulting discontinuities in the signal. They used biorthogonal wavelets.

3.3 Using Wavelets for Spectral Matching of Ground Motions

Wavelets have been used to modify actual ground motions to match a given response spectrum. Some methods start with an acceleration record and use an algorithm to alter the acceleration time history until the resulting response spectrum matches the target spectrum. Other methods use wavelet transforms in conjunction with neural networks to develop a ground motion based on a target spectrum that has similar time-varying frequency characteristics as a set of real ground motions.

Al Atik and Abrahamson (2010) presents a discussion of the need for spectral matching in reducing the number of response history analyses required to get an accurate measure of mean structural response while not compromising the accuracy and reliability of solutions. Also, spectral matching can be used to represent soil sites for which adequate ground motions representing the site conditions and hazard do not exist. They identify wavelet transform as an effective method for spectral matching because of its ability to preserve the non-stationary characteristics of real ground motions.

Algorithms for spectral matching through adjusting the frequency content are typically based on the methodology presented by Lilhanand and Tseng (1988). Suarez and Montejo (2005)

identified the selection of a proper wavelet basis as critical in the spectral matching process. Although the Littlewood-Paley (1937) wavelet was considered as a valid alternative, they developed their own wavelet based on the impulse response function. One of the challenges is adjusting the acceleration time history record in a way that the integrated velocity and displacement still have a zero value at the end. The wavelet used by Suarez and Montejo (2005) resulted in baseline shifts and thus required baseline correction as part of the implementation scheme. Al Atik and Abrahamson (2010) developed a method for spectral matching that does not require baseline correction. They use a tapered cosine wavelet that integrates to a velocity and displacement with zero value at large time. The method consists of creating acceleration time histories based on the difference between target and actual spectral ordinates. The created acceleration time histories are added to the original time history.

Nakhaei and Mohraz (2010) used spectral matching methods to create artificial ground motions that match the inelastic damage spectrum (damage index on the vertical axis, period on the horizontal axis). They used the Littlewood-Paley (1937) wavelet basis. They also compared the advantages and disadvantages of the genetic algorithm and wavelet transformation techniques for record scaling.

Several researchers have combined wavelet transforms with neural networks to create artificial ground motions to match a particular response spectrum. Rajasekaran et al. (2006) utilized Daubechies wavelet of order 2 with discrete wavelet transform. The Daubechies 2 wavelet was used because it was found to retain the shape of the signal even after three decomposition levels.

Asadi et al. (2010) combined wavelet transforms with neural networks to create artificial ground motions to match a particular response spectrum. The neural network was trained using a set of ground motions, which mapped their pseudo-velocity response spectrum to the corresponding wavelet coefficients (and resulting acceleration time history). New pseudo-velocity response spectra could then be input, and a ground motion with similar pseudo-velocity response spectrum and time-varying frequency content similar to realistic ground motions is created.

3.4 Moving Resonance and Effect of Spectral Nonstationarity on Structural Response

A number of studies in the past fifteen years have analyzed the effect of spectral nonstationarity on nonlinear structural response.

The need to consider the time-varying nature of earthquake ground motion frequency content and its effect on structural response has been identified by Cao and Friswell (2009). This paper also proposed the use of characteristic peak ground acceleration to quantify the difference between earthquake records (Record-to-Record Variability). A six-story reinforced concrete moment resisting frame structure was subjected to six ground motions. The ground motions were transformed to the frequency domain using the Littlewood-Paley (1937) mother wavelet and discrete wavelet transform. The frequency content of the ground motions were then changed by shifting the frequency content forward or backward in time. It was demonstrated that the peak roof drift could be significantly changed, in one case 45% reduction, when the frequency content occurs at different times.

Goggins et al. (2006) analyzed the results of shake table tests using wavelet transforms to compare the time-varying frequency content of the table acceleration to the time varying frequency content of the roof acceleration. This was done by comparing wavelet coefficients. Specifically, data from tests of a concentrically braced frame were analyzed in an attempt to examine stiffness changes due to brace buckling. Correlation coefficients were defined which indicate how well the wavelet coefficients for the ground motion correlate with the wavelet coefficients for the structural response. Also, the time-varying distributions of wavelet coefficients were used to make conclusions about the time in which nonlinearity in the system initiated. Comparisons were conducted for individual frequency bands, or for individual bands of time.

Koduru (2010) defined the envelope delay as a measure of when during the ground motion particular frequency content exists. It was shown that for a specific Loma Prieta ground motion, there is little variation of dominant frequency content, but for a specific Northridge ground motion, low frequency content occurs later in the ground motion. Koduru goes on to show that delayed low frequency content can cause significant increase in damage indices. The

conclusions although not based on wavelet transform, show that the nonstationary nature of ground motions is important.

Conte et al. (1990) & Conte et al. (1992) investigated the effect of time-varying ground motion frequency content on the inelastic response of structures. Conte et al. (1992) identified that ground motions exhibit nonstationarity in amplitude and frequency content. A time-varying auto-regressive moving average (ARMA) model was fit to earthquake ground motions. The ARMA model was then used to create artificial ground motions controlling the amplitude nonstationarity and the frequency nonstationarity of the ground motion signal. Based on the ARMA model of this ground motion, two sets of artificial ground motions were created, time invariant frequency content (TIF), and time varying frequency content (TVF). Three hysteretic SDOF models, bilinear, Clough, and a slip model, were subjected to the sets of ground motions. It was shown that for stiff structures, whose period (To)<0.3 sec, the time-varying frequency content ground motion produced larger response than the time invariant frequency content ground motions because of moving resonance. In some cases, the response was as much as 60% larger. Moving resonance occurs when the increasing effective structural period matches the increasing period of the ground motion frequency content. Conte et al. (1992) concludes that the effect of the moving resonance phenomenon depends on the time evolution of the difference in frequency between the effective structural frequency and the ground motion predominant frequency.

Mukherjee and Gupta (2002) used wavelet transforms to examine the variation in elastic-perfectly plastic single degree of freedom response due to nonstationarity of ground motions. Using 35 recorded ground motions, they found a ±20% from the mean to the 5% and 95% confidence levels for ductility demand. The ground motions were modified to match a target spectrum, so the variation was concluded to be due to spectral nonstationarity. It is concluded that the choice of accelogram, because of the spectral nonstationarity, can have a significant effect on structural response regardless of whether the accelogram are matched to a design spectrum.

In general, however, the studies discussed in this section have focused on developing stochastic ground motion models that can capture spectral nonstationarity and on exposing the effect of ground motion nonstationarity rather than developing means to quantify the effects. The novel approach taken in the research proposed herein is to focus on assessing the occurrence of moving resonance and also to develop methods for quantifying its effect on structural response which can be used in practical applications.

CHAPTER 4 : PROGRAM FOR CALCULATING WAVELET COEFFICIENTS

4.1 Introduction

This section describes the Matlab program written to calculate wavelet transforms. The program uses four different mother wavelet functions, namely Haar, Mexican Hat, Gabor (Complex Guassian), and the Complex Morlet wavelet. Separate codes have been written in Matlab for finding the coefficients using these different wavelet functions. These mother wavelet functions are incorporated in the code by using the Matlab inbuilt functions which are provided for each of these wavelets (The MathWorks 2010).

The Matlab wavelet toolbox has various tools for the analysis and synthesis of signals and images using wavelets and wavelet packets within the framework of Matlab. The wavelet toolbox was used for comparison and validation of the program developed herein.

The time-frequency plots that the wavelet toolbox shows are typically presented in terms of scale, instead of frequency or period. Although, scale is inversely proportional to frequency, this leads to some confusion interpreting the plots, as they pertain to structural response. Also, the wavelet toolbox doesn`t give the 3D representation of the wavelet coefficients. The amplitude of the coefficients can be better visualized in the 3D plots. With an idea of rectifying these limitations of the wavelet toolbox, and to facilitate expansion to further analyze signals, the Matlab programs were written. The validation will be described in a later section of this chapter in which these programs give the same wavelet coefficients obtained from the wavelet toolbox. The program also gives a provision for plotting the plots in 3D, amplitude (magnitude of the wavelet coefficient) being the third coordinate.

The following sub-sections describe the step wise procedure followed in the Matlab codes. Appendix B contains in-built functions of Matlab that are used in the self-programmed codes. It also contains the description of convolution theorem, the basis of which is used for multiplying the test signal with the wavelet basis function in the codes.

4.2 Mathematical Basis for the Program

This sub-section describes the mathematical basis behind wavelet analysis, which is also considered to be the underlying concept of most of the signal analysis techniques. Every vector *v* in a vector space V can be written as a linear combination of the summation of the basis vectors b_k in that vector space by multiplying with a scalar coefficient α_k as shown by Equation 4-1.

$$v = \sum_k \alpha_k b_k \qquad \textbf{4-1}$$

This concept, given in terms of vectors can be generalized to functions, by replacing the basis vectors b_k with basis functions φ_k and the vector *v* with function *f(t)*. Then equation 4-1 becomes

$$f(t) = \sum_k \mu_k \varphi_k \qquad \textbf{4-2}$$

The analysis of the signal involves the estimation of these constant numbers (wavelet coefficients).

If f(x) and g(x) are two functions in $L^2[a,b]$, (where $L^2[a,b]$ denotes the set of square-Integrable functions in [a,b]), then the inner product of two functions is defined by

$$< \mathrm{f(x)}, \mathrm{g(x)} > = \int_{\mathrm{a}}^{\mathrm{b}} \mathrm{f(x)g(x)dx} \qquad \textbf{4-3}$$

A function f(x) is said to be square-integrable function, if the integral of the square of the absolute value is finite which is given by Equation 4-4

$$\int_{-\infty}^{\infty} |f(x)|^2 dx < \infty \qquad \textbf{4-4}$$

According to the above definition of inner product as shown in Equation 4-3, the Continuos Wavelet Transform (CWT) can be treated as the inner product of the test signal *f(x)* (w.r.t time x), with the basic wavelet function $\Psi_{(s,\tau)}(x)$, which is defined by

$$CWT = < f(x), \Psi_{s,\tau}(x) > = \int_a^b f(x).\Psi_{s,\tau}(x)dx \qquad \textbf{4-5}$$

Where,

$$\Psi_{s,\tau}(x) = \frac{1}{\sqrt{s}}\Psi\left(\frac{x-\tau}{s}\right) \qquad \textbf{4-6}$$

Where [a,b] is the effective width of the wavelet function. The variables *s* and τ in Equation 4-6 corresponds to the scaling and shifting parameters respectively. The term $\frac{1}{\sqrt{s}}$ is the normalizing term and is used to maintain the same energy before and after the transformation process. The integral in the Equation 4-5 can be treated as the convolution of the test signal with the scaled and shifted versions of the mother wavelet.

A convolution is defined as the integral over all space of one function at x times another function at x-s. The integration is taken over the variable x, typically from minus infinity to infinity over all the dimensions. So the convolution is a function of a new variable s, as shown in the following equation 4-6. The cross in a circle is used to indicate the convolution operation.

$$C(s) = g(x) = f(x) \otimes h(x) = \int_{-\infty}^{+\infty} f(x)h(x-s)dx \qquad \textbf{4-7}$$

The operation given in the Equation 4-7 is considered as the area of the overlap between the function f(x) and the spatially reversed version of the function h(x). The following example demonstrates the concept of convolution.

If the functions f(s) and h(s) are defined as shown in Figure 4-1

Figure 4-1 Two functions f(s) and h(s) defined over an interval

then the convolution of two functions is given by the Figure 4-2

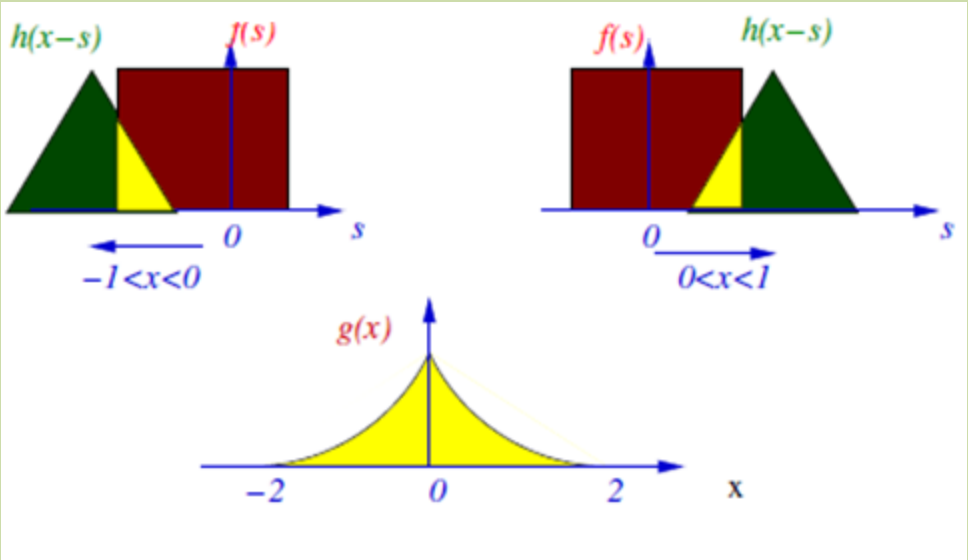

Figure 4-2 Convolution of two functions

In the Figure 4-2, it is shown that the spatially reversed function *h(s)* is convoluting with the function *f(s)* and giving the new function *g(x)*. This concept of convolution is applied in convoluting the spatially reversed wavelet basis function $\Psi_{s,\tau}(x)$ with the test signal *f(x)*.

4.3 Steps involved in calculating the wavelet coefficients:

The following are the five basic steps that are followed in the Matlab program for calculating CWT coefficients.

- Step 1: Choosing and defining an appropriate mother wavelet function

  The wavelet function appropriate for the signal to be analyzed must be chosen. The wavelet function chosen should be defined with in a range with specified increment. Usually, the range chosen should be the effective width/support of the wavelet function and increment will be the order of $\frac{1}{1024}$. The effective support varies with the wavelet function chosen i.e. For Mexican hat wavelet, the effective support is [-5, 5], for Complex Guassian it is [-8, 8] and for Haar is it [0, 1].
- Step 2: Start a loop over different scales and time increment

  The loop is created for different scales along each time increment.
- Step 3: Calculating the wavelet coefficient for different scales and shifts

- The wavelet function is spatially reversed and convoluted against the signal. This process of convolution and reversing is done by using the Matlab in-built functions (refer Appendix B). Thus the wavelet coefficients for different scales and shifts are calculated.

The result of the process is many wavelet coefficients, which are a function of scale and position. These coefficients represent how well the wavelet matches the signal with that scale and position. These wavelet coefficients are vectors in real-complex plane having both magnitude and phase.

4.4 Procedure involved in plotting of Wavelet Coefficients

The coefficients were plotted as a contour plot in 2D with period along the vertical axis and the time along the horizontal axis. The contour helps to differentiate the maximum value of coefficients with others. The following steps are followed in plotting the coefficients.

- Step 1: The absolute values (magnitudes for complex wavelets) of all the coefficients were taken.
- Step 2: The minimum and maximum values from the existing coefficients were obtained.
- Step 3: Normalization of wavelet coefficients: The minimum value is subtracted from all the coefficients and the ratio of all the newly obtained coefficients with respect to the maximum value is obtained.
- Step 4: These obtained values are multiplied with the code number chosen for the particular color, and by using image command; the required image of the coefficients is obtained. This way the color modulation is done with respect to the magnitude of the wavelet coefficient.

The color intensity at each x-y point is proportional to the absolute value of the normalized wavelet coefficients. It provides the signal energy distribution display with respect to the particular time and frequency information.

The 'surf' command, an in-built matlab function (refer Appendix B) is used to plot the wavelet coefficients in 3D. The normalization of the wavelet coefficients is not done in 3D plots unlike in 2D plots to show the original amplitude of the wavelet coefficients (which take sign into consideration). These 3D plots helps to locate and differentiate the peaks of frequency content easily.

4.5 Verification of Wavelet Analysis program with Matlab wavelet Toolbox

The matlab program was verified by comparing the results with the results of the Matlab Wavelet Toolbox. The results were compared in the following two ways:

- By doing numerical comparison of wavelet coefficients
- By plotting the coefficients and visually comparing their plots.

The wavelet analysis program enables more display options than the Matlab Wavelet Toolbox. Table 4-1 gives some of the additional information which can be extracted from the plots of wavelet analysis program when compared to wavelet toolbox.

Table 4-1 Comparison between Wavelet Analysis program and Matlab wavelet toolbox

S.No	Description of a section	Matlab Wavelet tool box	Wavelet Analysis program
1.	Vertical axis	Only displays scale values	Displays both scale and their corresponding period values by using the relationship given in equation 3-7
2.	Horizontal axis	Displays data point number	Displays time (duration) of the signal.
3.	Expandable for analyzing moving resonance	Not possible	Possible
4.	3D plots	Cannot be plotted	Can be plotted for the desired wavelet function

Tables 4-2 and 4-3 show the numerical comparison of wavelet coefficients of Mexican Hat wavelet and Complex Guassian wavelet of order 4 for Acceleration Time History (ATH) of Delta 352 component for a period of 0-10 sec. The Delta 352 is the horizontal 352^0 component of ground motion of Imperial Valley earthquake recorded at Delta station.

Table 4-2 Numerical comparison of wavelet coefficients for Mexican Hat wavelet

Method of comparison	Matlab Wavelet Toolbox	Wavelet Analysis program
Comparing the sum of all the coefficients	-83.3287	-83.1381
Comparing the peak values of all the coefficients	1.0669	1.0644
Ratio of avg. diff between coefficients and avg. of coefficients.	0.0023 (0.23 % variation)	

Table 4-3 Numerical comparison of wavelet coefficients for Complex Guassian wavelet of order 4

Method of comparison	Matlab Wavelet Toolbox	Wavelet Analysis program
Comparing the absolute sum of all the coefficients	36.9819	36.7812
Comparing the peak values of all the coefficients	0.8668	0.8637
Ratio of avg. diff between coefficients and avg. of coefficients.	0.0083 (0.83 % variation)	

Verification by comparing plots visually:

Comparison for Mexican Hat wavelet

This subsection shows the differences between the wavelet coefficient plots of Matlab wavelet toolbox and the wavelet analysis program shown in Figures 4-4 and 4-5 respectively. The signal analyzed is the Acceleration Time History of Delta 352 component of Imperial Valley earthquake shown in Figure 4-3.

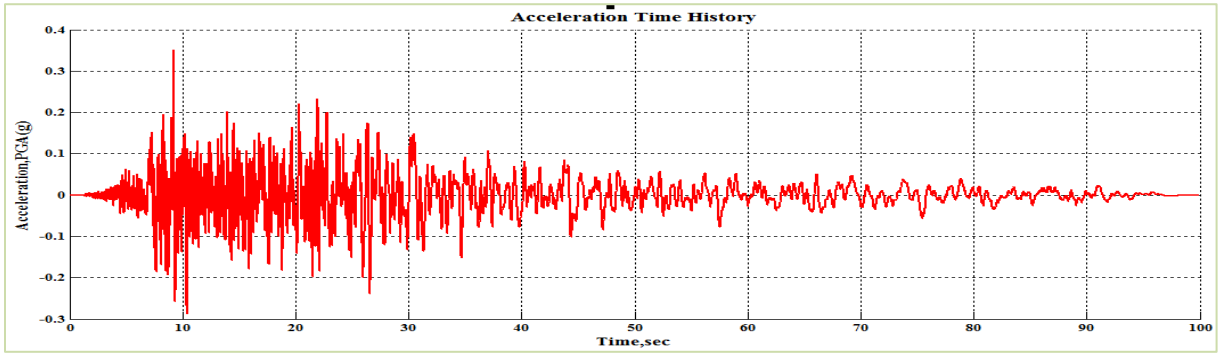

Figure 4-3 Acceleration Time History of Delta 352 component of Imperial Valley earthquake

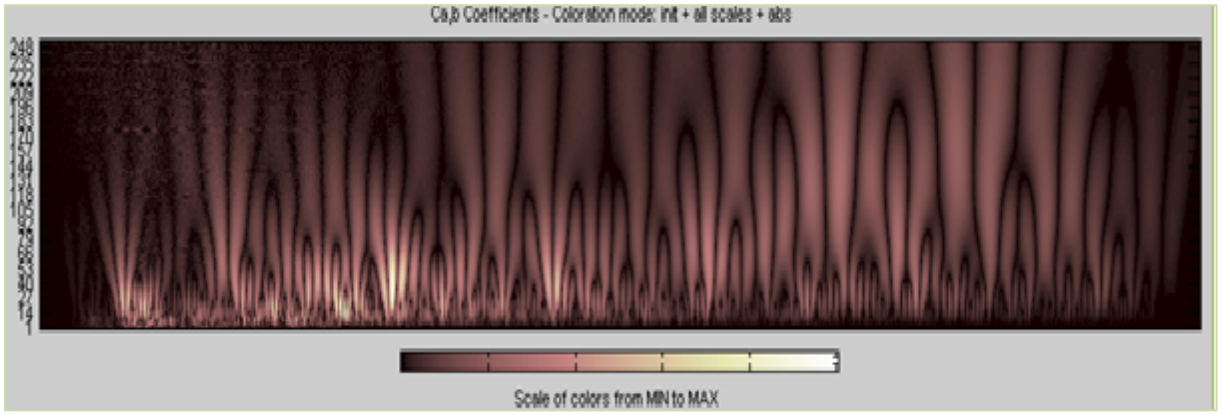

Figure 4-4 Wavelet coefficients plot from Matlab wavelet toolbox

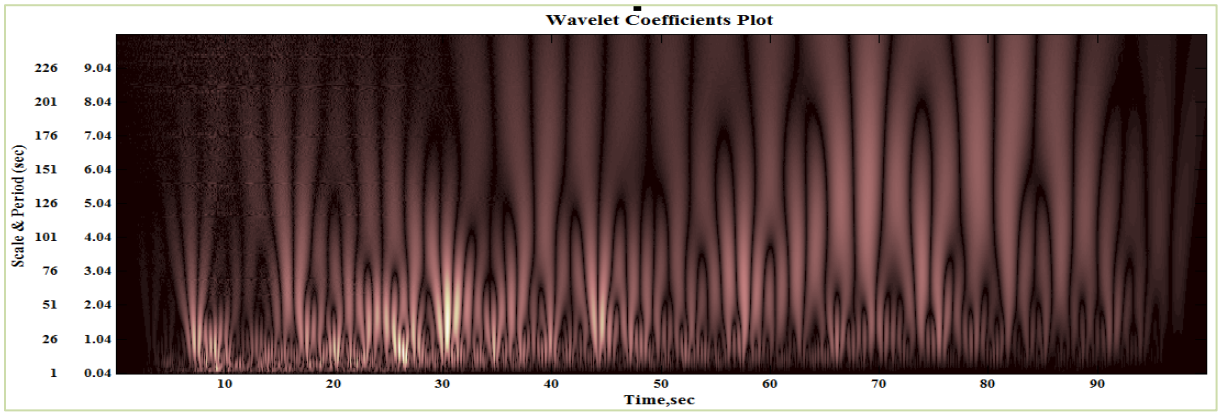

Figure 4-5 Wavelet coefficients plot from wavelet analysis program

Comparison for Complex Guassian wavelet of order 4

This subsection compares the wavelet coefficient plot of Matlab wavelet toolbox shown in Figure 4-7 with the wavelet coefficient plot of wavelet analysis program shown in Figure 4-8 for ATH of Delta 352 component of Imperial Valley earthquake shown in Figure 4-6. The vertical axis of Figure 4-8 shows two columns, the left column represents the scale values and the right column indicates their corresponding period.

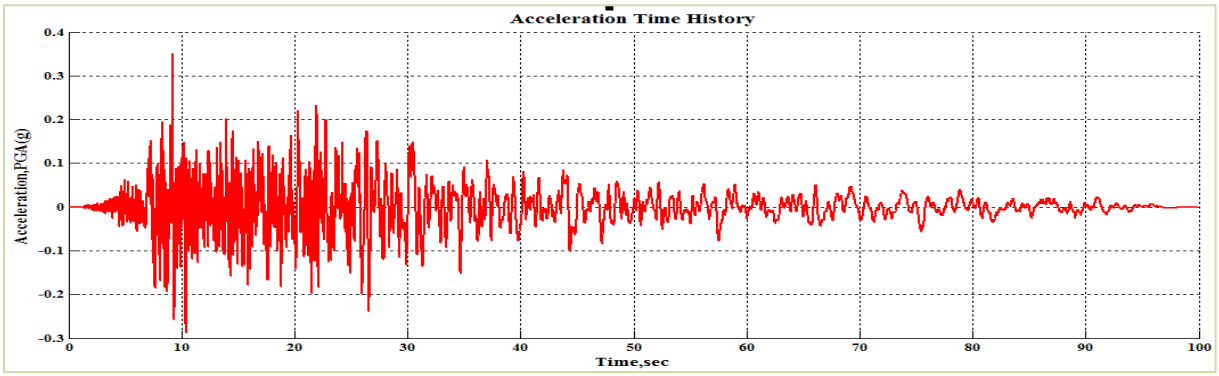

Figure 4-6 Acceleration Time History of Delta 352 component of Imperial Valley earthquake

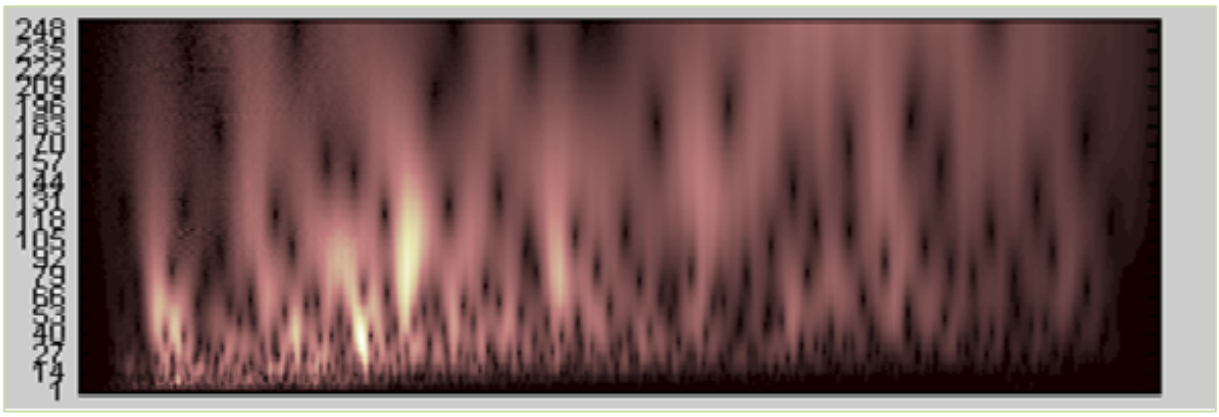

Figure 4-7 Wavelet coefficients plot from Matlab wavelet toolbox

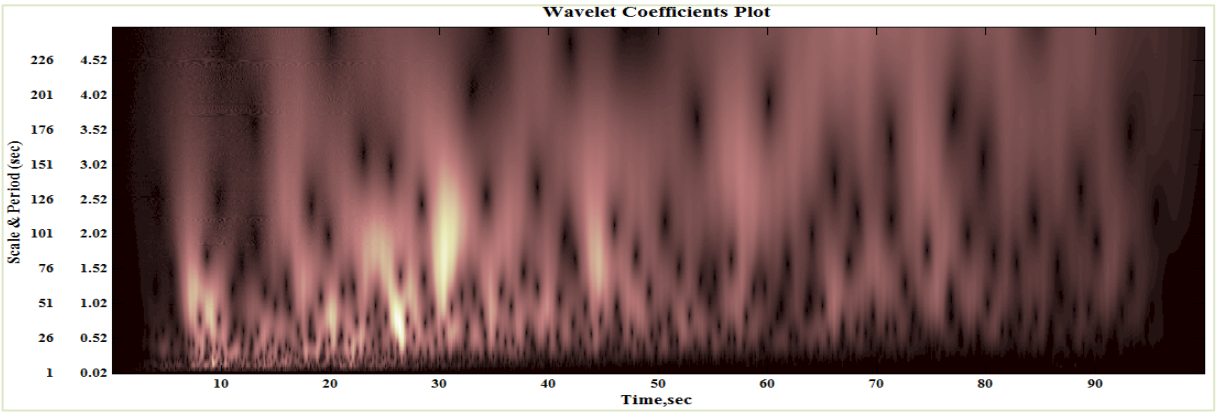

Figure 4-8 Wavelet coefficients plot from wavelet analysis program

3D plots using Wavelet analysis program for 'mexh' and 'cgau4'

This subsection shows the 3D wavelet coefficient plots using wavelet analysis program (which cannot be obtained from Matlab wavelet toolbox) for ATH of Delta 352 component of Imperial Valley earthquake shown in Figure 4-9.

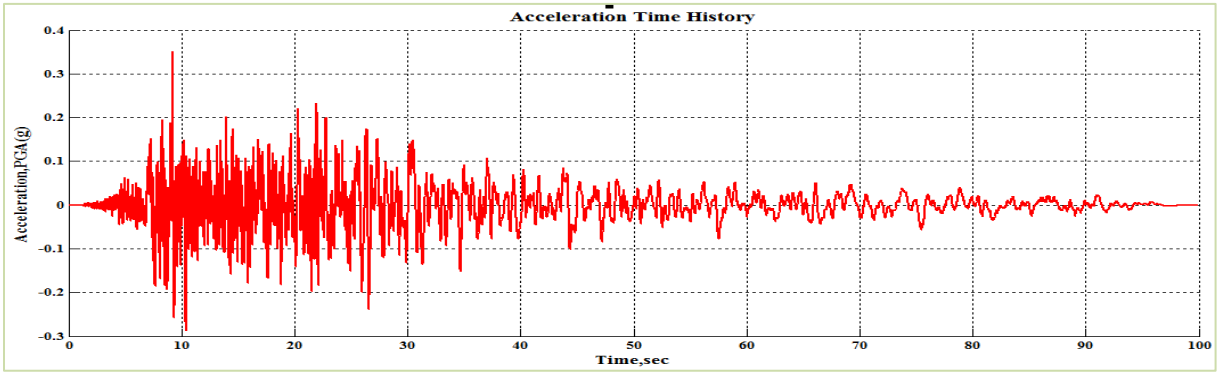

Figure 4-9 Acceleration Time History of Delta 352 component of Imperial Valley earthquake

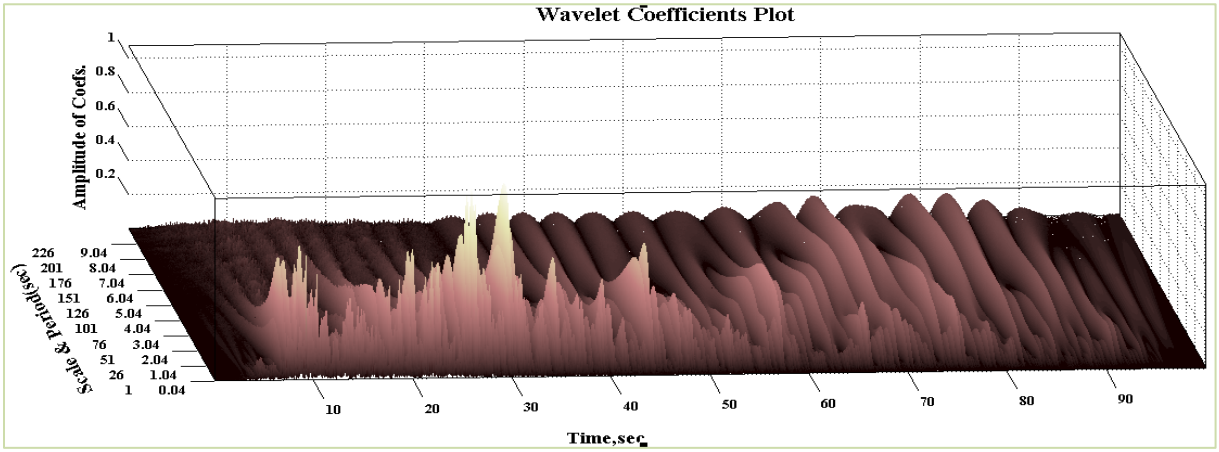

Figure 4-10 Wavelet coefficients plot in 3D using wavelet analysis program with Mexican hat wavelet

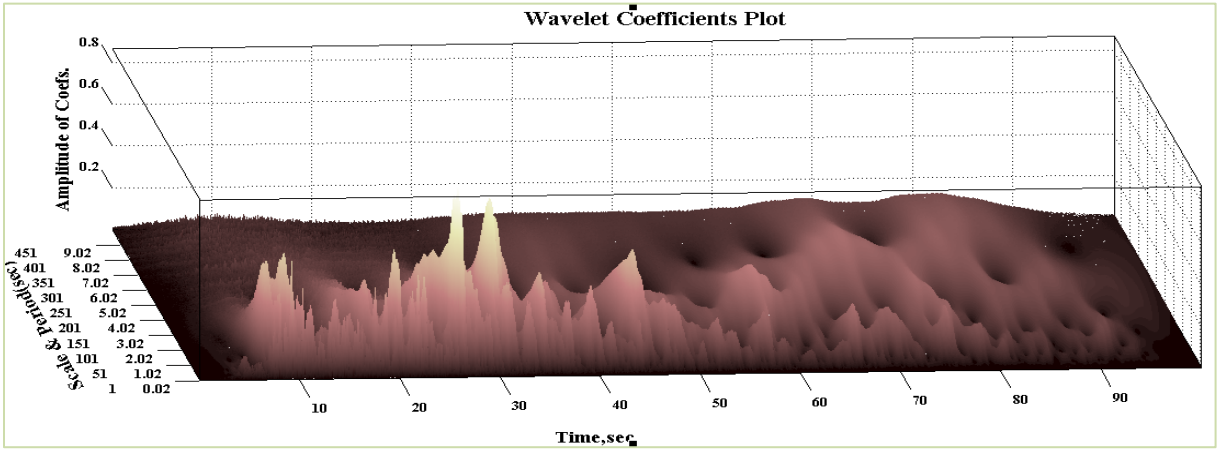

Figure 4-11 Wavelet coefficients plot in 3D using wavelet analysis program with Complex Guassian wavelet

CHAPTER 5 : REFINEMENT OF TIME-FREQUENCY REPRESENTATION OF EARTHQUAKE SIGNALS

5.1 Objectives and Methods

This chapter discusses the refinement of the time-frequency representation of ground motion signals. The Matlab program developed in the previous chapter was used to examine one randomly chosen ground motion in depth to refine the approach to wavelet decomposition and to investigate the character of the ground motion wavelet decomposition. The Mexican hat wavelet, Complex Guassian wavelet of different orders and Complex Morlet wavelet of band width 1 and center frequency 1.5 were used for analyzing the ground motion. Comparison of the analyses results of multiple components of this ground motion (such as Acceleration and Displacement Time histories) having varying frequency content helped in choosing a suitable wavelet function for the rest of the project. Existence of black holes (areas of low frequency content) in the analyses plots is examined by comparing the wavelet coefficients obtained using different wavelets.

The geographical location, site conditions and station details of the earthquake used in this chapter is given in Table 5-1 and the components and characteristics of the ground motions is given in Table 5-2. Section 5.1 shows Acceleration and Displacement response spectra plots of all the ground motion components listed in Table 5-1 for the three different damping ratios.

Table 5-1 Earthquake and station details

Earthquake and Station Details	
Imperial Valley 1979/10/15 23:16 Magnitude: M(6.5) MI (6.6)	Station: 6605 Delta Data Source: UNAM/UCSD
Distance closest to Fault rupture(km) - 43.6	Site conditions: USGS: C

Table 5-2 Ground motion components and their characteristics

Record /Component	PGA (g)	PGV (cm/s)	PGD (cm)
IMPVALL/ H-DLTDWN (vertical component)	0.145	14.8	8.62
IMPVALL/ H-DLT262 (horizontal component)	0.238	26.0	12.06
IMPVALL/ H-DLT352 (horizontal component)	0.351	33.0	19.02

5.1. Acceleration and Displacement Response Spectra for selected Ground Motion

The information in this section is provided as a context to the wavelet decomposition of upcoming sections. Response spectra represent one of the most popular forms of representing earthquake demands on structures. Figures 5-1 and 5-2 shows the acceleration and displacement response spectra plots for the horizontal 262^0 component of the Imperial valley earthquake at delta station (HDLT262) respectively. The maximum pseudo acceleration values for each % damping and the periods at which those values occur are given in Table 5-3. The plots for the remaining two ground motion components are shown in the Appendix C-1.

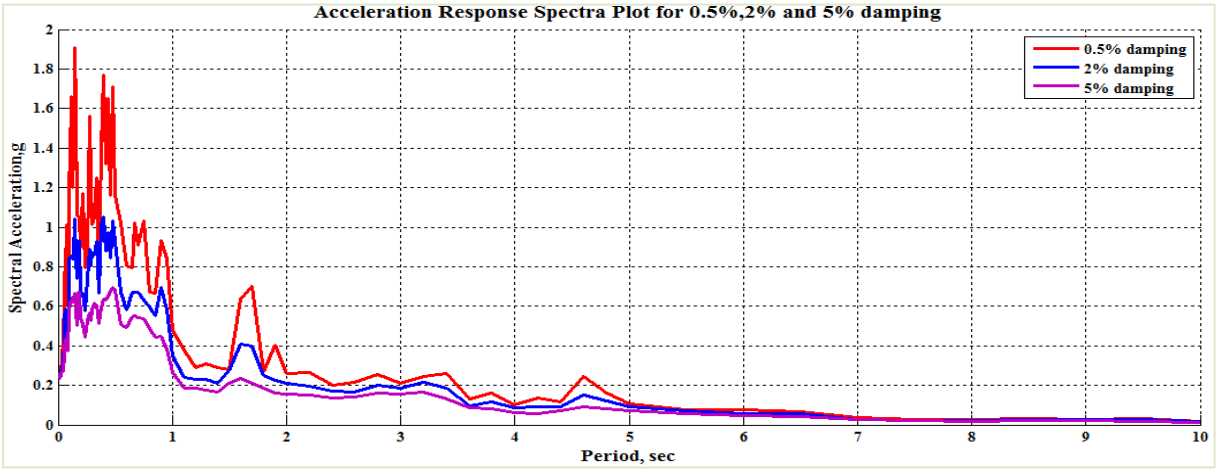

Figure 5-1 Acceleration Response Spectra plot of HDLT262 component for 0.5, 2, 5% damping

Table 5-3 Characteristics of Acceleration Response Spectra

% Damping	Maximum pseudo acceleration (g)	Occurring @ period (sec)
0.5	1.91	0.15
2	1.05	0.40
5	0.698	0.48

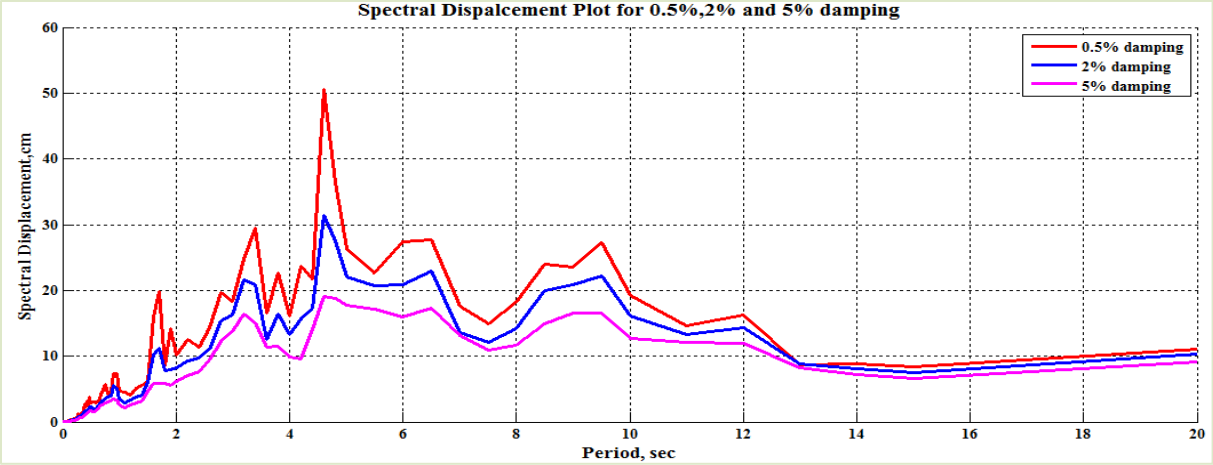

Figure 5-2 Displacement Response Spectra plot of HDLT262 component for 0.5, 2, 5% damping

The maximum relative displacement values for each % damping and the periods at which those values occur are given in Table 5-4.

Table 5-4 Characteristics of Displacement Response Spectra

% Damping	Maximum relative displacement (cm)	Occurring @ period (sec)
0.5	50.53	4.6
2	31.48	4.6
5	19.05	4.6

5.2. Wavelet Analysis of Acceleration Time History

This section is performed to choose a suitable wavelet function for the rest of the project. The frequency content of the acceleration time history is analyzed and compared by using two different wavelet functions namely Mexican hat wavelet and Complex Guassian (Gabor) wavelet of order 4 (shown in Figure 5-3 and Figure 5-4 respectively) .

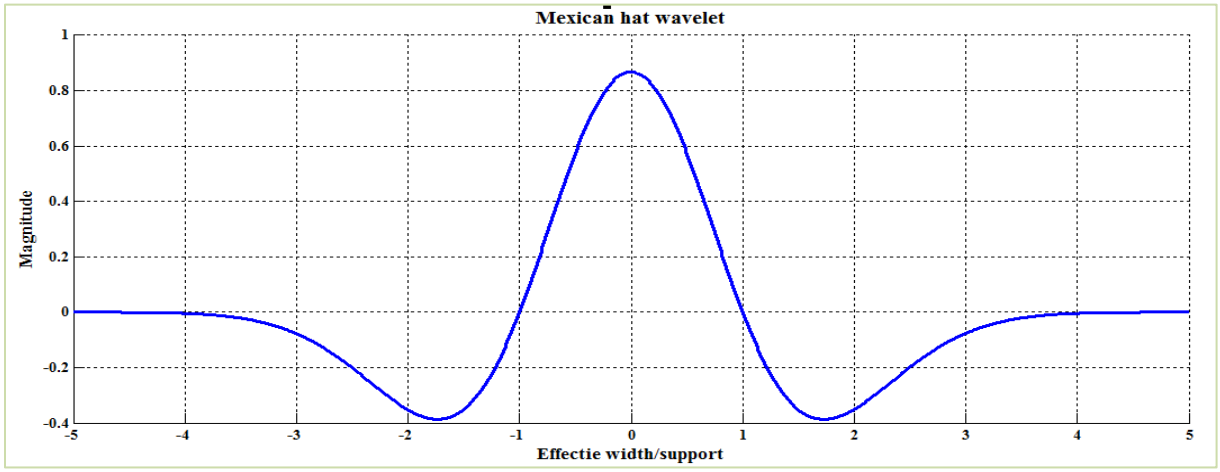

Figure 5-3 Mexican hat wavelet

The wavelet function of the Mexican hat wavelet is given by Equation 5-1.

$$\Psi(x) = \left(\frac{2}{\sqrt{3}}\pi^{-1/4}\right)(1-x^2)e^{-x^2/2} \qquad \textbf{5-1}$$

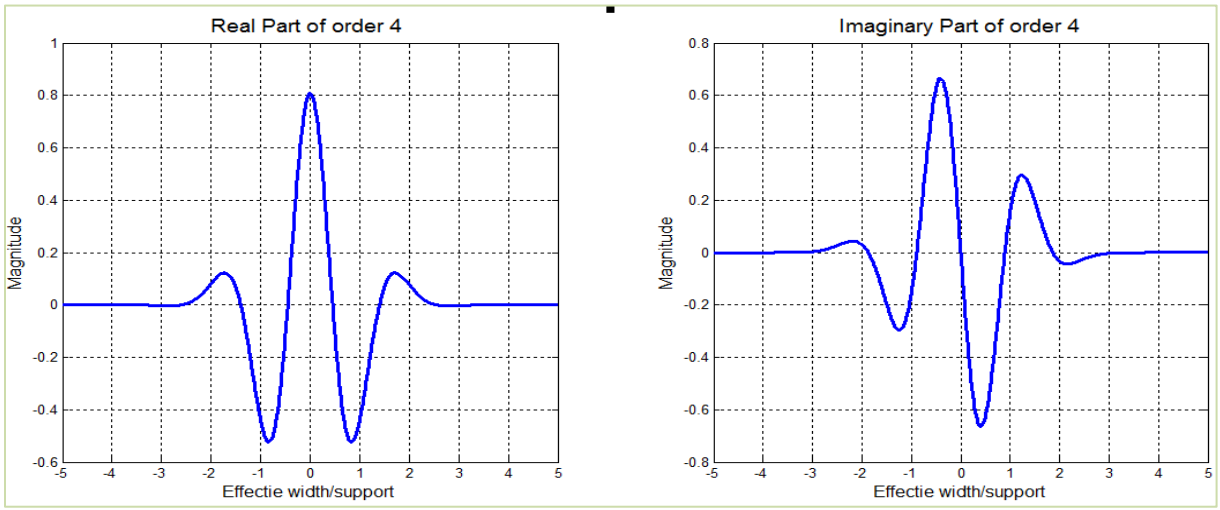

Figure 5-4 Real and Imaginary part of Complex Guassian wavelet of order 4

The wavelet function of the Complex Guassian wavelet is given by Equation 5-2.

$$\Psi(x,n) = C_n e^{-ix} e^{-x^2/2} \quad \textbf{5-2}$$

The n in the Equation 5-2 is the parameter of the Complex Guassian family and corresponds to the order of the wavelet function. i.e. n=4 corresponds to the 4th derivative (order) of the original function $\Psi(x)$. C_n is such that the 2-norm of the nth derivative of $\Psi(x)$ is 1 which is mathematically by Equation 5-3.

$$\left|\Psi^{(n)}\right|^2 = 1 \quad \textbf{5-3}$$

Where $\Psi^{(n)}$ is the nth derivative of $\Psi(x)$.

5.2.1 Comparing Two Different Types of wavelets

This sub-section shows the comparison between Mexican hat and Complex Guassian wavelets performed on acceleration time history of the horizontal 352^0 component as shown in Figure 5-5. The wavelet coefficient plots were compared for periods ranging from 0-10 sec. Figures 5-6 and 5-7 show the wavelet coefficient plots for wavelet transforms using Mexican Hat and Complex Guassian wavelets respectively. The values shown on the horizontal axis of both the plots corresponds to Time (in sec). Along the vertical axis, there are 2 columns of values. The first column (to the left) shows the scale values and the second column (to the right) represents period (in sec). The conversion to period from scale is done using the relation given by equation 3-8. The color modulation of the wavelet coefficients is shown in Figure 3-11. The plots for the remaining two ground motion components are shown in the Appendix C-2.

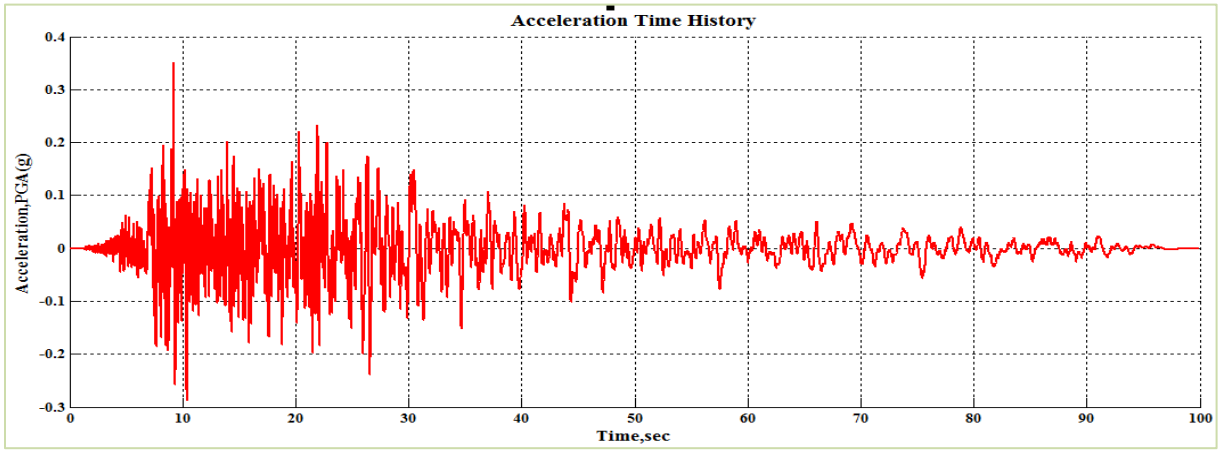

Figure 5-5 Acceleration Time History of HDLT352 component of Imperial Valley Earthquake

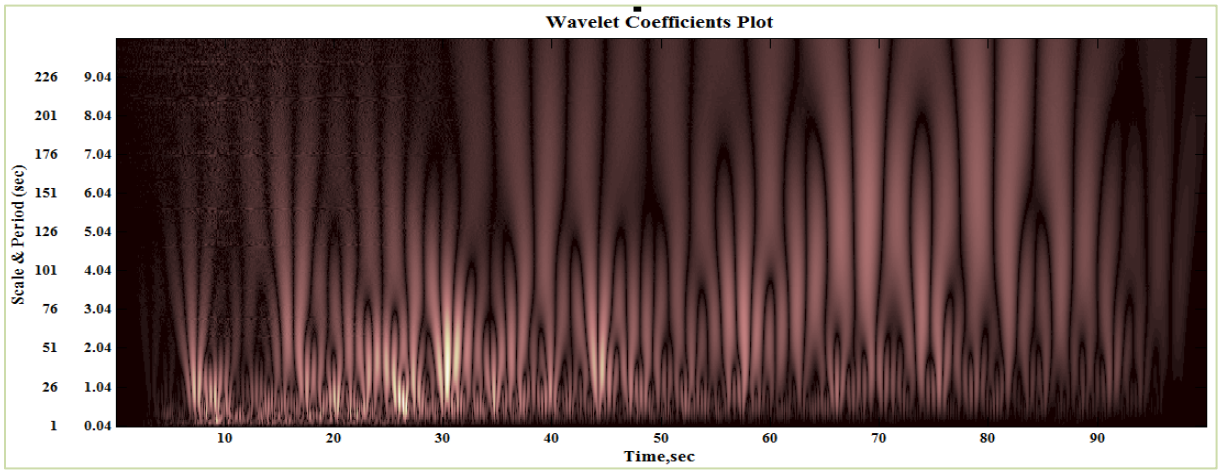

Figure 5-6 Wavelet coefficients plot using wavelet analysis program with Mexican hat wavelet

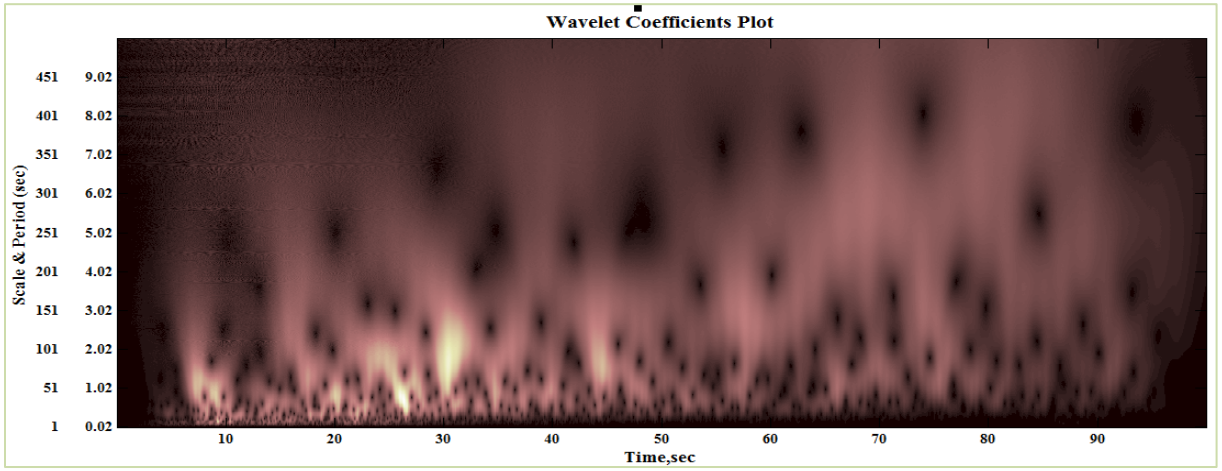

Figure 5-7 Wavelet coefficients plot using analysis program with Complex Guassian wavelet of order 4

One of the primary conclusions drawn from the comparison of Figures 5-6 and 5-7 are that the wavelet coefficients plotted using Mexican hat wavelet show interference bands. These interference bands occur when the wavelet is out of phase with the signal. The Complex Guassian wavelet rectifies this problem because it includes an imaginary part in its wavelet basis function that is 90 degrees out of phase with the real part. The magnitude of the resulting complex wavelet coefficients captures the energy in the signal regardless of phase. Though the Complex Guassian (Gabor) wavelet rectifies the problem of interference bands, it does have many time-period areas with unusually small wavelet coefficients. The following subsection will give more information about these areas of frequency content (termed as black holes here due to the color scale chosen and also to characterize the relatively localized lack of energy in the signal).

5.2.2 Examination of Order of Complex Guassian wavelet

The main purpose of this subsection is to investigate the black holes that were observed in the wavelet coefficient plots obtained using Complex Guassian wavelet of order 4. This subsection shows the comparison between wavelet coefficient plots of different orders of Complex Guassian wavelets (as shown in Figure 5-8) performed on acceleration time history data of downward component as shown in Figure 5-9.

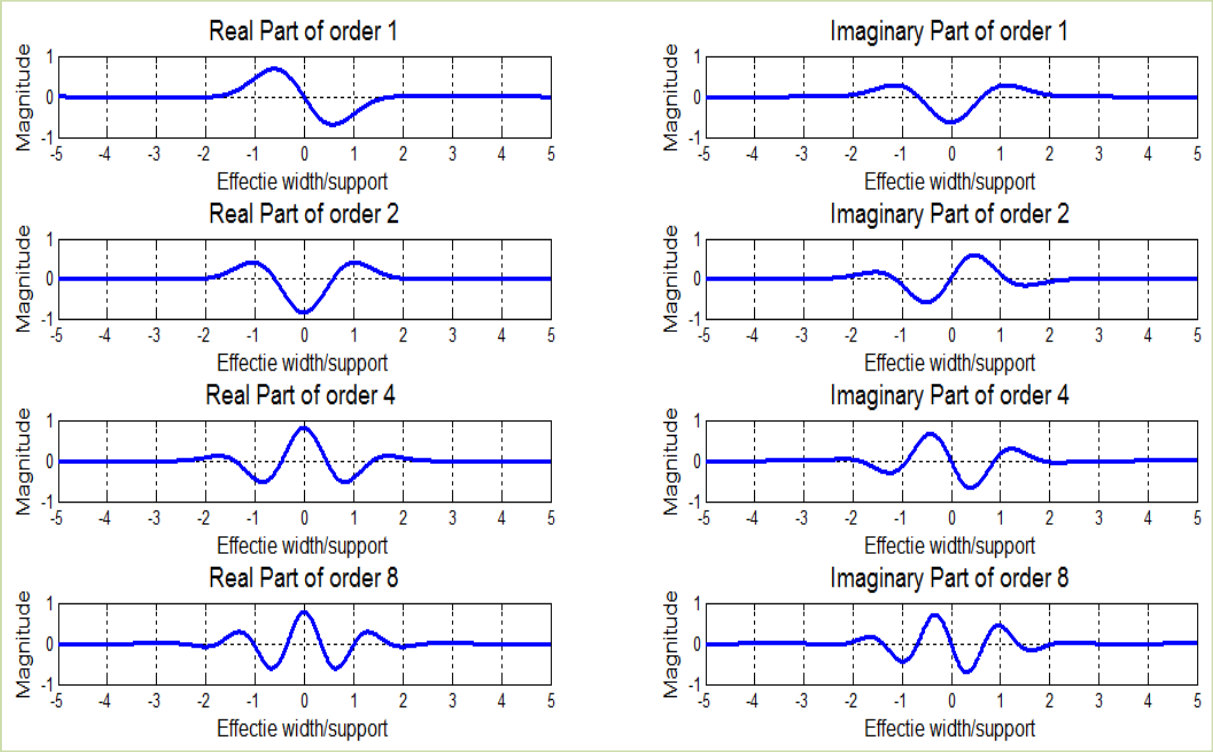

Figure 5-8 Complex Guassian wavelets of order 1, 2, 4 and 8

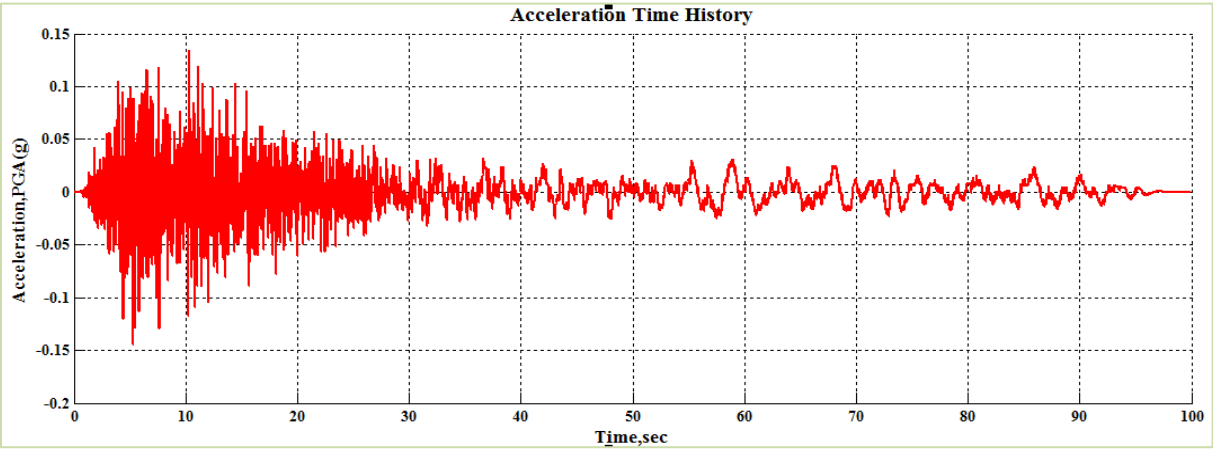

Figure 5-9 Acceleration Time History of HDLTDWN component of Imperial Valley Earthquake

Figures 5-10, 5-11, 5-12 and 5-13 shows the wavelet coefficient plots of Complex Guassian wavelet of order 1, 2, 4 and 8 respectively.

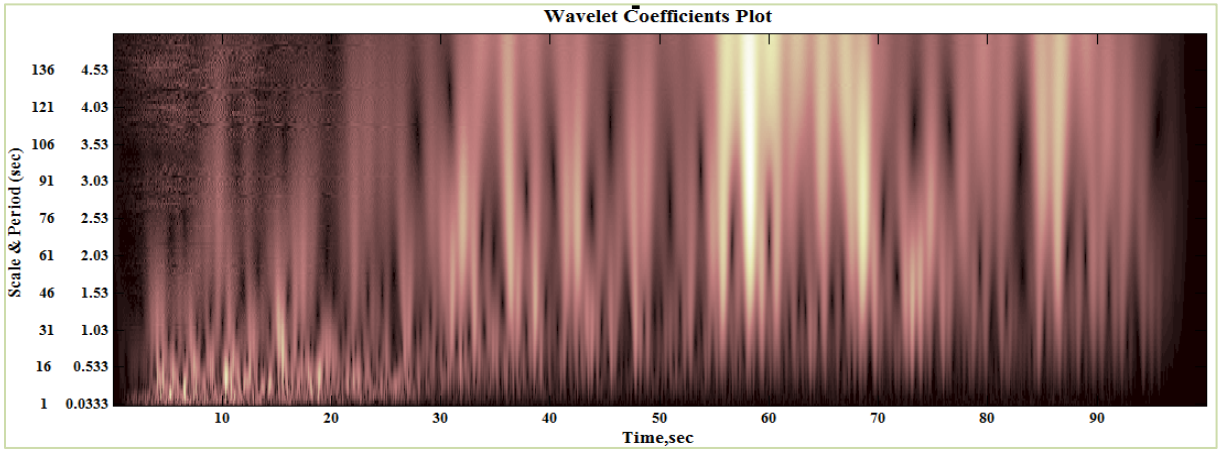

Figure 5-10 Wavelet coefficients plot using Complex Guassian wavelet of order 1

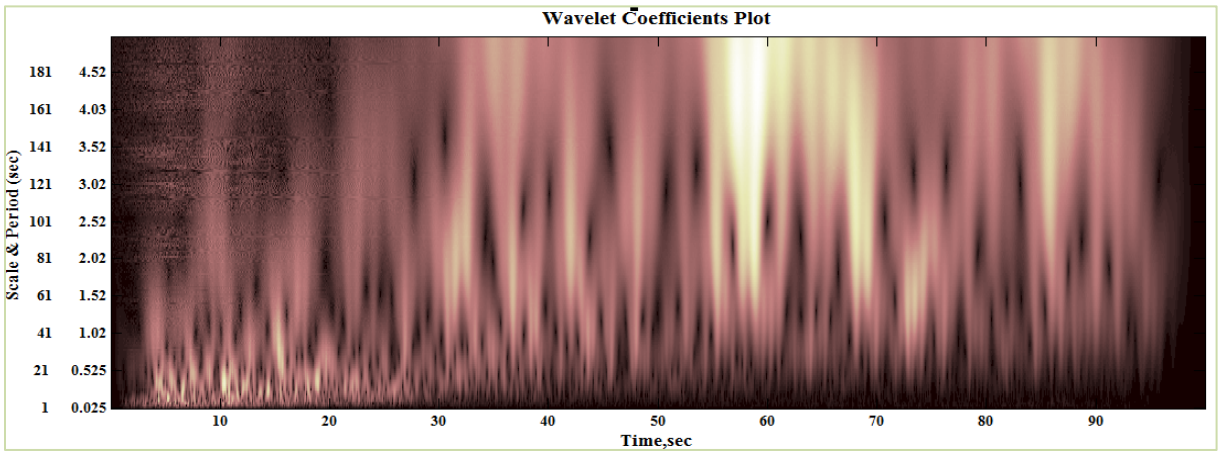

Figure 5-11 Wavelet coefficients plot using Complex Guassian wavelet of order 2

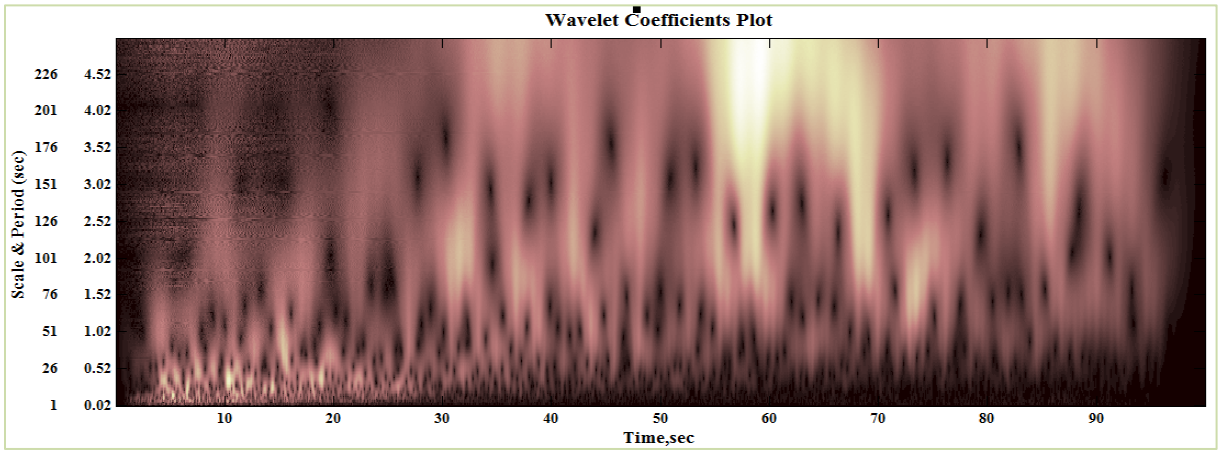

Figure 5-12 Wavelet coefficients plot using Complex Guassian wavelet of order 4

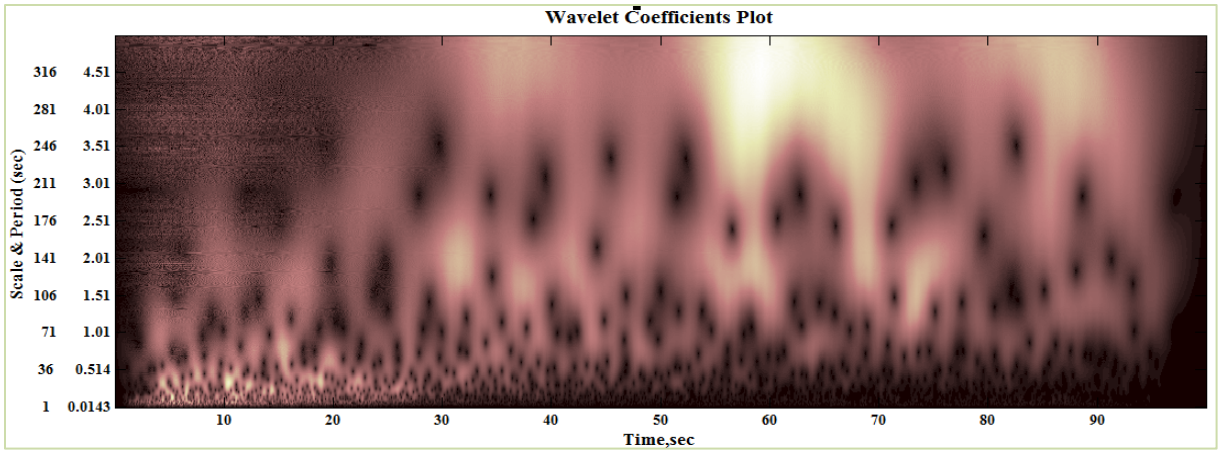

Figure 5-13 Wavelet coefficients plot using Complex Guassian wavelet of order 8

Increase in the order of Complex Guassian (Gabor) wavelet increases the number of areas with unusually small wavelet coefficients (black holes). These black holes get more sharply defined with the increase in the order of the Gabor wavelet. This is only because one black hole found with lower order Guassian wavelet is shown to contain (meld) multiple smaller black holes together. With the increase in the order of wavelets, the sharper resolution reveals more black holes. Hence, it is concluded that the changes observed in black holes with the increase in the order of wavelets is due to the resolution of the order of wavelet and the more about this is discussed in the later sections.

5.2.3 Comparison of 2D and 3D Wavelet Transform Plots

The main purpose of this subsection is to investigate the visualization of the wavelet coefficients that best show the data. It is also expected that wavelet coefficient plots in three dimensional (3D) may reveal some interesting characteristics about black holes.

This subsection shows the comparison between two dimensional (2D) and three dimensional (3D) wavelet coefficient plots for acceleration time history data of horizontal 352^0 component of Imperial Valley earthquake as shown in Figure 5-14 using wavelet analysis program with Complex Guassian wavelet of order 4. Figures 5-15 and 5-16 show the 2D and 3D wavelet coefficient plots respectively.

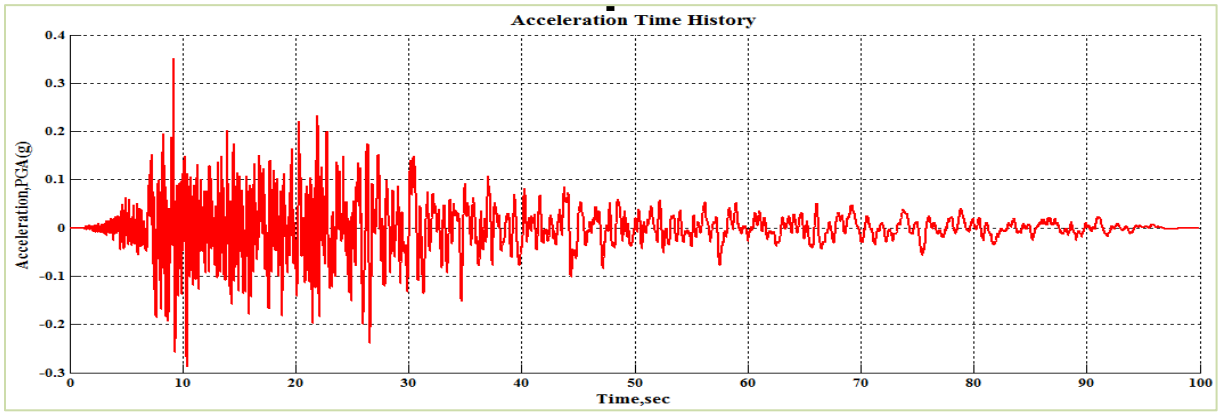

Figure 5-14 Acceleration Time History of HDLT352 component of Imperial Valley Earthquake

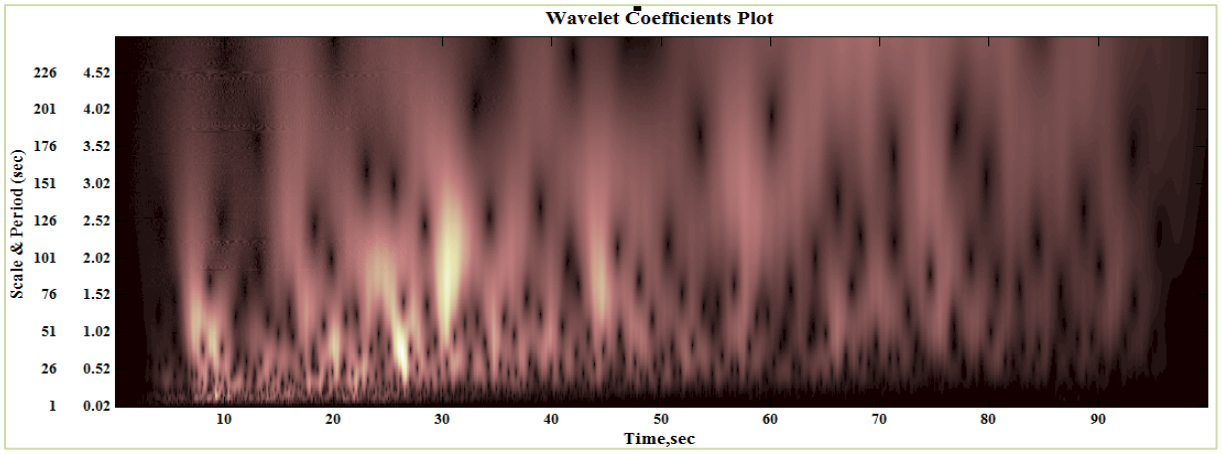

Figure 5-15 Wavelet coefficients plot using Complex Guassian wavelet of order 4

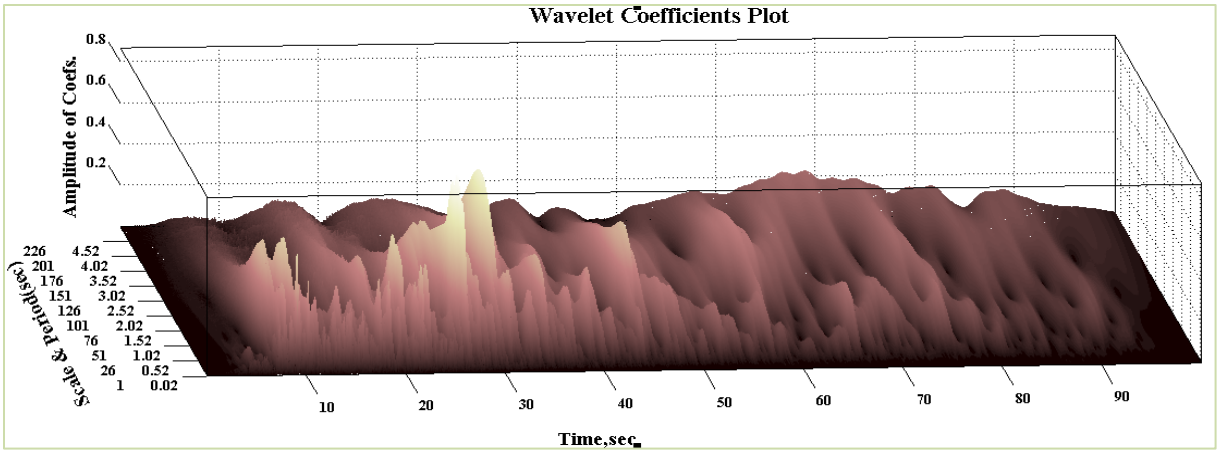

Figure 5-16 3D Wavelet coefficients plot using Complex Guassian wavelet of order 4

The 3D wavelet coefficient plot shown in Figure 5-16 is obtained by using the wavelet analysis program prepared for this purpose. Only the magnitude of the complex wavelet coefficients is considered in plotting and there is additional information contained in the complex wavelet coefficients regarding phase which is examined in the later chapters. The 2D plot in Figure 5-15 shows the location of peak wavelet coefficients and black holes (small wavelet coefficients) by the intensity of color, whereas 3D plot shows the magnitude of those coefficients. It can be observed from the 3D representation that the magnitudes of wavelet coefficients are small at the location of black holes seen in 2D plot.

5.3. Comparison of Wavelet Transforms of the Acceleration, Velocity, and Displacement Time Histories

The main purpose of this section is to see whether black holes exist in the wavelet coefficient plots of velocity and displacement time histories similar to acceleration time history. The section shows the comparison between the analysis of acceleration, velocity and displacement time histories of horizontal 352^0 component of Imperial Valley earthquake (shown in Figure 5-17) using wavelet analysis program with Complex Guassian wavelet of order 4.

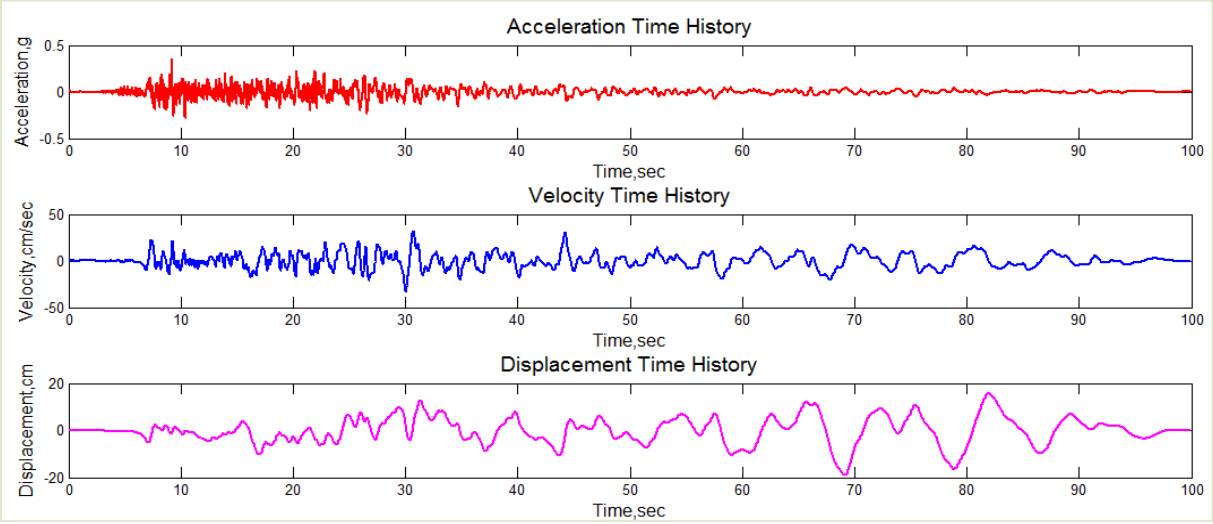

Figure 5-17 ATH, VTH, DTH of HDLT352 component of Imperial Valley Earthquake

Figures 5-18, 5-19 and 5-20 shows the wavelet coefficient plots for acceleration, velocity and displacement time histories respectively.

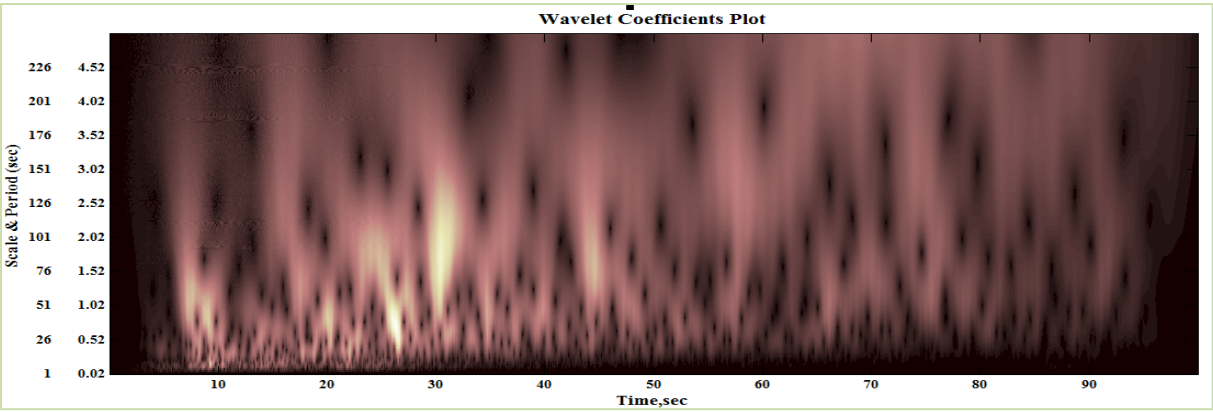

Figure 5-18 Wavelet coefficients plot of acceleration time history using Complex Guassian wavelet of order 4

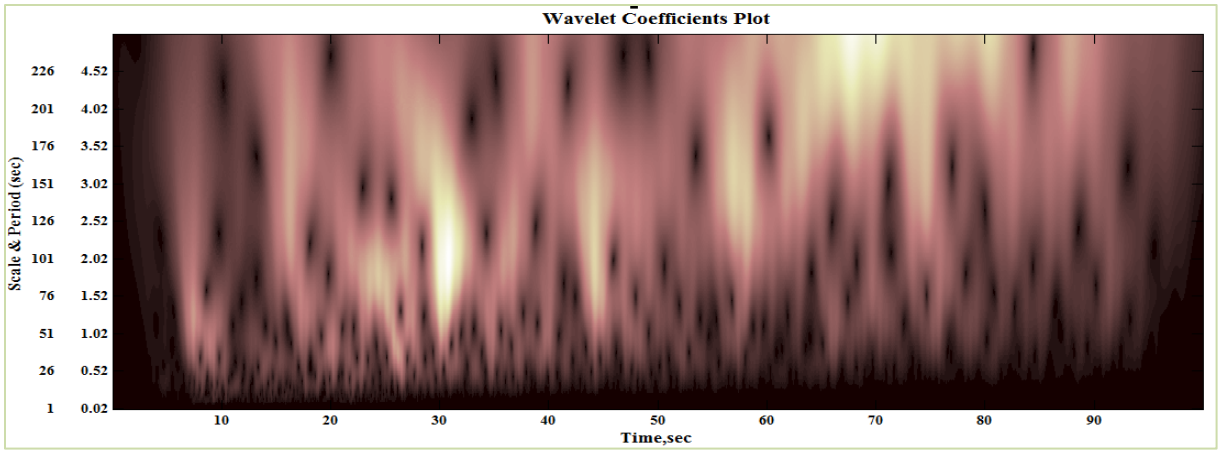

Figure 5-19 Wavelet coefficients plot of velocity time history using Complex Guassian wavelet of order 4

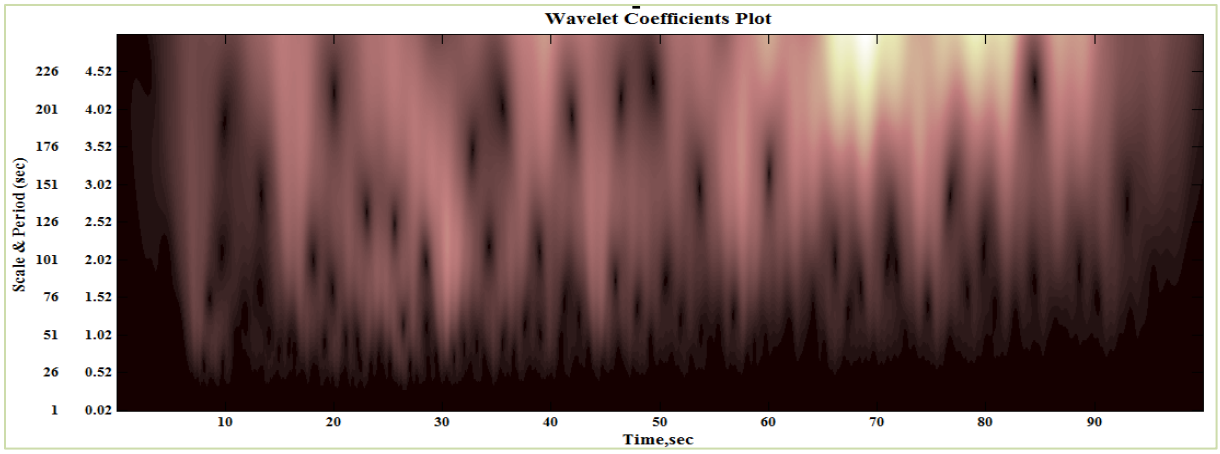

Figure 5-20 Wavelet coefficients plot of displacement time history using Complex Guassian wavelet of order 4

Though the frequency content of the three time histories are different, black holes are observed in all the three plots. This hints at black holes being a part of the signal and it leads to further investigation of the black holes which is discussed in the coming sections.

The sections 5.2 and 5.3 are repeated for the displacement time history of the horizontal 352^0 component of the Imperial Valley earthquake and can be seen in Appendix C-4.

5.4 Investigation into Black holes of Frequency Content

The areas of frequency content with unusually small wavelet coefficients are termed as black holes. It is concluded from previous sections that the changes observed in black holes with the increase in the order of wavelets is due to the resolution of the order of wavelet. From the 2D and 3D wavelet coefficient plots shown in section 5.3, it is observed that at the location of black holes, the wavelet coefficients are very small. But the exact location and the magnitude of the black hole is not known.

This section concentrates on finding the exact location of a particular black hole w.r.t to time and period to investigate their properties. This is achieved by plotting the wavelet coefficients in the vicinity of a black hole region for certain period range along the whole time series. The wavelet coefficient plot for horizontal 262^0 component of Imperial Valley earthquake analyzed by using the wavelet analysis program with Complex Guassian wavelet of order 4 as shown in Figure 5-21.The black hole circled in red is chosen to investigate its properties.

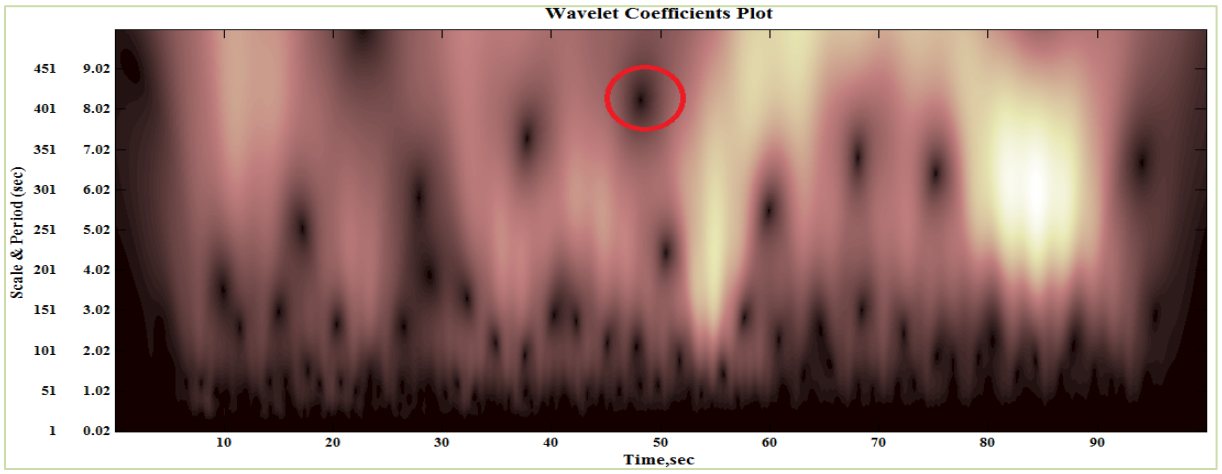

Figure 5-21 Wavelet coefficients plot for HDLT262 component using Complex Guassian wavelet function of order 4

The wavelet coefficients in the period range of 7.92-8.52 sec is selected and plotted along the whole time series as shown in Figure 5-22. It is evident from Figure 5-22 that all period values (shown in red lines) in this particular range has very low (near zero) magnitudes of wavelet coefficients at time t=48.18 sec. The period value corresponding to 8.24 sec (shown in blue line) has a wavelet coefficient of zero at time t=48.18 sec. Hence it is proved that at the location of black hole, the wavelet coefficients are near zero.

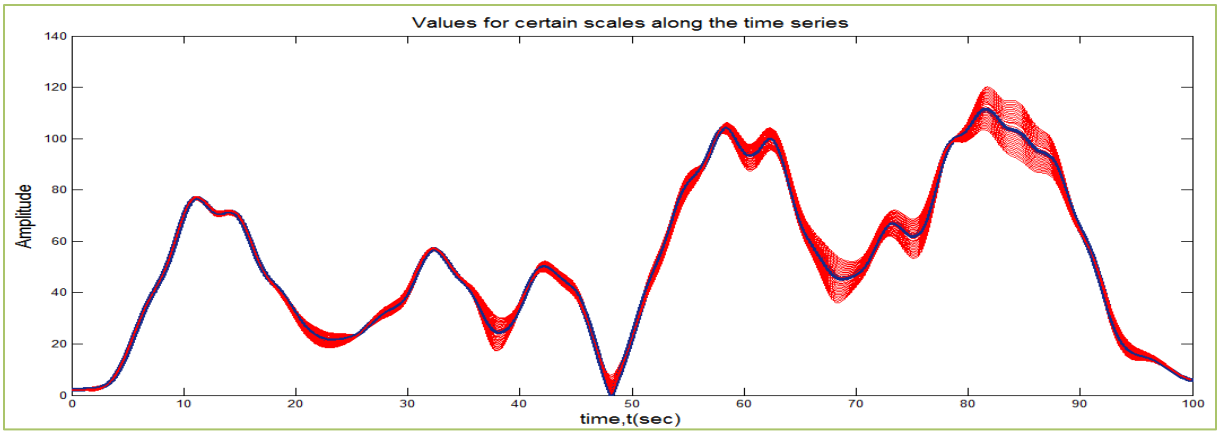

Figure 5-22 Plot for DLT262 DTH for periods between 7.92-8.52 sec near a black hole region

Wavelet coefficients near zero for the ground motion are not desirable because some functions using the wavelet coefficients such as transfer functions use the wavelet coefficients in their denominator. Having very low (near zero) values in the denominator will make the function approach infinity. This leads to further investigate these black holes.

The Approach for further investigation and treatment of black holes followed is as follows:

Determining whether the black hole of frequency content is a property of the signal being analysed, or a product of wavelet transform method. This can be achieved by examining the wavelet coefficients at the location of a black hole for varying complex wavelet bases which is discussed in section 5.5. If the black hole exists for all wavelet bases then it is an aspect of the signal.

5.5 Comparison of Complex Gaussian and Complex Morlet Wavelets

This section gives the comparison of wavelet transforms of the displacement time history data using wavelet analysis program with Complex Guassian and Complex Morlet wavelet functions.

The mother wavelet function of the Complex Morlet wavelet is given by Equation 5-4

$$\Psi(x) = \sqrt{\pi f_b} e^{2i\pi f_c x} e^{-x^2/f_b} \qquad \textbf{5-4}$$

Where

f_b is the bandwidth parameter

f_c is a wavelet center frequency

Bandwidth is the difference between upper and lower frequencies in a contiguous set of frequencies. It is typically measured in hertz. Wavelet center frequency is the number of oscillations the wavelet has in one sec. The Complex Morlet wavelet of different bandwidths and frequencies are compared with the Complex Guassian wavelet as shown in Figure 5-23. For simplicity, Complex Morlet wavelet is of bandwidth f_b and center frequency f_c is denoted by 'cmorf_b-f_c' throughout the document.

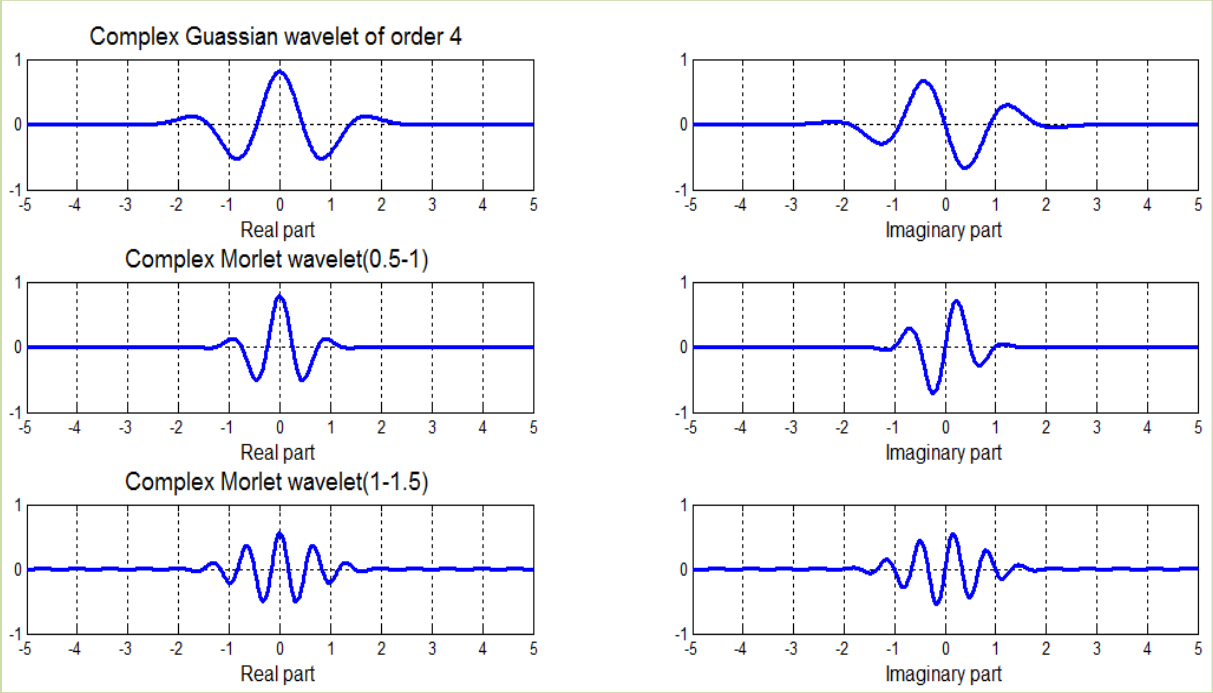

Figure 5-23 Real and Imaginary parts of different wavelets

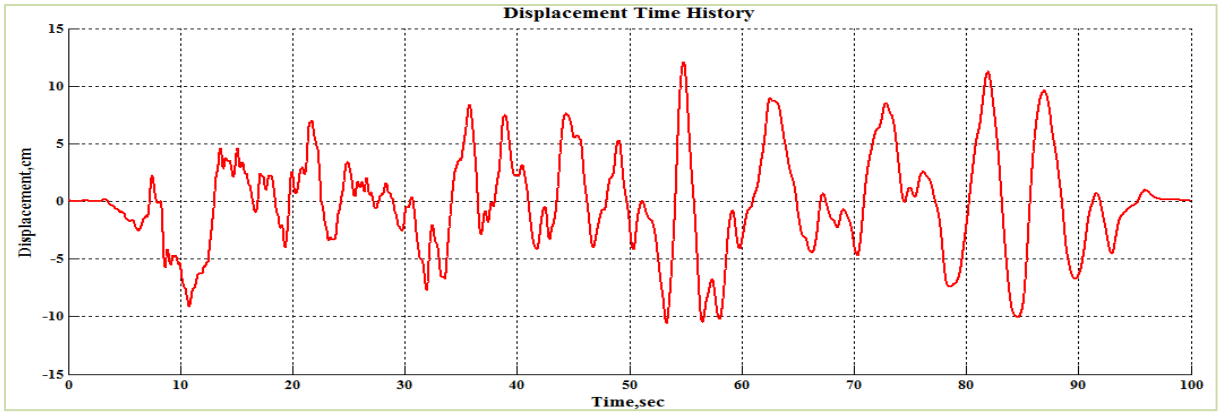

Figure 5-24 Displacement Time History of HDLT262 component of Imperial Valley Earthquake

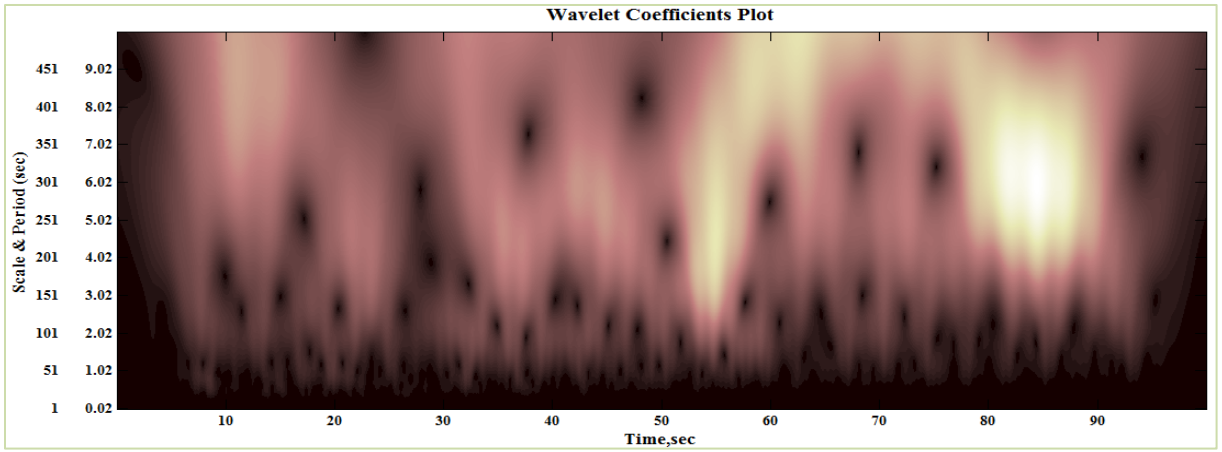

Figure 5-25 Wavelet coefficients plot using Complex Guassian wavelet of order 4

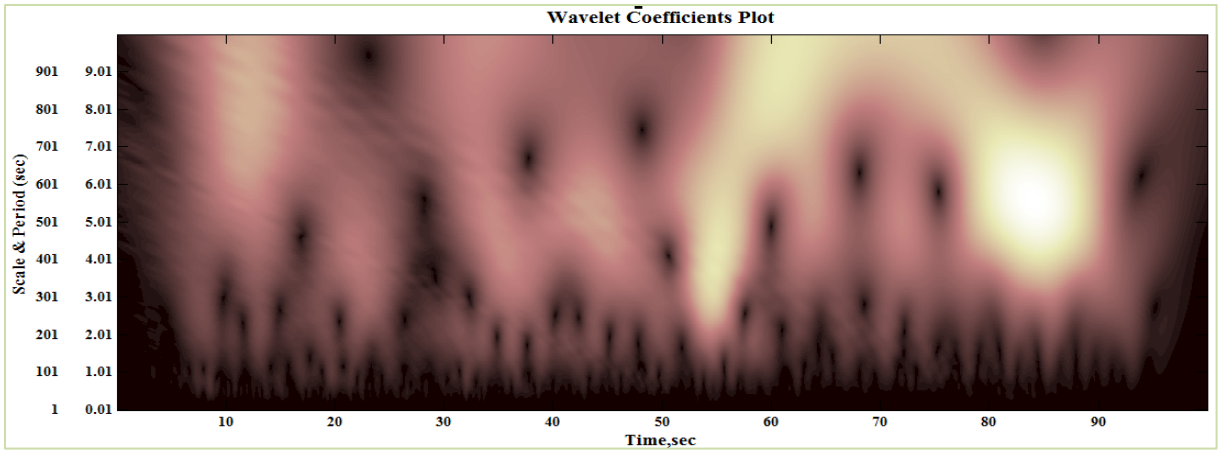

Figure 5-26 Wavelet coefficients plot using Complex Morlet wavelet (cmor0.5-1.5)

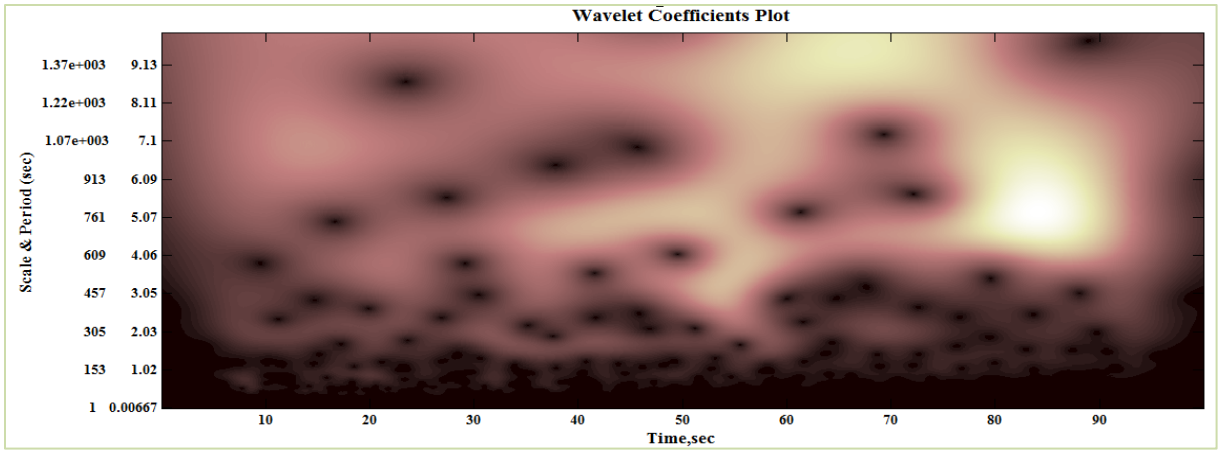

Figure 5-27 Wavelet coefficients plot using Complex Morlet wavelet (cmor1-1.5)

The black holes are also seen in the Complex Morlet wavelets of different bandwidths and frequencies as shown in Figures 5-26 and 5-27. This implies that the black holes are part of the signal and not part of the wavelet transform process. To conclude this analytically, a sample of the signal near black hole region is taken and analyzed using wavelet analysis program with 'cmor1-1.5'(refer to Appendix C-7). It is observed that near the black hole region, the integral of the signal*real part of wavelet and signal*complex part of wavelet is going to be near zero (approximately same area above the axis as below) whereas the integral of the signal*absolute part of the wavelet is not zero near the black hole region. This is significant because absolute values of the wavelet (obtained by taking square root of the sum of squares of real and complex part) neglect the sign. This concludes that black holes are the part of the signal but not the wavelet transform process.

The black holes are expanding horizontally, as shown in Figures 5-26 and 5-27 from'cmor0.5-1' to 'cmor1-1.5' of all the 3 components of ground motion. This is because cmor1-1.5 wavelet has good frequency resolution and poor time resolution when compared to good time resolution and poor frequency resolution of cmor0.5-1 wavelet. The wavelet bases of both cmor0.5-1 and cmor1-1.5 are shown in Figure 5-23 to have an idea of their time and frequency resolutions. Cmor1.5-1 has more oscillations and its spread over longer time, which is the reason for its good frequency resolution and poor time resolution, whereas cmor0.5-1 has very less oscillations and spread over short span of time resulting in very good time resolution and poor frequency resolution. This leads to the further investigation on the wavelet resolution in frequency and time which is explained in section 5.6.

5.6. Wavelet Resolution in Frequency and Time

It is observed from section 5.2.2 that the changes observed in black holes with the increase in the order of Complex Guassian wavelets is due to the resolution of the order of wavelet. It is observed from section 5.5 that the resolution of Complex Morlet wavelets depends on the frequency band under consideration. This concludes that different wavelet bases will have different resolution in frequency and time. Therefore, it is necessary to understand resolution to make valid conclusions about black holes or to interpret the meaning of a given wavelet coefficient.

The following described is the method to define the resolution of a particular wavelet function. Figure 5-28 shows the resolution box of the Complex Guassian wavelet of order 4.

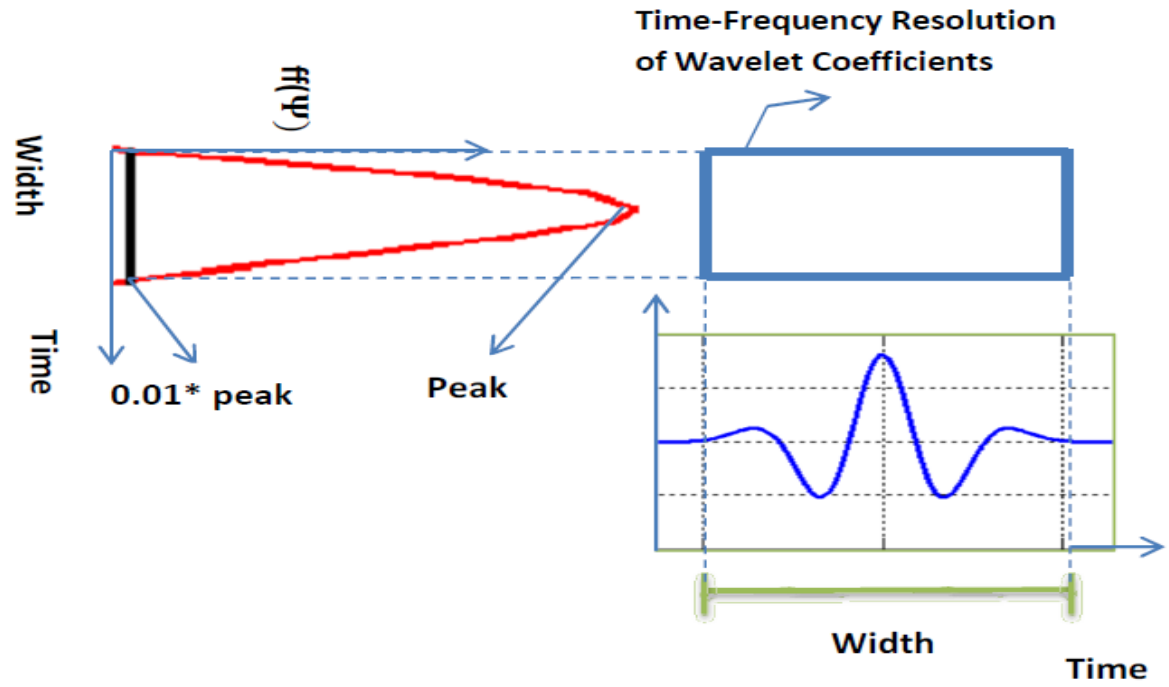

Figure 5-28 Resolution Plot for complex Guassian wavelet of order 4

The rectangular box in Figure 5-28 represents the time-frequency resolution of one wavelet coefficient of Complex Guassian wavelet of order 4. Width of the box along x-axis represents the time resolution and the height along the y axis represents the frequency resolution. The width of the box along x-axis (time resolution) corresponds to the effective width/support of the wavelet function and the width along the y-axis (frequency resolution) corresponds to the effective width

of the Fourier transform of the wavelet function. The effective width is the width taken at $1/100^{th}$ of the peak.

Table 5-5 shows the details of some randomly chosen black holes in the analysis plots of wavelet coefficients using wavelet analysis program with Complex Guassian wavelet of order 4. The signal analyzed is the acceleration time history of 352^0 component of Imperial Valley earthquake. The columns 4 and 6 of Table 5-5 correspond to the width of the resolution box along x and y axis at particular time and period given by columns 2 and 3 respectively whereas column 5 refers to the effective width of the fourier transform of the wavelet function.

Table 5-5 Width of Resolution plots for Complex Guassian wavelet of order 4

Scale	Period	Center of Black hole	Width (sec)	F width (sec)	T width (sec)
15	0.3	4.86	0.9	6.651	0.150
30	0.6	16.02	1.8	3.281	0.305
53	1.06	24.14	3.18	1.883	0.531
100	2	34.88	6	1.012	0.988
140	2.8	42.24	8.4	0.711	1.406
215	4.3	50.45	12.9	0.463	2.160
275	5.5	59.9	16.5	0.377	2.653
320	6.4	75.18	19.2	0.311	3.215
375	6.78	68.06	20.34	0.293	3.413

The resolution values corresponding to time and period shown in Table 5-5 were plotted as shown in Figure 5-29. It can be observed that the resolution of wavelet is changing in time and frequency. The energy in the signal that has a period and time within the box will contribute to the wavelet coefficient at the center of the box if the energy of the signal has a period and time outside this box will result in the smaller wavelet coefficients. Figure 5-30 shows the resolution plot for different periods at particular time t=4.86 sec. It can be observed that the resolution is changing with the change in period values.

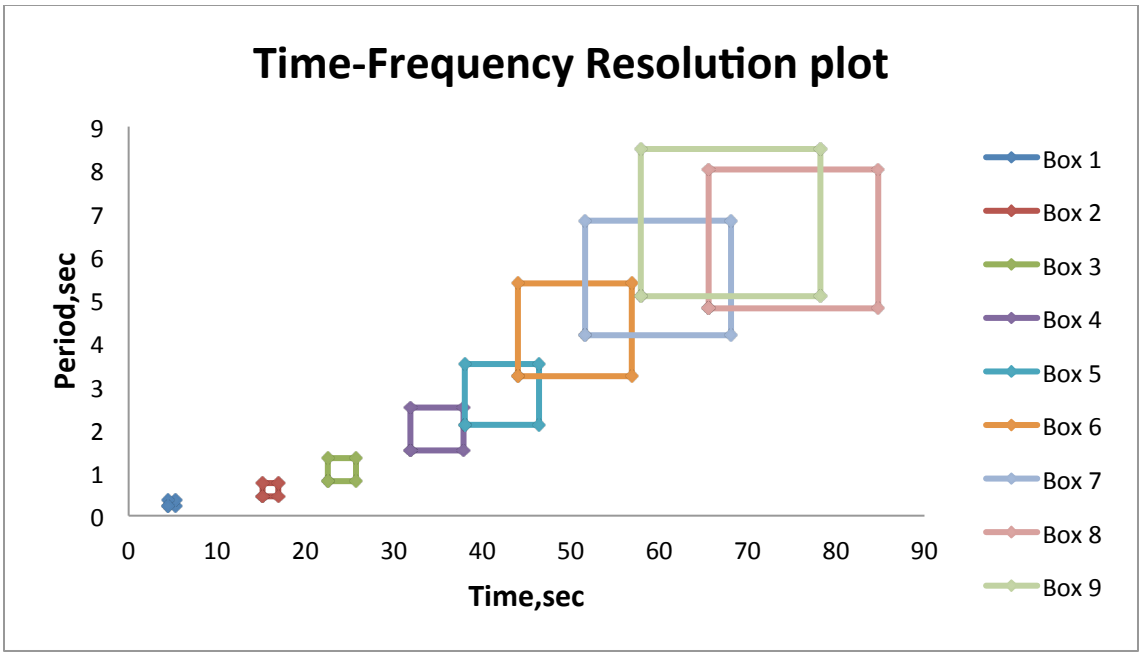

Figure 5-29 Time-Frequency Resolution varying w.r.t time and period

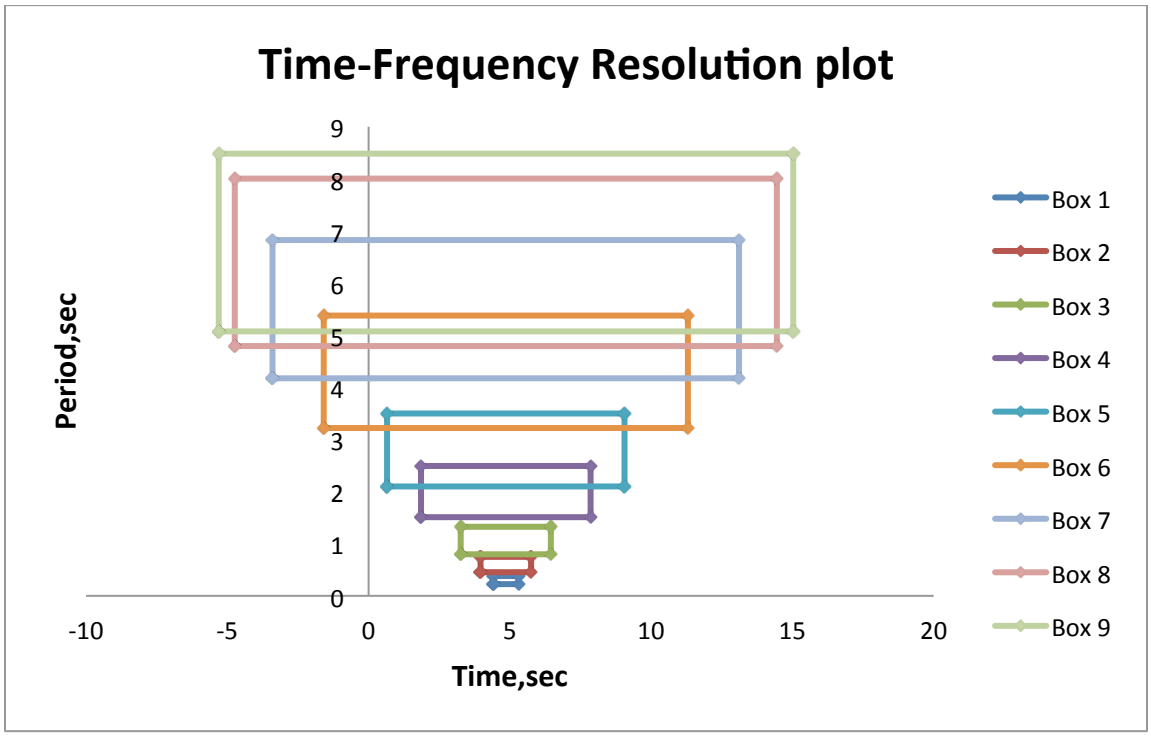

Figure 5-30 Time-Frequency Resolution varying w.r.t period (at particular time)

To spread out the resolution and to deal with the black hole issue, the wavelet coefficients of two different wavelet transforms are combined. The combination of frequency content of two wavelets namely 'cagu4' and 'cmor0.5-3.5' is done by taking the maximum absolute values from the two wavelets at the corresponding period(refer to Appendix C-8). It is observed that the combination of frequency content of two different wavelets results in the removal of black holes which can be seen from Figure 5-31. The signal being analyzed for this purpose is the displacement time history of the horizontal 262^{o} component of the Imperial Valley earthquake.

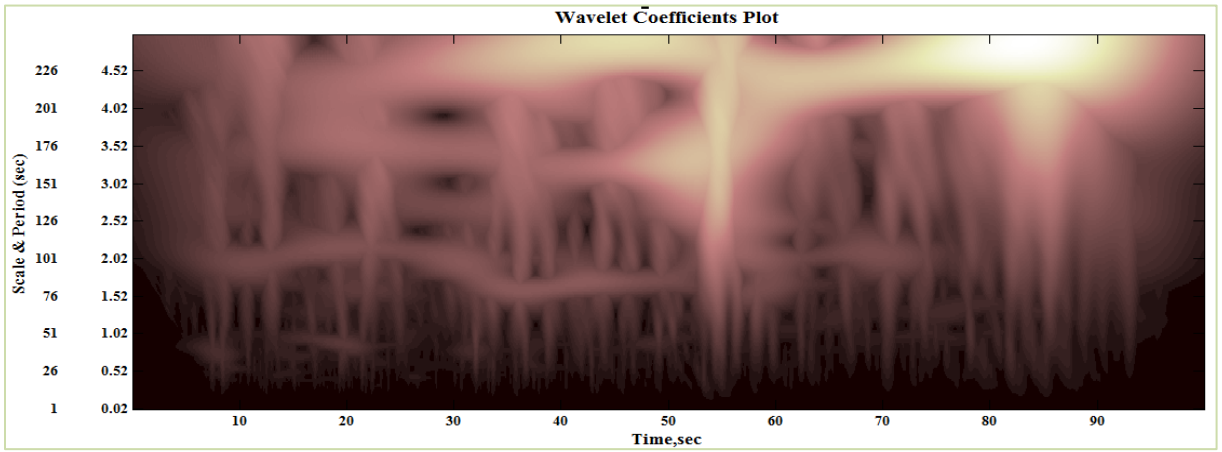

Figure 5-31 Combination of Complex Guassian of order 4 and Complex Morlet of bandwidth 0.5 and frequency 3.5 resulting in the removal of black holes

But the result is not as smooth as desired. Since the smoothness of the plot is a resolution problem, one possible solution suggested to the black hole issue is to use a wavelet that has very wide resolution both in time and frequency. That way the wavelet coefficients would not be near zero.

CHAPTER 6 : ASSESSING THE OCCURRENCE OF MOVING RESONANCE

6.1 Introduction

Real structures that are subjected to design level earthquake events are expected to experience nonlinearity in their structural response leading to time-varying structural properties. The natural frequencies of the structure shift to lower frequencies due to inelasticity and the resulting nonlinearity in the structural response. Inelasticity creates an effective softening of the system whereby the secant stiffness is smaller than the initial stiffness causing elongation of the structural period. When the frequency content of the ground motion shifts in a similar manner as the natural frequencies of the structural response, a phenomenon referred to as moving resonance occurs. Moving resonance is likely a contributor to the variability in the structural response and hence there is need to further understand the sources of variability due to this phenomenon. Lack of understanding could lead to the selection of ground motions that do not properly represent the potential for moving resonance at a site, or require a larger than necessary set of ground motions to appropriately capture the effect.

This section describes the details of analysis performed and related research to investigate the occurrence of moving resonance. These analyses are used to develop a measure of the correlation between the time-frequency content of the ground motion and the time-frequency content of the structural response. For simplicity and in order to maintain a non-specific approach, a generalized SDOF structure is considered. Two hysteretic models were considered in this study: bilinear elastic and the elastic-perfectly plastic. Elastic bilinear is used because it removes the effect of hysteretic damping and elastic-perfectly plastic is used to represent a generic ductile structural system. The chosen hysteretic SDOF system is generalized as a function of only two variables, initial fundamental period T_0 and strength ratio, η by choosing particular damping ratio ξ_0 which is given in the next section.

The following derivation demonstrates why the two parameters were chosen for this study. The equation of motion of a nonlinear SDOF system under seismic input is given by

$$m\ddot{u} + c\dot{u} + F(u) = -m\ddot{u}_g(t) \quad \textbf{6-1}$$

Where *m* is the mass of the system, *c* is the viscous damping coefficient and *F(u)* is the non-linear restoring force defined by the hysteretic model of the system. The displacement, velocity and acceleration of the system, relative to the ground are denoted by $u, \dot{u}$, and $\ddot{u}$ respectively. The ground acceleration at time t is designated by $\ddot{u}_g(t)$.

Two key parameters that are used in defining the dynamic response of the non-linear SDOF system are the initial period T_0 and the strength ratio η.

$$T_0 = 2\pi\sqrt{m/k_0} \quad \textbf{6-2}$$

$$\eta = \frac{F_y}{mg} \quad \textbf{6-3}$$

Where k_0 is the initial stiffness of the system, F_y is the yield force and g is the acceleration of gravity.

Using Eqn 6-2, Eqn 6-1 can be rewritten as

$$\ddot{u} + 2\xi_0\left(\frac{2\pi}{T_0}\right)\dot{u} + \left(\frac{2\pi}{T_0}\right)^2 \bar{f}\,(u) = -\ddot{u}_g \quad \textbf{6-4}$$

With ξ_0 denoting the initial fraction of critical damping of the system,

$$\xi_0 = \frac{c}{2\sqrt{k_0 m}} \quad \textbf{6-5}$$

and $\bar{f}\,(u)$ representing the non-linear pseudo-restoring force of the system,

$$\bar{f}\,(u) = \frac{F(u)}{k_0} \quad \textbf{6-6}$$

With this formulation, for a specified level of critical damping ξ_0, initial period T_0 and the strength ratio η, the SDOF is completely defined for both bilinear elastic and elastic-perfectly plastic. A post-yielding stiffness ratio α of 0.0001 is used for the bilinear hysteretic model.

The force deformation relationship for the bilinear elastic and elastic-perfectly plastic for a particular value of (T_0, η) is shown in Figures 6-1 and 6-2 respectively.

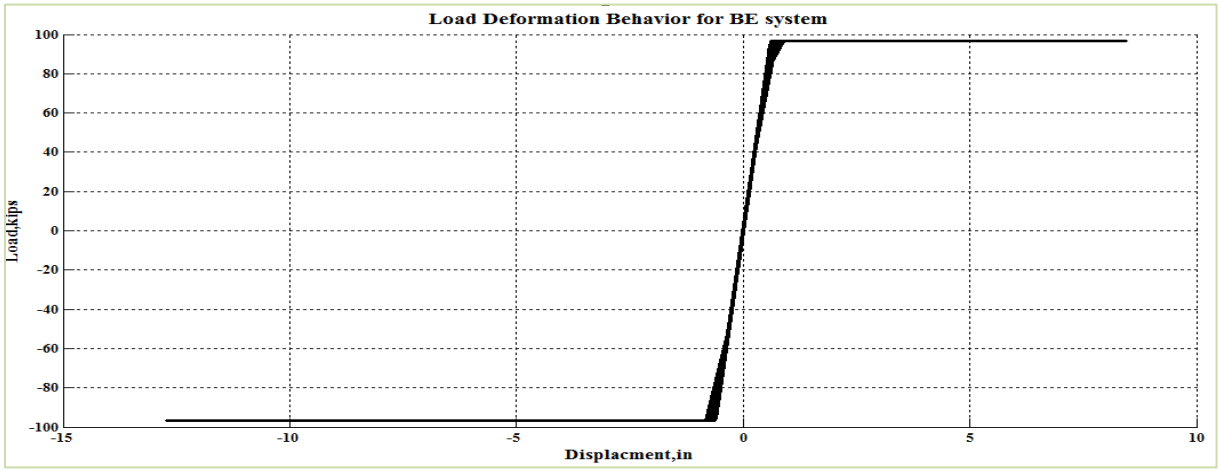

Figure 6-1 Force deformation behavior for BE systems

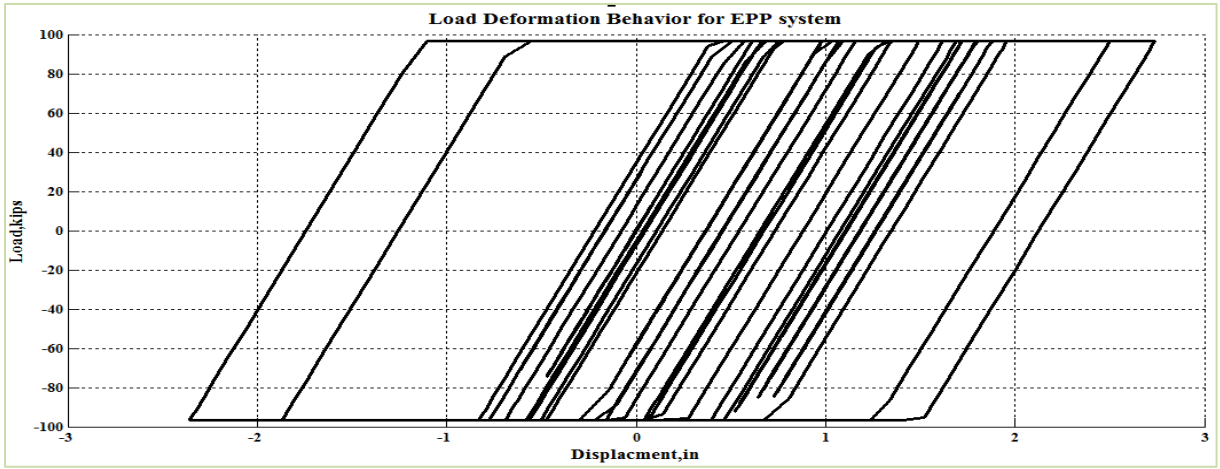

Figure 6-2 Force deformation behavior for EPP systems

6.2 Methods for Assessing and Quantifying Moving Resonance

This section discusses five tools for examining moving resonance and all of them were important in investigating instances of moving resonance. The methods will be developed first and will be applied to an example ground motion later in the section.

6.2.1 Parametric Peak Displacements

Opensees (2006) model is used to calculate the peak displacement of the structural response. The model uses Newmark integration with linear acceleration. Rayleigh damping is been implemented in the model and a damping ratio of 0.02 is chosen for a range of periods between T_0 and $3T_0$. The peak displacement is calculated for each system for a range of periods and strength ratios. The range of periods and strength ratios chosen for this study is from 0.25 to 2.00 with an interval of 0.25

6.2.2 Projecting Ground Motion Excitation on SDOF velocity

The method of assessing the occurrence of moving resonance focuses on calculating the effect of the component of ground motion represented by a wavelet coefficient on the structural response as represented by a wavelet coefficient. This can be achieved by finding the correlation between the wavelet coefficient of the ground motion and the wavelet coefficient of the structural response. The correlation can be obtained by means of projecting the wavelet coefficients of ground motion onto the wavelet coefficients of structural velocity. Before going into the concept of projection, it is important to discuss the basis behind this formulation. It is explained as follows:

The structure at any arbitrary time with current displacement and time which can be regarded as a SDOF system with initial displacement and initial velocity subjected to a set of harmonic excitations characterized by the wavelet coefficients of the ground motion is considered. The equations of motion for an elastic SDOF system subjected to resonant harmonic motion are examined. Although components of the excitation that are not at the natural frequency of the SDOF oscillator will also contribute to the response, the component in resonance will be the largest contributor and therefore deserves investigation. As for the nonlinearity in the SDOF oscillator, it is assumed that for a localized increment in time the system is linear (although the

natural frequency may not be the same as the initial natural frequency because of nonlinearity). The main purpose of this derivation is to define the conditions in which the ground motion wavelet coefficients cause the largest increase in structural response.

The equation of motion governing the relative displacement or deformation *u(t)* of linear system subjected to ground acceleration $\ddot{u}_g(t)$ is given by

$$m\ddot{u} + c\dot{u} + ku = -m\ddot{u}_g(t) \quad \textbf{6-7}$$

Equation 6-7 shows that the equations of motion for the structure subjected to ground acceleration $\ddot{u}_g(t)$ is the same as a system with external force$-m\ddot{u}_g(t)$. The ground motion can therefore be replaced by the effective earthquake force,

$$p_{eff}(t) = -m\ddot{u}_g(t) \quad \textbf{6-8}$$

To determine the effect of the component of ground motion represented by one wavelet coefficient, the ground acceleration can be approximated with a harmonic forcing function. The equation of motion governing the response of SDOF systems subjected to external harmonic forcing function $p_{forc}(t)$=$p_0 sin\omega t$ including viscous damping is given by

$$m\ddot{u} + c\dot{u} + ku = p_0 \sin\omega t \quad \textbf{6-9}$$

Where p_o is the amplitude or maximum value of the force and ω is the exciting or forcing frequency. In this case, the amplitude, p_o is considered analogous to the magnitude of the wavelet coefficient and the circular frequency, ω is the wavelet center frequency.

Hence the forcing function becomes,

$$p_{forc}(t) = p_0 sin\omega t = -m\ddot{u}_g(t) sin\omega t \quad \textbf{6-10}$$

The system initial conditions are analogous to the wavelet coefficient for the SDOF displacement response at the arbitrary time selected. Using the magnitude and phase of the complex wavelet coefficient, the current displacement and velocity could be approximated. The complete solution after solving the Equation 6-9 subject to the intial conditions $u = u(0)$ and $\dot{u} = \dot{u}(0)$ is given by

$$u(t) = e^{-\xi\omega_n t}(A cos\omega_D t + B sin\omega_D t) + C sin\omega t + D cos\omega t \quad \textbf{6-11}$$

Where $\omega_D = \omega_n\sqrt{1-\xi^2}$ Constants can be found by solving the homogenous form of the differential equation and C and D are given by

$$C = \frac{p_o}{k}\frac{1-\left(\frac{\omega}{\omega_n}\right)^2}{\left[1-\left(\frac{\omega}{\omega_n}\right)^2\right]+\left[2\xi\left(\frac{\omega}{\omega_n}\right)\right]^2} \quad \textbf{6-12}$$

$$D = \frac{p_o}{k}\frac{-2\xi\left(\frac{\omega}{\omega_n}\right)}{\left[1-\left(\frac{\omega}{\omega_n}\right)^2\right]+\left[2\xi\left(\frac{\omega}{\omega_n}\right)\right]^2} \quad \textbf{6-13}$$

Constants A and B can be solved by plugging in the values for constants C and D into equation 6-14 and using initial conditions. Considering the response for resonance (when $\omega=\omega_n$), C and D becomes 0 and the complete solution is given by

$$u(t) = \frac{(u_{st})_0}{2\xi}\left[e^{-\xi\omega_n t}(\cos\omega_D t + \sin\omega_D t) - \cos\omega_n t\right] \quad \textbf{6-14}$$

For lightly damped systems the sinusoidal term in equation 6-14 is small and $\omega_D = \omega_n$; thus

$$u(t) = \frac{(u_{st})_0}{2\xi}\left(e^{-\xi\omega_n t} - 1\right)\cos\omega_n t \quad \textbf{6-15}$$

Envelope function

The deformation shown in Equation 6-16 varies with time as a cosine function, with its amplitude increasing with time according to the envelope function.

Differentiating Equation 6-15, the velocity can be obtained as

$$\dot{u}(t) = \left(\omega_n - \omega_n e^{-\xi\omega_n t}\right)\sin\omega_n t \quad \textbf{6-16}$$

Equations 6-15 and 6-16 shows that the displacement $u(t)$ is **out of phase** and velocity $\dot{u}(t)$is **in phase** with the forcing function given by Equation 6-10. Also, since the effective excitation is the opposite sign of the ground acceleration time the mass, the criterion for maximum system

response is when the ground motion wavelet coefficient is in phase with the opposite of the system velocity wavelet coefficient.

This criterion plays an important role and forms the basis behind the concept of projecting the wavelet coefficients of ground motion onto the wavelet coefficients of structural velocity. If the ground motion wavelet coefficient is in phase with the opposite of the structural velocity wavelet coefficient that component of the ground motion has the maximum effect on increasing the structural response. In other words, the structural response is expected to be the largest when the frequency content of ground motion is in *phase* with the opposite of the frequency content of the structural velocity.

The vector projection of wavelet coefficients of ground motion (W_{GM}) on the wavelet coefficients of structural velocity (W_{SV}) is calculated by Equation 6-17 given below. These wavelet coefficients are vectors in real-complex plane having both magnitude and phase.

$$proj_{\overrightarrow{SV}}\ \overrightarrow{GM} = \frac{\overrightarrow{W_{SV}}.\overrightarrow{W_{GM}}}{\left|\overrightarrow{W_{SV}}\right|^2}\ \overrightarrow{W_{SV}} \qquad \textbf{6-17}$$

6.2.3 Weighted Ground Motion Component Projections

The components of the ground motion that will most affect structural response are the ones that are closest to the systems current effective natural frequency. There could be energy in the ground motion at low frequency that is not going to affect structural response very much because it doesn`t match the systems natural frequency at all. The purpose of the weighted projection is to isolate the components of the ground motion that will have the largest effect on structural response and determine if they are in phase or out of phase with the system.

The weighted effect of the ground motion projection on structural velocity which is given by

$$F_{proj}(t,T) = |W_{SV}| * proj_{\overrightarrow{SV}}\ \overrightarrow{GM} \qquad \textbf{6-18}$$

Where:

F_{proj} (t, T) = weighted forcing function as a function of time and period

Where $|W_{SV}|$ = magnitude of the complex wavelet coefficients of the structural velocity

$proj_{\overrightarrow{SV}}\ \overrightarrow{GM}$ = projection of frequency content of ground motion onto structural velocity as calculated in previous section.

For better understanding, the weighted effect of projected frequency content of ground motion on the structural velocity as a function of time is calculated as

$$F_{proj}(t) = \sum_{s} |W_{SV}| * proj_{\overrightarrow{SV}}\ \overrightarrow{GM} \qquad \textbf{6-19}$$

The weighted forcing function shown in Equation 6-19 is meant to be a way to tell whether the ground motion excitation is increasing the system response (constructive) or decreasing the system response (destructive) at any given time. For positive values the forcing function is out of phase with velocity (destructive), and for negative values, it is in phase (constructive).

6.2.4 Degree of Correlation between Ground Motion and SDOF Response

If the time-varying dominant frequencies in the structural response for a nonlinear system match up well with the time-frequency distribution of energy in the ground motion signal, then the occurrence of moving resonance is more likely. The purpose of this method is to determine how well.

The correlation coefficient is calculated as follows. If a series of n measurements of X and Y written as x_i and y_i where i = 1, 2, ..., n, then the sample correlation coefficient can be used to estimate the correlation r between X and Y. The sample correlation coefficient (C.C) is given by

$$\mathrm{C.C} = \frac{\sum_{\mathrm{i}=1}^{\mathrm{n}}(\mathrm{x_i} - \bar{\mathrm{x}})(\mathrm{y_i} - \bar{\mathrm{y}})}{\sqrt{(\sum_{\mathrm{i}=1}^{\mathrm{n}}(\mathrm{x_i} - \bar{\mathrm{x}})^2)}.\sqrt{(\sum_{\mathrm{i}=1}^{\mathrm{n}}(\mathrm{y_i} - \bar{\mathrm{y}})^2)}} \qquad \textbf{6-20}$$

Where x_i and y_i are the magnitudes of the wavelet coefficients of SR and GM

$\bar{x}$ and $\bar{y}$ are the sample means of the wavelet coefficients of SR and GM

The Equation 6-20 can also be written as:

$$\mathrm{C.C} = \frac{n\sum_{\mathrm{i}=1}^{\mathrm{n}}\mathrm{x_i}\mathrm{y_i} - \sum_{i=1}^{n}x_i\sum_{i=1}^{n}y_i}{\sqrt{(n\sum_{\mathrm{i}=1}^{\mathrm{n}}\mathrm{x_i}^2 - (\sum_{i=1}^{n}x_i)^2)}.\sqrt{(n\sum_{\mathrm{i}=1}^{\mathrm{n}}\mathrm{y_i}^2 - (\sum_{i=1}^{n}y_i)^2)}} \qquad \textbf{6-21}$$

The correlation between the frequency content of ground motion and frequency content was calculated using Equation 6-21.

The correlation coefficient (C.C) ranges from −1 to 1. A value of 1 implies that a linear equation describes the relationship between *X (ground motion)* and *Y (structural response)* perfectly, with all data points lying on a line for which *Y* increases as *X* increases. A value of −1 implies that all data points lie on a line for which *Y* decreases as *X* increases. A value of 0 implies that there is no linear correlation between the variables.

It is also noted that $(x_i - \bar{x})\ (y_i - \bar{y})$ is positive if and only if x_i and y_i lie on the same side of their respective means. Thus the correlation coefficient is positive if x_i and y_i tend to be simultaneously greater than or simultaneously less than their respective means. The correlation coefficient is negative if x_i and y_i tend to lie on opposite sides of their respective means.

Based on the interpretation explained above, the significance of correlation coefficient when its value is -1, 0 or 1 is well defined. In most physical systems, however, these ideal correlation cases are unusual. It is necessary to identify criteria to define a particular C.C. value as good correlation with respect to the type of application. The criterion shown in Table 6-1 is followed in the current study.

Table 6-1 Criteria for correlation coefficients

Correlation Coefficient (C.C)	**Type of Correlation**
0	No Correlation
+1	Perfect Positive Correlation
-1	Perfect Negative Correlation
+0.7 to +1	Good Positive Correlation
-0.7 to -1	Good Negative Correlation
0<C.C<0.7 or 0>C.C>-0.7	Poor Correlation

6.2.5. Calculation of Amplification in Peak Displacement for Moving Resonance

The effect of moving resonance is investigated by comparing the structural response due to the original ground motion with the structural response due to a modified ground motion that will not cause moving resonance. The ratio of these peak displacements, which is considered as a moving resonance amplification factor, is intended to quantify the effect of moving resonance. An amplification factor of 3 signifies that the peak displacement is increased by 3 times due to the effect of moving resonance.

The method followed for calculating the structural response without moving resonance is analogous to modal response history analysis in which multiple time history analyses are performed and the results are combined. The procedure is explained in the following steps.

- Breaking the ground motion acceleration signal into its constituent signals with isolated frequency bands using Discrete Wavelet Analysis from Matlab wavelet toolbox. The discrete 'meyer' wavelet function is chosen for decomposing the ground motion in the current study.

- The structural response of the system under consideration (given T_o and η values and either bilinear elastic or elastic plastic hysteretic behavior) is calculated as subjected to each component of the ground motion. This component of the structural response is not capable of experiencing moving resonance because the excitation only contains energy in one frequency band. The total structural response of the system is as the sum of the components of the structural response. This calculated structural response will be taken as the response of the structure without moving resonance. Different methods were considered for combining the results as described below, but a simple sum of the time histories was selected because it results in same total structural response for an elastic system as the displacement history obtained from subjecting the system to the original ground motion.

As mentioned above, the peak structural response of the nonlinear system was calculated by the three methods to determine the best method for combining components of the structural response. The three methods considered include:

- Adding the peak structural response of each individual component

  In this method, the peak structural response of the nonlinear system without moving resonance would be calculated by adding the peak structural response of each individual component.

- Performing SRSS of the peak displacements due to each component

  In this method, the peak structural response of the nonlinear system without moving resonance is calculated by performing square root of sum of squares (SRSS) of the peak displacements due to each component.

- Adding the individual structural response to obtain a total structural response and recording the peak displacement.

  In this method, the peak structural response of the nonlinear system without moving resonance is calculated by adding the individual structural responses and then taking peak response from the total displacement history.

The most appropriate method for calculating structural response is chosen among the three methods explained above by performing an example analysis as shown below.

The acceleration time history of component 1 of Northridge earthquake at Beverly Hills is taken and decomposed into 8 constituent frequency bands using discrete Meyer wavelet from Matlab wavelet toolbox. The time integration is performed using each component as excitation incorporating either bilinear elastic or elasto- plastic behavior and period T_0=0.5 sec with set of η values as shown in Table 6-2 and Table 6-3. Columns 3, 4, 5 of Table 6-2 and Table 6-3 show the peak structural response of the nonlinear system calculated from the three methods explained above.

Table 6-2 Calculation of peak structural response for bilinear behavior

T_0 (sec)	η	Peak Disp (in)	Cum. sum of peaks (1)	S.R.S.S. of Peak Disp (2)	Peak Disp after adding all comp. (3)
0.5	0.25	12.725	23.278	14.895	9.284
	0.50	17.222	7.765	4.737	2.933
	0.75	7.495	9.530	5.943	3.807
	1.00	5.888	13.204	8.493	5.357
	1.25	8.198	13.142	8.450	6.082
	1.50	4.607	10.331	6.496	4.190
	1.75(elastic)	**4.122**	**10.317**	**6.486**	**4.122**
	2.00	**4.122**	**10.317**	**6.486**	**4.122**

Table 6-3 Calculation of peak structural response for elastoplastic behavior

T_0 (sec)	η	Peak Disp (in)	Cum. sum of peaks (1)	S.R.S.S. of Peak Disp (2)	Peak Disp after adding all comp. (3)
0.5	0.25	2.738	3.499	2.287	1.666
	0.50	3.729	3.071	1.976	2.152
	0.75	4.430	3.551	2.406	2.774
	1.00	3.955	4.106	2.922	3.332
	1.25	4.125	4.782	3.568	3.964
	1.50	4.122	5.162	3.935	4.224
	1.75(elastic)	**4.122**	**5.159**	**3.932**	**4.122**
	2.00	**4.122**	**5.159**	**3.932**	**4.122**

From the tabular values shown in Table 6-2 and Table 6-3, it is evident that at elastic stage, the peak displacement values calculated by using method 3 as explained above is matching with the peak displacement values of the original ground motion.

The verification of the method 3 in calculating the structural response is done by comparing the plots which is shown as follows:

The acceleration time history of component 1 of Northridge earthquake at Beverly Hills is taken as shown in Figure 6-3 and decomposed into 8 constituent frequency bands using discrete Meyer wavelet from matlab wavelet toolbox as shown in Figure 6-4.

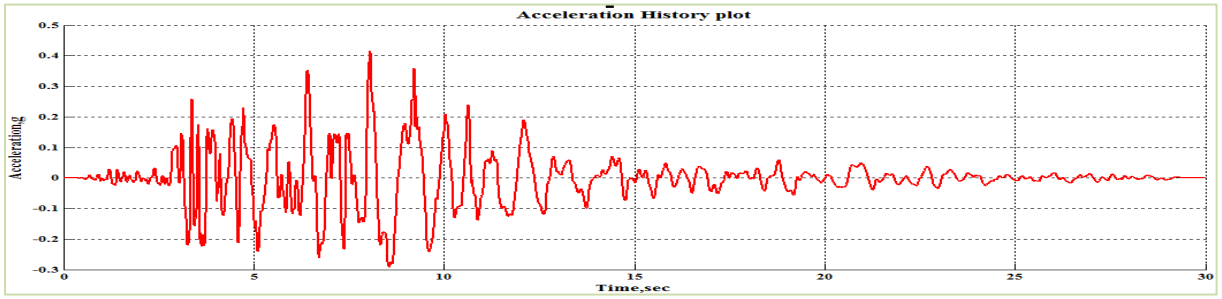

Figure 6-3 Ground Motion Acceleration Time History of horizontal component of Northridge Earthquake at Beverly Hills

The total structural response calculated as the sum of the structural response of the individual components by following method 3 as explained above for elastic system is shown in Figure 6-5. The structural response of the original ground motion for an elastic system is shown in Figure 6-6 and it is evident that both the structural responses are same for elastic system. This proves that the peak displacement values at elastic stage obtained from method 3 is not affected by moving resonance. Hence, method 3 is used to calculate the structural response that is intended to be representative of how the structure would respond without the effect of moving resonance.

This is expected as the natural period of the structure is not changing. The systems that experience inelasticity have values for peak displacement that are often similar to peak displacement of the nonlinear system subjected to the original ground motion. Instances in which the peak displacement of the response built from components is greater than the response of the system subjected to the original ground motion imply that the way the system's dominant natural period varies in time is an important factor in the peak displacement of the system.

Hence, method 3 is used to calculate the structural response that is intended to be representative of how the structure would respond without the effect of moving resonance.

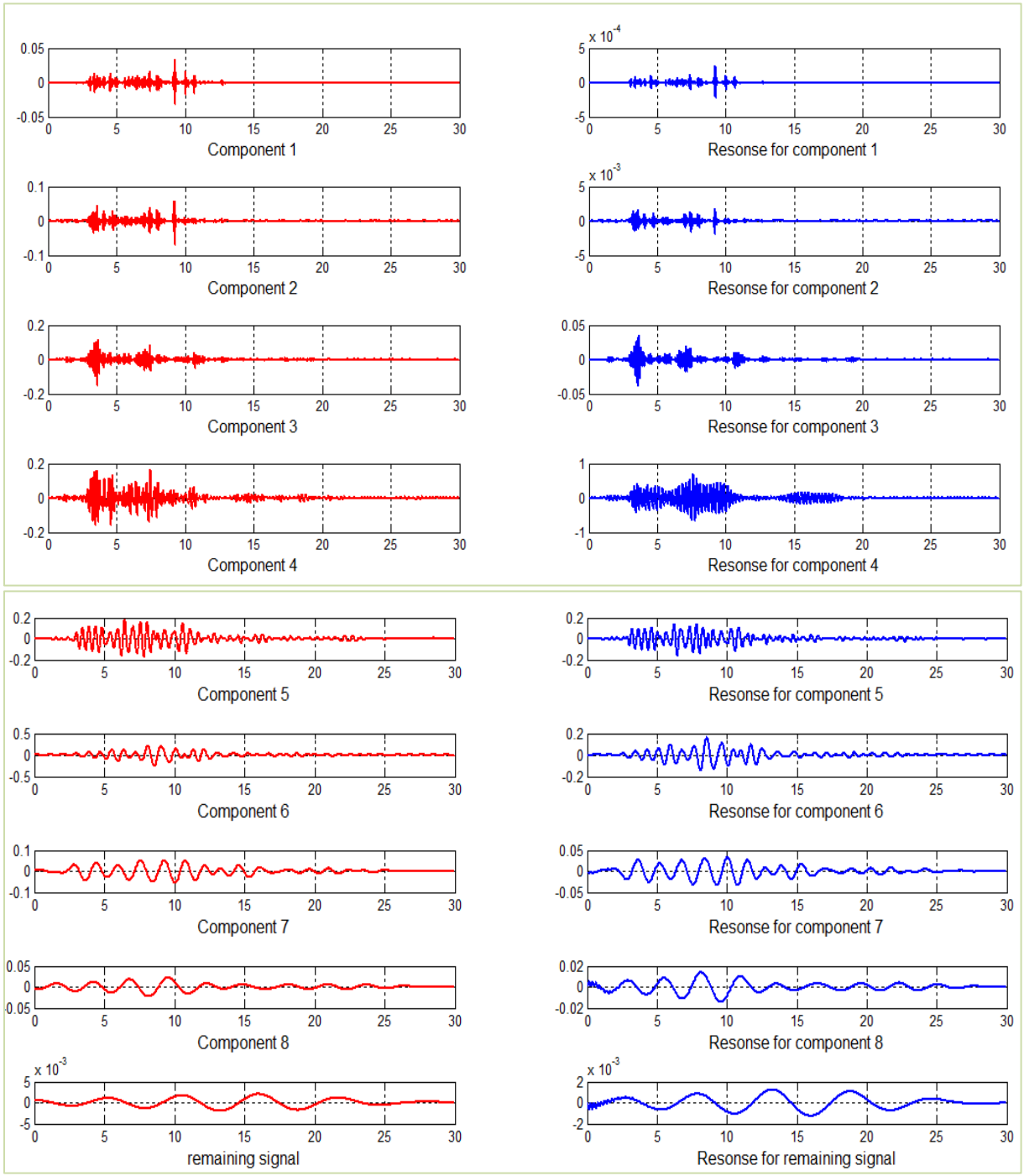

Figure 6-4 Components of Ground Motion and their responses

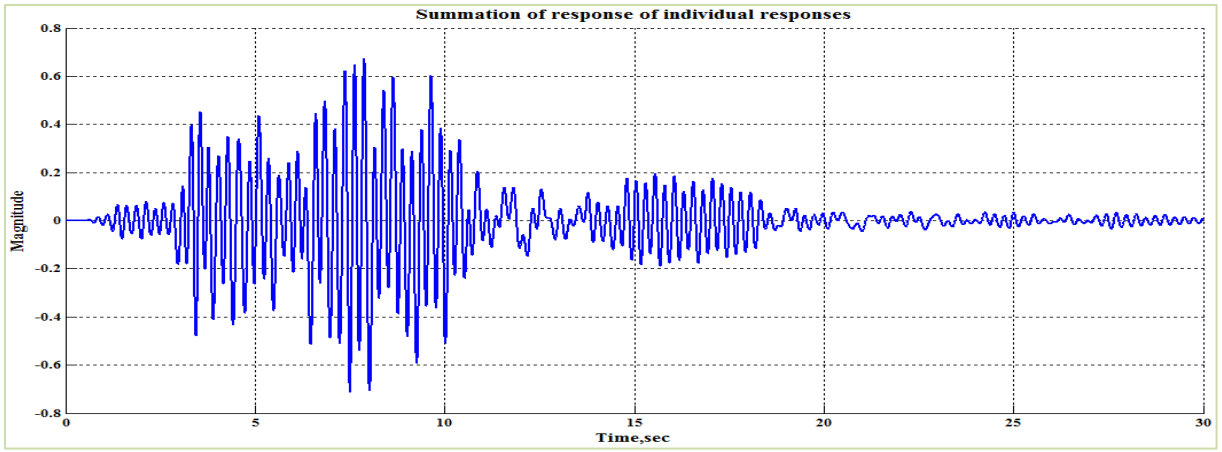

Figure 6-5 Summation of response of individual responses

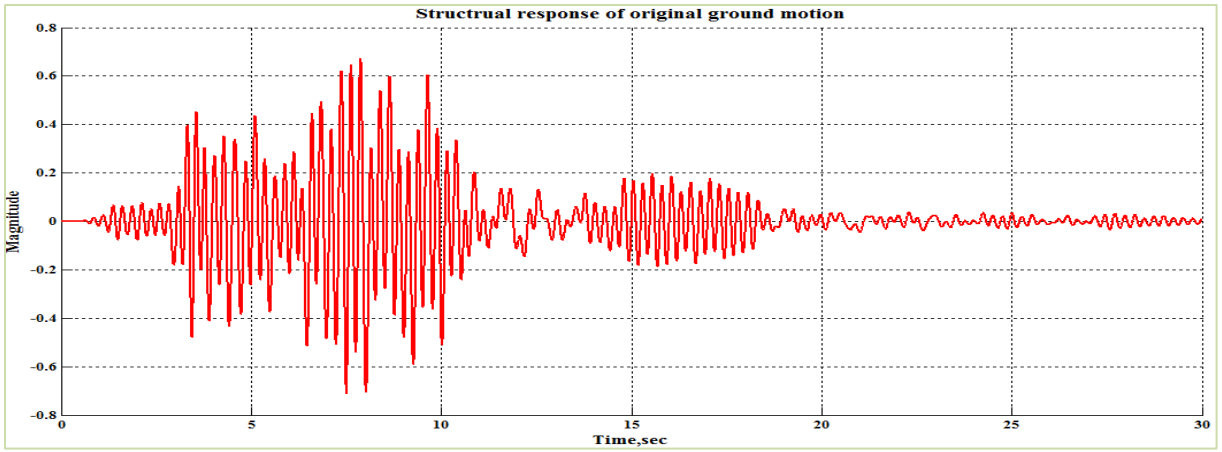

Figure 6-6 Structural response of original ground motion

6.3 Study Assessing the Occurrence of Moving Resonance

This section analyzes one ground motion in depth that is suspected of exhibiting moving resonance. Each of the tools described in the preceding section are used to investigate. In the following chapter, the tools developed and demonstrated in this section are applied to a set of ground motions. The procedure followed for the current study is explained as follows

6.3.1 Selection of Ground Motion for the Study:

The ground motion chosen for this study was the Acceleration Time History of horizontal component of Northridge Earthquake at Beverly Hills as shown in Figure 6-7.

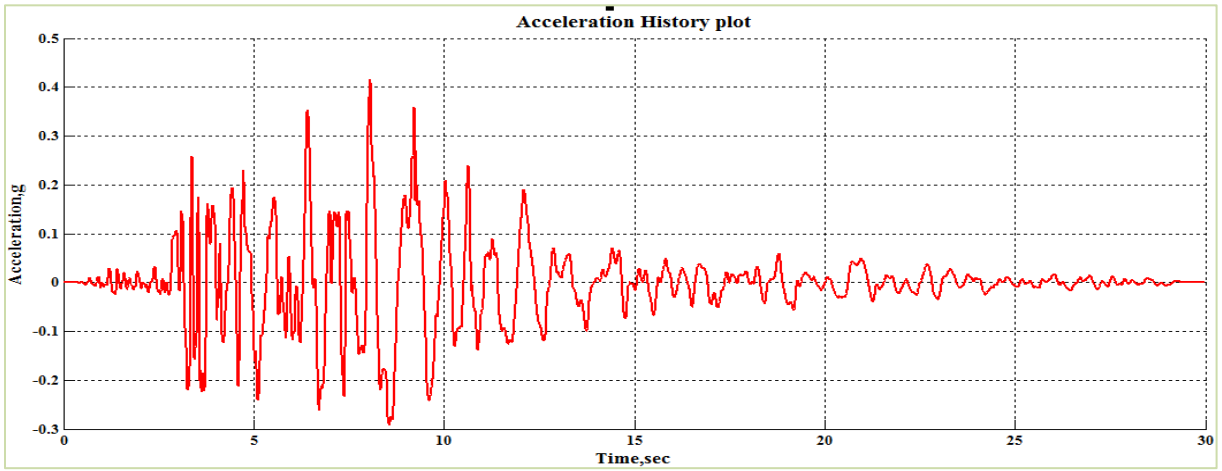

Figure 6-7 Ground Motion Acceleration Time History of horizontal component of Northridge Earthquake at Beverly Hills

It is observed from Figure 6-7 that the significant cycles of this particular ground motion are starting at around 3 sec and the intensity of excitation is increasing as time increases. It can be seen that the large cycles are reaching a period of approximately T_0=1 sec at around 9 sec but this is not clear from an examination of Figure 6-7. These two aspects of the frequency content of this particular ground motion can be clearly seen in the wavelet coefficient plots shown in Figures 6-8 and 6-9 respectively. These coefficient plots were the result of analyzing the ground motion acceleration record using Complex Morlet wavelet of bandwidth 1 and frequency 1.5.

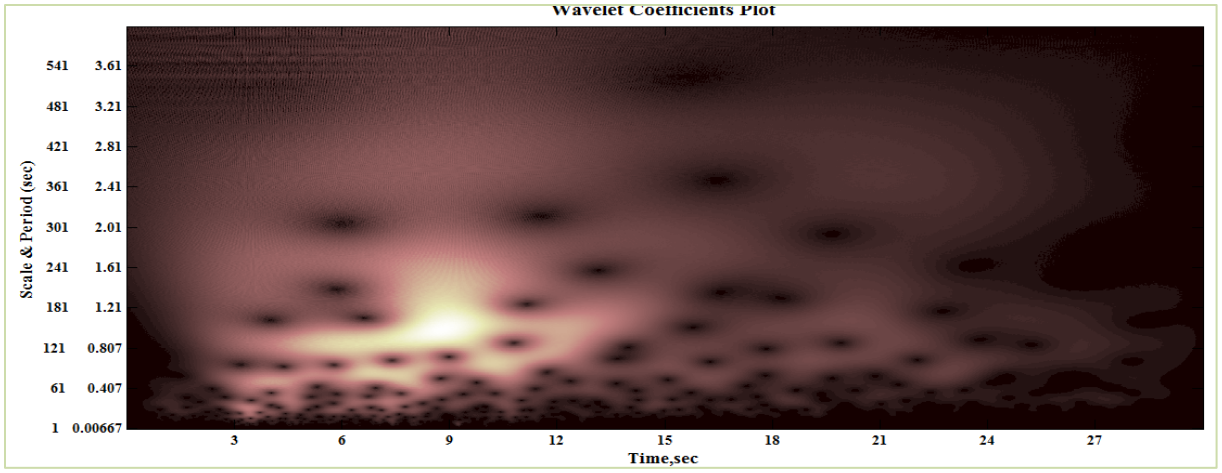

Figure 6-8 Wavelet coefficients plot of the Ground Motion using Complex Morlet wavelet

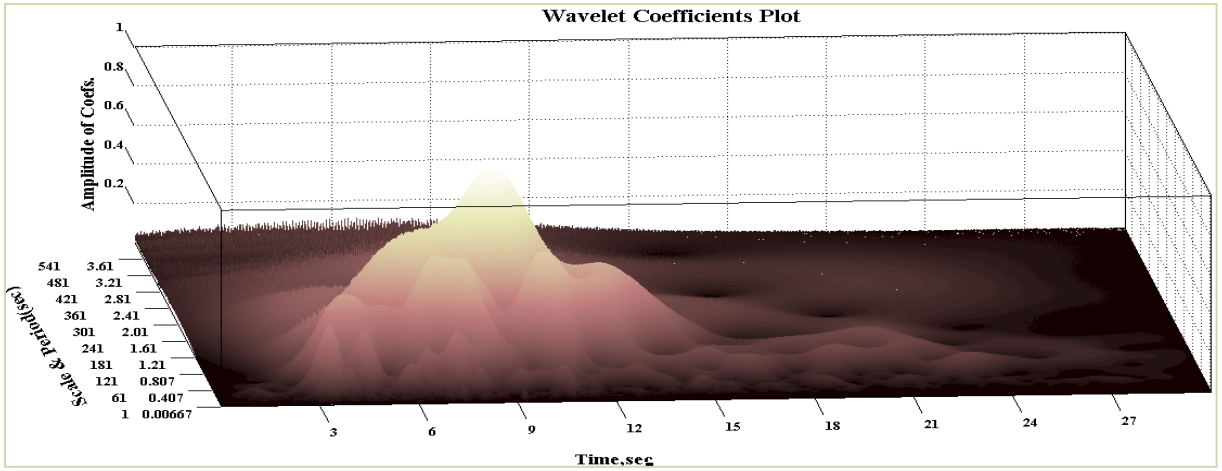

Figure 6-9 Wavelet coefficients plot of the Ground Motion in 3D using Complex Morlet wavelet

It is observed from the wavelet coefficients that the significant frequency content is starting at around time=3.6 sec with a period of 0.467(nearly 0.5) sec and is hitting the period of 1 sec at time= 9 sec. This can be clearly seen from the wavelet coefficients plot shown in Figures 6-8 and 6-9 respectively.

6.3.2 Selection of Range of Variables for the Study

It is observed from the Figure 6-8 that the large amount of energy in the ground motion lies in the period range of 0-2 sec. Hence, this period range at an interval of every 0.25 sec was considered for the analysis of SDOF systems. Strength reduction ratio η at the same interval of 0.25 is varied until the elastic behavior is observed. A damping ratio (ξ_0) equal to 0.02 is selected for this study.

6.3.3 Peak Displacements and Amplification Factors for the Bilinear Elastic System

The seismic response of a SDOF system is analyzed considering bilinear elastic hysteretic behavior and peak displacement is obtained at every interval of period and strength reduction ratio. The peak displacement values obtained for a range of periods and strength levels were plotted in 3D and 2D plots as shown in Figure 6-10 and Figure 6-11 respectively.

The peak displacement plot in 2D shown in Figure 6-11 is done for a subset of the period values i.e., 0.25 sec-1.25 sec for better visualization of specific data. This range of period values was kept uniform for all 2D peak displacement plots in this document for consistency.

The 2D peak displacement plot as shown in Figure 6-11 have bumps (localized high points) in peak displacement at corresponding (T_0,η) values of (0.50,0.50) and (0.50,1.25).This localized increase in peak displacement is hypothesized to be the result of occurrence of moving resonance and hence an increase in amplification factor is expected for these combinations of period and strength. The hypothesis makes sense because of the trend in the dominant frequencies of the ground motion. Also moving resonance is a likely conclusion because slight changes in period or strength have smaller peak displacement.

The 3D and 2D peak amplification plots of the structural system incorporating bilinear elastic behavior are shown in Figures 6-12 and 6-13 respectively. It is evident from Figure 6-13 that the amplification values corresponding to (T_0,η) values of (0.5,0.5) and (0.5,1.25) (at similar places where localized high points of peak displacement were observed in Figure 6-11) are greater than 1 leading to the increase in peak displacement. This increase in peak displacement is considered to be the effect of moving resonance. A maximum effect of moving resonance is seen at T_0=0.5 sec and η=0.5 where the peak displacement is increased by 6 times.

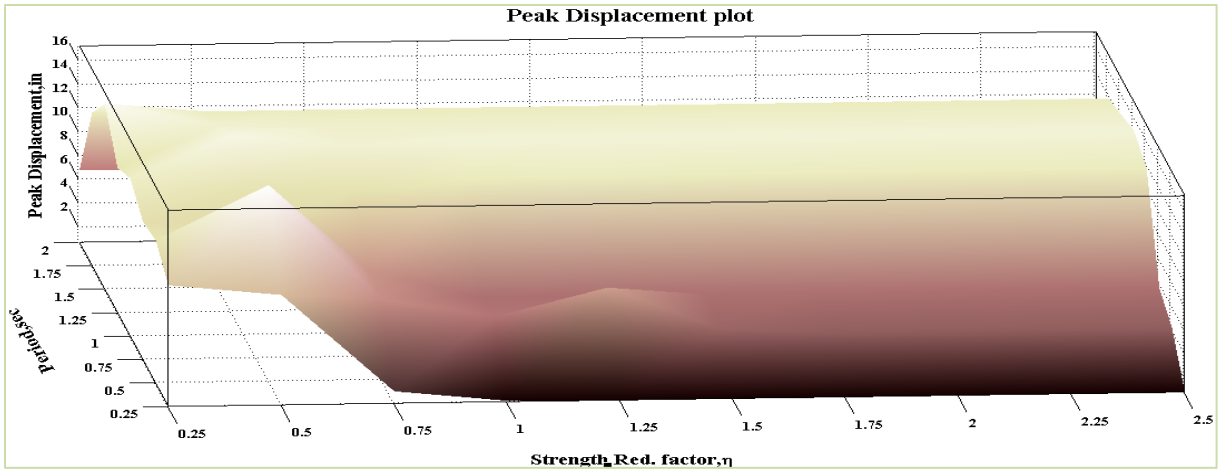

Figure 6-10 Peak Displacement plot in 3D for bilinear hysteretic behavior

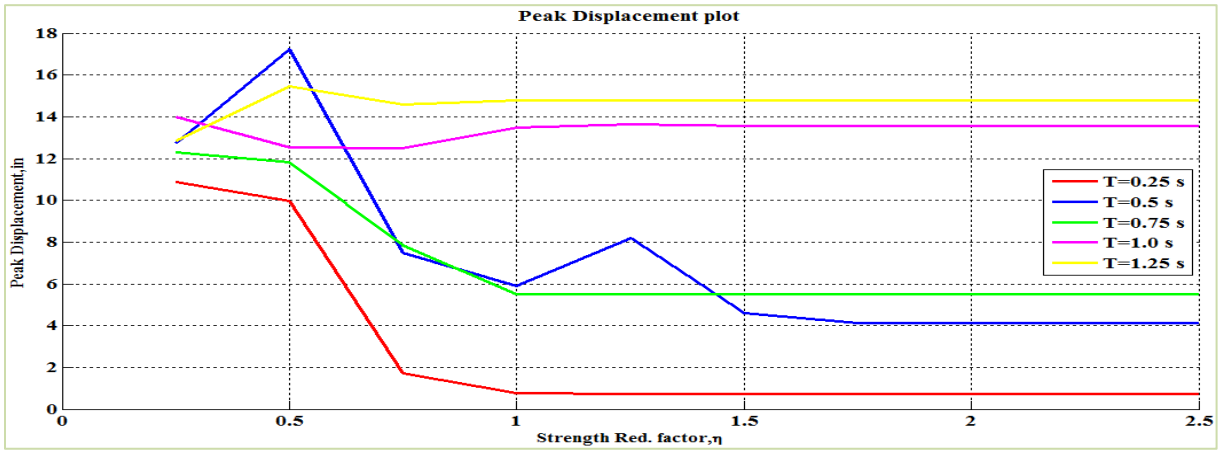

Figure 6-11 Peak Displacement plot in 2D for bilinear hysteretic behavior

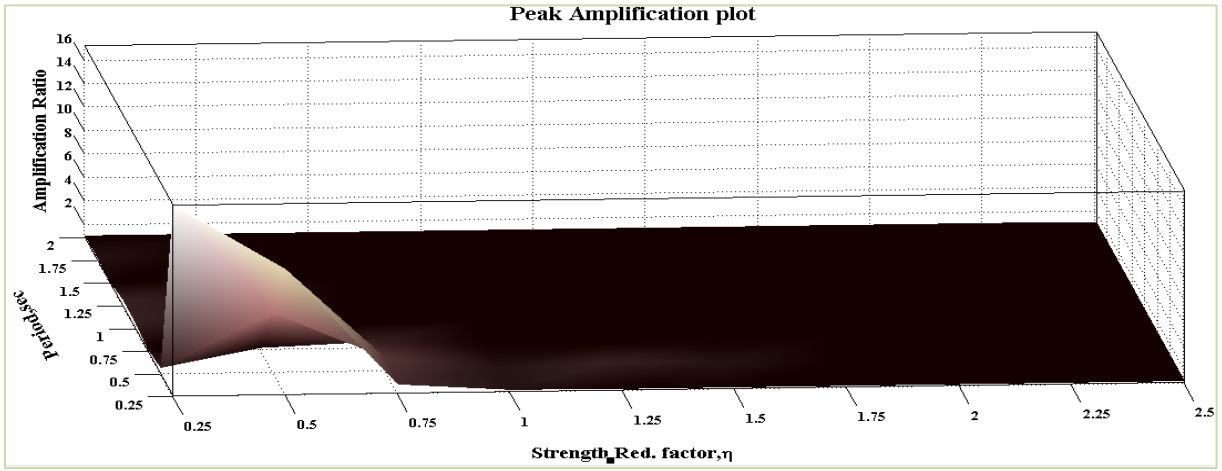

Figure 6-12 3D Peak Amplification plot for bilinear elastic behavior

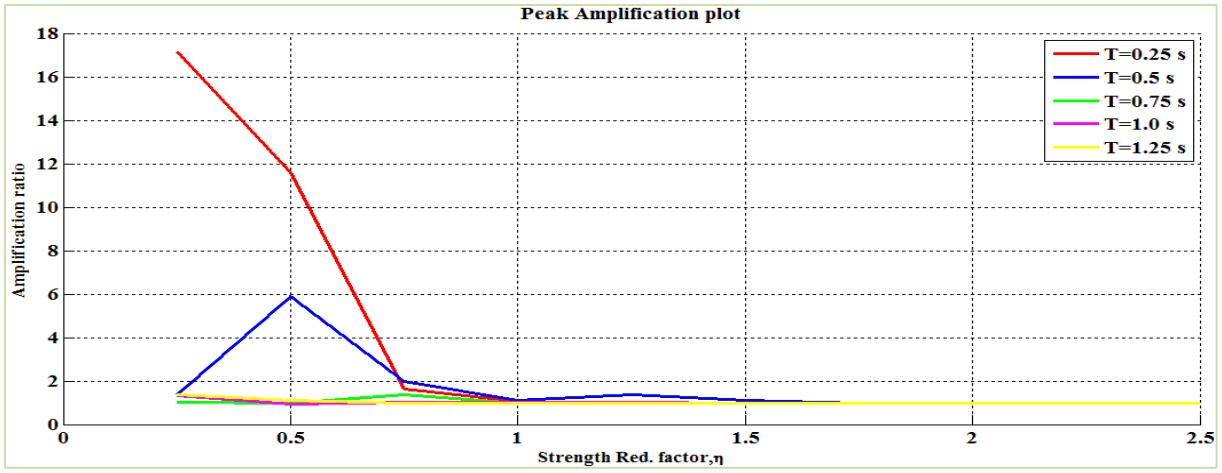

Figure 6-13 2D Peak Amplification Plot for bilinear elastic behavior

It is noted that systems with low periods (e.g. *To*=0.25 sec) are shown to exhibit large amplification factors. It is not surprising that especially low period structures with nonlinear hysteretic behavior experience large peak displacements. Previous studies on systems with short periods have shown that short period structures with yield strength less than the elastic forces will experience excessive inelastic displacements (Veletsos et al. 1965). The current study does not focus on this effect, but instead focuses on systems that experience larger peak displacement than systems with similar system parameters (T_0,η).

The calculation of peak displacements was verified against the spectral displacements. The peak displacement values corresponding to large strength reduction factors in which the system exhibited elastic response were compared with the spectral displacement values for the ground motion with damping ratio of 2%. The result is plotted as shown in the Figure 6-14. The peak displacement plot shown in Figure 6-14 (in blue) is plotted for a period values of 0.25-2 sec with an interval of 0.25 sec and spectral displacement plot (in red) is plotted for a period values of 0.25-5 sec with an interval of 0.25 sec. The variation in the range of periods is chosen to make it clear that both plots overlap each other. Since, both plots are identical it can be concluded that the accuracy of the calculations for peak displacement were partially verified.

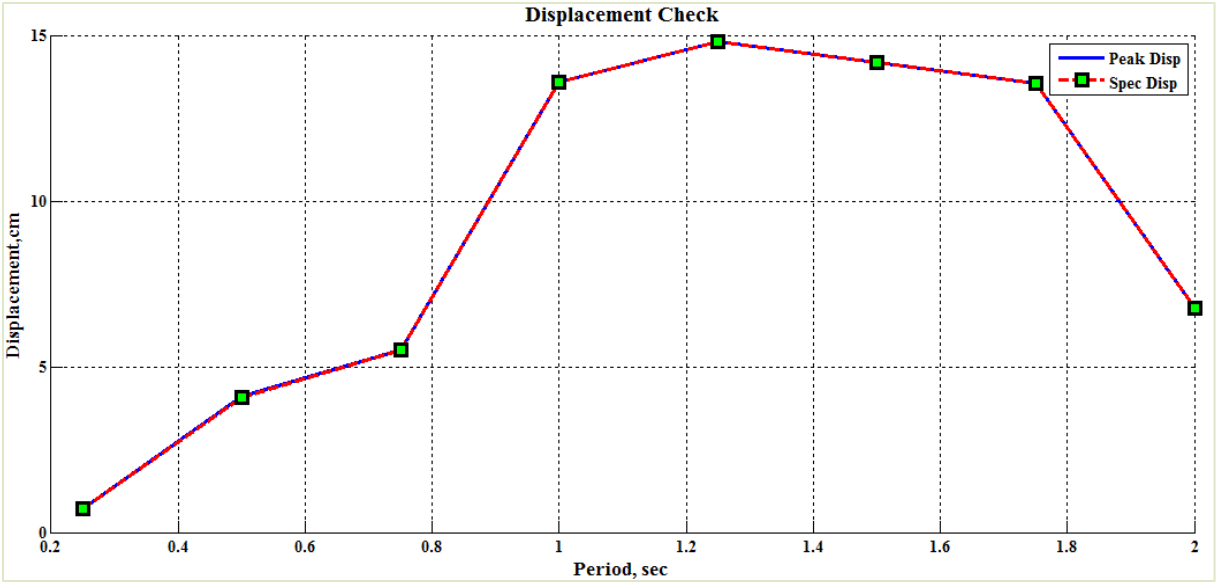

Figure 6-14 Peak Displacement vs Spectral Displacement plot

The spectral displacement values were obtained by using the equation 6-22 given below.

$$S_D = \frac{S_a * T^2 * 386.4}{4 * \pi^2} \qquad \textbf{6-22}$$

Where S_D is the spectral displacement

S_a is the spectral acceleration value

T is the corresponding period.

The peak displacement plots and amplification factors provide information about moving resonance for the full range of periods and strength ratios. On the other hand, the other tools for assessing the occurrence of moving resonance are more applicable to specific values of period T_0, strength reduction ratio η and critical damping ξ_0. Therefore, a period of 0.5 sec and a critical damping of 0.02 is chosen for bilinear elastic hysteretic behavior to measure the correlation with the frequency content of the ground motion. The results of the analysis are described in the following subsections.

The two main reasons for applying the other tools for assessing moving resonance to a period of T_0=0.5 sec and specific values of the strength reduction factor are as follows:

- As discussed above, the two bumps observed in the 2D peak displacement plot as shown in Figure 6-11 corresponding to period= 0.5 sec at strength reduction factor of 0.5 and 1.25 are hypothesized to be the result of moving resonance.
- This is the period at which the significant frequency content of the ground motion started which can be seen in Figure 6-7.
- The two bumps hypothesized to be moving resonance occur at strength reduction ratios of 0.5 and 1.25. The values of the strength reduction factor between these two values were selected for further investigation, η = 0.5, 0.75, 1.0, 1.25.

6.3.4 Application of Other Tools for Selected Bilinear Elastic Systems

The frequency content of the structural response shown in the following sections is analyzed using Complex Morlet wavelet of band width 1 and frequency 1.5. This was one of the systems that is suspected of exhibiting moving resonance as determined from the peak displacement and amplification factor results.

6.3.4.1 Projection plots for T_0=0.50 sec and η=0.50

The displacement time history of the structural response is shown in Figure 6-15 and the 2D and 3D wavelet coefficients of the structural response is shown in Figures 6-16 and 6-17 respectively. Figures 6-15 and 6-17 shows a clear concentration of energy at a fundamental period of T_0=0.5 sec starting from time t=3 sec and returning to that period between time t=16 sec and t=27 sec. The dominant frequency content reaches higher periods from time t=6 sec to t=15 sec showing the period elongation as the system becomes nonlinear. More interestingly, a hot spot of frequency content of structural velocity is seen similar to that of ground motion`s frequency content as shown in Figure 6-8. Though this hot spot of frequency content of structural velocity shifts in time with respect to ground motion`s energy content, both hit the same period of around 1 sec at around time t=8-9 sec. The dominant natural period of the system is shown to start at 0.5 sec which corresponds to the energy early in the ground motion. The system then

becomes nonlinear and the dominant period of the system shifts to approximately 1 sec matching the high energy in the ground motion. The occurrence of moving resonance is confirmed.

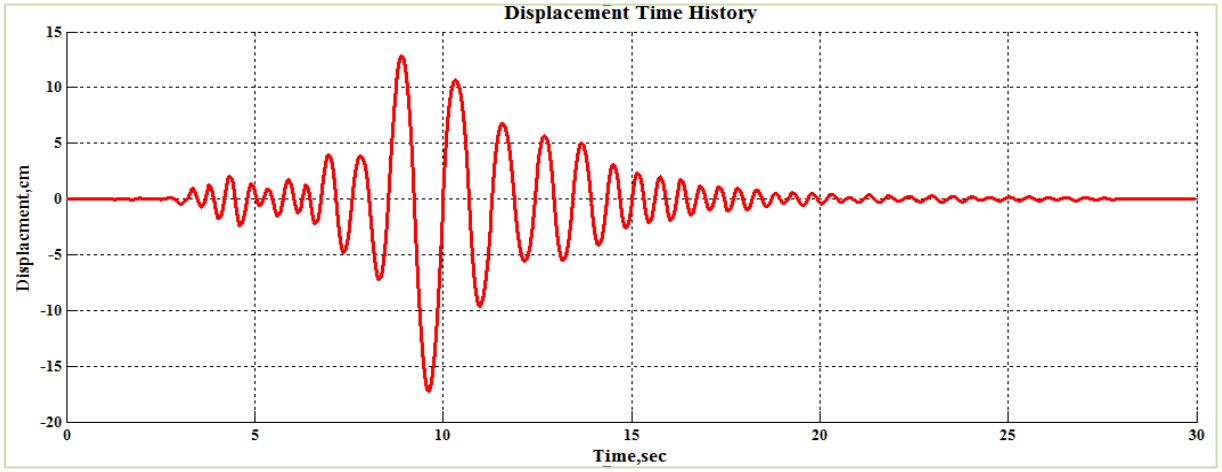

Figure 6-15 Displacement Time History for the structural response

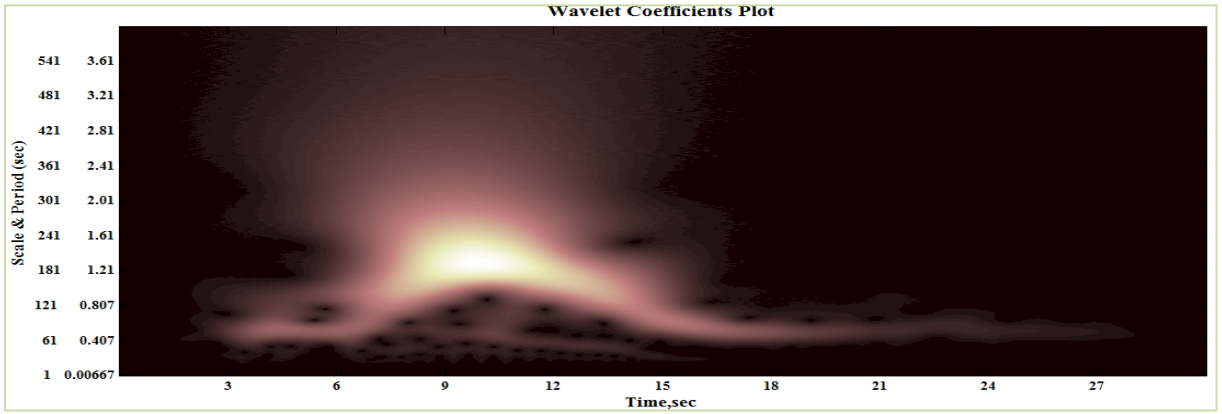

Figure 6-16 Wavelet coefficients plot of the Structural Response

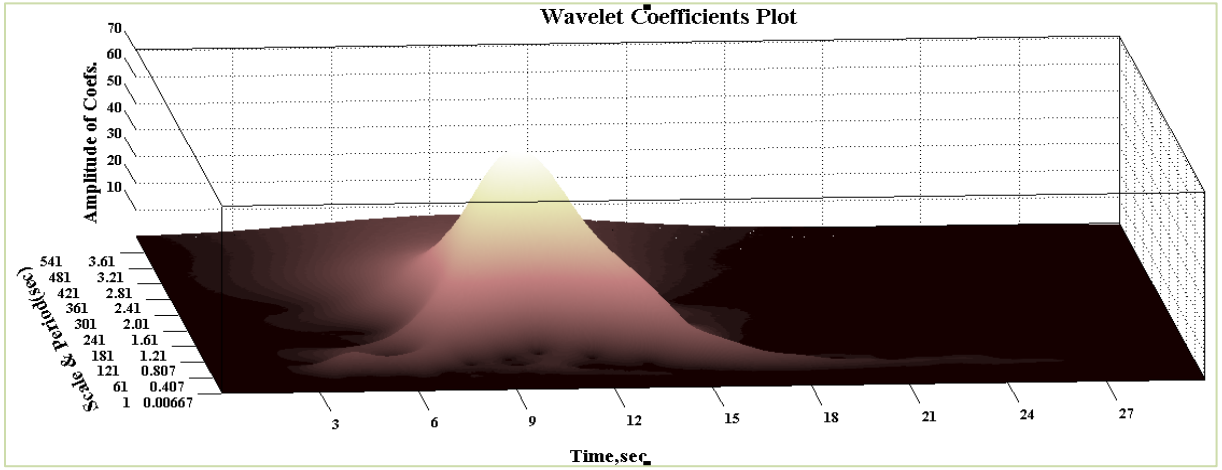

Figure 6-17 Wavelet coefficients plot of the Structural Response in 3D

The projection of the ground motion wavelet coefficients in the direction of the SDOF system velocity is shown in Figure 6-18. The calculations of both are discussed in section 6.2.3.

Figure 6-18 shows that there is significant variation in the ground motion projections. This implies that the components of the ground motion represented by the wavelet coefficients are sometimes in phase and sometimes out of phase with the system velocity. From Figure 6-18, it is evident that the frequency content of ground motion is generally *in phase* with the frequency content of the structural response as the weighted effect of projection is seen in the negative axis. As described in section 6.2.2, the maximum potential for increasing structural response occurs when the projection values are negative. It is also observed that the weighted effect of projection is maximum at time t=8-9 sec where both the dominant energy of the two signals are hitting the same period as seen from Figures 6-8 and 6-16.

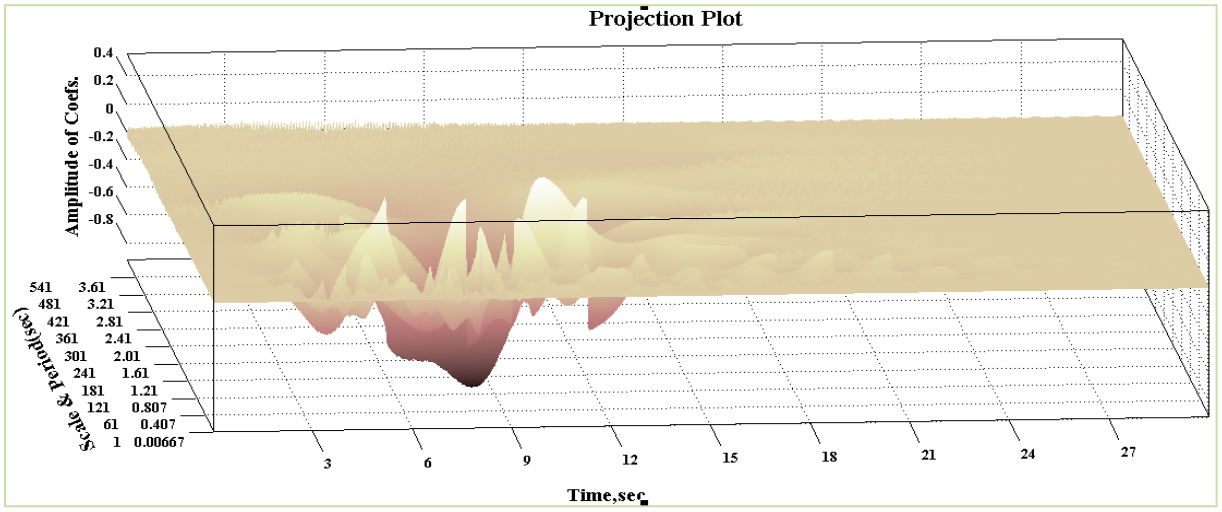

Figure 6-18 3D Projection of Ground Motion on Structural Velocity

The weighed effect of projection of ground motion on structural velocity as shown in Figure 6-20 is calculated by using Equation 6-18.It is clear from the Figure 6-20 that the frequency content of ground motion is *in phase* with the frequency content of the structural response as the weighted effect is seen in the negative axis(refer Equation 6-10). It is also observed from Figure 6-20 that the weighted effect of projection is maximum at time t=8-9 sec where both the frequency contents are hitting the same period (as seen from Figures 6-8 and 6-16).The y- axis on the Figure 6-20 shows the intensity of the effect of ground motion frequency content on structural response. This proves that for this T_0 and η at time around 9 sec, the frequency content of ground motions shifts is in phase (shifts in a similar manner) with the structural velocity and

this is the reason for the larger peak displacement as compared to slightly different values of T_0 and η.

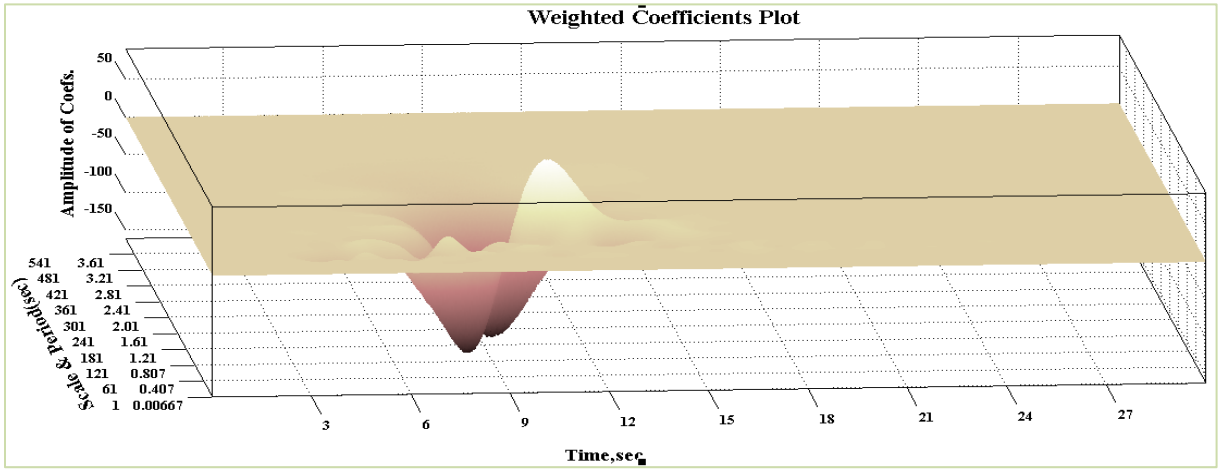

Figure 6-19 3D Comparison of weighted effect of Ground Motion on Structural Velocity

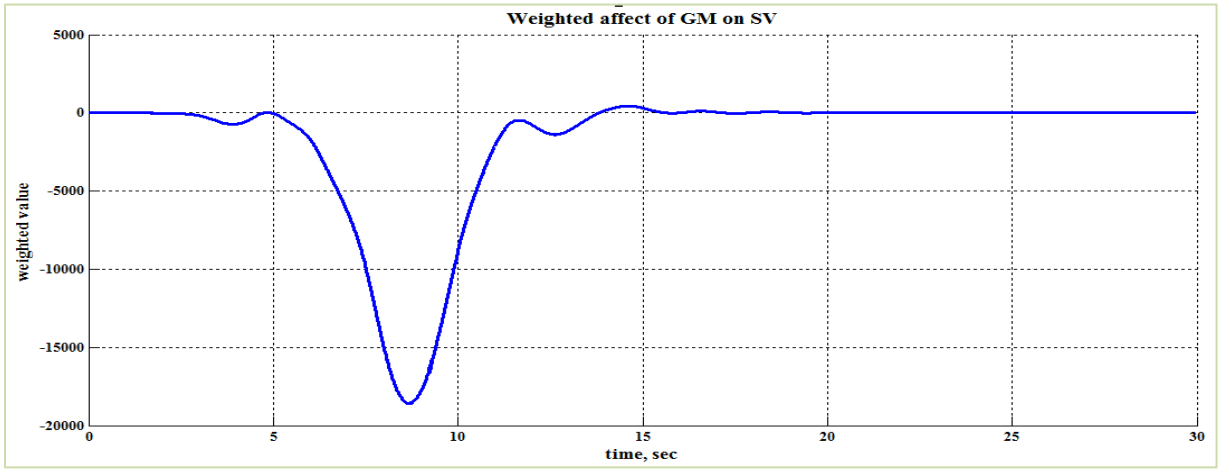

Figure 6-20 2D Comparison of weighted effect of Ground Motion on Structural Velocity

The correlation coefficients as shown in Figure 6-21 is calculated by using equation 6-21. Any correlation value that falls outside the red solid lines shown in Figure 6-21 were considered to be a good correlation value(as per criteria given in Table 6-1). It can be clearly seen from Figure 6-21 that there exists some good correlation values at around 9 sec, which tells the existence of correlation between the frequency content at that particular time.

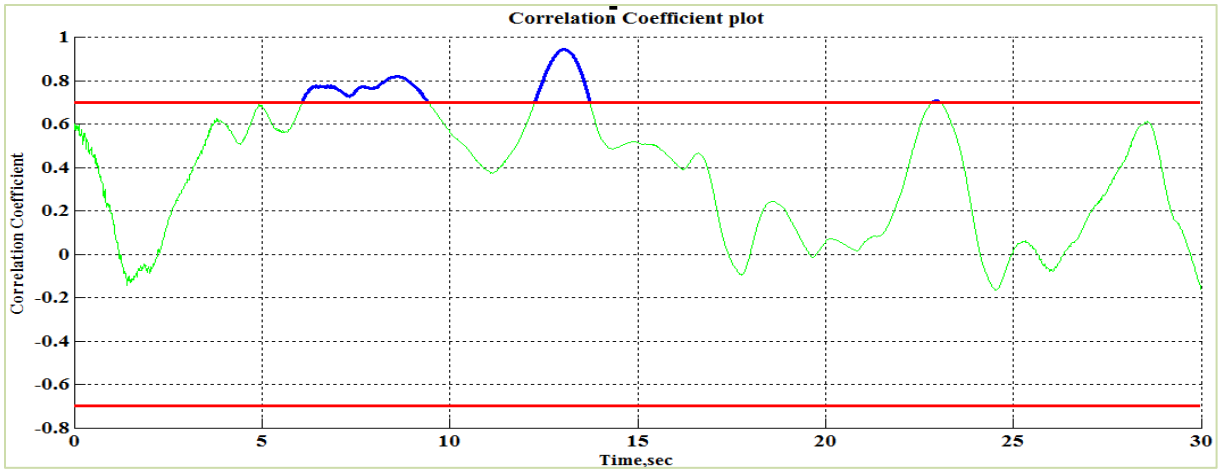

Figure 6-21 Correlation coefficients plot

6.3.4.2 Further Analysis of the Bilinear Elastic System with T_0=0.50 sec and η=0.75

The displacement time history of the structural response is shown in Figure 6-22 and the 2D and 3D wavelet coefficients of the structural response is shown in Figures 6-23 and 6-24 respectively. Figures 6-22 and 6-24 shows a clear trace of fundamental period of T_0=0.5 sec starting from time t=3 sec. Though there is a clear period of large amplitude oscillations in the structural response between 10 and 17 seconds, the energy in the ground motion is shown to occur at different dominant periods as shown in Figure 8. The system is therefore not undergoing moving resonance.

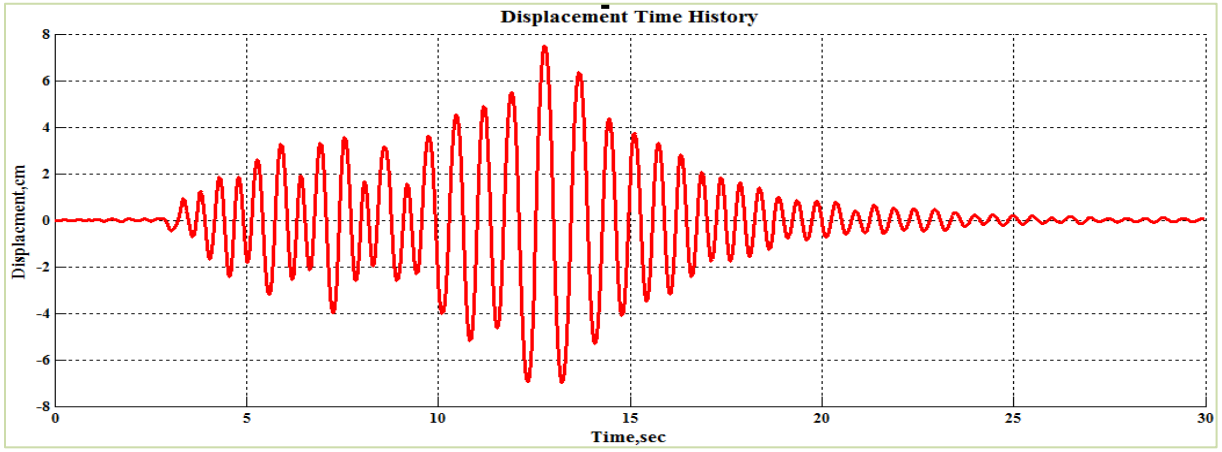

Figure 6-22 Displacement time history of structural response

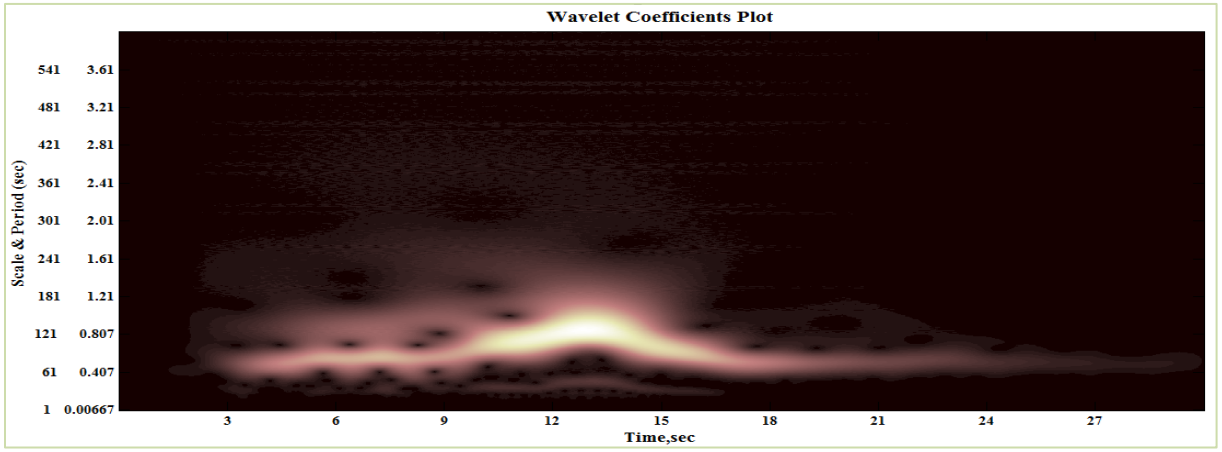

Figure 6-23 2D Wavelet coefficients plot of the Structural Response

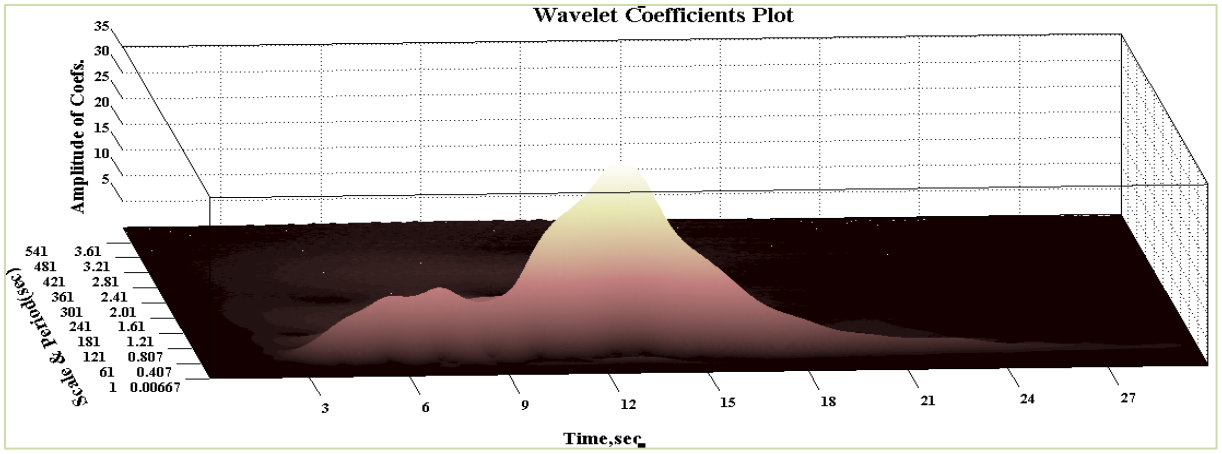

Figure 6-24 3D Wavelet coefficients plot of the Structural Response

It is observed from the projection of ground motion on structural velocity plot shown in Figure 6-25 that the frequency content of ground motion is *in phase* with the frequency content of the structural response as the weighted effect of projection is seen in the negative axis.

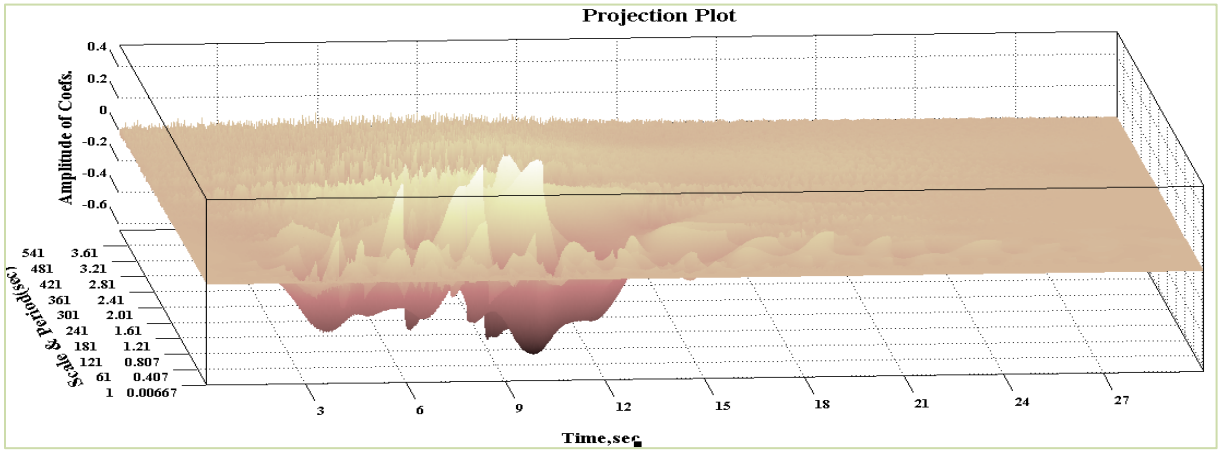

Figure 6-25 3D Projection of Ground Motion on Structural Velocity

The 3D and 2D weighted effect of ground motion on structural velocity plots were shown in Figures 6-26 and 6-27 respectively. Though the frequency content of ground motion is generally in phase with that of the structural velocity (as evidenced by negative values in Figure 6-25), the intensity of the weighted effect is not large at time t=9 sec (where the largest energy content occurs in ground motion). This is a contrast the system with η=0.5. Since, the effect of ground motion on structural response is therefore expected to be less, the effect of moving resonance is less, and the peak displacement is smaller for this particular η value.

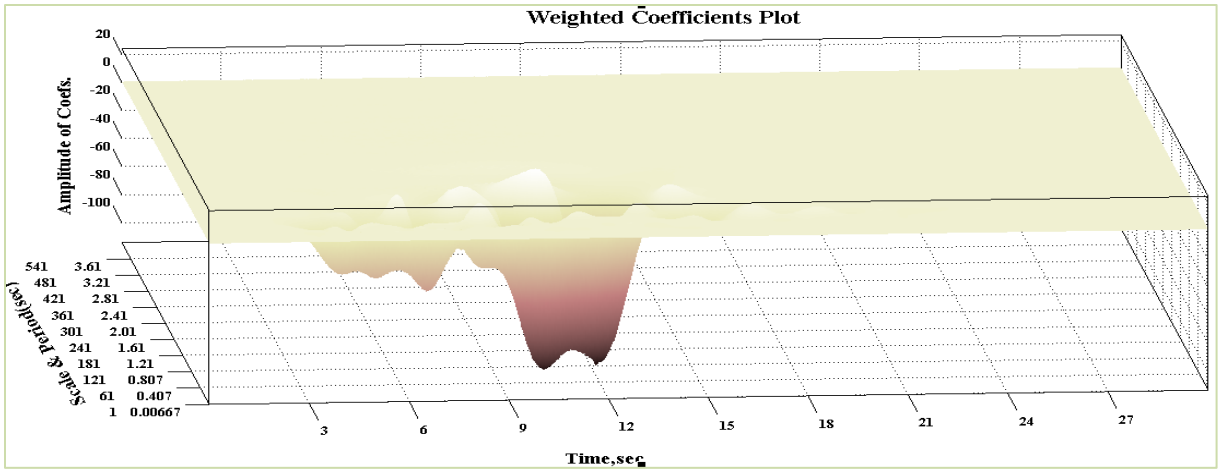

Figure 6-26 3D Comparison of weighted effect of Ground Motion on Structural Velocity

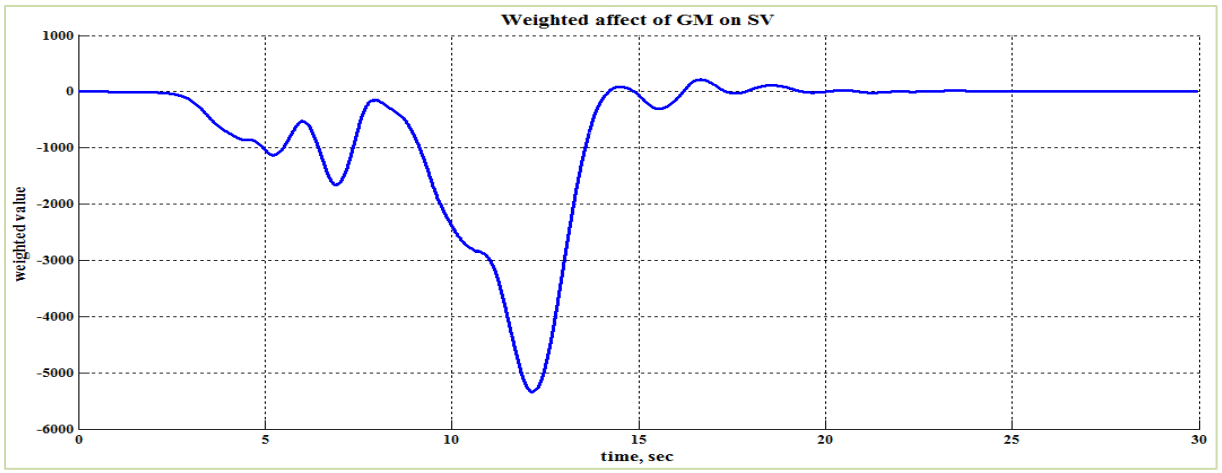

Figure 6-27 2D Comparison of weighted effect of Ground Motion on Structural Velocity

The correlation coefficient plot shown in Figure 6-28 also shows that there exists some correlation at time t= 6 sec and time t=12 sec but there is no correlation at time t=8 to 9 sec(where there is large amount frequency content in the ground motion as shown in Figure 6-8).

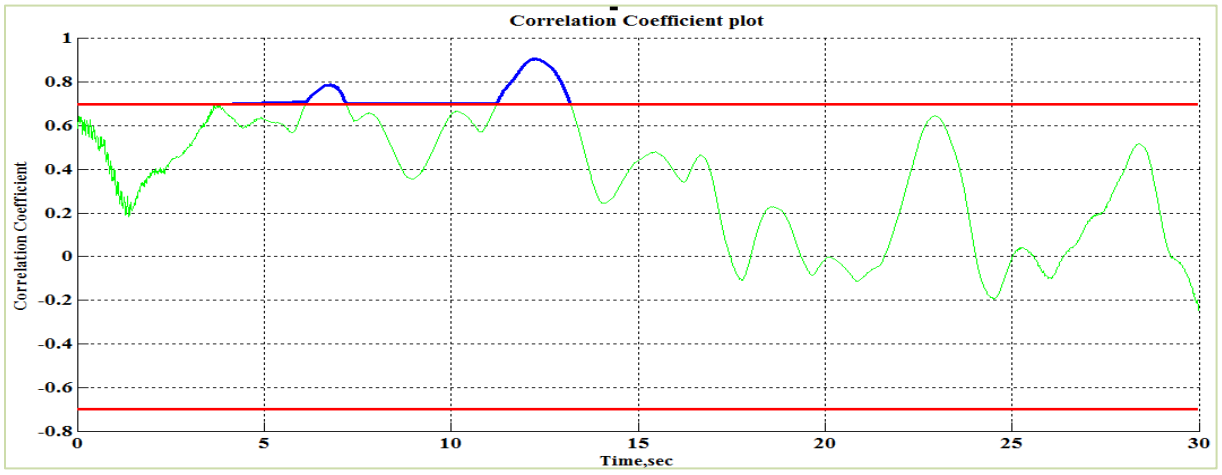

Figure 6-28 Correlation coefficients plot

6.3.4.3 Further Analysis of the Bilinear Elastic System with T_0=0.50 sec and η=1.0

The displacement time history of the structural response is shown in Figure 6-29 and the 2D and 3D wavelet coefficients of the structural response is shown in Figures 6-30 and 6-31 respectively. The trace of fundamental period of 0.5 sec can be seen clearly in the Figure 6-29. There is not much variation in the dominant structural period and little frequency content at time t=9 sec unlike in ground motion as shown in Figure 6-8.

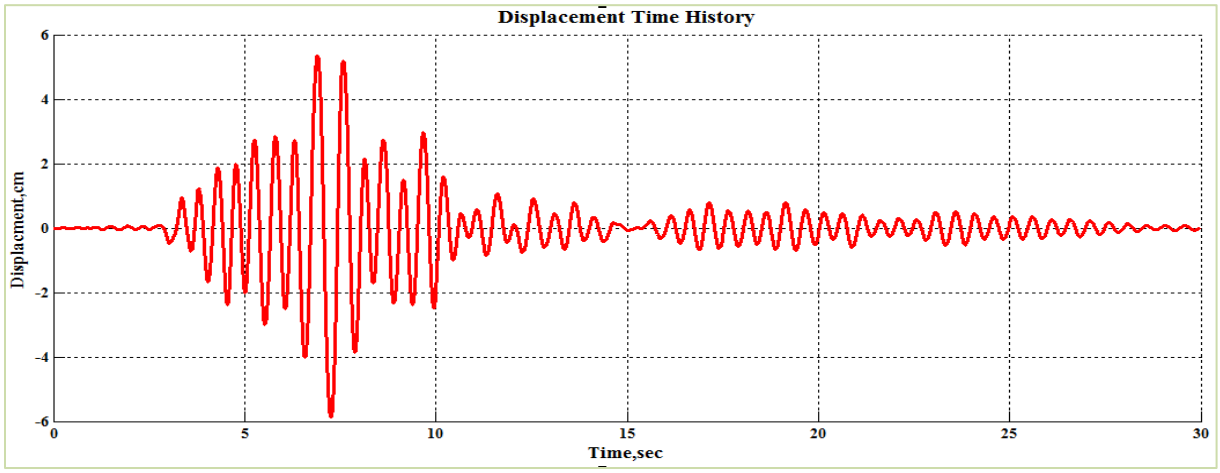

Figure 6-29 Displacement time history of structural response

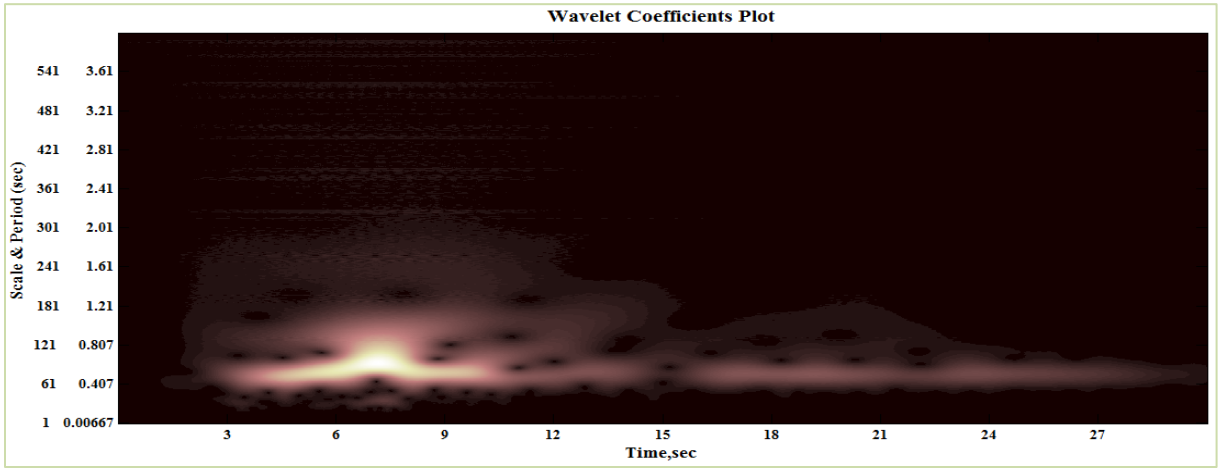

Figure 6-30 Wavelet coefficients plot of the Structural Response

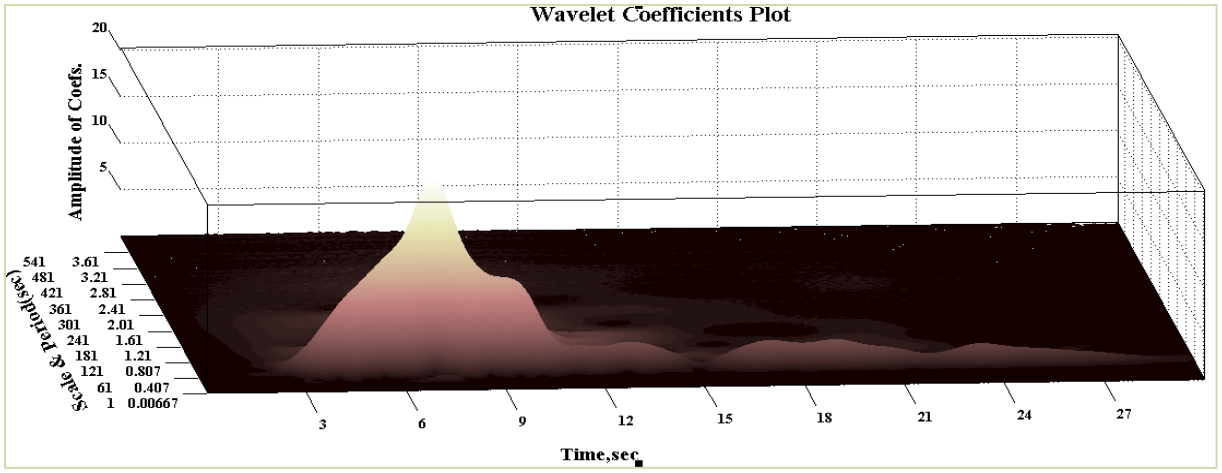

Figure 6-31 Wavelet coefficients plot of the Structural Response in 3D

The frequency content of ground motion is in phase with the structural velocity up to t=6 sec and then the frequency content is *out of phase* with the structural velocity. At time t=8 to 9 sec (where there is a hot spot of frequency content in the ground motion), the frequency content of the ground motion is *out of phase* with the structural velocity which can be seen from Figure 6-32. This proves that there is no correlation between their frequency contents and hence there doesn`t exist moving resonance.

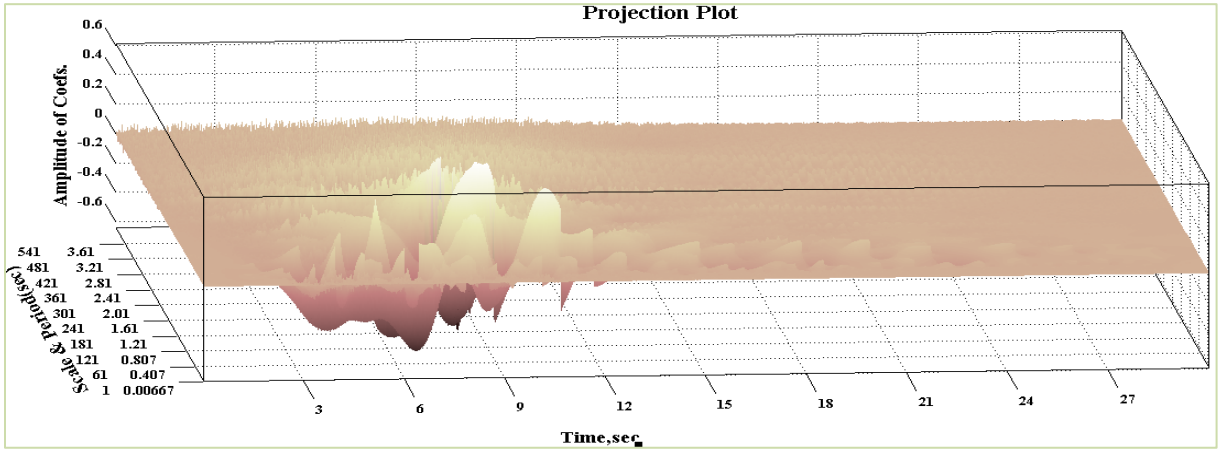

Figure 6-32 3D Projection of Ground Motion on Structural Velocity

The 3D and 2D weighted effect of ground motion on structural velocity plots were shown in Figures 6-33 and 6-34 respectively. The integral of the intensity of the weighted effect of ground motion on structural velocity is near zero at time t=8-9 sec (approximately same area above the axis as below) where there is large amount of frequency content in the ground motion. This implies that oscillations of the ground motion acceleration are nearly out of phase with the oscillations of the structural velocity. The large energy in the ground motion at 9 sec does not

have significant affect on the structure, therefore, for this particular η value. This is the reason behind having less peak displacement value at this particular η value, as there is no effect of moving resonance.

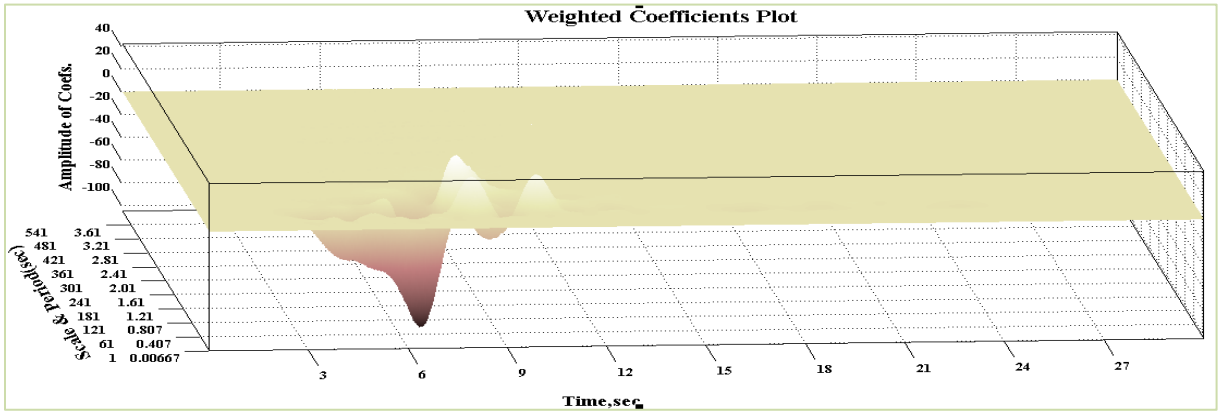

Figure 6-33 3D Comparison of weighted effect of Ground Motion on Structural Velocity

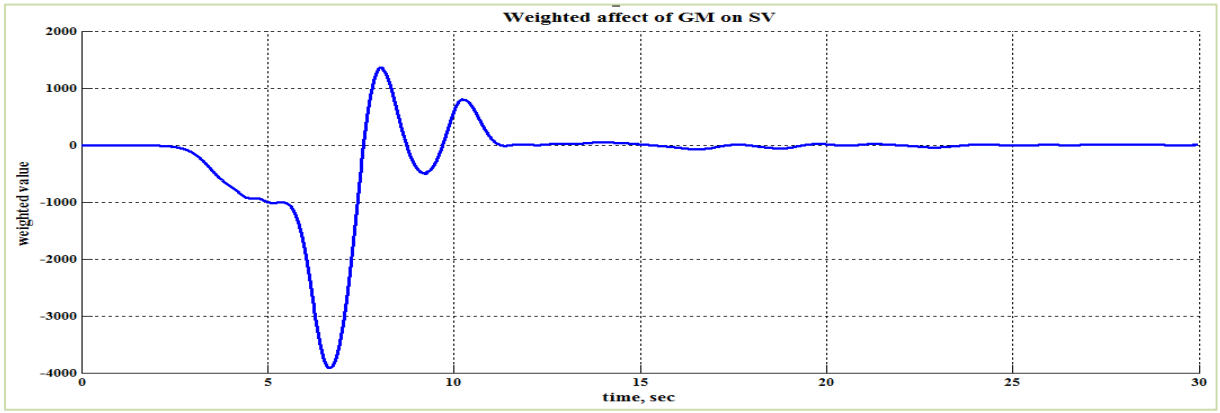

Figure 6-34 3D Comparison of weighted effect of Ground Motion on Structural Velocity

The correlation coefficient plot shown in Figure 6-35 also shows that there exists some correlation at time t= 6 sec but there is less correlation at time t=8 to 9 sec (at the time when there is large amount of energy content in the ground motion as shown in Figure 6-8).

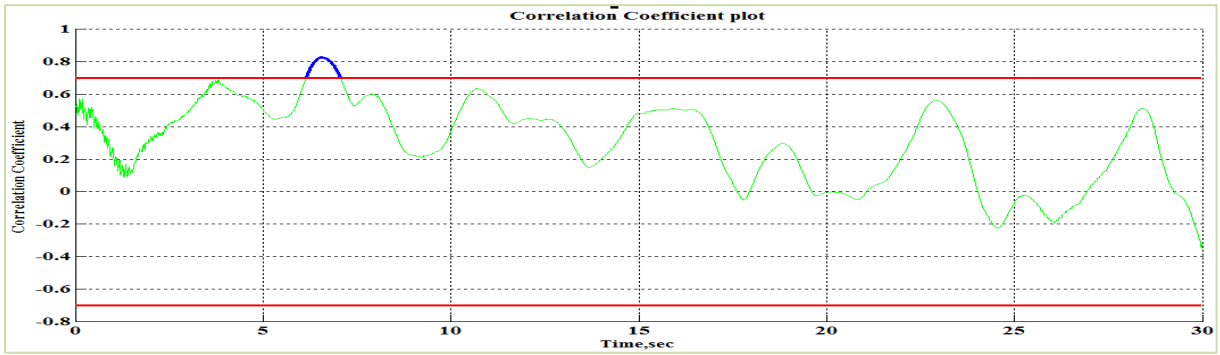

Figure 6-35 Correlation coefficient plot

6.3.4.4 Further Analysis of the Bilinear Elastic System with T_0=0.50 sec and η=1.25

The displacement time history of the structural response is shown in Figure 6-36 and the 2D and 3D wavelet coefficients of the structural response is shown in Figures 6-37 and 6-38respectively. The trace of fundamental period of 0.5 sec is clearly seen in Figures 6-36 to 6-38. More interestingly, a hot spot of frequency content is evident at around time t=8-9 sec and 12 sec similar to that of ground motion as shown in Figure 6-8. The occurrence of moving resonance is confirmed.

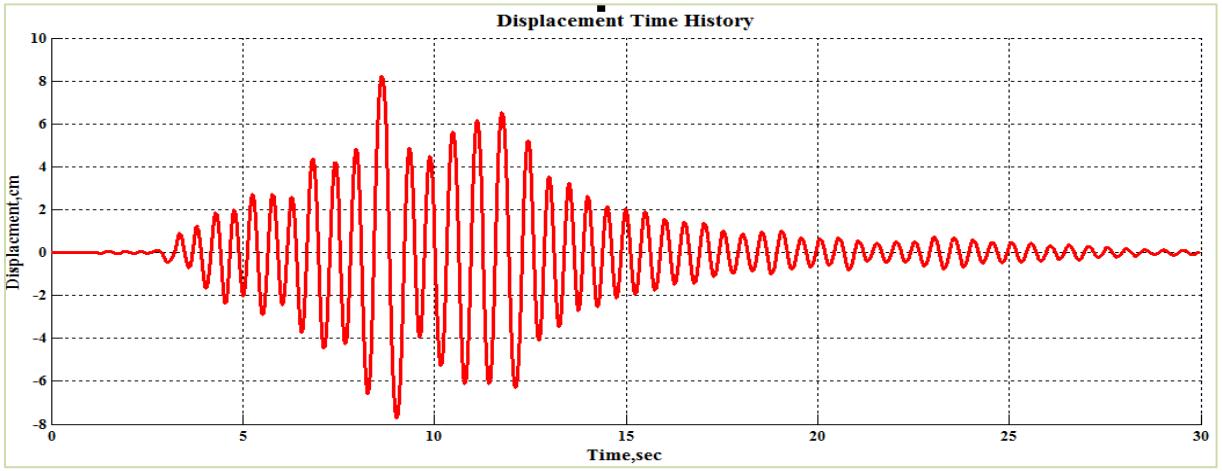

Figure 6-36 Displacement time history of structural response

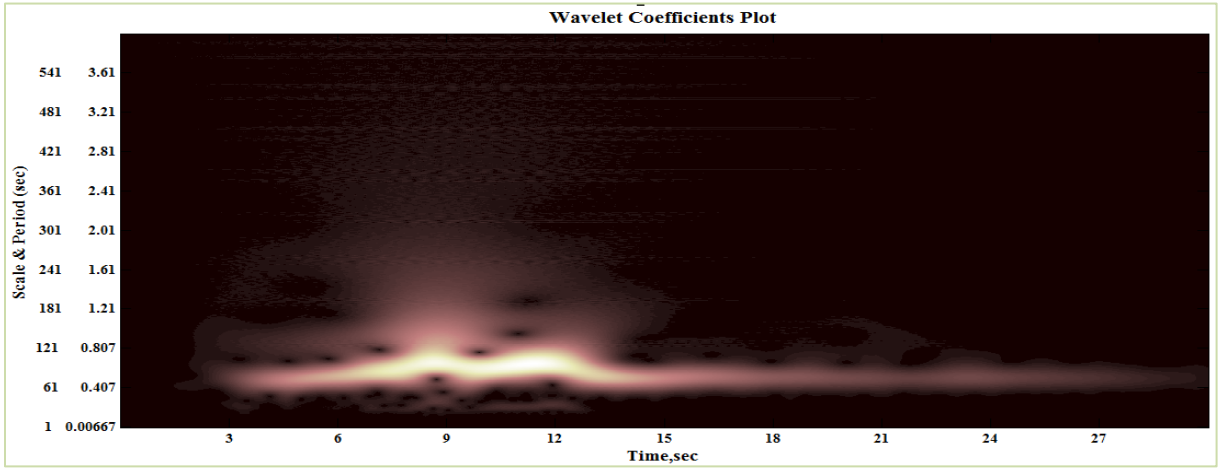

Figure 6-37 Wavelet coefficients plot of the Structural Response

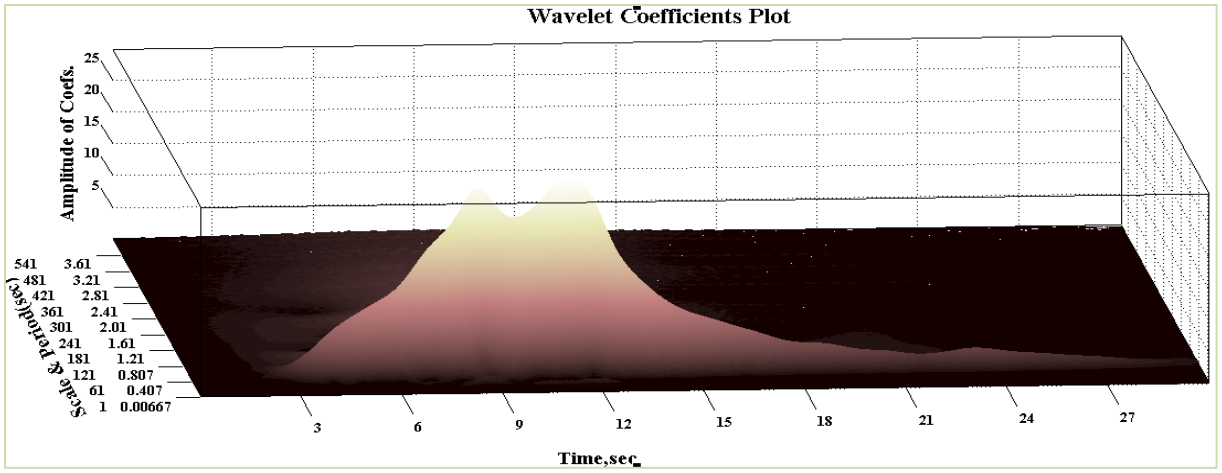

Figure 6-38 Wavelet coefficients plot of the Structural Response in 3D

The projection plot as shown in Figure 6-39 shows that the frequency content of ground motion is in phase with the frequency content of the structural velocity at time t=8-9 sec and 12 sec.

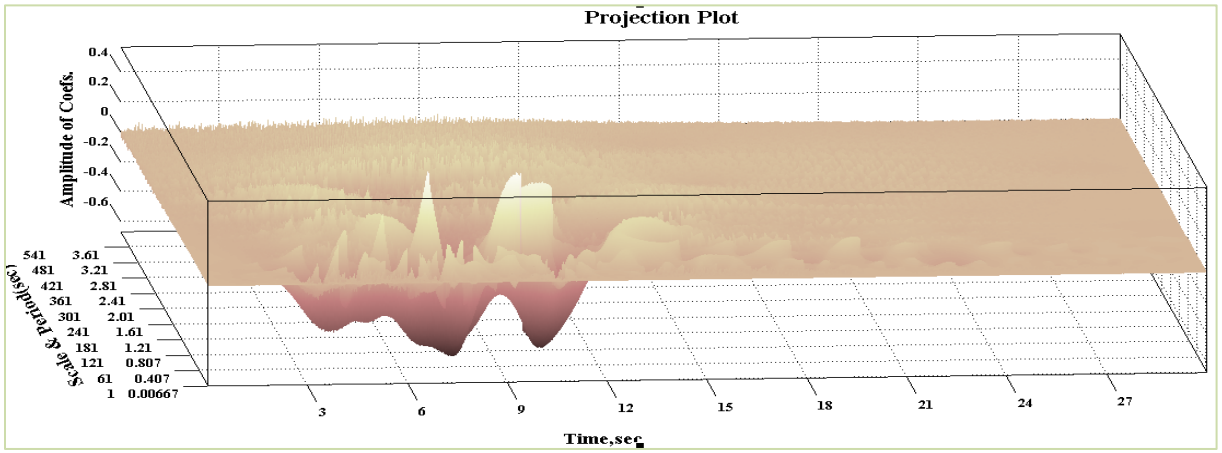

Figure 6-39 3D Projection of Ground Motion on Structural Velocity

The 3D and 2D weighted effect of ground motion on structural velocity plots were shown in Figures 6-40 and 6-41respectively. The intensity of the weighted effect of ground motion on structural velocity as shown in Figure 6-41 is negative and maximum at the time t=8-9 sec which tells that there is effect of moving resonance for this particular value of η and as a result there is increase in the peak displacement value as seen from Figure 6-11.

As expected, the integral portion of area which is *in phase* in the projection plot (projection of ground motion on structural velocity) decreased from η=0.5 to η=1.0 and again increase for η=1.25.

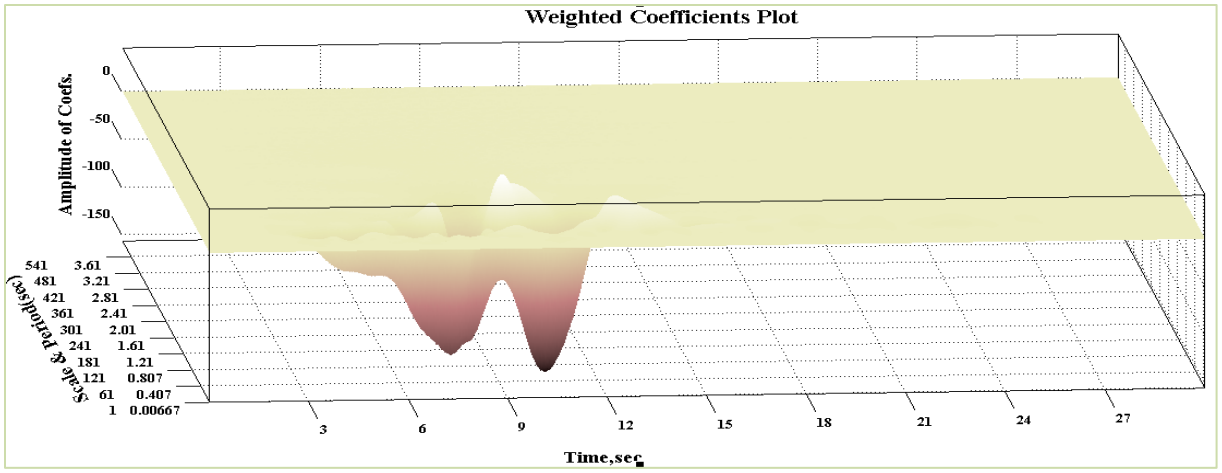

Figure 6-40 3D Comparison of weighted effect of Ground Motion on Structural Velocity

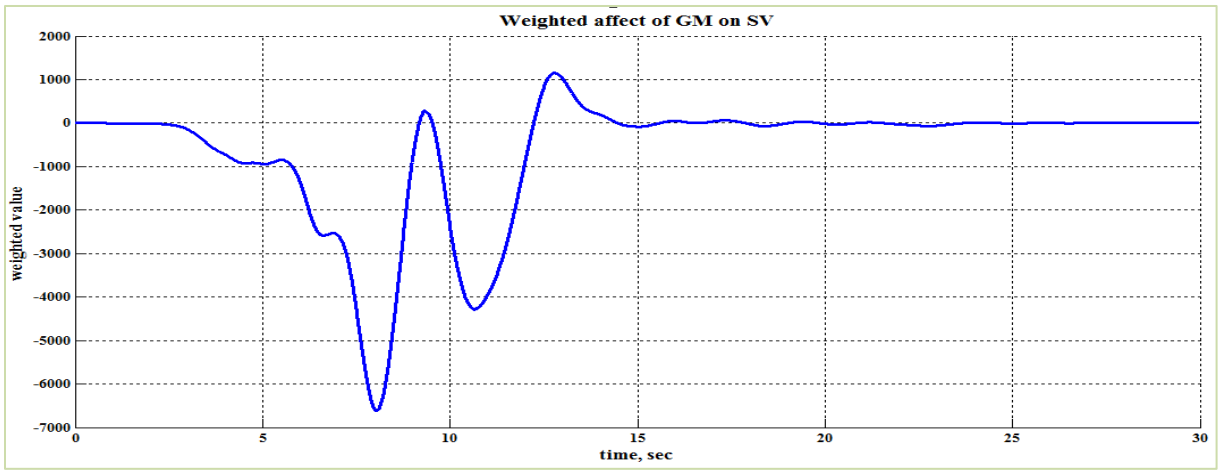

Figure 6-41 3D Comparison of weighted effect of Ground Motion on Structural Velocity

If the bumps (localized high points) in peak displacement observed in Figure 6-11 are the result of moving resonance, it is expected that the integral portion of area which is *in phase* in the projection plot (projection of ground motion on structural velocity) should decrease from η=0.5 to η=1.0 and again increase for η=1.25. This criterion is observed from the previous plots and hence the instances of moving resonance affecting bilinear elastic system are concluded.

6.3.5 Peak Displacements and Amplification Factors for the Elastic-Perfectly Plastic System

The seismic response of SDOF system is analyzed considering elastic-perfectly plastic behavior and peak displacement is obtained at every interval of period and strength reduction ratio. The peak displacement values obtained for a range of periods and strength levels were plotted in 3D and 2D plots are shown in Figure 6-42 and Figure 6-43 respectively. The difference between the SDOF system in this section and the SDOF system of the last section is that this system has hysteretic damping. Hysteretic damping is expected to reduce the peak displacements of the nonlinear systems as compared to the bilinear elastic system.

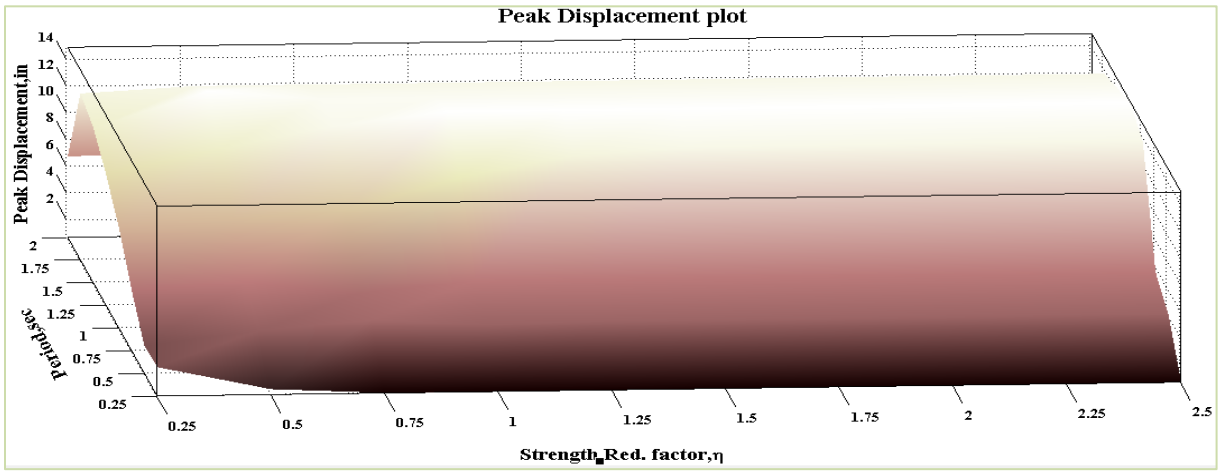

Figure 6-42 Peak Displacement for Ground Motion 1 for EPP Behavior

Figure 6-43 Peak Displacement for Ground Motion 1 for EPP Behavior

From Figure 6-42, it can be seen that, for low periods (for T=0.25 sec) the peak displacement of the inelastic system is greater than the associated elastic system. This shows that the peak displacement values are in accordance with findings from previous studies of EPP systems (Newmark, 1983).

The 2D peak displacement plot of the structural system incorporating elasto-plastic behavior as shown in Figure 6-43 have bumps (localized high point) in peak displacement at corresponding (T_0,η) values of (0.50,0.75) whereas there is a valley (localized low point) in peak displacement at corresponding (T_0,η) values of (0.75,0.75). The bumps are hypothesized to be the result of occurrence of moving resonance and hence a larger amplification factor is expected for these combinations of period and strength whereas the valleys are hypothesized to be the absence of moving resonance (frequency content of ground motion being *out of phase* with the structural response and thus constitutes destructive interference) and hence results in lower amplification factor is expected.

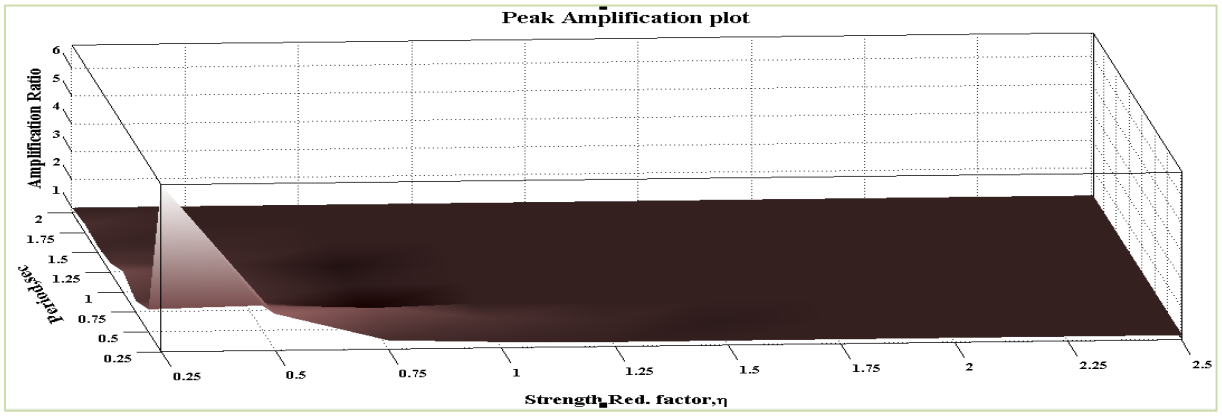

Figure 6-44 3D Peak Amplification plot for EPP behavior

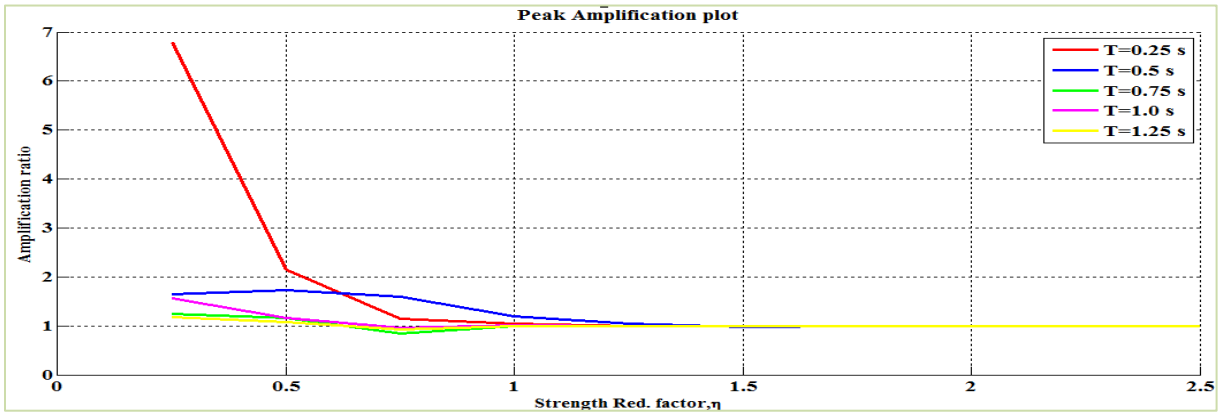

Figure 6-45 Peak Amplification plot for EPP behavior

It is observed from the peak amplification plot shown in Figure 6-45 that the amplification factors corresponding to (T_0,η) values of (0.50,0.75) (at similar places where bumps of peak displacement were observed as shown in Figure 6-43) are greater than 1 leading to the increase in peak displacement. This increase in peak displacement is considered to be the effect of moving resonance. It is also observed from Figure 6-45 that the amplification value corresponding to (T_0,η) value of (0.75,0.75) (at similar place where valley of peak displacement is observed from Figure 6-43) is less than 1, which implies that there is destructive interference effect (frequency content of ground motion being *out of phase* with the structural response) of moving resonance for that particular (T_0,η) value.

It is noted that systems with low periods (e.g. To=0.25 sec) are shown to exhibit large amplification factors. It is not surprising that especially low period structures with nonlinear hysteretic behavior experience large peak displacements. Previous studies on systems with short periods have shown that short period structures with yield strength less than the elastic forces will experience excessive inelastic displacements (Veletsos et al. 1965). The current study does not focus on this effect, but instead focuses on systems that experience larger peak displacement than systems with similar system parameters (T_0,η).

The effect of moving resonance on elasto-plastic systems is muted, likely because of hysteretic damping. This is the primary reason for examining bilinear elastic systems.

The calculation of peak displacements was verified against the spectral displacements. The peak displacement values corresponding to large strength reduction factors in which the system exhibited elastic response were compared with the spectral displacement values for the ground motion with damping ratio of 2%. The result is plotted as shown in the Figure 6-46. The peak displacement plot shown in Figure 6-46 (in blue) is plotted for a period values of 0.25-2 sec with an interval of 0.25 sec and spectral displacement plot (in red) is plotted for a period values of 0.25-5 sec with an interval of 0.25 sec. The variation in the range of periods is chosen to make it clear that both plots overlap each other. Since, both plots are identical it can be concluded that the accuracy of the calculations for peak displacement were partially verified.

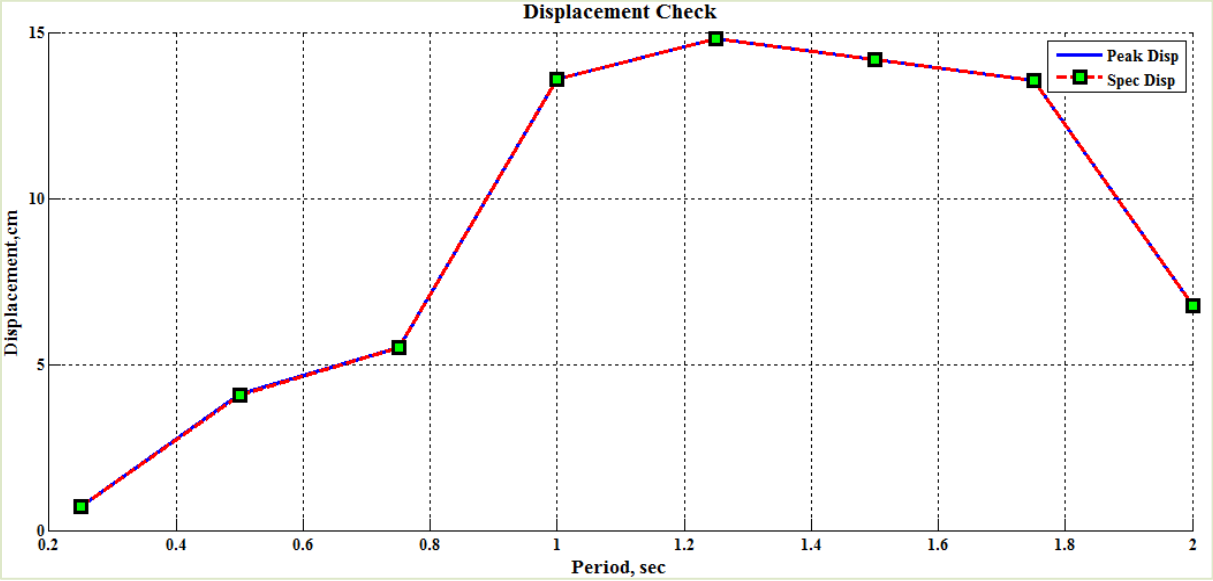

Figure 6-46 Peak Displacement vs Spectral Displacement plot

Similar to the previous sections regarding the bilinear elastic system, the other tools for analyzing moving resonance were applied to specific system configurations. A period of 0.5, 0.75 sec were chosen for the elasto-plastic behavior to measure the correlation with the frequency content of the ground motion.

The peak displacement plot corresponding to periods T_0=0.5 sec and 0.75 sec as shown in Figure 6-43 has bumps (localized increases in the peak displacement) at strength reduction ratio of 0.75 and 1.00 respectively. This increase in the peak displacement is hypothesized to be the result of

occurrence of moving resonance, and hence projection plots for these two values of η are compared with the projection plots of η values that precede these values.

6.3.6 Application of Other Tools for Selected Elastic-Perfectly Plastic Systems

The frequency content of the structural response shown in the following sections were analyzed using Complex Morlet wavelet of frequency 1.5

6.3.6.1 Further Analysis for the Elastic Perfectly Plastic System with T_0=0.50 sec and η=0.75

The displacement time history of the structural response is shown in Figure 6-47 and the 2D and 3D wavelet coefficients of the structural response is shown in Figures 6-48 and 6-49 respectively. A trace of fundamental period of 0.5 sec is observed in Figures 6-47 to 6-49 and there also exists a hot spot of frequency content from time t=3 sec to time t=9 sec. This frequency content matches with the frequency content of the ground motion. So, some correlation between both the frequency contents is expected.

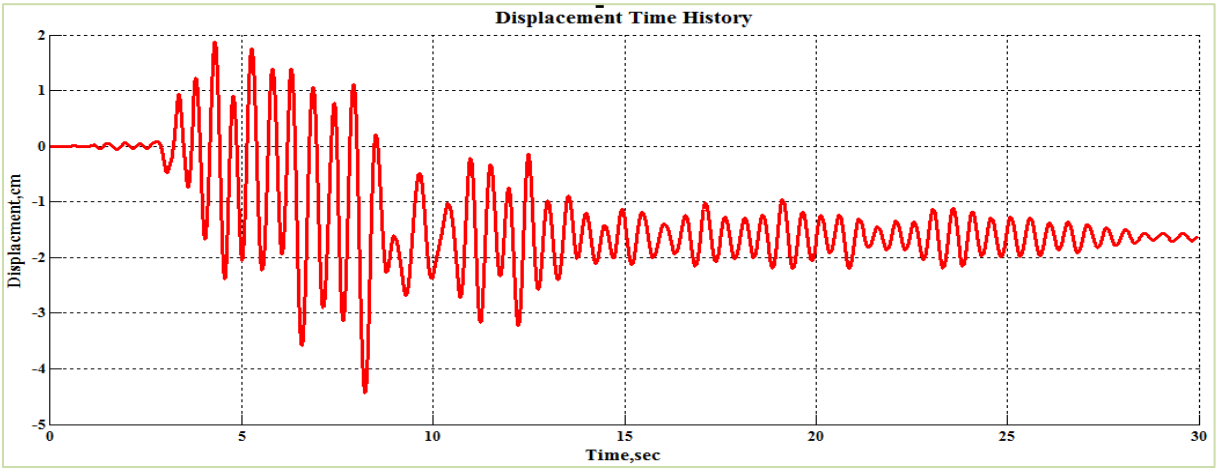

Figure 6-47 Displacement time history of structural response

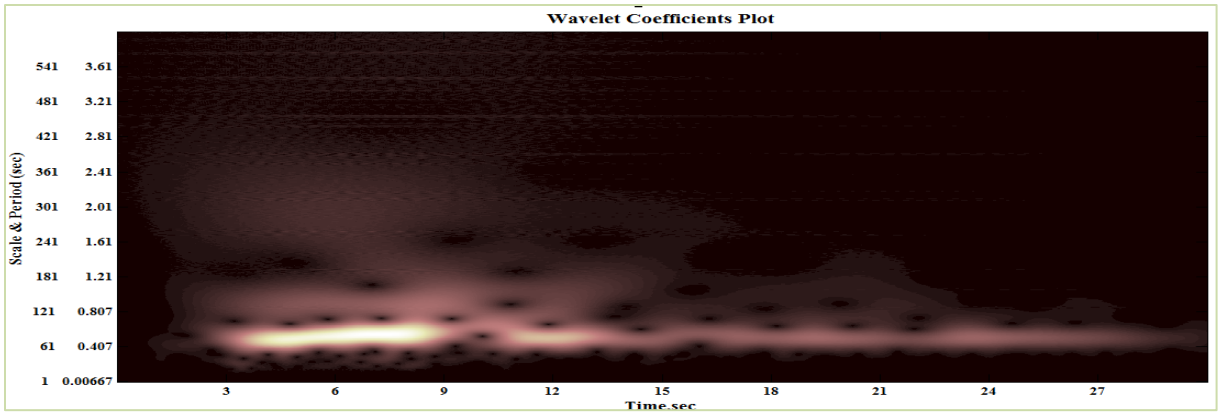

Figure 6-48 Wavelet coefficients plot of the Structural Response

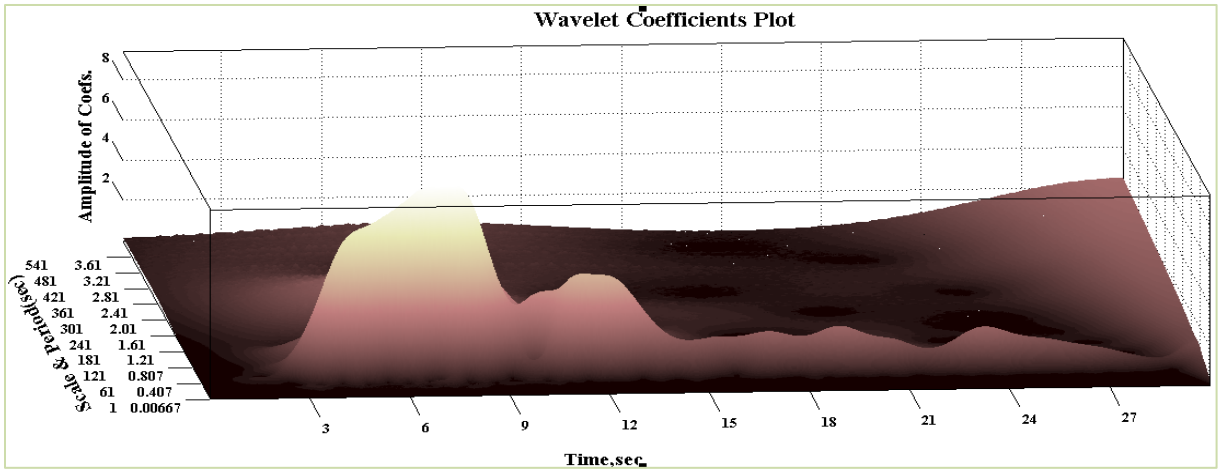

Figure 6-49 Wavelet coefficients plot of the Structural Response in 3D

From Figures 6-50, since the projection plot is in the negative axis at time t=3 to t=8 sec (where both ground motion and structural velocity have hot spot of frequency contents), it is evident that their frequency contents are in phase with each other and moving resonance is expected.

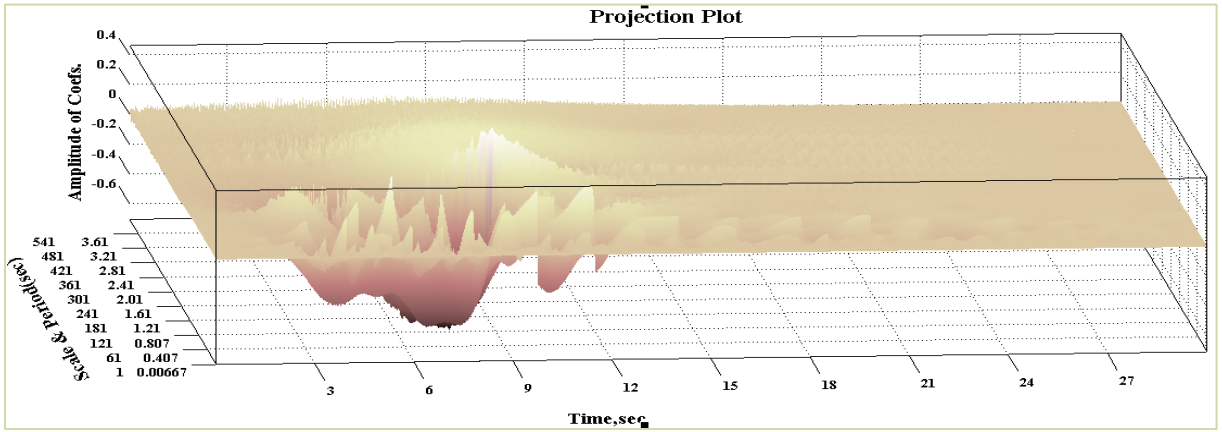

Figure 6-50 3D Projection of Ground Motion on Structural Velocity

The 3D and 2D weighted effect of ground motion on structural velocity plots were shown in Figures 6-51 and 6-52 respectively. From the weighted effect of ground motion on structural velocity plot as shown in Figure 6-51, it can be seen that the intensity is maximum at the time t=3 to t=8 sec showing the occurrence of moving resonance.

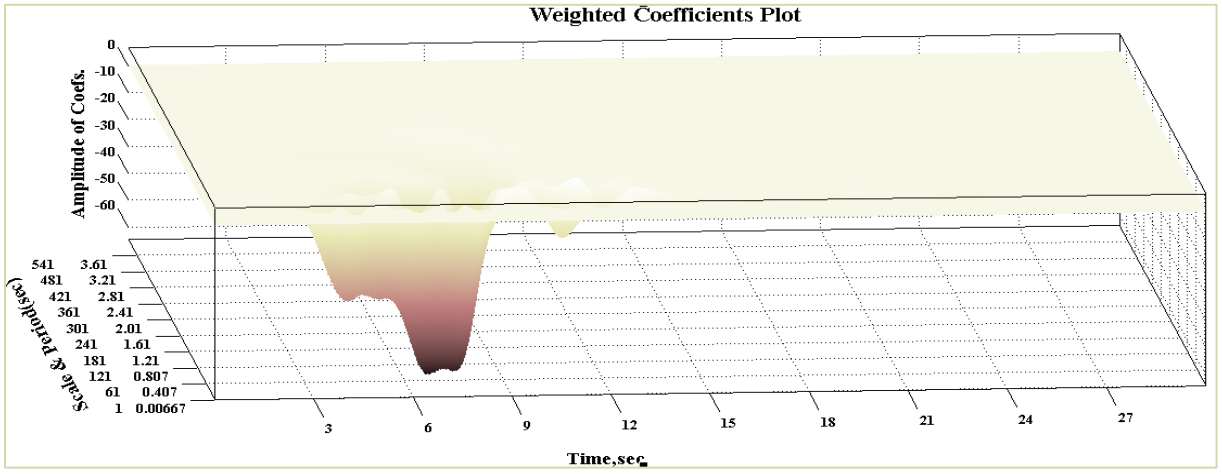

Figure 6-51 3D Comparison of weighted effect of Ground Motion on Structural Velocity

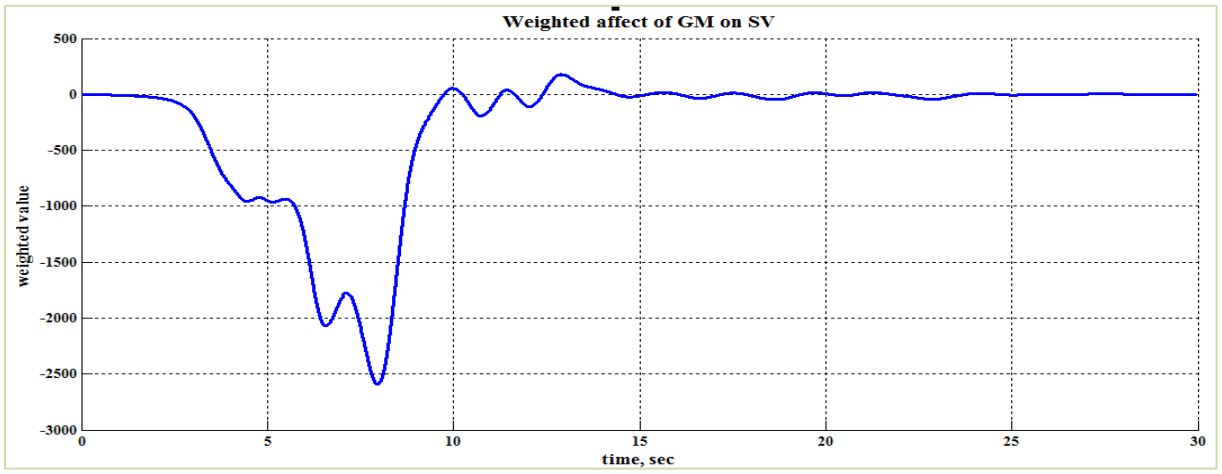

Figure 6-52 2D Comparison of weighted effect of Ground Motion on Structural Velocity

Correlation coefficient plot as shown in Figure 6-53 doesn`t tells much story in this case, but it can be seen that the correlation values are closer to 0.7 during the time t=3 to t=8 sec, whereas at remaining times those values are far from 0.7. This tells there is some good correlation between the two frequency contents at that particular time. Since 0.7 is taken arbitrarily to consider a correlation value as good, it may not work for all cases.

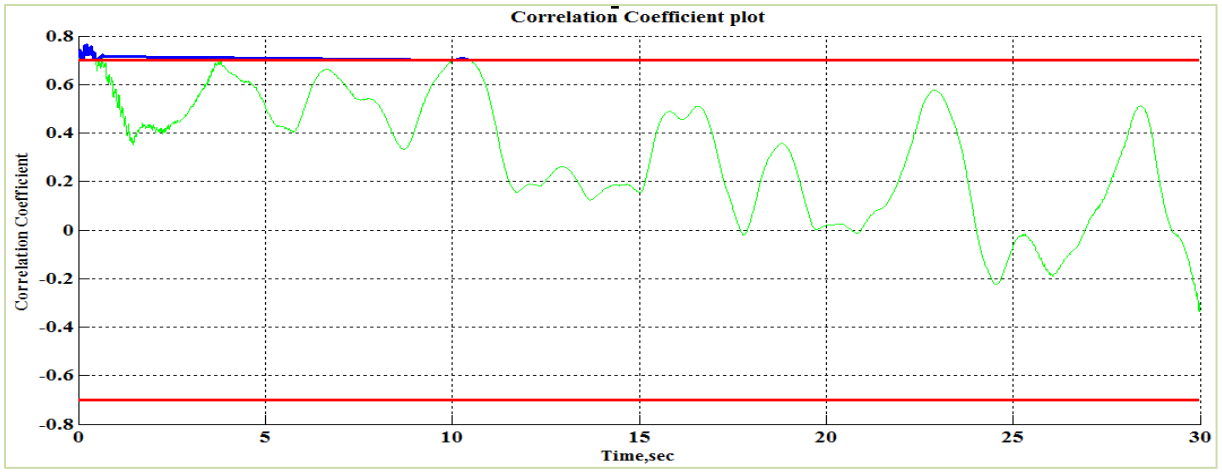

Figure 6-53 Correlation coefficient plot

6.3.6.2 Further Analysis for the Elastic Perfectly Plastic System with T_0=0.75 sec and η=0.75

The displacement time history of the structural response is shown in Figure 6-54 and the 2D and 3D wavelet coefficients of the structural response is shown in Figures 6-55 and 6-56 respectively. A clear trace of fundamental period of 0.75 sec is seen from Figures 6-54 to 6-56 and there is some discontinuity in the frequency content at time t=9 sec(time where there is hot spot of frequency content in ground motion as shown in Figure 6-8). Hence there may not be much effect of moving resonance.

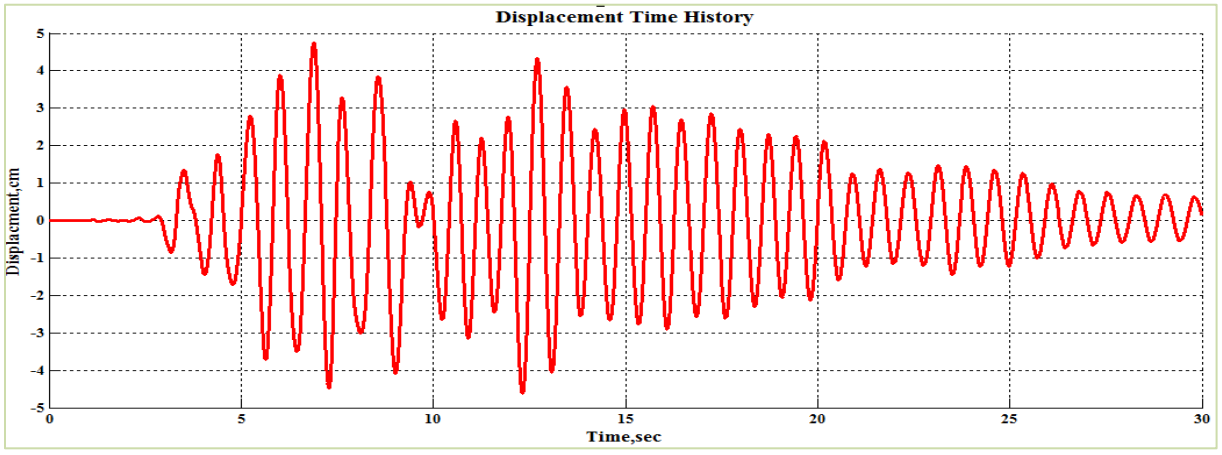

Figure 6-54 Displacement time history of structural response

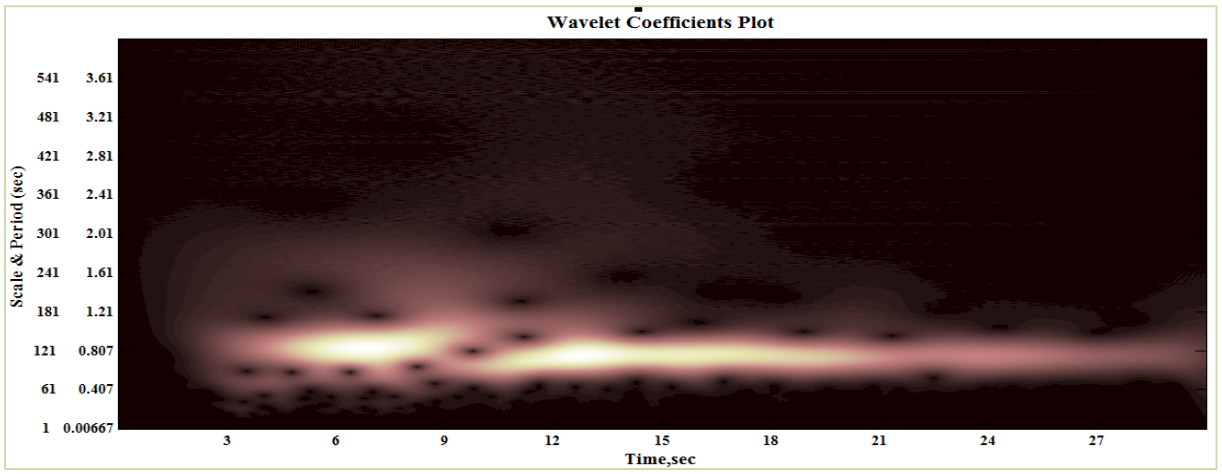

Figure 6-55 Wavelet coefficients plot of the Structural Response

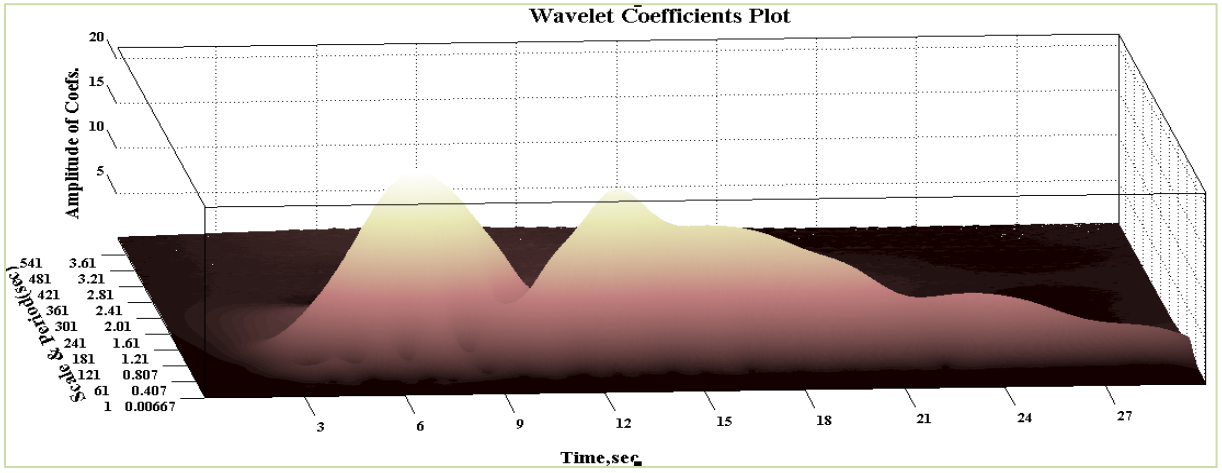

Figure 6-56 Wavelet coefficients plot of the Structural Response in 3D

It is clear from the projection plot shown in Figure 6-57 that the frequency content of ground motion is *in phase* with the frequency content of the structural velocity.

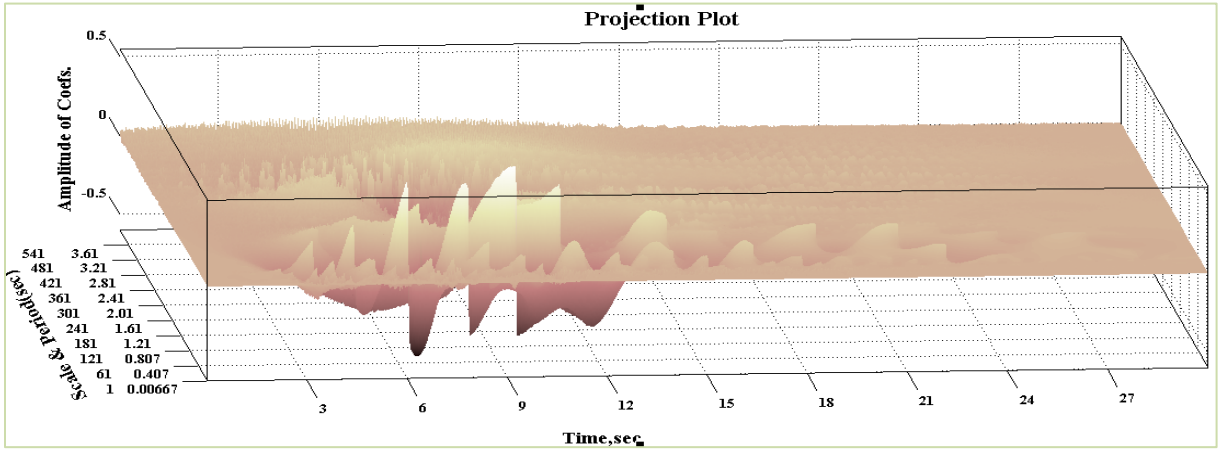

Figure 6-57 3D Projection of Ground Motion on Structural Velocity

The 3D and 2D weighted effect of ground motion on structural velocity plots were shown in Figures 6-58 and 6-59 respectively. From the weighted effect of ground motion on structural velocity shown in Figure 6-59, it is clear that the both the frequency contents are out of phase with each other at time t=8-9 sec and this shows there is no effect of moving resonance on peak displacement at this particular η value. This statement is strengthened by the correlation coefficient plot shown in Figure 6-60

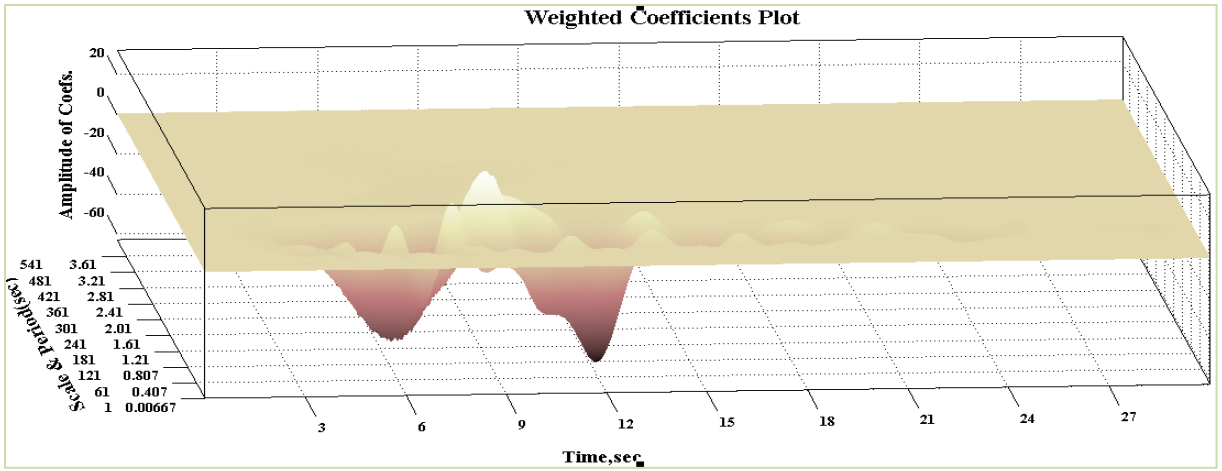

Figure 6-58 3D Comparison of weighted effect of Ground Motion on Structural Velocity

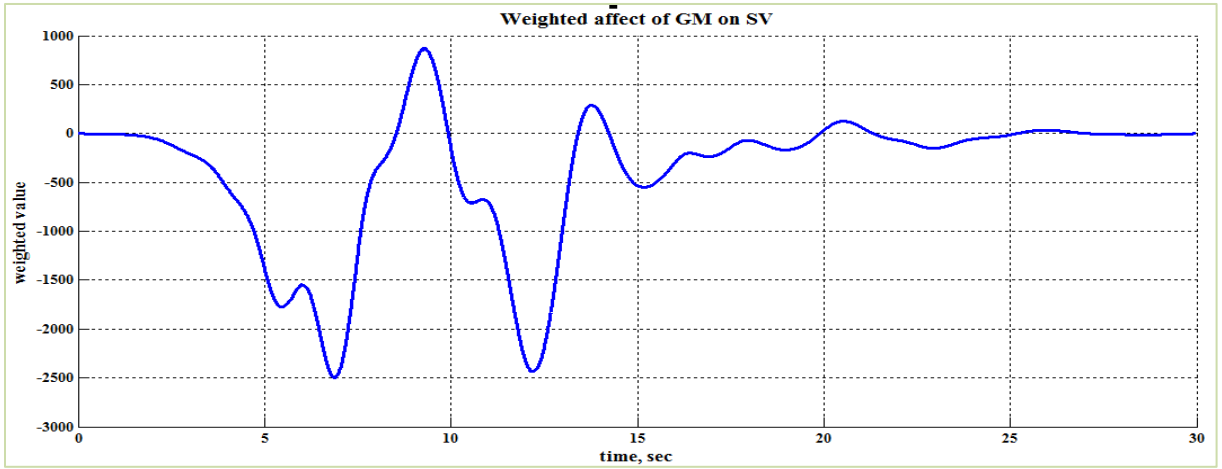

Figure 6-59 3D Comparison of weighted effect of Ground Motion on Structural Velocity

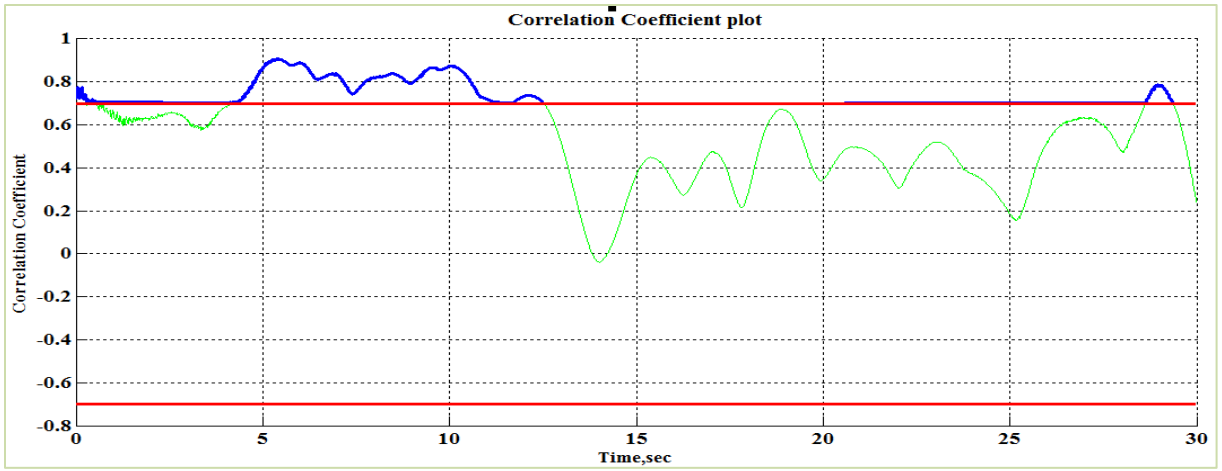

Figure 6-60 Correlation coefficient plot

6.5.6.3 Further Analysis for the Elastic Perfectly Plastic System with T_0=0.75 sec and η=0.50

The displacement time history of the structural response is shown in Figure 6-61 and the 2D and 3D wavelet coefficients of the structural response is shown in Figures 6-62 and 6-63respectively. A clear trace of fundamental period of 0.75 sec and a hot spot of frequency content similar to that of ground motion is seen in the wavelet coefficients plot shown in Figure 6-8.

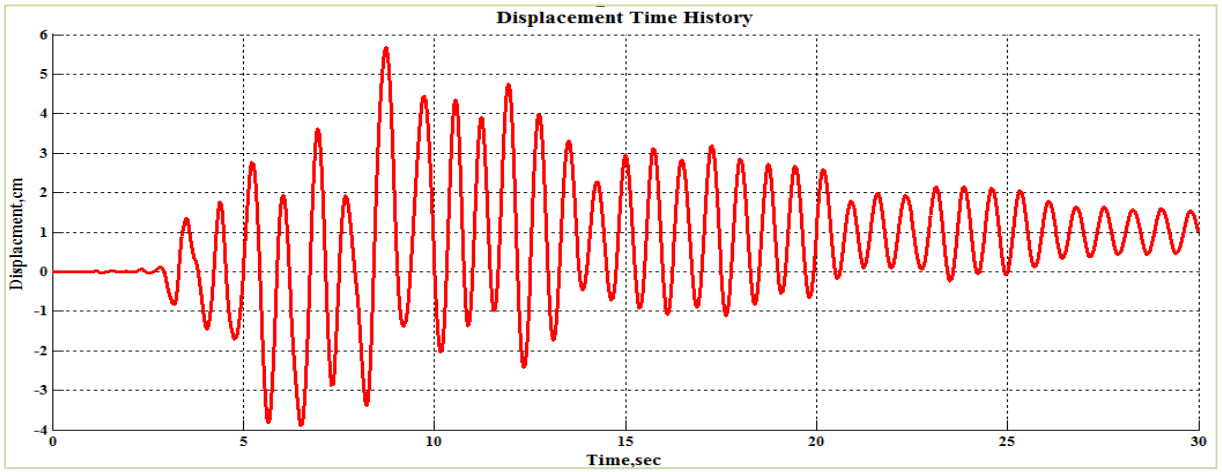

Figure 6-61 Displacement time history of structural response

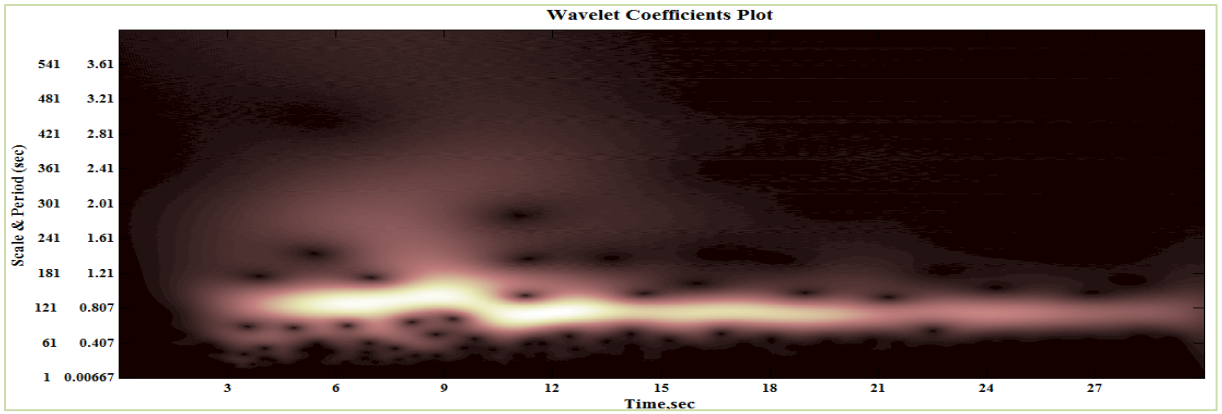

Figure 6-62 Wavelet coefficients plot of the Structural Response

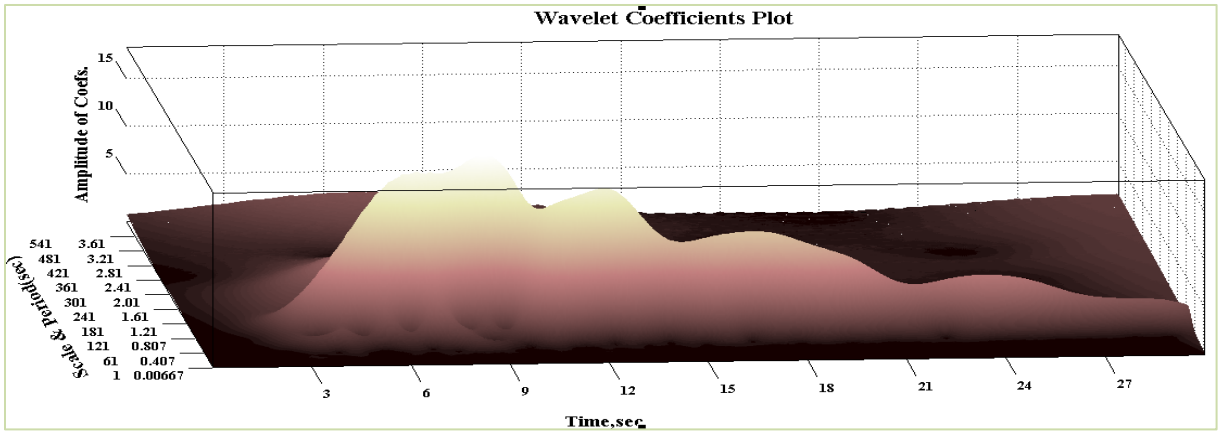

Figure 6-63 Wavelet coefficients plot of the Structural Response in 3D

It is clear from the projection plot shown in Figure 6-64 that the frequency content of ground motion is *in phase* with the frequency content of the structural velocity. This statement is strengthened by the weighted effect of ground motion on structural velocity plots shown in Figure 6-65 and Figure 6-66 and the correlation coefficient plot shown in Figure 6-67.As expected the area of projection plot which is in phase decreases from η=0.5 to η=0.75

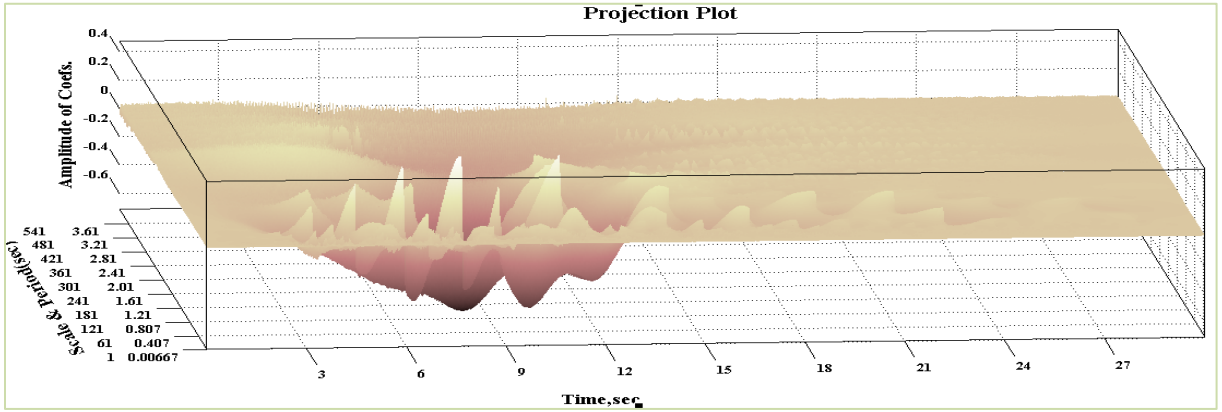

Figure 6-64 3D Projection of Ground Motion on Structural Velocity

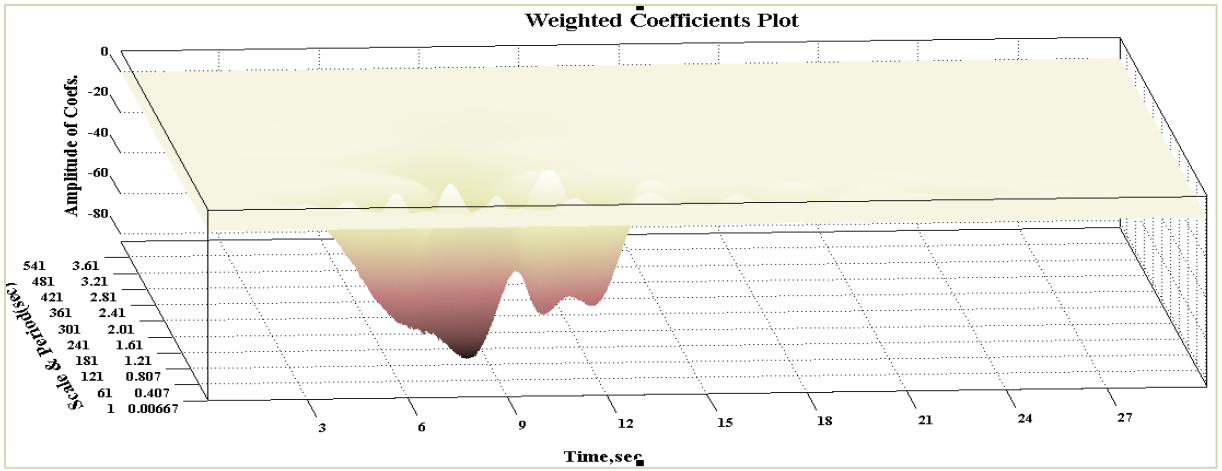

Figure 6-65 3D Comparison of weighted effect of Ground Motion on Structural Velocity

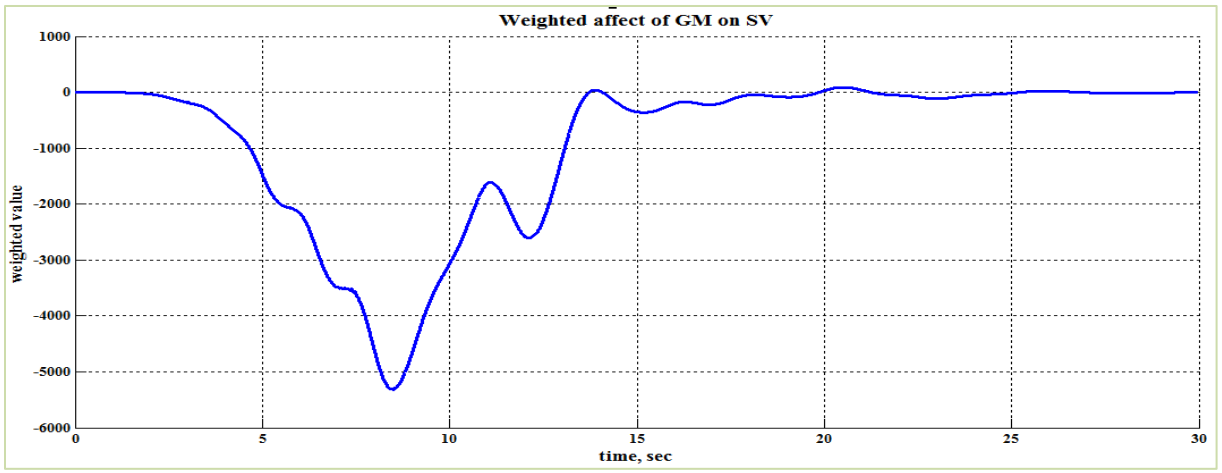

Figure 6-66 3D Comparison of weighted effect of Ground Motion on Structural Velocity

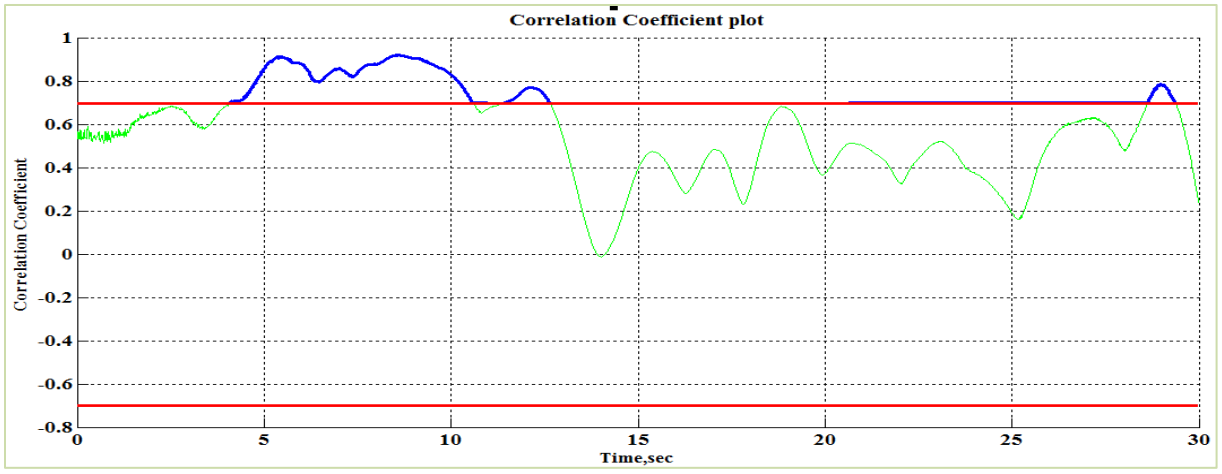

Figure 6-67 Correlation coefficient plot

If the bumps (localized high points) in peak displacement observed in Figure 6-43 are the result of moving resonance, it is expected that the integral portion of area which is *in phase* in the projection plot (projection of ground motion on structural velocity) should be maximum for η=0.75 for T_0=0.5 sec and should decrease from η=0.50 to η=0.75 for T_0=0.75 sec. This criterion is observed from the previous plots and hence the instances of moving resonance affecting bilinear elastic system are concluded.

6.4 Conclusions

The instances of moving resonance were found and the different tools corroborated the hypothesis. The effect of moving resonance is significant in bilinear elastic systems and is muted in elasto-plastic systems likely because of hysteretic damping.

CHAPTER 7 : INVESTIGATING MOVING RESONANCE FOR A SUITE OF GROUND MOTIONS

Chapter 6 gave some specific instances of moving resonance. This chapter is meant to extend the study to investigate the occurrence of moving resonance for a suite of ground motions. The goal is to determine how the potential for moving resonance changes from one ground motion to the next. This chapter focuses on two of the tools used in the previous chapter to explain the effect of moving resonance- the peak displacements and the amplification factors.

7.1 Extending the method of analysis over a range of Ground Motions

7.1.1 Details of Analysis

The quantification of the effect of moving resonance on the structures incorporating bilinear elastic and elasto-plastic behavior is intended to extend over a large range of ground motion records. The ground motions records were selected from FEMA p695 (FEMA 2009) and the details of the records are provided in section 7.1.2. For the chosen ground motion records, the wavelet coefficient plots of the ground motion, the peak displacement plots and the peak amplification plots of the structural response incorporating bilinear elastic and elasto-plastic behavior are shown. The other three tools used in chapter 6 are meant for investigating specific systems (given to T_0 and η). The tools used in this chapter allow investigation of the full range of those variables. The ground motion records were analyzed with the help of complex Morlet wavelet of band width 1 and frequency 1.5.

7.1.2 Selection of Ground Motions

The ground motions from FEMA p695 (FEMA 2010) are selected for use in this study. A total of 22 Far field ground motions were chosen. These ground motions are chosen because the magnitude of record to record variability has been investigated (Ibarra and Krawinkler 2011, FEMA 2010).

Far Field Sets:

The Far-Field record set includes twenty-two records selected from the PEER NGA database. For each record, Table 7-1 summarizes the magnitude, year, and name of the event, name of the

station, component and PGA. The twenty-two records are taken from 14 events that occurred between 1971 and 1999. Of the 14 events, eight were California earthquakes and six were from five different foreign countries.

Table 7-1Summary of details of Far Field record set

No.	Mag.	Year	Name	Station	Horizontal records	PGA
1	6.7	1994	Northridge	Beverly Hills	Component 1	0.52
2	6.7	1994	Northridge	Canyon Country	Component 1	0.48
3	7.1	1999	Duzce, Turkey	Bolu	Component 1	0.82
4	7.1	1999	Hector Mine	Hector	Component 1	0.34
5	6.5	1979	Imperial Valley	Delta	Component 1	0.35
6	6.5	1979	Imperial Valley	El CentroArray#11	Component 1	0.38
7	6.9	1995	Kobe, Japan	Nishi-Akashi	Component 1	0.51
8	6.9	1995	Kobe, Japan	Shin-Osaka	Component 1	0.24
9	7.5	1999	Kocaeli, Turkey	Duzce	Component 1	0.36
10	7.5	1999	Kocaeli, Turkey	Arcelik	Component 1	0.22
11	7.3	1992	Landers	Yermo Fire station	Component 1	0.24
12	7.3	1992	Landers	Cool water	Component 1	0.42
13	6.9	1989	Loma Prieta	Capitola	Component 1	0.53
14	6.9	1989	Loma Prieta	Gilroy Array #3	Component 1	0.56
15	7.4	1990	Manjil, Iran	Abbar	Component 1	0.51
16	6.5	1987	Superstition Hills	El Centro Imp.co	Component 1	0.36
17	6.5	1987	Superstition Hills	Poe road (temp)	Component 1	0.45
18	7.0	1992	Cape Mendocino	Rio dell overpass	Component 1	0.55
19	7.6	1999	Chi-Chi, Taiwan	CHY 101	Component 1	0.44
20	7.6	1999	Chi-Chi, Taiwan	TCU 045	Component 1	0.51
21	6.6	1971	San Fernando	LA- Hollywood	Component 1	0.21
22	6.5	1976	Friuli, Italy	Tolmezzo	Component 1	0.35

Event magnitudes range from M6.5 to M7.6 with an average magnitude of M7.0 for the Far-Field record set. Site characteristics include shear wave velocity and the corresponding *NEHRP* Site Class. Sixteen sites are classified as Site Class D (stiff soil sites) and the remaining six are classified as Site Class C (very stiff soil sites). Fifteen records are from events of predominantly strike-slip faulting and the remaining seven are from events of predominantly thrust (or reverse faulting). Scaling of ground motions is not done but the effect of scaling the ground motion is captured by reducing the system strength ratio η.

7.2 Analyzing the Effect of Moving Resonance on a range of Ground Motions

7.2.1 Ground Motion 1: Northridge Earthquake at Beverly Hills

This particular ground motion (a repeat from chapter 6) is included for completeness and to provide context for the other ground motions. It provides good context because some of the specific cases were investigated in chapter 6 and were able to conclude that moving resonance was occurring. The two tools – peak displacements and amplification factors has been shown capable of finding instances of moving resonance.

The acceleration time history and the acceleration response spectra for 2 % damping of the component 1 of Northridge earthquake at Beverly Hills is shown in Figures 7-1 and 7-2 respectively. The 2D and 3D wavelet coefficient plot of this particular ground motion performed using Complex Morlet wavelet of band width 1 and frequency 1.5 is shown in Figures 7-3 and 7-4 respectively.

It is observed from Figure 7-1 that the significant energy content of the ground motion is starting at around time t=3 sec at low periods and the intensity of excitation is increasing and then again decreasing as time increases. It is clearly seen from the acceleration response spectra plot shown in Figure 7-2 that there are three distinct peaks of periods with periods ranging from 0.25 sec – 1.00 sec. But it is unclear whether these periods occur at same time or not. These two aspects of the frequency content of this particular ground motion are evident from the wavelet coefficient plots shown in Figures 7-3 and 7-4 respectively. It can be clearly seen that there is a transition of dominant periods starting with lower periods (i.e. 0.25 sec) and shifting to moderate periods (i.e.0.50, 1.00 sec) between time t=3 sec to time t=12 sec and the significant frequency content is

starting exactly at time t=3.6 sec with a period of 0.467(nearly 0.5) sec and is shifting to a period of 1 sec at time t= 9 sec.

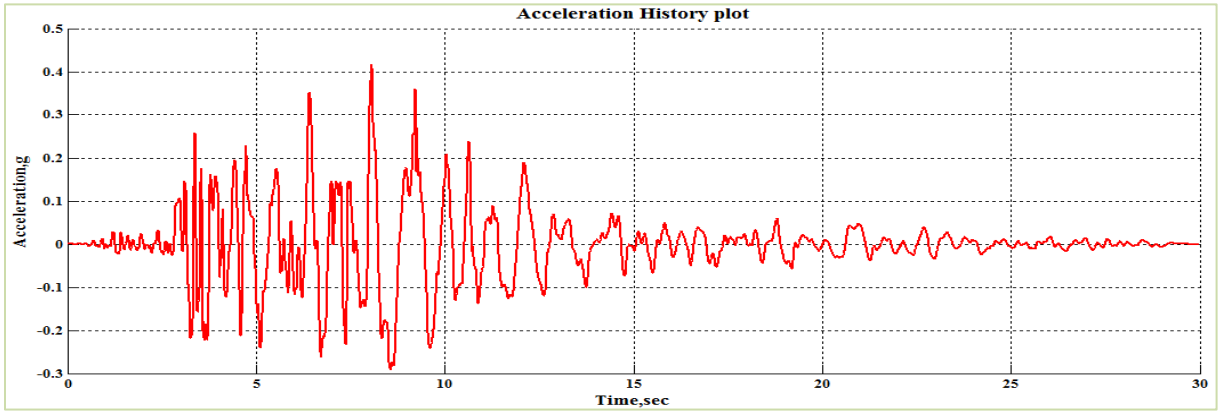

Figure 7-1 Acceleration Time History of Ground Motion 1

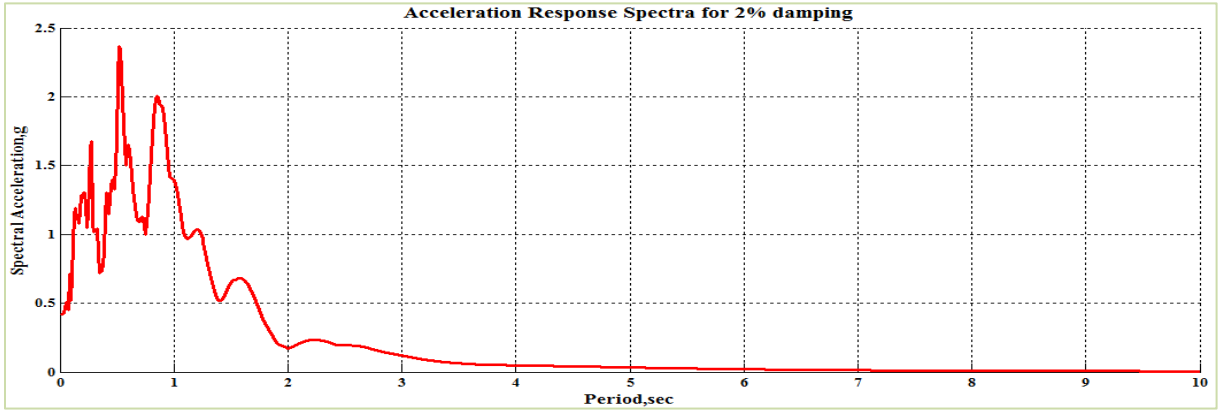

Figure 7-2 Acceleration Response Spectra for 2% Damping

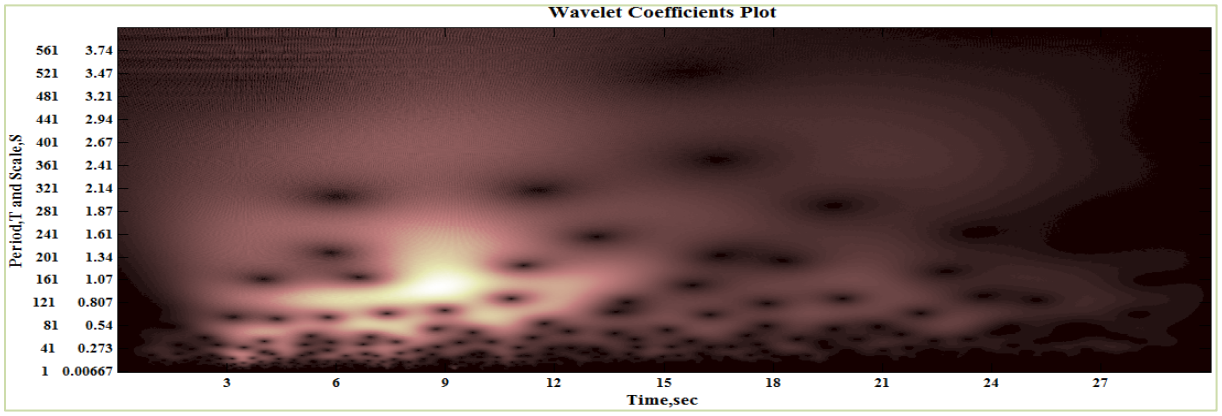

Figure 7-3 Wavelet coefficients plot of Ground Motion 1 (Northridge –Beverly Hills)

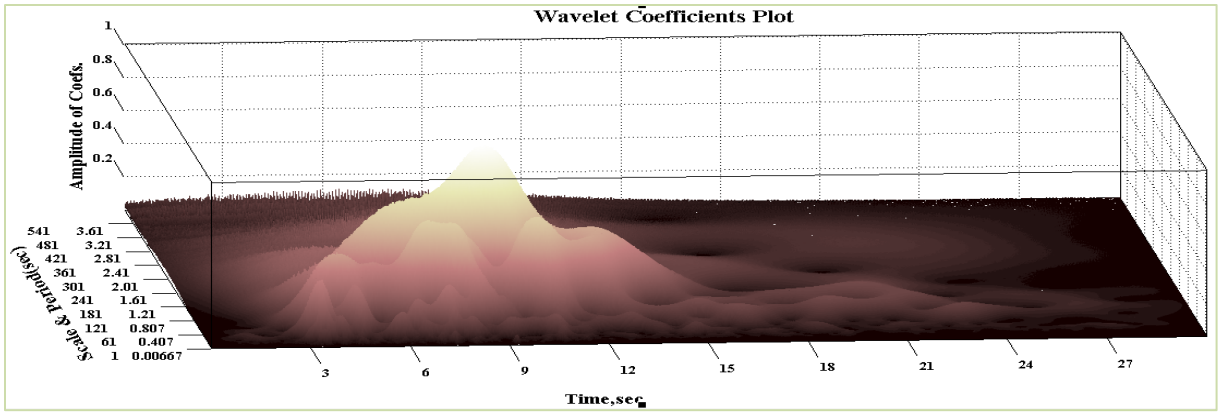

Figure 7-4 3D Wavelet coefficients plot of Ground Motion 1 (Northridge –Beverly Hills)

The 3D and 2D peak displacement plot of the structural system incorporating bilinear elastic behavior is shown in Figures 7-5 and 7-6 respectively. The 2D peak displacement plot as shown in Figure 7-6 have bumps (localized high points) in peak displacement at corresponding (T_0,η) values of (0.50,0.50) and (0.50,1.25).This localized increase in peak displacement is hypothesized to be the result of occurrence of moving resonance and hence an increase in amplification factor is expected for these combinations of period and strength. The hypothesis makes sense because of the trend in the dominant frequencies of the ground motion. Also moving resonance is a likely conclusion because slight changes in period or strength have smaller peak displacement.

The 3D and 2D peak amplification plot of the structural system incorporating bilinear elastic behavior is shown in Figures 7-7 and 7-8 respectively. It is evident from Figure 7-8 that the amplification values corresponding to (T_0,η) values of (0.5,0.5) and (0.5,1.25) (at similar places where localized high points of peak displacement were observed in Figure 7-6) are greater than 1 leading to the increase in peak displacement. This increase in peak displacement is considered to be the effect of moving resonance. A maximum effect of moving resonance is seen at T_0=0.5 sec and η=0.5 where the peak displacement is increased by 6 times. In chapter 6, these bumps were analyzed in detail and all of the tools used pointed toward moving resonance. It is concluded that therefore that the use of these tools (peak displacement plots and amplification factor) are good for quick view of which system properties are likely to be experiencing moving resonance.

It is noted that systems with low periods (e.g. To=0.25 sec) are shown to exhibit large amplification factors. It is not surprising that especially low period structures with nonlinear hysteretic behavior experience large peak displacements. Previous studies on systems with short

periods have shown that short period structures with yield strength less than the elastic forces will experience excessive inelastic displacements (Veletsos et al. 1965). The current study does not focus on this effect, but instead focuses on systems that experience larger peak displacement than systems with similar system parameters (T_0,η).

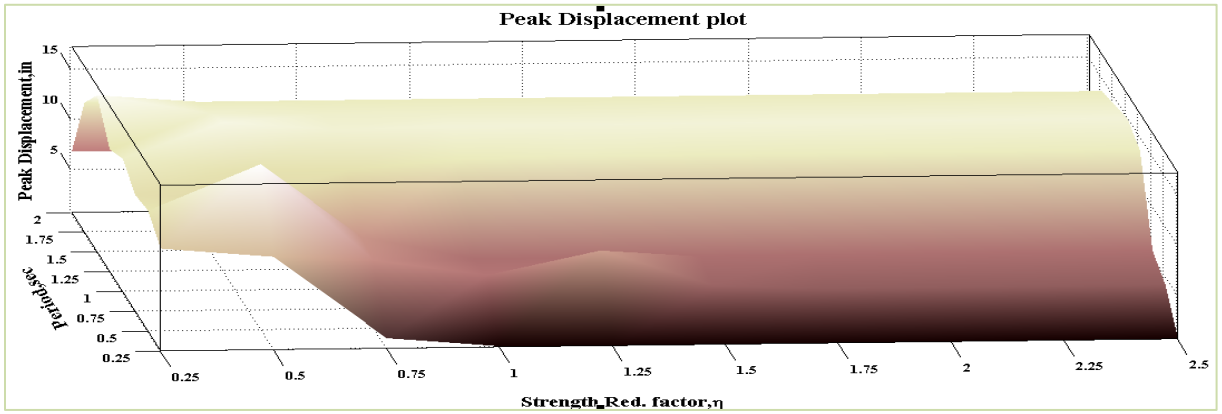

Figure 7-5 3D Peak Displacement plot for Ground Motion 1 for Bilinear Elastic Behavior

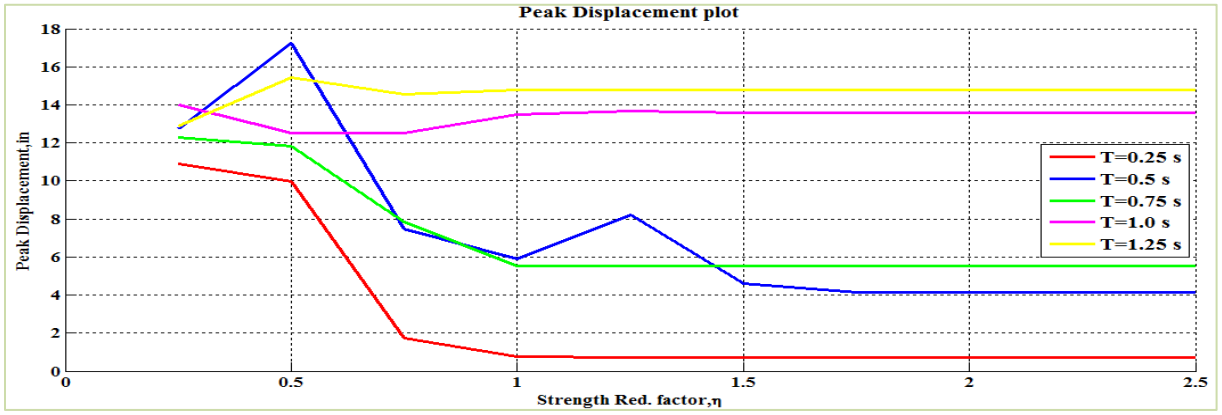

Figure 7-6 2D Peak Displacement plot for Ground Motion 1 for Bilinear Elastic Behavior

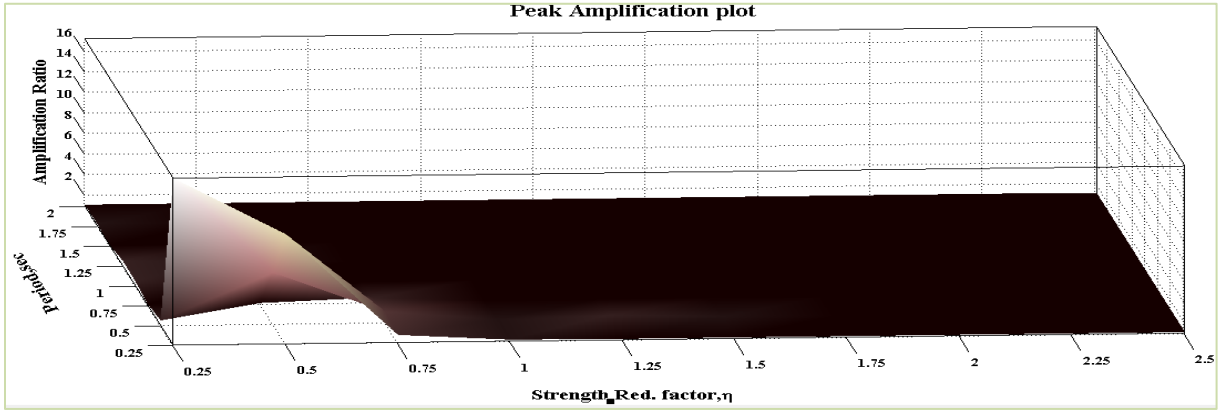

Figure 7-7 3D Peak Amplification plot for Ground Motion 1 (Bilinear Elastic Behavior)

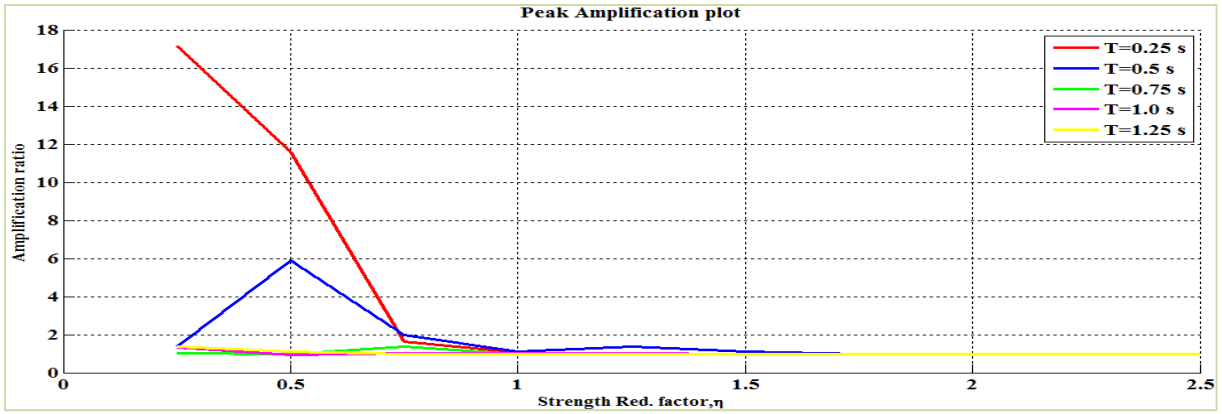

Figure 7-8 2D Peak Amplification plot for Ground Motion 1 (Bilinear Elastic Behavior)

The 3D and 2D peak displacement plot of the structural system incorporating elasto-plastic behavior is shown in Figures 7-9 and 7-10 respectively. From Figure 7-10, it can be seen that, for low periods (for T=0.25 sec) the peak displacement of the inelastic system is greater than the associated elastic system. This shows that the peak displacement values are in accordance with findings from previous studies of EPP systems (Newmark, 1983).

The 2D peak displacement plot for elasto-plastic behavior as shown in Figure 7-10 have bumps (localized high point) in peak displacement at corresponding (T_0,η) values of (0.50,0.75) whereas there is a valley (localized low point) in peak displacement at corresponding (T_0,η) values of (0.75,0.75). The bumps are hypothesized to be the result of occurrence of moving resonance and hence a larger amplification factor is expected for these combinations of period and strength whereas the valleys are hypothesized to be the absence of moving resonance (frequency content of ground motion being *out of phase* with the structural response and thus constitutes destructive interference) and hence results in lower amplification factor is expected.

The 3D and 2D peak amplification plot of the structural system incorporating elasto-plastic behavior is shown in Figures 7-11 and 7-12 respectively. It is evident from the peak amplification plot shown in Figure 7-12 that the amplification factors corresponding to (T_0,η) values of (0.50,0.75) (at similar places where localized high points of peak displacement were observed as shown in Figure 7-10) are greater than 1 leading to the increase in peak displacement. This increase in peak displacement is considered to be the effect of moving resonance. It is also observed from Figure 7-12 that the amplification value corresponding to (T_0,η) value of (0.75,0.75) (at similar place where valley of peak displacement is observed from

Figure 7-10) is less than 1, which implies that there is destructive interference effect (frequency content of ground motion being *out of phase* with the structural response) of moving resonance for that particular (T_0,η) value.

It is noted that systems with low periods (e.g. To=0.25 sec) are shown to exhibit large amplification factors. It is not surprising that especially low period structures with nonlinear hysteretic behavior experience large peak displacements. Previous studies on systems with short periods have shown that short period structures with yield strength less than the elastic forces will experience excessive inelastic displacements (Veletsos et al. 1965). The current study does not focus on this effect, but instead focuses on systems that experience larger peak displacement than systems with similar system parameters (T_0,η).

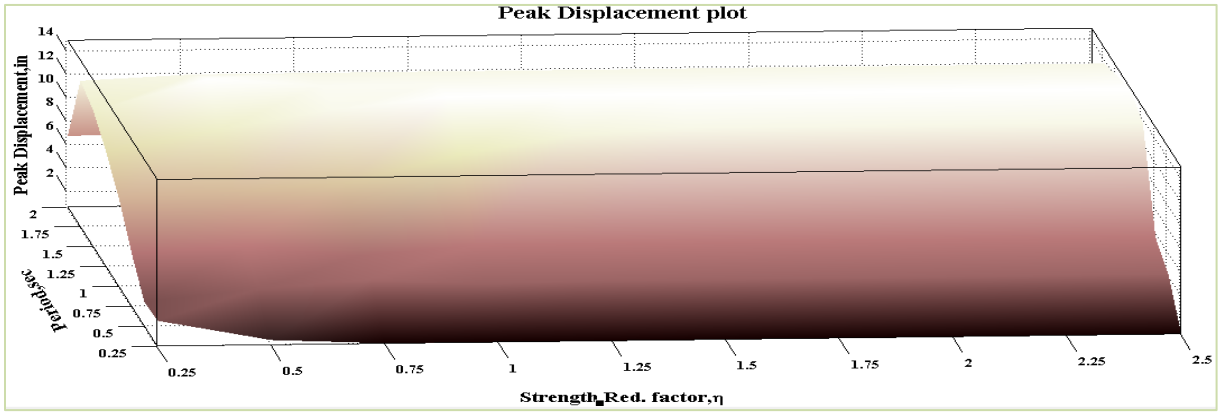

Figure 7-9 3D Peak Displacement for Ground Motion 1 for EPP Behavior

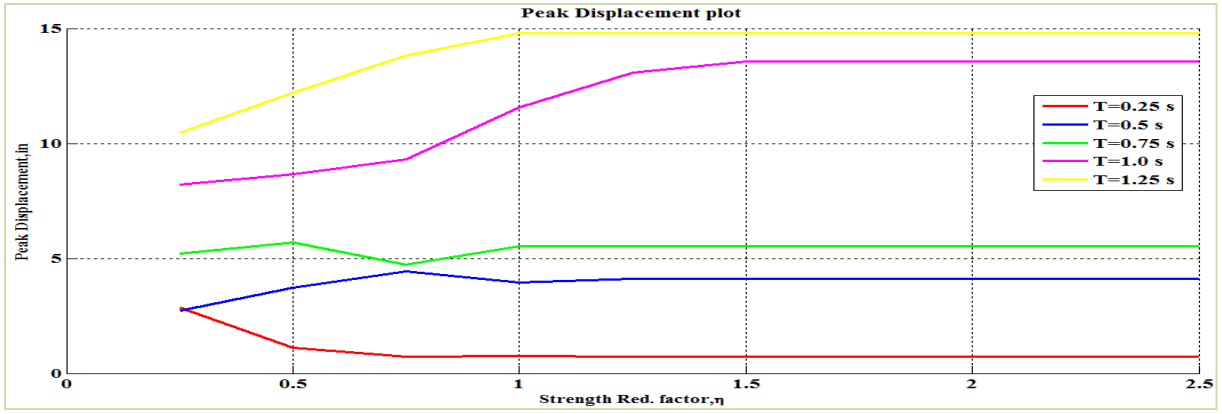

Figure 7-10 2D Peak Displacement for Ground Motion 1 for EPP Behavior

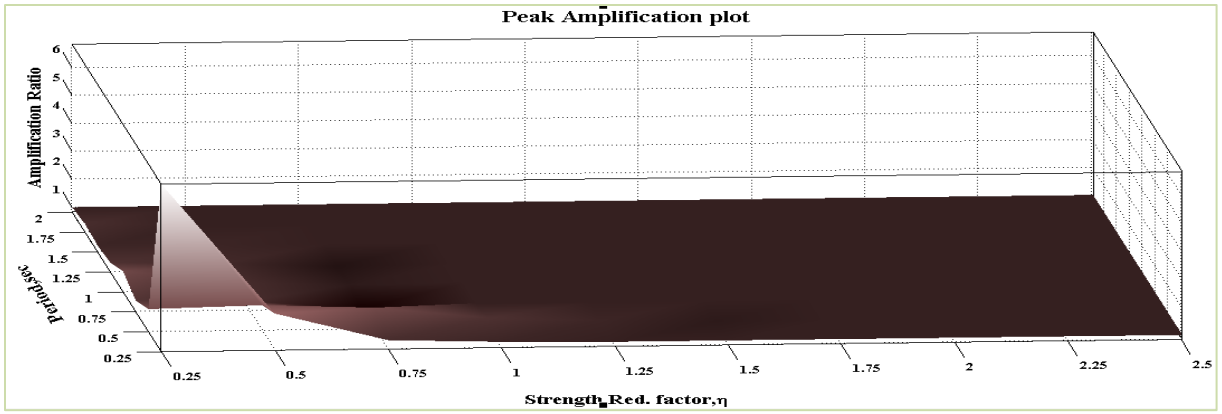

Figure 7-11 3D Peak Amplification plot for Ground Motion 1 (EPP Behavior)

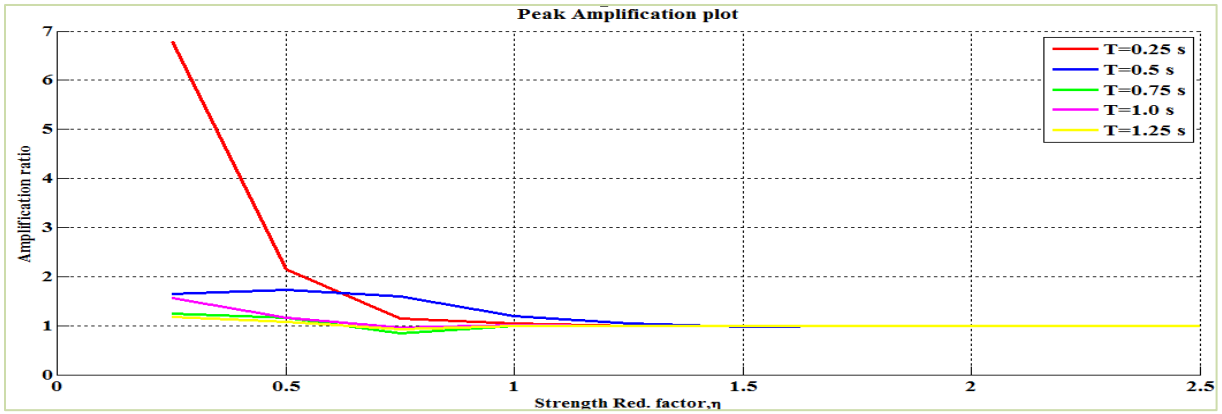

Figure 7-12 2D Peak Amplification plot for Ground Motion 1 (EPP Behavior)

The effect of moving resonance on elasto-plastic systems is muted, likely because of hysteretic damping. This is the primary reason for examining bilinear elastic systems.

One of the primary conclusions from the investigation of this particular ground motion is that moving resonance can have significant effect on the structural systems incorporating bilinear elastic and elasto-plastic behavior having initial periods of 0.5 sec. This is also corroborated by other tools in chapter 6.

7.2.2 Ground Motion 2: Northridge Earthquake at Canyon Country

The acceleration time history and the acceleration response spectra for 2 % damping of the component 1 of Northridge earthquake at Canyon County is shown in Figures 7-13 and 7-14 respectively. The 2D and 3D wavelet coefficient plot of this particular ground motion performed using Complex Morlet wavelet of band width 1 and frequency 1.5 is shown in Figures 7-15 and 7-16 respectively.

It is shown in Figure 7-13 that the significant frequency content is starting at around time t=4 sec hitting low periods and the intensity of excitation is increasing and then again decreasing as time increases. It is observed that there is some energy at lower periods (i.e. 0.25 sec) at 4 sec that then shifts to strong shaking at moderate periods (i.e.0.50,0.75 sec) between time t=4 sec to time t=8 sec. These aspects of the frequency content can be clearly seen in the wavelet coefficient plots shown in Figures 7-15 and 7-16 respectively. Knowing this, it can be assumed that there may be effect of moving resonance on structures having periods starting below 0.75 sec.

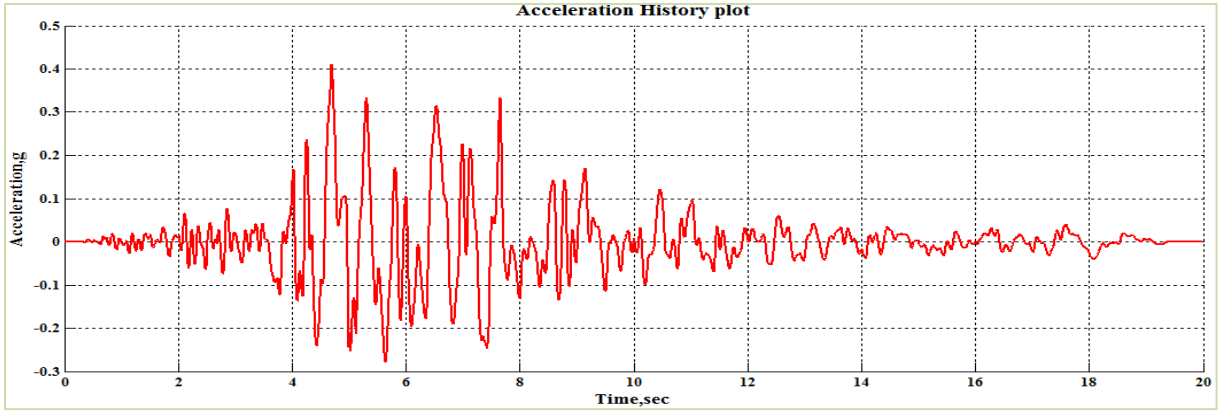

Figure 7-13 Acceleration Time History of Ground Motion 2 (Northridge-Canyon Country)

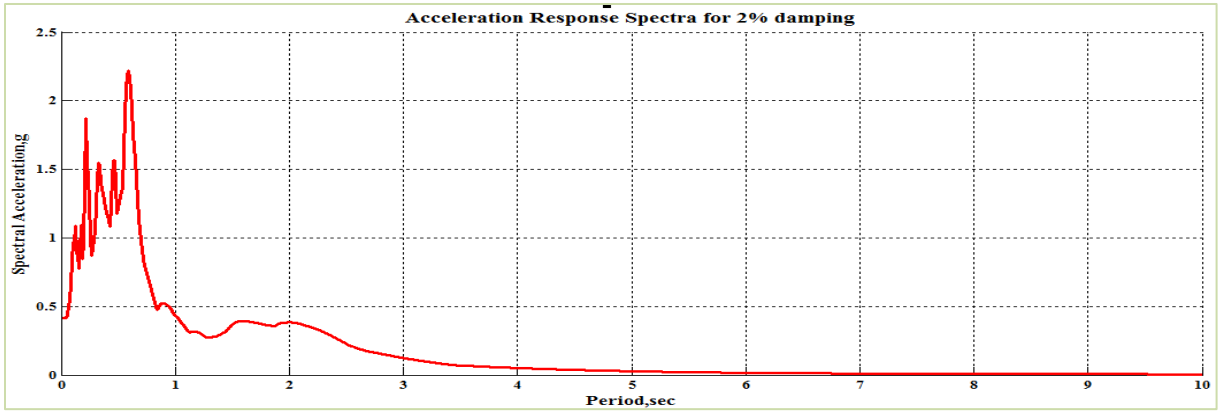

Figure 7-14 Acceleration Response Spectra for 2% Damping

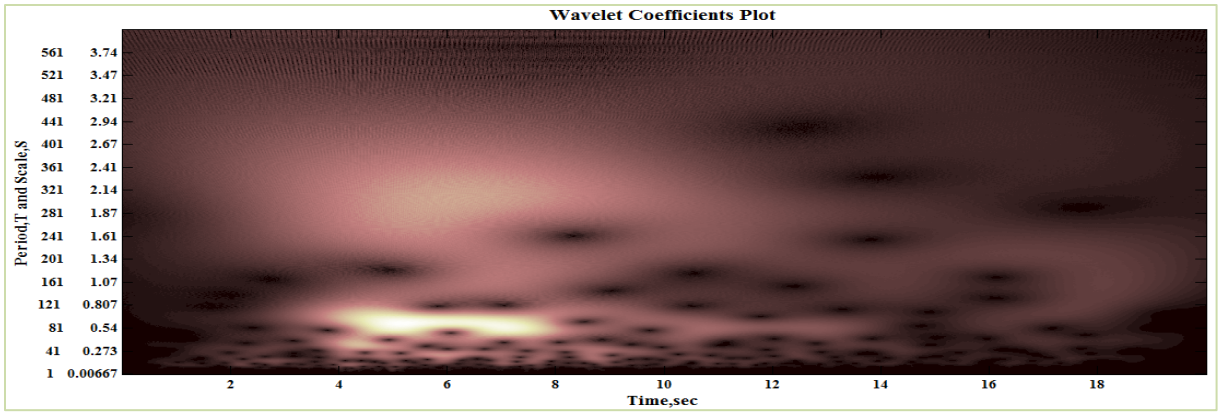

Figure 7-15 2D Wavelet coefficients plot of Ground Motion 2 (Northridge –Canyon Country)

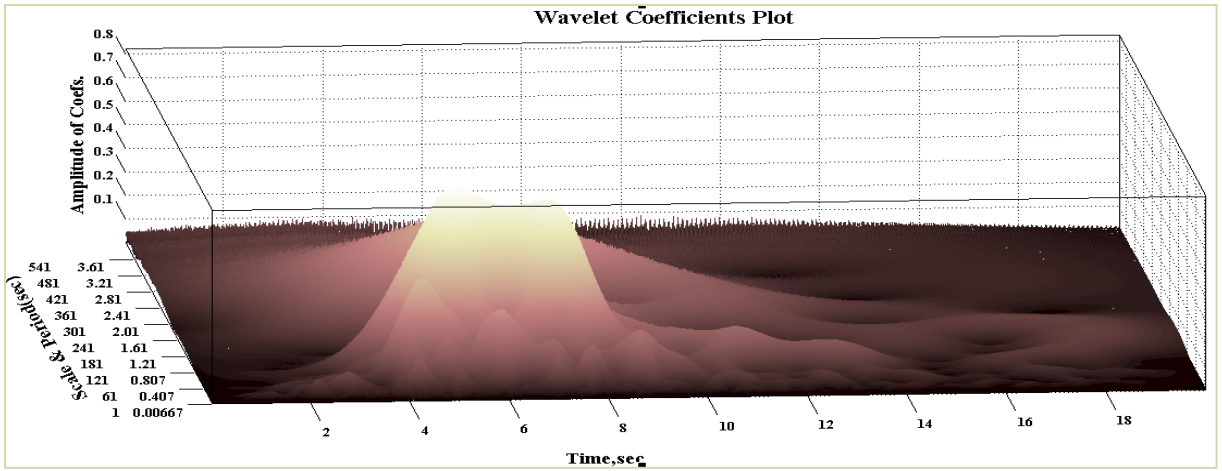

Figure 7-16 3D Wavelet coefficients plot of Ground Motion 2 (Northridge –Canyon Country)

The 3D and 2D peak displacement plot of the structural system incorporating bilinear elastic behavior is shown in Figures 7-17 and 7-18 respectively. The 2D peak displacement plot as shown in Figure 7-18 have bumps (localized high points) in peak displacement at corresponding (T_0,η) values of (0.50,0.50) and (0.50,0.75).This localized increase in peak displacement is hypothesized to be the result of occurrence of moving resonance and hence an increase in amplification factor is expected for these combinations of period and strength.

The 3D and 2D peak amplification plot of the structural system incorporating bilinear elastic behavior is shown in Figures 7-19 and 7-20 respectively. It is evident from Figure 7-20 that the amplification values corresponding to (T_0,η) values of (0.50,0.50) and (0.50,75) (at similar places where localized high points of peak displacement were observed in Figure 7-18) are greater than 1 leading to the increase in peak displacement. This increase in peak displacement is considered to be the effect of moving resonance.

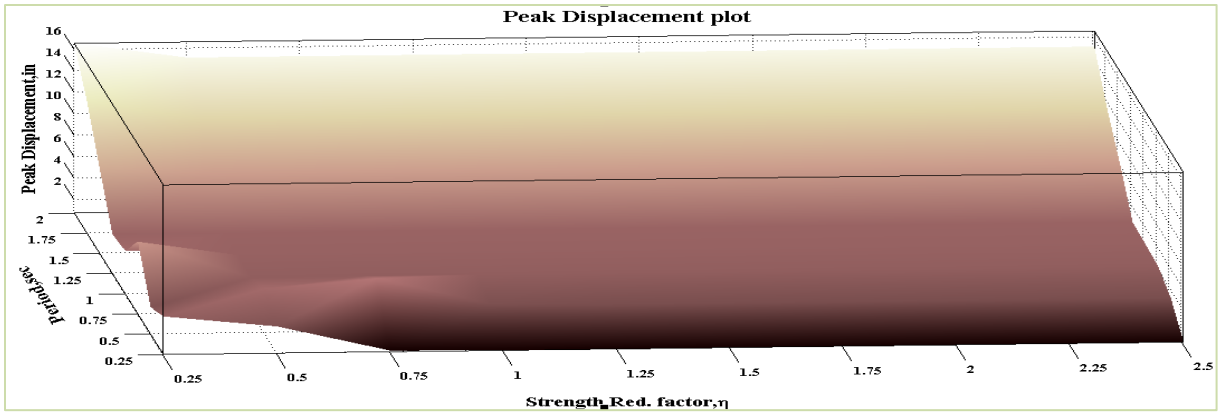

Figure 7-17 3D Peak Displacement plot for Ground Motion 2 (Bilinear Behavior)

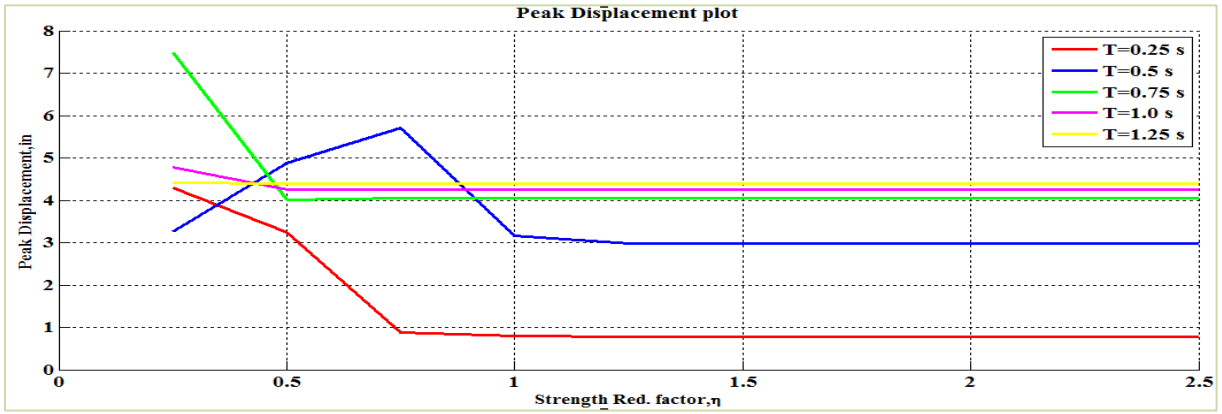

Figure 7-18 2D Peak Displacement plot for Ground Motion 2 (Bilinear Behavior)

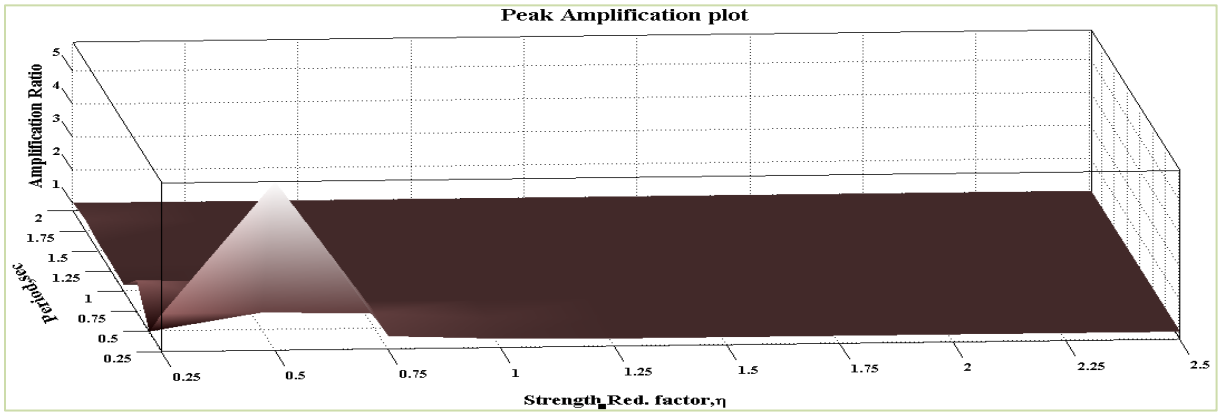

Figure 7-19 3D Peak Amplification plot for Ground Motion 2 (Bilinear Behavior)

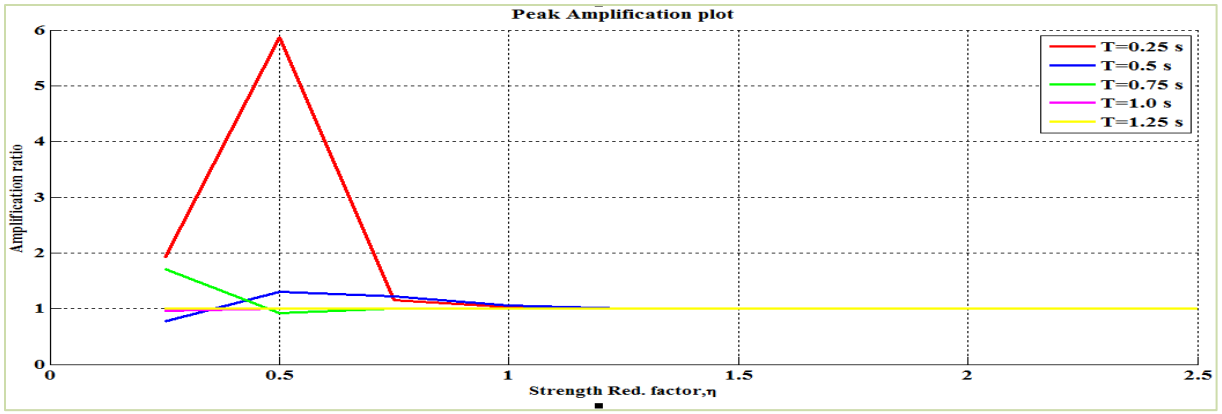

Figure 7-20 2D Peak Amplification plot for Ground Motion 2 (Bilinear Behavior)

The 3D and 2D peak displacement plot of the structural system incorporating elasto-plastic behavior is shown in Figures 7-21 and 7-22 respectively. The 2D peak displacement plot for elasto-plastic behavior as shown in Figure 7-22 have bumps (localized high point) in peak displacement at corresponding (T_0,η) values of (0.50,1.00) .This localized increase in peak displacement is hypothesized to be the result of occurrence of moving resonance and hence a amplification factor greater than 1 is expected for these combinations of period and strength.

The 3D and 2D peak amplification plot of the structural system incorporating elasto-plastic behavior is shown in Figures 7-23 and 7-24 respectively. It is evident from the peak amplification plot shown in Figure 7-24 that the amplification factors corresponding to (T_0,η) values of (0.50,1.00) (at similar places where localized high points of peak displacement were observed as shown in Figure 7-22) are greater than 1 leading to the increase in peak displacement. This increase in peak displacement is considered to be the effect of moving resonance. It is also observed from Figure 7-24 that the amplification value corresponding to (T_0,η) value of (0.50,0.75) (at similar place where valley of peak displacement is observed from Figure 7-22) is less than 1, which implies that there is destructive interference effect (frequency content of ground motion being *out of phase* with the structural response) of moving resonance for that particular (T_0,η) value.

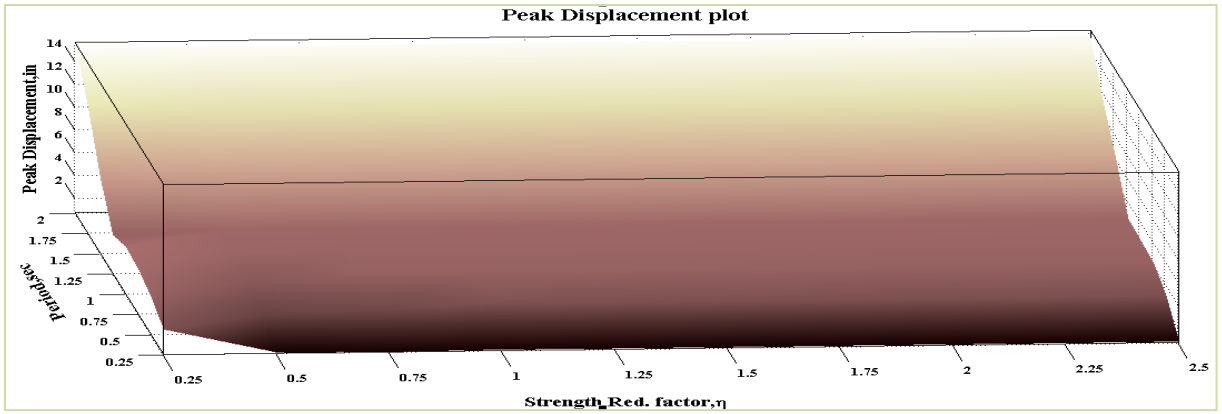

Figure 7-21 3D Peak Displacement plot for Ground Motion 2 (EPP Behavior)

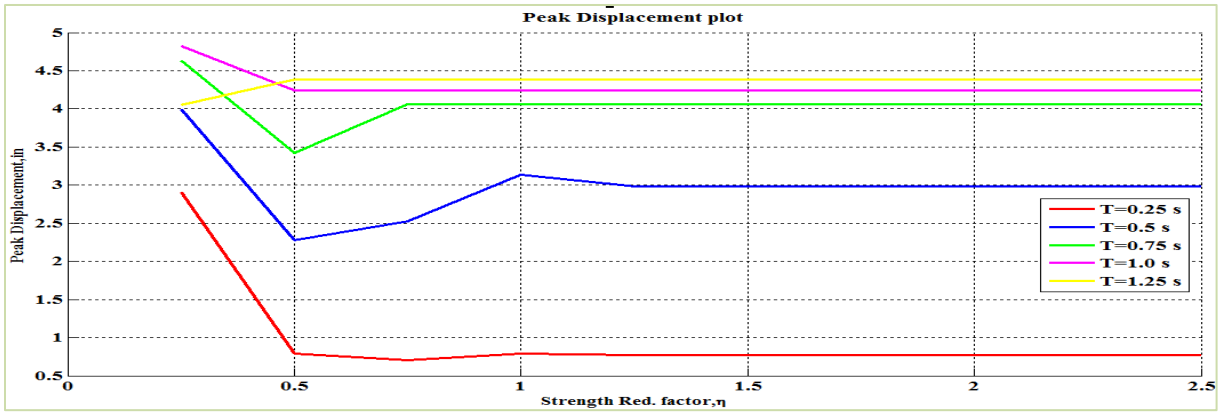

Figure 7-22 2D Peak Displacement plot for Ground Motion 2 (EPP Behavior)

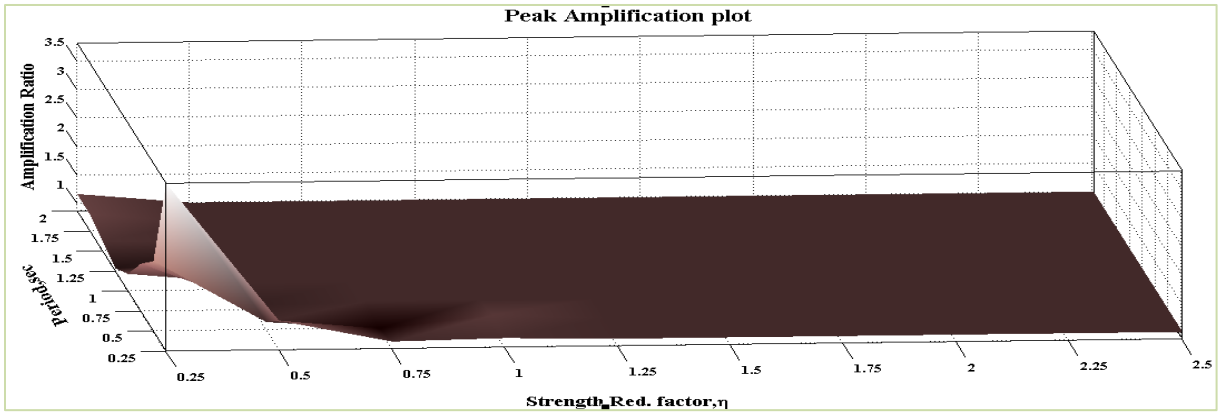

Figure 7-23 3D Peak Amplification plot for Ground Motion 2 (EPP Behavior)

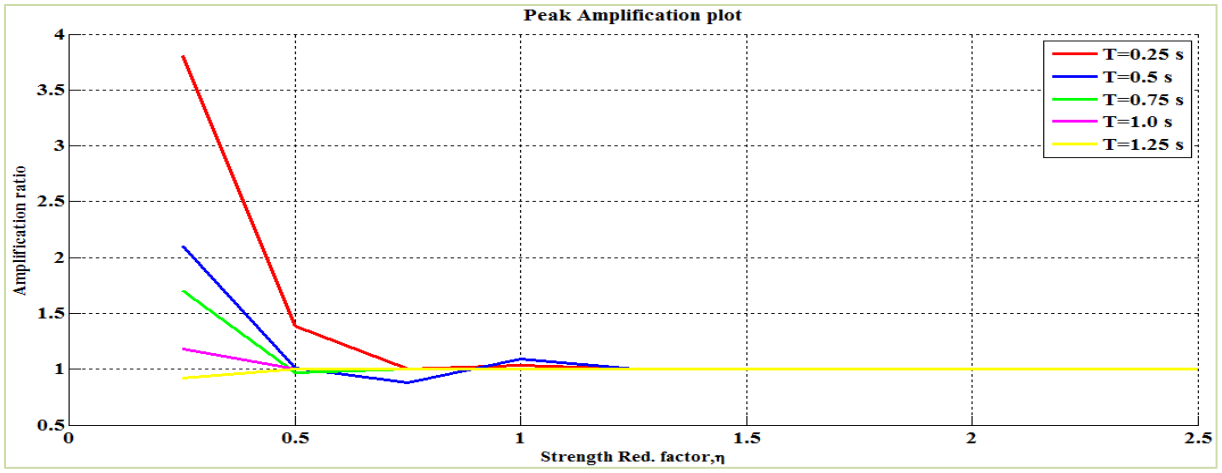

Figure 7-24 2D Peak Amplification plot for Ground Motion 2 (EPP Behavior)

Hence, it is concluded that for this particular ground motion, moving resonance has little effect on the structural systems. The possible reason might be because the energy in the ground motion is so well centered on one period and the dominant frequency does not change much.

7.2.3 Ground Motion 3: Duzce Turkey at Bolu station

The acceleration time history and the acceleration response spectra for 2 % damping of the component 1 of Duzce Turkey earthquake at Bolu station is shown in Figures 7-25 and 7-26 respectively. The 2D and 3D wavelet coefficient plot of this particular ground motion performed using Complex Morlet wavelet of band width 1 and frequency 1.5 is shown in Figures 7-27 and 7-28 respectively.

The ground motion shown in Figure 7-25 has strong shaking for a short period of time. The energy in the ground motion appears to be centered at time t=10-12 sec with most of the energy at approximately 0.5 sec period (as seen in Figure 7-26) with a lesser peak in energy at a period of about 0.9 sec. These aspects of the frequency content can be clearly seen in the wavelet coefficient plots shown in Figures 7-27 and 7-28 respectively. Knowing this, it can be assumed that there may be effect of moving resonance on structures having periods between 0.25-0.5 sec.

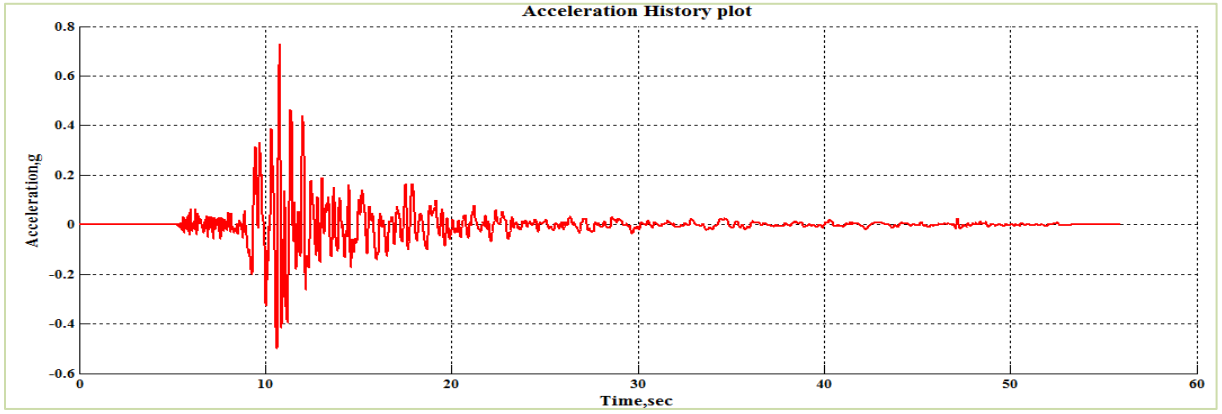

Figure 7-25 Acceleration Time History of Ground Motion 3 (Duzce, Turkey-Bolu)

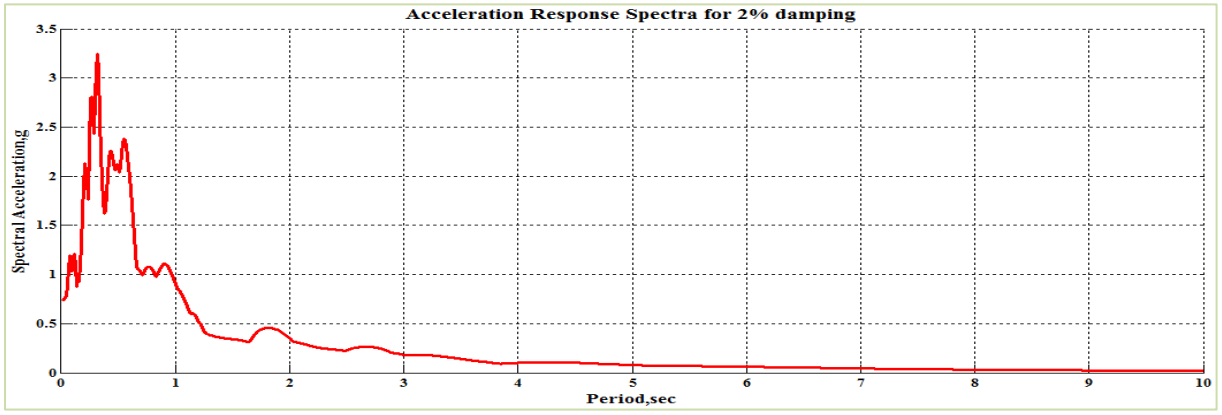

Figure 7-26 Acceleration Response Spectra for 2% Damping

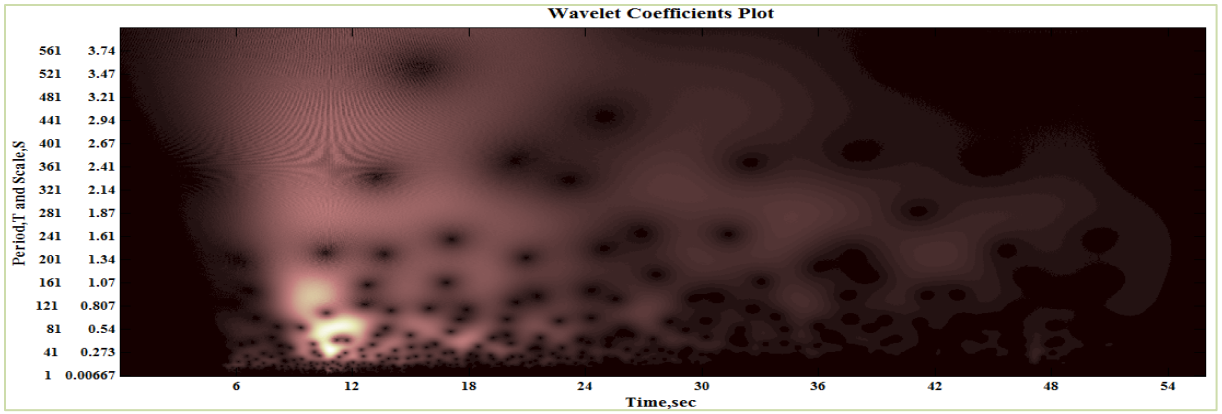

Figure 7-27 2D Wavelet coefficients plot of Ground Motion 3 (Duzce, Turkey-Bolu)

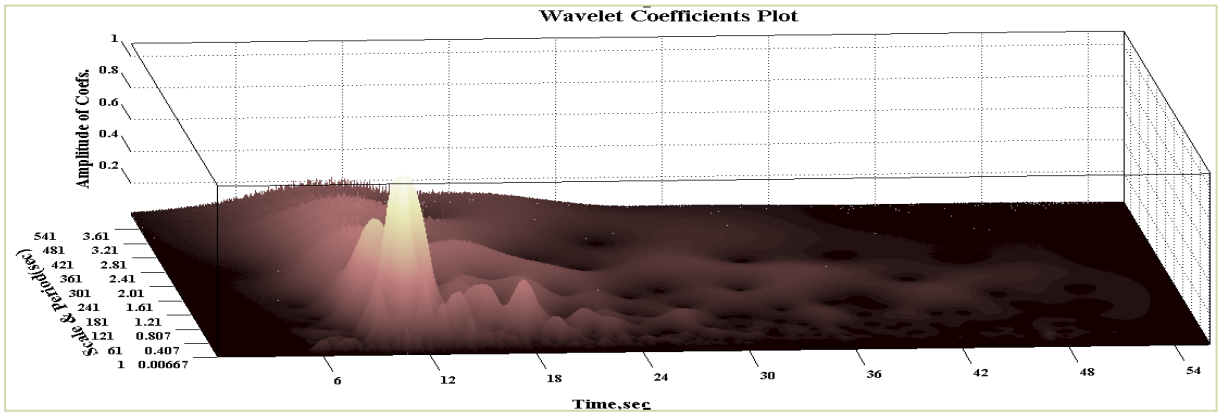

Figure 7-28 3D Wavelet coefficients plot of Ground Motion 3 (Duzce, Turkey-Bolu)

The 3D and 2D peak displacement plot of the structural system incorporating bilinear elastic behavior is shown in Figures 7-29 and 7-30 respectively. The 2D peak displacement plot as shown in Figure 7-30 have bumps (localized high points) in peak displacement at corresponding (T_0,η) values of (0.25,0.50), (0.25,1.25),(0.50,1.25) and (0.75,0.5). This localized increase in peak displacement is hypothesized to be the result of occurrence of moving resonance and hence amplification factor greater than 1 is expected for these combinations of period and strength.

The 3D and 2D peak amplification plot of the structural system incorporating bilinear elastic behavior is shown in Figures 7-31 and 7-32 respectively. It is observed from Figure 7-32 that the amplification values corresponding to (T_0,η) values of (0.25,0.50), (0.25,1.25),(0.50,1.25) and (0.75,0.5) (at similar places where localized high points of peak displacement were observed in Figure 7-30) are greater than 1 leading to the increase in peak displacement. This increase in peak displacement is considered to be the effect of moving resonance. These amplification factors aren`t as large as the first ground motion, but an interesting conclusion is that even though the ground motion is pulse like, it still creates moving resonance.

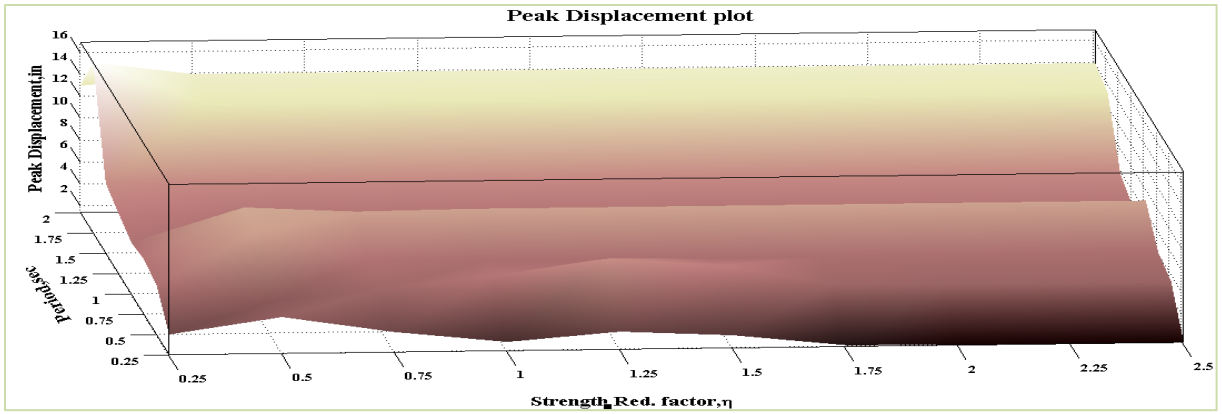

Figure 7-29 3D Peak Displacement plot for Ground Motion 3 (Bilinear Behavior)

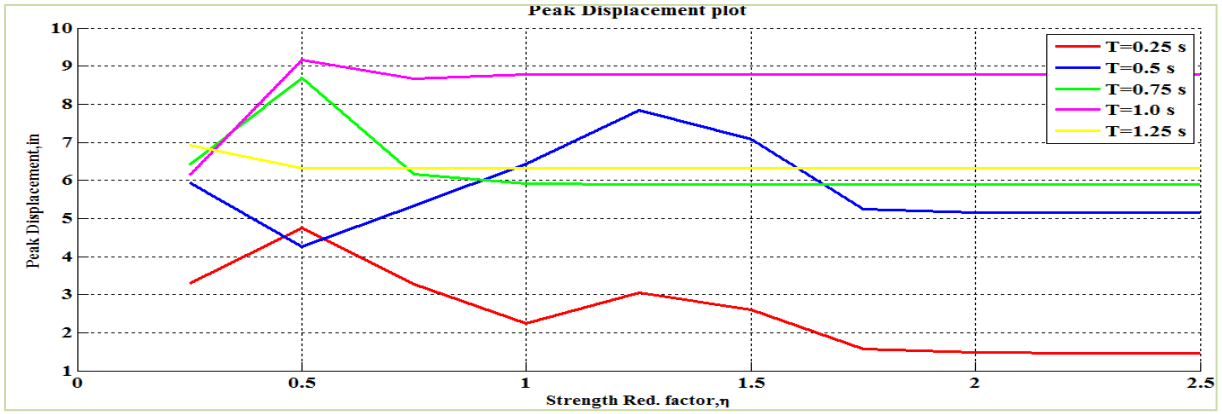

Figure 7-30 2D Peak Displacement plot for Ground Motion 3 (Bilinear Behavior)

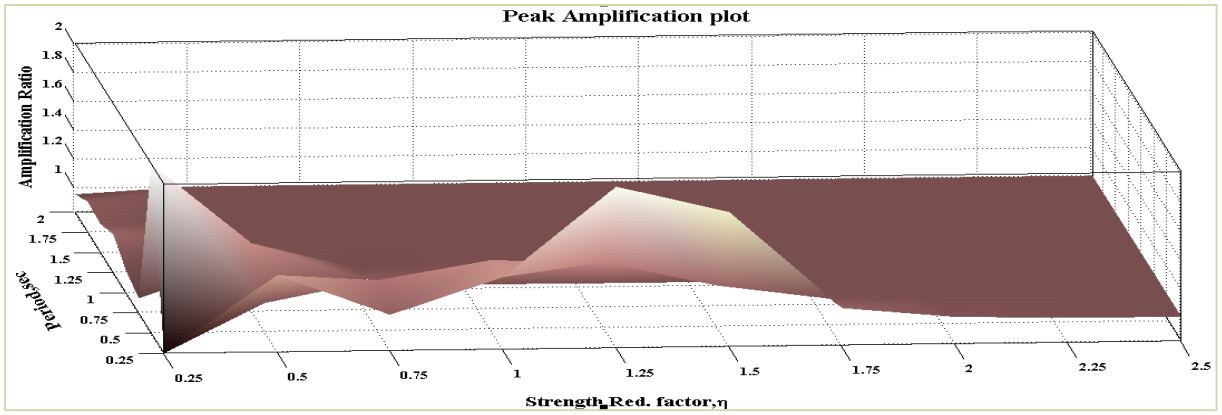

Figure 7-31 3D Peak Amplification plot for Ground Motion 3 (Bilinear Behavior)

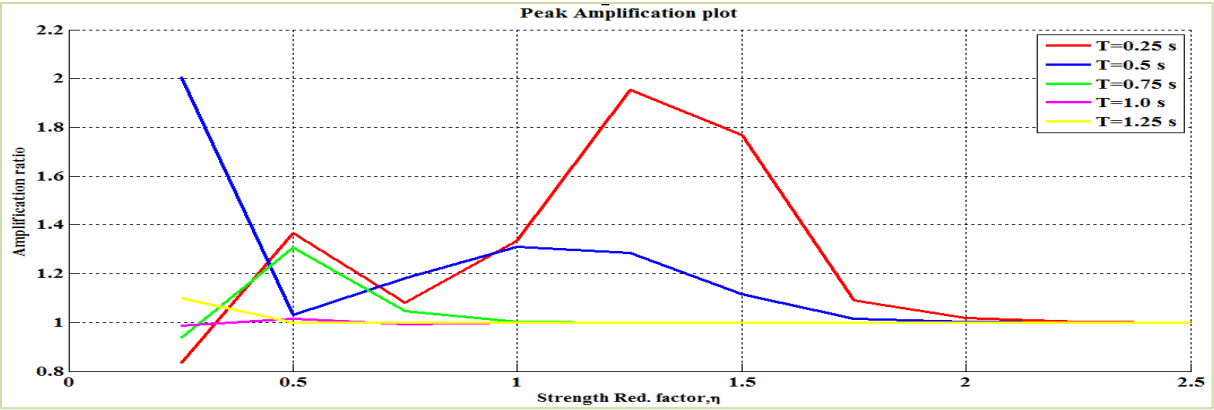

Figure 7-32 2D Peak Amplification plot for Ground Motion 3 (Bilinear Behavior)

The 3D and 2D peak displacement plot of the structural system incorporating elasto-plastic behavior is shown in Figures 7-33 and 7-34 respectively. The 2D peak displacement plot for elasto-plastic behavior as shown in Figure 7-34 have bumps (localized high point) in peak displacement at corresponding (T_0,η) values of (0.25,1.5),(0.50,1.00) and (1.00,0.50) whereas there is a valley (steep decrease) in peak displacement at corresponding (T_0,η) values of (0.75,0.50).This localized increase in peak displacement is hypothesized to be the result of occurrence of moving resonance and hence a amplification factor greater than 1 is expected for these combinations of period and strength whereas the valleys are hypothesized to be the absence of moving resonance(frequency content of ground motion being *out of phase* with the structural response) and hence amplification factor less than 1 is expected.

The 3D and 2D peak amplification plot of the structural system incorporating elasto-plastic behavior is shown in Figures 7-35 and 7-36 respectively. It is evident from the peak amplification plot shown in Figure 7-36 that the amplification factors corresponding to (T_0,η) values of (0.25,1.5),(0.50,1.00) and (1.00,0.50) (at similar places where localized high points of peak displacement were observed as shown in Figure 7-34) are greater than 1 leading to the increase in peak displacement. This increase in peak displacement is considered to be the effect of moving resonance. It is also observed from Figure 7-36 that the amplification value corresponding to (T_0,η) value of (0.75,0.50) (at similar place where valley of peak displacement is observed from Figure 7-34) is less than 1, which implies that there is destructive interference effect (frequency content of ground motion being *out of phase* with the structural response) of moving resonance for that particular (T_0,η) value. Over all, the effect of moving resonance for EPP system is minimal.

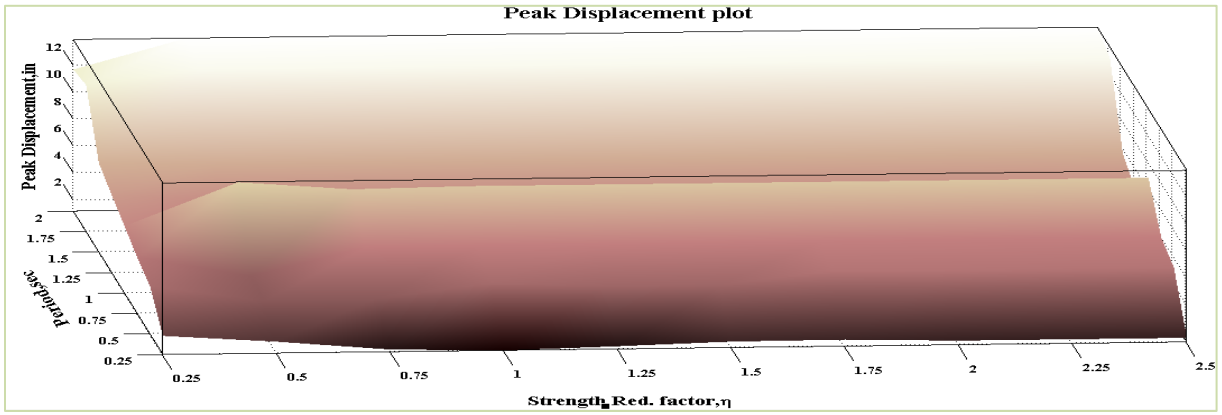

Figure 7-33 3D Peak Displacement plot for Ground Motion 3 (EPP Behavior)

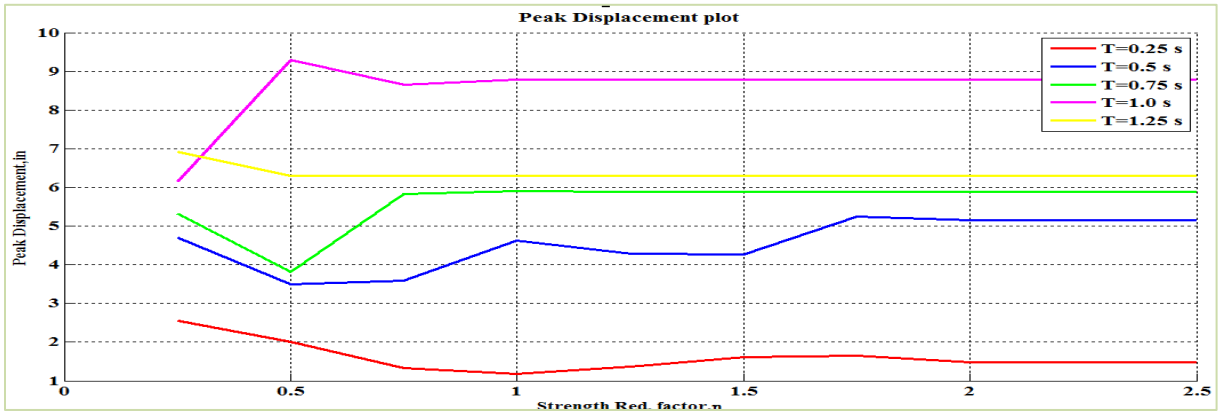

Figure 7-34 2D Peak Displacement plot for Ground Motion 3 (EPP Behavior)

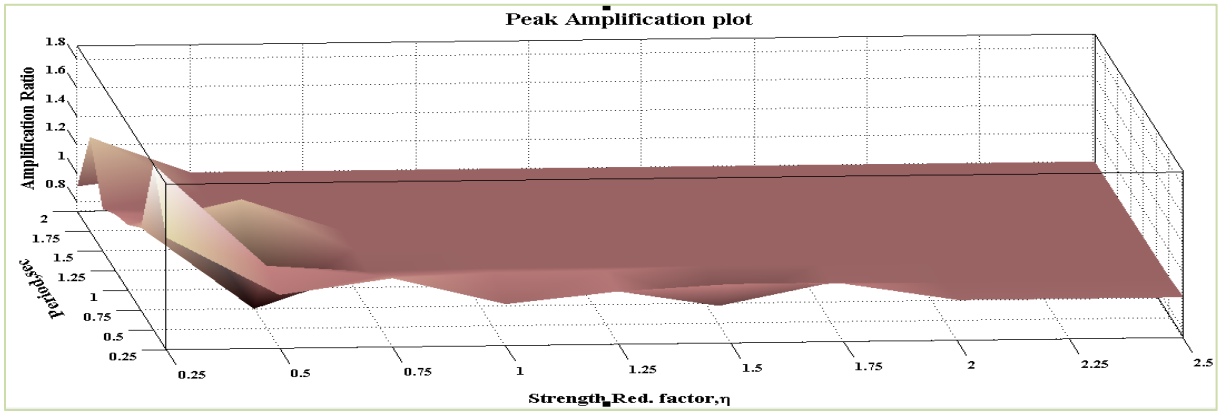

Figure 7-35 3D Peak Amplification plot for Ground Motion 3 (EPP Behavior)

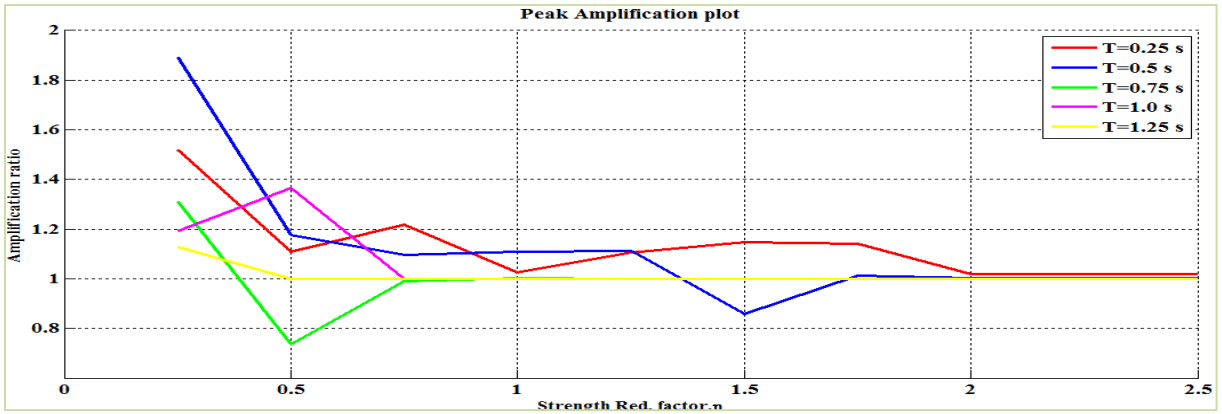

Figure 7-36 2D Peak Amplification plot for Ground Motion 3 (EPP Behavior)

Overall, it is concluded that even pulse like ground motion creates moving resonance. There was some propensity for moving resonance in the T_0= 0.25 sec bilinear elastic system, but other than that moving resonance did not have a huge effect. The elastic-perfectly system showed very little amplification in general.

7.2.4 Ground Motion 4: Hector Mine at Hector station

The acceleration time history and the acceleration response spectra for 2 % damping of the component 1 of Hector Mine earthquake at Hector station is shown in Figures 7-37 and 7-38 respectively. The 2D and 3D wavelet coefficient plot of this particular ground motion performed using Complex Morlet wavelet of band width 1 and frequency 1.5 is shown in Figures 7-39 and 7-40 respectively.

The ground motion shown in Figure 7-37 has some miscellaneous energy in the ground motion at lower periods, but a significant amount of energy is present in the signal at a period of about 1.25 sec occurring at about 6 sec. A secondary peak is present at a period of about 0.9 sec at about 12 sec. One interesting aspect of this ground motion is that the dominant period goes down from around 1.25 sec to 0.9 sec. These aspects of the frequency content can be clearly seen in the wavelet coefficient plots shown in Figures 7-39 and 7-40 respectively.

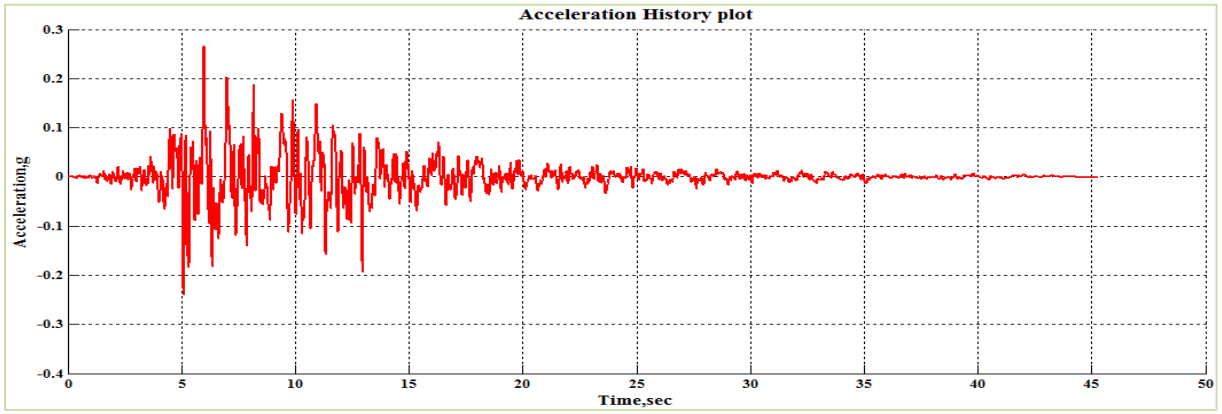

Figure 7-37 Acceleration Time History of Ground Motion 4 (Hector Mine-Hector)

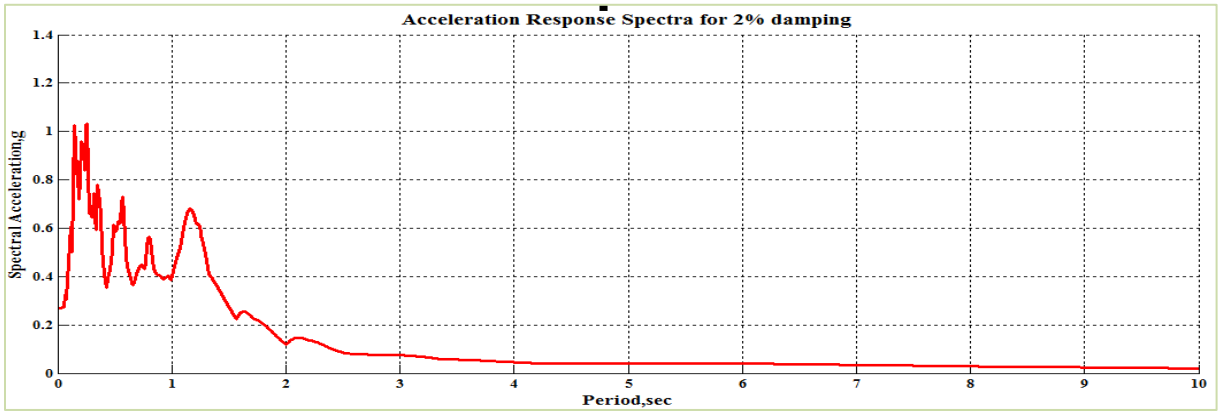

Figure 7-38 Acceleration Response Spectra for 2% Damping

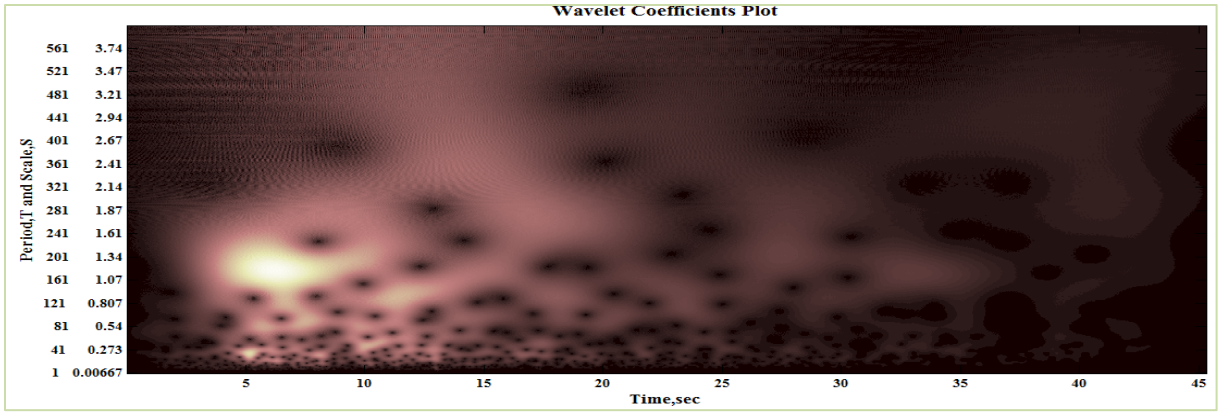

Figure 7-39 2D Wavelet coefficients plot of Ground Motion 4 (Hector Mine)

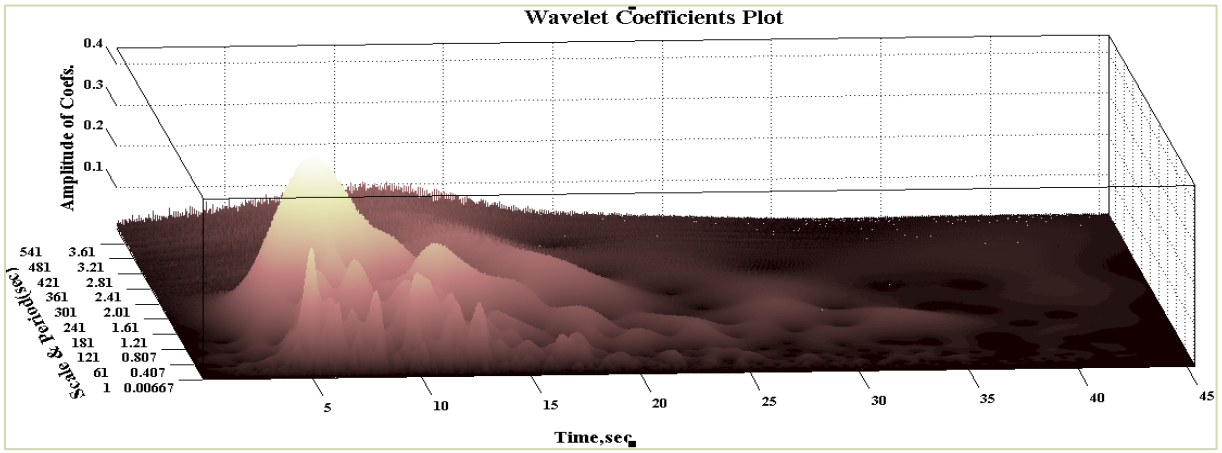

Figure 7-40 3D Wavelet coefficients plot of Ground Motion 3 (Hector Mine)

The 3D and 2D peak displacement plot of the structural system incorporating bilinear elastic behavior is shown in Figures 7-41 and 7-42 respectively. The 2D peak displacement plot as shown in Figure 7-42 doesn`t have bumps (localized high points) in peak displacement. Hence, the amplification factor is expected to be equal to 1. It is observed from Figure 7-42 that the system becomes elastic for relatively low strength reduction factor.

The 3D and 2D peak amplification plot of the structural system incorporating bilinear elastic behavior is shown in Figures 7-43 and 7-44 respectively. It is observed from Figure 7-44 that the amplification factor for all periods is nearer to 1 which proves that the the moving resonance doesn`t have significant effect on the structural systems incorporating bilinear elastic behavior. Since the dominant periods in the ground motion were decreasing with time rather than increasing, moving resonance did not have much effect. At (T_0,η) value of (0.75,0.25) a very low amplification factor is observed and this implies that there was significant destructive interference in the way the structure responds to the ground motion.

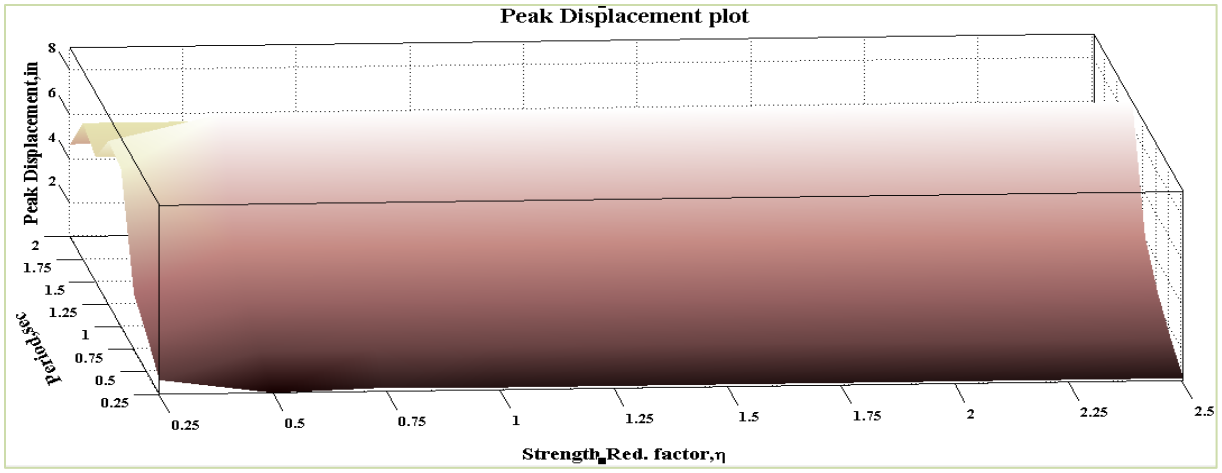

Figure 7-41 3D Peak Displacement plot for Ground Motion 4 (Bilinear Behavior)

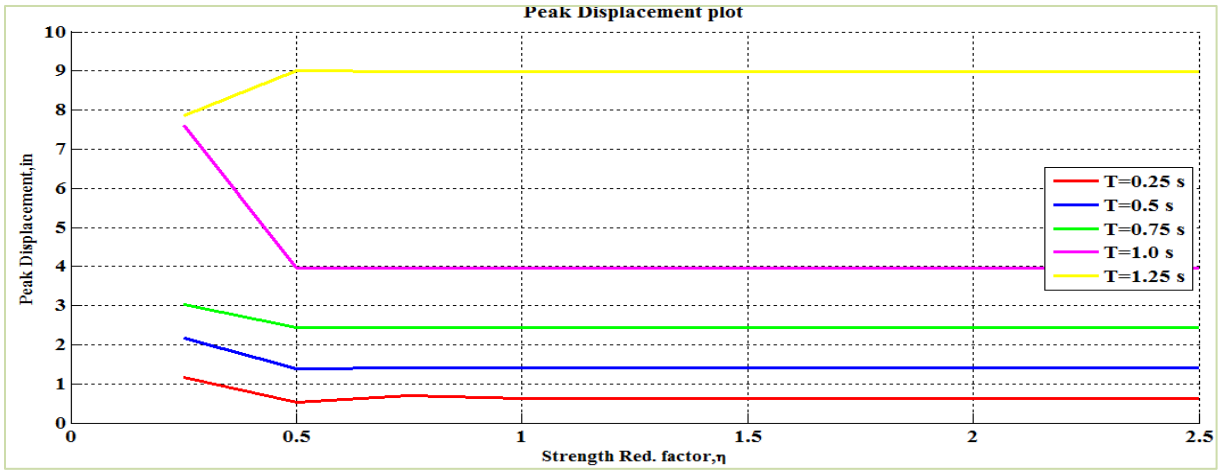

Figure 7-42 2D Peak Displacement plot for Ground Motion 4 (Bilinear Behavior)

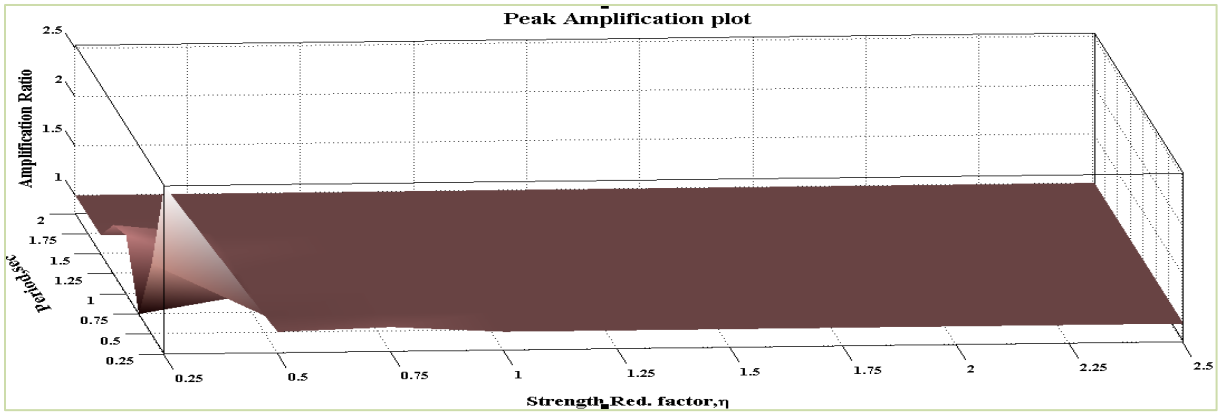

Figure 7-43 3D Peak Amplification plot for Ground Motion 4 (Bilinear Behavior)

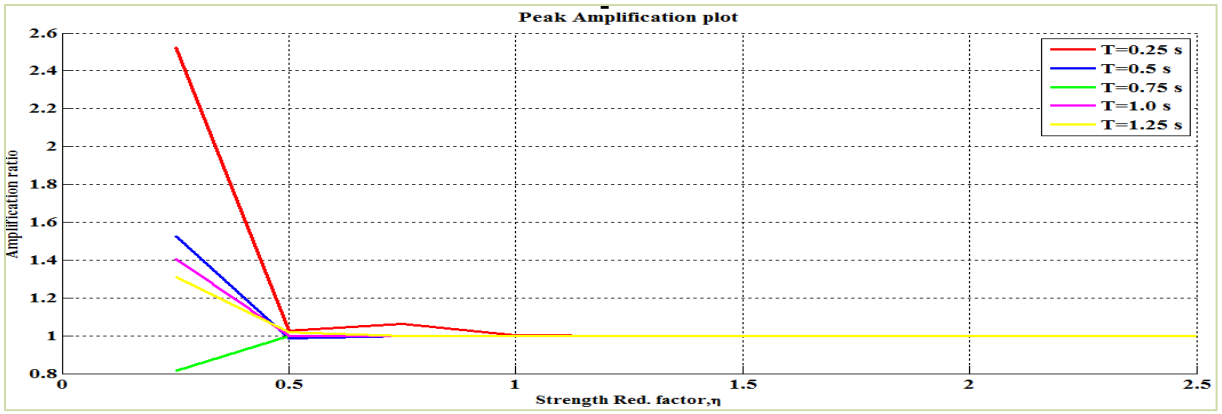

Figure 7-44 2D Peak Amplification plot for Ground Motion 4 (Bilinear Behavior)

The 3D and 2D peak displacement plot of the structural system incorporating elasto-plastic behavior is shown in Figures 7-45 and 7-46 respectively. The 2D peak displacement plot as shown in Figure 7-46 doesn`t have bumps (localized high points) in peak displacement. Hence, the amplification factor is expected to be equal to 1. It is observed from Figure 7-46 that the system becomes elastic for relatively low strength reduction factor.

The 3D and 2D peak amplification plot of the structural system incorporating bilinear elastic behavior is shown in Figures 7-47 and 7-48 respectively. It can be clearly seen from Figure 7-48 that the amplification factor for all periods is nearer to 1 which proves that the the moving resonance doesn`t have any effect on the structural systems incorporating bilinear elastic behavior. Since the dominant periods in the ground motion were decreasing with time rather than increasing, moving resonance did not have much effect.

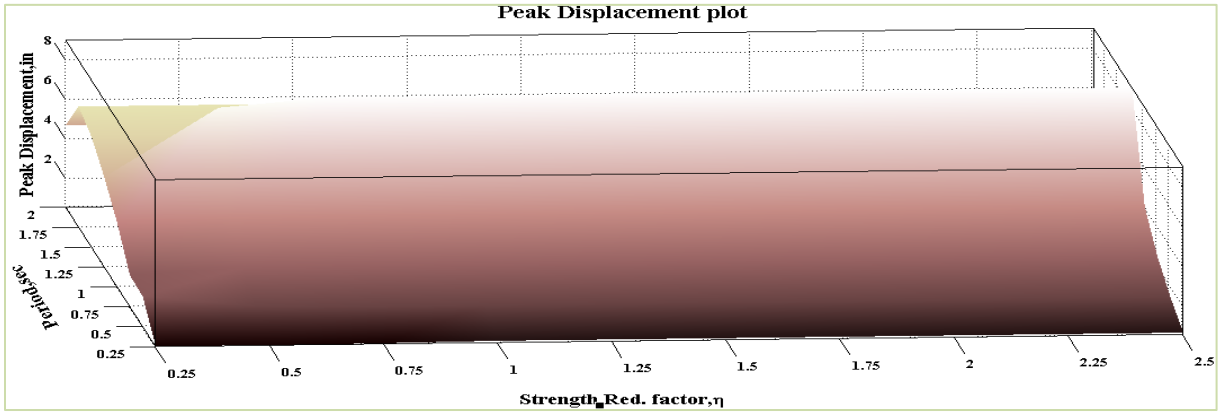

Figure 7-45 3D Peak Displacement plot for Ground Motion 4 (EPP Behavior)

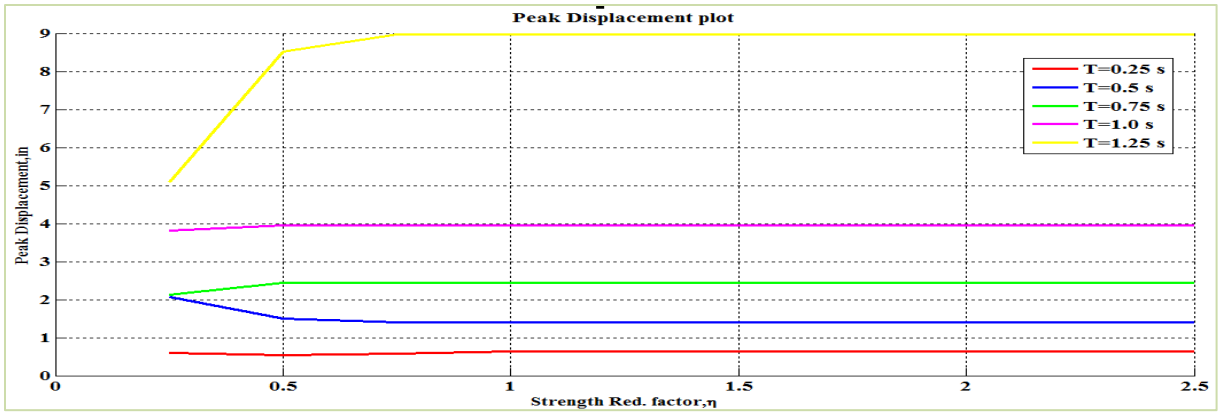

Figure 7-46 2D Peak Displacement plot for Ground Motion 4 (EPP Behavior)

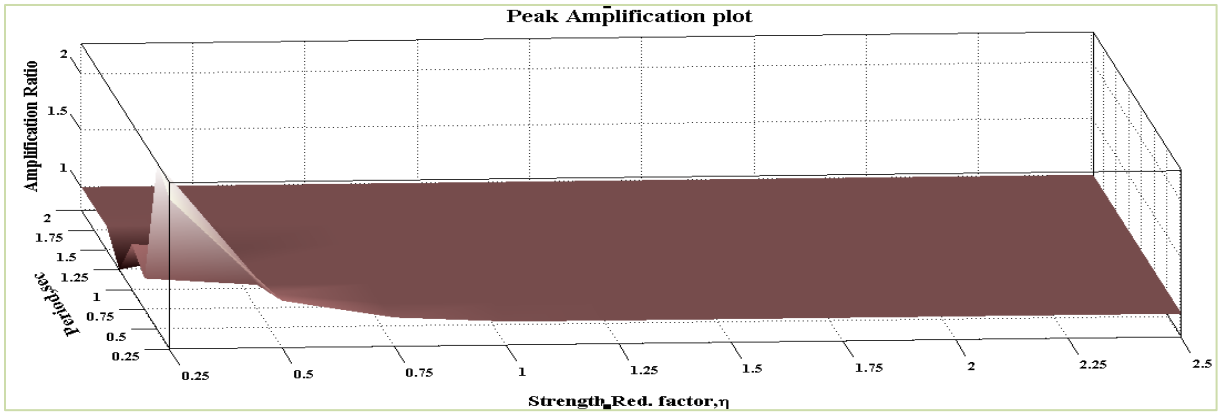

Figure 7-47 3D Peak Amplification plot for Ground Motion 4 (EPP Behavior)

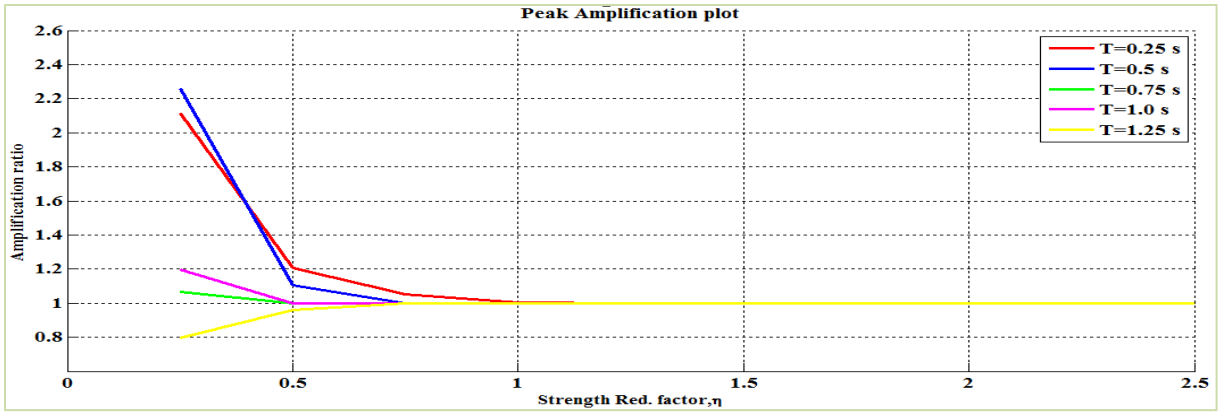

Figure 7-48 2D Peak Amplification plot for Ground Motion 4 (EPP Behavior)

Overall, it is concluded that this particular ground motion doesn`t creates moving resonance. The main reason is being the dominant periods in the ground motion were decreasing with time rather than increasing and this trend is significant. Also, both the systems are reaching elastic behavior for relatively very small strength values.

7.2.5 Ground Motion 5: Imperial Valley at Delta station

The acceleration time history and the acceleration response spectra for 2 % damping of the component 1 of Imperial valley earthquake at Delta station is shown in Figures 7-49 and 7-50 respectively. The 2D and 3D wavelet coefficient plot of this particular ground motion performed using Complex Morlet wavelet of band width 1 and frequency 1.5 is shown in Figures 7-51 and 7-52 respectively.

Figures 7-49 to 7-52 shows that this ground motion has lot of energy at many different periods and they have significant amplitude for a long period of time. It is a long ground motion with a lot of strong shaking.

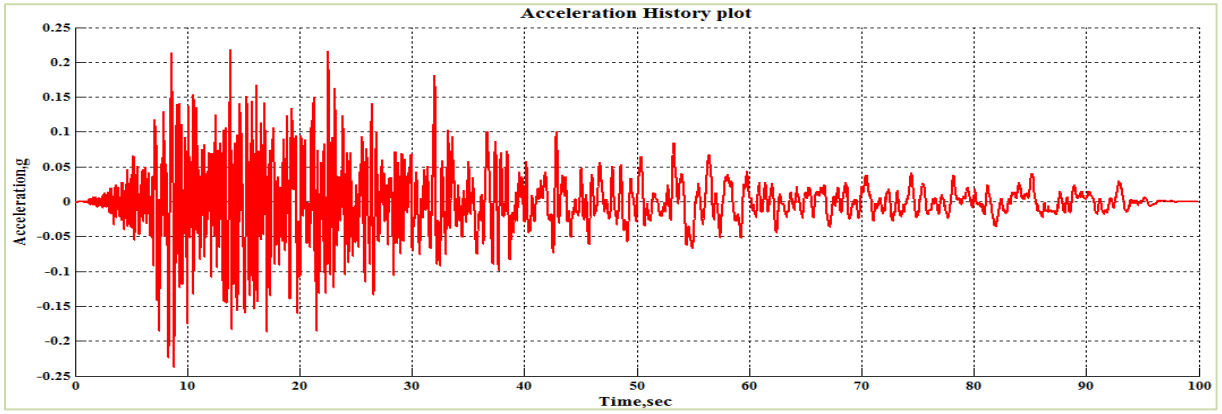

Figure 7-49 Acceleration Time History of Ground Motion 5 (Imperial Valley-Delta)

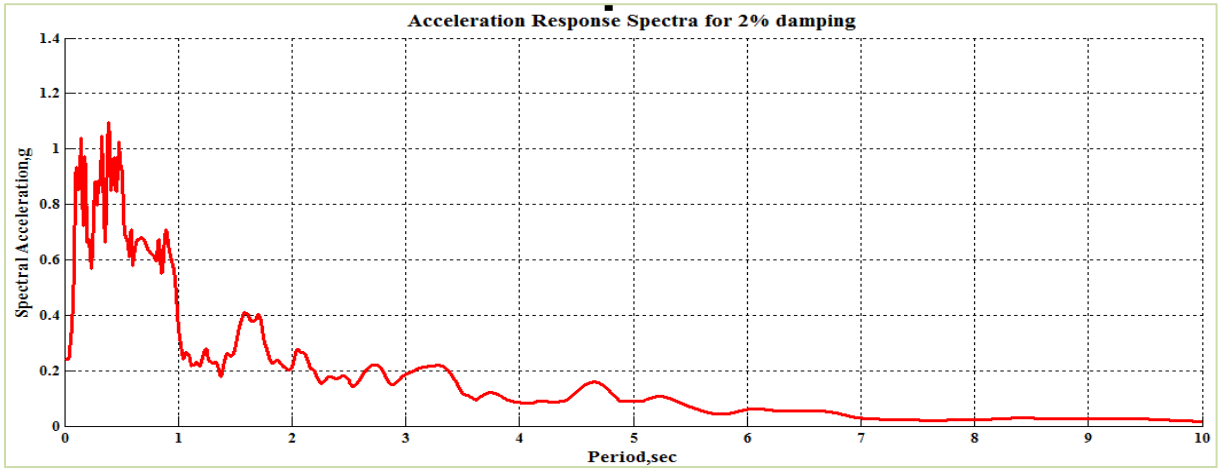

Figure 7-50 Acceleration Response Spectra for 2% Damping

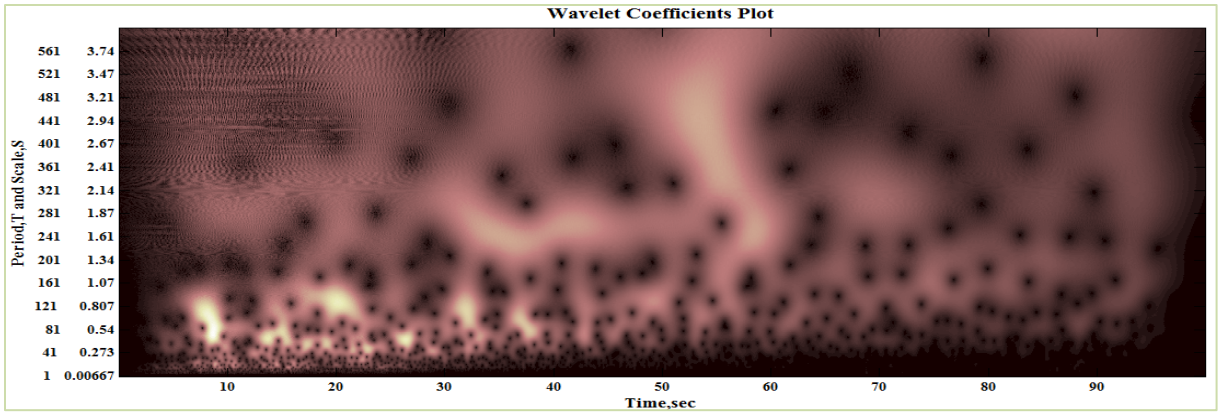

Figure 7-51 2D Wavelet coefficients plot of Ground Motion 5 (Imperial Valley-Delta)

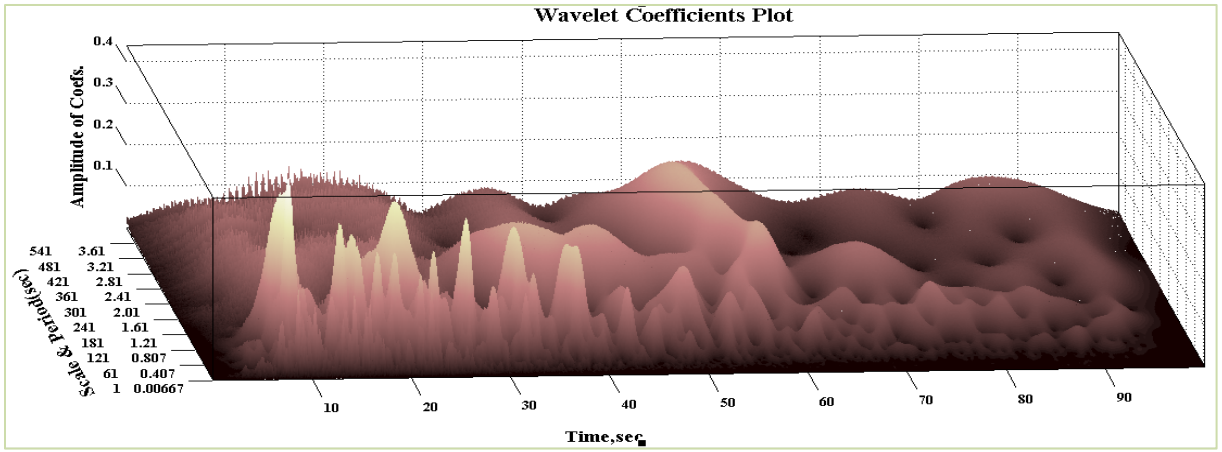

Figure 7-52 3D Wavelet coefficients plot of Ground Motion 5 (Imperial Valley-Delta)

The 3D and 2D peak displacement plot of the structural system incorporating bilinear elastic behavior is shown in Figures 7-53 and 7-54 respectively. The 2D peak displacement plot for bilinear elastic behavior as shown in Figure 7-54 doesn`t have any bumps in peak displacement. Hence it is expected that the amplification factor will be equal to 1 for these combinations of period and strength.

The 3D and 2D peak amplification plot of the structural system incorporating bilinear elastic behavior is shown in Figures 7-55 and 7-56 respectively. It is observed from Figure 7-56 that the amplification factor for all periods is nearer to 1 which proves that the the moving resonance doesn`t have any effect on the structural systems incorporating bilinear elastic behavior.

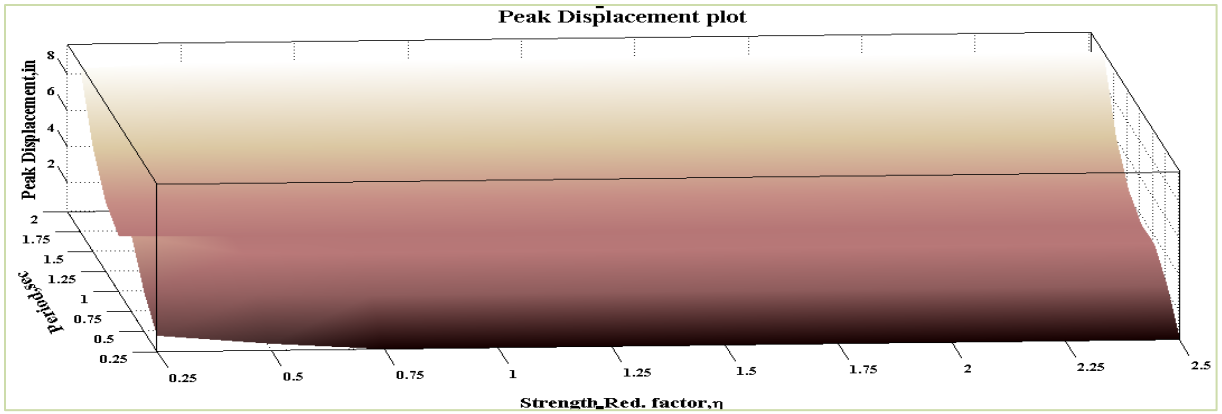

Figure 7-53 3D Peak Displacement plot for Ground Motion 5 (Bilinear Behavior)

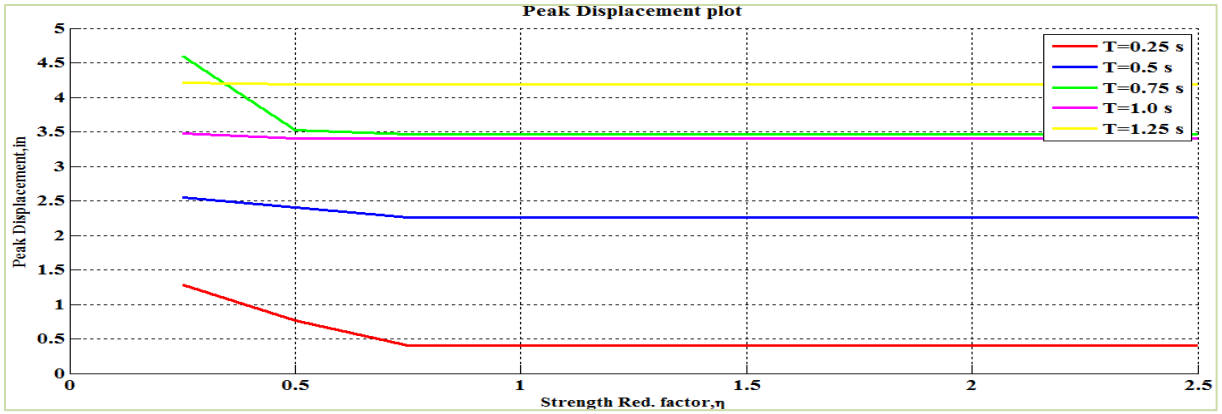

Figure 7-54 2D Peak Displacement plot for Ground Motion 5 (Bilinear Behavior)

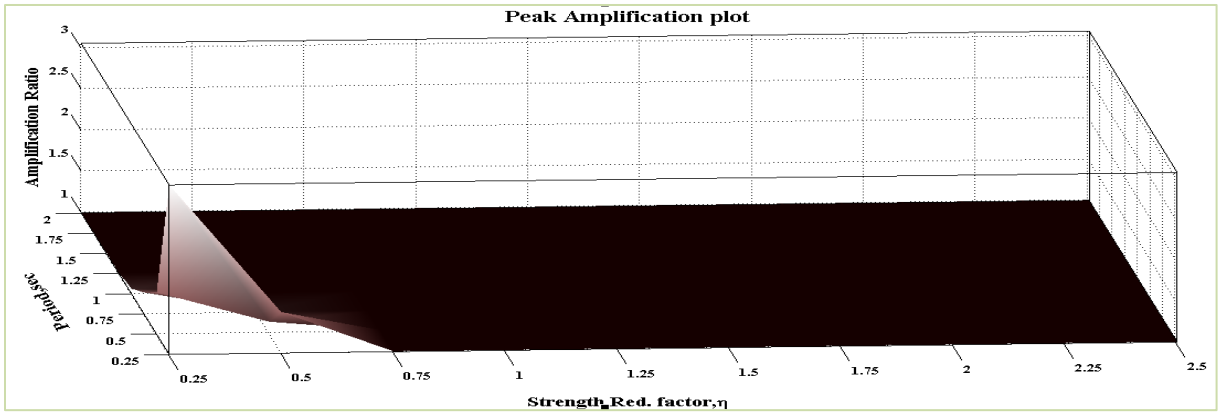

Figure 7-55 3D Peak Amplification plot for Ground Motion 5 (Bilinear Behavior)

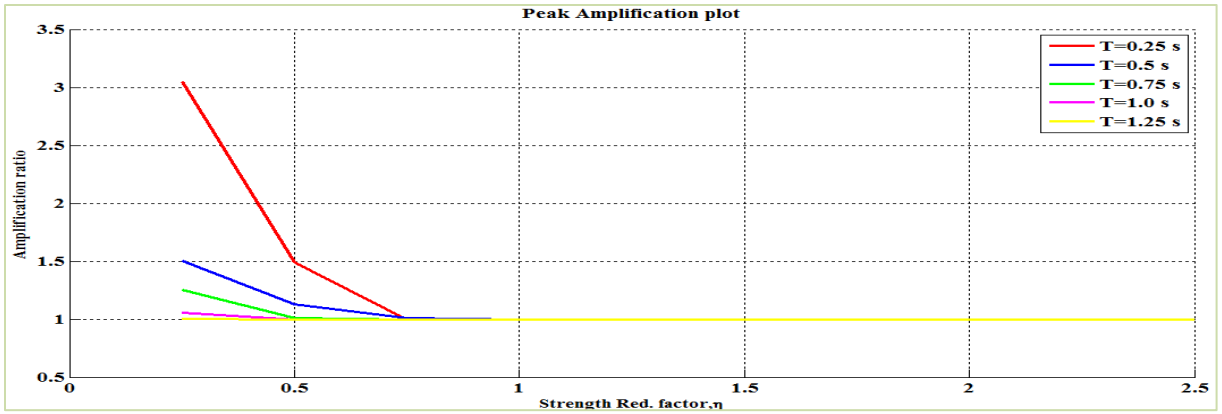

Figure 7-56 2D Peak Amplification plot for Ground Motion 5 (Bilinear Behavior)

The 3D and 2D peak displacement plot of the structural system incorporating elasto-plastic behavior is shown in Figures 7-57 and 7-58 respectively. The 2D peak displacement plot for bilinear elastic behavior as shown in Figure 7-58 doesn`t have any significant bumps in peak displacement. Though there is a bump in peak displacement at (T_0,η) value of (0.75,0.50), it is not prevalent.Hence it is expected that the amplification factor will be equal to 1 for these combinations of period and strength.

The 3D and 2D peak amplification plot of the structural system incorporating bilinear elastic behavior is shown in Figures 7-59 and 7-60 respectively. It is observed from Figure 7-60 that the amplification factor for all periods is nearer to 1 which proves that the the moving resonance doesn`t have any effect on the structural systems incorporating elasto-plastic behavior.

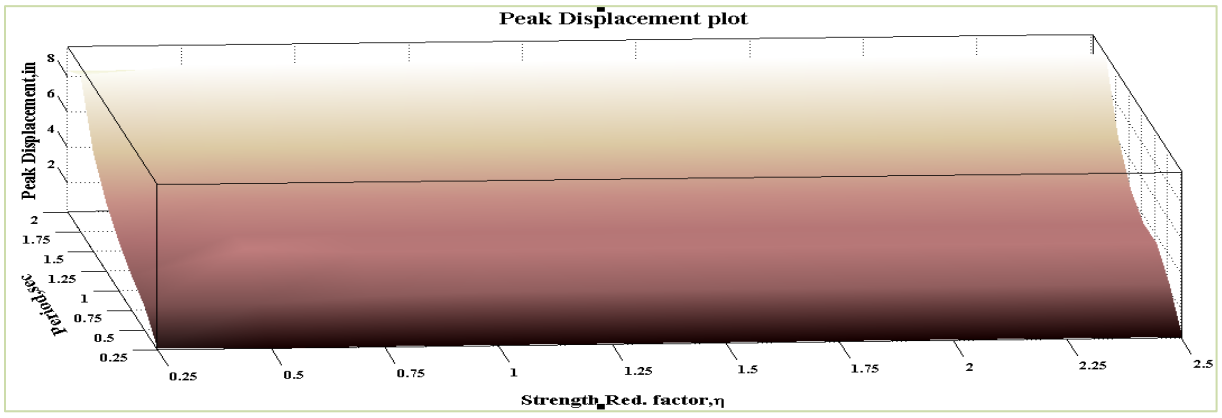

Figure 7-57 3D Peak Displacement plot for Ground Motion 5 (Elasto-plastic Behavior)

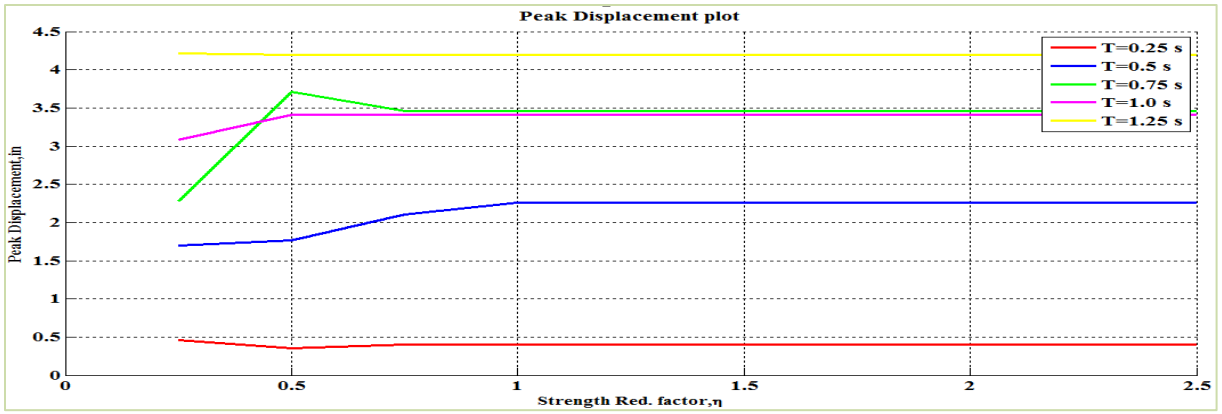

Figure 7-58 2D Peak Displacement plot for Ground Motion 5 (Elasto-plastic Behavior)

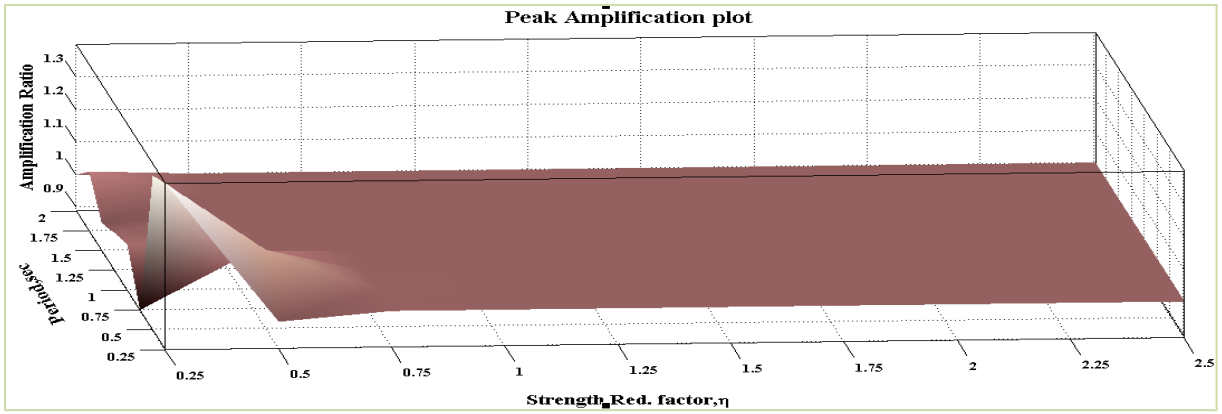

Figure 7-59 2D Peak Amplification plot for Ground Motion 5 (EPP Behavior)

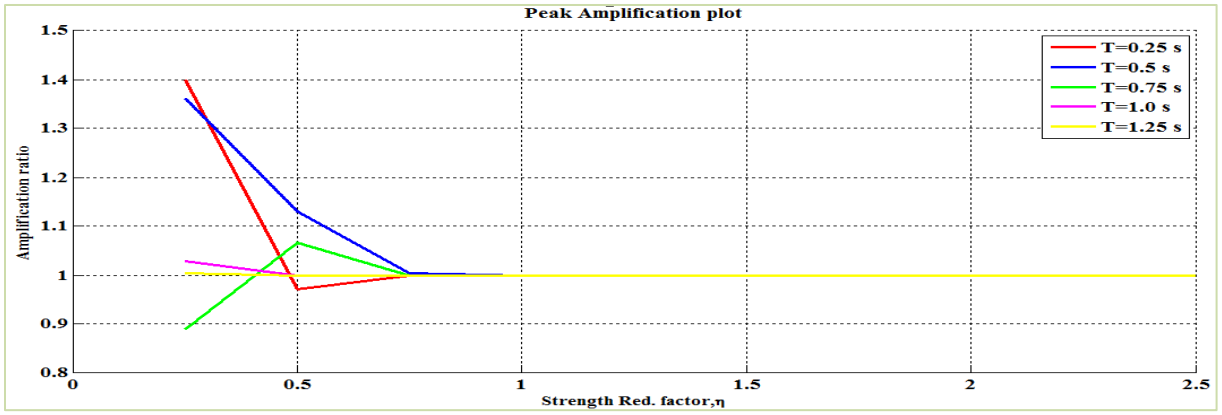

Figure 7-60 2D Peak Amplification plot for Ground Motion 5 (EPP Behavior)

Hence, it is concluded that though the ground motion has a strong shaking, it doesn`t create moving resonance because the intensity of the energy was well spread out in frequency and time.

7.2.6 Ground Motion 6: Imperial Valley at El Centro station

The acceleration time history and the acceleration response spectra for 2 % damping of the component 1 of Imperial valley earthquake at El Centro station is shown in Figures 7-61 and 7-62 respectively. The 2D and 3D wavelet coefficient plot of this particular ground motion performed using Complex Morlet wavelet of band width 1 and frequency 1.5 is shown in Figures 7-63 and 7-64 respectively.

The salient features of this ground motion which can be seen from Figures 7-61 to 7-64 is that there is burst of energy with period of 0.4 sec at 6 sec and then a fairly steady strong shaking with period of 0.25 sec between 7 and 12 sec. The fact that the dominant frequency content goes down as time increases is similar to ground motion 4 and then remains fairly constant similar to ground motion 2. So a similar result of not having moving resonance is expected.

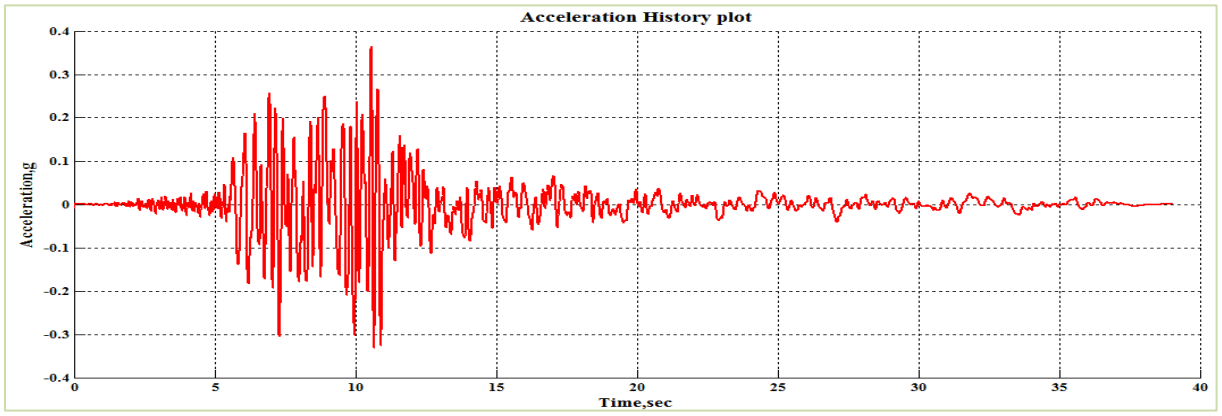

Figure 7-61 Acceleration Time History of Ground Motion 6 (Imperial Valley-El Centro)

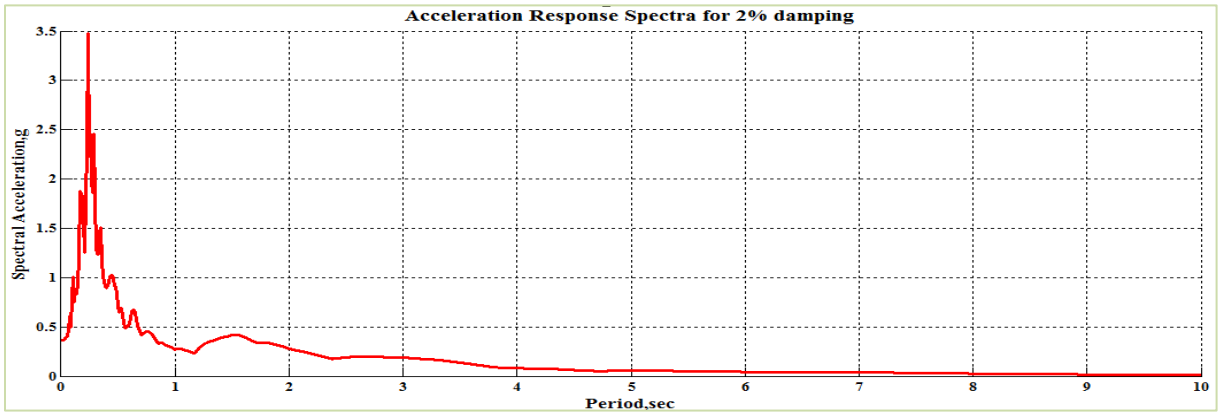

Figure 7-62 Acceleration Response Spectra for 2% Damping

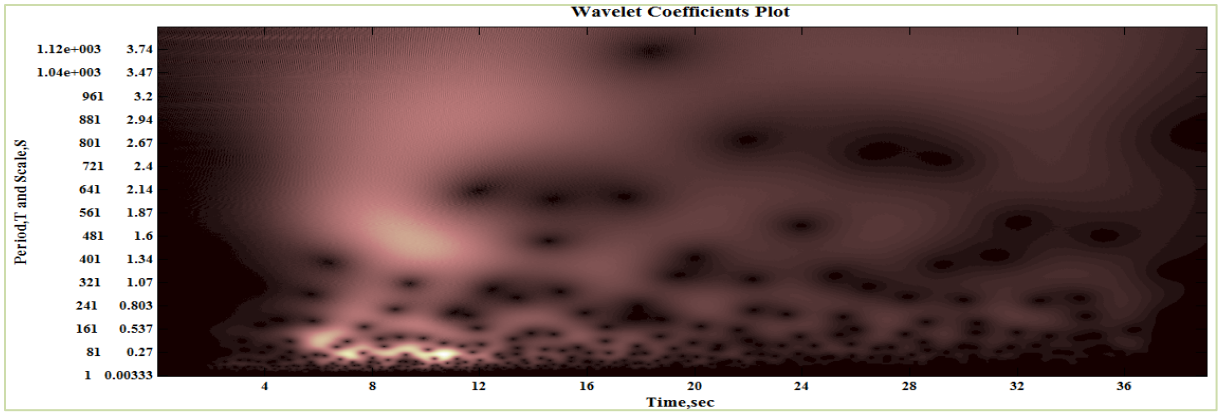

Figure 7-63 2D Wavelet coefficients plot of Ground Motion 6 (Imperial Valley-El Centro)

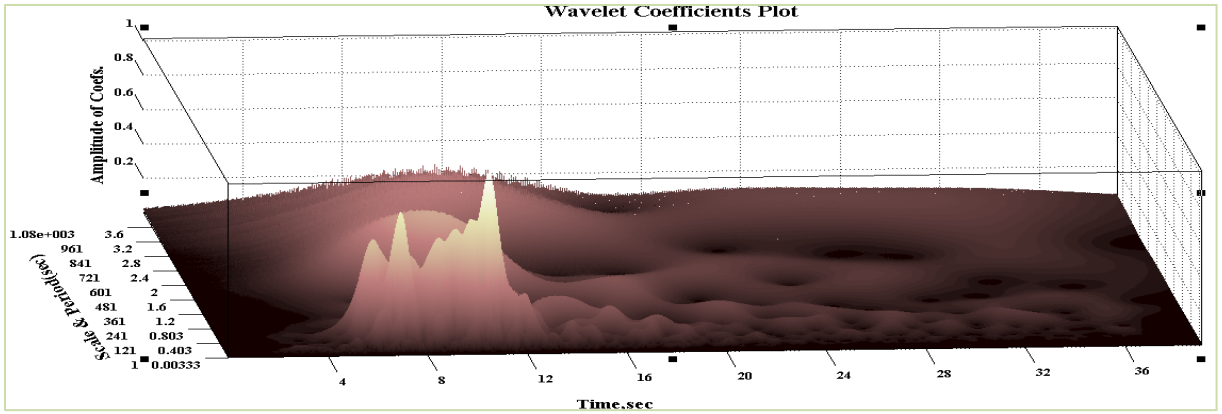

Figure 7-64 3D Wavelet coefficients plot of Ground Motion 6 (Imperial Valley-El Centro)

The 3D and 2D peak displacement plot of the structural system incorporating bilinear elastic behavior is shown in Figures 7-65 and 7-66 respectively. The 2D peak displacement plot as shown in Figure 7-66 have bumps in peak displacement at corresponding (T_0,η) values of (0.25,0.75) and (0.25,1.5).This localized increase in peak displacement is hypothesized to be the result of occurrence of moving resonance and hence amplification factor greater than 1 is expected for these combinations of period and strength.

The 3D and 2D peak amplification plot of the structural system incorporating bilinear elastic behavior is shown in Figures 7-67 and 7-68 respectively. It is observed from Figure 7-68 that the amplification values corresponding to (T_0,η) values of (0.25,0.75) and (0.25,1.5) (at similar places where localized high points of peak displacement were observed in Figure 7-66) are greater than 1 leading to the increase in peak displacement. This increase in peak displacement is considered to be the effect of moving resonance.

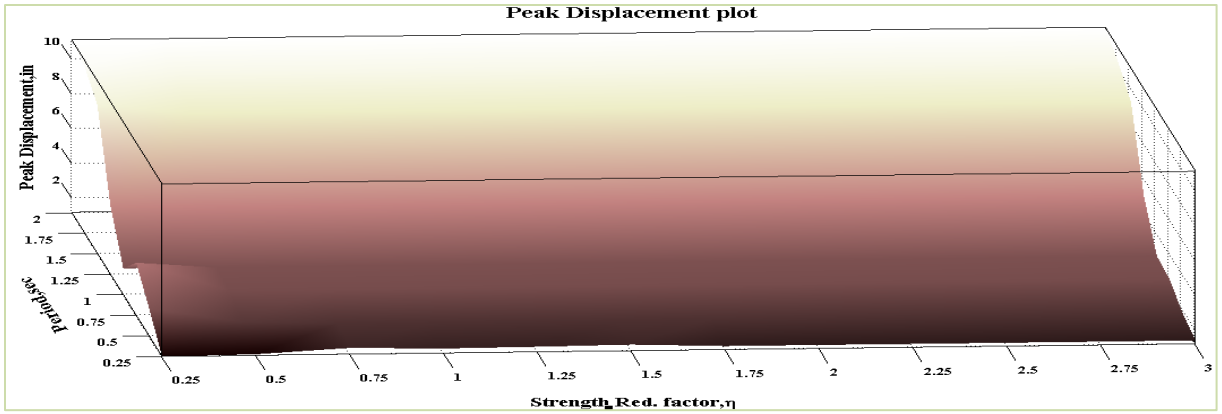

Figure 7-65 3D Peak Displacement plot for Ground Motion 6 (Bilinear Behavior)

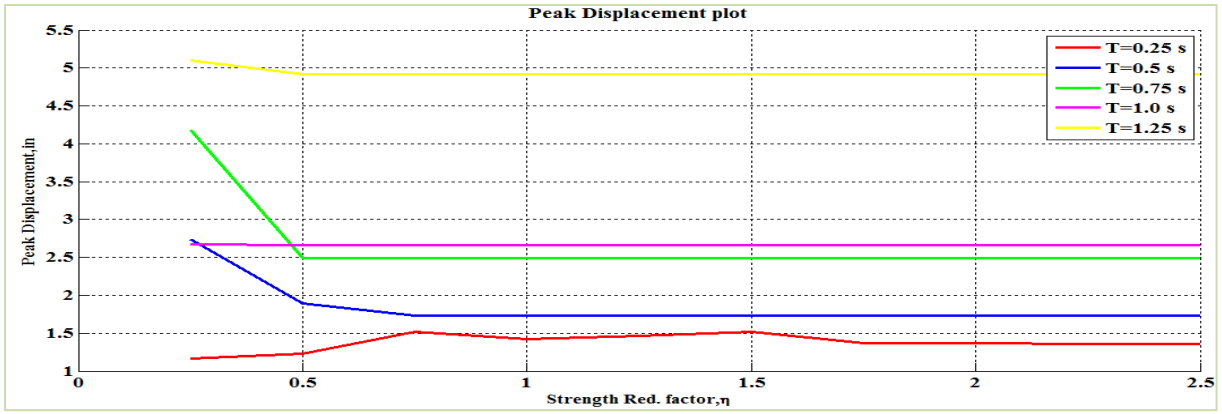

Figure 7-66 2D Peak Displacement plot for Ground Motion 6 (Bilinear Behavior)

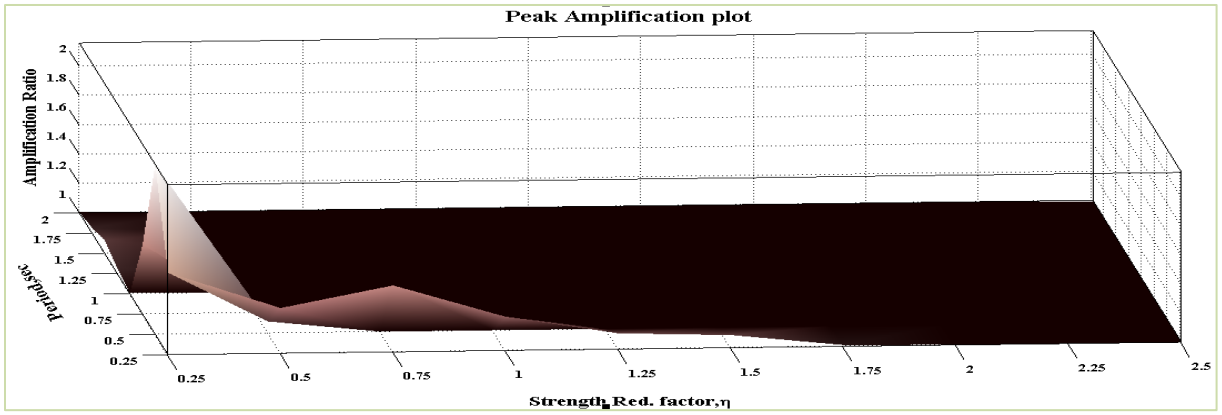

Figure 7-67 3D Peak Amplification plot for Ground Motion 6 (Bilinear Behavior)

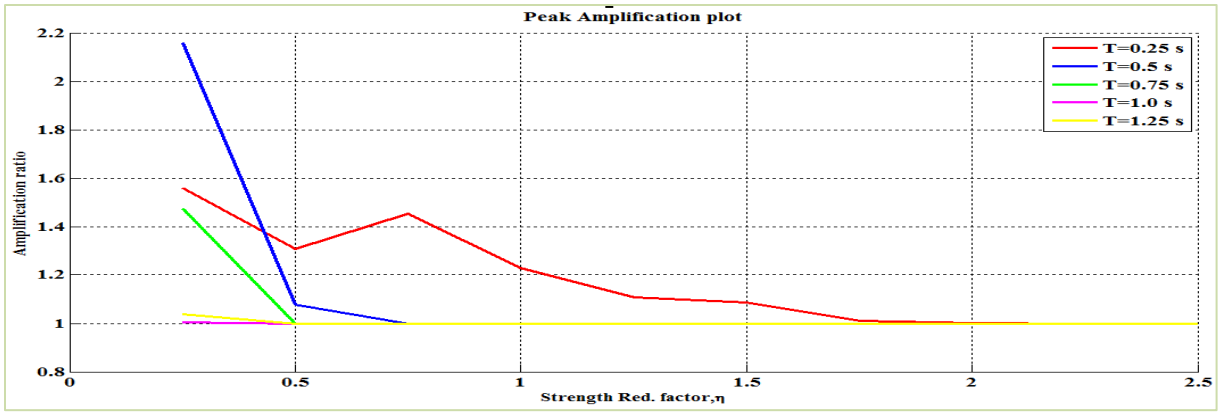

Figure 7-68 2D Peak Amplification plot for Ground Motion 6 (Bilinear Behavior)

The 3D and 2D peak displacement plot of the structural system incorporating elasto-plastic behavior is shown in Figures 7-69 and 7-70 respectively. The 2D peak displacement plot as shown in Figure 7-70 have bumps in peak displacement at corresponding (T_0,η) values of (0.25,0.75) and (0.25,1.75).This localized increase in peak displacement is hypothesized to be the result of occurrence of moving resonance and hence amplification factor greater than 1 is expected for these combinations of period and strength.

The 3D and 2D peak amplification plot of the structural system incorporating elasto-plastic behavior is shown in Figures 7-71 and 7-72 respectively. It is observed from Figure 7-72 that the amplification values corresponding to (T_0,η) values of (0.25,0.75) and (0.25,1.75) (at similar places where localized high points of peak displacement were observed in Figure 7-70) are greater than 1 leading to the increase in peak displacement. This increase in peak displacement is considered to be the effect of moving resonance.

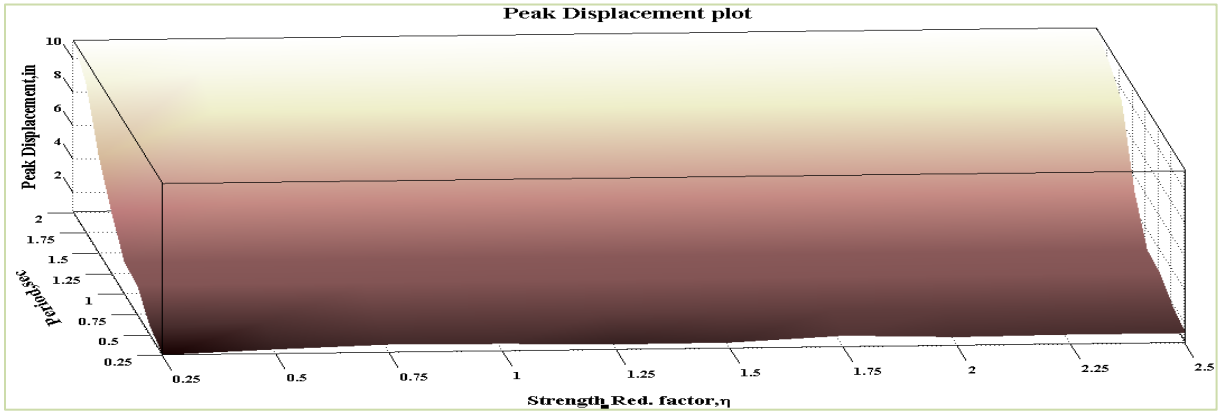

Figure 7-69 3D Peak Displacement plot for Ground Motion 6 (EPP Behavior)

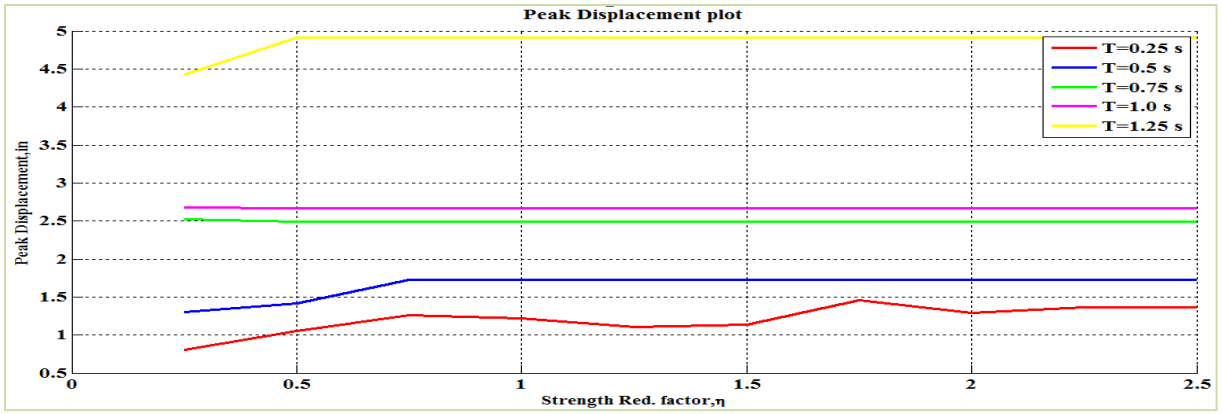

Figure 7-70 2D Peak Displacement plot for Ground Motion 6 (EPP Behavior)

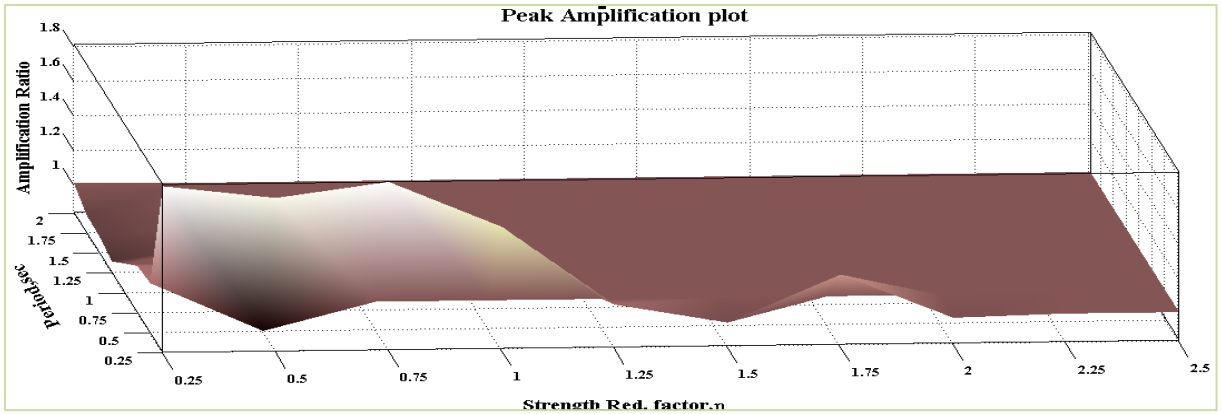

Figure 7-71 3D Peak Amplification plot for Ground Motion 6 (EPP Behavior)

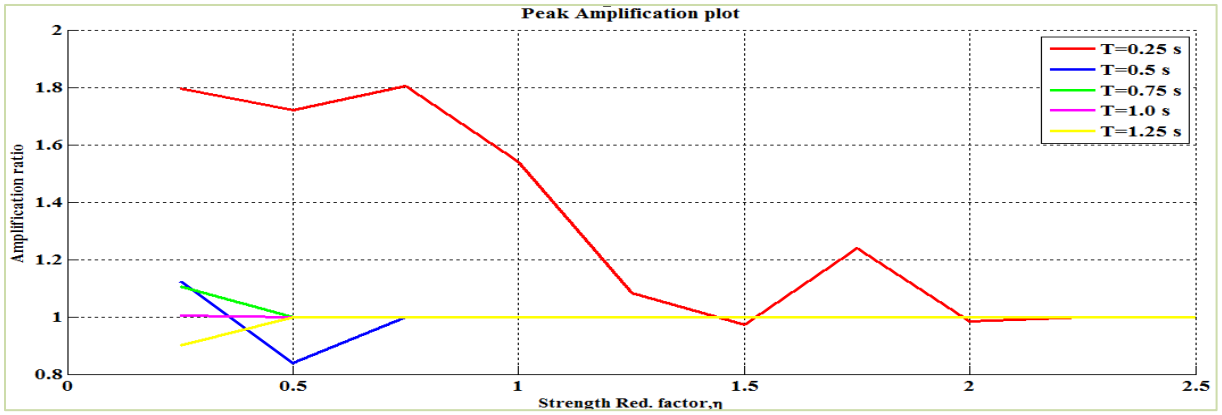

Figure 7-72 2D Peak Amplification plot for Ground Motion 6 (EPP Behavior)

Though the ground motion`s dominant frequency content shifts downwards and doesn`t have longer periods, amplification was observed indicating moving resonance. This is because even it shifts to lower periods, it has very strong frequency content unlike ground motion 4 which has very little frequency content when shifted to lower periods.

7.2.7 Ground Motion 7: Kobe Japan at Nishi Akashi station

The acceleration time history and the acceleration response spectra for 2 % damping of the component 1 of Kobe Japan earthquake at Nishi Akashi station is shown in Figures 7-73 and 7-74 respectively. The 2D and 3D wavelet coefficient plot of this particular ground motion performed using Complex Morlet wavelet of band width 1 and frequency 1.5 is shown in Figures 7-75 and 7-76 respectively.

The characteristic features of this ground motion which can be seen from Figures 7-73 to 7-74 is that it has concentrated energy in the time frequency space. There is a suitable increase in the dominant period during the concentrated energy portion. This character of the ground motion can be seen clearly from the acceleration response spectra shown in Figure 7-74. It is expected that the structures with slightly lower periods would be more susceptible to moving resonance because they are more likely to hit the hot spot as they become nonlinear.

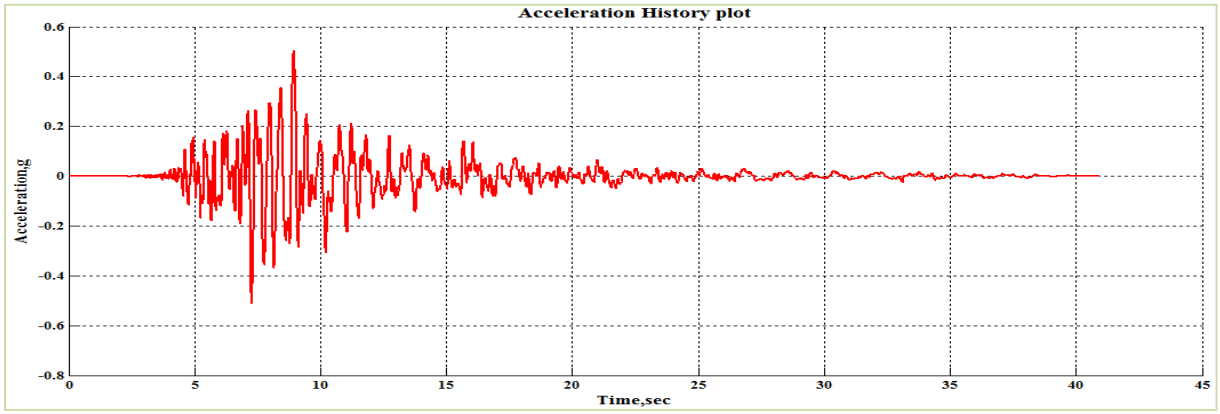

Figure 7-73 Acceleration Time History of Ground Motion 7 (Kobe Japan-Nishi Akashi)

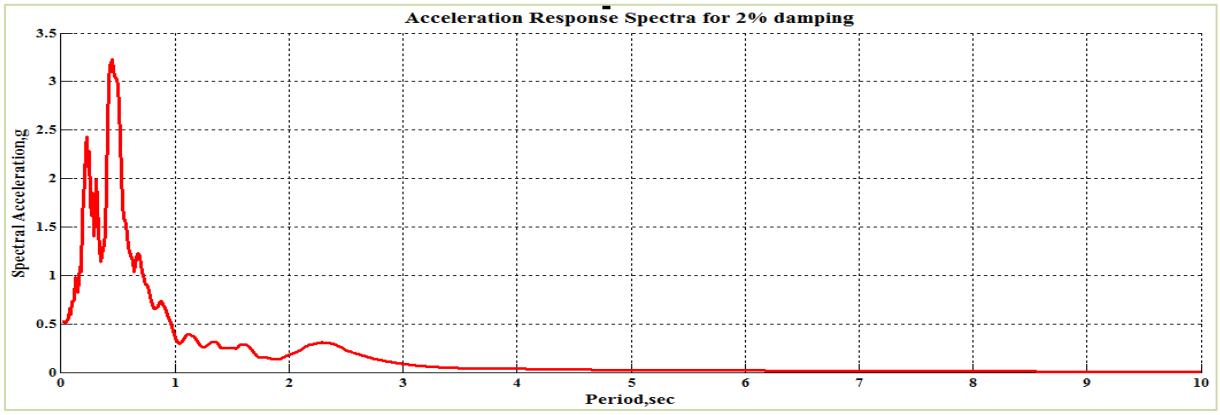

Figure 7-74 Acceleration Response Spectra for 2% Damping

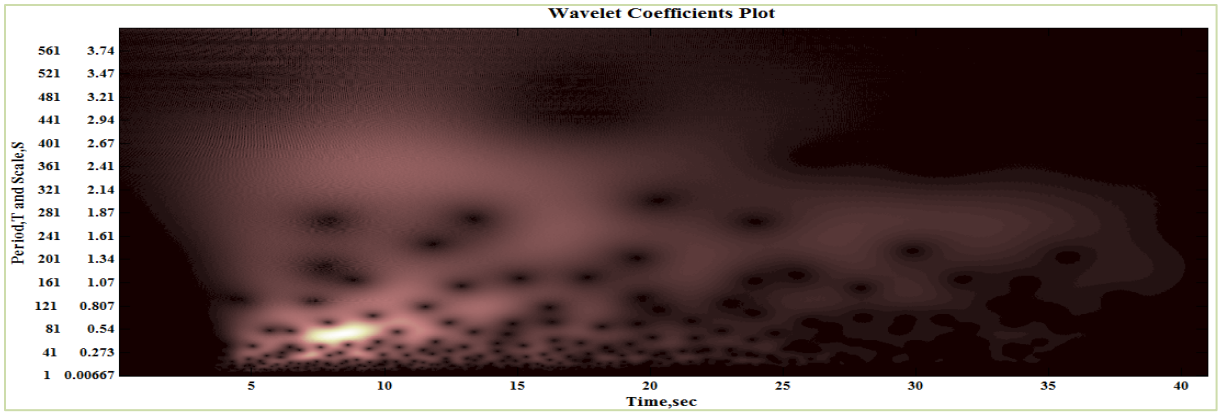

Figure 7-75 2D Wavelet coefficients plot of Ground Motion 7 (Kobe Japan-Nishi Akashi)

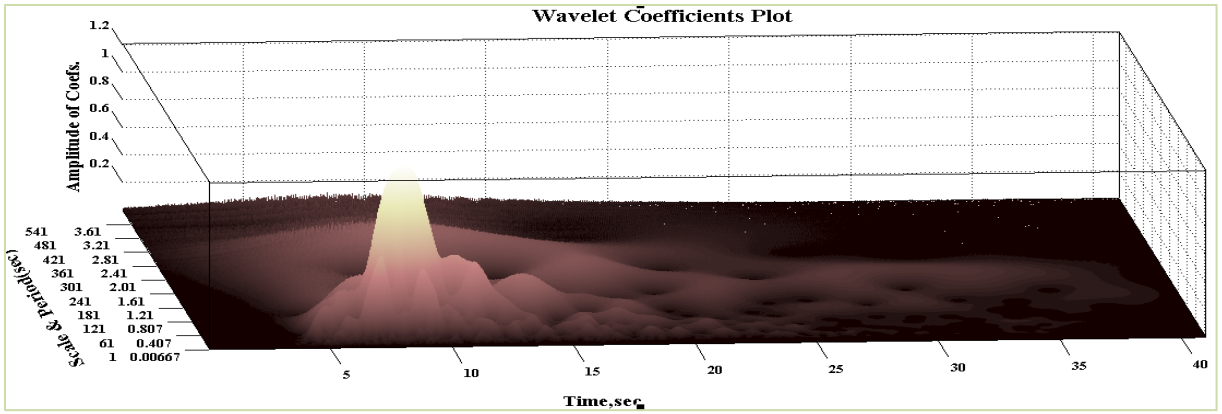

Figure 7-76 3D Wavelet coefficients plot of Ground Motion 7 (Kobe Japan-Nishi Akashi)

The 3D and 2D peak displacement plot of the structural system incorporating bilinear elastic behavior is shown in Figures 7-77 and 7-78 respectively. The 2D peak displacement plot as shown in Figure 7-78 have bumps in peak displacement at corresponding (T_0,η) values of (0.25,0.5),(0.25,1.75),(0.5,1.0) and (0.5,1.5).This localized increase in peak displacement is hypothesized to be the result of occurrence of moving resonance and hence amplification factor greater than 1 is expected for these combinations of period and strength.

The 3D and 2D peak amplification plot of the structural system incorporating bilinear elastic behavior is shown in Figures 7-79 and 7-80 respectively. It is observed from Figure 7-80 that the amplification values corresponding to (T_0,η) values of (0.25,0.5),(0.25,1.75),(0.5,1.0) and (0.5,1.5) (at similar places where localized high points of peak displacement were observed in Figure 7-78) are greater than 1 leading to the increase in peak displacement. This increase in peak displacement is considered to be the effect of moving resonance.

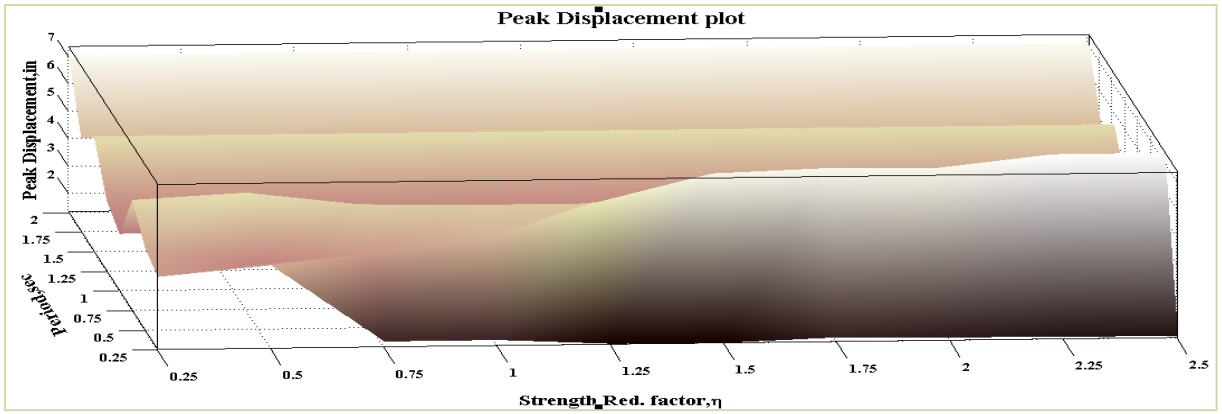

Figure 7-77 3D Peak Displacement plot for Ground Motion 7 (Bilinear Behavior)

Figure 7-78 2D Peak Displacement plot for Ground Motion 7 (Bilinear Behavior)

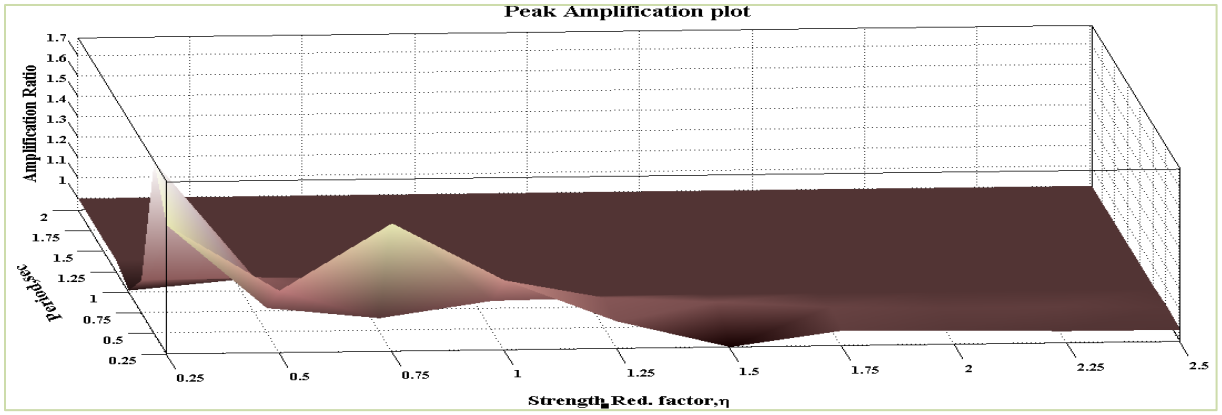

Figure 7-79 3D Peak Amplification plot for Ground Motion 7 (Bilinear Behavior)

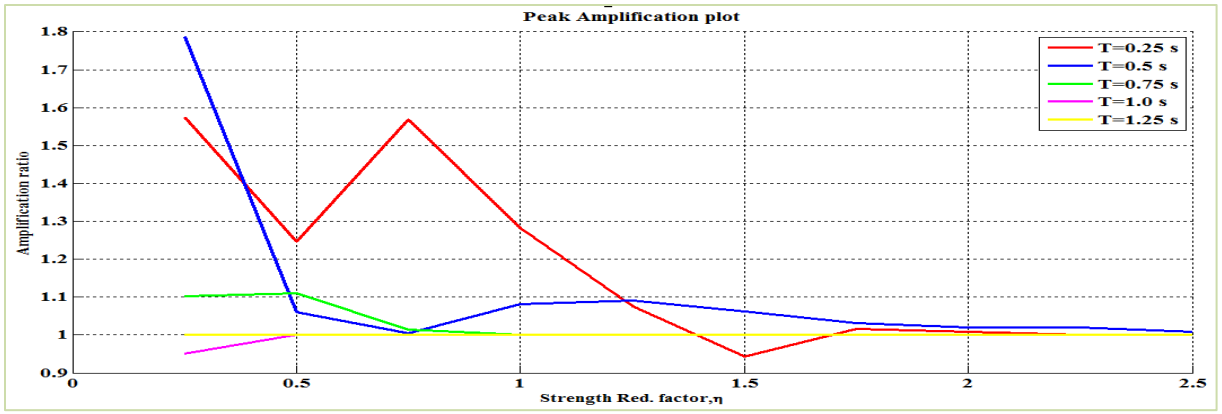

Figure 7-80 2D Peak Amplification plot for Ground Motion 7 (Bilinear Behavior)

The 3D and 2D peak displacement plot of the structural system incorporating elasto-plastic behavior is shown in Figures 7-81 and 7-82 respectively. The 2D peak displacement plot as shown in Figure 7-82 have bumps in peak displacement at corresponding (T_0,η) values of (0.25,1.5),(0.5,1.25) and(0.5,2.0). This localized increase in peak displacement is hypothesized to be the result of occurrence of moving resonance and hence amplification factor greater than 1 is expected for these combinations of period and strength.

The 3D and 2D peak amplification plot of the structural system incorporating elasto-plastic behavior is shown in Figures 7-83 and 7-84 respectively. It is observed from Figure 7-84 that the amplification values corresponding to (T_0,η) values of (0.25,1.5),(0.5,1.25) and(0.5,2.0) (at similar places where localized high points of peak displacement were observed in Figure 7-82) are greater than 1 leading to the increase in peak displacement. This increase in peak displacement is considered to be the effect of moving resonance. It is interesting that this ground motion has larger amplification factors for the EPP system than BE system.

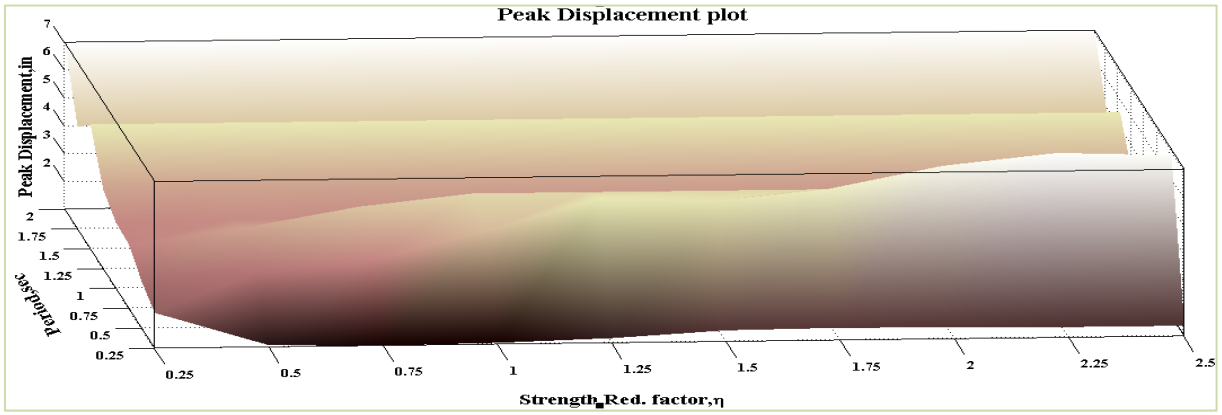

Figure 7-81 3D Peak Displacement plot for Ground Motion 7 (EPP Behavior)

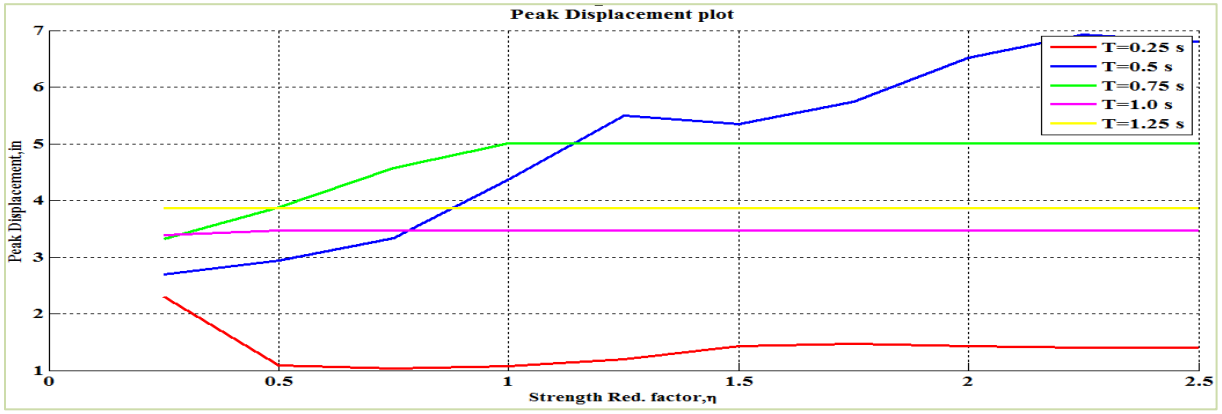

Figure 7-82 3D Peak Displacement plot for Ground Motion 7 (EPP Behavior)

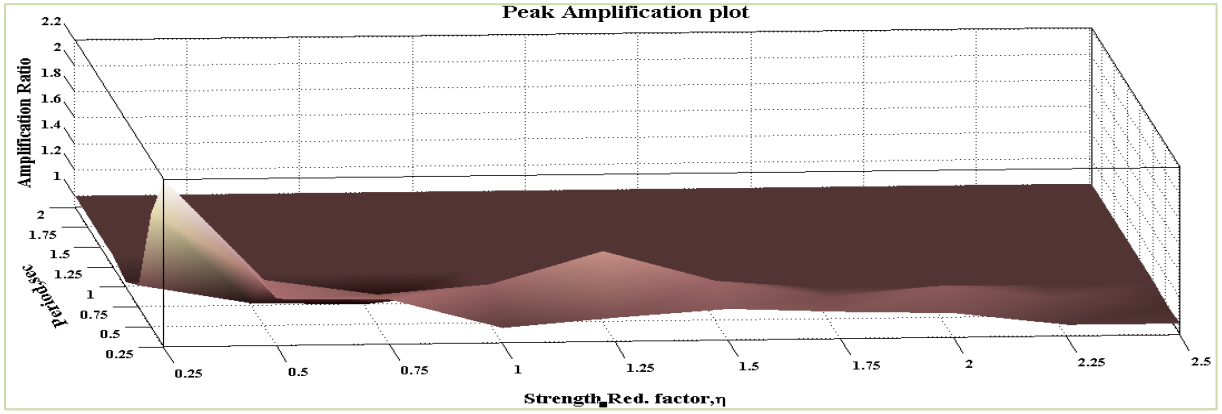

Figure 7-83 3D Peak Amplification plot for Ground Motion 7 (EPP Behavior)

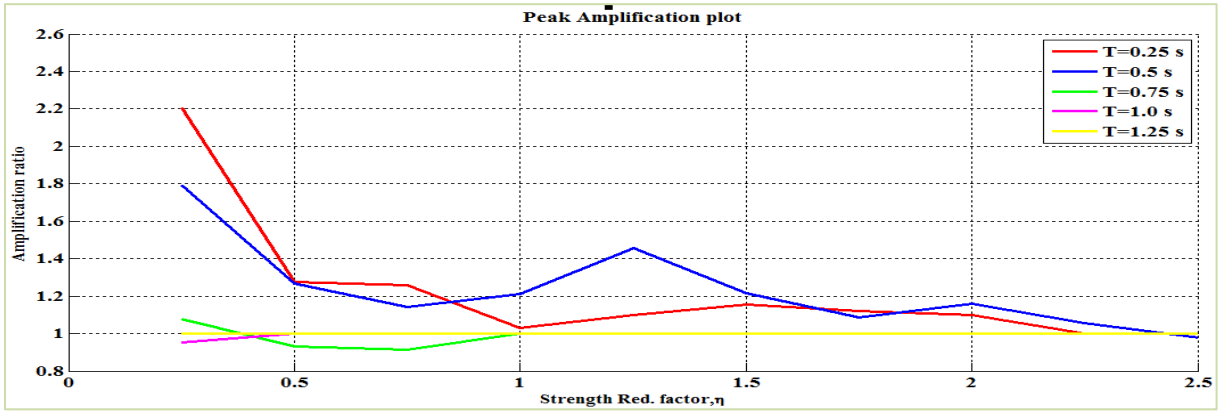

Figure 7-84 2D Peak Amplification plot for Ground Motion 7 (EPP Behavior)

The energy in the ground motion was fairly concentrated with a subtle increase in period. The effect of moving resonance was not as strong as other ground motions. It is interesting that this ground motion has larger amplification factors for EPP system than BE system.

7.2.8 Ground Motion 8: Kobe Japan at Shin Osaka station

The acceleration time history and the acceleration response spectra for 2 % damping of the component 1 of Kobe Japan earthquake at Shin Osaka station is shown in Figures 7-85 and 7- 86 respectively. The 2D and 3D wavelet coefficient plot of this particular ground motion performed using Complex Morlet wavelet of band width 1 and frequency 1.5 is shown in Figures 7-87 and 7-88 respectively.

The salient features of this ground motion which can be seen from Figures 7-85 to 7-88 is that there are two dominant ridges of energy in the ground motion. The one with larger period is just slightly delayed compared to the lower period range. It might be expected that there would be some potential for moving resonance.

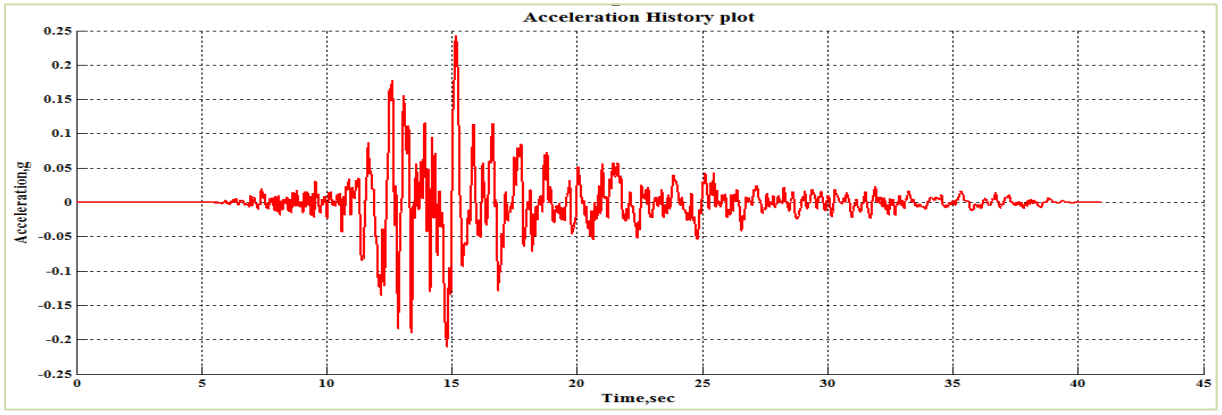

Figure 7-85 Acceleration Time History of Ground Motion 8 (Kobe Japan-Shin Osaka)

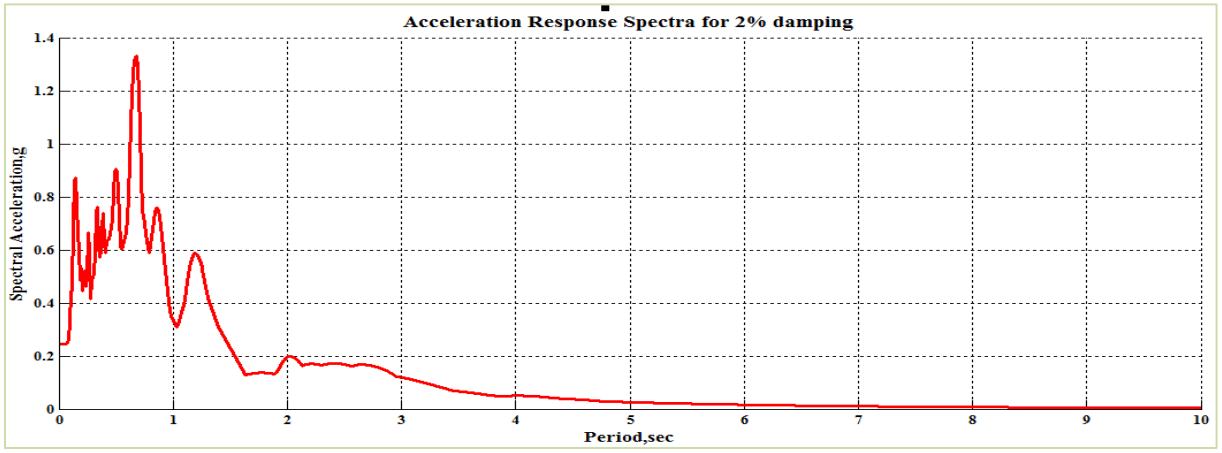

Figure 7-86 Acceleration Response Spectra for 2% Damping

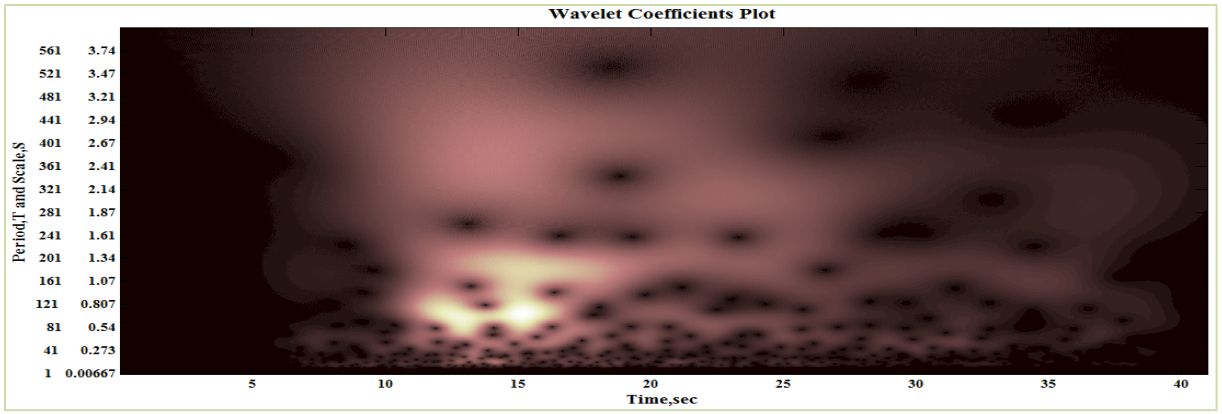

Figure 7-87 2D Wavelet coefficients plot of Ground Motion 8 (Kobe Japan-Shin Osaka)

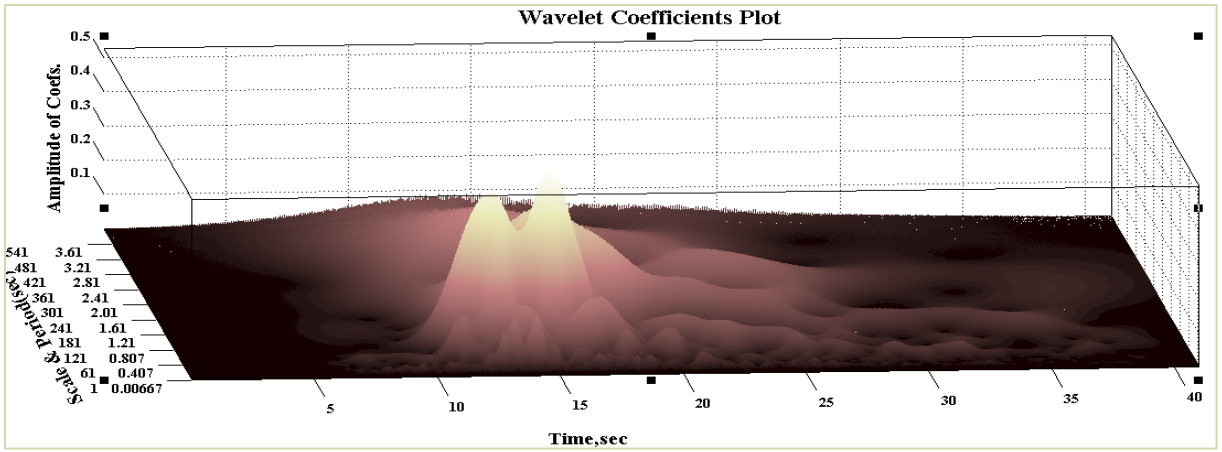

Figure 7-88 3D Wavelet coefficients plot of Ground Motion 8 (Kobe Japan-Shin Osaka)

The 3D and 2D peak displacement plot of the structural system incorporating bilinear elastic behavior is shown in Figures 7-89 and 7-90 respectively. The 2D peak displacement plot as shown in Figure 7-90 doesn`t have significant bumps (localized high points) in peak displacement. Hence, the amplification factor is expected to be equal to 1. It is observed from Figure 7-90 that the system becomes elastic for relatively low strength reduction factor.

The 3D and 2D peak amplification plot of the structural system incorporating bilinear elastic behavior is shown in Figures 7-91 and 7-92 respectively. It is observed from Figure 7-92 that the amplification factor for all periods is nearer to 1 which proves that the the moving resonance doesn`t have significant effect on the structural systems incorporating bilinear elastic behavior.

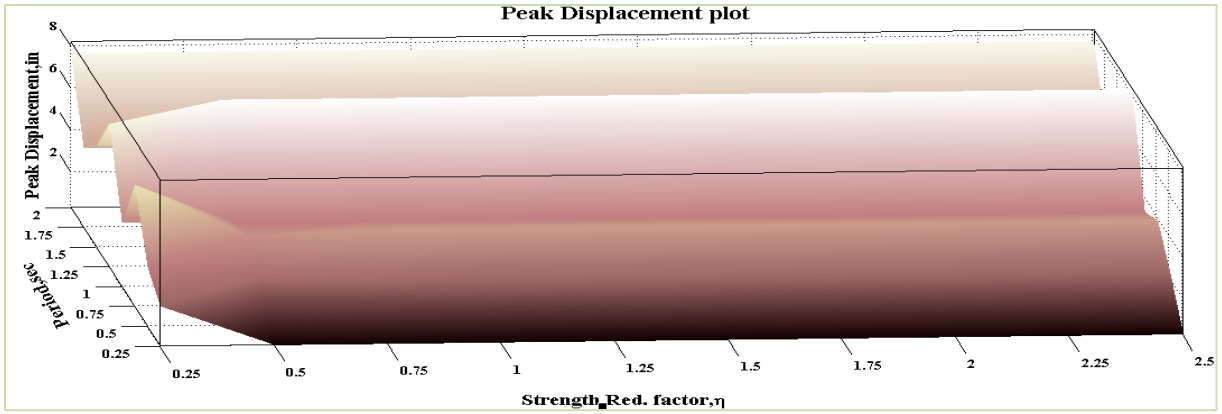

Figure 7-89 3D Peak Displacement plot for Ground Motion 8 (Bilinear Behavior)

Figure 7-90 2D Peak Displacement plot for Ground Motion 8 (Bilinear Behavior)

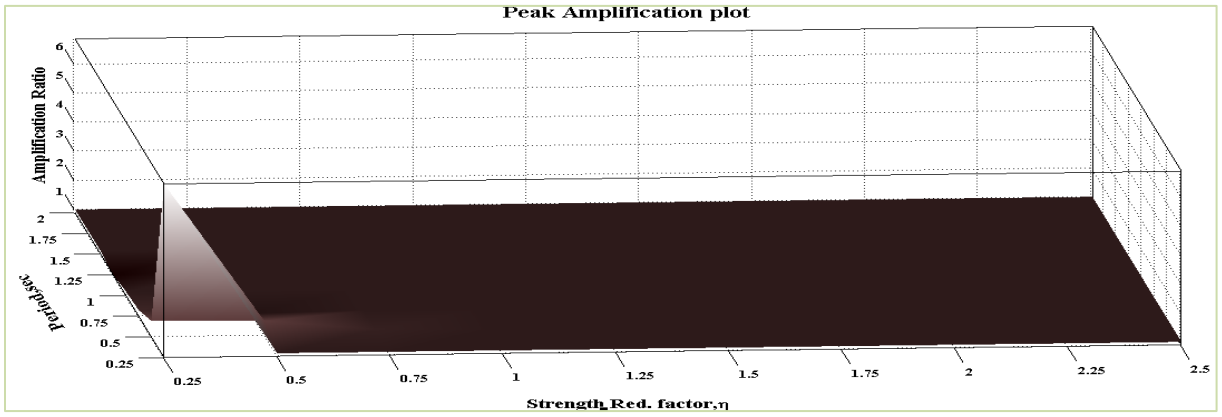

Figure 7-91 3D Peak Amplification plot for Ground Motion 8 (Bilinear Behavior)

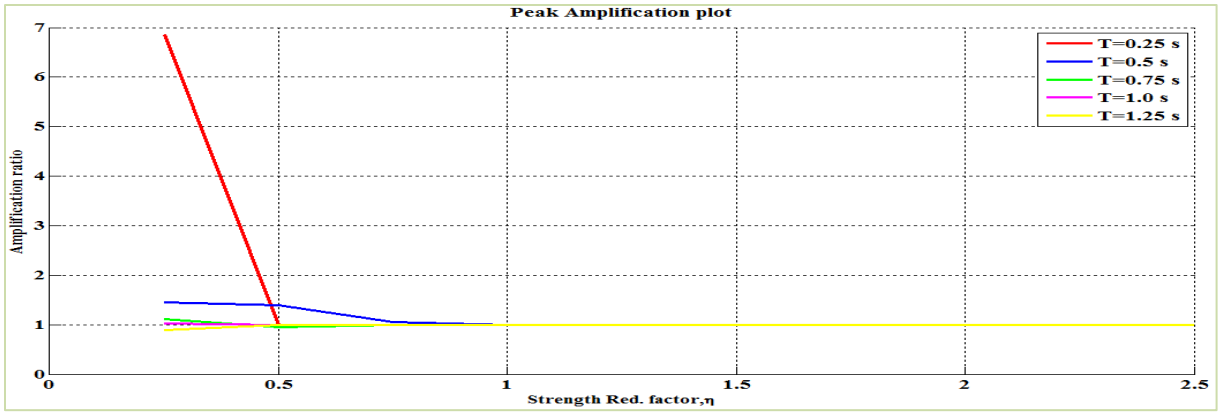

Figure 7-92 2D Peak Amplification plot for Ground Motion 8 (Bilinear Behavior)

The 3D and 2D peak displacement plot of the structural system incorporating elasto plastic behavior is shown in Figures 7-93 and 7-94 respectively. The 2D peak displacement plot as shown in Figure 7-94 doesn`t have significant bumps (localized high points) in peak displacement. Hence, the amplification factor is expected to be equal to 1. It is observed from Figure 7-92 that the system becomes elastic for relatively low strength reduction factor.

The 3D and 2D peak amplification plot of the structural system incorporating elasto plastic behavior is shown in Figures 7-93 and 7-94 respectively. It is observed from Figure 7-94 that the amplification factor for all periods is nearer to 1 which proves that the the moving resonance doesn`t have significant effect on the structural systems incorporating elasto plastic behavior.

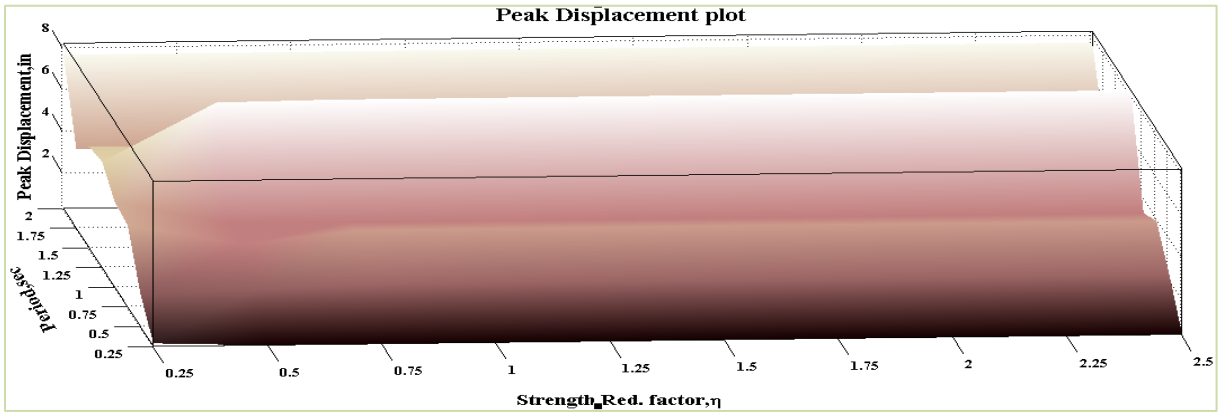

Figure 7-93 3D Peak Displacement plot for Ground Motion 8 (EPP Behavior)

Figure 7-94 2D Peak Displacement plot for Ground Motion 8 (EPP Behavior)

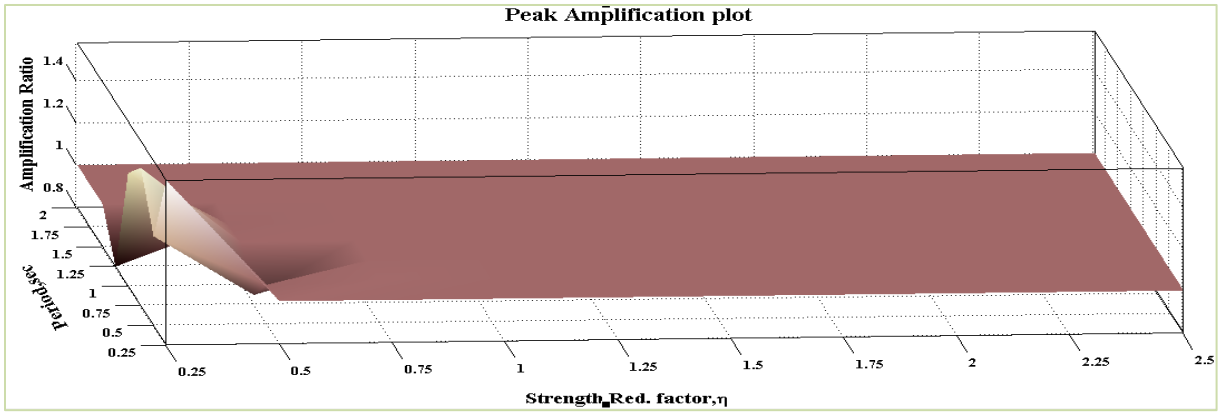

Figure 7-95 3D Peak Amplification plot for Ground Motion 8 (EPP Behavior)

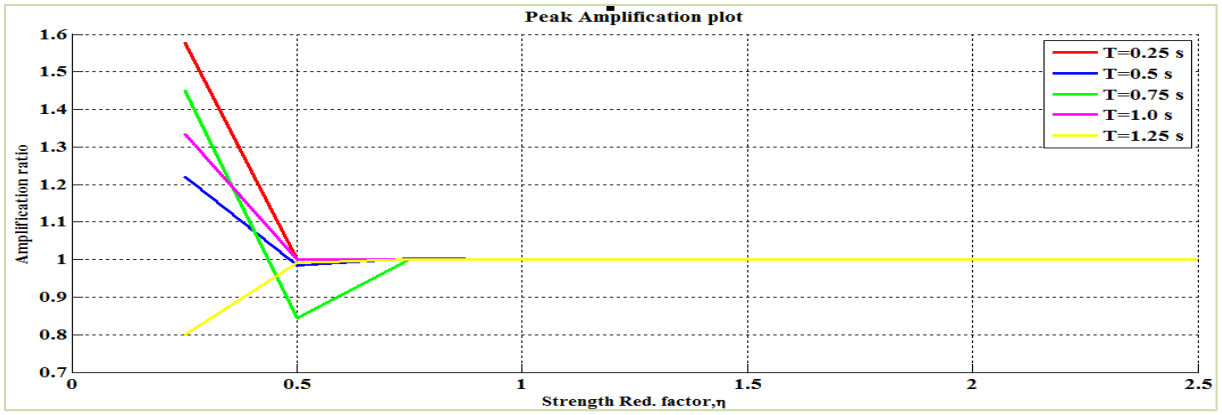

Figure 7-96 2D Peak Amplification plot for Ground Motion 8 (EPP Behavior)

This ground motion had two ridges of ground motion energy in which the higher period energy ridge was slightly delayed compared to the lower period ridge. Although, some effect of moving resonance was expected, only small effect was observed. It is observed that both the systems become elastic for relatively small strength values.

7.2.9 Ground Motion 9: Kocaeli, Turkey at Duzce station

The acceleration time history and the acceleration response spectra for 2 % damping of the component 1 of Kocaeli Turkey earthquake at Duzce station is shown in Figures 7-97 and 7-98 respectively. The 2D and 3D wavelet coefficient plot of this particular ground motion performed using Complex Morlet wavelet of band width 1 and frequency 1.5 is shown in Figures 7-99 and 7-100 respectively.

The interesting characteristics of this ground motion which can be observed from Figures 7-97 to 7-100 are that there is a late coming portion of energy in the ground motion at a higher period than the previous dominant period, but there is an 8 sec gap in between. It is interesting to know whether the gap in time will negate the importance of moving resonance.

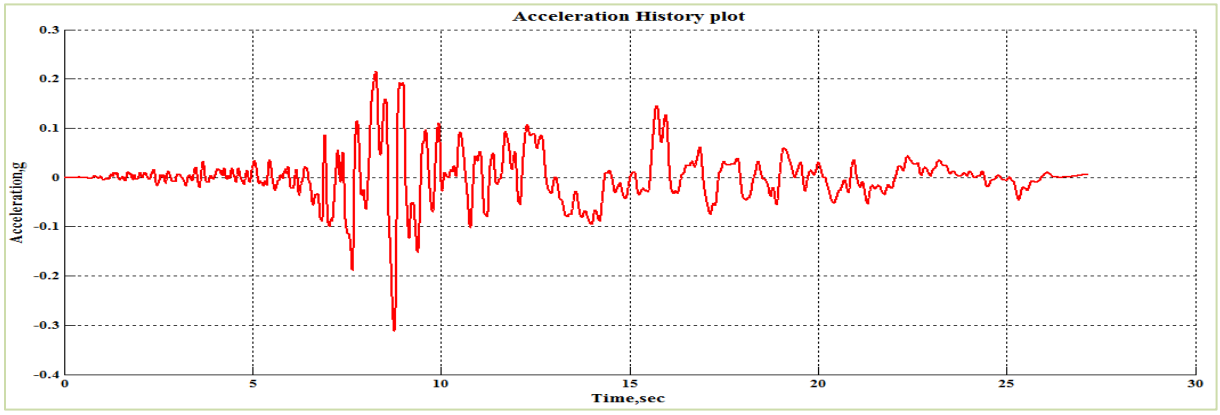

Figure 7-97 Acceleration Time History of Ground Motion 9 (Kocaeli Turkey-Duzce)

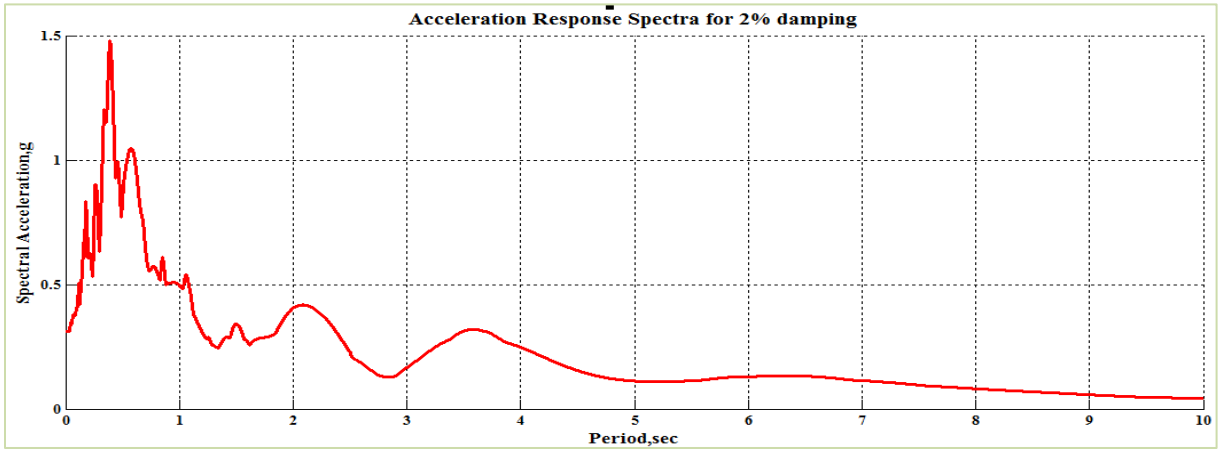

Figure 7-98 Acceleration Response Spectra for 2% Damping

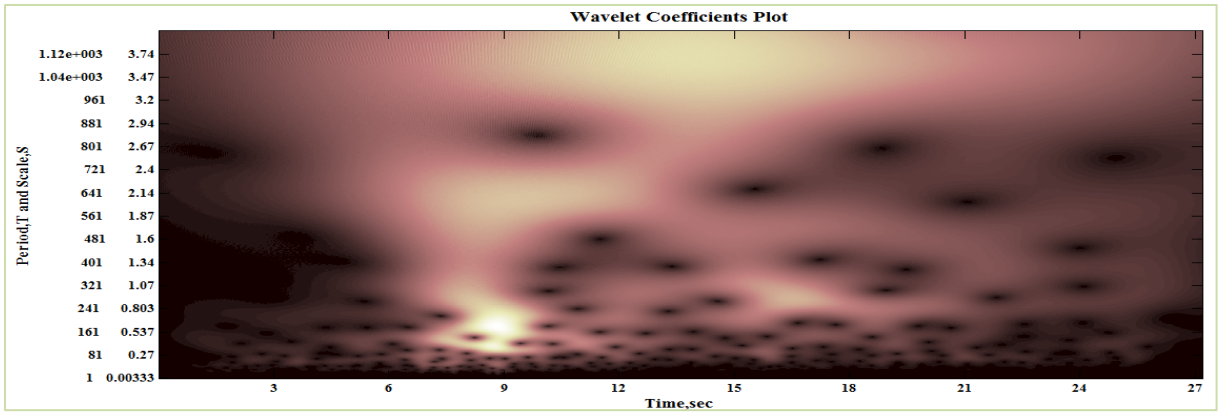

Figure 7-99 2D Wavelet coefficients plot of Ground Motion 9 (Kocaeli Turkey-Duzce)

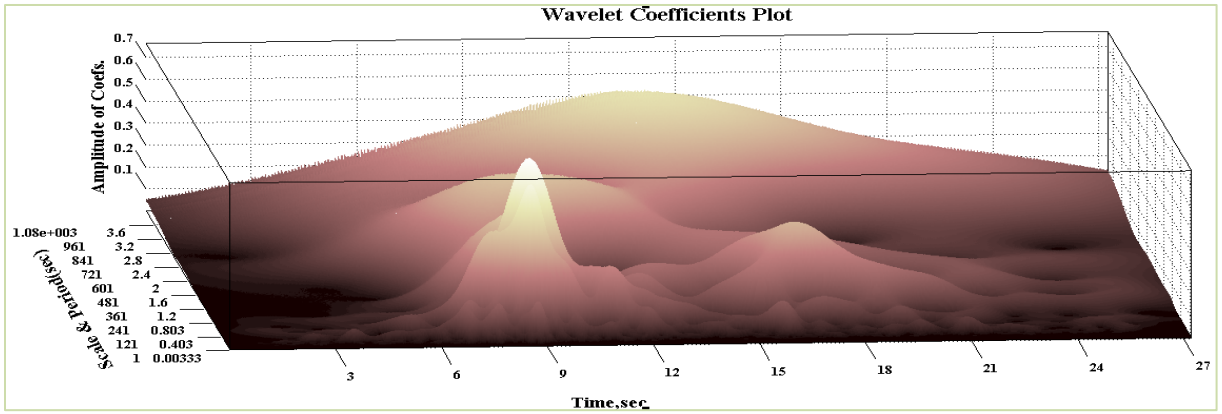

Figure 7-100 3D Wavelet coefficients plot of Ground Motion 9 (Kocaeli Turkey-Duzce)

The 3D and 2D peak displacement plot of the structural system incorporating bilinear elastic behavior is shown in Figures 7-101 and 7-102 respectively. The 2D peak displacement plot as shown in Figure 7-102 doesn`t have significant bumps (localized high points) in peak displacement. Hence, the amplification factor is expected to be equal to 1. It is observed from Figure 7-102 that the system becomes elastic for relatively low strength reduction factor.

The 3D and 2D peak amplification plot of the structural system incorporating bilinear elastic behavior is shown in Figures 7-103 and 7-104 respectively. It is observed from Figure 7-104 that the amplification factor for all periods is nearer to 1 which proves that the the moving resonance doesn`t have significant effect on the structural systems incorporating bilinear elastic behavior.

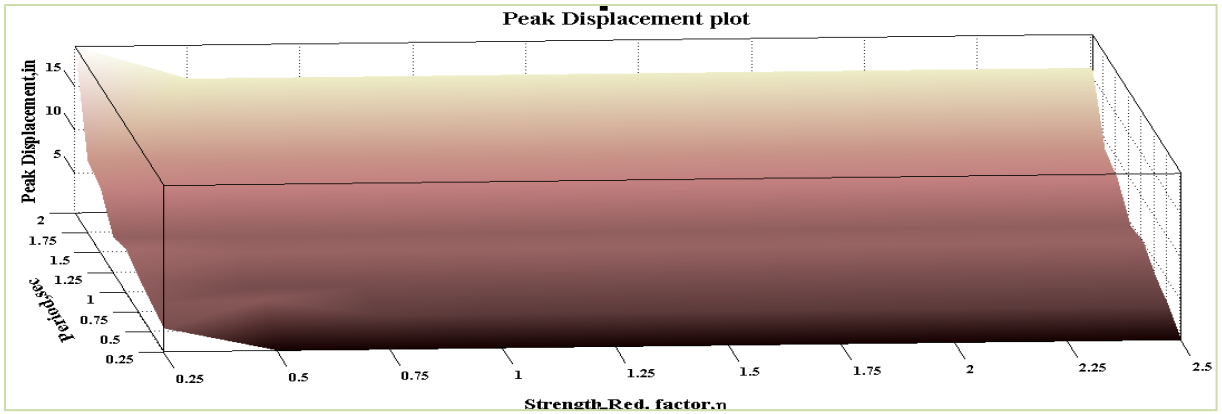

Figure 7-101 3D Peak Displacement plot for Ground Motion 9 (Bilinear Behavior)

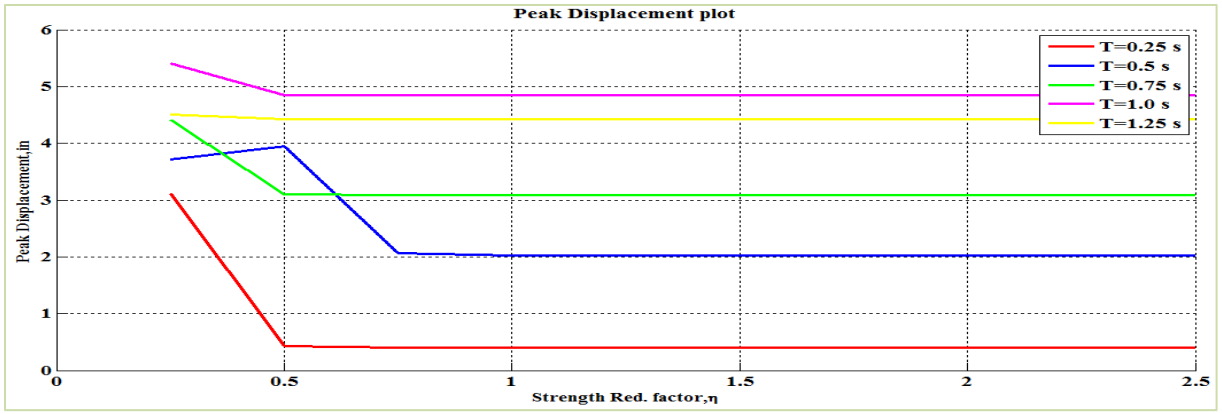

Figure 7-102 2D Peak Displacement plot for Ground Motion 9 (Bilinear Behavior)

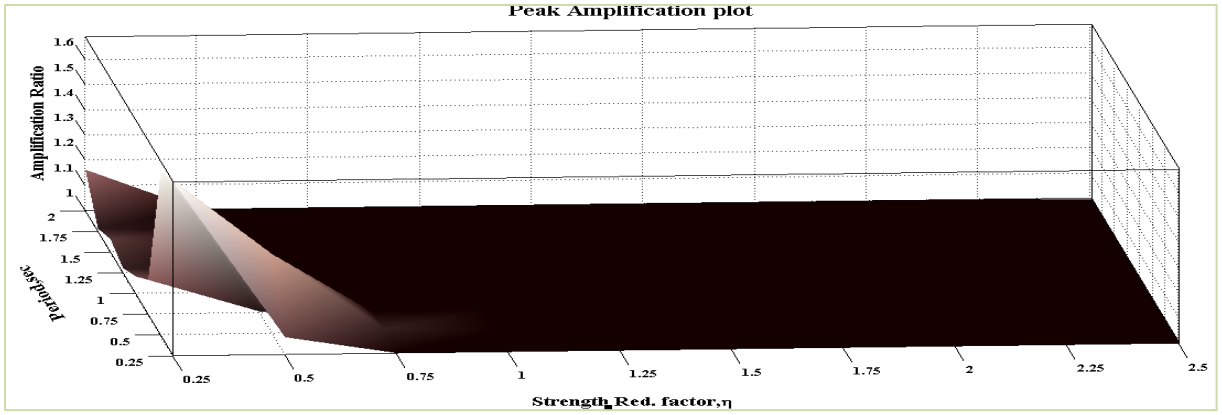

Figure 7-103 3D Peak Amplification plot for Ground Motion 9 (Bilinear Behavior)

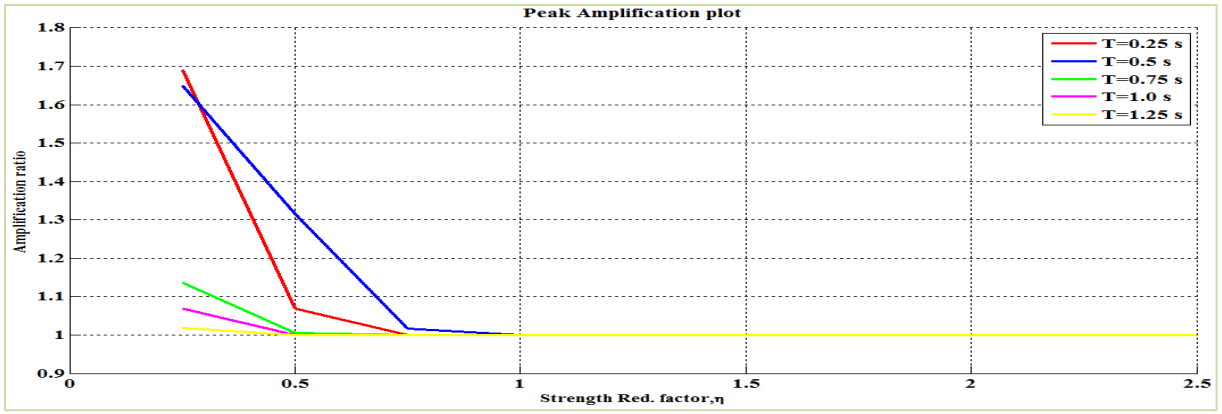

Figure 7-104 2D Peak Amplification plot for Ground Motion 9 (Bilinear Behavior)

The 3D and 2D peak displacement plot of the structural system incorporating elasto-plastic behavior is shown in Figures 7-105 and 7-106 respectively. The 2D peak displacement plot as shown in Figure 7-106 have bumps in peak displacement at corresponding (T_0,η) values of (0.5,0.5).This localized increase in peak displacement is hypothesized to be the result of occurrence of moving resonance and hence amplification factor greater than 1 is expected for these combinations of period and strength.

The 3D and 2D peak amplification plot of the structural system incorporating bilinear elastic behavior is shown in Figures 7-107 and 7-108 respectively. It is observed from Figure 7-108 that the amplification values corresponding to (T_0,η) values of (0.5,0.5) (at similar places where localized high points of peak displacement were observed in Figure 7-106) are greater than 1 leading to the increase in peak displacement. This increase in peak displacement is considered to be the effect of moving resonance.

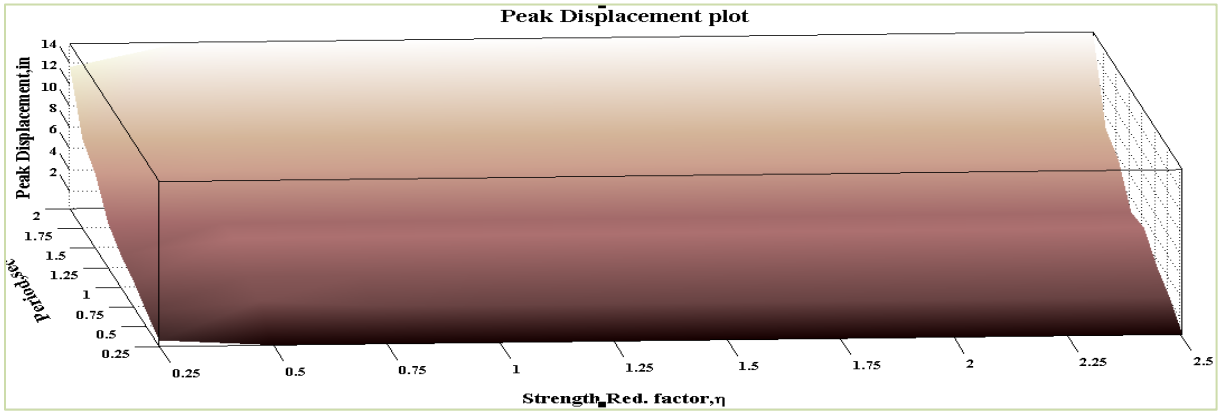

Figure 7-105 3D Peak Displacement plot for Ground Motion 9 (EPP Behavior)

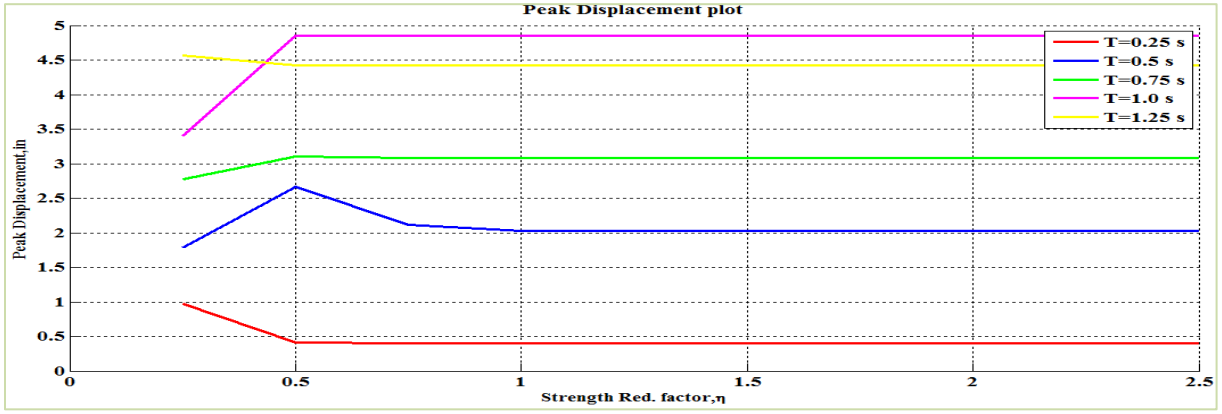

Figure 7-106 2D Peak Displacement plot for Ground Motion 9 (EPP Behavior)

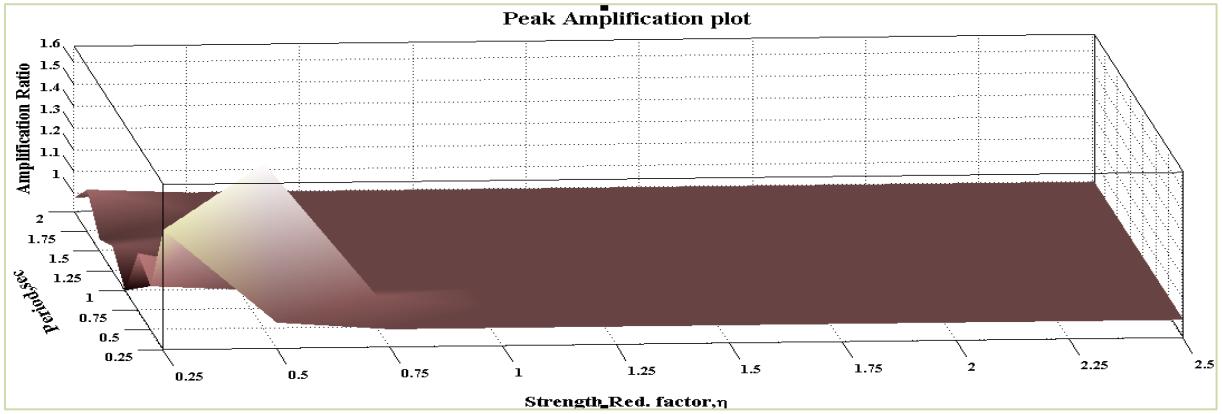

Figure 7-107 3D Peak Amplification plot for Ground Motion 9 (EPP Behavior)

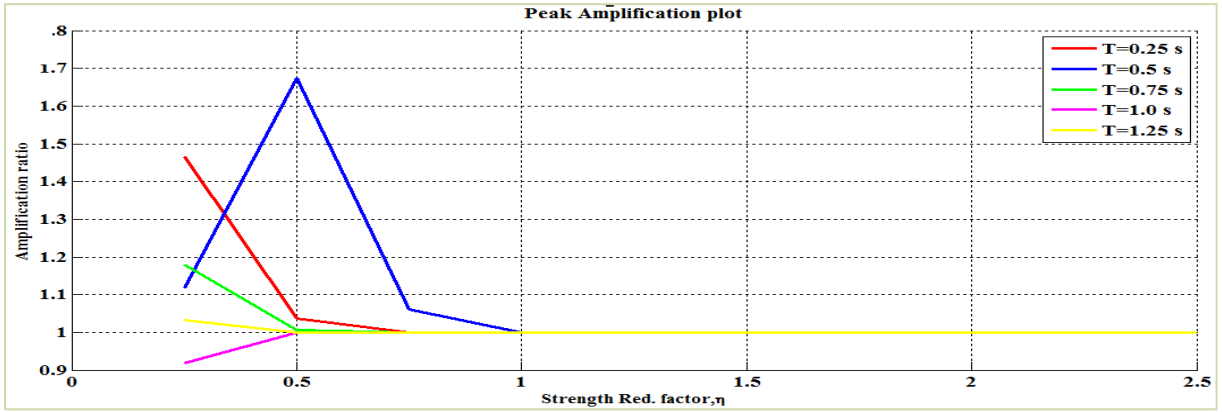

Figure 7-108 2D Peak Amplification plot for Ground Motion 9 (EPP Behavior)

There was an 8 sec gap between two ridges of energy in the ground motion and that proved to be too long to excite large moving resonance.

7.2.10 Ground Motion 10: Kocaeli, Turkey at Arcelik station

The acceleration time history and the acceleration response spectra for 2 % damping of the component 1 of Kocaeli Turkey earthquake at Arcelik station is shown in Figures 7-109 and 7-110 respectively. The 2D and 3D wavelet coefficient plot of this particular ground motion performed using Complex Morlet wavelet of band width 1 and frequency 1.5 is shown in Figures 7-111 and 7-112 respectively.

It can be observed from Figures 7-97 to 7-100 that this ground motion has strong shaking at a very short period with some concentrations of energy at longer periods occurring in the middle of the ground motion.

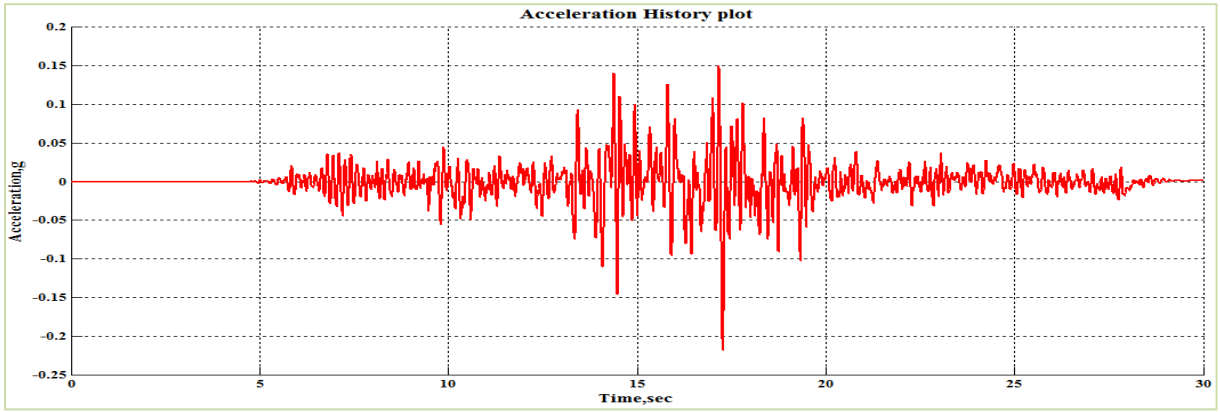

Figure 7-109 Acceleration Time History of Ground Motion 10 (Kocaeli Turkey-Arcelik)

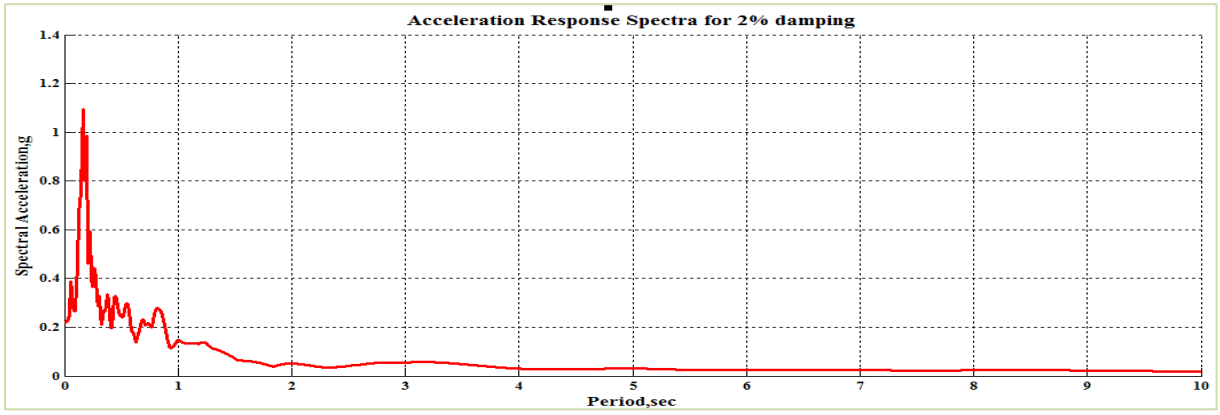

Figure 7-110 Acceleration Response Spectra for 2% Damping

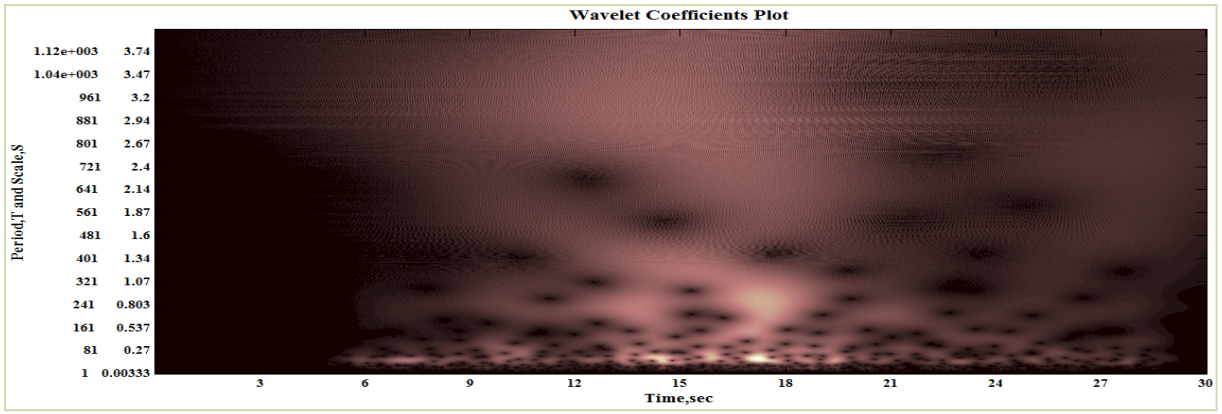

Figure 7-111 2D Wavelet coefficients plot of Ground Motion 10 (Kocaeli Turkey-Arcelik)

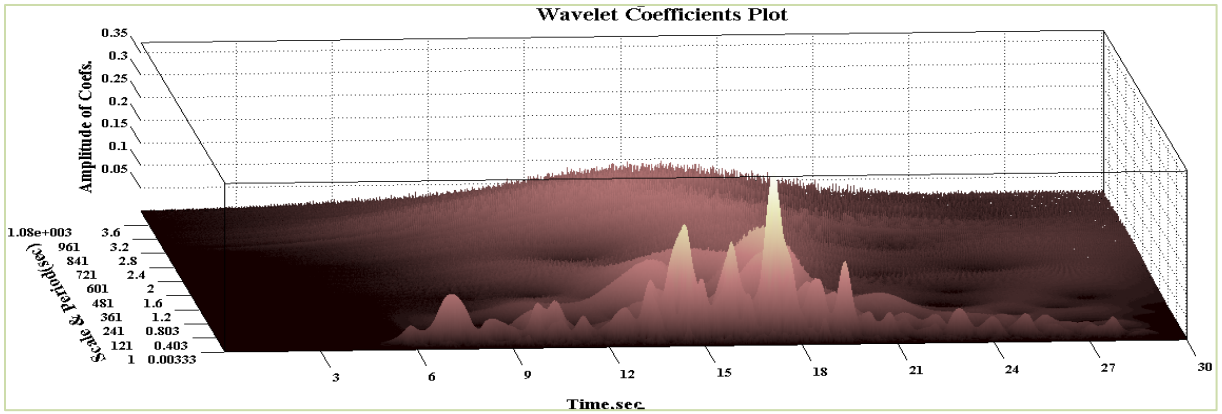

Figure 7-112 3D Wavelet coefficients plot of Ground Motion 10 (Kocaeli Turkey-Arcelik)

The 3D and 2D peak displacement plot of the structural system incorporating bilinear elastic behavior is shown in Figures 7-113 and 7-114 respectively. The 2D peak displacement plot as shown in Figure 7-114 doesn`t have significant bumps (localized high points) in peak displacement. Hence, the amplification factor is expected to be equal to 1. It is observed from Figure 7-114 that the system becomes elastic for relatively very low strength reduction factor.

The 3D and 2D peak amplification plot of the structural system incorporating bilinear elastic behavior is shown in Figures 7-115 and 7-116 respectively. It is observed from Figure 7-116 that the amplification factor for all periods is nearer to 1 which proves that the the moving resonance doesn`t have significant effect on the structural systems incorporating bilinear elastic behavior.

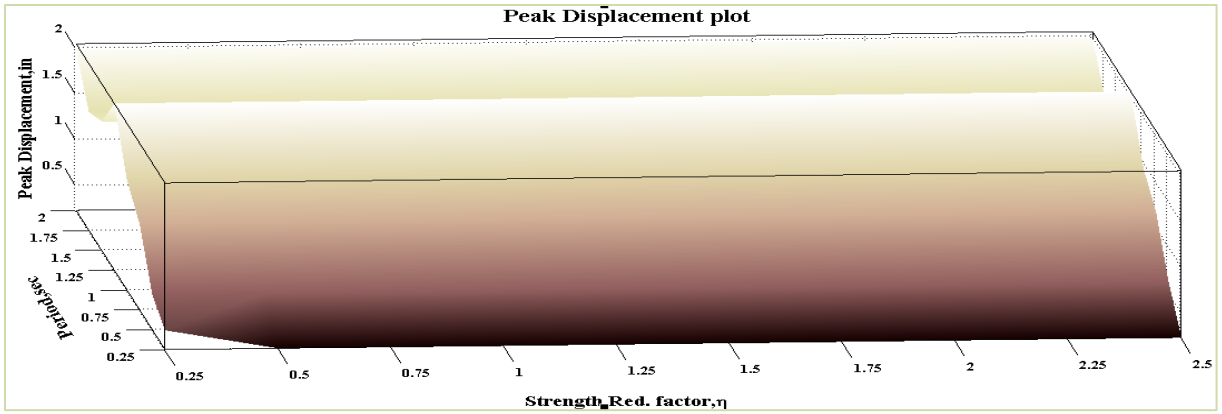

Figure 7-113 3D Peak Displacement plot for Ground Motion 10 (Bilinear Behavior)

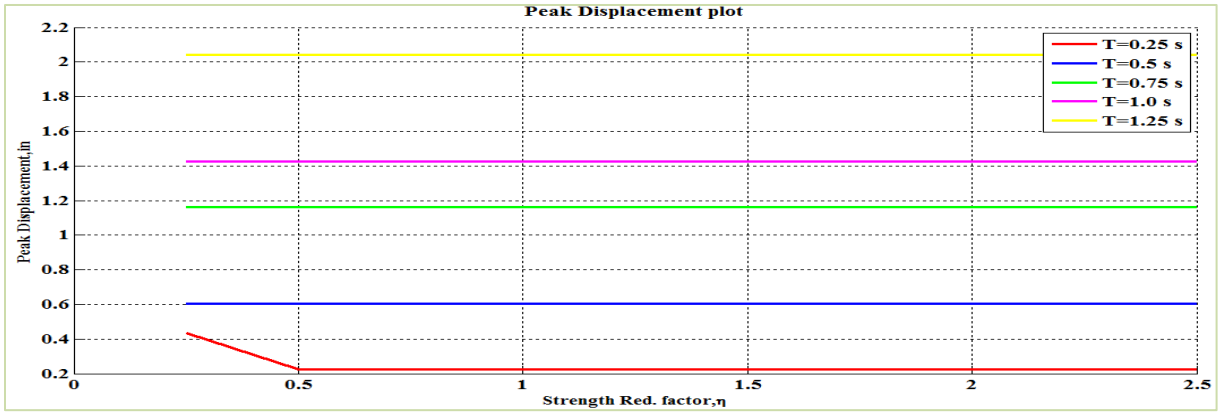

Figure 7-114 2D Peak Displacement plot for Ground Motion 10 (Bilinear Behavior)

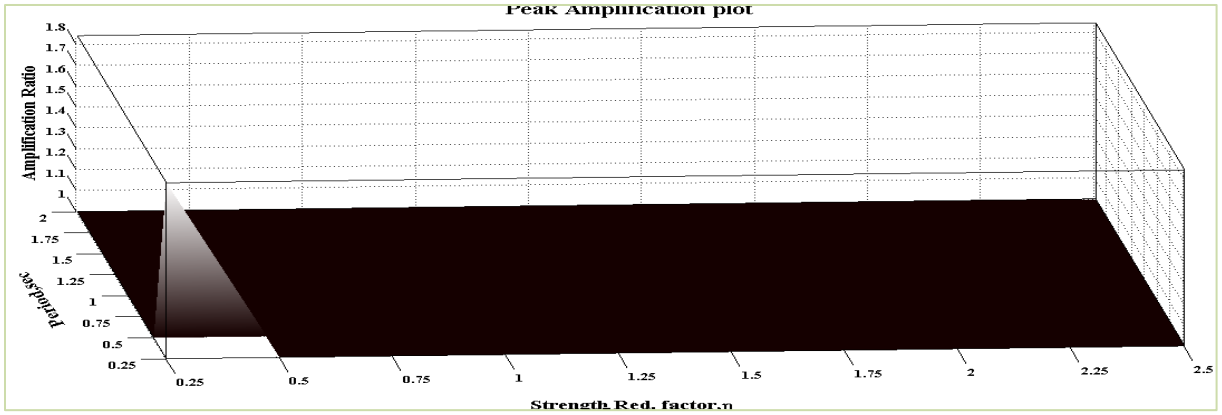

Figure 7-115 3D Peak Amplification plot for Ground Motion 10 (Bilinear Behavior)

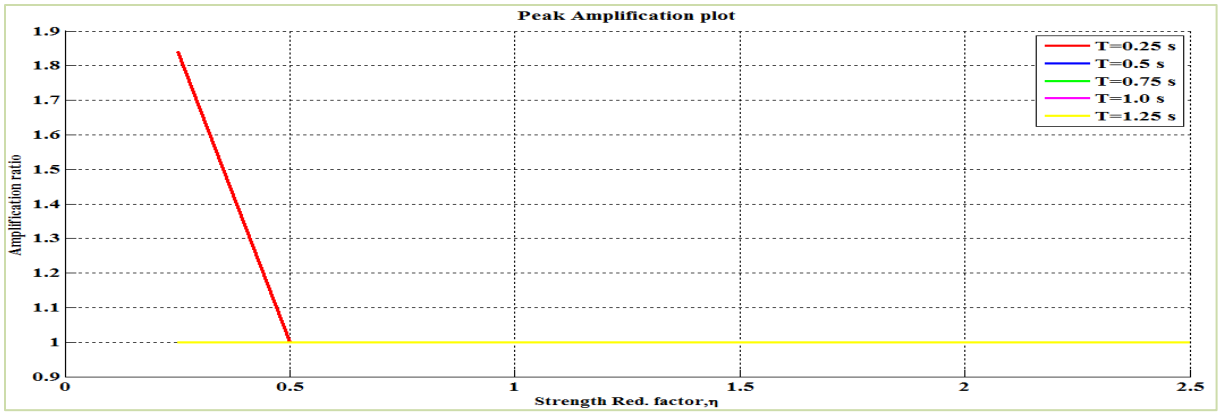

Figure 7-116 2D Peak Amplification plot for Ground Motion 10 (Bilinear Behavior)

The 3D and 2D peak displacement plot of the structural system incorporating elasto plastic behavior is shown in Figures 7-117and 7-118 respectively. The 2D peak displacement plot as shown in Figure 7-118 doesn`t have significant bumps (localized high points) in peak displacement. Hence, the amplification factor is expected to be equal to 1. It is observed from Figure 7-118 that the system becomes elastic for relatively very low strength reduction factor.

The 3D and 2D peak amplification plot of the structural system incorporating elasto plastic behavior is shown in Figures 7-119 and 7-120 respectively. It is observed from Figure 7-120 that the amplification factor for all periods is nearer to 1 which proves that the the moving resonance doesn`t have significant effect on the structural systems incorporating elasto plastic behavior. It is interesting that the short period system with small η and an initial natural period similar to that of the ground motion experienced larger peak dispalcements when subjected to the components of the gorund motion than when it was subjected to the original ground motion. This implies that there is destrcutive interference when the low period system experiences period elongation and must be out of phase with the ground motion energy at the larger periods.

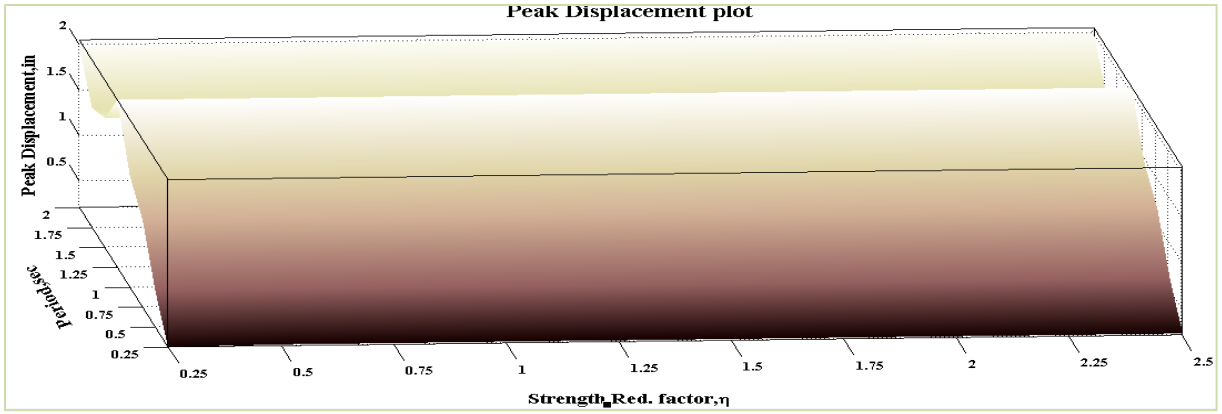

Figure 7-117 3D Peak Displacement plot for Ground Motion 10 (EPP Behavior)

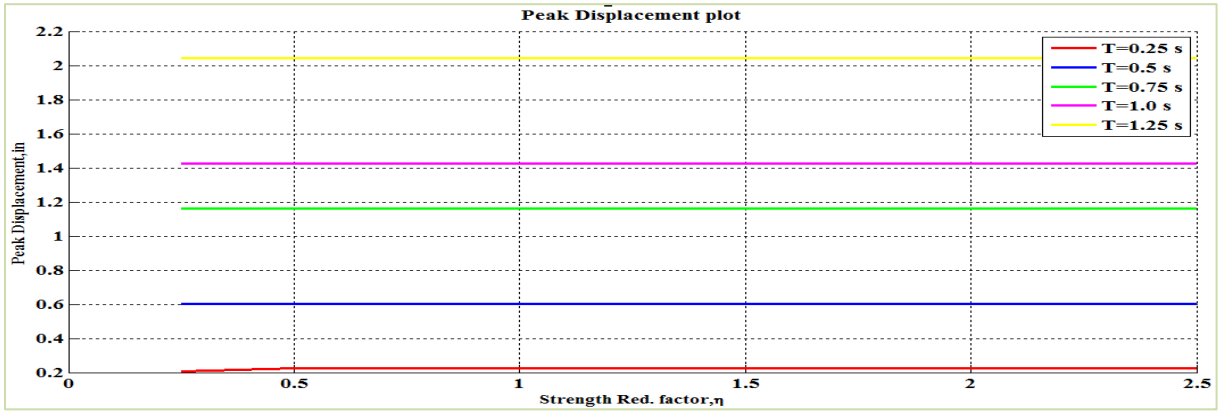

Figure 7-118 3D Peak Displacement plot for Ground Motion 10 (EPP Behavior)

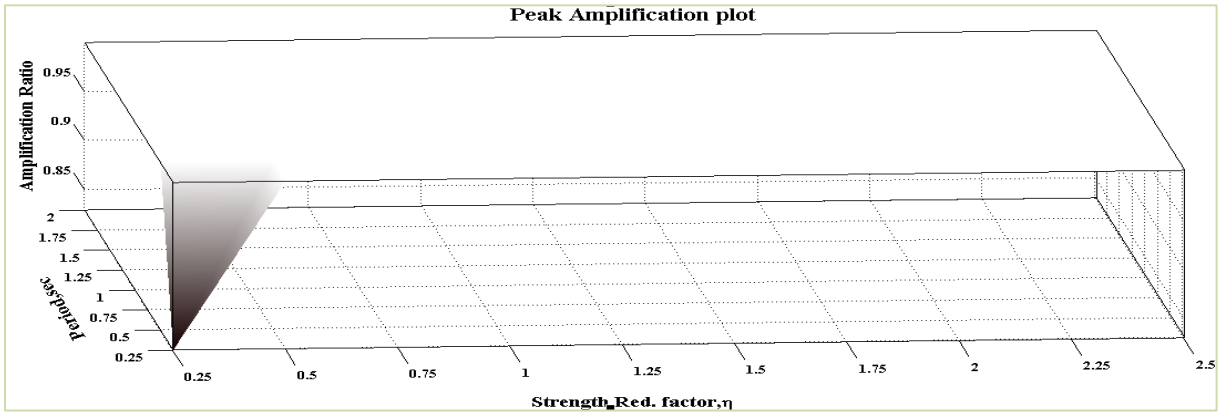

Figure 7-119 3D Peak Amplification plot for Ground Motion 9 (EPP Behavior)

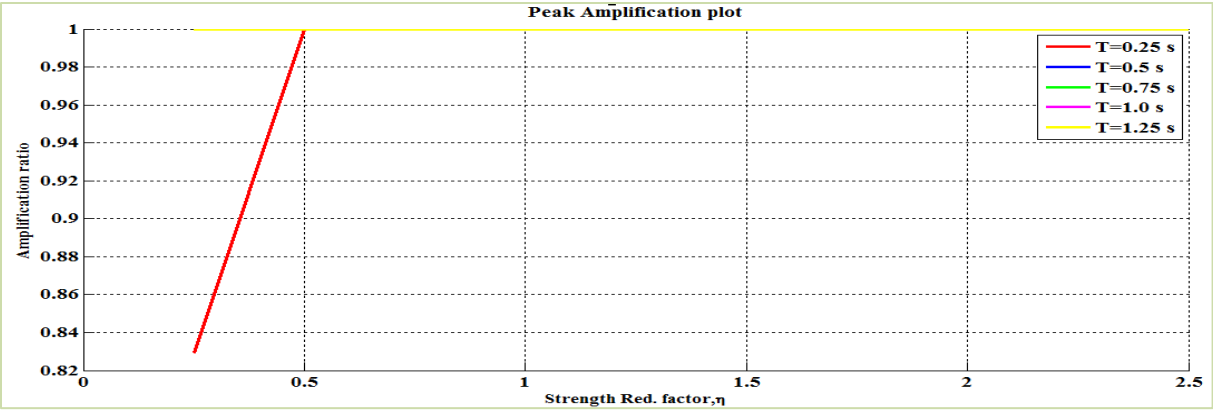

Figure 7-120 3D Peak Amplification plot for Ground Motion 9 (EPP Behavior)

The bulk of the energy in this ground motion occurred at very short periods. Therefore, there was not much opportunity for the system to experience moving resonance. There were some ridges of energy at longer periods, but the two areas of frequency content did not cause moving resonance. However, the short period system with small η experienced amplified response with a bilinear elastic hysteretic behavior and a reduction in response with the EPP behavior.

7.2.11 Ground Motion 11: Landers at Yermo Fire station

The acceleration time history and the acceleration response spectra for 2 % damping of the component 1 of Landers earthquake at Yermo Fire station is shown in Figures 7-121 and 7-122 respectively. The 2D and 3D wavelet coefficient plot of this particular ground motion performed using Complex Morlet wavelet of band width 1 and frequency 1.5 is shown in Figures 7-123 and 7-124 respectively.

It can be observed from Figures 7-121 to 7-124 that most of the energy in the ground motion is concentrated in a short length of time – about five seconds. It is observed that there is some energy at moderate periods (i.e. 0.5 sec) at 14 sec that then shifts to strong shaking at high periods (i.e.1.25,1.50 sec) between time t=15 sec to time t=18 sec.

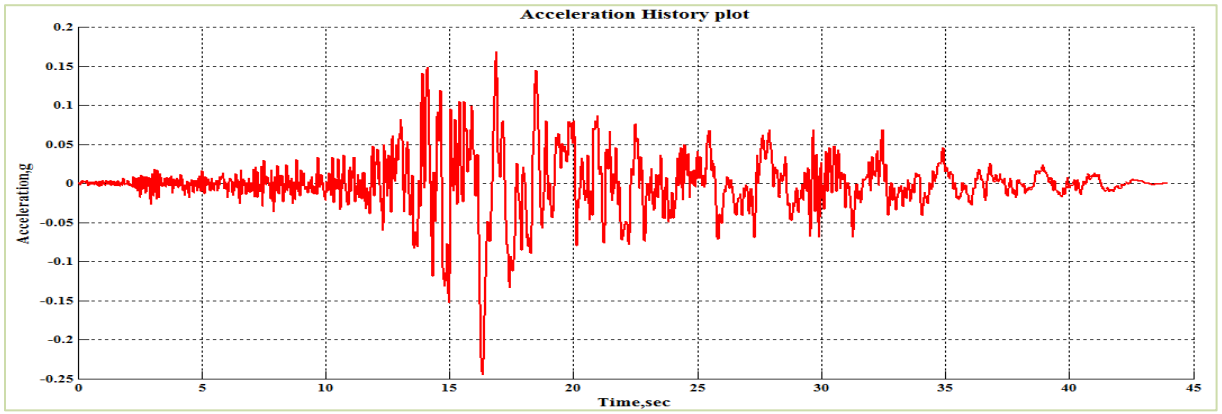

Figure 7-121 Acceleration Time History of Ground Motion 11 (Landers- Yermo Fire station)

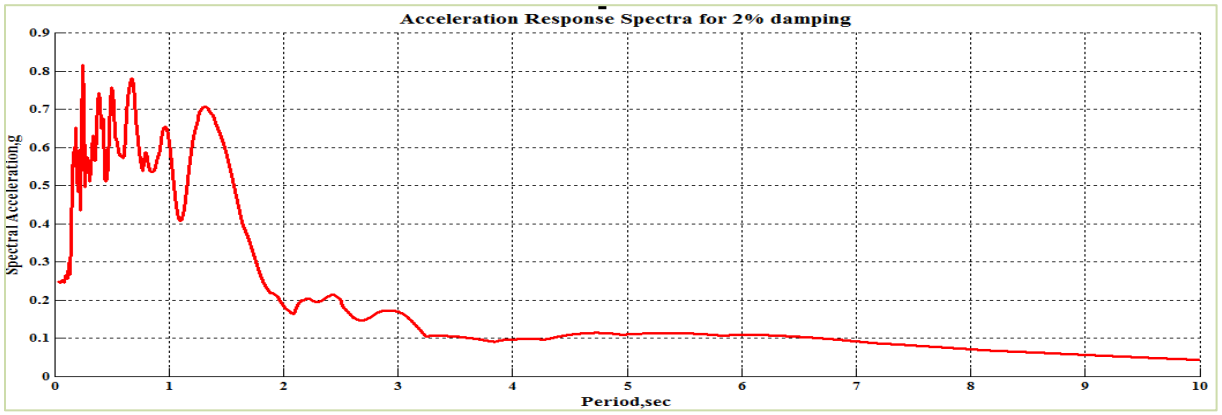

Figure 7-122 Acceleration Response Spectra for 2% Damping

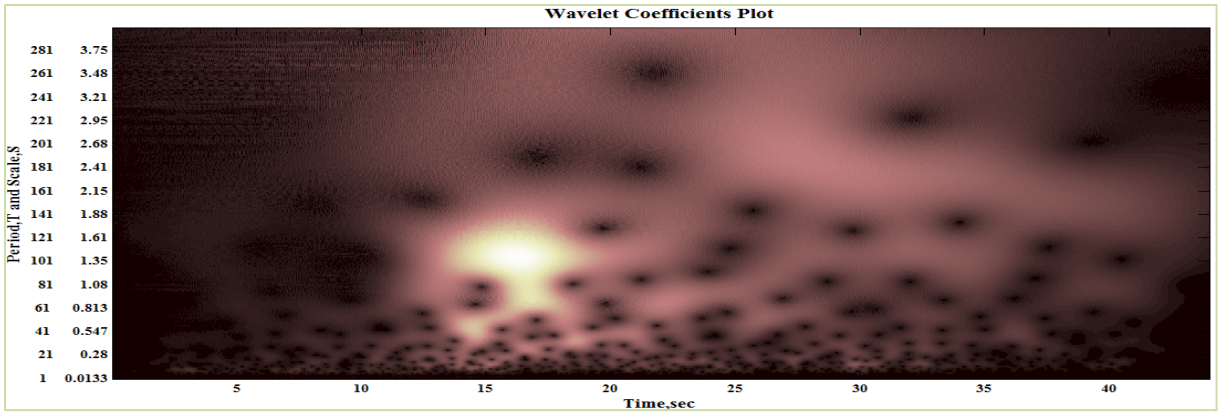

Figure 7-123 2D Wavelet coefficients plot of Ground Motion 11 (Landers- Yermo Fire station)

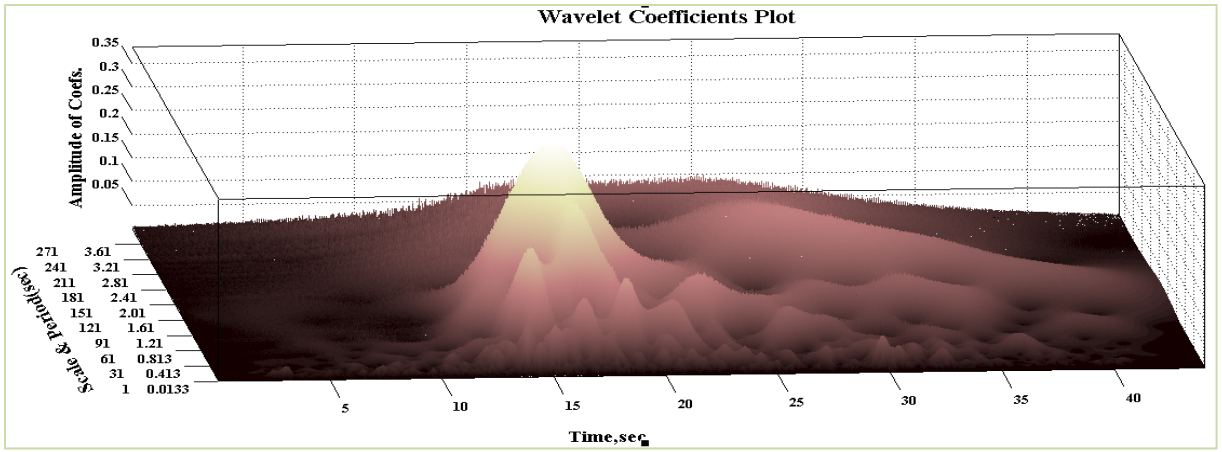

Figure 7-124 3D Wavelet coefficients plot of Ground Motion 11 (Landers- Yermo Fire station)

The 3D and 2D peak displacement plot of the structural system incorporating bilinear elastic behavior is shown in Figures 7-125 and 7-126 respectively. The 2D peak displacement plot as shown in Figure 7-126 doesn`t have significant bumps (localized high points) in peak displacement. Hence, the amplification factor is expected to be equal to 1. It is observed from Figure 7-126 that the system becomes elastic for relatively very low strength reduction factor.

The 3D and 2D peak amplification plot of the structural system incorporating bilinear elastic behavior is shown in Figures 7-127 and 7-128 respectively. It is observed from Figure 7-128 that though there are no significant bumps in peak displacement, for small eta systems, the amplification factors are greater than 1.

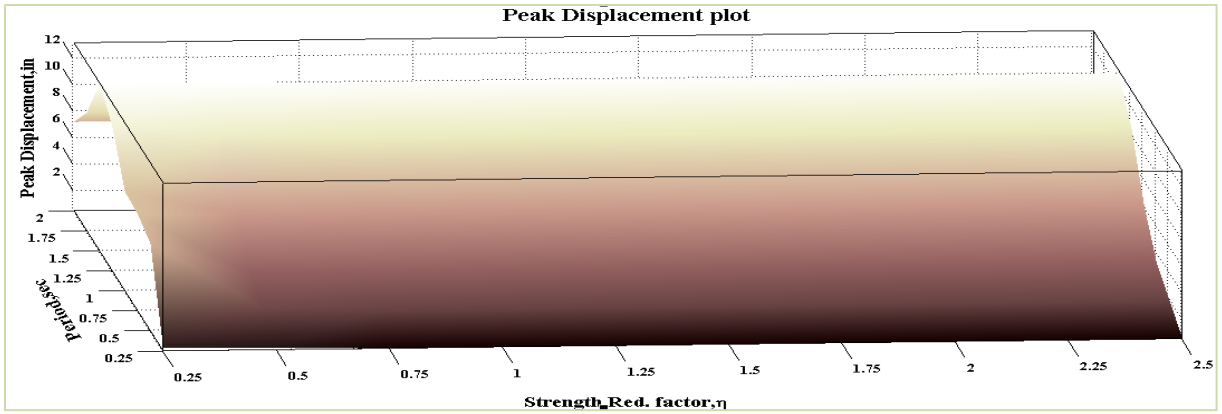

Figure 7-125 3D Peak Displacement plot for Ground Motion 11 (Bilinear Behavior)

Figure 7-126 2D Peak Displacement plot for Ground Motion 11 (Bilinear Behavior)

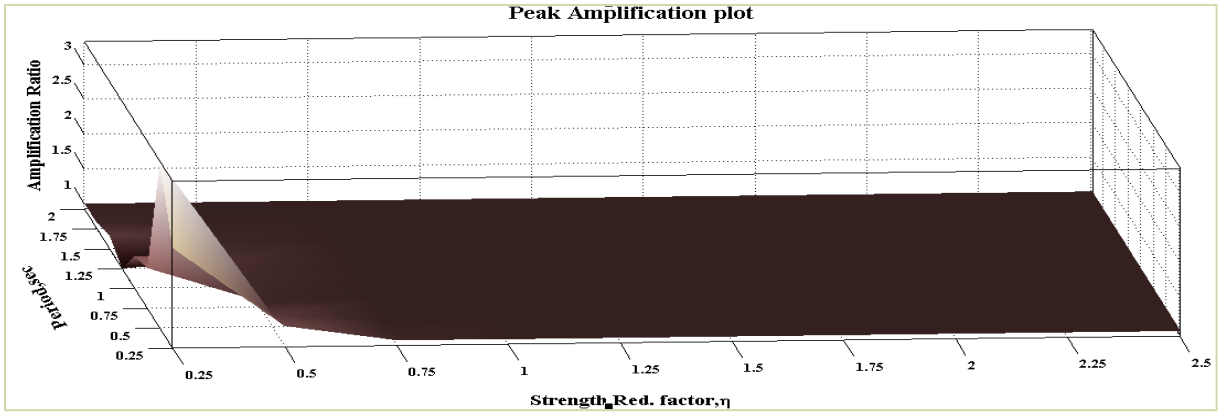

Figure 7-127 3D Peak Amplification plot for Ground Motion 11 (Bilinear Behavior)

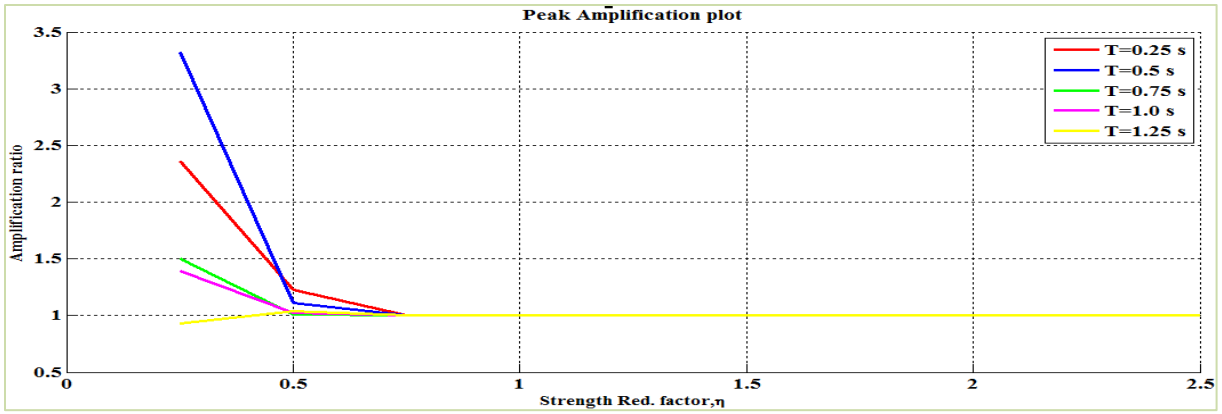

Figure 7-128 2D Peak Amplification plot for Ground Motion 11 (Bilinear Behavior)

The 3D and 2D peak displacement plot of the structural system incorporating elasto-plastic behavior is shown in Figures 7-129 and 7-130 respectively. The 2D peak displacement plot as shown in Figure 7-130 doesn`t have significant bumps (localized high points) in peak displacement. Hence, the amplification factor is expected to be equal to 1. It is observed from Figure 7-130 that the system becomes elastic for relatively very low strength reduction factor.

The 3D and 2D peak amplification plot of the structural system incorporating bilinear elastic behavior is shown in Figures 7-131 and 7-132 respectively. It is observed from Figure 7-132 though there are no significant bumps in peak displacement, for small eta systems, the amplification factors are greater than 1.

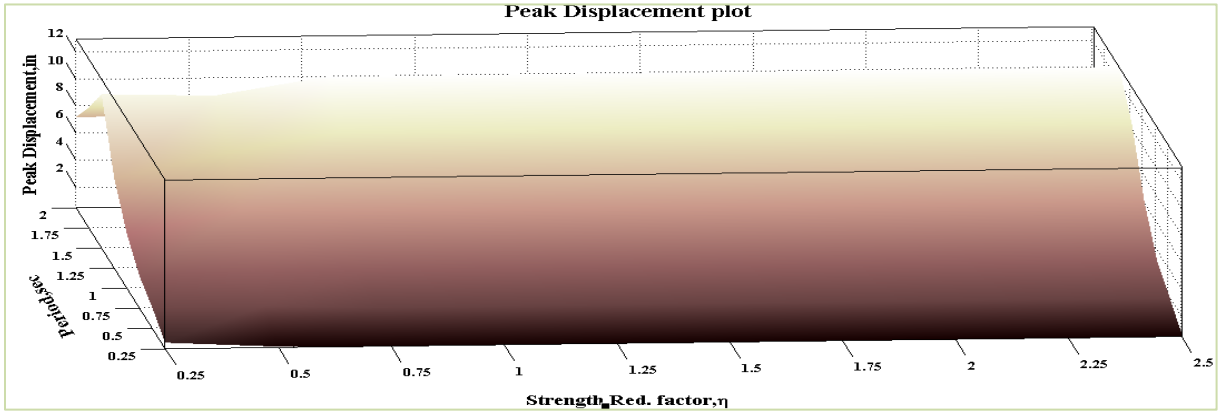

Figure 7-129 3D Peak Displacement plot for Ground Motion 11 (EPP Behavior)

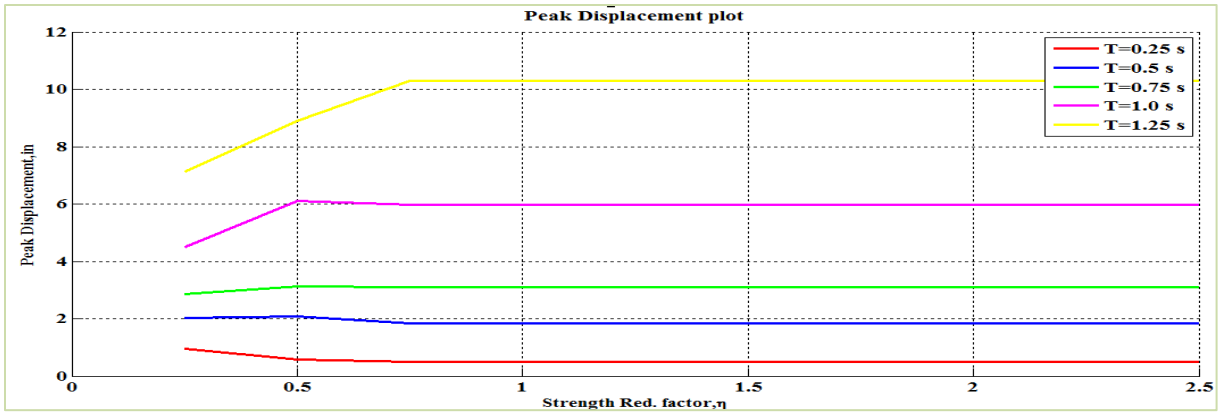

Figure 7-130 2D Peak Displacement plot for Ground Motion 11 (EPP Behavior)

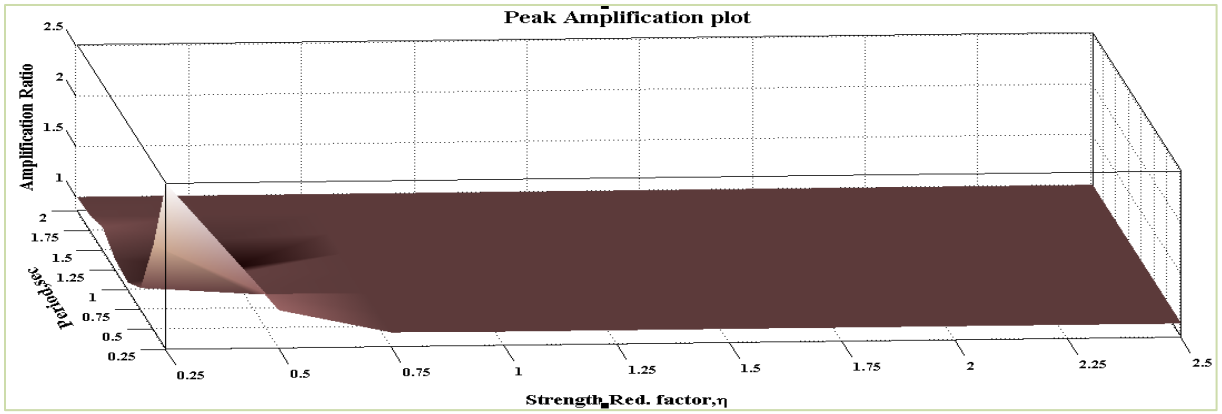

Figure 7-131 3D Peak Amplification plot for Ground Motion 11 (Bilinear Behavior)

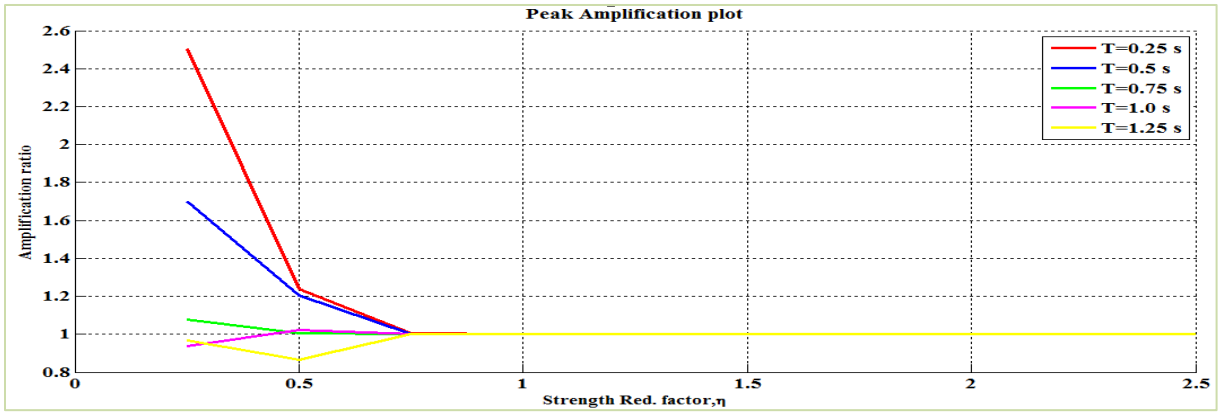

Figure 7-132 2D Peak Amplification plot for Ground Motion 11 (Bilinear Behavior)

The frequency content is concentrated in a short length of time and its energy is spread out in the period range that it covers. The systems with small eta values experienced significant amplification factors.

7.2.12 Ground Motion 12: Landers at Cool water station

The acceleration time history and the acceleration response spectra for 2 % damping of the component 1 of Landers earthquake at Cool water station is shown in Figures 7-133 and 7-134 respectively. The 2D and 3D wavelet coefficient plot of this particular ground motion performed using Complex Morlet wavelet of band width 1 and frequency 1.5 is shown in Figures 7-135 and 7-136 respectively.

It can be observed from Figures 7-133 to 7-136 that the significant frequency content of this ground motion is starting very late at around time t=12 sec with low periods and the intensity of excitation is increasing and then again decreasing as time increases. A sequence of three ridges of energy in the ground motion at gradually increasing period is observed between time t=13 sec to time t=20 sec. It is expected that this trend in the ground motion is conducive to moving resonance.

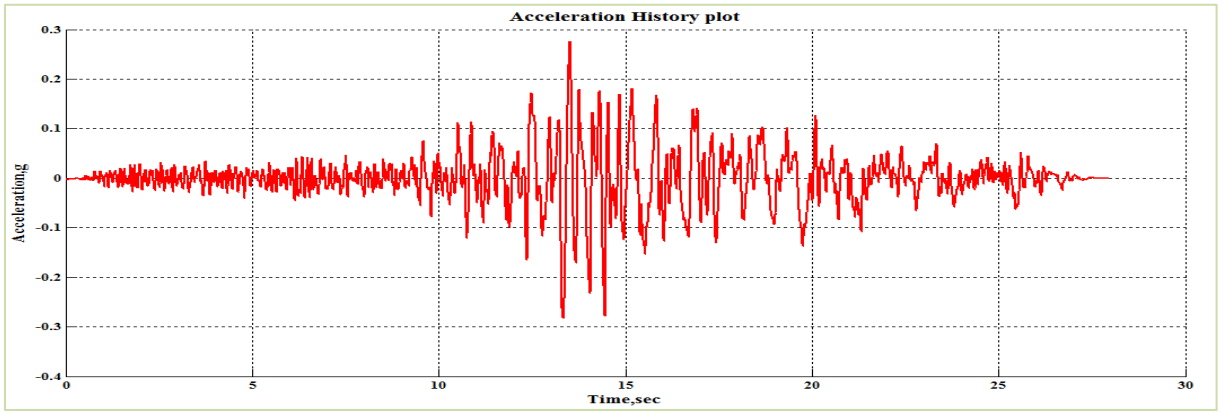

Figure 7-133 Acceleration Time History of Ground Motion 12 (Landers-Cool water)

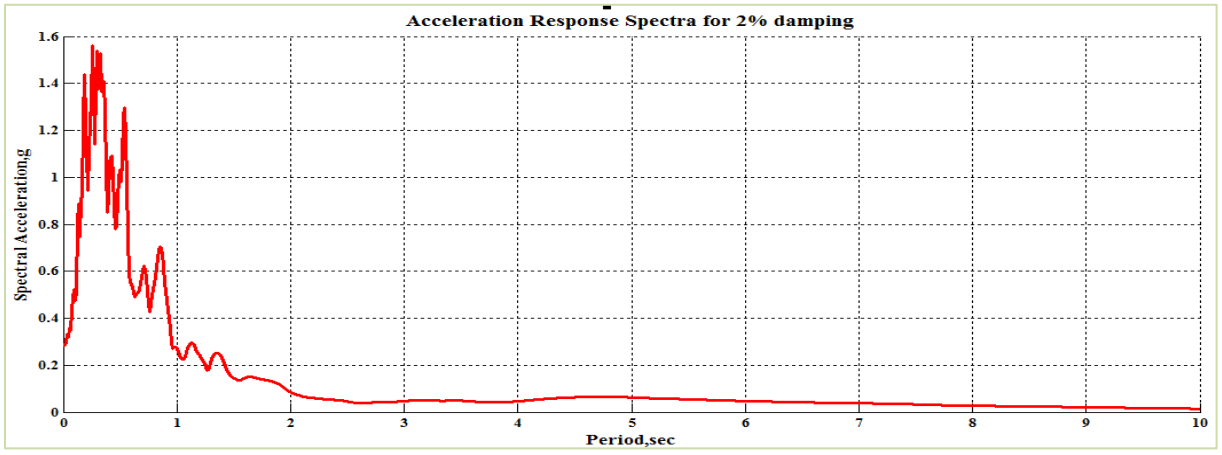

Figure 7-134 Acceleration Response Spectra for 2% Damping

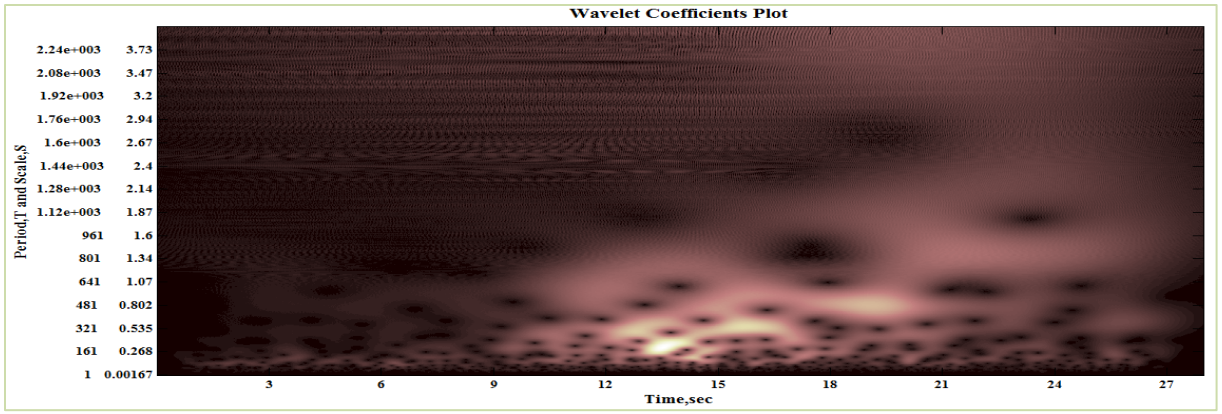

Figure 7-135 2D Wavelet coefficients plot of Ground Motion 12 (Landers-Cool water)

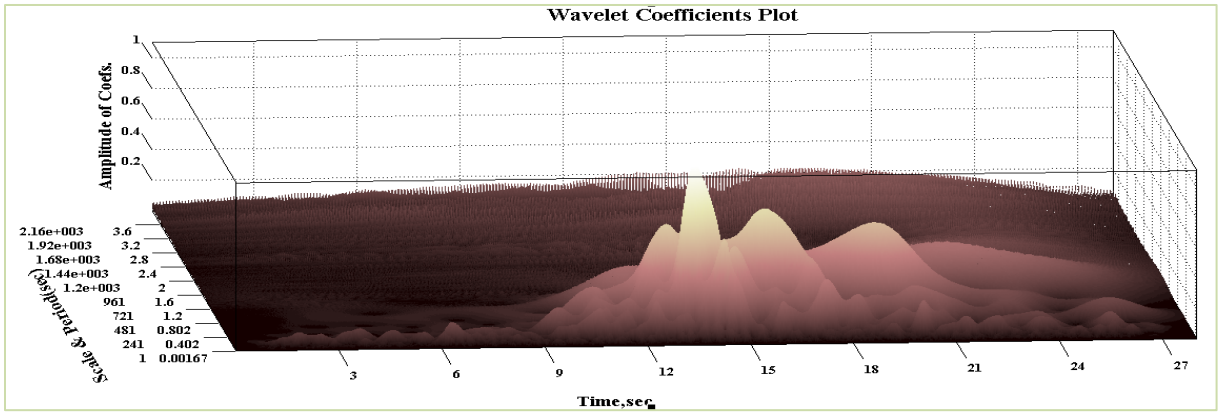

Figure 7-136 3D Wavelet coefficients plot of Ground Motion 12 (Landers-Cool water)

The 3D and 2D peak displacement plot of the structural system incorporating bilinear elastic behavior is shown in Figures 7-137 and 7-138 respectively. The 2D peak displacement plot as shown in Figure 7-138 have bumps in peak displacement at corresponding (T_0,η) values of (0.25,0.75), and (0.50,0.50).This localized increase in peak displacement is hypothesized to be the result of occurrence of moving resonance and hence amplification factor greater than 1 is expected for these combinations of period and strength.

The 3D and 2D peak amplification plot of the structural system incorporating bilinear elastic behavior is shown in Figures 7-139 and 7-140 respectively. It is observed from Figure 7-140 that the amplification values corresponding to (T_0,η) values of (0.25,0.75), and (0.50,0.50) (at similar places where localized high points of peak displacement were observed in Figure 7-138) are greater than 1 leading to the increase in peak displacement. This increase in peak displacement is considered to be the effect of moving resonance.

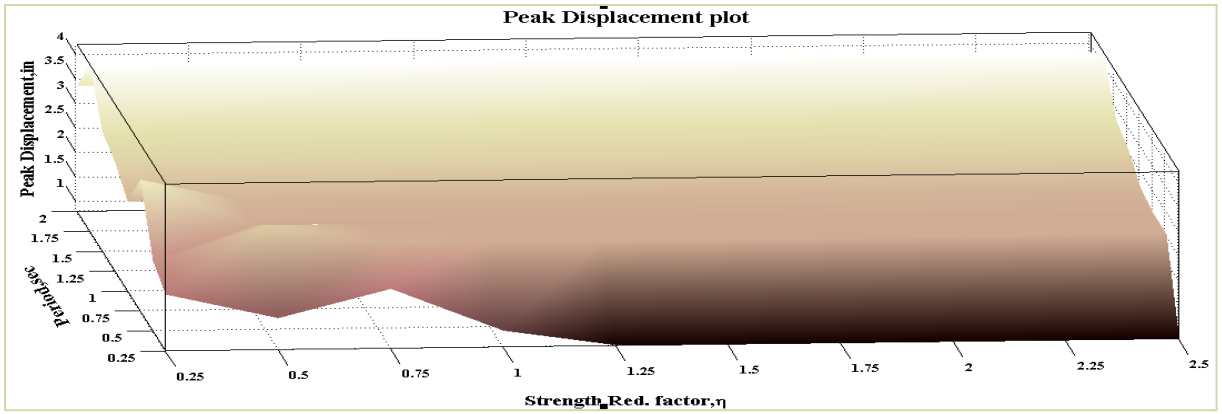

Figure 7-137 3D Peak Displacement plot for Ground Motion 12 (Bilinear Behavior)

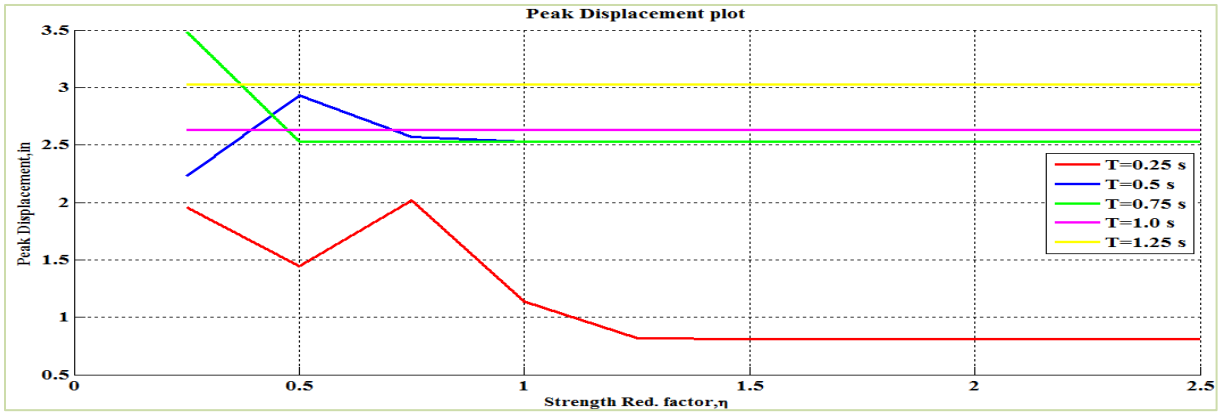

Figure 7-138 2D Peak Displacement plot for Ground Motion 12 (Bilinear Behavior)

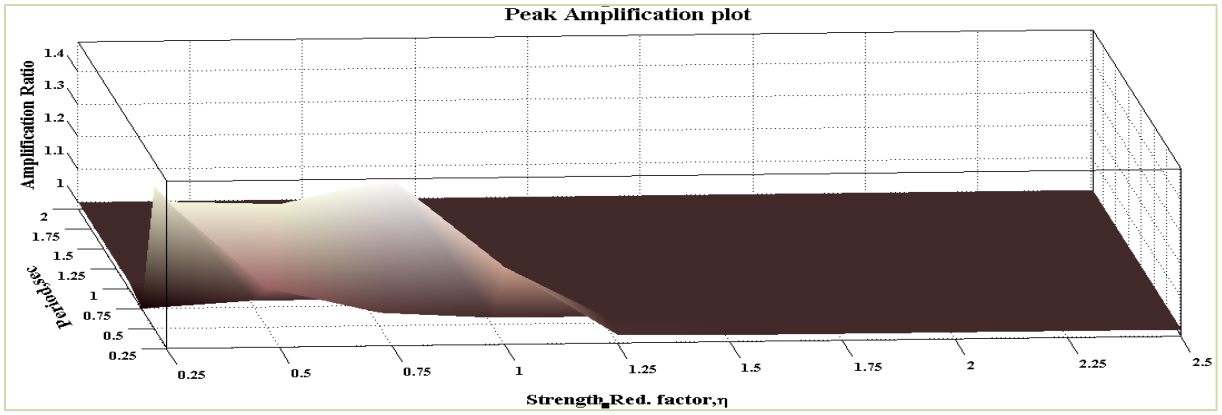

Figure 7-139 3D Peak Amplification plot for Ground Motion 12 (Bilinear Behavior)

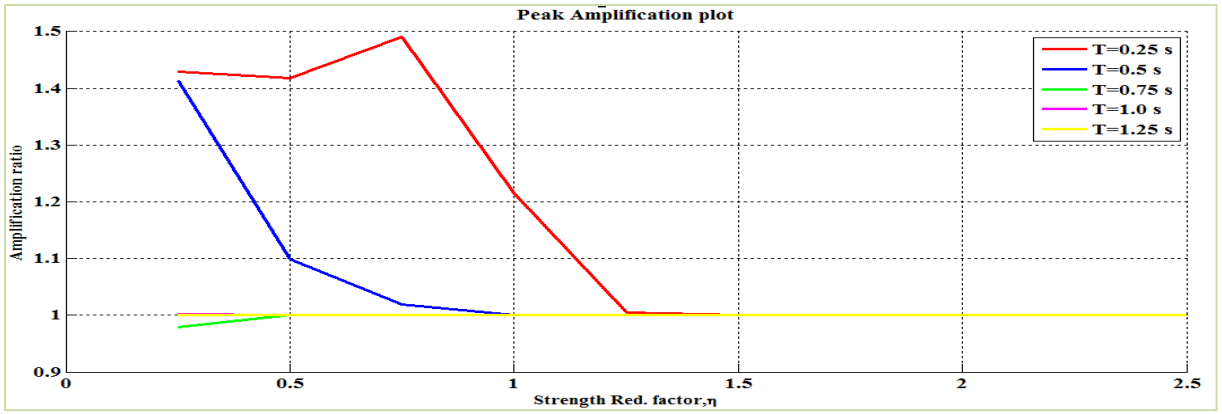

Figure 7-140 2D Peak Amplification plot for Ground Motion 12 (Bilinear Behavior)

The 3D and 2D peak displacement plot of the structural system incorporating elasto-plastic behavior is shown in Figures 7-141 and 7-142 respectively. The 2D peak displacement plot as shown in Figure 7-142 have bumps in peak displacement at corresponding (T_0,η) values of (0.25,0.5), and (0.50,0.50).This localized increase in peak displacement is hypothesized to be the result of occurrence of moving resonance and hence amplification factor greater than 1 is expected for these combinations of period and strength.

The 3D and 2D peak amplification plot of the structural system incorporating bilinear elastic behavior is shown in Figures 7-143 and 7-144 respectively. It is observed from Figure 7-144 that the amplification values corresponding to (T_0,η) values of (0.25,0.5), and (0.50,0.50) (at similar places where localized high points of peak displacement were observed in Figure 7-142) are greater than 1 leading to the increase in peak displacement. This increase in peak displacement is considered to be the effect of moving resonance.

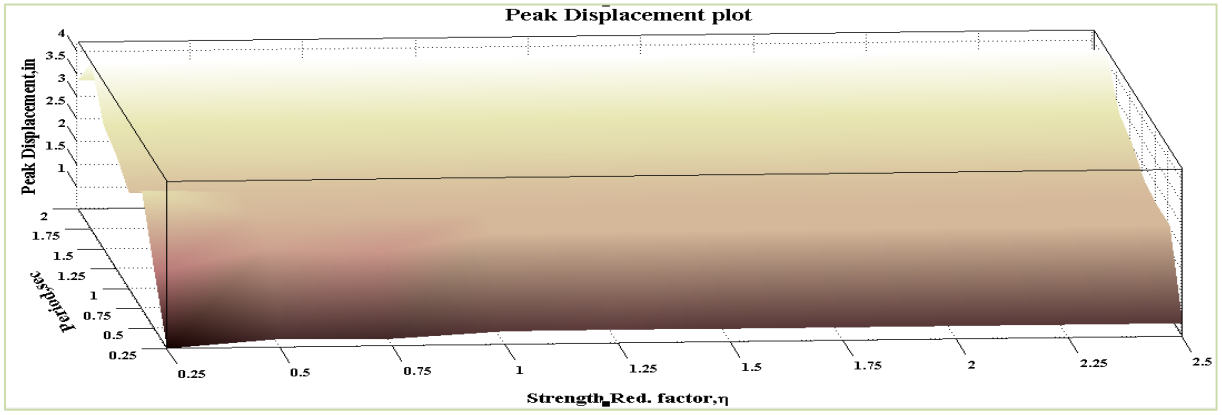

Figure 7-141 3D Peak Displacement plot for Ground Motion 12 (EPP Behavior)

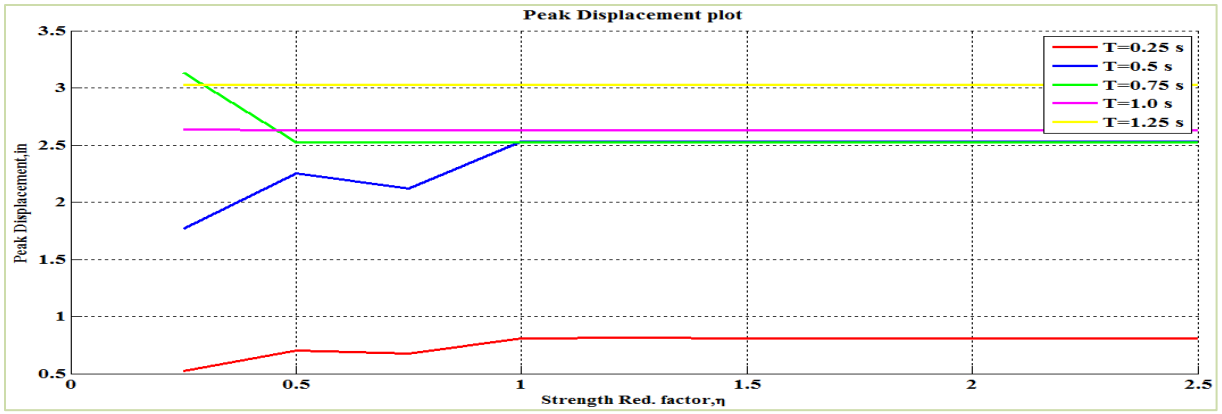

Figure 7-142 2D Peak Displacement plot for Ground Motion 12 (EPP Behavior)

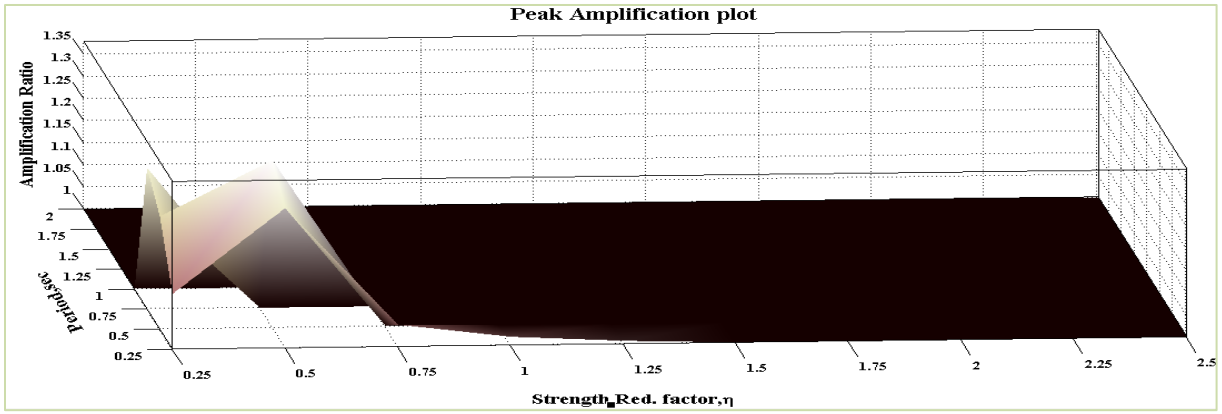

Figure 7-143 3D Peak Amplification plot for Ground Motion 12 (EPP Behavior)

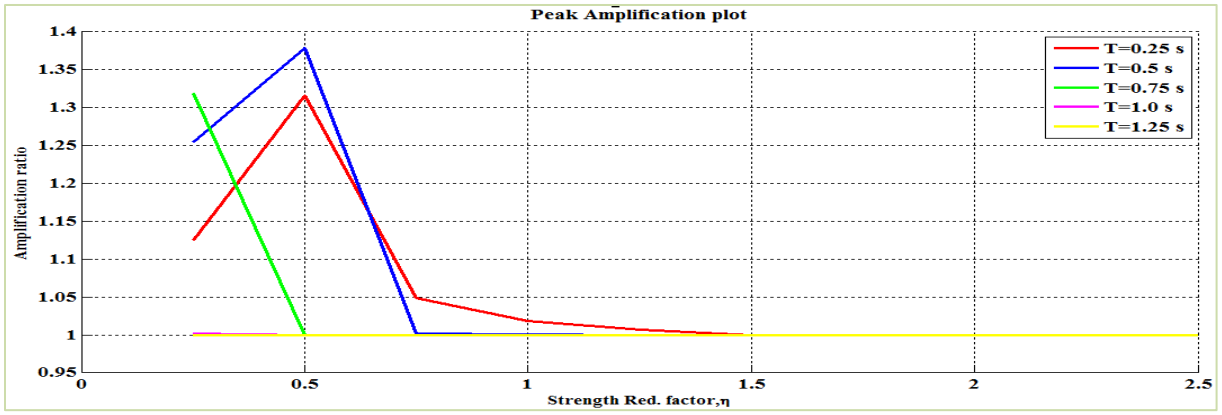

Figure 7-144 2D Peak Amplification plot for Ground Motion 12 (EPP Behavior)

It is concluded that the sequence of ridges at gradually increasing period of the ground motion energy was well suited for moving resonance in both the systems. Some effect of moving resonance was observed. However, the effect was not as strong as that for ground motion 1.

7.2.13 Ground Motion 13: Loma Prieta Earthquake at Capitola

The acceleration time history and the acceleration response spectra for 2 % damping of the component 1 of Loma Prieta earthquake at Capitola station is shown in Figures 7-145 and 7-146 respectively. The 2D and 3D wavelet coefficient plot of this particular ground motion performed using Complex Morlet wavelet of band width 1 and frequency 1.5 is shown in Figures 7-147 and 7-148 respectively.

It can be observed from Figures 7-145 to 7-147 that the significant frequency content is starting at around time t=4 sec hitting low periods and the intensity of excitation is increasing and then again decreasing as time increases. The energy of the ground motion split up into three ridges at gradually increasing period is observed between time t=4 sec to time t=12 sec. It is expected that this trend in the ground motion is conducive to moving resonance.

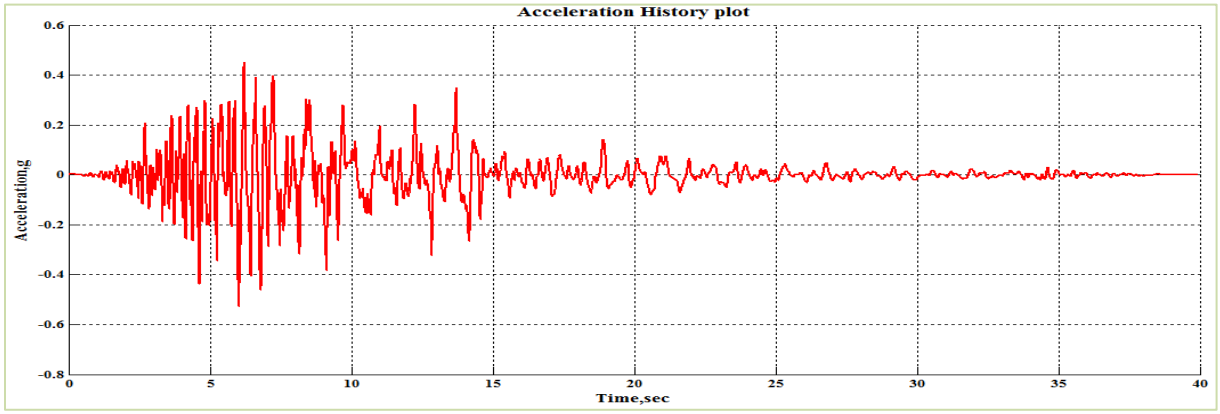

Figure 7-145 Acceleration Time History of Ground Motion 13 (Loma Prieta-Capitola)

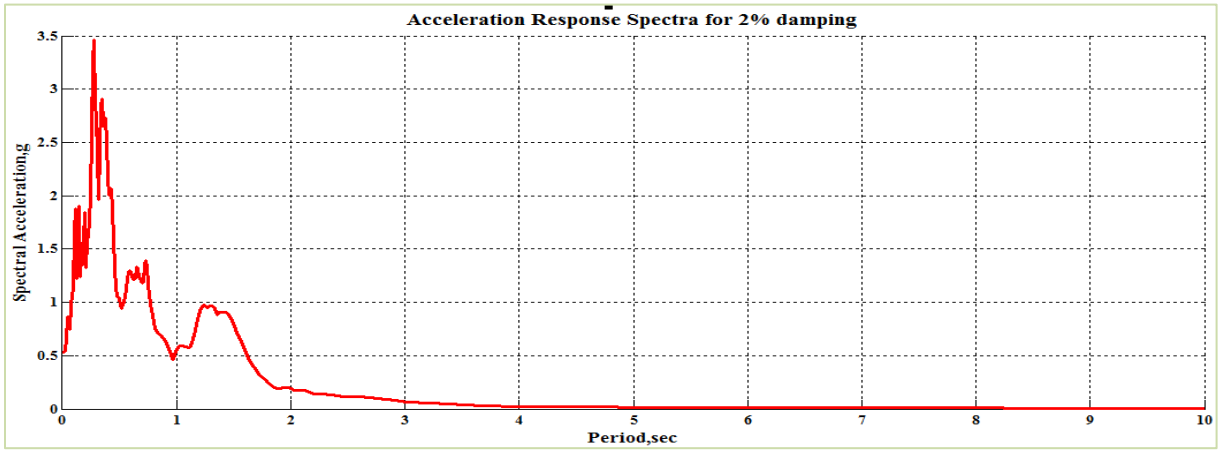

Figure 7-146 Acceleration Response Spectra for 2% Damping

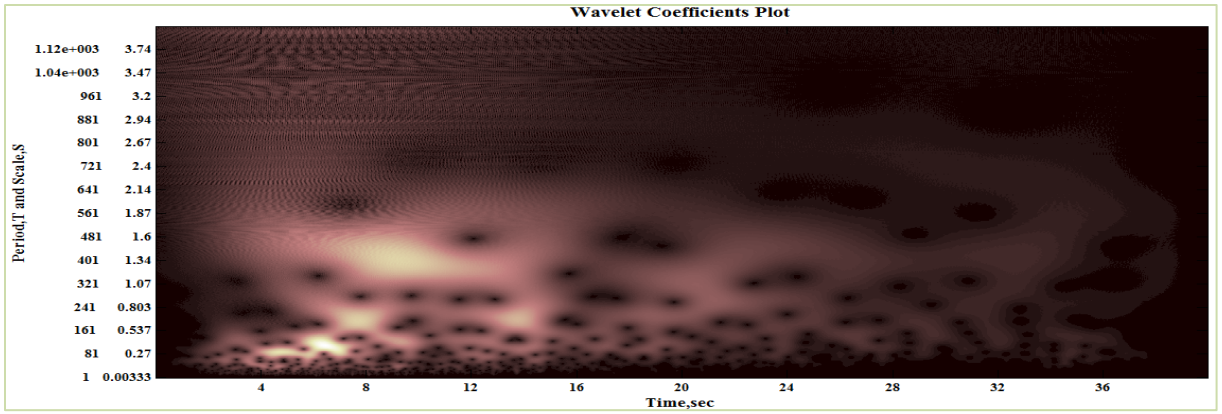

Figure 7-147 2D Wavelet coefficients plot of Ground Motion 13 (Loma Prieta-Capitola)

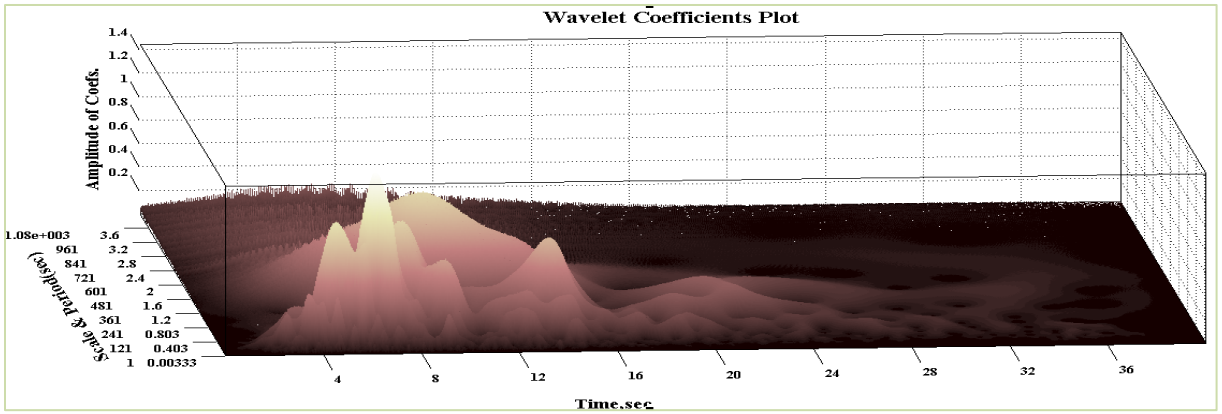

Figure 7-148 3D Wavelet coefficients plot of Ground Motion 13 (Loma Prieta-Capitola)

The 3D and 2D peak displacement plot of the structural system incorporating bilinear elastic behavior is shown in Figures 7-149 and 7-150 respectively. The 2D peak displacement plot as shown in Figure 7-150 have bumps in peak displacement at corresponding (T_0,η) values of (0.75,0.75). This localized increase in peak displacement is hypothesized to be the result of occurrence of moving resonance and hence amplification factor greater than 1 is expected for these combinations of period and strength.

The 3D and 2D peak amplification plot of the structural system incorporating bilinear elastic behavior is shown in Figures 7-151 and 7-152 respectively. It is observed from Figure 7-152 that the amplification values corresponding to (T_0,η) values (0.75,0.75) (at similar places where localized high points of peak displacement were observed in Figure 7-150) are greater than 1 leading to the increase in peak displacement. This increase in peak displacement is considered to be the effect of moving resonance.

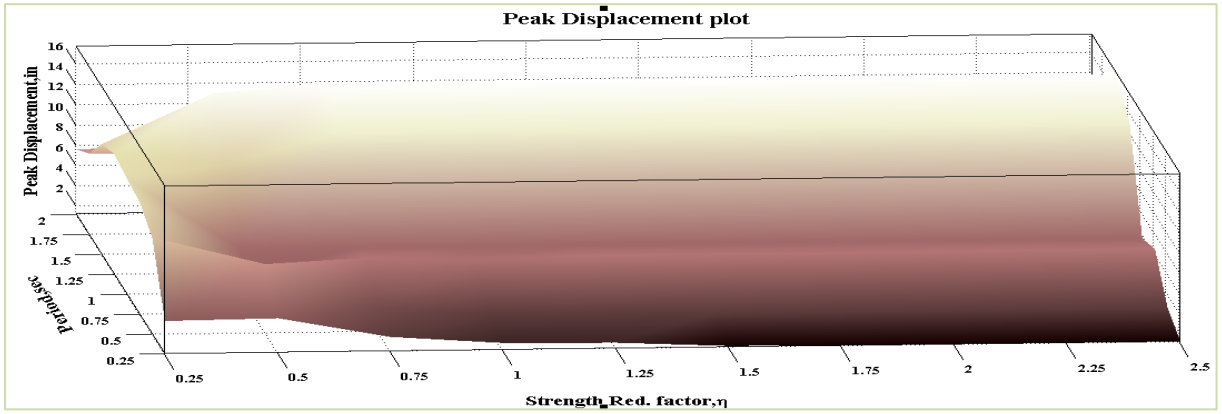

Figure 7-149 3D Peak Displacement plot for Ground Motion 13 (Bilinear Behavior)

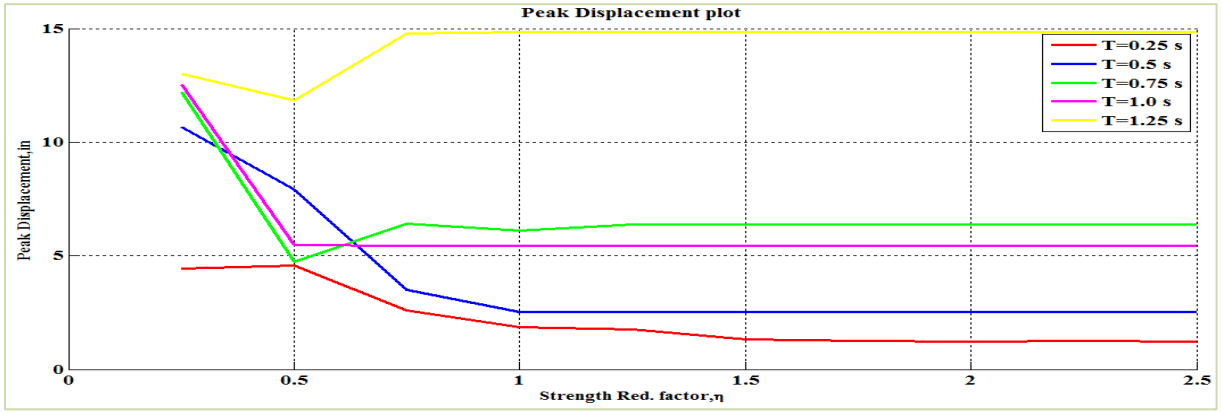

Figure 7-150 2D Peak Displacement plot for Ground Motion 13 (Bilinear Behavior)

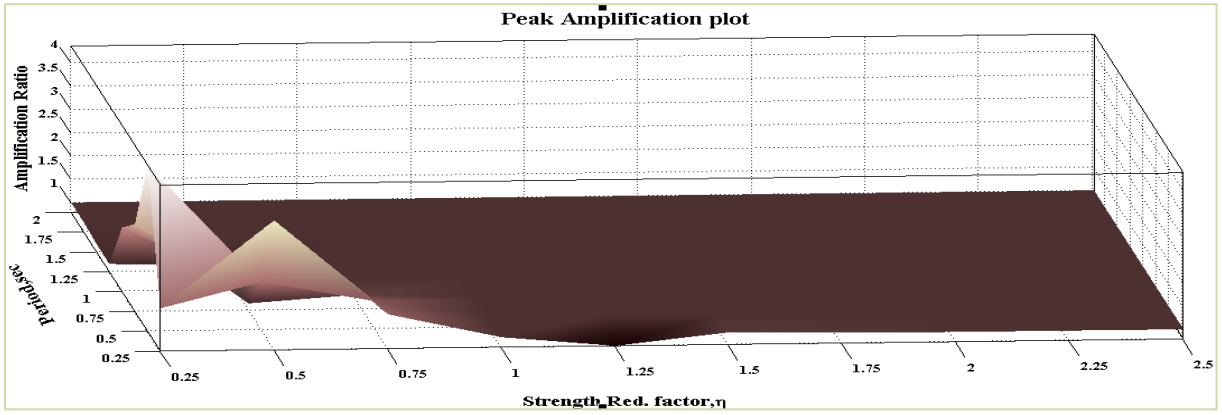

Figure 7-151 3D Peak Amplification plot for Ground Motion 13 (Bilinear Behavior)

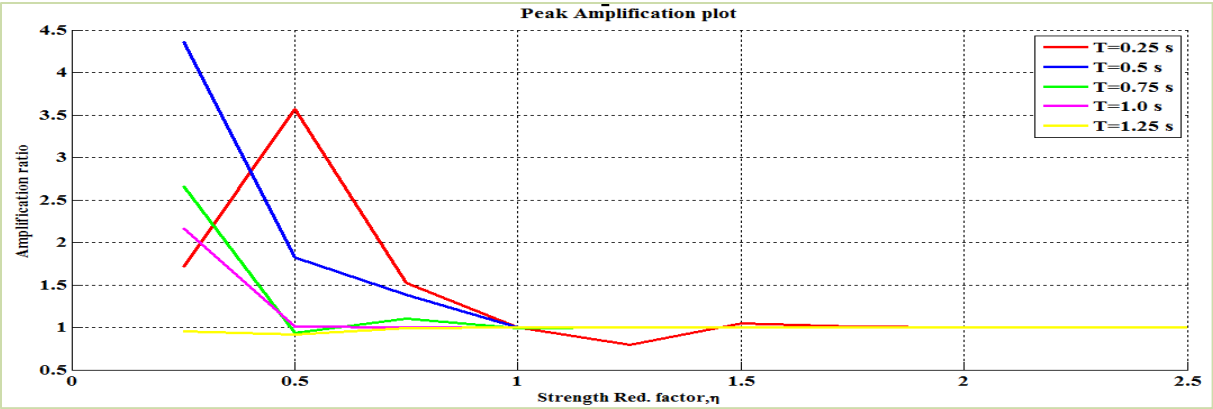

Figure 7-152 2D Peak Amplification plot for Ground Motion 13 (Bilinear Behavior)

The 3D and 2D peak displacement plot of the structural system incorporating elasto-plastic behavior is shown in Figures 7-153 and 7-154 respectively. The 2D peak displacement plot as shown in Figure 7-154 have bumps in peak displacement at corresponding (T_0,η) values of (0.25,1.00),(0.75,0.50) and (0.75,1.00). This localized increase in peak displacement is hypothesized to be the result of occurrence of moving resonance and hence amplification factor greater than 1 is expected for these combinations of period and strength.

The 3D and 2D peak amplification plot of the structural system incorporating elasto-plastic behavior is shown in Figures 7-155 and 7-156 respectively. It is observed from Figure 7-156 that the amplification values corresponding to (T_0,η) values (0.25,1.00),(0.75,0.50) and (0.75,1.00) (at similar places where localized high points of peak displacement were observed in Figure 7-154) are greater than 1 leading to the increase in peak displacement. This increase in peak displacement is considered to be the effect of moving resonance.

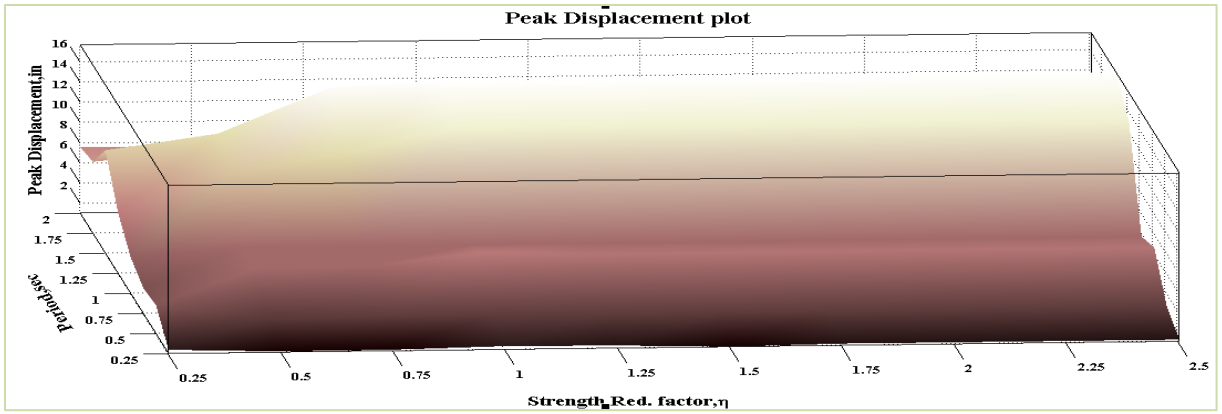

Figure 7-153 3D Peak Displacement plot for Ground Motion 13 (EPP Behavior)

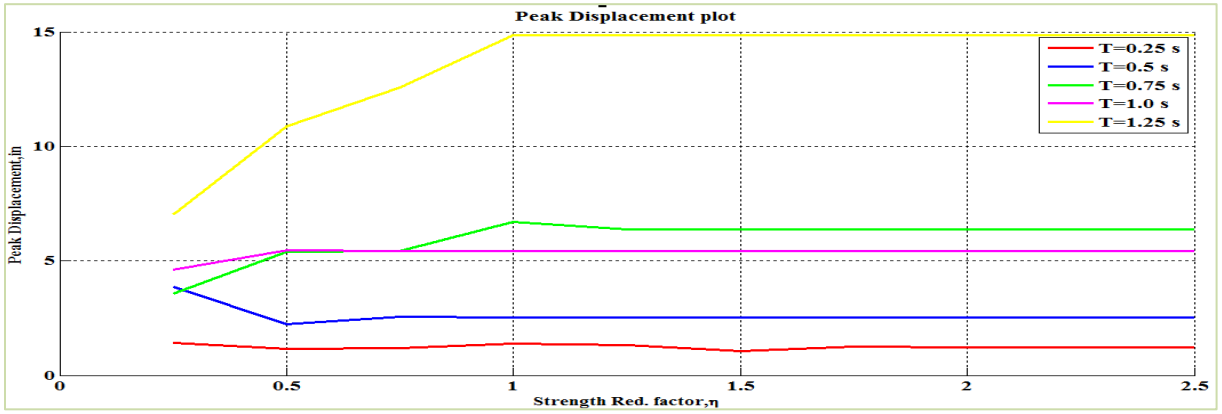

Figure 7-154 2D Peak Displacement plot for Ground Motion 13 (EPP Behavior)

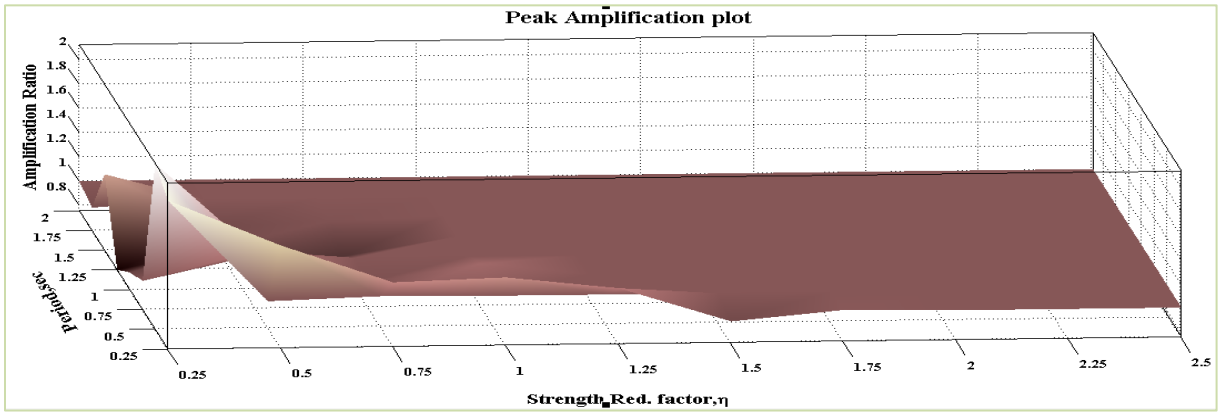

Figure 7-155 3D Peak Amplification plot for Ground Motion 13 (EPP Behavior)

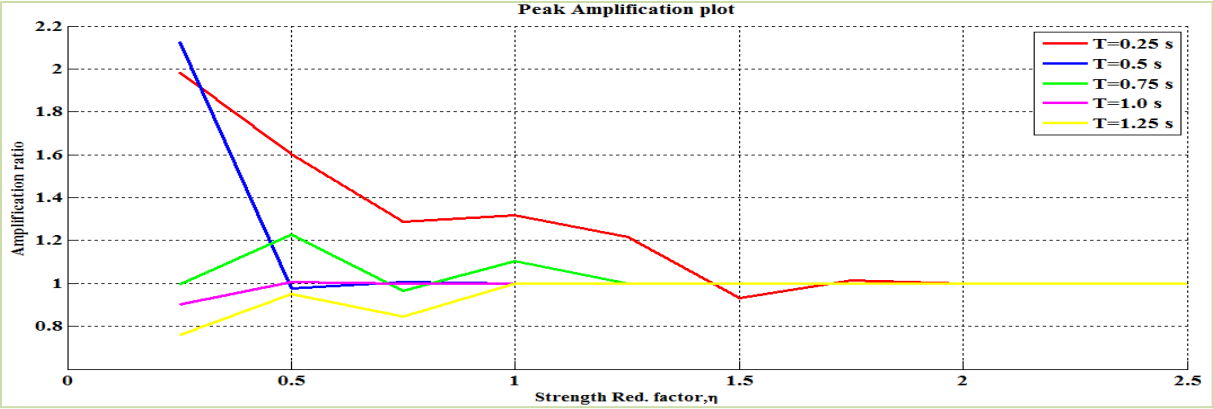

Figure 7-156 2D Peak Amplification plot for Ground Motion 13 (EPP Behavior)

It is concluded that the sequence of energy ridges at gradually increasing period of the ground motion was well suited for moving resonance in both the systems. More significant effect is observed in BE system than the EPP system.

7.2.14 Ground Motion 14: Loma Prieta Earthquake at Gilroy Array

The acceleration time history and the acceleration response spectra for 2 % damping of the component 1 of Loma Prieta earthquake at Gilroy Array station is shown in Figures 7-157 and 7-158 respectively. The 2D and 3D wavelet coefficient plot of this particular ground motion performed using Complex Morlet wavelet of band width 1 and frequency 1.5 is shown in Figures 7-159 and 7-160 respectively.

It can be observed from Figures 7-157 to 7-160 that the energy of this ground motion is concentrated in short time. There are two primary ridges of energy in this ground motion, the second has longer period than the first, but smaller intensity.

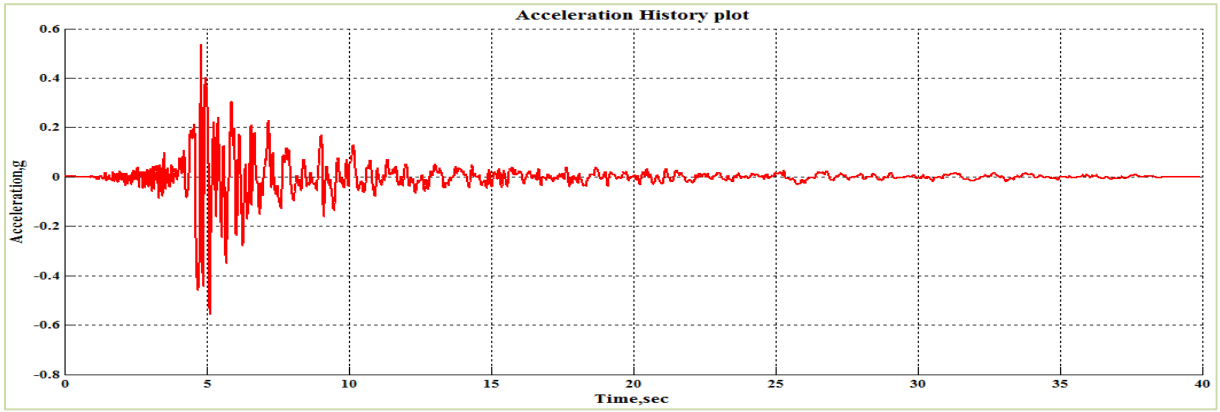

Figure 7-157 Acceleration Time History of Ground Motion 14 (Loma Prieta-Gilroy Array)

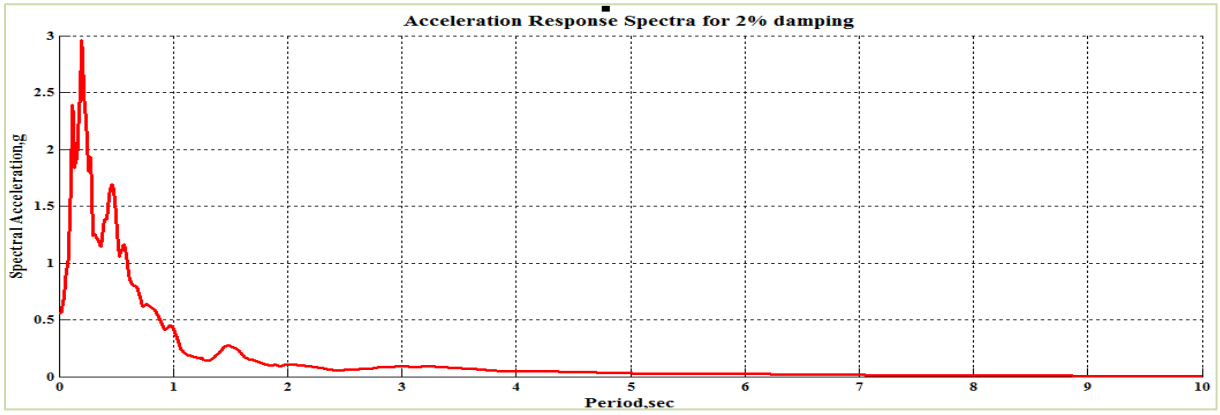

Figure 7-158 Acceleration Response Spectra for 2% Damping

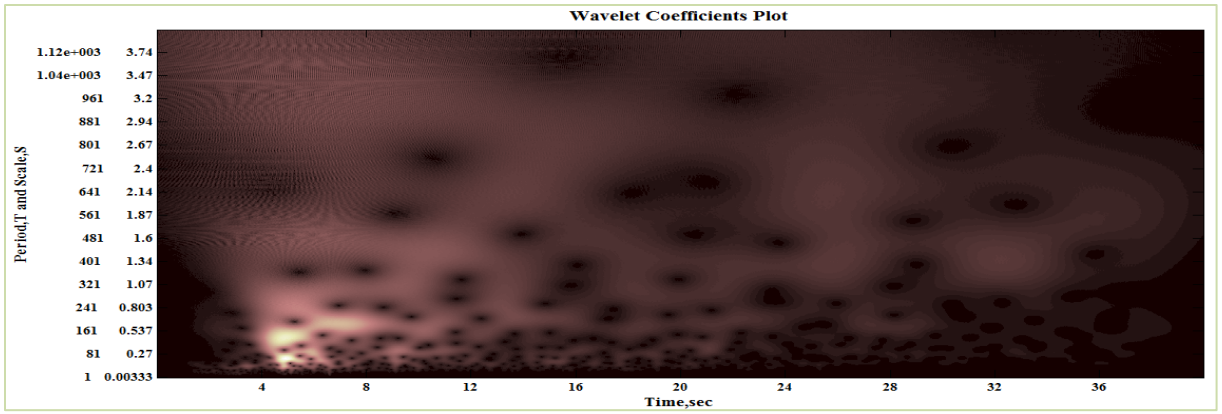

Figure 7-159 2D Wavelet coefficients plot of Ground Motion 14 (Loma Prieta-Gilroy Array)

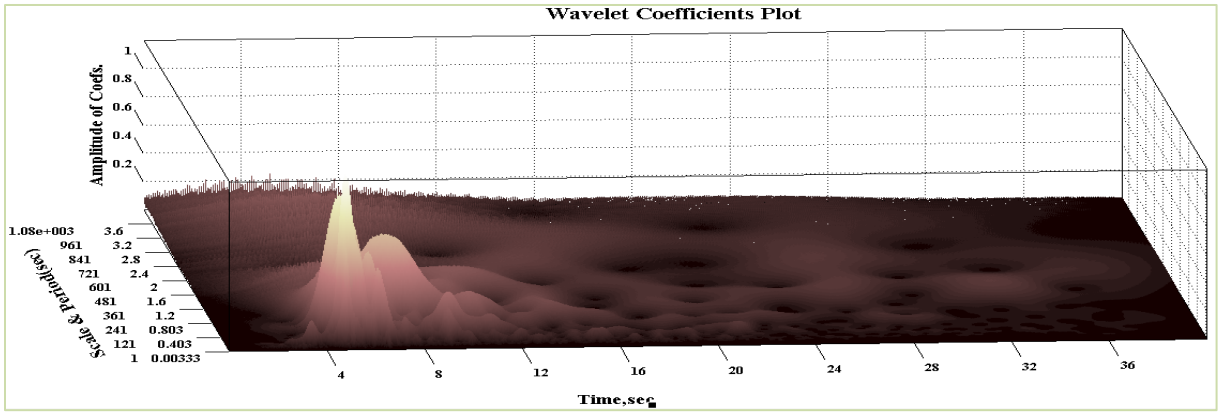

Figure 7-160 3D Wavelet coefficients plot of Ground Motion 14 (Loma Prieta-Gilroy Array)

The 3D and 2D peak displacement plot of the structural system incorporating bilinear elastic behavior is shown in Figures 7-161 and 7-162 respectively. The 2D peak displacement plot as shown in Figure 7-152 have bumps in peak displacement at corresponding (T_0,η) values of (0.5,0.75) and(0.25,1.25). This localized increase in peak displacement is hypothesized to be the result of occurrence of moving resonance and hence amplification factor greater than 1 is expected for these combinations of period and strength.

The 3D and 2D peak amplification plot of the structural system incorporating bilinear elastic behavior is shown in Figures 7-163 and 7-164 respectively. It is observed from Figure 7-164 that the amplification values corresponding to (T_0,η) values (0.5,0.75) and(0.25,1.25) (at similar places where localized high points of peak displacement were observed in Figure 7-162) are greater than 1 leading to the increase in peak displacement. This increase in peak displacement is considered to be the effect of moving resonance.

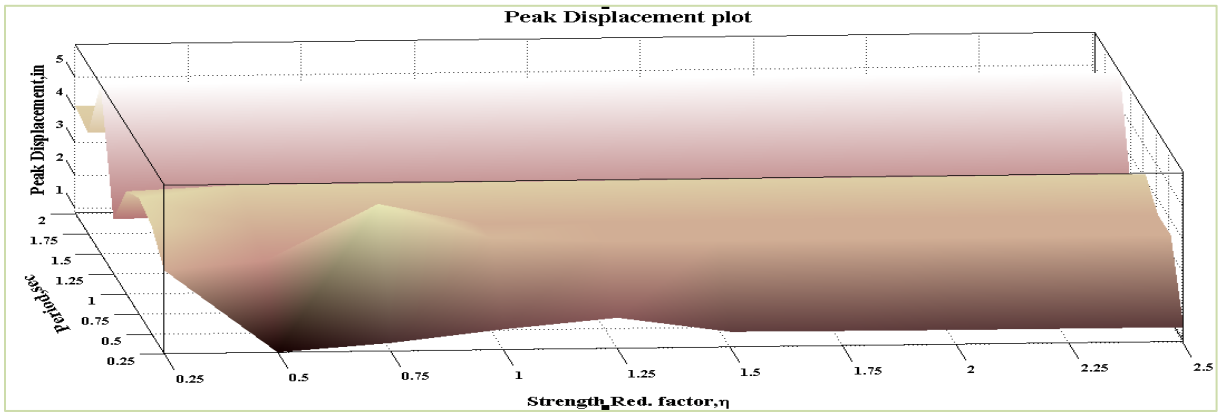

Figure 7-161 3D Peak Displacement plot for Ground Motion 14 (Bilinear Behavior)

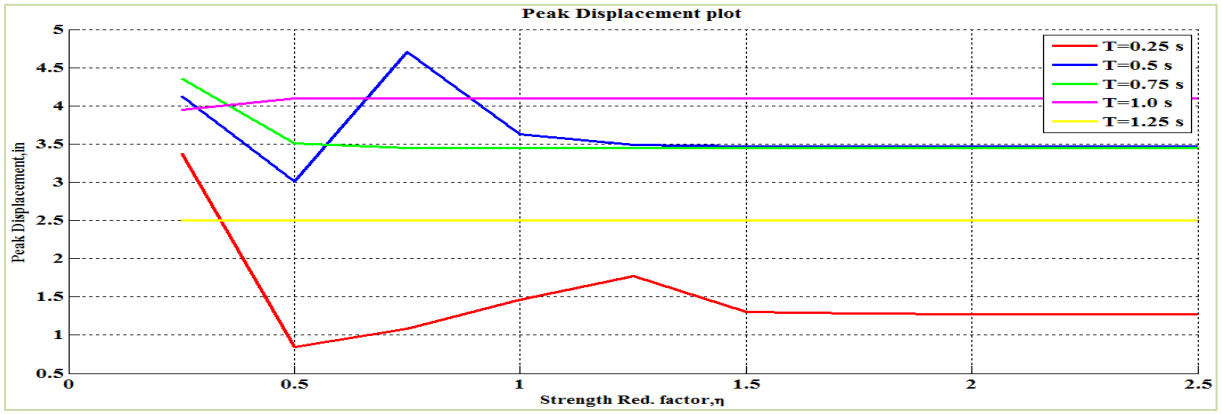

Figure 7-162 2D Peak Displacement plot for Ground Motion 14 (Bilinear Behavior)

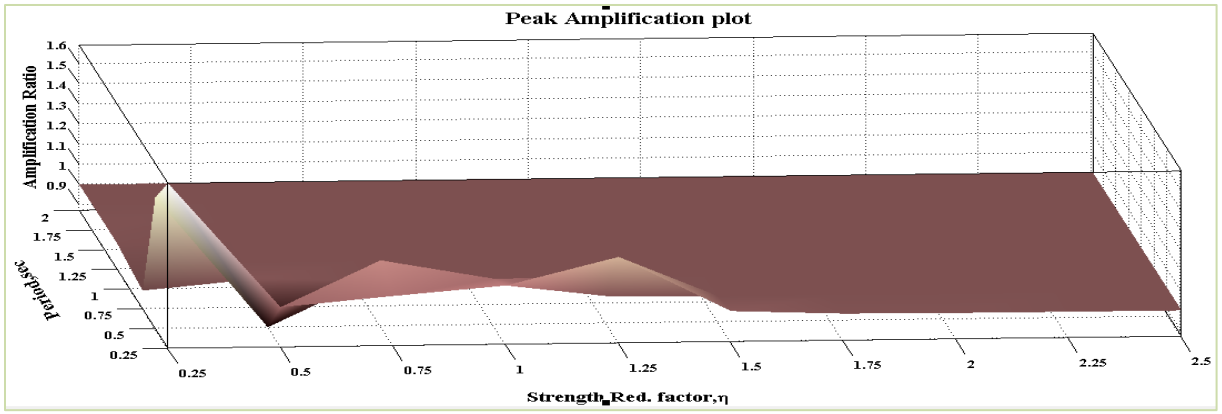

Figure 7-163 3D Peak Amplification plot for Ground Motion 14 (Bilinear Behavior)

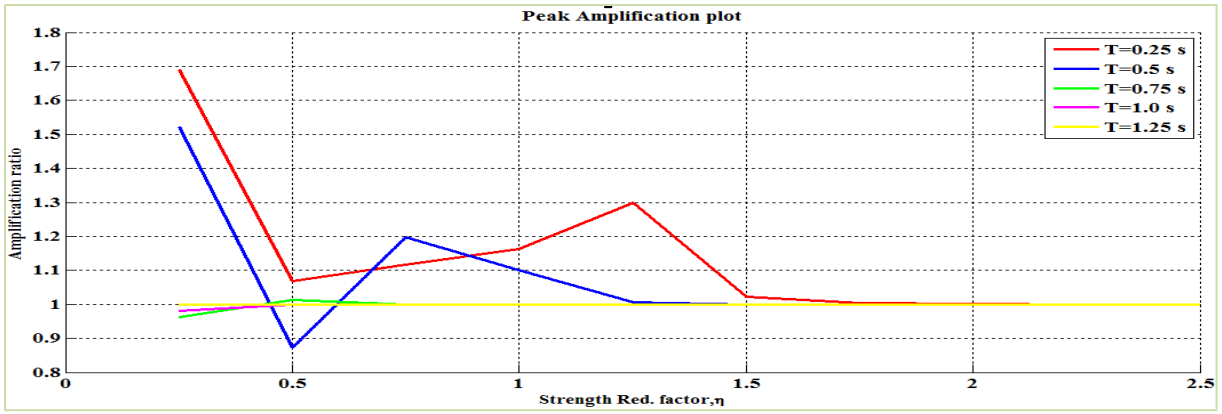

Figure 7-164 2D Peak Amplification plot for Ground Motion 14 (Bilinear Behavior)

The 3D and 2D peak displacement plot of the structural system incorporating elasto-plastic behavior is shown in Figures 7-165 and 7-166 respectively. The 2D peak displacement plot as shown in Figure 7-166 have bumps in peak displacement at corresponding (T_0,η) values of (0.5,0.75) (0.25,1.5) and (0.25,0.75). This localized increase in peak displacement is hypothesized to be the result of occurrence of moving resonance and hence amplification factor greater than 1 is expected for these combinations of period and strength.

The 3D and 2D peak amplification plot of the structural system incorporating elasto-plastic behavior is shown in Figures 7-167 and 7-168 respectively. It is observed from Figure 7-168 that the amplification values corresponding to (T_0,η) values (0.5,0.75) (0.25,1.5) and (0.25,0.75) (at similar places where localized high points of peak displacement were observed in Figure 7-166) are greater than 1 leading to the increase in peak displacement. This increase in peak displacement is considered to be the effect of moving resonance.

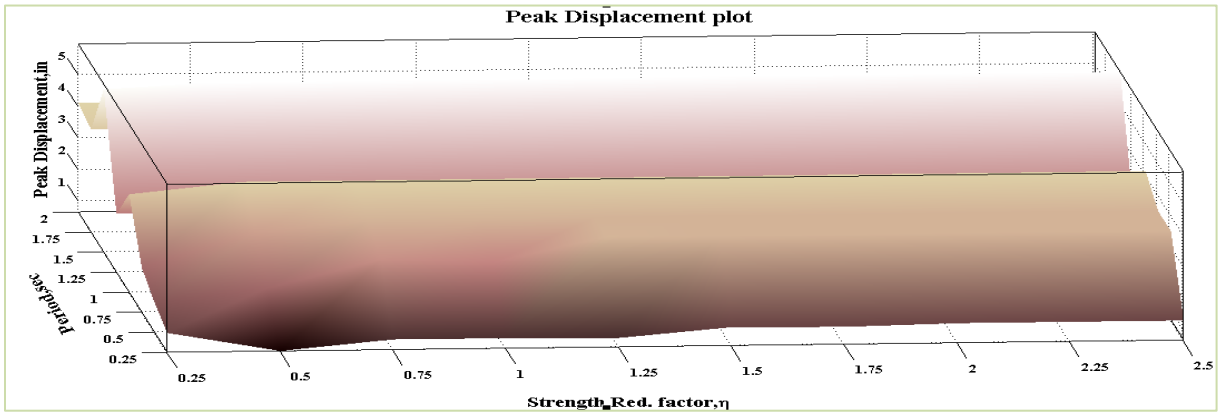

Figure 7-165 3D Peak Displacement plot for Ground Motion 14 (EPP Behavior)

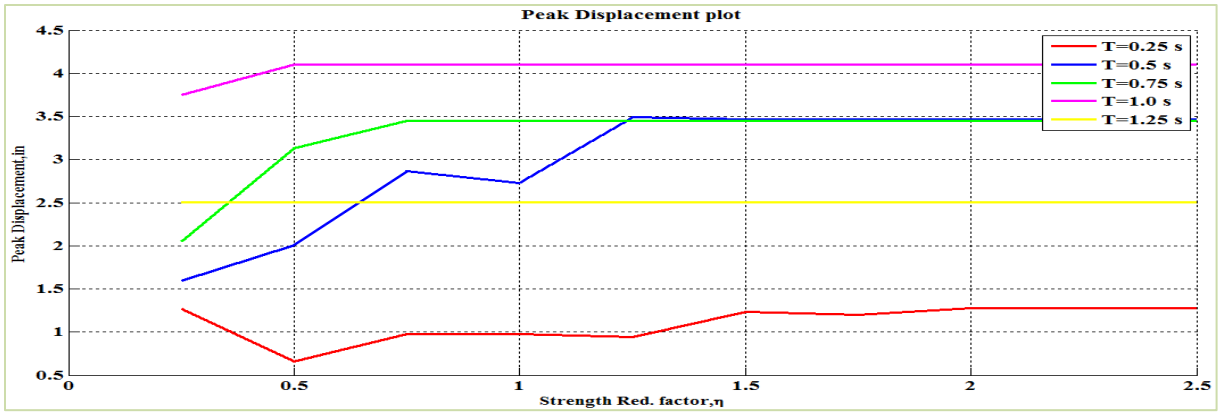

Figure 7-166 2D Peak Displacement plot for Ground Motion 14 (EPP Behavior)

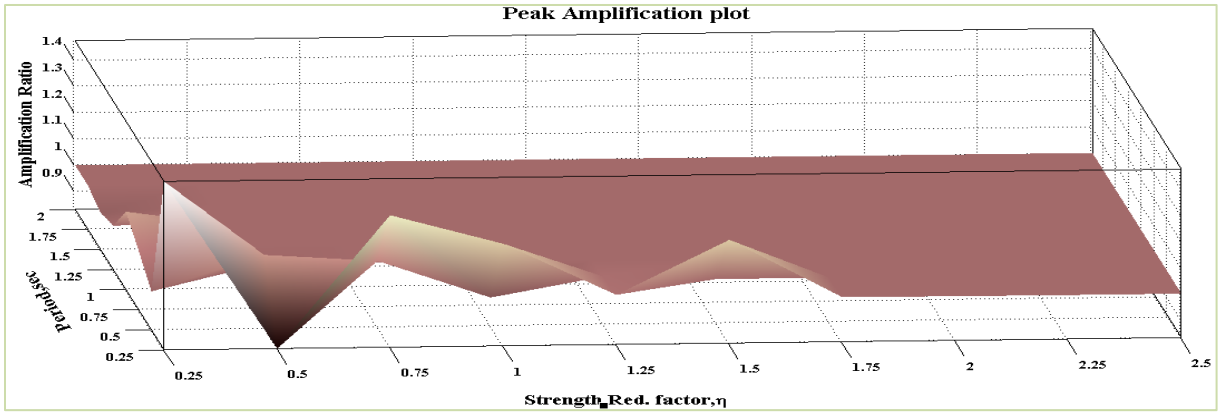

Figure 7-167 3D Peak Amplification plot for Ground Motion 14 (EPP Behavior)

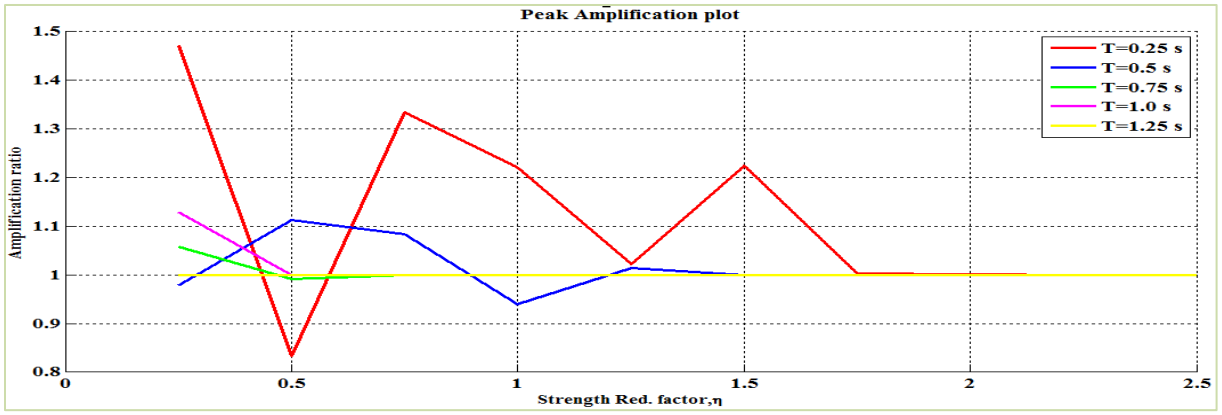

Figure 7-168 2D Peak Amplification plot for Ground Motion 14 (EPP Behavior)

This ground motion had two ridges of energy in which the latter has longer period than the first, but smaller intensity. These ridges located at periods of 0.25 and 0.5 sec (shown in Figure 7-158) are conducive to moving resonance. Expected moving resonance is observed in both the systems with these periods. The effect of moving resonance on EPP systems with periods 0.5 sec is lessened due to hysteretic damping compared to BE system with similar period.

7.2.15 Ground Motion 15: Manjil, Iran Earthquake at Abbas station

The acceleration time history and the acceleration response spectra for 2 % damping of the component 1 of Manjil, Iran earthquake at Abbas station is shown in Figures 7-169 and 7-170 respectively. The 2D and 3D wavelet coefficient plot of this particular ground motion performed using Complex Morlet wavelet of band width 1 and frequency 1.5 is shown in Figures 7-171 and 7-172 respectively.

It is observed from Figures 7-169 to 7-172 that there is a transition of frequency content with lower periods (i.e. 0.25 sec) to moderate periods (i.e.0.50,0.75 sec) between time t=6 sec to time t=12 sec. There is a potential for moving resonance if a system with short period, T_0=0.25 sec experiences the energy in the ground motion at 6 sec then experiences a period elongation to a dominant natural period of 0.75 sec.

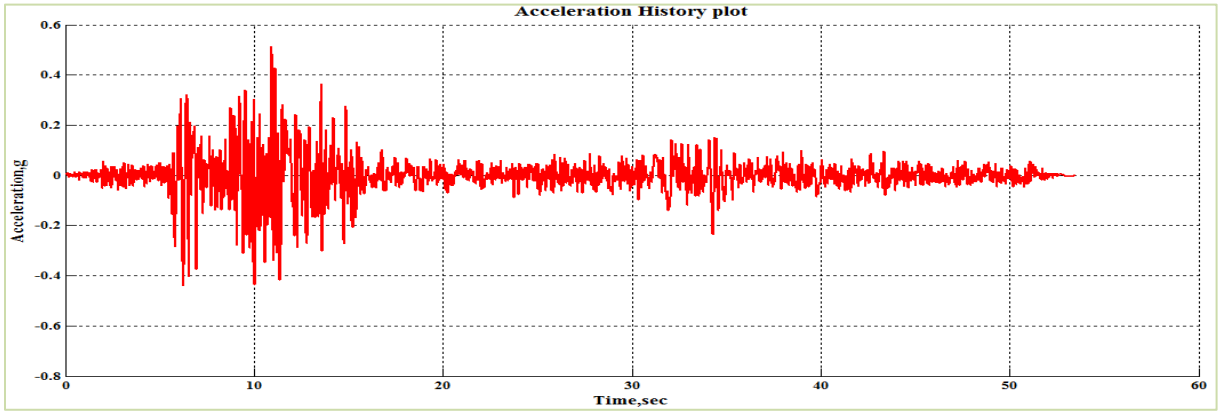

Figure 7-169 Acceleration Time History of Ground Motion 15 (Manjil, Iran-Abbas)

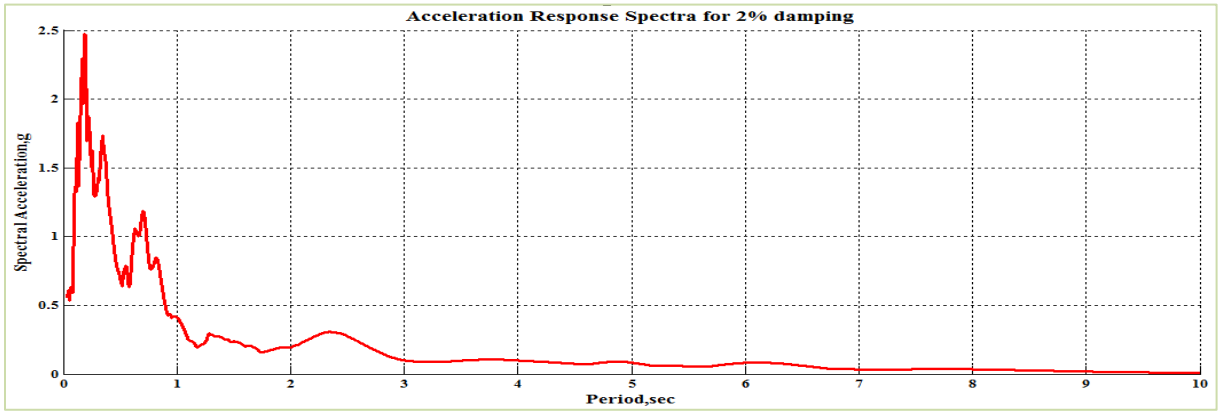

Figure 7-170 Acceleration Response Spectra for 2% Damping

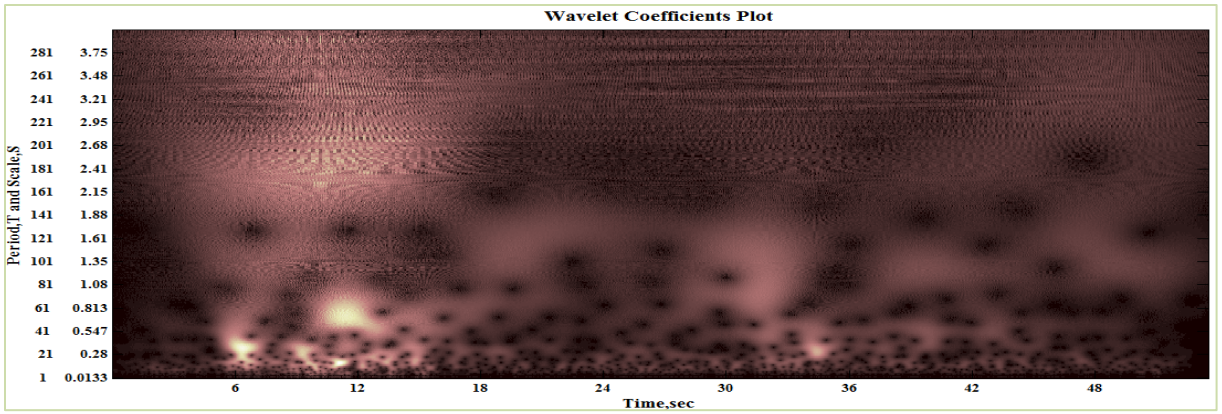

Figure 7-171 2D Wavelet coefficients plot of Ground Motion 15 (Manjil, Iran-Abbas)

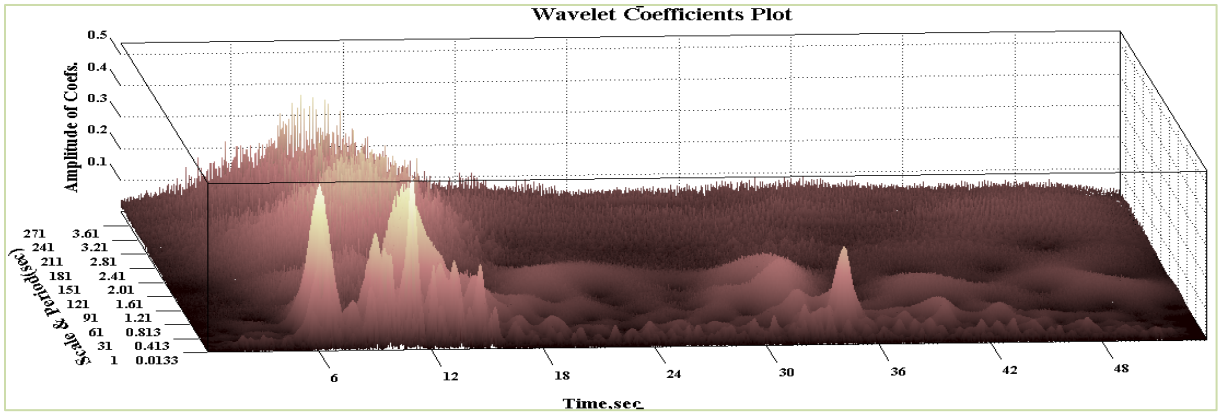

Figure 7-172 3D Wavelet coefficients plot of Ground Motion 15 (Manjil, Iran-Abbas)

The 3D and 2D peak displacement plot of the structural system incorporating bilinear elastic behavior is shown in Figures 7-173 and 7-174 respectively. The 2D peak displacement plot as shown in Figure 7-174 have bumps in peak displacement at corresponding (T_0,η) values of (0.25,0.75). This localized increase in peak displacement is hypothesized to be the result of occurrence of moving resonance and hence amplification factor greater than 1 is expected for these combinations of period and strength.

The 3D and 2D peak amplification plot of the structural system incorporating bilinear elastic behavior is shown in Figures 7-175 and 7-176 respectively. It is observed from Figure 7-176 that the amplification values corresponding to (T_0,η) values (0.25,0.75) (at similar places where localized high points of peak displacement were observed in Figure 7-174) are greater than 1 leading to the increase in peak displacement. This increase in peak displacement is considered to be the effect of moving resonance.

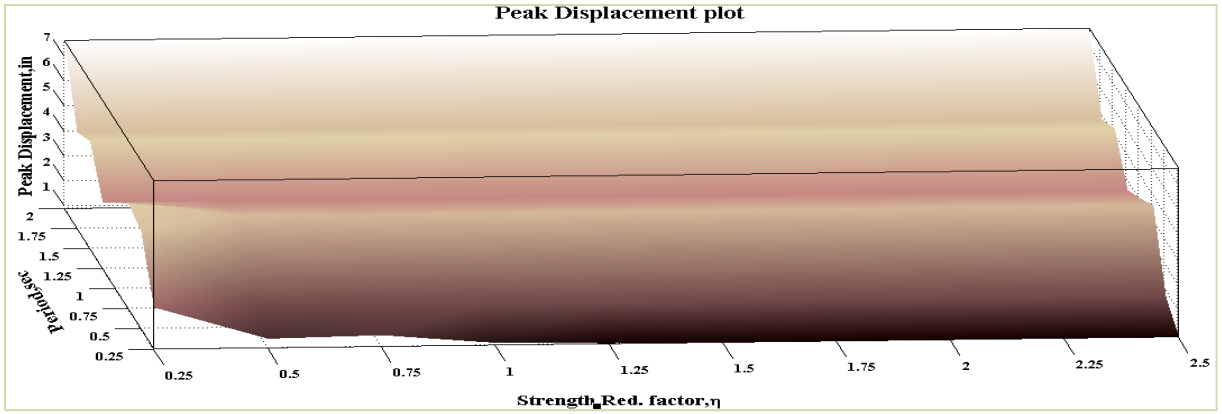

Figure 7-173 3D Peak Displacement plot for Ground Motion 15 (Bilinear Behavior)

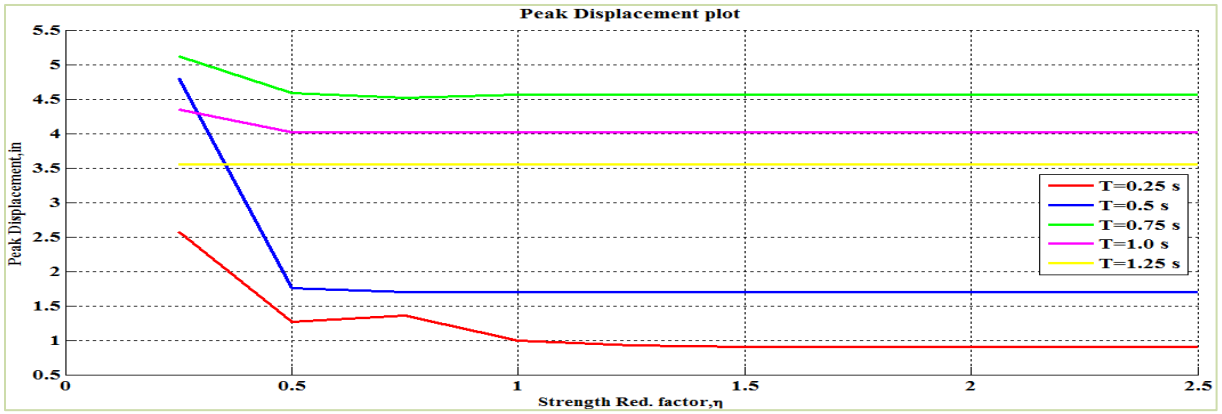

Figure 7-174 2D Peak Displacement plot for Ground Motion 15 (Bilinear Behavior)

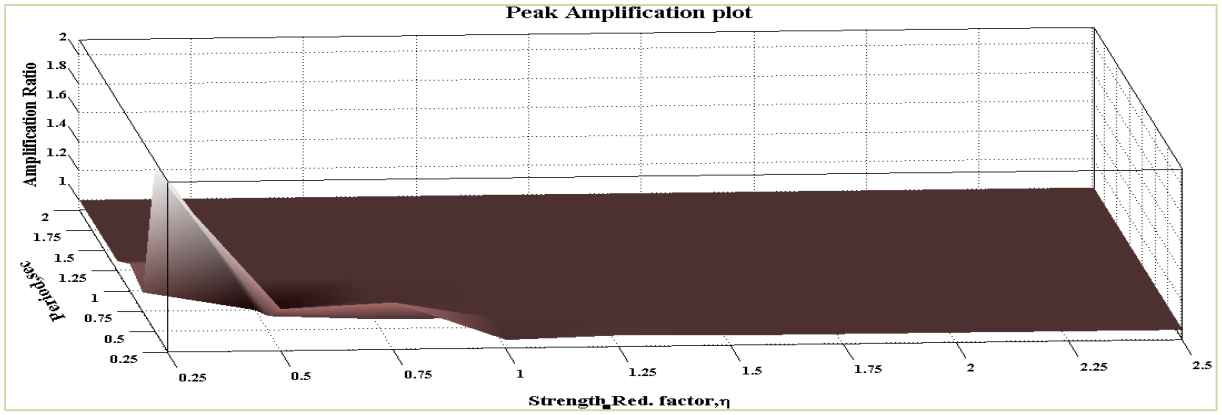

Figure 7-175 3D Peak Amplification plot for Ground Motion 15 (Bilinear Behavior)

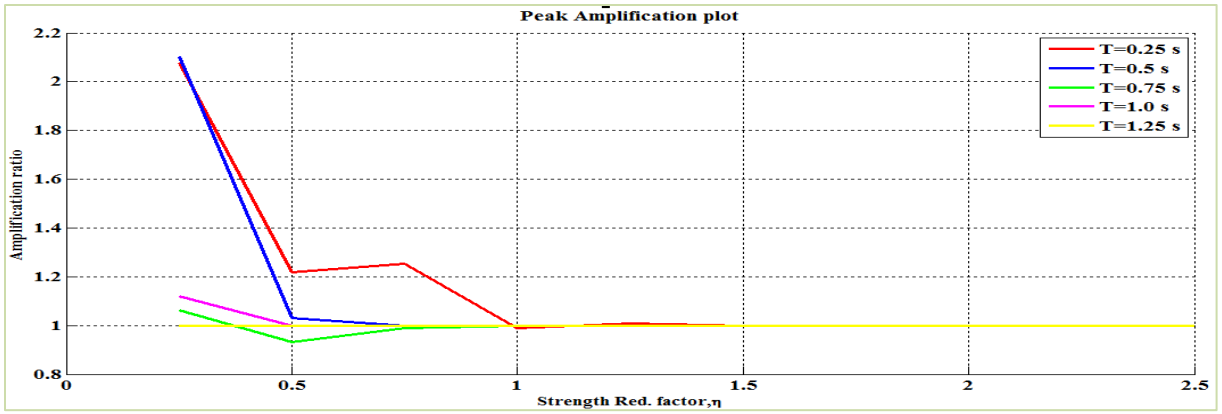

Figure 7-176 2D Peak Amplification plot for Ground Motion 15 (Bilinear Behavior)

The 3D and 2D peak displacement plot of the structural system incorporating elasto-plastic behavior is shown in Figures 7-177 and 7-178 respectively. The 2D peak displacement plot as shown in Figure 7-178 have bumps in peak displacement at corresponding (T_0,η) values of (0.75,0.50). This localized increase in peak displacement is hypothesized to be the result of occurrence of moving resonance and hence amplification factor greater than 1 is expected for these combinations of period and strength.

The 3D and 2D peak amplification plot of the structural system incorporating elasto-plastic behavior is shown in Figures 7-179 and 7-180 respectively. It is observed from Figure 7-180 that the amplification values corresponding to (T_0,η) values (0.75,0.50) (at similar places where localized high points of peak displacement were observed in Figure 7-178) are greater than 1 leading to the increase in peak displacement. This increase in peak displacement is considered to be the effect of moving resonance.

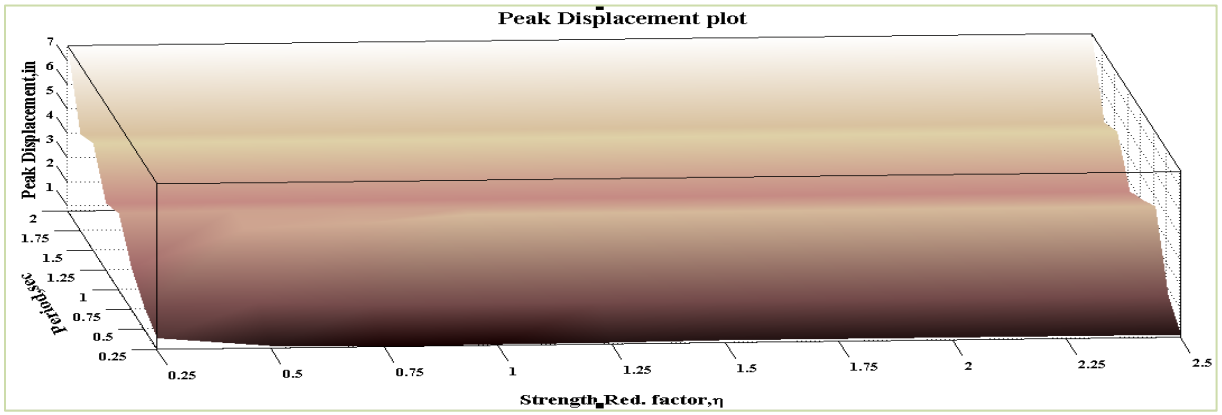

Figure 7-177 3D Peak Displacement plot for Ground Motion 15 (EPP Behavior)

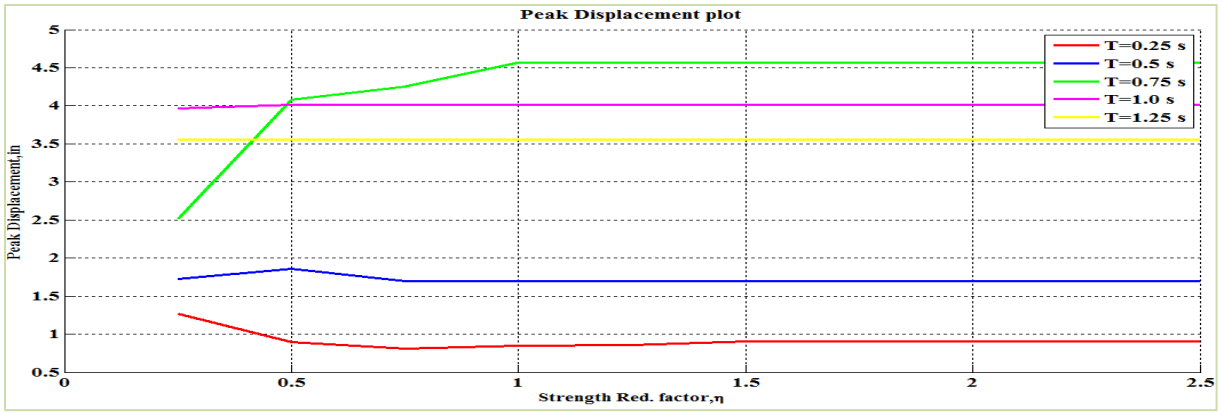

Figure 7-178 2D Peak Displacement plot for Ground Motion 15 (EPP Behavior)

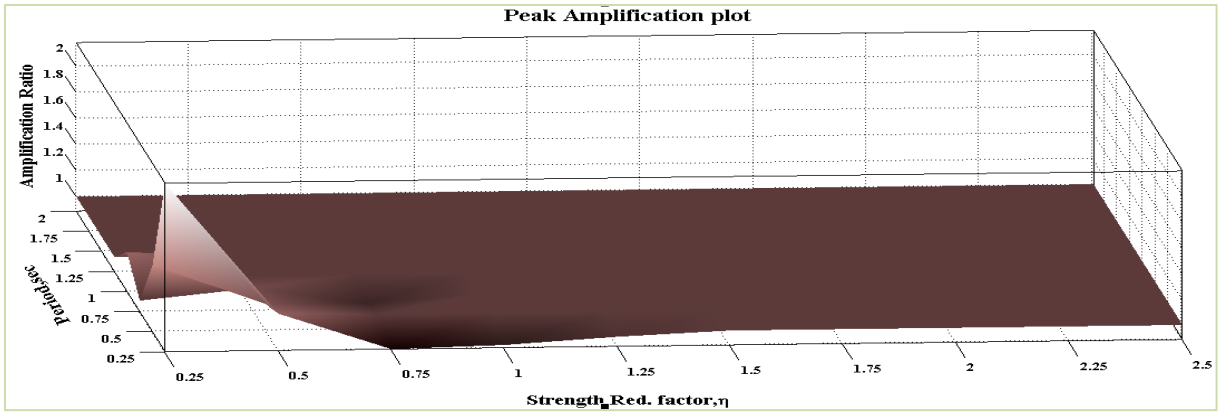

Figure 7-179 3D Peak Amplification plot for Ground Motion 15 (EPP Behavior)

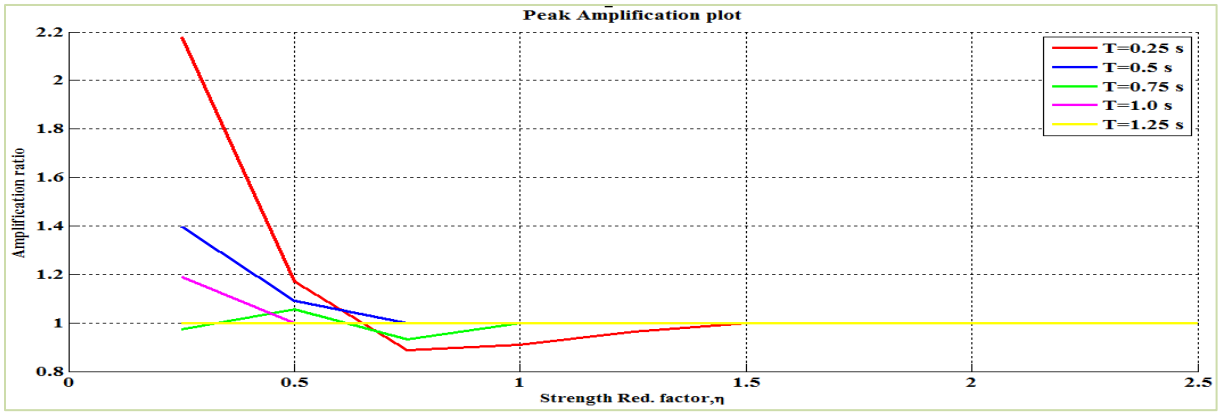

Figure 7-180 2D Peak Amplification plot for Ground Motion 15 (EPP Behavior)

As expected in the discussion of the ground motion characteristics, there was a significant effect of moving resonance for short period structures. Both the BE and EPP systems with period 0.25 sec experienced significant moving resonance.

7.2.16 Ground Motion 16: Superstition Hills Earthquake at El Centro station

The acceleration time history and the acceleration response spectra for 2 % damping of the component 1 of Superstition Hills earthquake at El Centro station is shown in Figures 7-181 and 7-182 respectively. The 2D and 3D wavelet coefficient plot of this particular ground motion performed using Complex Morlet wavelet of band width 1 and frequency 1.5 is shown in Figures 7-183 and 7-184 respectively.

It can be observed from Figures 7-181 to 7-184 that most of the energy in the ground motion is concentrated in a short length of time – about three seconds. Though the energy is concentrates in a narrow time band, it is spread out in dominant period.

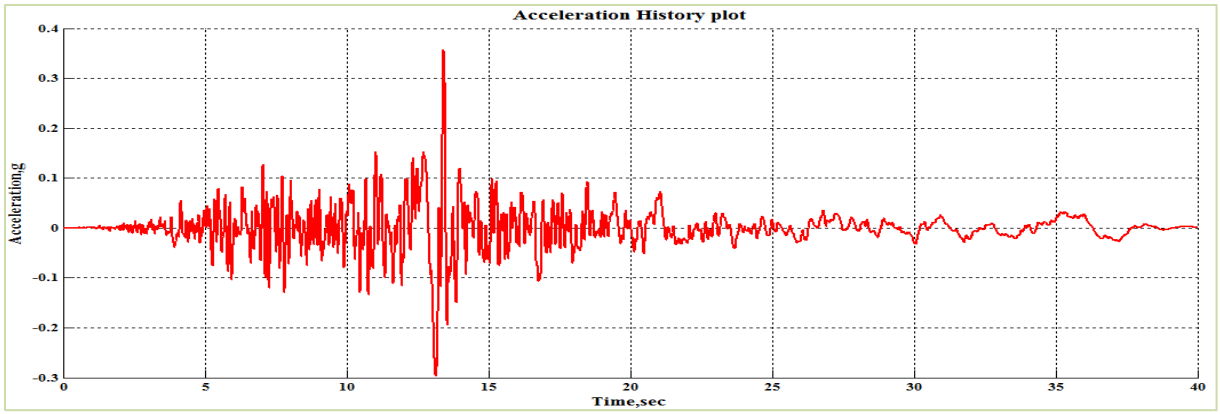

Figure 7-181 Acceleration Time History of Ground Motion 16 (Superstition Hills, El Centro)

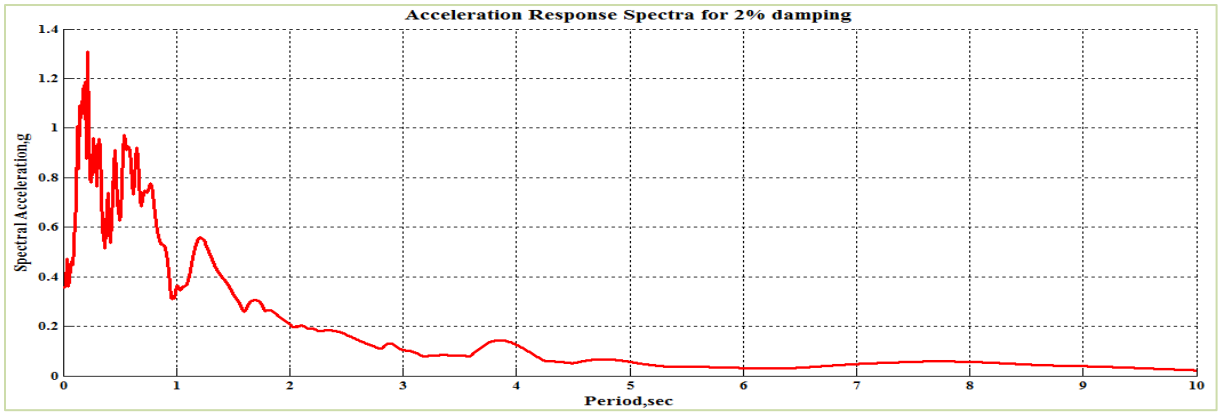

Figure 7-182 Acceleration Response Spectra for 2% Damping

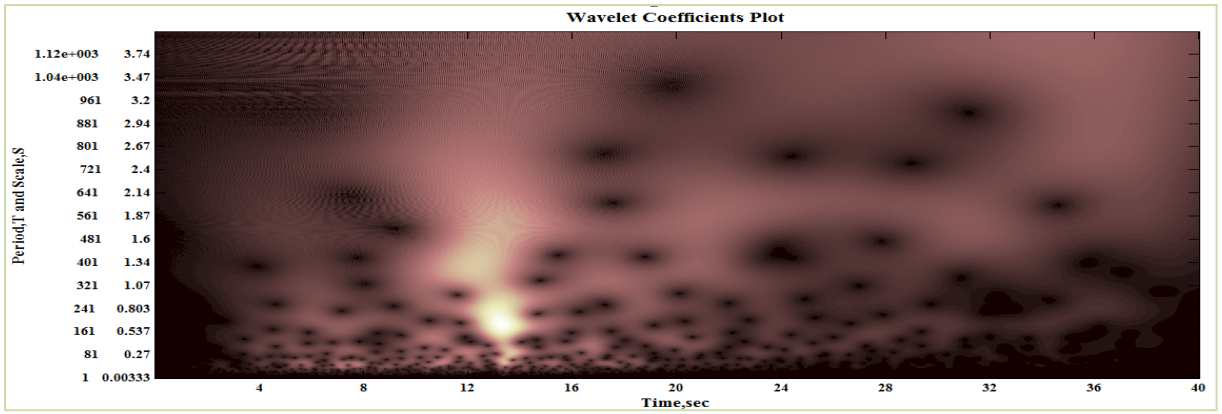

Figure 7-183 2D Wavelet coefficients plot of Ground Motion 16 (Superstition Hills, El Centro)

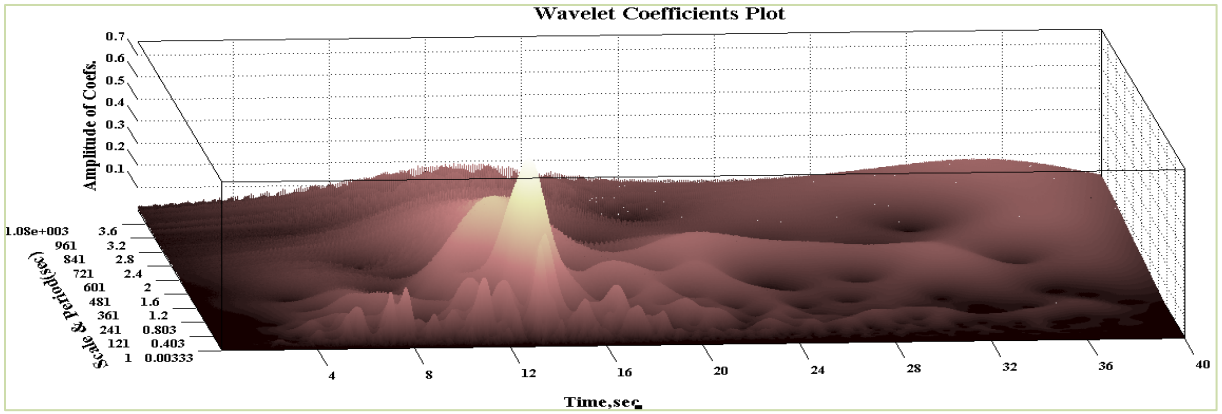

Figure 7-184 2D Wavelet coefficients plot of Ground Motion 16 (Superstition Hills, El Centro)

The 3D and 2D peak displacement plot of the structural system incorporating bilinear elastic behavior is shown in Figures 7-185 and 7-186 respectively. The 2D peak displacement plot as shown in Figure 7-186 doesn`t have significant bumps (localized high points) in peak displacement. Hence, the amplification factor is expected to be equal to 1. It is observed from Figure 7-186 that the system becomes elastic for relatively very low strength reduction factor.

The 3D and 2D peak amplification plot of the structural system incorporating bilinear elastic behavior is shown in Figures 7-187 and 7-188 respectively. It is observed from Figure 7-188 that though there are no significant bumps in peak displacement, for small eta systems, the amplification factors are greater than 1. The possible reason for this is that the period is likely elongating such that the dominant period matches the ridge in ground motion energy.

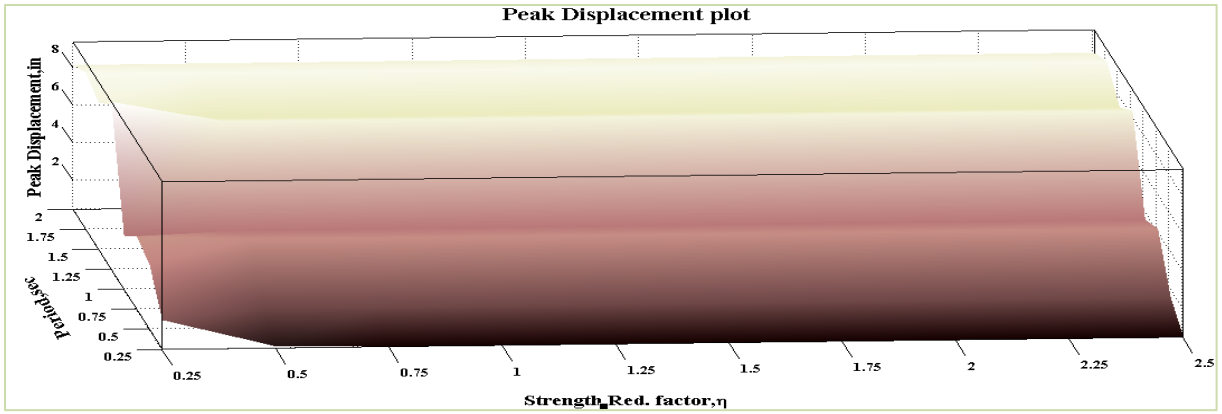

Figure 7-185 3D Peak Displacement plot for Ground Motion 16 (Bilinear Behavior)

Figure 7-186 2D Peak Displacement plot for Ground Motion 16 (Bilinear Behavior)

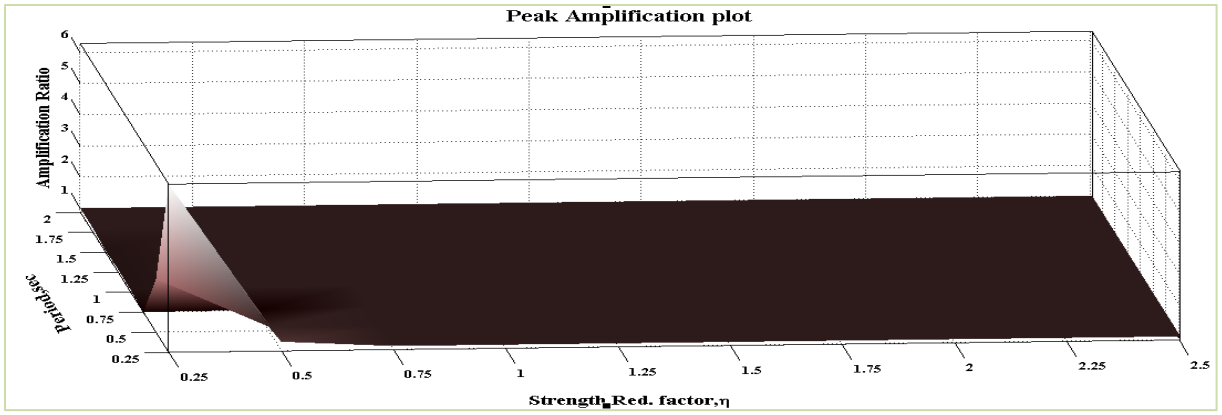

Figure 7-187 3D Peak Amplification plot for Ground Motion 16 (Bilinear Behavior)

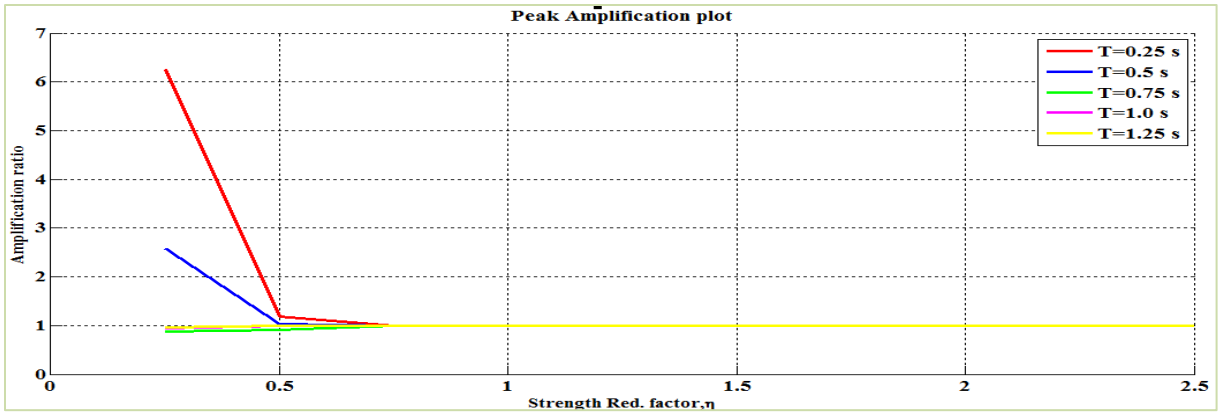

Figure 7-188 2D Peak Amplification plot for Ground Motion 16 (Bilinear Behavior)

The 3D and 2D peak displacement plot of the structural system incorporating elasto-plastic behavior is shown in Figures 7-189 and 7-190 respectively. The 2D peak displacement plot as shown in Figure 7-190 doesn`t have significant bumps (localized high points) in peak displacement. Hence, the amplification factor is expected to be equal to 1. It is observed from Figure 7-190 that the system becomes elastic for relatively very low strength reduction factor.

The 3D and 2D peak amplification plot of the structural system incorporating elasto-plastic behavior is shown in Figures 7-191 and 7-192 respectively. It is observed from Figure 7-192 that though there are no significant bumps in peak displacement, for small eta systems, the amplification factors are greater than 1. It is interesting that period of 0.75 sec system has large amplification for small eta. It is more likely that the system is undergoing period elongation and hitting the ground motion energy at period of 1.25 sec.

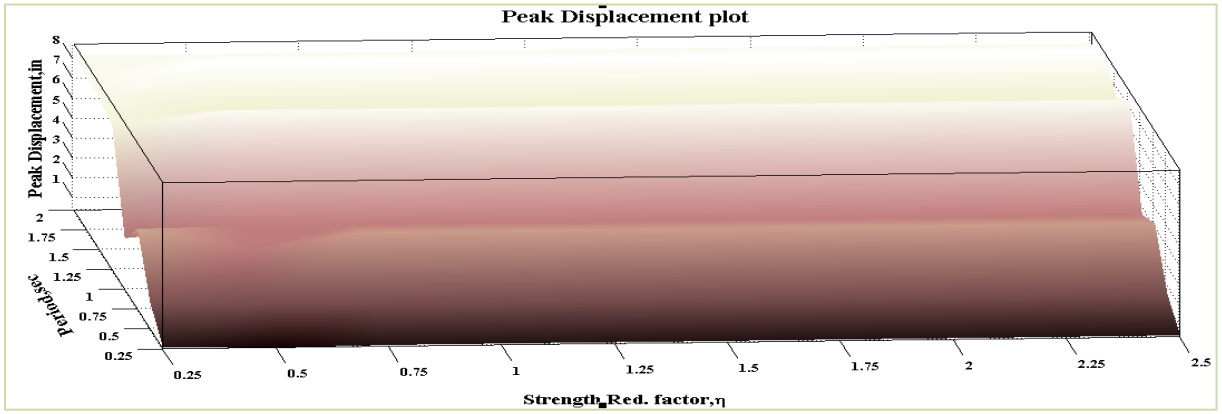

Figure 7-189 3D Peak Displacement plot for Ground Motion 16 (EPP Behavior)

Figure 7-190 2D Peak Displacement plot for Ground Motion 16 (EPP Behavior)

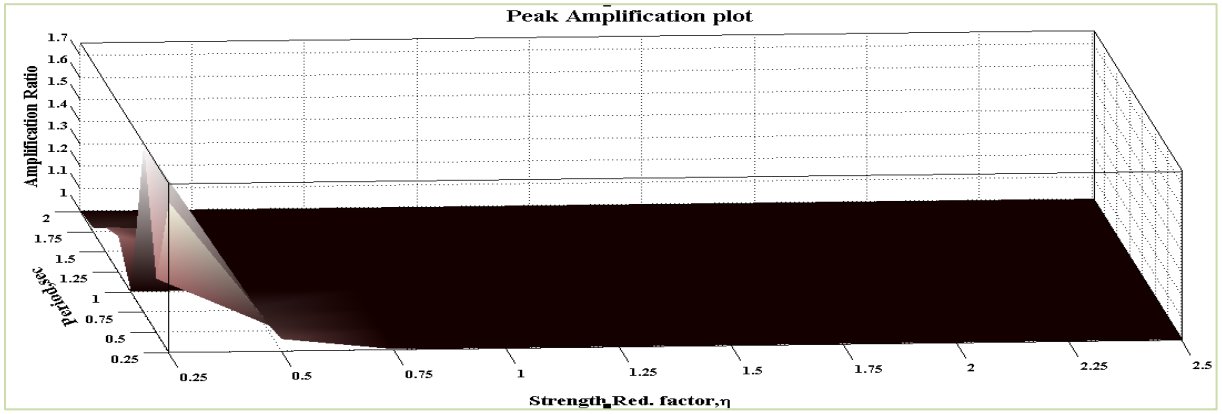

Figure 7-191 3D Peak Amplification plot for Ground Motion 16 (EPP Behavior)

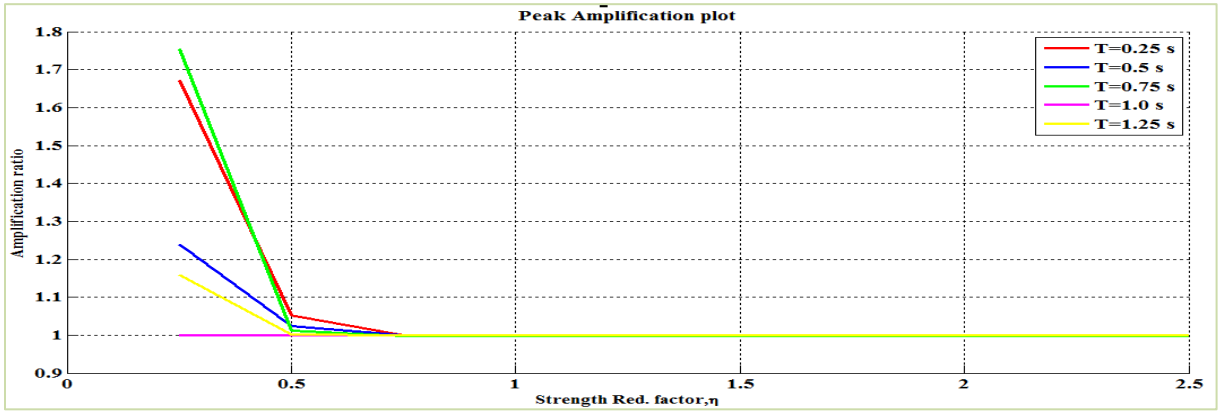

Figure 7-192 2D Peak Amplification plot for Ground Motion 16 (EPP Behavior)

The frequency content is concentrated in a short length of time and its energy is spread out in the period range that it covers. The systems with small eta values experienced significant amplification factors similar to the ground motion 11 which has similar characteristics like this one.

7.2.17 Ground Motion 17: Superstition Hills Earthquake at Poe road

The acceleration time history and the acceleration response spectra for 2 % damping of the component 1 of Superstition Hills earthquake at Poe road station is shown in Figures 7-193 and 7-194 respectively. The 2D and 3D wavelet coefficient plot of this particular ground motion performed using Complex Morlet wavelet of band width 1 and frequency 1.5 is shown in Figures 7-195 and 7-196 respectively.

It can be observed from Figures 7-193 to 7-196 that the ground motion has two distinct ridges of energy, each about two seconds long, both at approximately the same dominant period(around 0.5 sec), but separated by about five seconds. It might be expected that there would be some potential for moving resonance for systems with periods starting below 0.5 sec.

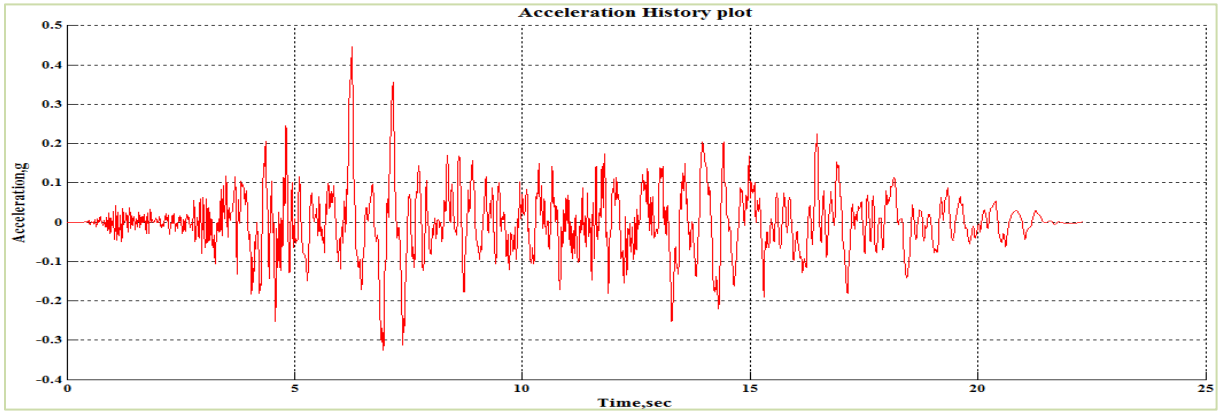

Figure 7-193 Acceleration Time History of Ground Motion 17 (Superstition Hills-Poe road)

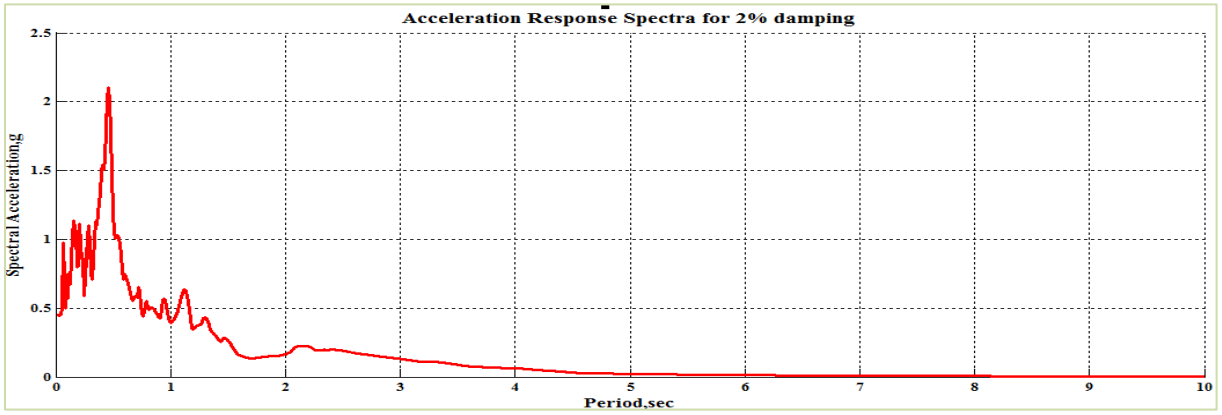

Figure 7-194 Acceleration Response Spectra for 2% Damping

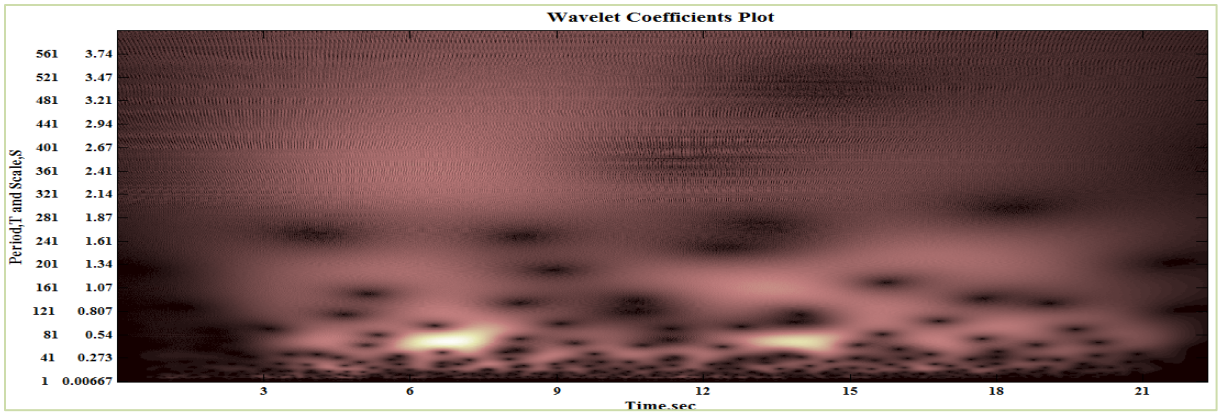

Figure 7-195 2D Wavelet coefficients plot of Ground Motion 17 (Superstition Hills-Poe road)

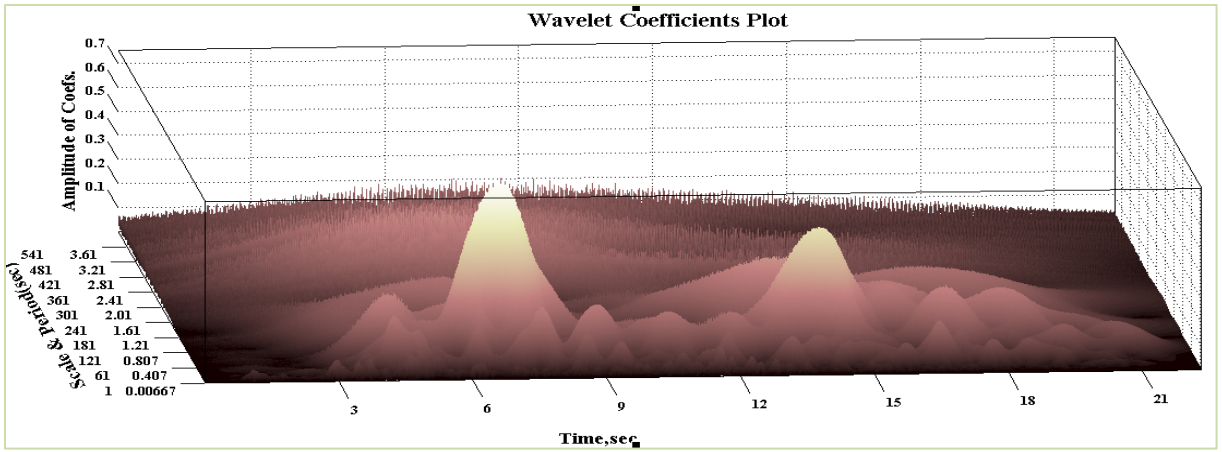

Figure 7-196 3D Wavelet coefficients plot of Ground Motion 17 (Superstition Hills-Poe road)

The 3D and 2D peak displacement plot of the structural system incorporating bilinear elastic behavior is shown in Figures 7-197 and 7-198 respectively. The 2D peak displacement plot as shown in Figure 7-198 doesn`t have significant bumps (localized high points) in peak displacement. Hence, the amplification factor is expected to be equal to 1. It is observed from Figure 7-198 that the system becomes elastic for relatively very low strength reduction factor.

The 3D and 2D peak amplification plot of the structural system incorporating bilinear elastic behavior is shown in Figures 7-199 and 7-200 respectively. It is observed from Figure 7-128 that though there are no significant bumps in peak displacement, for small eta systems, the amplification factors are greater than 1.

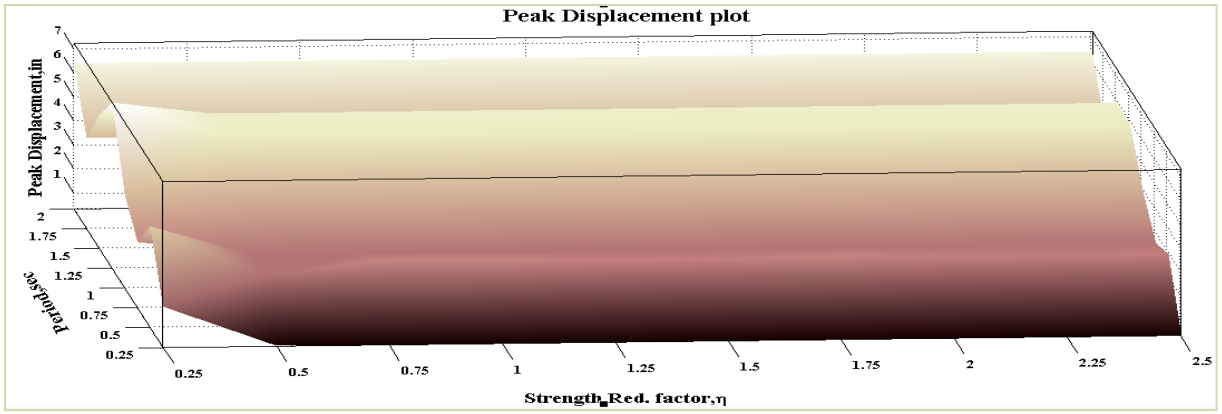

Figure 7-197 3D Peak Displacement plot for Ground Motion 17 (Bilinear Behavior)

Figure 7-198 2D Peak Displacement plot for Ground Motion 17 (Bilinear Behavior)

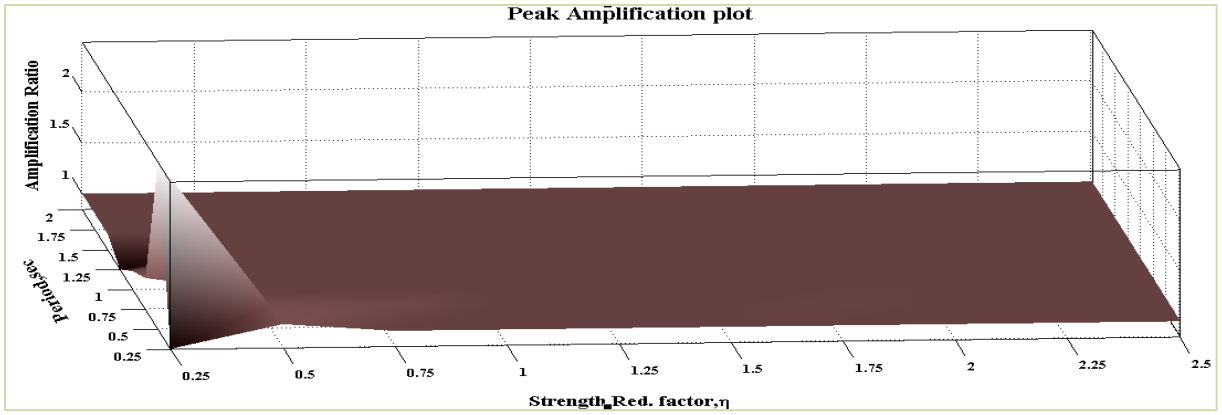

Figure 7-199 3D Peak Amplification plot for Ground Motion 17 (Bilinear Behavior)

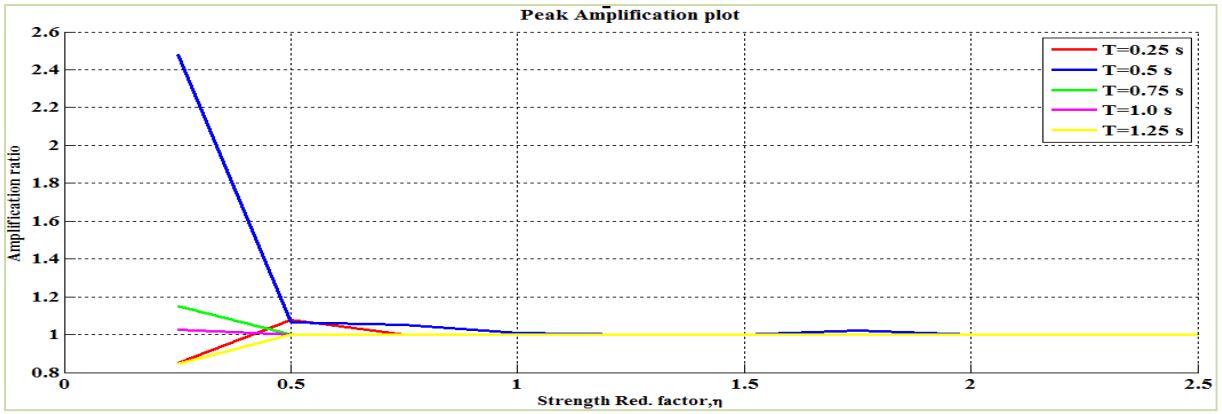

Figure 7-200 2D Peak Amplification plot for Ground Motion 17 (Bilinear Behavior)

The 3D and 2D peak displacement plot of the structural system incorporating elasto-plastic behavior is shown in Figures 7-201 and 7-202 respectively. The 2D peak displacement plot as shown in Figure 7-202 doesn`t have significant bumps (localized high points) in peak displacement. Hence, the amplification factor is expected to be equal to 1. It is observed from Figure 7-202 that the system becomes elastic for relatively very low strength reduction factor.

The 3D and 2D peak amplification plot of the structural system incorporating elasto-plastic behavior is shown in Figures 7-203 and 7-204 respectively. It is observed from Figure 7-204 that though there are no significant bumps in peak displacement, for small eta systems, the amplification factors are greater than 1.

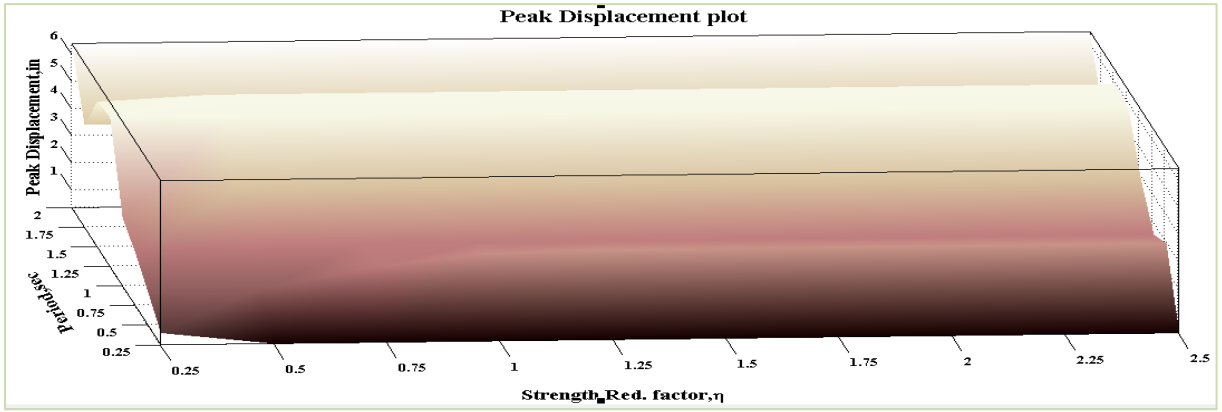

Figure 7-201 3D Peak Displacement plot for Ground Motion 17 (EPP Behavior)

Figure 7-202 2D Peak Displacement plot for Ground Motion 17 (EPP Behavior)

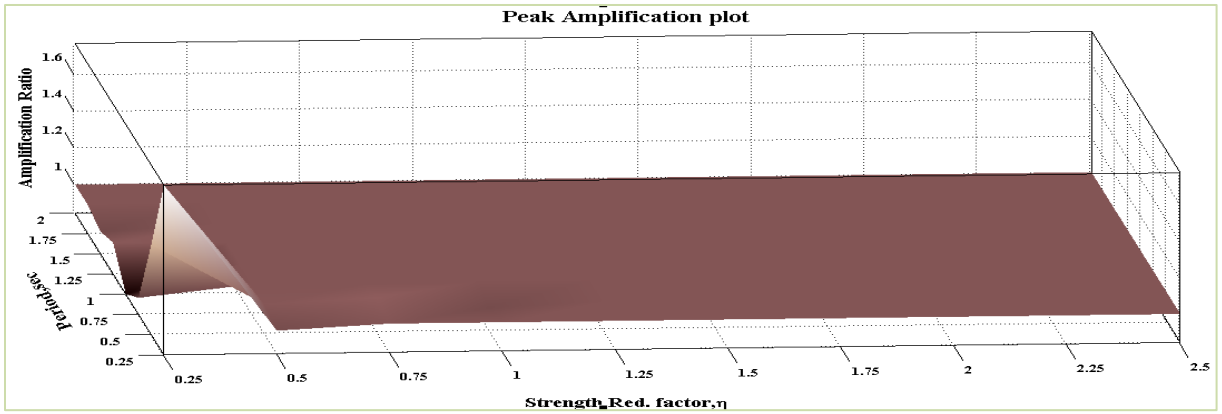

Figure 7-203 3D Peak Amplification plot for Ground Motion 17 (EPP Behavior)

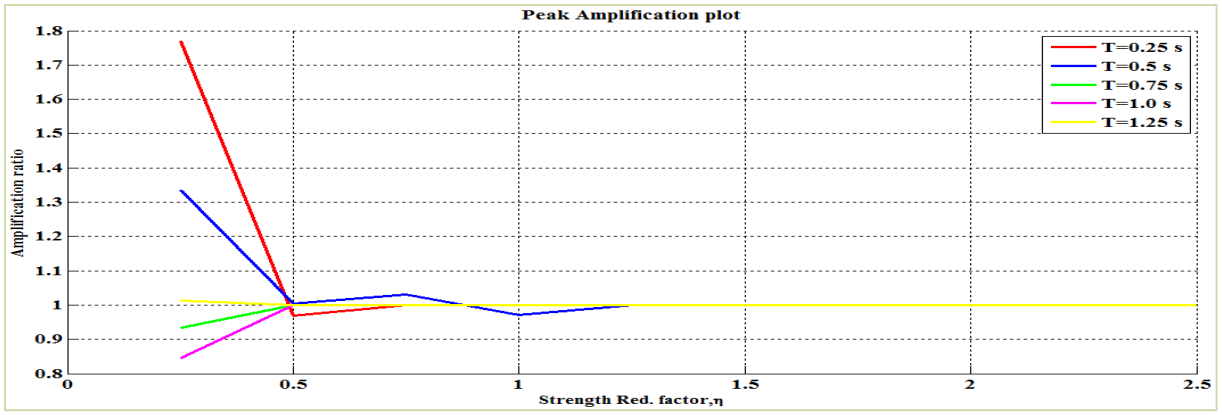

Figure 7-204 2D Peak Amplification plot for Ground Motion 17 EPP Behavior)

This ground motion has two ridges of energy at approximately the same period, but separated by five seconds. Since the bursts of energy are at essentially the same period, there is not much potential for moving resonance. Instead it is the short period structure that can period elongates to match the energy in the ground motion that is most susceptible to moving resonance.

7.2.18 Ground Motion 18: Cape Mendocino Earthquake at Rio Dell overpass

The acceleration time history and the acceleration response spectra for 2 % damping of the component 1 of Cape Mendocino earthquake at Rio Dell overpass station is shown in Figures 7-205 and 7-206 respectively. The 2D and 3D wavelet coefficient plot of this particular ground motion performed using Complex Morlet wavelet of band width 1 and frequency 1.5 is shown in Figures 7-207 and 7-208 respectively.

The salient features of this ground motion which can be seen from Figures 7-205 to 7-208 is that this has as a strong burst of energy concentrated in time with a wide band of periods with a trailing ridge of energy at a higher period of approximately 1.5 sec. It might be expected that there would be some potential for moving resonance.

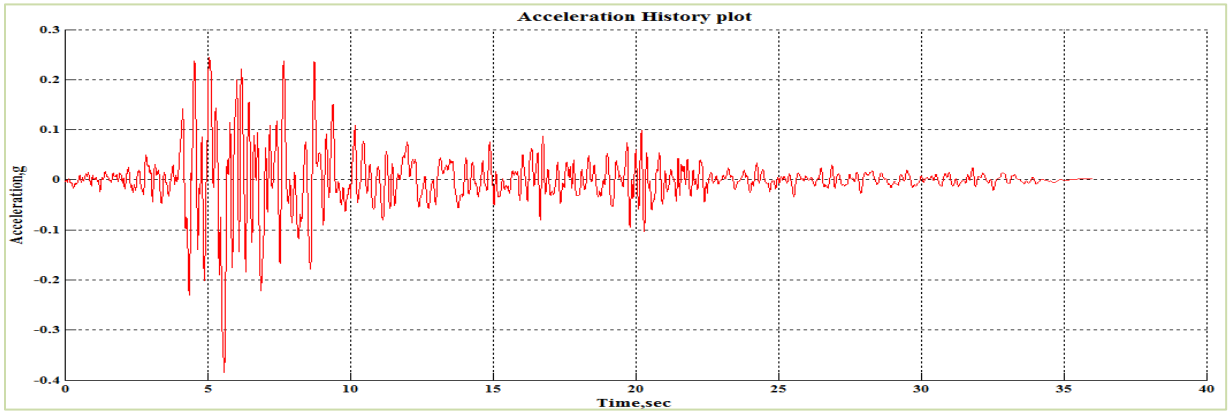

Figure 7-205 Acceleration Time History of Ground Motion 18 (Cape Mendocino-Rio Dell Overpass)

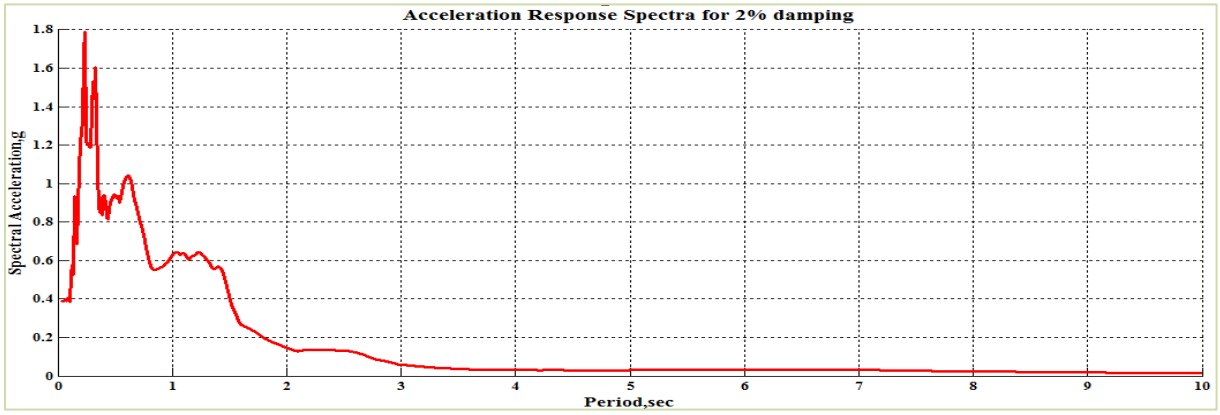

Figure 7-206 Acceleration Response Spectra for 2% Damping

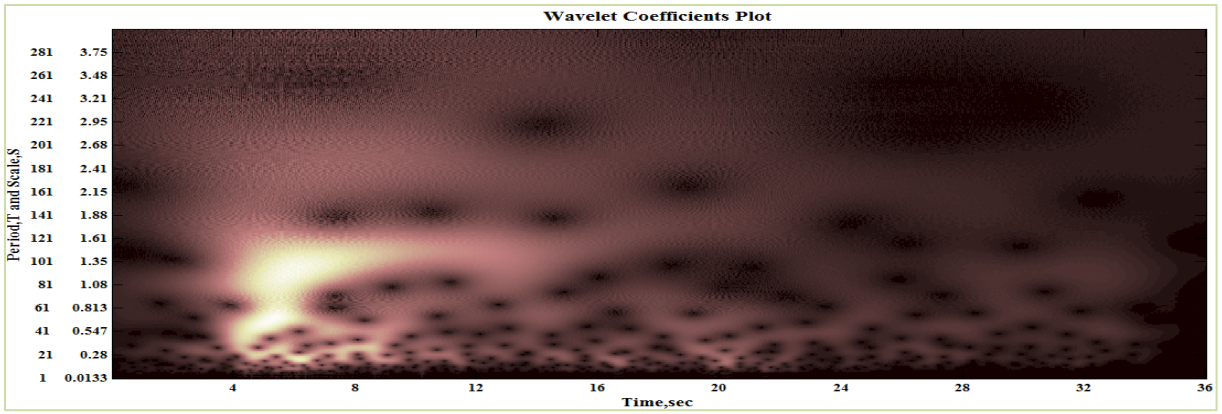

Figure 7-207 2D Wavelet coefficients plot of Ground Motion 18 (Cape Mendocino-Rio Dell Overpass)

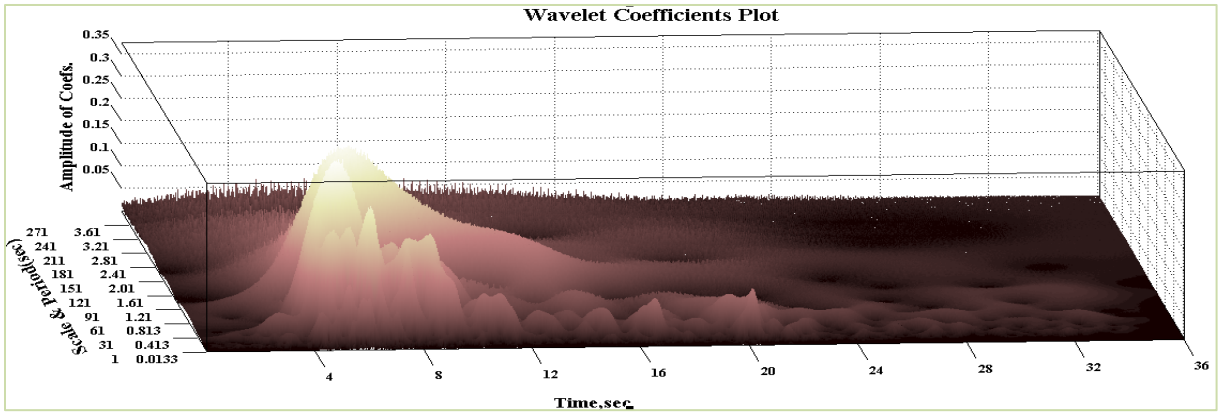

Figure 7-208 3D Wavelet coefficients plot of Ground Motion 18 (Cape Mendocino-Rio Dell Overpass)

The 3D and 2D peak displacement plot of the structural system incorporating bilinear elastic behavior is shown in Figures 7-209 and 7-210 respectively. The 2D peak displacement plot as shown in Figure 7-210 have no significant bumps in peak displacement. Hence the amplification factor will be near to 1 for these combinations of period and strength.

The 3D and 2D peak amplification plot of the structural system incorporating bilinear elastic behavior is shown in Figures 7-211 and 7-212 respectively. It is observed from Figure 7-212 that though no bumps in peak displacement, the amplification values corresponding to (T_0,η) of (0.5,0.5) are greater than 1. It might be conjectured that the larger amplification factors might correspond to systems that experience enough period elongation that their dominant natural period matches the trailing strong energy in the ground motion.

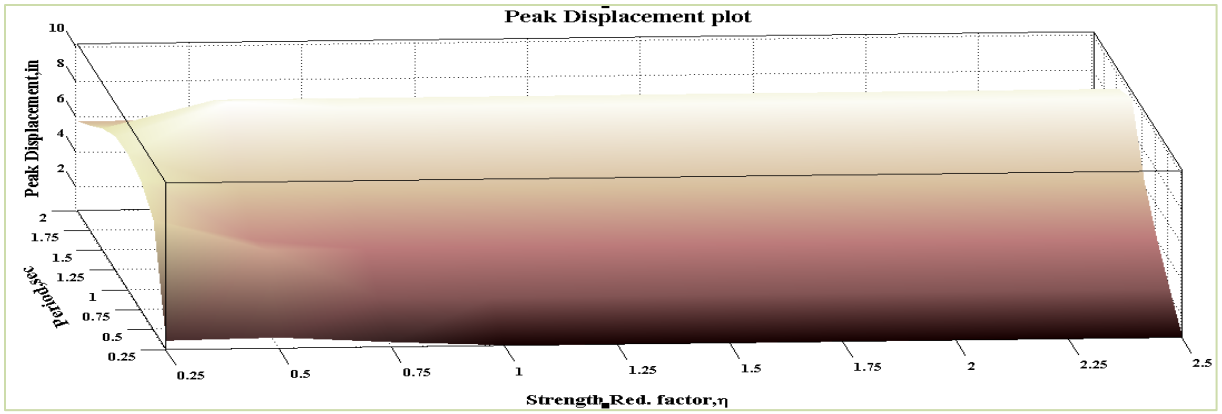

Figure 7-209 3D Peak Displacement plot for Ground Motion 18 (Bilinear Behavior)

Figure 7-210 2D Peak Displacement plot for Ground Motion 18 (Bilinear Behavior)

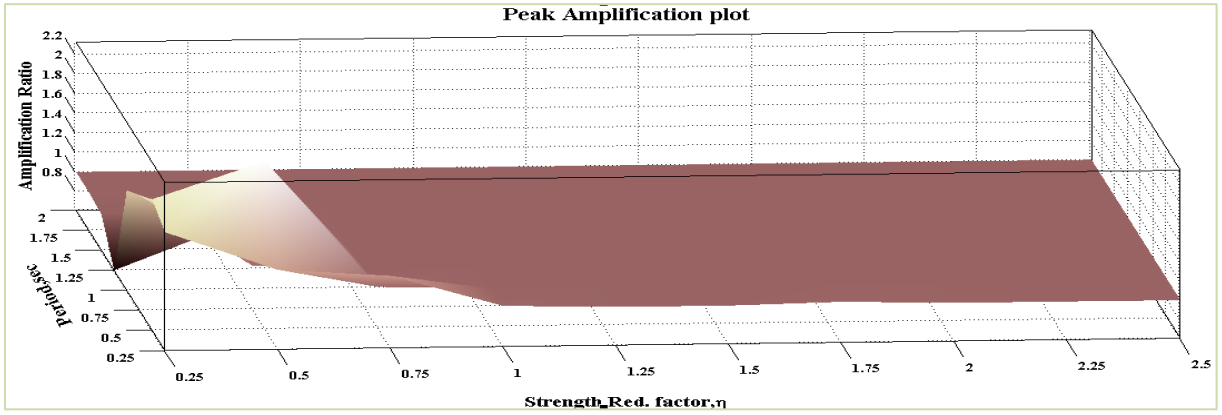

Figure 7-211 3D Peak Amplification plot for Ground Motion 18 (Bilinear Behavior)

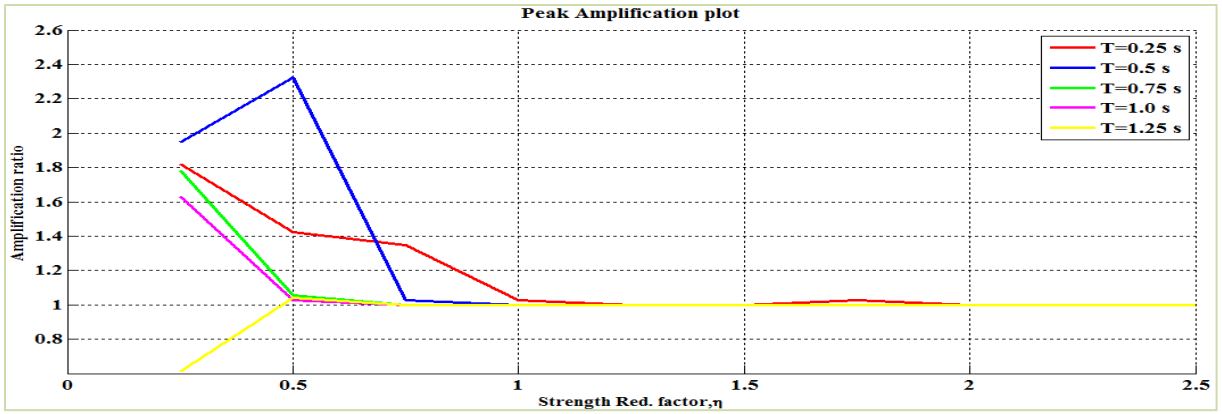

Figure 7-212 2D Peak Amplification plot for Ground Motion 18 (Bilinear Behavior)

The 3D and 2D peak displacement plot of the structural system incorporating elasto-plastic behavior is shown in Figures 7-213 and 7-214 respectively. The 2D peak displacement plot as shown in Figure 7-214 have no significant bumps in peak displacement.

The 3D and 2D peak amplification plot of the structural system incorporating elasto-plastic behavior is shown in Figures 7-215 and 7-216 respectively. It is observed from Figure 7-216 that though no bumps in peak displacement, the amplification values corresponding to systems with small eta are significant. It leads to hypothesize that the systems which hit the strong shaking experience period elongation are affected by the trailing energy at long period in the ground motion. More interestingly, the amplification factors found larger for EPP systems than BE systems.

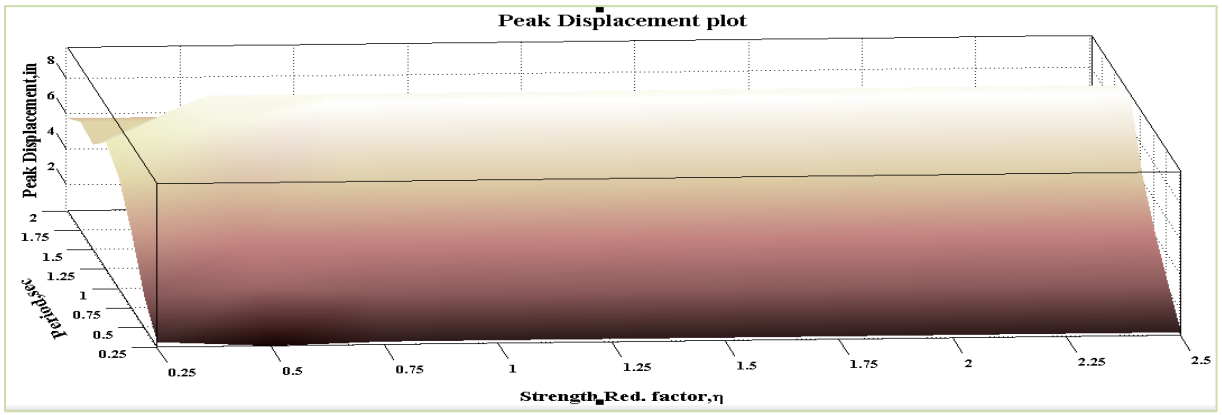

Figure 7-213 3D Peak Displacement plot for Ground Motion 18 (EPP Behavior)

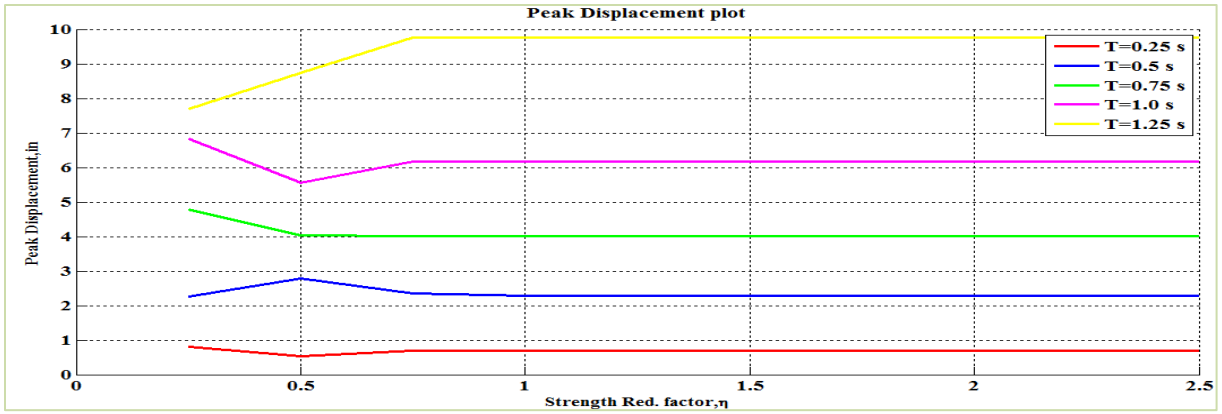

Figure 7-214 2D Peak Displacement plot for Ground Motion 18 (EPP Behavior)

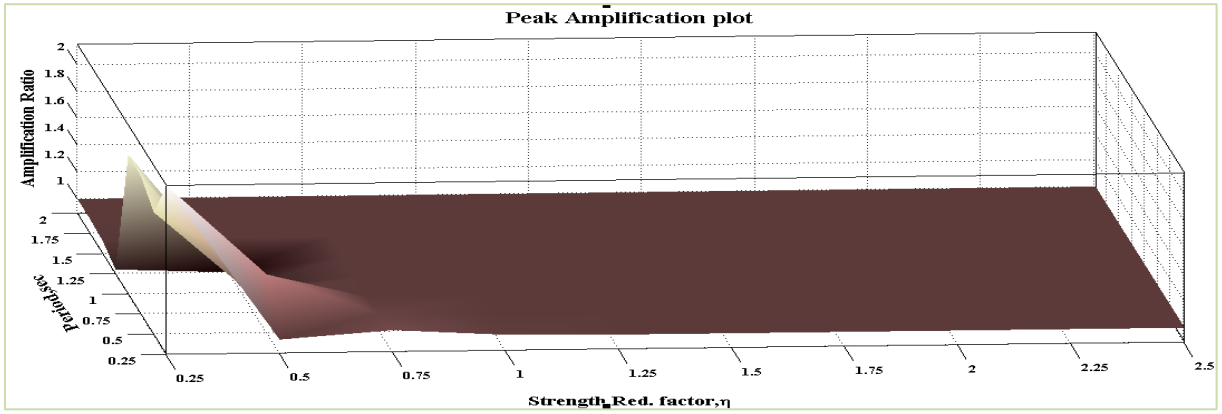

Figure 7-215 3D Peak Amplification plot for Ground Motion 18 (EPP Behavior)

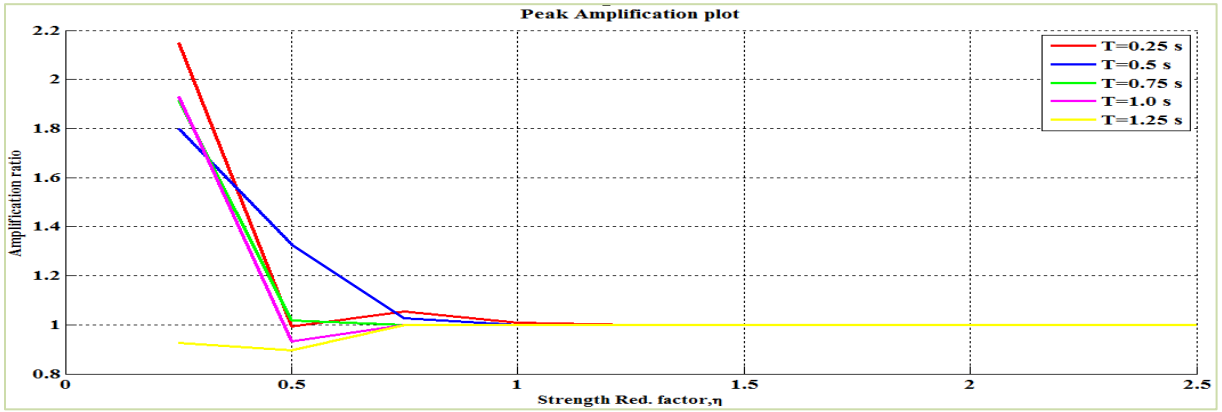

Figure 7-216 2D Peak Amplification plot for Ground Motion 18 (EPP Behavior)

This ground motion has strong burst of energy concentrated in time with a wide band of periods with a trailing ridge of energy at a higher periods. Potential moving resonance was expected, but the effect is seen only for the systems with small η value.

7.2.19 Ground Motion 19: Chi-Chi Taiwan Earthquake at CHY 101

The acceleration time history and the acceleration response spectra for 2 % damping of the component 1 of Chi-Chi Taiwan earthquake at CHY 101 station is shown in Figures 7-217 and 7-218 respectively. The 2D and 3D wavelet coefficient plot of this particular ground motion performed using Complex Morlet wavelet of band width 1 and frequency 1.5 is shown in Figures 7-219 and 7-220 respectively.

It can be observed from the Figures 7-217 to 7-220 that the largest energy in this ground motion is at a period (3 sec) well beyond the systems that are studied. It may be difficult to investigate the η values small enough that the nonlinear systems interact with this strong energy content in the ground motion. So, the study focuses on the two bursts of energy at periods around 0.75 sec and 0.9 sec at time approximately 30 and 37 seconds respectively. These are the components that are probably contributing to the response in the range of periods that are studied here.

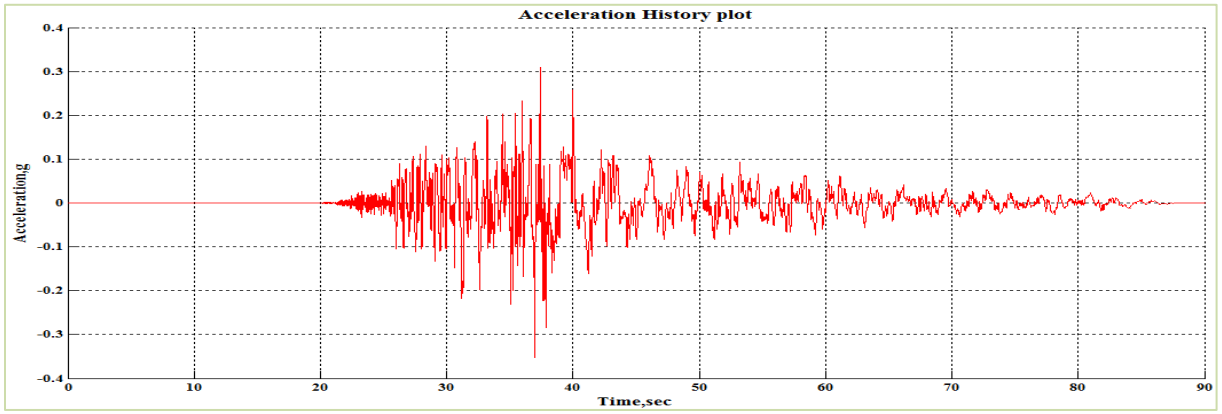

Figure 7-217 Acceleration Time History of Ground Motion 19 (Chi-Chi Taiwan-CHY 101)

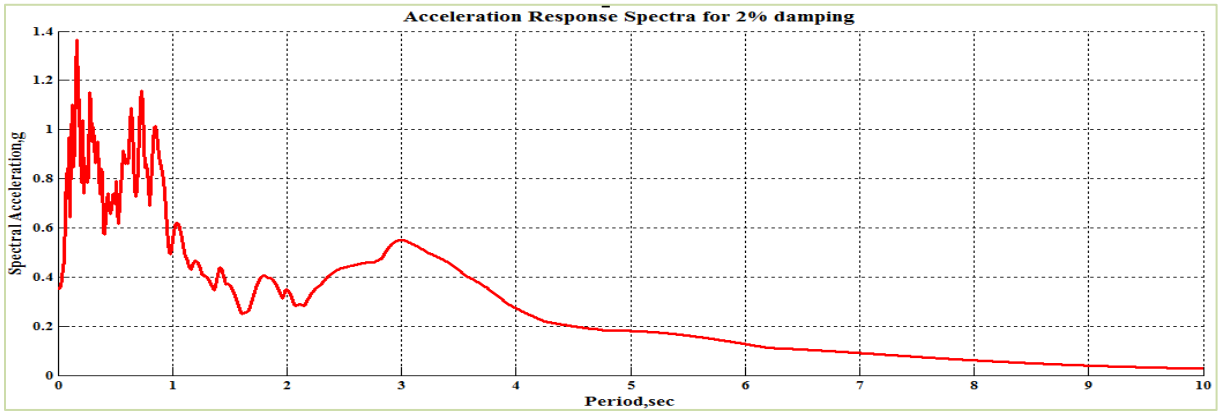

Figure 7-218 Acceleration Response Spectra for 2% Damping

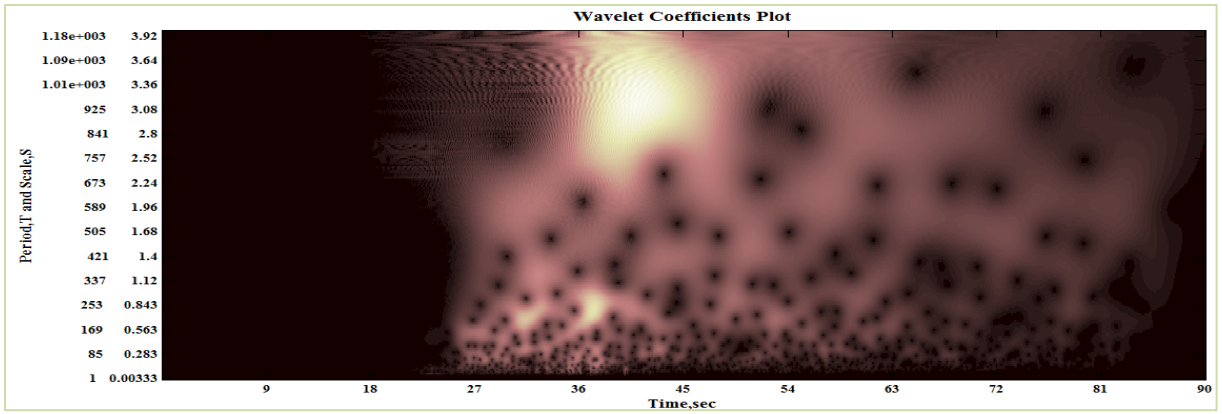

Figure 7-219 2D Wavelet coefficients plot of Ground Motion 19 (Chi-Chi Taiwan-CHY 101)

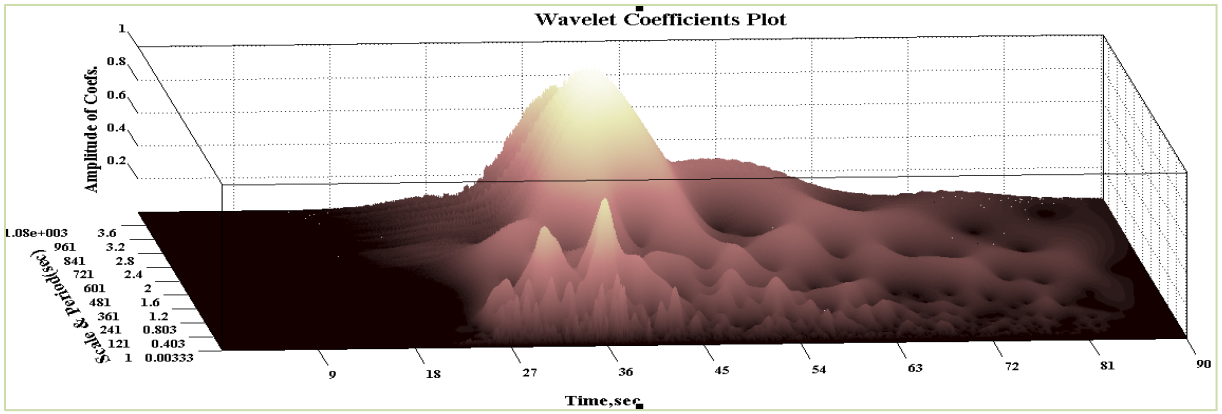

Figure 7-220 3D Wavelet coefficients plot of Ground Motion 19 (Chi-Chi Taiwan-CHY 101)

The 3D and 2D peak displacement plot of the structural system incorporating bilinear elastic behavior is shown in Figures 7-221 and 7-222 respectively. The 2D peak displacement plot as shown in Figure 7-222 have bumps in peak displacement at corresponding (T_0,η) values of (0.50,0.50). This localized increase in peak displacement is hypothesized to be the result of occurrence of moving resonance and hence amplification factor greater than 1 is expected for these combinations of period and strength.

The 3D and 2D peak amplification plot of the structural system incorporating bilinear elastic behavior is shown in Figures 7-223 and 7-224 respectively. It is observed from Figure 7-224 that the amplification values corresponding to (T_0,η) values (0.50,0.50) are greater than 1 leading to the increase in peak displacement. This increase in peak displacement is considered to be the effect of moving resonance.

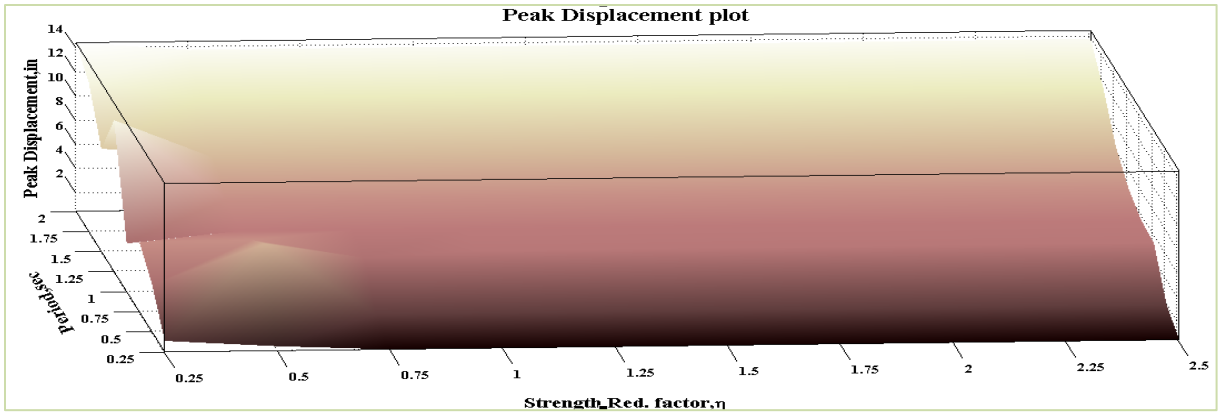

Figure 7-221 3D Peak Displacement plot for Ground Motion 19 (Bilinear Behavior)

Figure 7-222 2D Peak Displacement plot for Ground Motion 19 (Bilinear Behavior)

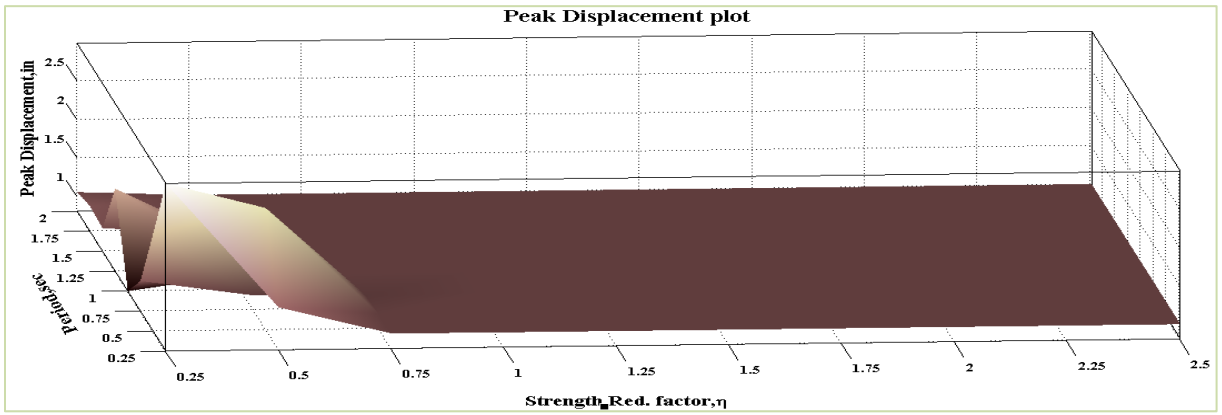

Figure 7-223 3D Peak Amplification plot for Ground Motion 19 (Bilinear Behavior)

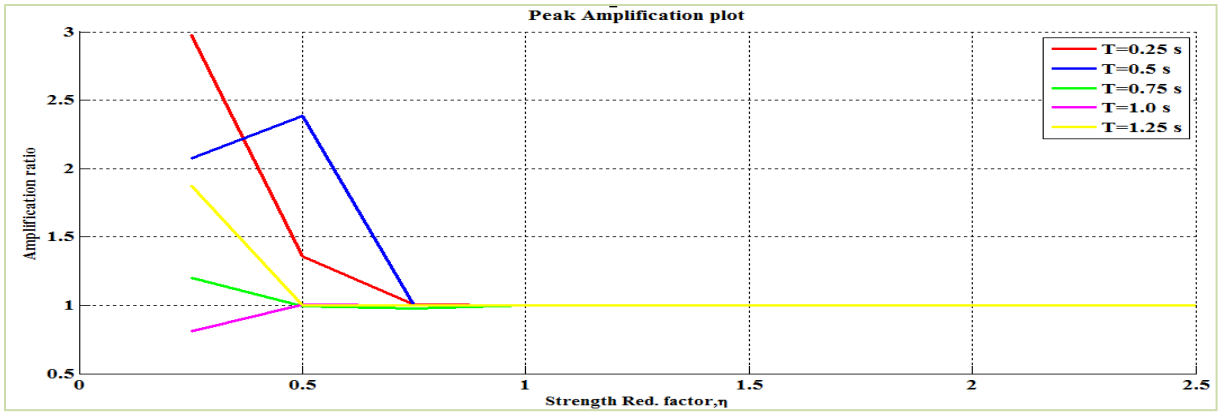

Figure 7-224 2D Peak Amplification plot for Ground Motion 19 (Bilinear Behavior)

The 3D and 2D peak displacement plot of the structural system incorporating elasto-plastic behavior is shown in Figures 7-225 and 7-226 respectively. The 2D peak displacement plot as shown in Figure 7-226 have bumps in peak displacement at corresponding (T_0,η) values of (0.75,0.75). This localized increase in peak displacement is hypothesized to be the result of occurrence of moving resonance and hence amplification factor greater than 1 is expected for these combinations of period and strength.

The 3D and 2D peak amplification plot of the structural system incorporating elasto-plastic behavior is shown in Figures 7-227 and 7-228 respectively. It is observed from Figure 7-228 that the amplification values corresponding to (T_0,η) values (0.75,0.75) are greater than 1 leading to the increase in peak displacement. This increase in peak displacement is considered to be the effect of moving resonance.

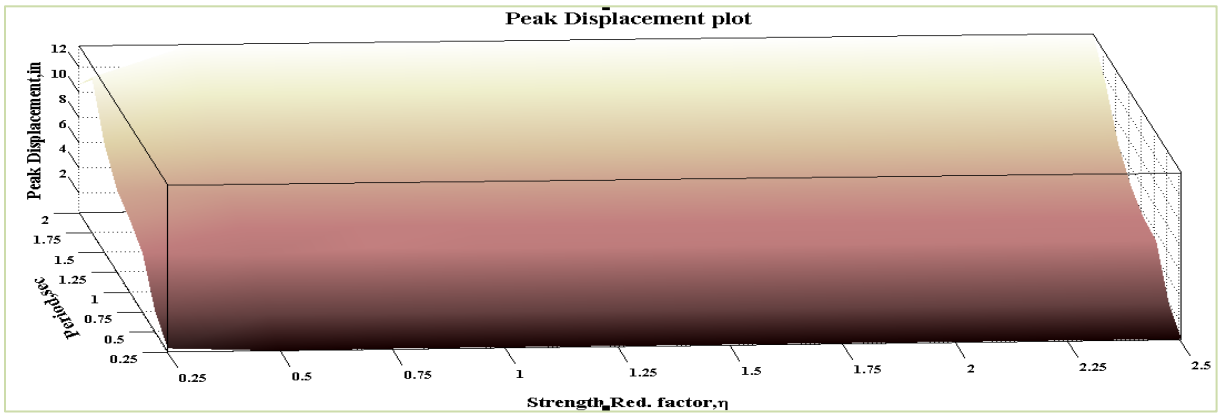

Figure 7-225 3D Peak Displacement plot for Ground Motion 19 (EPP Behavior)

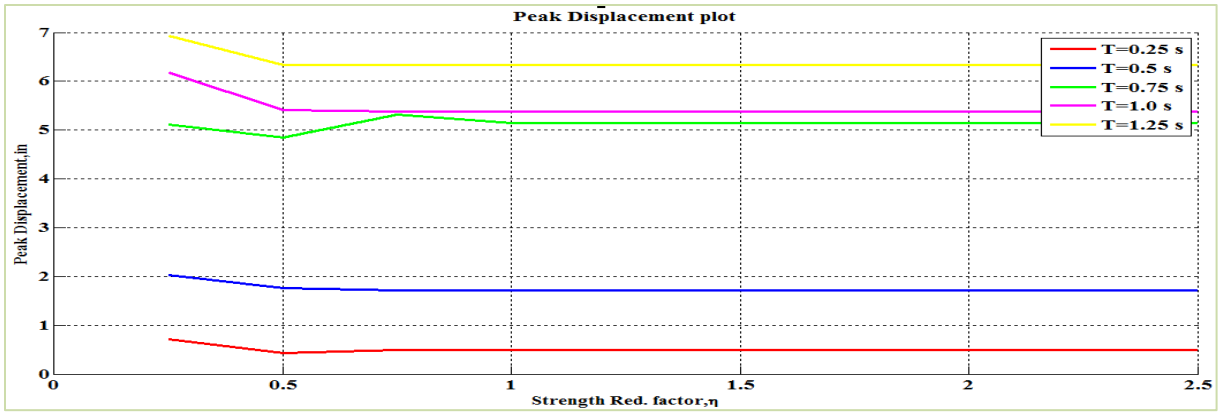

Figure 7-226 2D Peak Displacement plot for Ground Motion 19 (EPP Behavior)

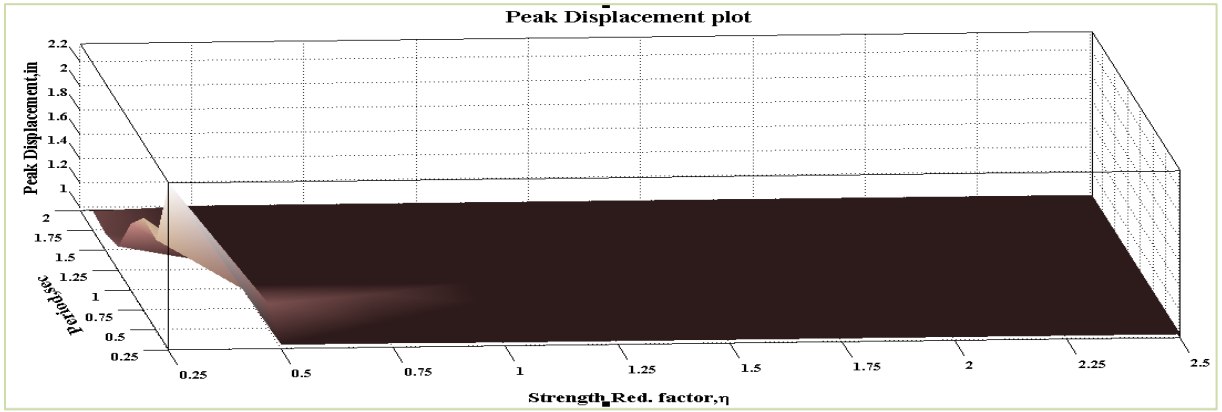

Figure 7-227 3D Peak Amplification plot for Ground Motion 19 (EPP Behavior)

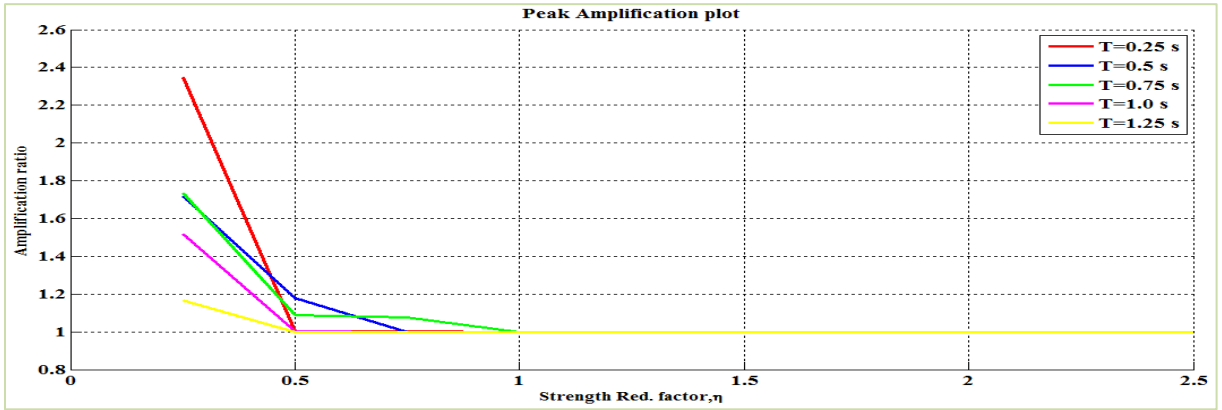

Figure 7-228 2D Peak Amplification plot for Ground Motion 19 (EPP Behavior)

The large energy content in the ground motion at 3 sec period does not contribute much to moving resonance. Instead, it is concluded that the two peaks in ground motion that have increasing period from one to the other contributed to the moving resonance.

7.2.20 Ground Motion 20: Chi-Chi Taiwan Earthquake at TCU 045

The acceleration time history and the acceleration response spectra for 2 % damping of the component 1 of Chi-Chi Taiwan earthquake at TCU 045 station is shown in Figures 7-229 and 7-230 respectively. The 2D and 3D wavelet coefficient plot of this particular ground motion performed using Complex Morlet wavelet of band width 1 and frequency 1.5 is shown in Figures 7-231 and 7-232 respectively.

It can be seen from Figures 7-229 to 7-232 that the energy in the ground motion is extremely concentrated in time and period and is considered as pulse like.

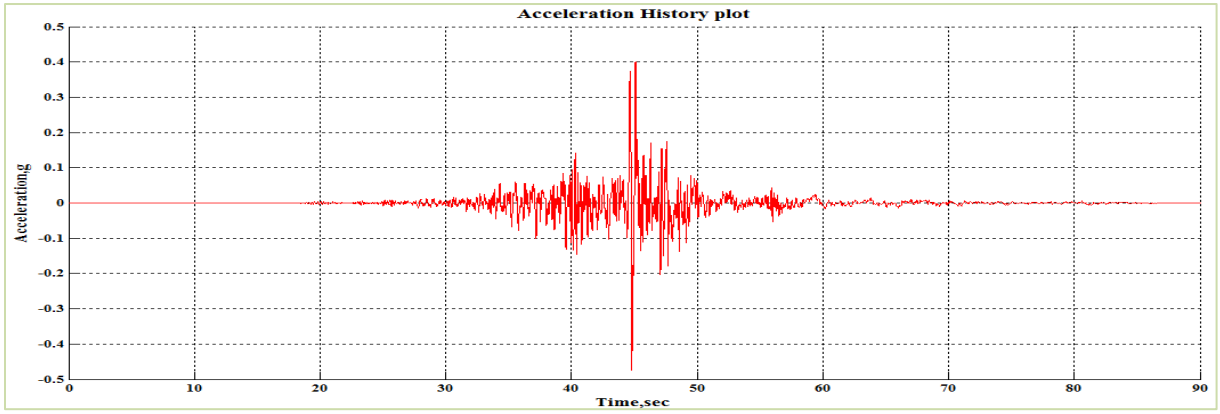

Figure 7-229 Acceleration Time History of Ground Motion 20 (Chi-Chi Taiwan, TCU 045)

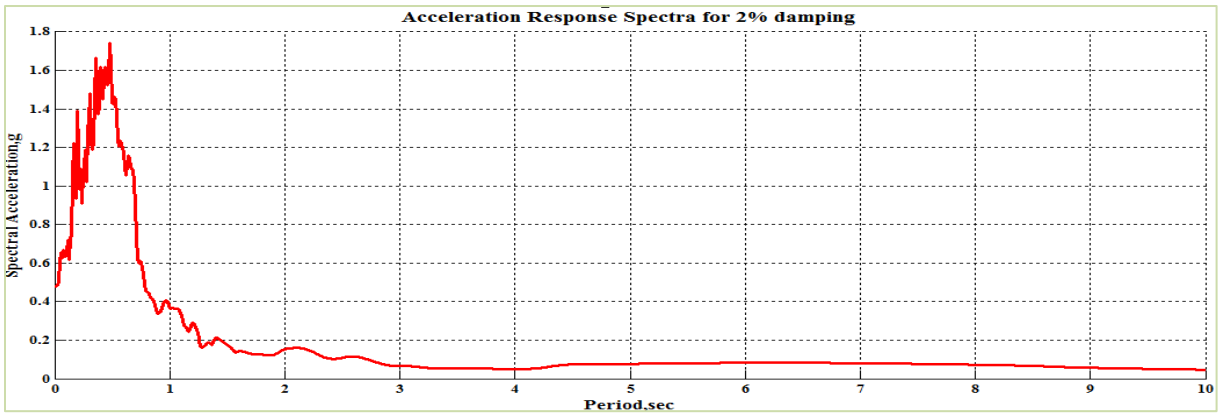

Figure 7-230 Acceleration Response Spectra for 2% Damping

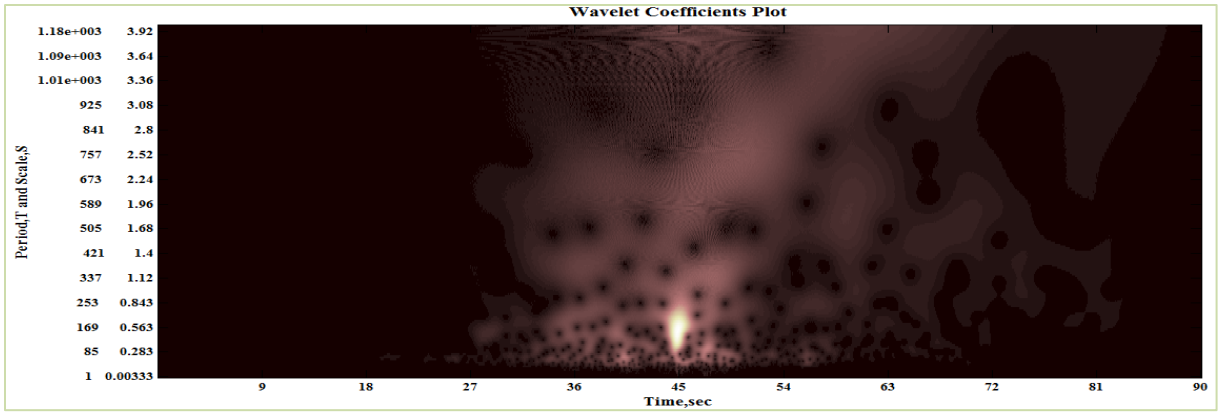

Figure 7-231 2D Wavelet coefficients plot of Ground Motion 20 (Chi-Chi Taiwan, TCU 045)

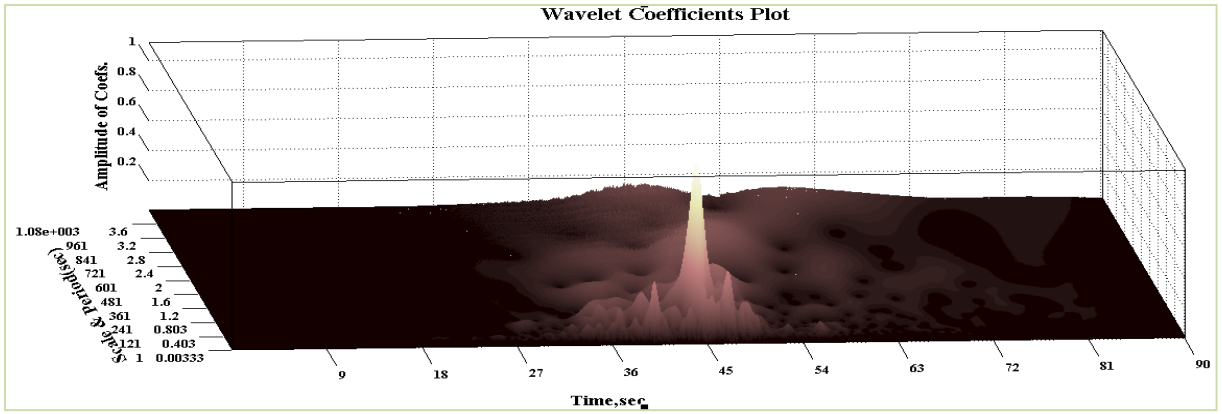

Figure 7-232 3D Wavelet coefficients plot of Ground Motion 20 (Chi-Chi Taiwan, TCU 045)

The 3D and 2D peak displacement plot of the structural system incorporating bilinear elastic behavior is shown in Figures 7-233 and 7-234 respectively. The 2D peak displacement plot as shown in Figure 7-234 have bumps in peak displacement at corresponding (T_0,η) values of (0.50,0.50). This localized increase in peak displacement is hypothesized to be the result of occurrence of moving resonance and hence amplification factor greater than 1 is expected for these combinations of period and strength.

The 3D and 2D peak amplification plot of the structural system incorporating bilinear elastic behavior is shown in Figures 7-235 and 7-236 respectively. It is observed from Figure 7-236 that the amplification values corresponding to (T_0,η) values (0.50,0.50) are greater than 1 causing moving resonance but not that significant when compared to the amplification factor at (0.25,0.50). The short period system (T_0=0.25sec) undergoes period elongation for the right values of η such that the effective system period matches the pulse of energy that dominates this ground motion. This causes significant amplification factor due to moving resonance.

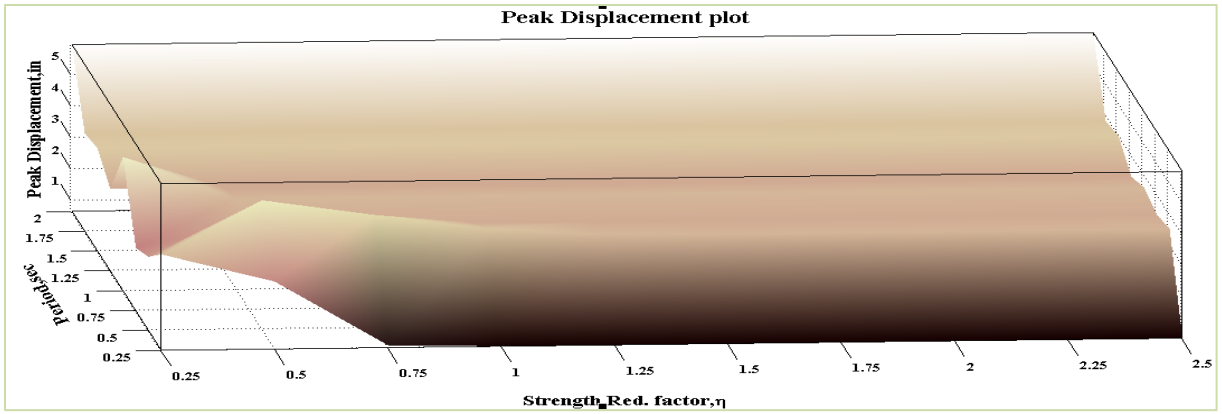

Figure 7-233 3D Peak Displacement plot for Ground Motion 20 (Bilinear Behavior)

Figure 7-234 2D Peak Displacement plot for Ground Motion 20 (Bilinear Behavior)

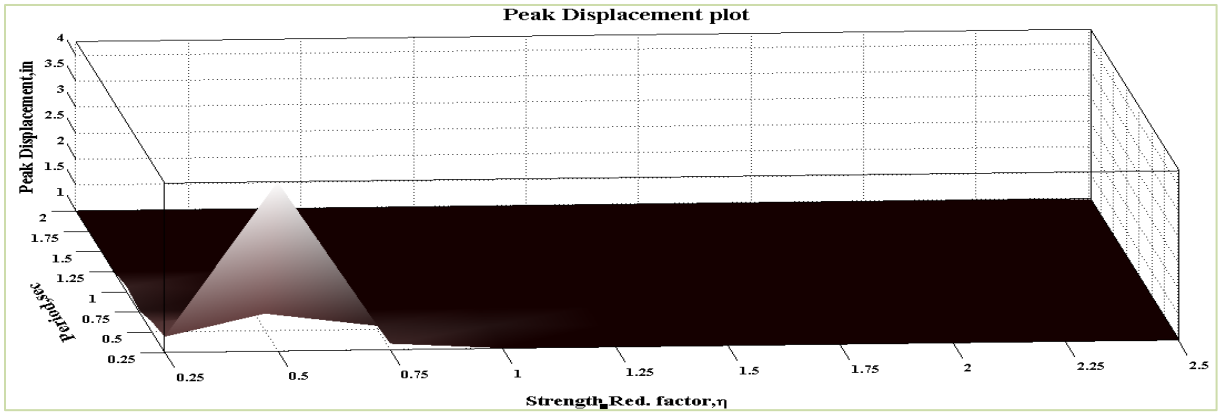

Figure 7-235 3D Peak Amplification plot for Ground Motion 20 (Bilinear Behavior)

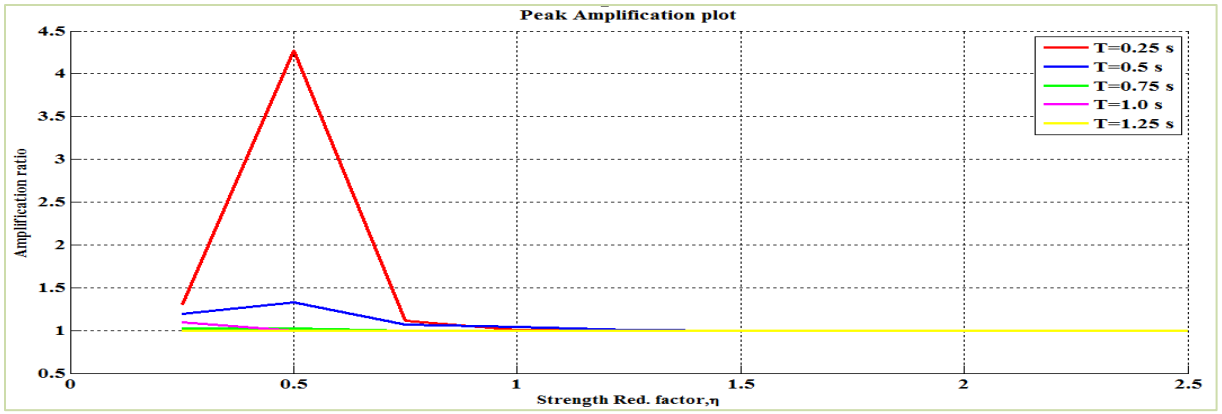

Figure 7-236 2D Peak Amplification plot for Ground Motion 20 (Bilinear Behavior)

The 3D and 2D peak displacement plot of the structural system incorporating elasto-plastic behavior is shown in Figures 7-237 and 7-238 respectively. The 2D peak displacement plot as shown in Figure 7-238 have bumps in peak displacement at corresponding (T_0,η) values of (0.25,0.5), (0.5,0.5) and (0.5,1.0). This localized increase in peak displacement is hypothesized to be the result of occurrence of moving resonance and hence amplification factor greater than 1 is expected for these combinations of period and strength.

The 3D and 2D peak amplification plot of the structural system incorporating elasto-plastic behavior is shown in Figures 7-239 and 7-240 respectively. It is observed from Figure 7-240 that the amplification values corresponding to (T_0,η) values of (0.25,0.5), (0.5,0.5) and (0.5,1.0) are greater than 1 leading to increase in peak displacement. Similar to BE systems, it is observed that the amplification due to moving resonance is greatest for this type of pulse like ground motion when the shorter period structures experience period elongation and hit the energy contained in the ground motion pulse.

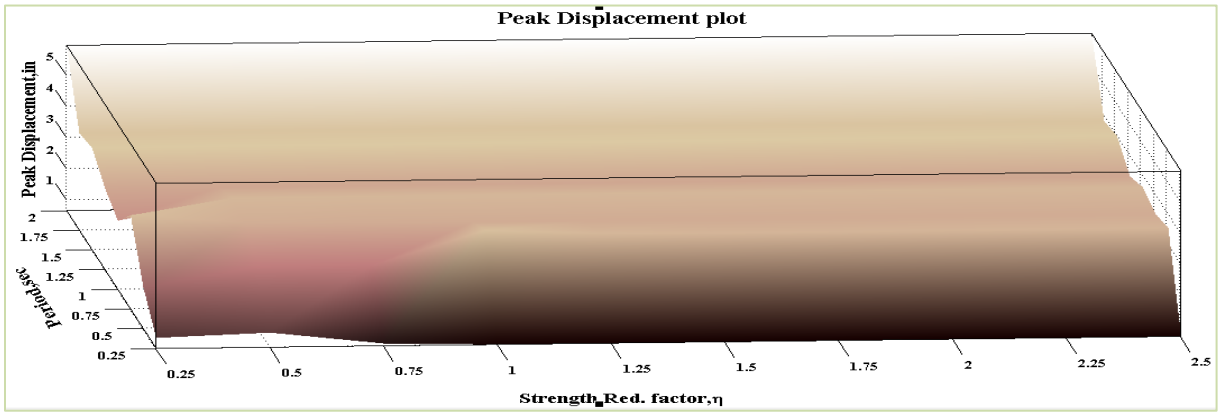

Figure 7-237 3D Peak Displacement plot for Ground Motion 20 (EPP Behavior)

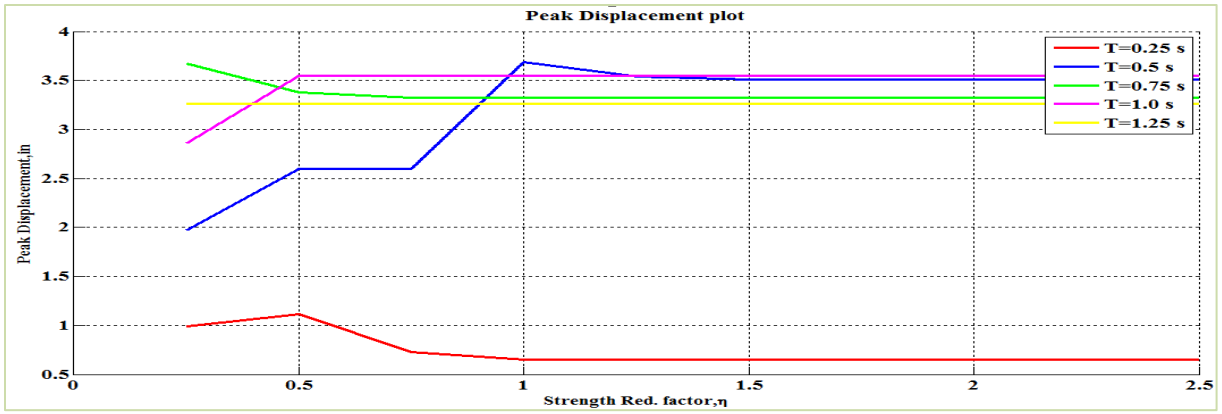

Figure 7-238 2D Peak Displacement plot for Ground Motion 20 (EPP Behavior)

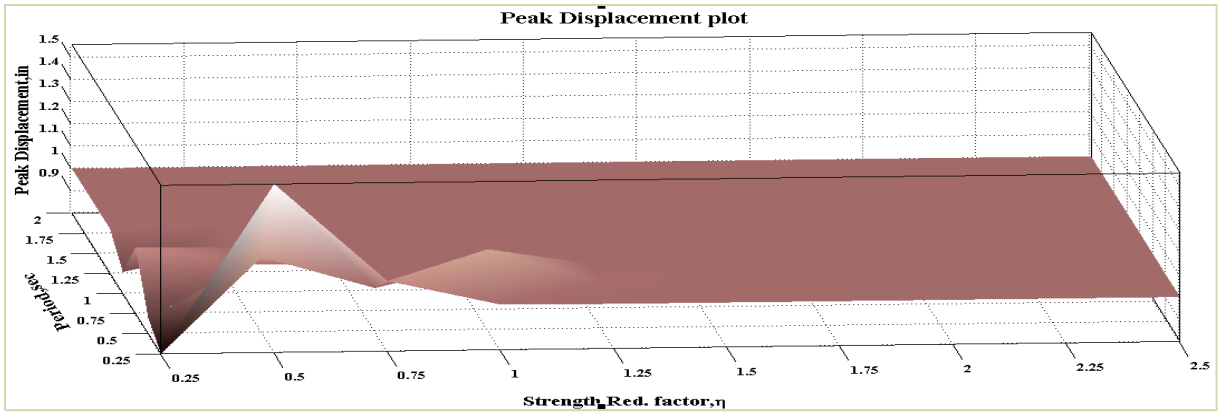

Figure 7-239 3D Peak Amplification plot for Ground Motion 20 (EPP Behavior)

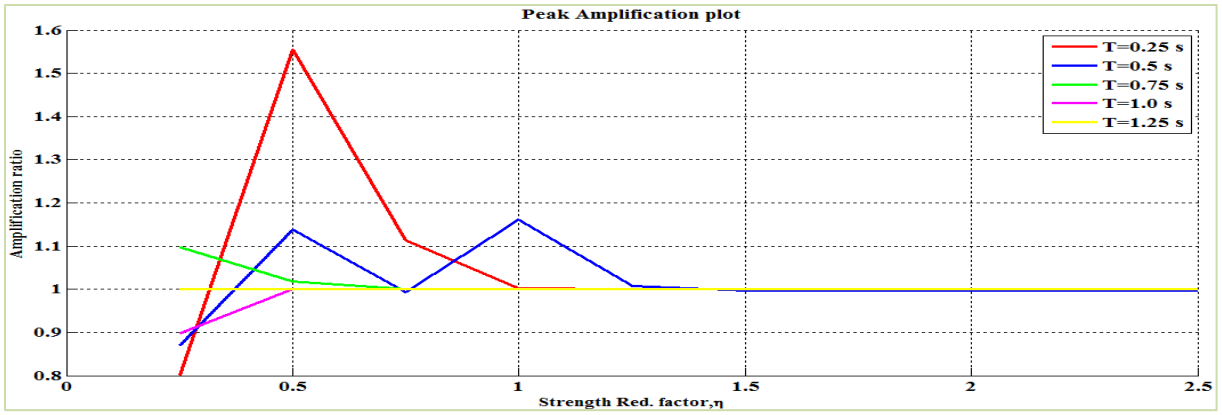

Figure 7-240 3D Peak Amplification plot for Ground Motion 20 (EPP Behavior)

The energy in the ground motion is extremely concentrated and perhaps the most pulse like ground motion in the suite of ground motions studies here. For pulse like motions, the shorter period structures experience period elongation and hit the energy contained in the ground motion pulse.

7.2.21 Ground Motion 21: San Fernando Earthquake at LA Hollywood

The acceleration time history and the acceleration response spectra for 2 % damping of the component 1 of San Fernando earthquake at LA Hollywood station is shown in Figures 7-241 and 7-242 respectively. The 2D and 3D wavelet coefficient plot of this particular ground motion performed using Complex Morlet wavelet of band width 1 and frequency 1.5 is shown in Figures 7-243 and 7-244 respectively.

The salient features of this ground motion which can be seen from Figures 7-241 to 7-244 is that this has as a strong burst of energy concentrated in time with a wide band of periods with a trailing ridge of energy at a higher period of approximately 1.5 sec. It might be expected that there would be some potential for moving resonance.

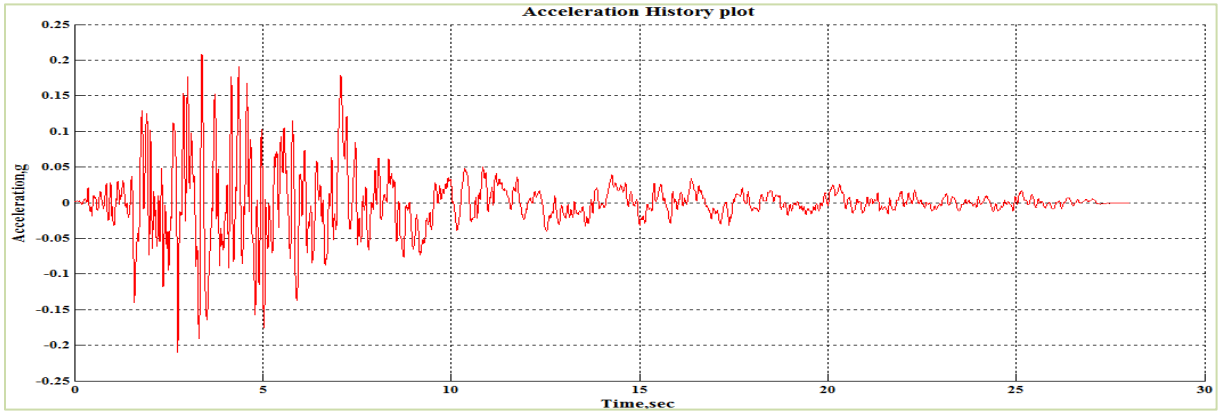

Figure 7-241 Acceleration Time History of Ground Motion 21 (San Fernando-LA Hollywood)

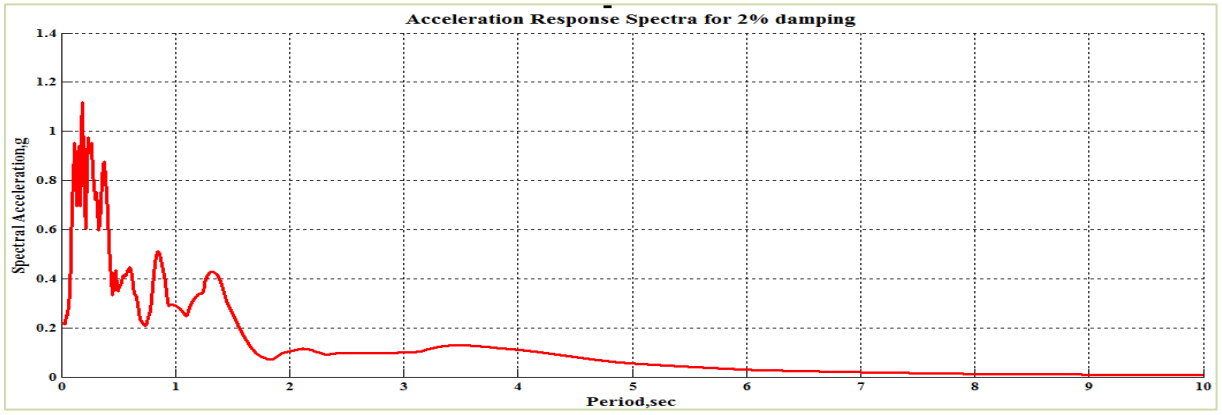

Figure 7-242 Acceleration Response Spectra for 2% Damping

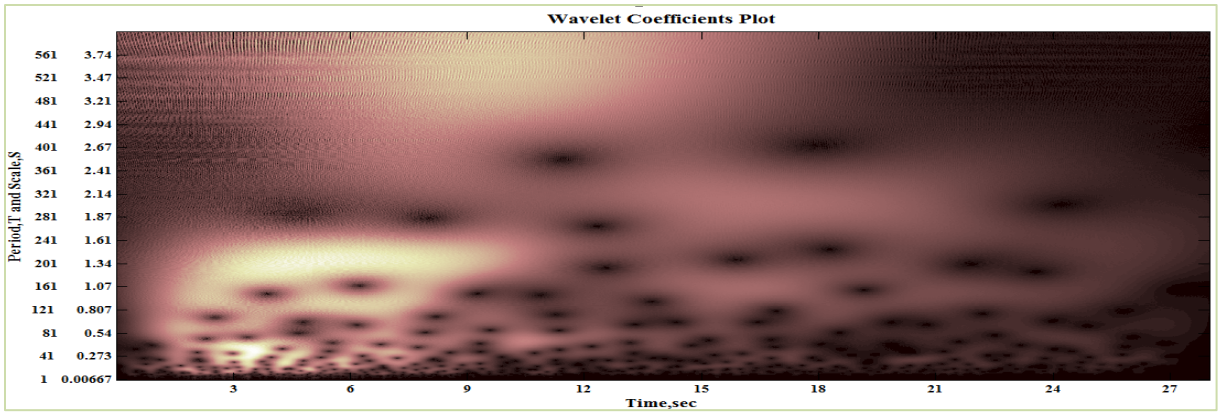

Figure 7-243 2D Wavelet coefficients plot of Ground Motion 21 (San Fernando-LA Hollywood)

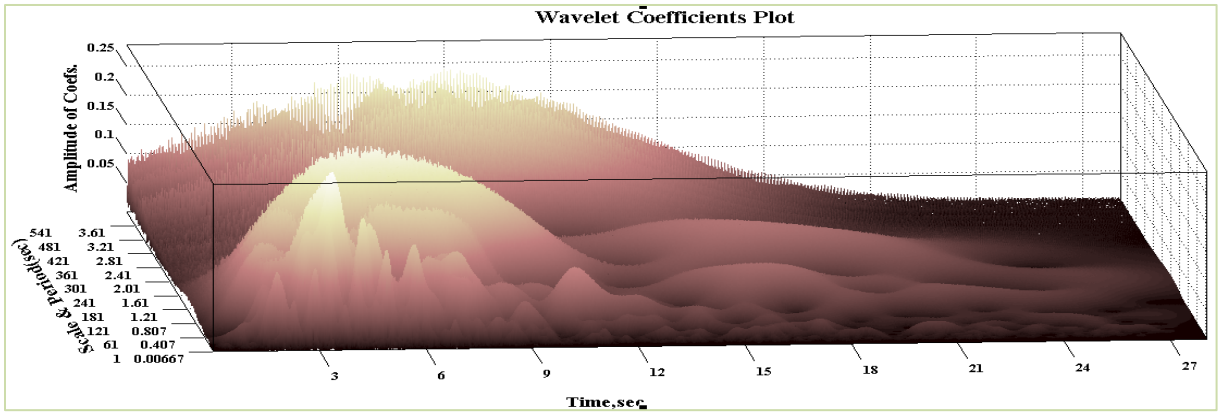

Figure 7-244 3D Wavelet coefficients plot of Ground Motion 21 (San Fernando-LA Hollywood)

The 3D and 2D peak displacement plot of the structural system incorporating bilinear elastic behavior is shown in Figures 7-245 and 7-246 respectively. The 2D peak displacement plot as shown in Figure 7-246 have no significant bumps in peak displacement. Hence the amplification factor will be near to 1 for these combinations of period and strength.

The 3D and 2D peak amplification plot of the structural system incorporating bilinear elastic behavior is shown in Figures 7-247 and 7-248 respectively. It is observed from Figure 7-248 that though no bumps in peak displacement, the amplification values corresponding to 0.25 sec at small eta values are greater than 1. It might be conjectured that the larger amplification factors might correspond to systems that experience enough period elongation that their dominant natural period matches the trailing strong energy in the ground motion.

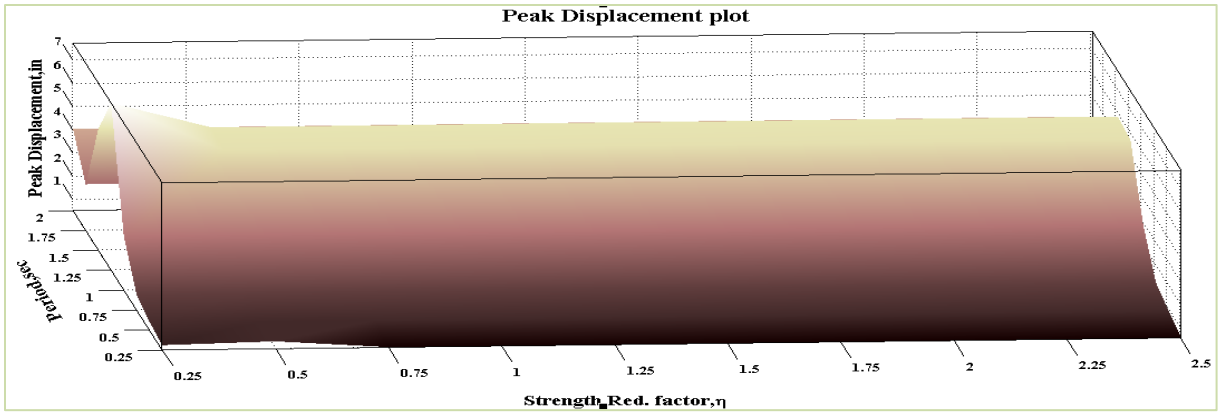

Figure 7-245 3D Peak Displacement plot for Ground Motion 21 (Bilinear Behavior)

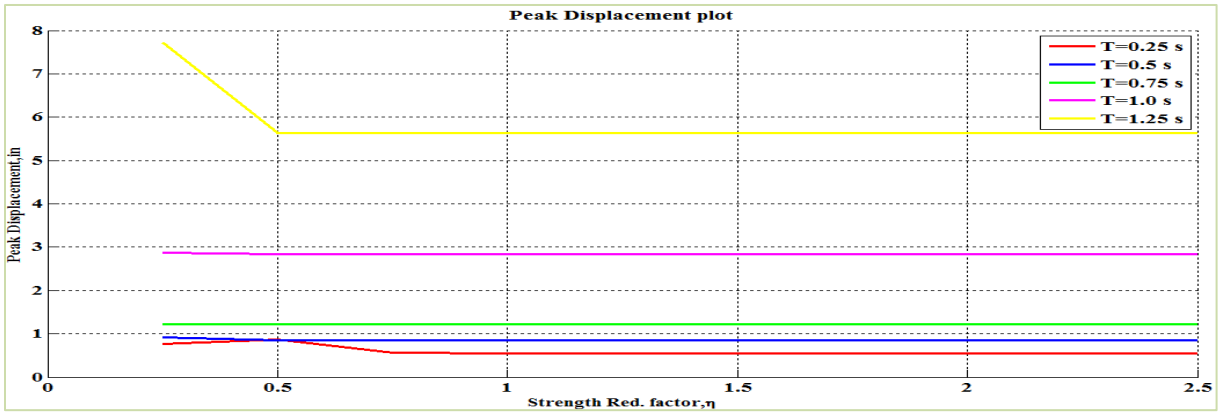

Figure 7-246 2D Peak Displacement plot for Ground Motion 21 (Bilinear Behavior)

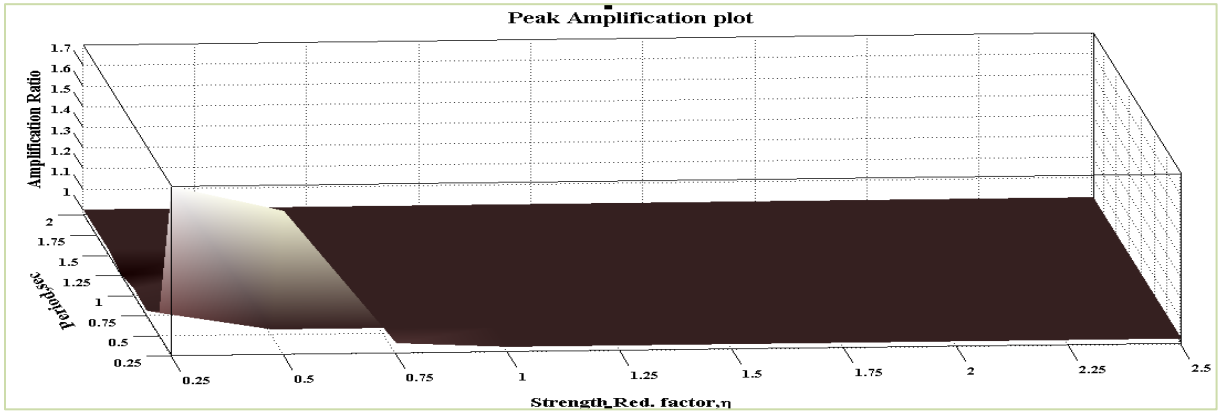

Figure 7-247 3D Peak Amplification plot for Ground Motion 21 (Bilinear Behavior)

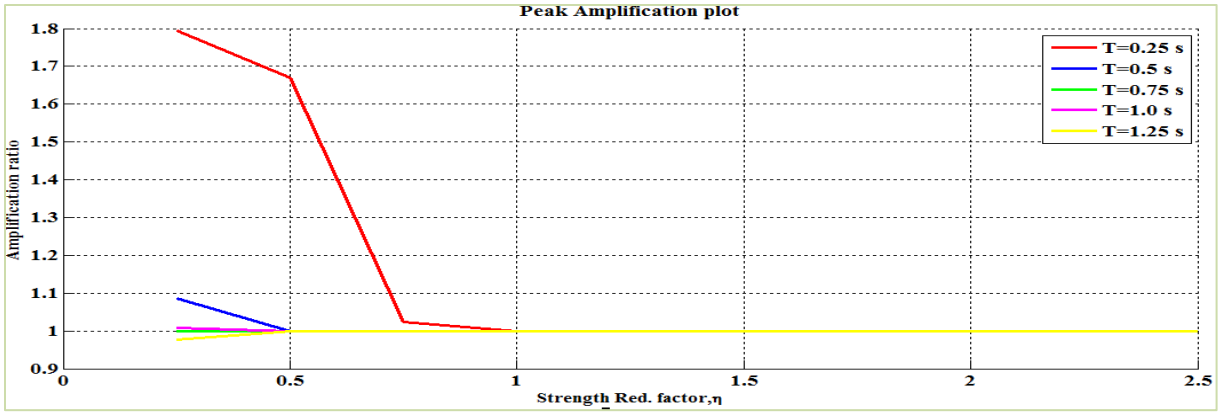

Figure 7-248 2D Peak Amplification plot for Ground Motion 21 (Bilinear Behavior)

The 3D and 2D peak displacement plot of the structural system incorporating elasto-plastic behavior is shown in Figures 7-249 and 7-250 respectively. The 2D peak displacement plot as shown in Figure 7-250 have no significant bumps in peak displacement. Hence the amplification factor will be near to 1 for these combinations of period and strength.

The 3D and 2D peak amplification plot of the structural system incorporating elasto-plastic behavior is shown in Figures 7-251 and 7-252 respectively. It is observed from Figure 7-252 that the amplification factors are very nearer to 1 and this shows that this ground motion does not cause moving resonance on EPP systems.

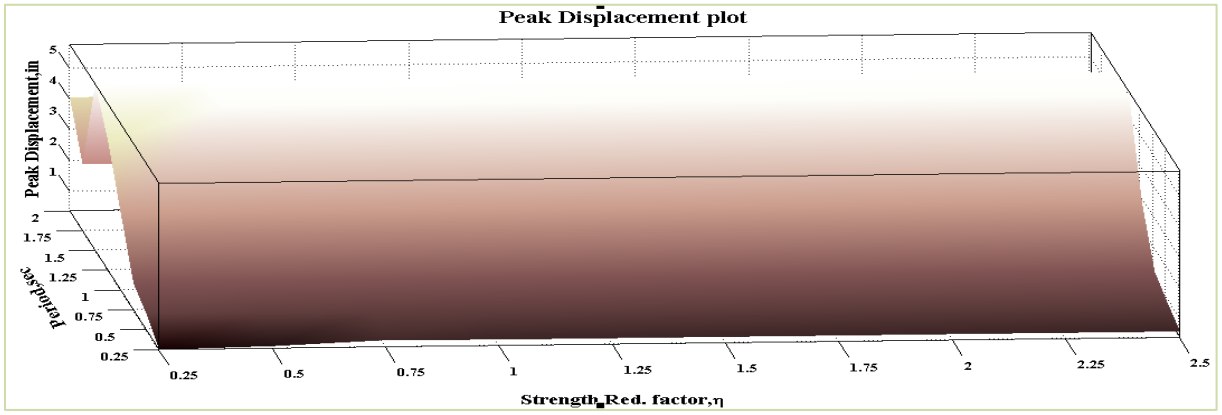

Figure 7-249 3D Peak Displacement plot for Ground Motion 21 (EPP Behavior)

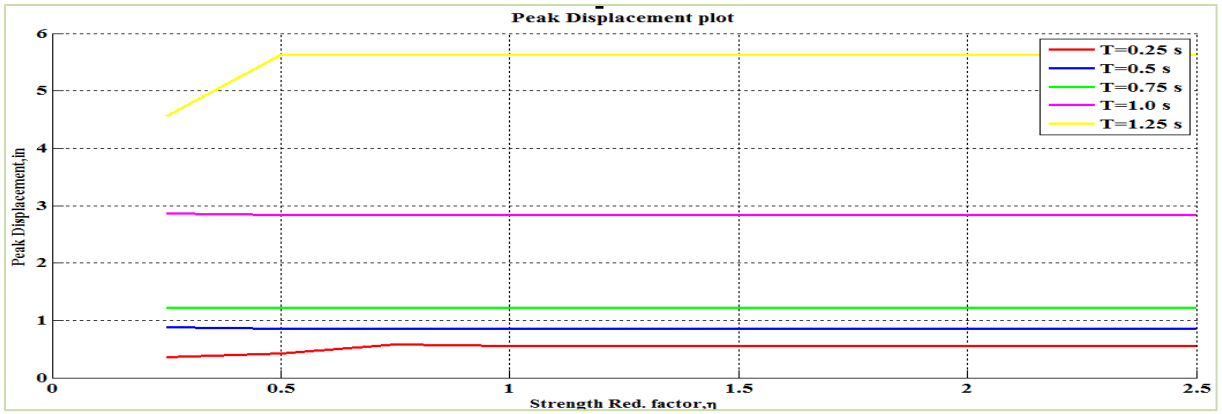

Figure 7-250 2D Peak Displacement plot for Ground Motion 21 (EPP Behavior)

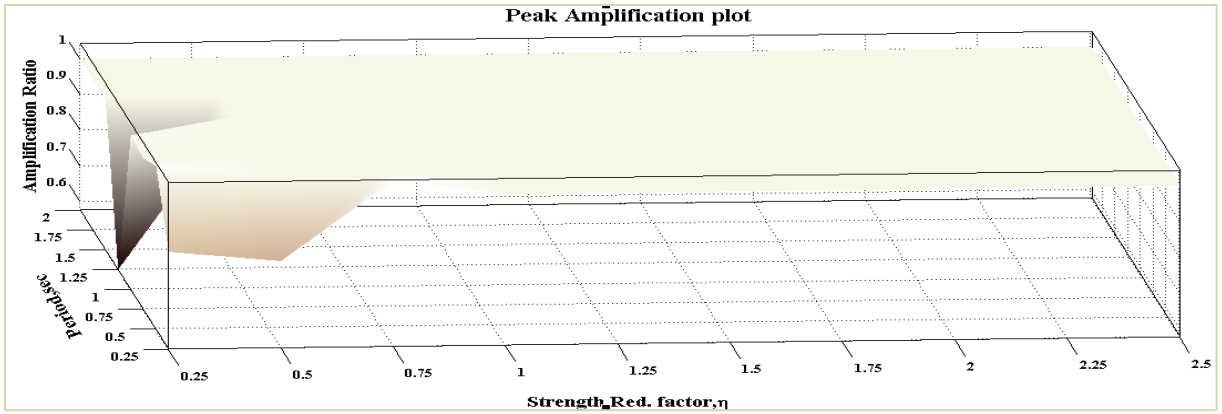

Figure 7-251 3D Peak Amplification plot for Ground Motion 21 (Bilinear Behavior)

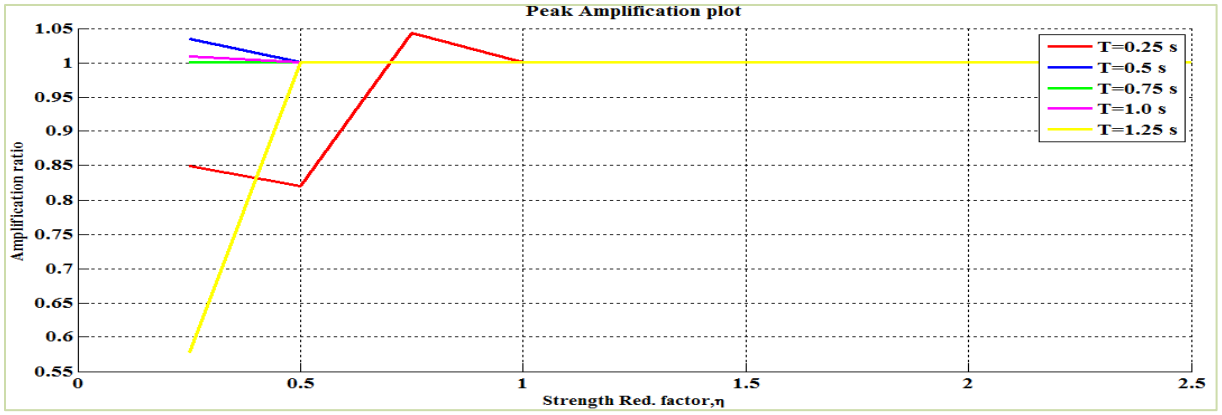

Figure 7-252 2D Peak Amplification plot for Ground Motion 21 (Bilinear Behavior)

This ground motion has strong burst of energy concentrated in time with a wide band of periods with a trailing ridge of energy at a higher periods similar to ground motion 18. Though the characteristics of ground motion are similar, different trend of moving resonance is observed. In this case none of the systems, (with the exception of T=0.25 sec and BE hysteretic) experienced appreciable moving resonance. The possible reason may be that the trailing ridge of energy was too high for most of the systems to period elongate.

7.2.22 Ground Motion 22: Friuli, Italy Earthquake at Tolmezzo

The acceleration time history and the acceleration response spectra for 2 % damping of the component 1 of Friuli, Italy earthquake at Tolmezzo station is shown in Figures 7-253 and 7-254 respectively. The 2D and 3D wavelet coefficient plot of this particular ground motion performed using Complex Morlet wavelet of band width 1 and frequency 1.5 is shown in Figures 7-255 and 7-256 respectively.

The ground motion shown in Figure 7-253 has strong shaking for a short period of time. It is clearly seen that there is a transition of frequency content hitting lower periods (i.e. 0.25 sec) to moderate periods (i.e.0.50 sec) between time t=4 sec to time t=8 sec. It is expected that the only systems likely to experience moving resonance are short period structures.

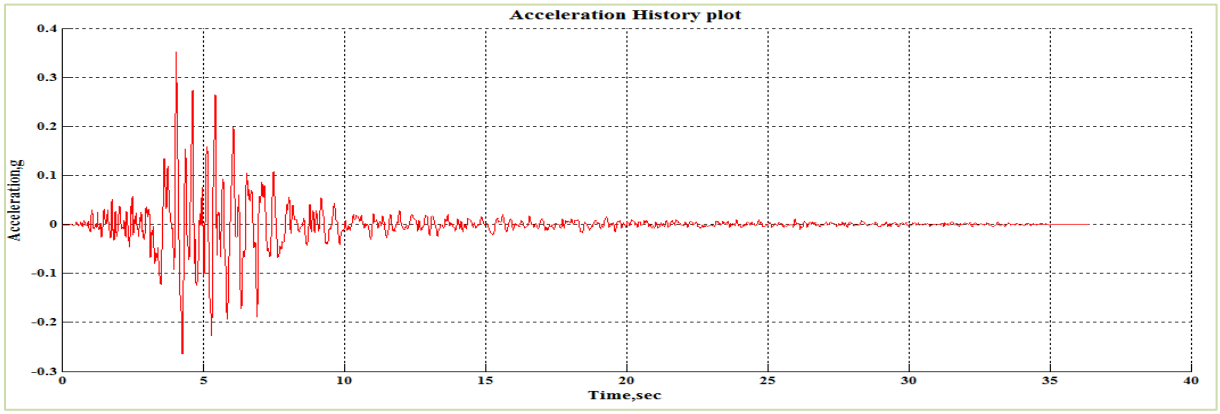

Figure 7-253 Acceleration Time History of Ground Motion 22 (Friuli, Italy-Tolmezzo)

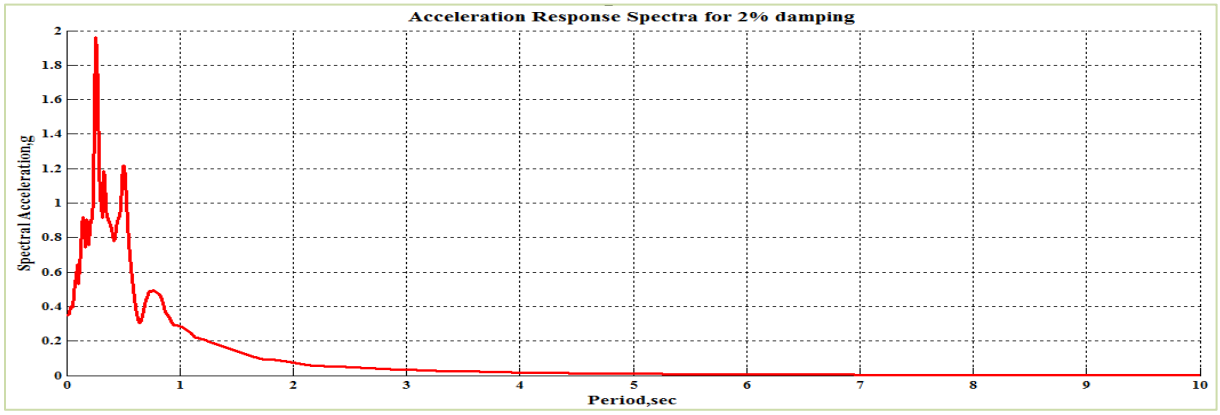

Figure 7-254 Acceleration Response Spectra for 2% Damping

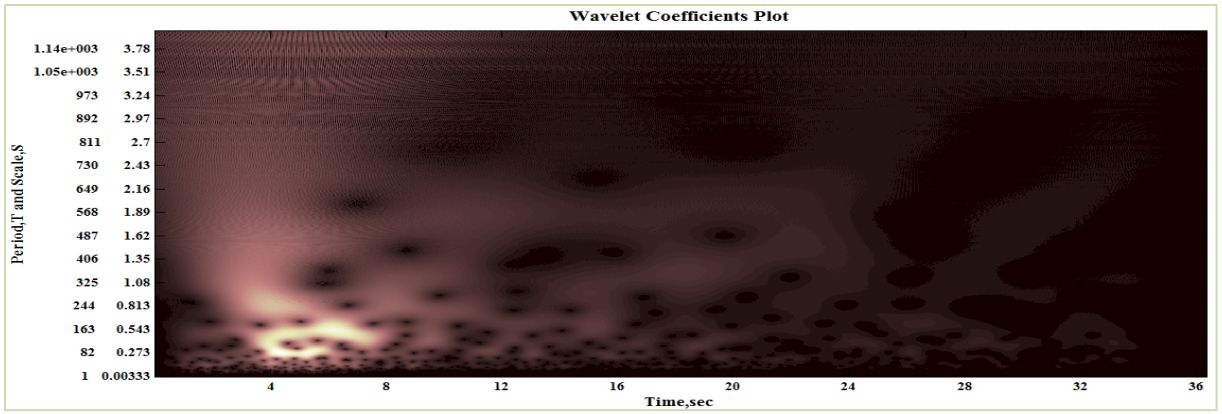

Figure 7-255 2D Wavelet coefficients plot of Ground Motion 22 (Friuli, Italy-Tolmezzo)

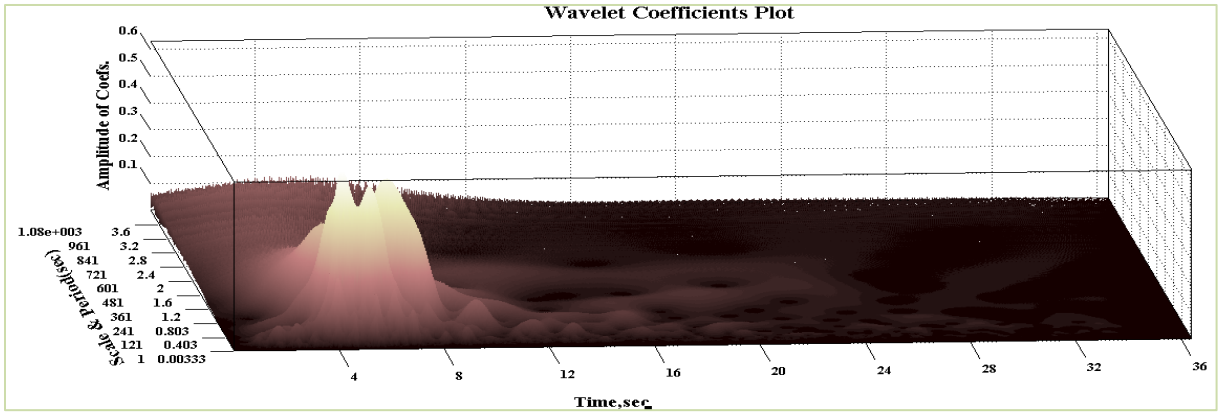

Figure 7-256 3D Wavelet coefficients plot of Ground Motion 22 (Friuli, Italy-Tolmezzo)

The 3D and 2D peak displacement plot of the structural system incorporating bilinear elastic behavior is shown in Figures 7-257 and 7-258 respectively. The 2D peak displacement plot as shown in Figure 7-258 have bumps in peak displacement at corresponding (T_0,η) values of (0.25,1.00) and(0.50,0.75). This localized increase in peak displacement is hypothesized to be the result of occurrence of moving resonance and hence amplification factor greater than 1 is expected for these combinations of period and strength.

The 3D and 2D peak amplification plot of the structural system incorporating bilinear elastic behavior is shown in Figures 7-259 and 7-260 respectively. It is observed from Figure 7-260 the amplification values corresponding to (T_0,η) values of (0.25,01.00), and (0.50,0.75) are greater than 1 leading to the increase in peak displacement. Though the effect of moving resonance is observed, it is very minimal for period 0.5 sec.

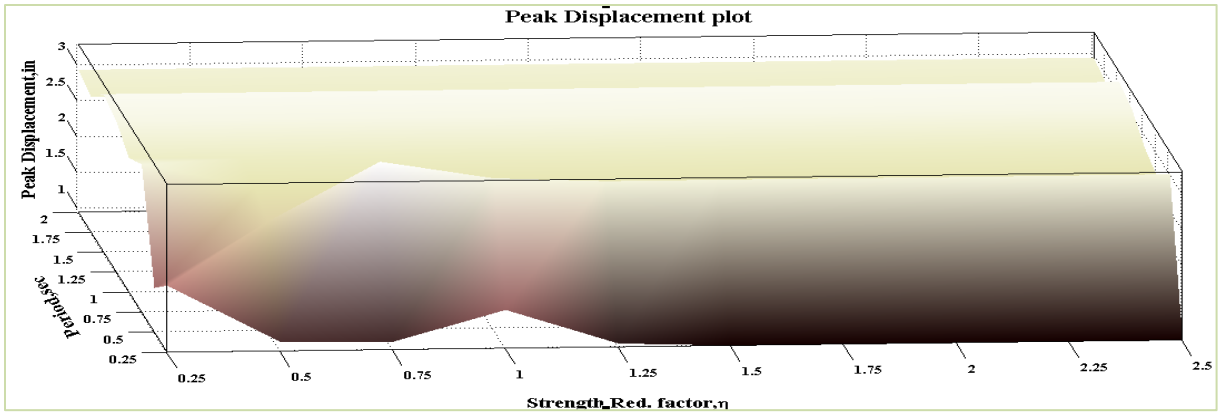

Figure 7-257 3D Peak Displacement plot for Ground Motion 22 (Bilinear Behavior)

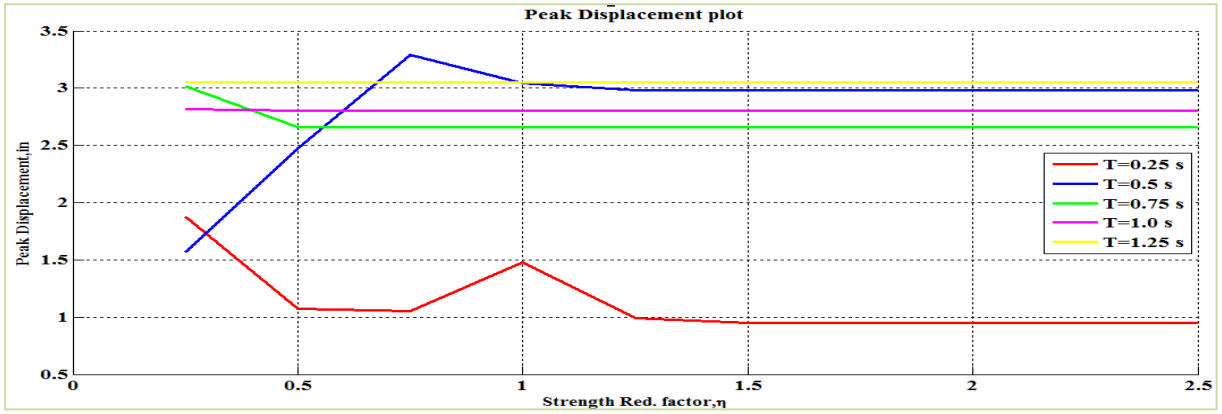

Figure 7-258 2D Peak Displacement plot for Ground Motion 22 (Bilinear Behavior)

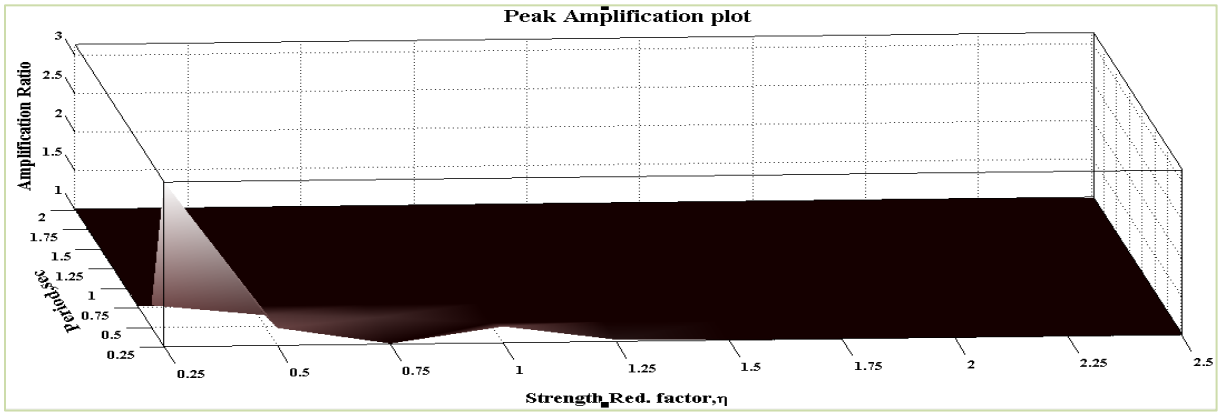

Figure 7-259 3D Peak Amplification plot for Ground Motion 22 (Bilinear Behavior)

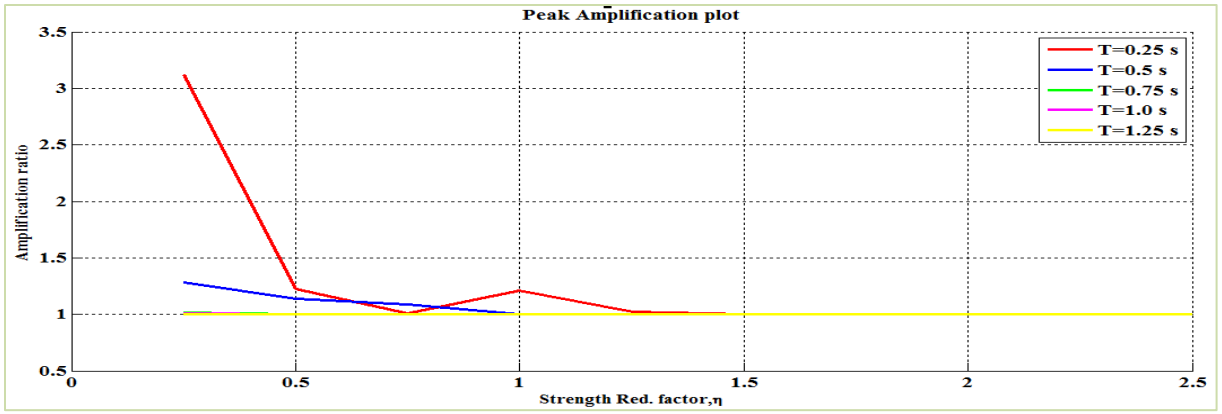

Figure 7-260 2D Peak Amplification plot for Ground Motion 22 (Bilinear Behavior)

The 3D and 2D peak displacement plot of the structural system incorporating elasto-plastic behavior is shown in Figures 7-261 and 7-262 respectively. The 2D peak displacement plot as shown in Figure 7-262 have bumps in peak displacement at corresponding (T_0,η) values of (0.25,0.75) and(0.25,1.25). This localized increase in peak displacement is hypothesized to be the result of occurrence of moving resonance and hence amplification factor greater than 1 is expected for these combinations of period and strength.

The 3D and 2D peak amplification plot of the structural system incorporating bilinear elastic behavior is shown in Figures 7-263 and 7-264 respectively. It is observed from Figure 7-264 the amplification values corresponding to (T_0,η) values of (0.25,01.00), and (0.50,0.75) are greater than 1 leading to the increase in peak displacement. The significant effect is observed for systems with period 0.25 sec with small η values.

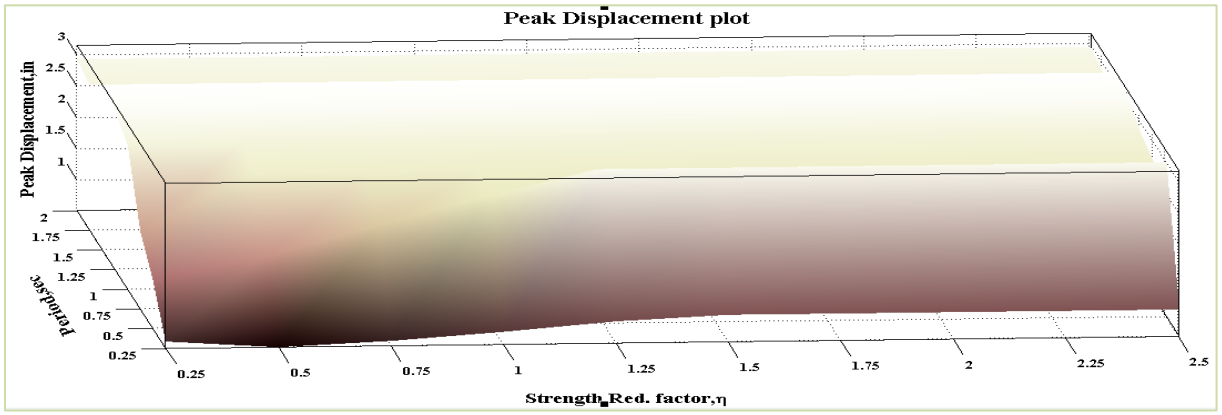

Figure 7-261 3D Peak Displacement plot for Ground Motion 22 (EPP Behavior)

Figure 7-262 2D Peak Displacement plot for Ground Motion 22 (EPP Behavior)

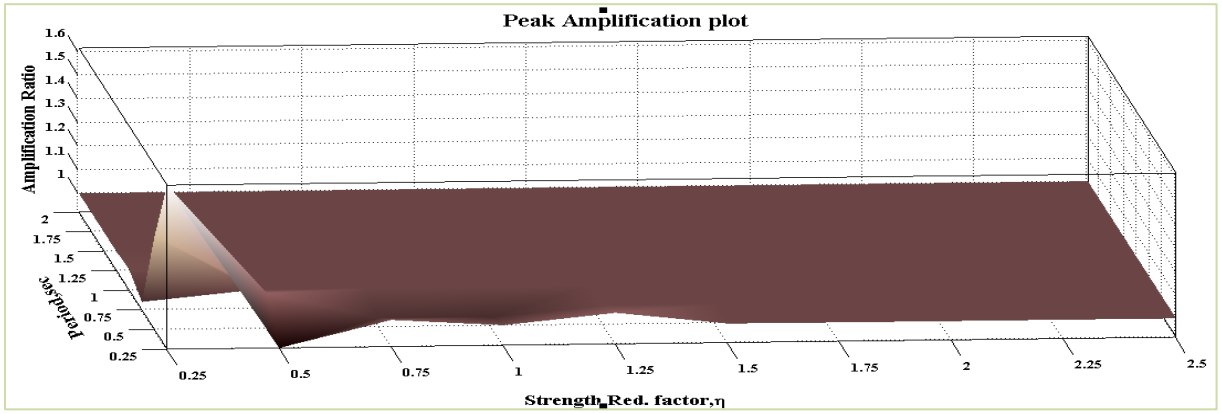

Figure 7-263 3D Peak Amplification plot for Ground Motion 22 (EPP Behavior)

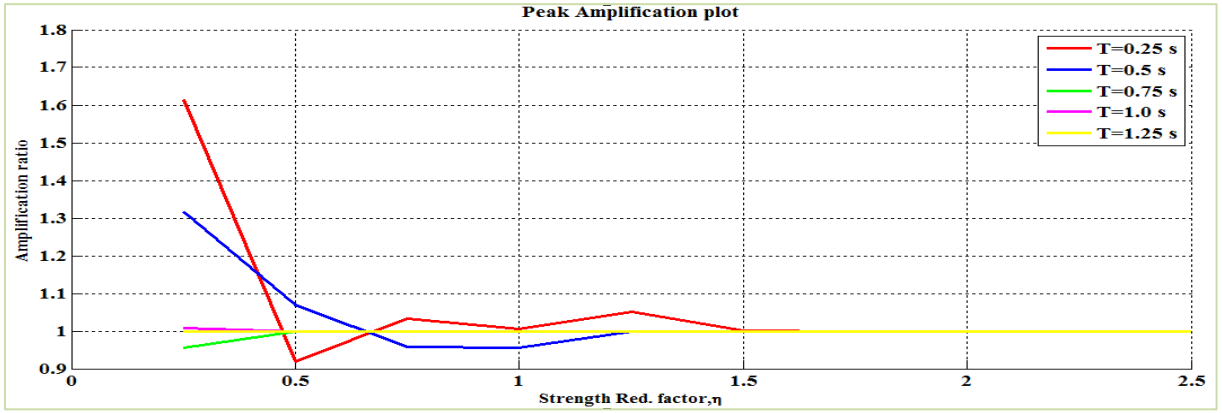

Figure 7-264 2D Peak Amplification plot for Ground Motion 22 (EPP Behavior)

Moving resonance is concentrated in systems with short period because the energy in the ground motion is at relatively short periods.

7.3 Summary

Through observing the trends in the ground motion energy content as a function of time, it is possible to understand the potential for moving resonance. This gives a base and hope for future research to characterize the trends in ground motion energy to predict the potential for moving resonance. The detailed analysis to quantify the effect of moving resonance on structural systems due to 22 Far Field ground motion records has been studied. Based on the analyses results, the characteristics of the ground motion records that don't cause significant moving resonance effect on structural systems were observed. Similarly, the characteristics of the ground motions that do cause moving resonance effect on structural systems were examined.

Table 7-2 shows the characteristics of ground motions that made them especially well-suited to produce moving resonance and the characteristics that made them not conducive to moving resonance.

Table 7-2 Categorization of a suite of ground motions

Ground Motion	Ground Motion Characteristics	Largest Amplification Factors	Comment on Effect of Moving Resonance
1	Well defined ridges of energy with increasing period	17 BE 6.5 EPP	Strong Effect of Moving Resonance, See Ch. 6 for Additional Details
2	Well Defined Ridge of Energy of Constant Period	5.8 BE 3.8 EPP	Lesser effect of moving resonance, small η systems most effected
3	Concentrated energy in time and dominant period	2.0 BE 1.9 EPP	Distinct effect on short period systems
4	Energy follows reducing dominant period	2.5 BE 2.2 EPP	Small effect except for small η systems.
5	Long strong shaking with well distributed energy in time and period	3.0 BE 1.4 EPP	Small effect except for small η systems.
6	Dominant energy has decreasing period and then long constant period	2.2 BE 1.8 EPP	General small except for To=0.25 sec for EPP, and small η for BE
7	Concentrated energy burst with subtle increase in dominant period	1.8 BE 2.2 EPP	Generally small
8	Two dominant ridges of energy, the one with larger period is slightly delayed.	6.9 BE 1.6 EPP	Small effect except for To=0.25 sec for BE

9	Late coming portion of energy at a higher period than previous, with a gap of 8 sec	1.7 BE 1.7 EPP	Generally small
10	Strong shaking at a very short period	1.8 BE 1.0 EPP	Generally small for BE and no effect for EPP
11	Concentrated energy in short length of time –about five seconds	3.3 BE 2.5 EPP	Small effect except for small η=0.25 systems
12	Strong energy with increasing dominant period(similar to ground motion 1)	1.5 BE 1.4 EPP	Distinct effect on short period systems
13	Energy split into several peaks, generally increasing dominant period	4.3 BE 2.1 EPP	More significant effect for BE than EPP system
14	Energy concentrated in time with two ridges	1.7 BE 1.5 EPP	Small effect except for To=0.25,0.5 sec
15	Transition of frequency content with lower to moderate periods	2.2 BE 2.2 EPP	Small effect except for small η systems
16	Concentrated energy in time and dominant period	6.2 BE 1.7 EPP	Small effect except for To=0.25 sec for BE
17	Two distinct ridges of energy with same dominant period	2.5 BE 1.7 EPP	Small effect except for To=0.25 sec for BE
18	Concentrated energy burst with a trailing ridge of energy	2.3 BE 2.1 EPP	Small effect except for small η systems
19	Two bursts of energy	3.0 BE 2.3 EPP	Small effect except for small η systems
20	Concentrated energy in time-Pulse like	4.2 BE 1.5 EPP	Significant effect for To=0.25,0.5 sec
21	Concentrated energy burst with a trailing ridge of energy	1.8 BE 1.0 EPP	Generally small for BE and no effect for EPP
22	Transition of frequency content with lower to moderate periods	3.2 BE 1.6 EPP	Small effect except for small η systems

CHAPTER 8 : SUMMARY, CONCLUSIONS AND RECOMMENDATIONS

8.1 Introduction

Nonlinear structures, when subjected to multiple ground motion records that are scaled to consistent ground motion intensity show significant variation in their response. This effect of ground motion randomness on the variation of structural response is defined as Record-to-Record (RTR) Variability. IDA results reveal additional aspects of RTR variability. It is not uncommon that the peak displacements do not increase monotonically with ground motion intensity. Instead, the peak displacement for one intensity level is sometimes smaller than the peak displacement from a lower intensity level. This hints at the complex interaction between a nonlinear structure and the ground motion excitation. Ground motion characteristics that contribute to the variability in response includes the variation of signal composition with time in particular how the dominant frequencies change with time (spectral nonstationarity). Although RTR variability is identified as important in many references related to nonlinear response history studies and the effects of RTR variability have been analyzed statistically by some researchers, there is a gap in the research in analyzing the sources of this variability. This brings the need to further understand the sources of the variability. The phenomenon of moving resonance which occurs when the frequency content of the ground motion shifts in a similar manner as the natural frequencies of the structural response, is likely a contributor to variability.

8.2 Summary

The present study was carried out to develop a method to analyze the time-frequency content of a ground motion to assess the occurrence of moving resonance and to quantify its potential in effecting the structural systems. Bilinear elastic and elasto-plastic hysteretic behavior was considered. Wavelet transforms have been used to analyze the time-frequency content of the ground motion and structural response.

First, a thorough understanding of the mathematical basis behind wavelet transforms characteristics of different wavelet families and the literature review which includes their

application in the field of earthquake engineering was presented. Further, the literature review has been extended to know the previous research done in the area of moving resonance and its effect on structural response. Though, a number of studies in the past fifteen years have analyzed the effect of spectral nonstationarity on nonlinear structural response, these studies have focused developing stochastic ground motion models that can capture spectral nonstationarity and on exposing the effect of ground motion nonstationarity rather than developing means to quantify the effects. The need to consider the time-varying nature of earthquake ground motion frequency content and its effect on structural response was therefore identified.

After the wavelet analysis program was developed, it was then used to investigate the phenomenon of moving resonance. The present study was done in three phases:

Phase I mainly focused on refining the time-frequency representation of the earthquake signals using wavelet transforms. The properties of wavelet families and the differences between various wavelet transforms were studied. The complex continuous wavelet function was chosen for the study because it captures the frequency content irrespective of the signal being in phase or out of phase. The complex wavelet transforms also rectifies the problem of interference bands. To perform the wavelet transforms and facilitate expansion to further analyze signals, a Matlab program was written and validated against commercially available wavelet transform software. This Matlab program was used to choose a suitable wavelet function (Complex Morlet) by comparing the analyses results of different ground motions with varying frequency content. Existence of black holes (areas of low frequency content) in the analysis plots was investigated and it was concluded that they were a property of the signal. Wavelet coefficients near zero for the ground motion are not desirable because some functions using the wavelet coefficients such as transfer functions use the wavelet coefficients in their denominator. It was concluded that although localized holes in the frequency content of the signal exist that the problem might be mitigated by using a wavelet function having wide resolution both in time and frequency. This would effectively smooth out energy in the ground motion signal and therefore mitigate the effect of localized low energy content in the ground motion signal.

Phase II of the present study focused on developing methods to assess the occurrence of moving resonance and to quantify its potential in effecting structural response. One method of assessing

the occurrence of moving resonance is performed by means of finding correlation between the time-frequency content of the ground motion and the structural response. The correlation is obtained by projecting the wavelet coefficients of ground motion onto the wavelet coefficients of structural velocity. The occurrence of moving resonance concluded from the correlation plots is validated with the increase in the peak displacement values at the corresponding locations. The quantification of the effect of moving resonance is investigated by comparing the peak displacement caused due to the original ground motion with the peak displacement caused due to modified ground motion.The peak displacement plots at elastic stage were validated with the spectral displacement plots. One ground motion which was expected to produce significant moving resonance was analyzed in depth using all five tools.

Phase III of the study involved examining the potential for moving resonance from a suite of ground motions. Detailed analysis is done to quantify the effect of moving resonance on structural systems due to 22 Far Field ground motion records. Based on the analyses results, the characteristics of the ground motion records that don't cause significant moving resonance effect on structural systems were observed. Similarly, the characteristics of the ground motions that do cause moving resonance effect on structural systems were examined.

8.3 Conclusions

The wavelet coefficient plots gave very good detail of the characteristics of the ground motions that were not clear from the acceleration time histories and response spectra plots. Instances of moving resonance were found out to be significant. Amplification due to moving resonance was found to be quite large. One instance studied in detail(accelerogram of Northridge earthquake) had peak displacement amplified by 6 times compared to the amount of peak displacement expected if the system did not exhibit moving resonance. The five tools developed presented corroborating evidence and demonstrated in detail how the system (bilinear elastic and elastic perfectly plastic) natural period elongates and matches dominant energy of this particular ground motion. It was found that phase is important. The ground motion which is seen out of phase with the system (elastic perfectly plastic) for a (T_o,η) value of (0.75,0.75) resulted in destructive interference.

The effect of moving resonance was significant in some cases for bilinear elastic and this effect was muted for elastic perfectly plastic behavior likely because of hysteretic damping. For instance, a peak amplification factor of 17 for bilinear elastic systems is observed for Northridge earthquake at Beverly Hills when compared to a peak amplification factor of 6.5 for elastic perfectly plastic. Also, it is observed that the average peak amplification factor of bilinear elastic systems for all ground motions is more than the elastic perfectly plastic systems.

The ground motions with increasing dominant period (as observed from Northridge earthquake) shows significant effect of moving resonance when compared to ground motions with decreasing dominant period (as observed from Hector Mine earthquake) . It is concluded that even pulse like ground motions (e.g., Chi-Chi Taiwan earthquake) has some propensity towards moving resonance. The ground motions with energy concentrated in time and dominant frequency did cause moving resonance but primarily for systems with initial natural period lower than the ground motion dominant period (as e.g., Duzce Turkey, Kobe Japan and Superstition Hills earthquakes). Significant effect of moving resonance is observed for ground motions with energy that was concentrated in a narrow period band, but spread out in time (e.g., Northridge at Canyon County, Kobe Japan at Nishi-Asaki and Imperial Valley earthquake).

8.4 Recommendations for Future Work

The following are some of the recommendations for future research work in this area:

1. Black holes (areas of low frequency content) can be mitigated in the wavelet transform by using a wavelet function that has very wide resolution both in time and frequency. This will result in significantly improved ability to apply transfer functions (which have these values in the denominator).

2. The ground motion records used for the present study were not scaled. Scaling all the ground motions to the same design response spectrum and then analyzing in detail to assess the effect of moving resonance may give interesting results.

3. The present study conducted on far field ground motion records can be extended to Near field ground motions and can identify the effect of moving resonance on Pulse and No-pulse signals.

4. Development of a method for predicting the potential for moving resonance. The purpose is to characterize how the dominant frequencies in the ground motion vary with time.

5. Trying different hysteretic models to determine the sensitivity of the system to hysteretic behavior.

6. Further investigation of the short period structures. Is that huge amplification values are due to moving resonance?

7. Compare results with the studies done on RTR variability of the FEMA P695 set. Develop better understanding of the RTR variability.

REFERENCES

Al Atik, L., and Abrahamson, N. (2010). "An Improved Method for Nonstationary Spectral Matching." *Earthquake Spectra*, 26(3), 601

Asadi, A., Fadavi, M., Bagheri,A., and Ghodrati Amiri,G., (2011). "Application of Neural Networks and an Adapted Wavelet Packet for Generating Artificial Ground Motion." *Structural Engineering and Mechanics*, 37(6), p 575-592.

Baker, J. W. (2007). "Quantitative Classification of Near-Fault Ground Motions Using Wavelet Analysis." *Bulletin of the Seismological Society of America*, 97(5), 1486-1501

Cao, H., and Friswell, M. (2009). "The Effect of Energy Concentration of Earthquake Ground Motions on the Nonlinear Response of RC Structures." *Soil Dynamics and Earthquake Engineering*, 29(2), 292-299

Chakraborty, A., and Okaya, D. (1995). "Frequency-Time Decomposition of Seismic Data using Wavelet-Based Method." *Geophysics*, 60, 1906-1916

Chanerley, A.A, and Alexander, N.A (2010). "Obtaining Estimates of the Low-Frequency 'Fling',Instrument Tilts and Displacement Timeseries using Wavelet Decomposition." *Bulletin of Earthquake Engineering*, 8(2), p231-255

Conte,J.P., Pister, K.S., Mahin, S.A., (1992). "Nonstationarity ARMA Modeling of Seismic Motions." *Soil Dynamics and Earthquake Engineering*, 11(7), p411-426

Conte,J.P., Pister, K.S., Mahin, S.A., (1990). "Influence of the Earthquake Ground Motion Process and Structural Properties on Response Characteristics of Simple Structures ." *Earthquake Engineering Research Center*, 90(9), p362

ElGawady, M. Sehhati R.,Rodriguez Marek A., William cofer F., (2010). "Response of Multi-Story Structures to Near-Fault Ground Motions and Equivalent Pulses." Proceedings of the 9th U.S. National and 10th Canadian Conference on Earthquake Engineering

FEMA, 2009, NEHRP Recommended Provisions for Seismic Regulations for New Buildings and other Structures. FEMA p695, "Quantification of Building Seismic Performance Factors."

Gaupillaud, P., Grossmann, A., and Morlet, J. (1984). "Cycle-Octave and Related Transforms in Seismic Signal Analysis." *Geo-exploration*, 23, 85–102

Goggins, J.,Basu B., Elghazouli A.Y. (2006). "Earthquake Damage Detection in Concentrically-Braced Frames using Wavelet Analysis." *Earthquake Engineering & Structural Dynamics*, 33(9), 1023-1049

Grossmann, A., & Morlet, J. (1984). “Decomposition of Hardy Functions into Square-Integrable Wavelets of constant Shape.” *SIAM Journal on Mathematical Analysis*, 15(4), 723-36.

Ibarra, L., and Krawinkler, H. (2011). "Variance of Collapse Capacity of SDOF Systems under Earthquake Excitations" *Earthquake Engineering & Structural Dynamics*, 31(3), 491-514

Kareem A., Gurley K., (1999). "Applications of Wavelet Transforms in Earthquake, Wind and Ocean Engineering." *Engineering Structures*, 26(3), 601

Koduru (2010). "Influence of Spectral Nonstationairty On Structural Damage." Proceedings of the 9th U.S. National and 10th Canadian Conference on Earthquake Engineering

Lihanand K.,Tseng W.S, (1988). "Development and Application of Realistic Earthquake Time Histories Compatible with Multiple-Damping Design Spectra." Proceedings of the 9th World Conference on Earthquake Engineering

Littlewood J., & Paley P., (1937). "Theorems on Fourier Series and Power Series." *Proceedings of London Math Society*. 42(2)

Matlab, 7.10.0 (R2010a). “The Langauage of Technical Computing.” *The Mathworks, Inc.*

Mavroeidis, G. P., Dong, G., and Papageorgiou, A. S. (2004). "Near-fault ground motions, and the Response of Elastic and Inelastic Single-Degree-of-Freedom(SDOF) Systems." *Earthquake Engineering & Structural Dynamics*, 33(9), 1023-1049

Mukherjee, S., & Gupta, V. K. (2002b). "Wavelet-Based Characterization of Design Ground Motions." *Earthquake Engineering & Structural Dynamics*, 31(5), 1173-1190

Nakhaei, M., and Mohraz, B. (2010). "Comparing the Robustness of genetic Algorithms and Wavelet Transformations for Ground Motion scaling." *Structures Congress*.

Newmark, N.M. and W.J. Hall (1982), “Earthquake Spectra and Design.”*Earthquake Engineering research Institute*.

NONLIN, 7.05 (2003). “Computer Program for Nonlinear Dynamic Time History Analysis of Single- and Multi-Degree-of-Freedon Systems.” *Advanced Structural Concepts, Inc.*

OpenSees ,2006. *Open System for earthquake engineerign Simulation,* Pacific Earthquake Engineering Research Center, University of California, Berkeley.

Rajasekaran,S.,Latha Vasuki., and Lee S.C. (2006) ”Generation of Artificial Earthquake Motion Records using Wavelets and Principal Component Analysis.”*Journal of Earthquake Engineering*,10(5),p 665-691

Saurez, L.E., and Montejo,L.A. (2005) ”Generation of Artificial Earthquakes via the Wavelet Transform.”*International Journal of Solid and Structures*,21-22,p 5905-5919

Shannon, C.E.(1949)“Communication in the presence of noise.” *Proc. Institute of Radio Engineers*,37(1),10-21.

Vamvatsikos, D., and Cornell, M. P. (2002). "Incremental Dynamic Analysis." *Earthquake Engineering & Structural Dynamics*, 31(3), 491-514.

Veletsos, A.S.,Newmark, N.M., Chelapati, C.V. (1965). "Deformation Spectra for Elastic and Elastoplastic Systems Subjected to Ground Shock and Earthquake Motions."*Proceedings of the 3rd World Conference on Earthquake Engineering ,Wellington,New Zealand*, 663-680.

Zhou, Z.,& Adeli, H., (2003). "Time-Frequency Signal Analysis of Earthquake Records Using Mexican Hat Wavelets." *Computer Aided Civil and Infrastructure Engineering.* 18(5), 379-89

APPENDIX A: WAVELET FUNCTIONS

A.1 Properties of wavelet functions

Wavelet functions Ψ(x) should satisfy the following prescribed conditions:

- Continuity;

- A zero mean amplitude (the integral of the function is equal to zero)

$$\int \Psi(x) dx = 0$$

The equation A-1 implies that a wavelet function has at least some oscillations;

- The wavelet function Ψ(x) takes either null value out-side a given real domain of R (it has a finite duration of energy, and consequently is known as compactly supported) or Ψ(x) approaches zero quickly as independent variable *x* approaches infinity. This property prevents the propagation of any local transient signal features through time indefinitely; and

- Relatively less energy for lower frequencies compared with that for higher frequencies.

The following are other properties that classify wavelet functions into different categories.

- **Orthogonality**: Orthogonal wavelets are one type of compactly supported wavelet functions where the same basis function is used for both decomposition and reconstruction.

  Orthogonal wavelet functions will have no overlap with each other (zero correlation) when computing the wavelet transform, while non-orthogonal wavelets will have some overlap (nonzero correlation). Using an orthogonal wavelet, one can transform to wavelet space and back with no loss of information.
  Non-orthogonal wavelet functions tend to artificially add in energy (due to the overlap) and require renormalization to conserve the information. In general, discrete wavelets are orthogonal while continuous wavelets are non-orthogonal.

- **Biorthogonality**: Biorthogonal wavelets are another type of finite duration wavelet functions where there is a pair of basis wavelet functions that are dual to each other.

- **Admissibility**: It ensures the perfect reconstruction of the original signal from the transformed wavelet coefficients; It can be shown that square Integrable functions Ψ(x) satisfying the admissibility condition,

$$\int \frac{|\Psi(\omega)|^2}{|\omega|} d\omega \ < +\infty$$

can be used to first analyse and then reconstruct a signal without loss of information. In the above equation Ψ(ω) stands for the Fourier transform of Ψ(x). The admissibility condition implies that the Fourier transform of Ψ(x) vanishes at the zero frequency, which can be shown as follows:

$$||\Psi(\omega)|^2|_{\omega=0} = 0$$

This means that wavelets must have a band-pass like spectrum. This is a very important observation, which will be helpful to build an efficient wavelet transform. A zero at the zero frequency also means that the average value of the wavelet in the time domain must be zero.

$$\int \Psi(x)\ dx = 0$$

and therefore it must be oscillatory. In other words, Ψ(x) must be a wave.

The admissibility property can be explained better with the following example.

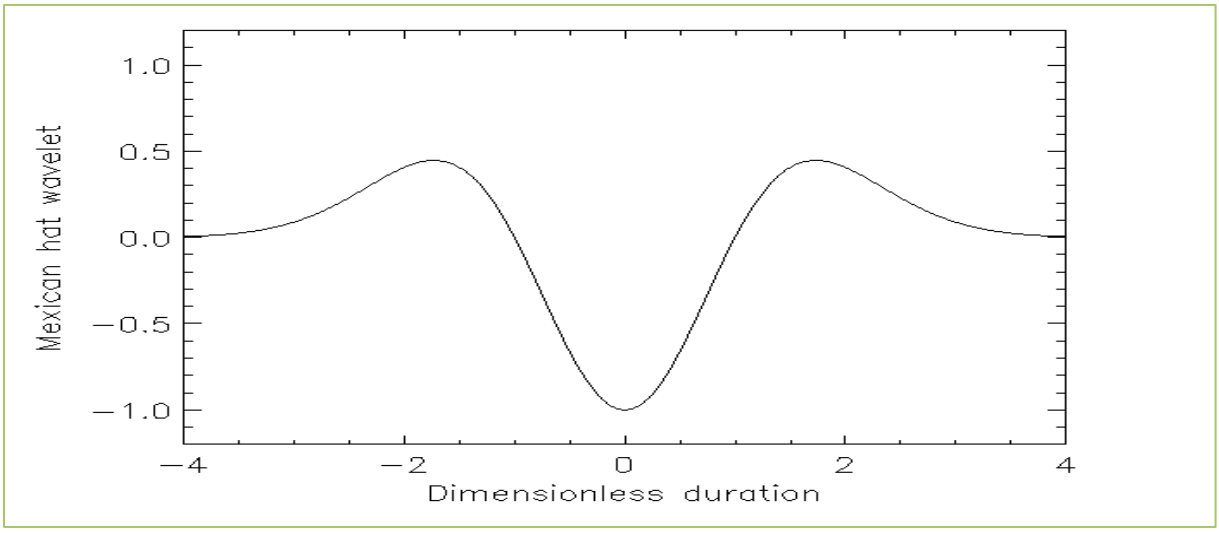

Figure A-1 Mexican hat wavelet

The figure A-1 represents the Mexican hat wavelet function upside-down with a central trough (top of the hat) and two symmetric bumps on either side. It is important to note

that, for this to be a wavelet, the positive and negative areas under the curve must cancel out. This is known as the admissibility condition.

- **Compact support**: This value measures the effective width of the wavelet function. A narrow wavelet function such as the Daubechies order 2 (compact support=3) is fast to compute, but the narrowness in "time" implies a very large width in "frequency." Conversely, wavelets with large compact support such as the Daubechies order 24 (compact support=47) are smoother, have finer frequency resolution and are usually more efficient at denoising.

- **Symmetry or anti-symmetry**: It refers to the shape of the wavelet; Symmetric wavelets show no preferred direction in "time," while asymmetric wavelets give unequal weighting to different directions.

  For eg: Mexican wavelets as shown in the Figure A-1 is symmetric in nature. Haar's wavelet is the only orthogonal wavelet which is anti-symmetric. It has s simple form of a step function and is not continuously differentiable consequently; the application of Haar's wavelet is quite limited.

- **Regularity**: It refers to the degree of differentiability of the wavelet function, which is essential when smooth representation of signals is needed.

A.2 Selection of Wavelet Functions

Most strong earthquakes of interest to structural engineers are caused by a sudden rupture or slip of a geological fault. An earthquake generated from a single point rupture can be described ideally as a penny-shaped crack located on the hypocenter (Housner, 1970). When the stress in the area inside the crack zone exceeds the rupture point, strain is released with the rupture and a displacement occurs between the two sides of the rupture as idealized in the following figure.

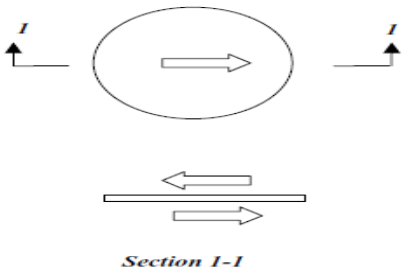

Figure A-2 Penny-shaped rupture to model single-source earthquakes (Housner,1970)

A displacement wave is created by this rupture and propagates radially from the source. Vibrations are produced when this displacement wave reaches the earth's surface at the site of a structure. The single-source displacement of ground motion is idealized by a Gaussian function

in the following form:

$$d(t) = e^{-t^2/2}$$

The general shape of such a simple single-source displacement wave is shown as follows:

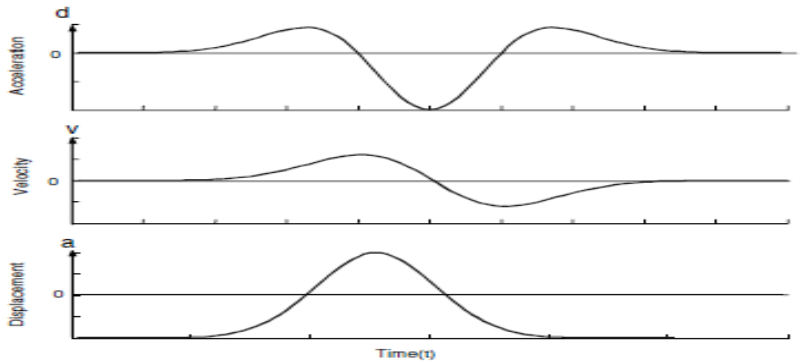

Figure A-3 Idealized ground motion wave generated by a single-source earthquake (Zhou and Adeli, 2003)

Such a simple displacement wave has in fact been recorded at seismographic stations. There have been a number of small earthquakes with primarily one displacement wave similar to that shown in Figure A-3. The first such simple-source ground motion was observed in Port Hueneme earthquake on March 18, 1957 (with magnitude $M = 4.7$), as shown in Figure A-4.

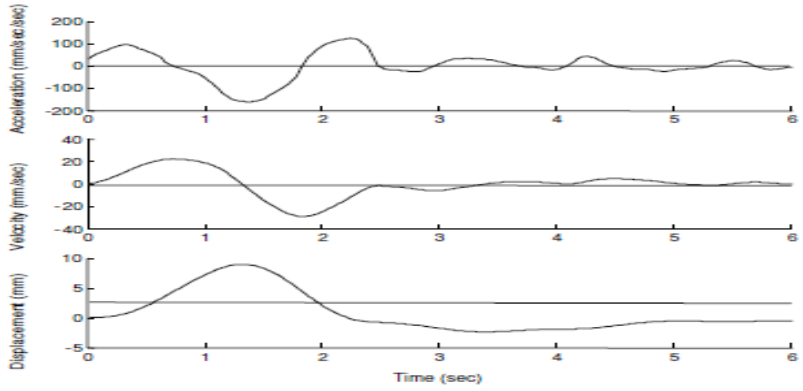

Figure A-4 East-West component of ground motions recorded in the Port Hueneme earthquake (Zhou and Adeli, 2003)

Most earthquakes of engineering significance are generated by a more complicated source mechanism and their ground motion appears more complex. The time histories of the El Centro earthquake of 1940 ($M = 6.9$) is shown in Figure A-5

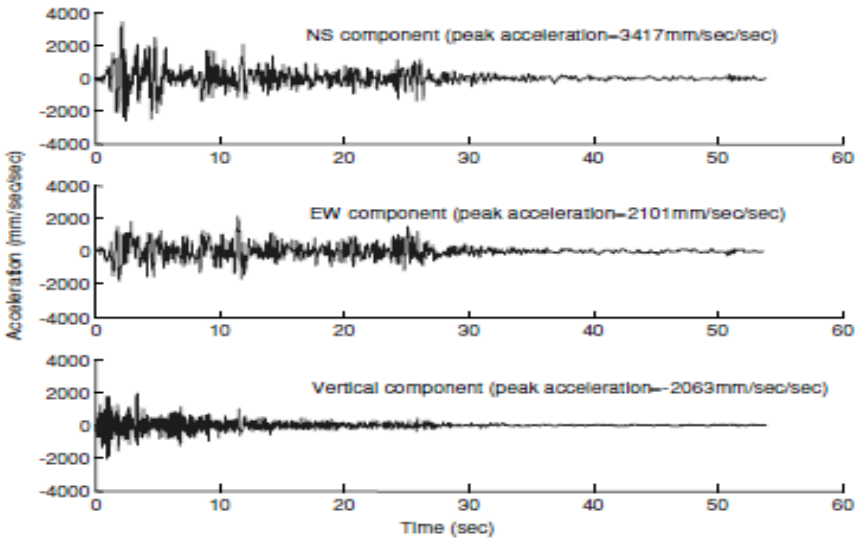

Figure A-5 El Centro earthquake accelerograms (Zhou and Adeli, 2003)

It is postulated that ground motions in such earthquakes are produced by a sequence of the simple penny-shaped ruptures at different locations along a fault line. These simple ruptures occur at different locations and time, resulting in a series of simple records combined to create a complicated earthquake record such as that of the El Centro earthquake. The existence of single-displacement earthquake wave supports the hypothesis of the decomposition of earthquakes into many single-source ground motions of the kind shown in Figure A-2.

For the purpose of signal analysis of accelerograms (Seismograms or earthquake signals), the ground motion record generated by a simple penny-shaped rupture is used to form the basis wavelet function. After a careful study of the characteristics of various wavelet functions, the corresponding wavelet function will be chosen.

The selection of the most appropriate wavelet basis function is based on the following considerations. Some more conditions have to be considered based up on the signal, but these are the basic ones to be considered.

- Since the mother wavelet should characterize the acceleration wave generated from a single rupture source, its initial and final values should approach zero. Consequently, the wavelet basis function has to be compactly supported with a finite duration, or nearly compactly supported.
- The goal of the wavelet decomposition of the earth-quake accelerograms is to extract time-frequency features from the signal. As such, no reconstruction of the original accelerograms from the transformed wavelet coefficients is required. Therefore, the orthogonally or Biorthogonality properties are not required.
- The acceleration generated by an ideal single displacement wave has a symmetric shape.

Orthogonal wavelets are asymmetric in general (Daubechies, 1992) and therefore not suitable for the above application.

- Since in response spectrum analysis a second-order structural vibrations differential equation has to be solved, a wavelet with an analytical expression is preferred because it is more amenable to mathematical manipulation.

APPENDIX B: MATLAB PROGRAMMING

B.1 Matlab Inbuilt Functions used for developing the code:

B.1.1 RESHAPE

RESHAPE(X, M, N) returns the M-by-N matrix whose elements are taken column wise from X. An error results if X does not have M*N elements.

B.1.2 CGAUWAVF (Complex Gaussian wavelet)

[PSI,X] = CGAUWAVF(LB,UB,N,P) returns values of the Pth derivative of the complex Gaussian function F = Cp*exp(-i*x)*exp(-x^2) on an N point regular grid for the interval [LB,UB]. Cp is such that the 2-norm of the Pth derivative of F is equal to 1. P can be integer values from 1 to 8.

B.1.3 CMORWAVF (Complex Morlet wavelet)

[PSI,X] = CMORWAVF (LB,UB, N,FB,FC) returns values of the complex Morlet wavelet defined by a positive bandwidth parameter FB, a wavelet center frequency FC, and the expression

PSI(X) = ((pi*FB)^(-0.5))*exp(2*i*pi*FC*X)*exp(-(X^2)/FB)

on an N point regular grid in the interval [LB,UB].

B.1.4 MEXIHAT (Mexican hat wavelet)

[PSI, X] = MEXIHAT (LB, UB, N) returns values of the Mexican hat wavelet on an N point regular grid in the interval [LB, UB]. Output arguments are the wavelet function PSI computed on the grid X.

B.1.5 CUMSUM (Cumulative sum of elements)

For vectors, CUMSUM(X) is a vector containing the cumulative sum of the elements of X. For matrices, CUMSUM(X) is a matrix the same size as X containing the cumulative sums over each column.

B.1.6 FLIPLR (Flip matrix in left/right direction)

FLIPLR(X) returns X with row preserved and columns flipped in the left/right direction

X = [1 2 3 becomes [3 2 1

4 5 6] 6 5 4]

B.1.7 CONV2 (Two dimensional convolution)

C = CONV2 (A, B) performs the 2-D convolution of matrices A and B.

If [ma,na] = size(A), [mb,nb] = size(B), and [mc,nc] = size(C), then

mc = max([ma+mb-1,ma,mb]) and nc = max([na+nb-1,na,nb]).

B.1.8 IMAGE (Display image)

IMAGE(C) displays matrix C as an image. Each element of C specifies the color of a rectilinear patch in the image. C can be a matrix of dimension MxN or MxNx3.

B.1.9 CENTFRQ (Wavelet center frequency)

FREQ = CENTFRQ ('wname') returns the center frequency in hertz of the wavelet function 'wname'.

B.1.10 SET (Set object properties)

SET (H,'PropertyName', PropertyValue) sets the value of the specified property for the graphics object with handle H. H can be a vector of handles, in which case SET sets the properties' values for all the objects.

B.1.11 SURF (3-D colored surface)

SURF(X, Y, Z, C) plots the colored parametric surface defined by four matrix arguments. The view point is specified by VIEW. The axis labels are determined by the range of X, Y and Z,or by the current setting of AXIS. The color scaling is determined by the range of C, or by the current setting of CAXIS. The scaled color values are used as indices into the current COLORMAP.The shading model is set by SHADING.
SURF(X, Y, Z) uses C = Z, so color is proportional to surface height.

B.1.12 SHADING (Color shading mode)

SHADING controls the Color shading of SURFACE and PATCH objects.
Surface and Patch objects are created by the functions SURF, MESH.

B.1.13 HANDLE (Superclass of all handle classes)

A handle is an object that indirectly references its data. When a handle is constructed, an object with storage for property values is created. The constructor returns a handle to this object. When a handle object is copied, for example during assignment or when passed to a MATLAB function, the handle is copied but not the underlying object property values.

B.2 Convolution theorem

A convolution is defined as the integral over all space of **one function at x times another function at u-x**. The integration is taken over the variable x, typically from minus infinity to infinity over all the dimensions. So the convolution is a function of a new variable u, as shown in the following equations. The cross in a circle is used to indicate the convolution operation.

$$C = f(x) \otimes g(x) = \int f(x)g(u-x)dx$$

$$C = g(x) \otimes f(x) = \int g(x)f(u-x)dx$$

The **convolution operation is commutative**. The following figure shows the convolution, as giving a **weighted sum of shifted copies of one function**: the weights are given by the function value of the second function at the shift vector.

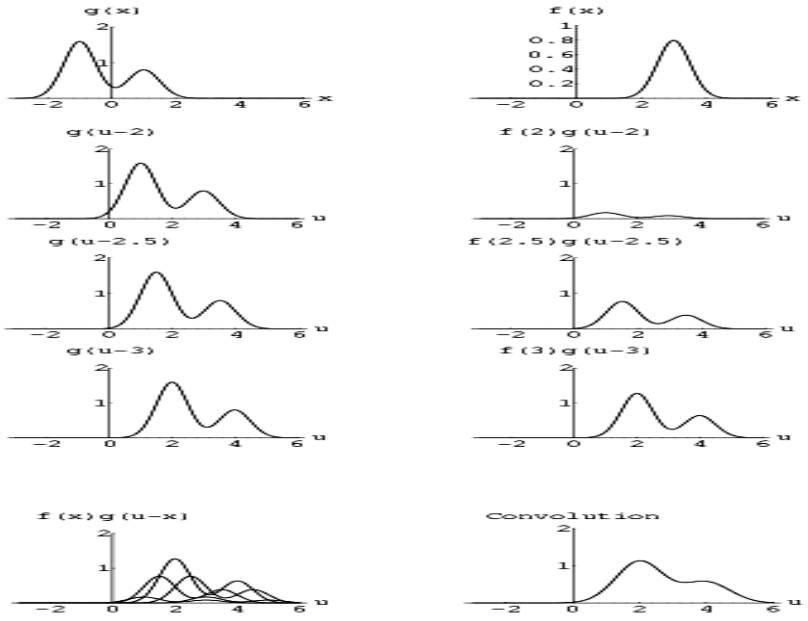

Figure B-1 Graphs explaining convolution theorem

In the figure B-1, the top pair of graphs shows the original functions. The next three pairs of graphs show (on the left) the function g shifted by various values of x and, on the right, that shifted function g multiplied by f at the value of x.

The bottom pair of graphs shows, on the left, the superposition of several weighted and shifted copies of g and, on the right, the integral (*i.e.* the sum of all the weighted, shifted copies

of g). It can be noticed that the biggest contribution comes from the copy shifted by 3, *i.e.* the position of the peak of f.

APPENDIX C: REFINEMENT OF TIME-FREQUENCY PLOTS

C.1. Acceleration and Displacement Response Spectra plots

C.1.1. HDLT352 Component of Imperial Valley Earthquake

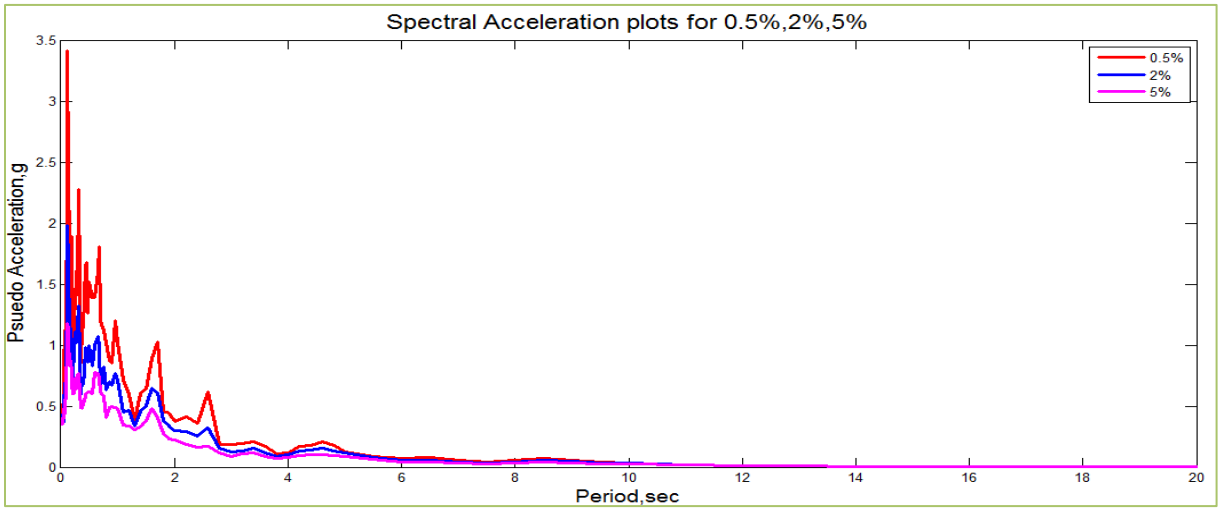

Figure C-1 Acceleration Response Spectra plot of HDLT352 component for 0.5,2 and 5% damping

max(PAA0.5%)=3.41g @period=0.12 sec

max(PAA2%)=1.98g @period=0.12 sec

max(PAA5%)=1.18 @period=0.12 sec

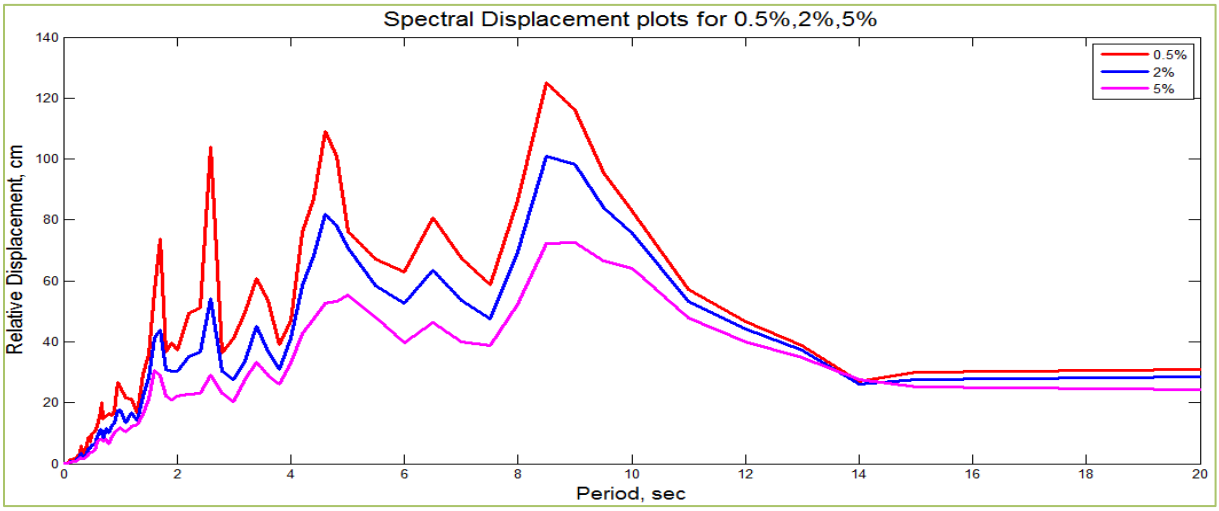

Figure C-2 Displacement Response Spectra plot of HDLT352 component for 0.5,2 and 5% damping

max(RD0.5%)=125 cm @period= 8.5 sec

max(RD2%)=101 cm @period= 8.5 sec

max(RD5%)=72.5 cm @period= 9 sec

C.1.2 HDLTDWN Component of Imperial Valley Earthquake

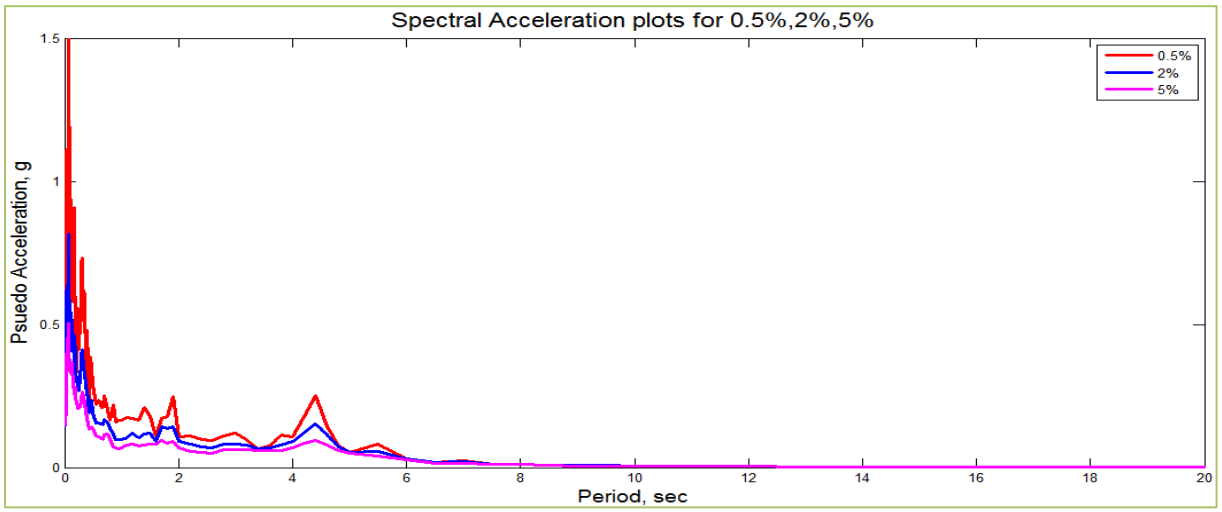

Figure C-3 Acceleration Response Spectra plot of HDLTDWN component for 0.5,2 and 5% damping

max(PAA0.5%)=1.5 g @period=0.075 sec

max(PAA2%)=0.8170 g @period=0.075 sec

max(PAA5%)=0.505g @period=0.075 sec

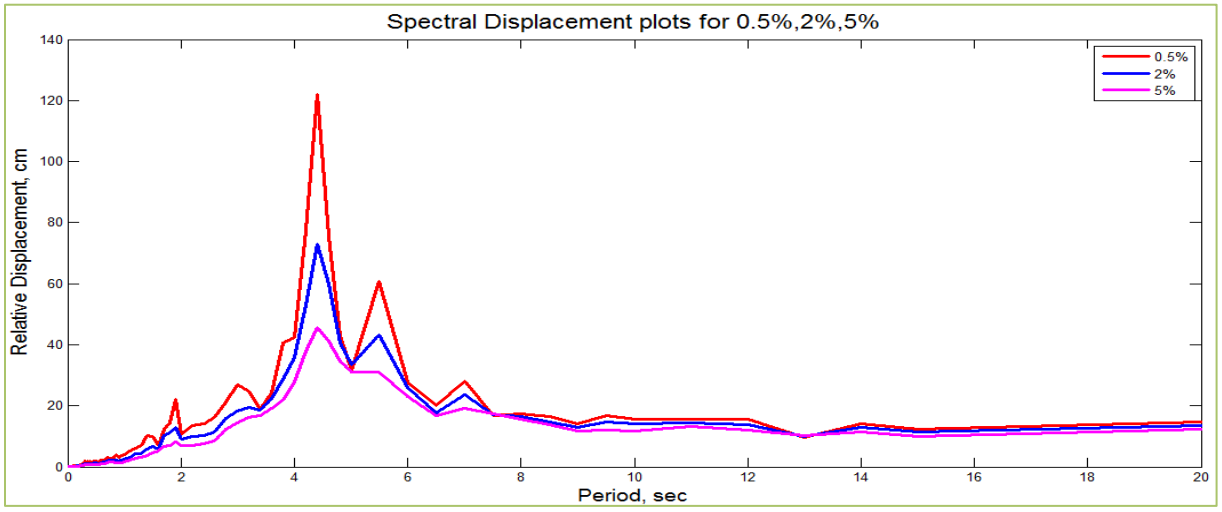

Figure C-4 Displacement Response Spectra plot of HDLTDWN component for 0.5,2 and 5% damping

max(RD0.5%)=122 cm @period=4.4 sec

max(RD2%)=73.1 cm @period=4.4 sec

max(RD5%)=45.5 cm @period=4.4 sec

C.2 Wavelet Transforms of Acceleration Time History Data:

C.2.1. HDLT262 ATH for periods ranging between 0-10 sec of ‘mexh’, ‘cgau4’

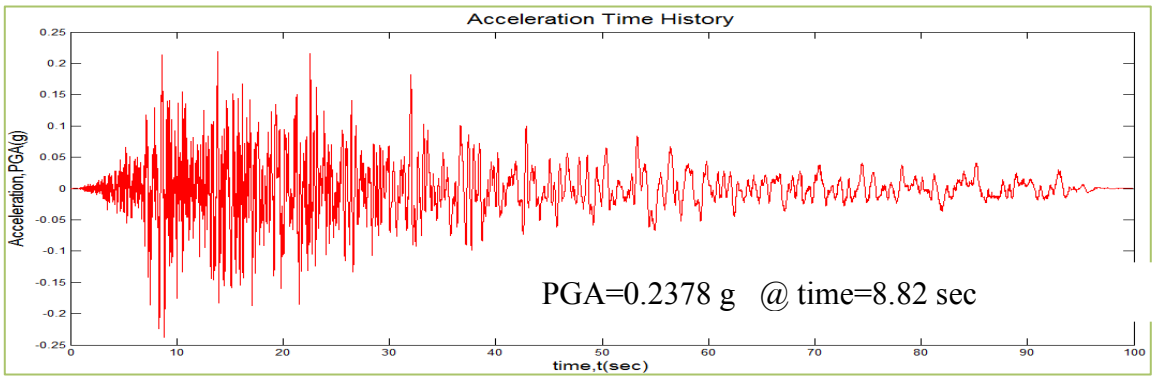

Figure C-5 Acceleration Time History of HDLT262 component of Imperial Valley Earthquake

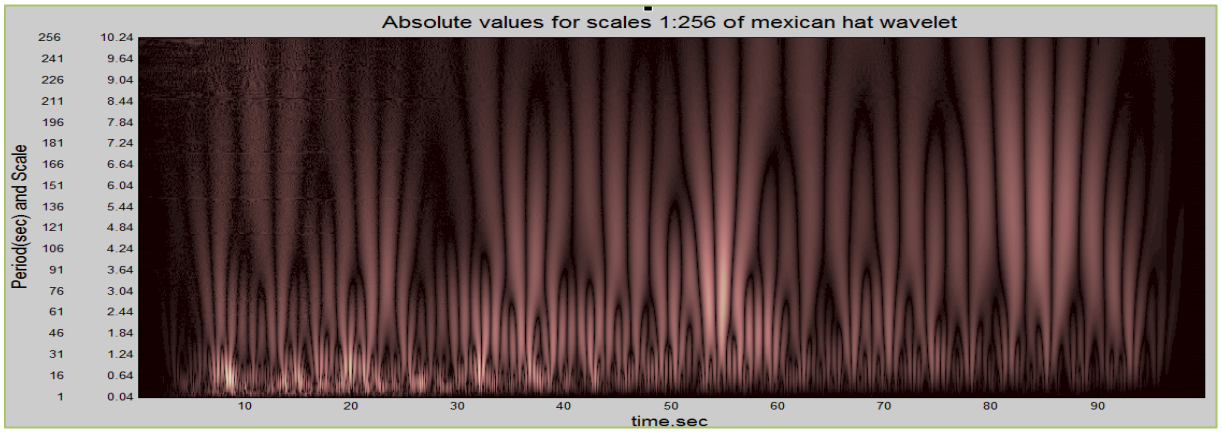

Figure C-6 Wavelet coefficients plot using Mexican hat wavelet analysis program

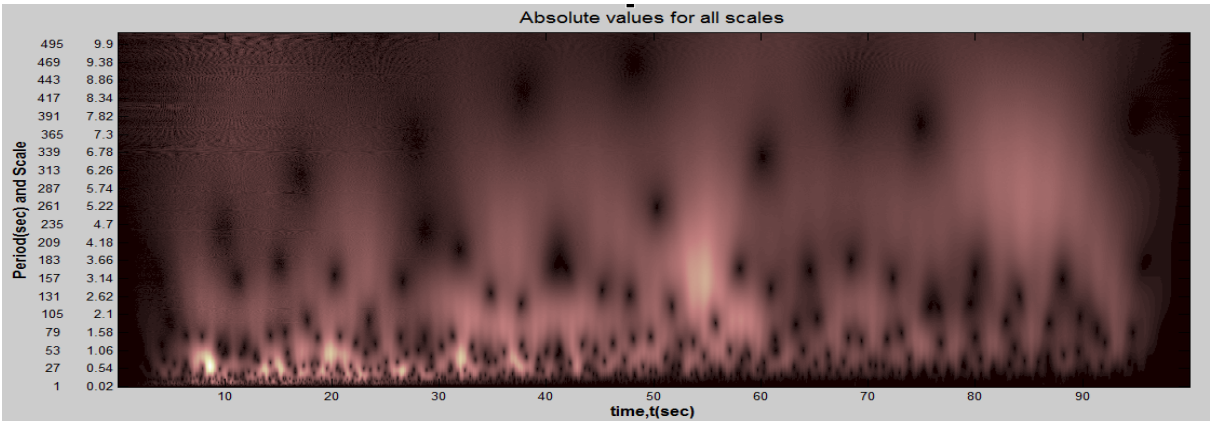

Figure C-7 Wavelet coefficients plot using Complex Guassian wavelet analysis program

C.2.2. HDLTDWN ATH for periods ranging between 0-10 sec of ‘mexh’, ‘cgau4’

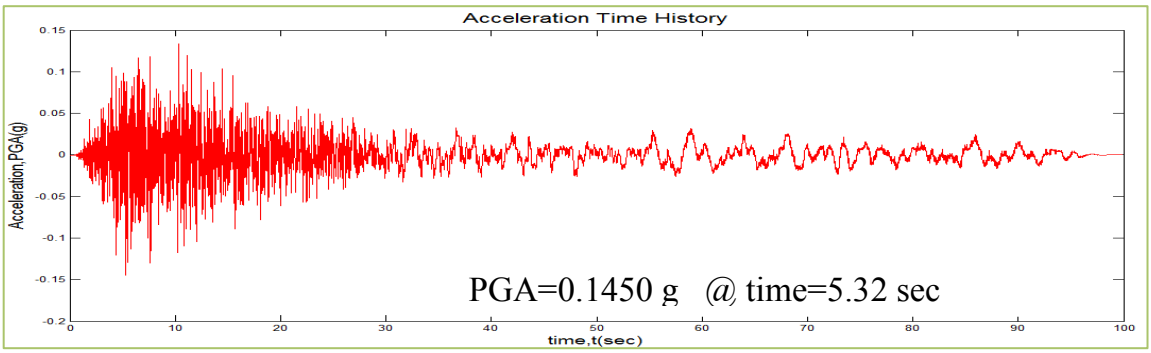

Figure C-8 Acceleration Time History of HDLTDWN component of Imperial Valley Earthquake

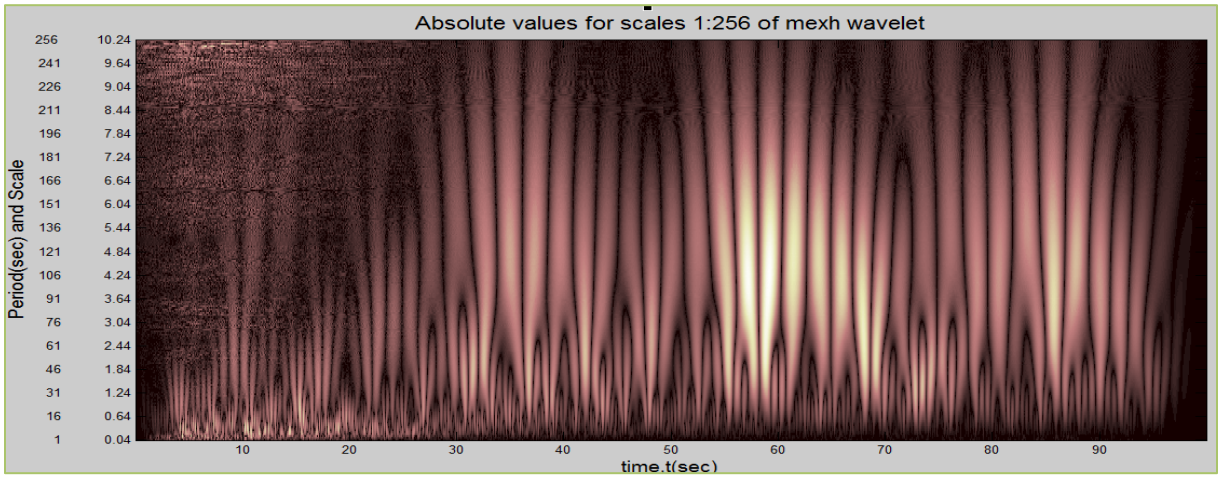

Figure C-9 Wavelet coefficients plot using Mexican hat wavelet analysis program

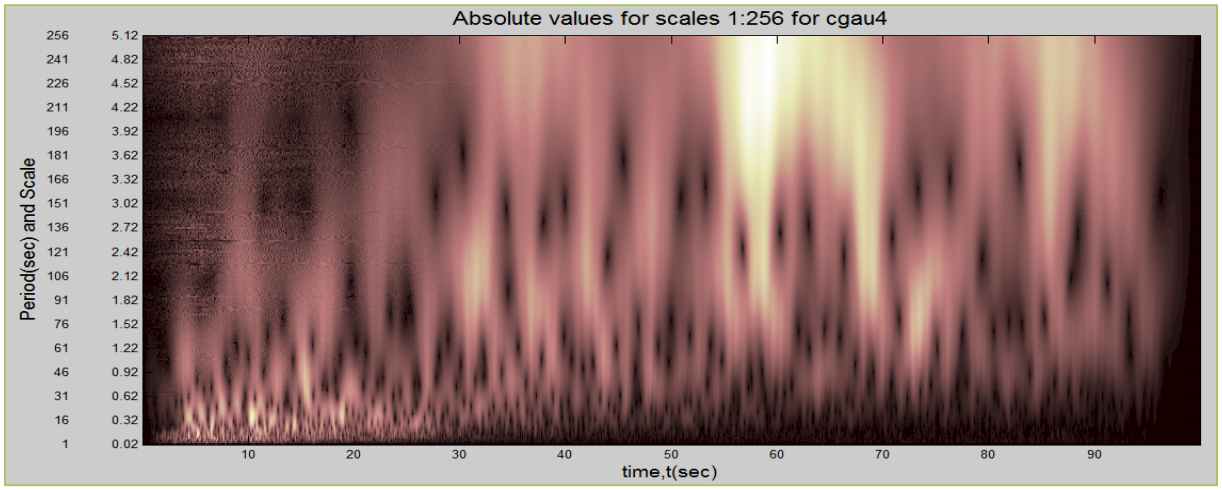

Figure C-10 Wavelet coefficients plot using Complex Guassian wavelet analysis program

C.3. Comparison of 2D and 3D wavelet transform plots using Mexican hat wavelet

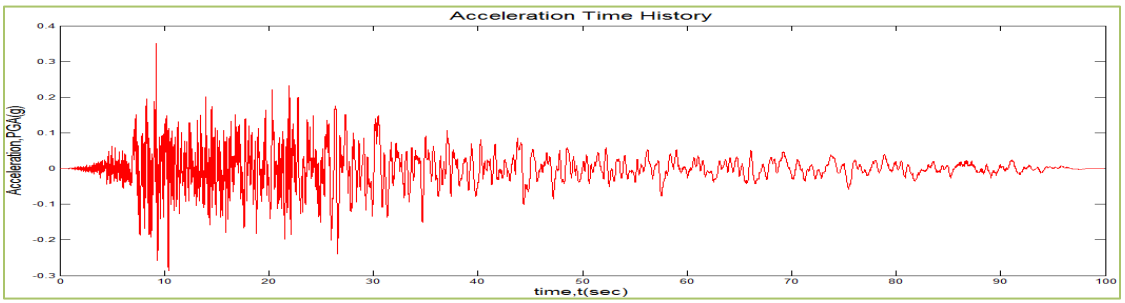

Figure C-11 Acceleration Time History of HDLT352 component of Imperial Valley Earthquake

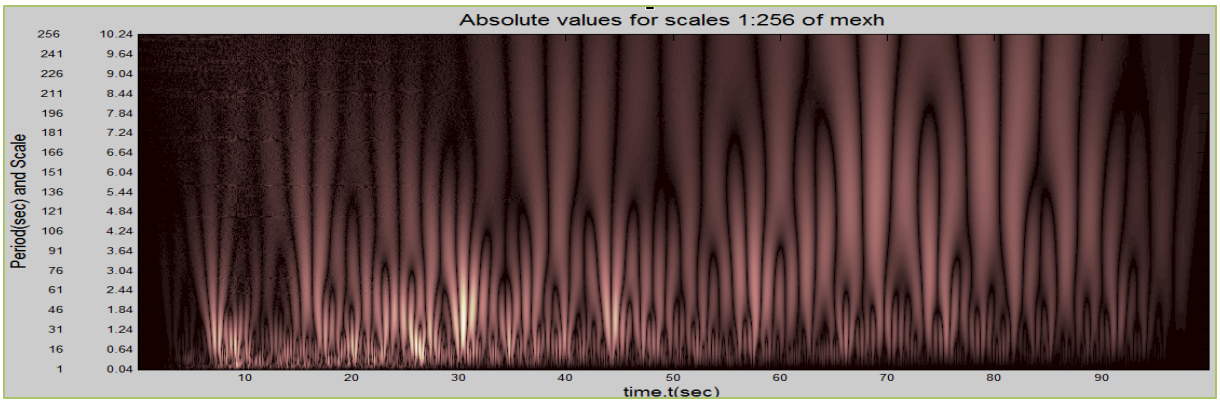

Figure C-12 Wavelet coefficients plot in 2D using Mexican hat wavelet analysis program

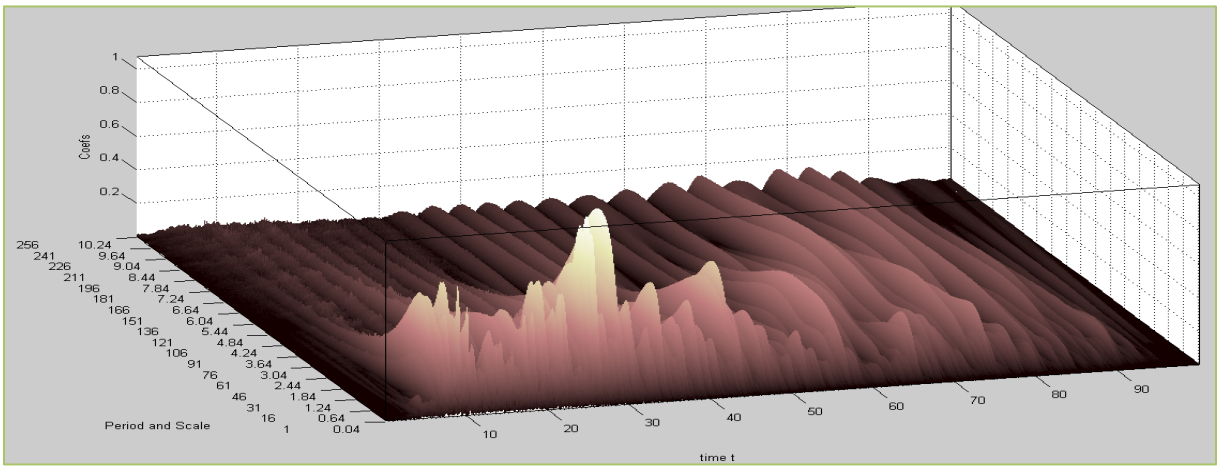

Figure C-13 Wavelet coefficients plot in 3D using Mexican hat wavelet analysis program

C.4 Wavelet analysis on Displacement Time History (DTH) data:

The section 5.4 and its sub-sections are the repetition of section 5.2 and its sub-sections on Displacement Time History data. The frequency content is very well displayed in the Gabor wavelet. The black spots are also reduced by large number from section 5.2 where Acceleration Time History data used.

C.4.1 Wavelet analysis on HDLT262 component of Imperial Valley Earthquake

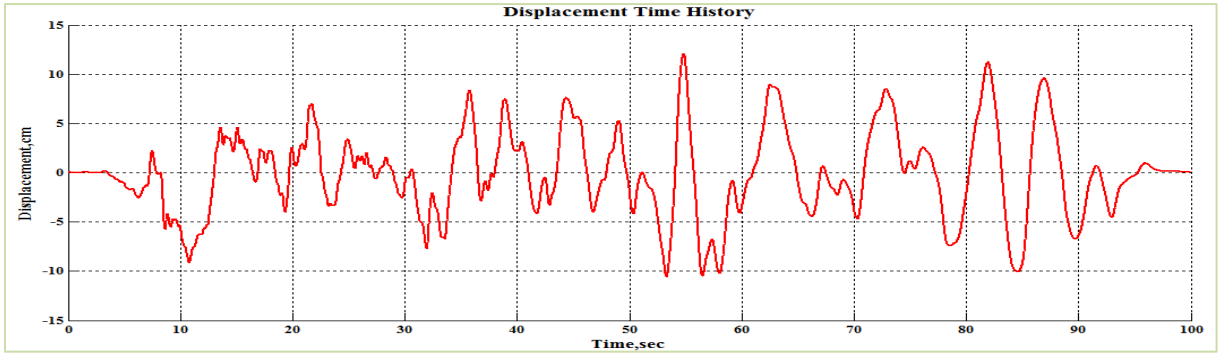

Figure C-14 Displacement Time History of HDLT352 component of Imperial Valley Earthquake

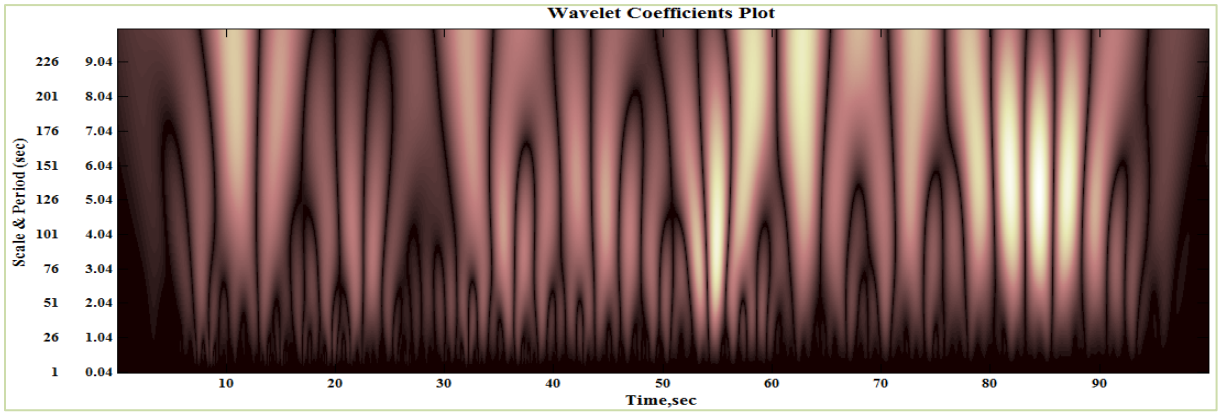

Figure C-15 Wavelet coefficients plot using Mexican hat wavelet analysis program

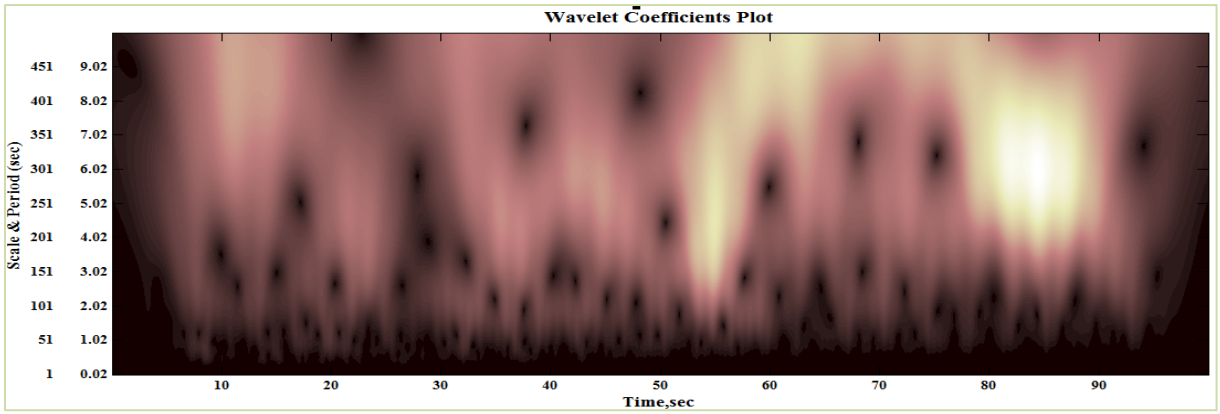

Figure C-16 Wavelet coefficients plot using Complex Guassian wavelet analysis program of order 4

C.4.2 Wavelet analysis on HDLT262 component by using varying orders of Complex Guassian wavelet

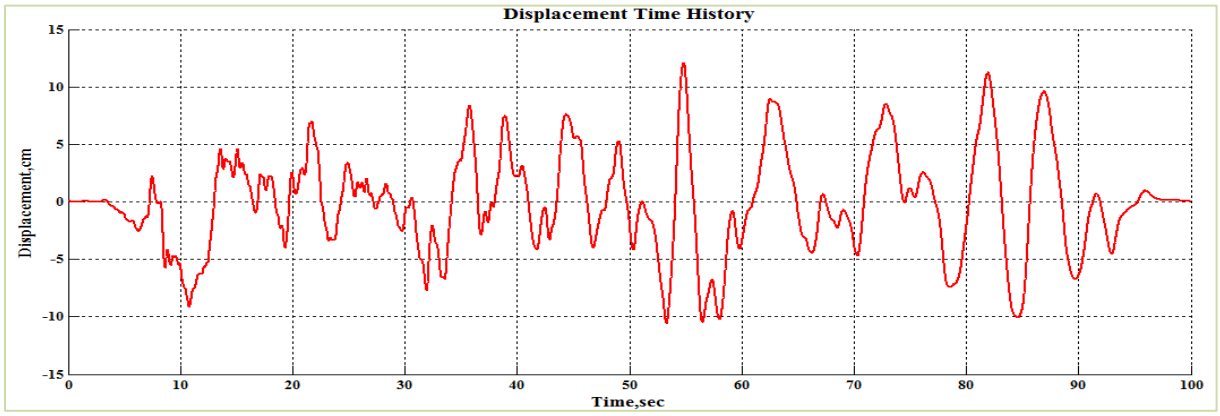

Figure C-17 Displacement Time History of HDLT 262 component of Imperial Valley Earthquake

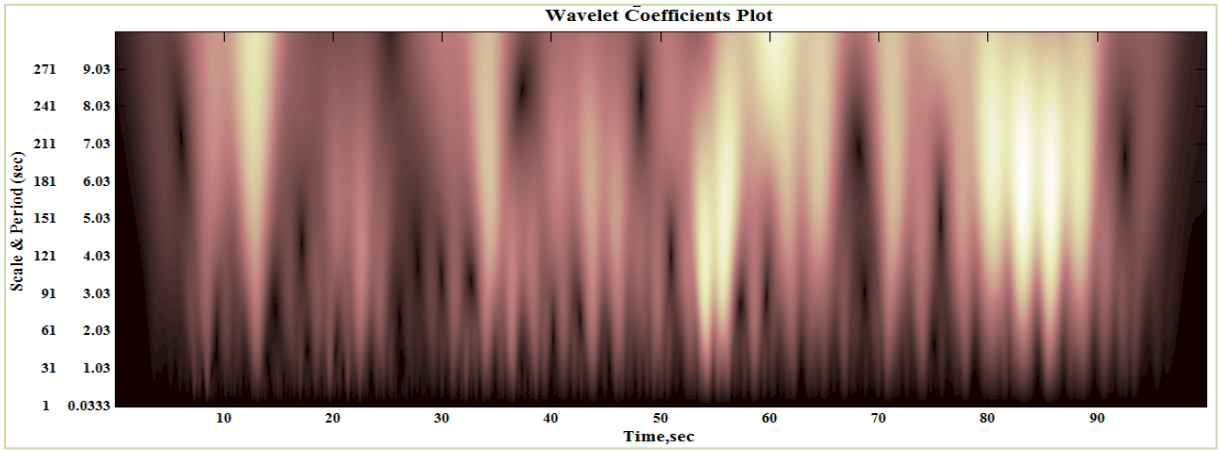

Figure C-18 Wavelet coefficients plot using Complex Guassian wavelet analysis program of order 1

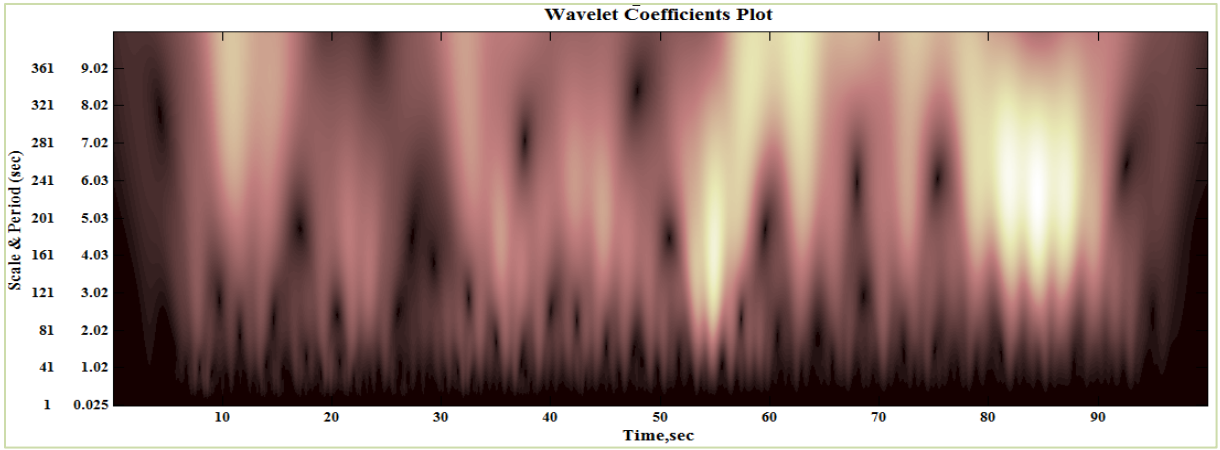

Figure C-19 Wavelet coefficients plot using Complex Guassian wavelet analysis program of order 2

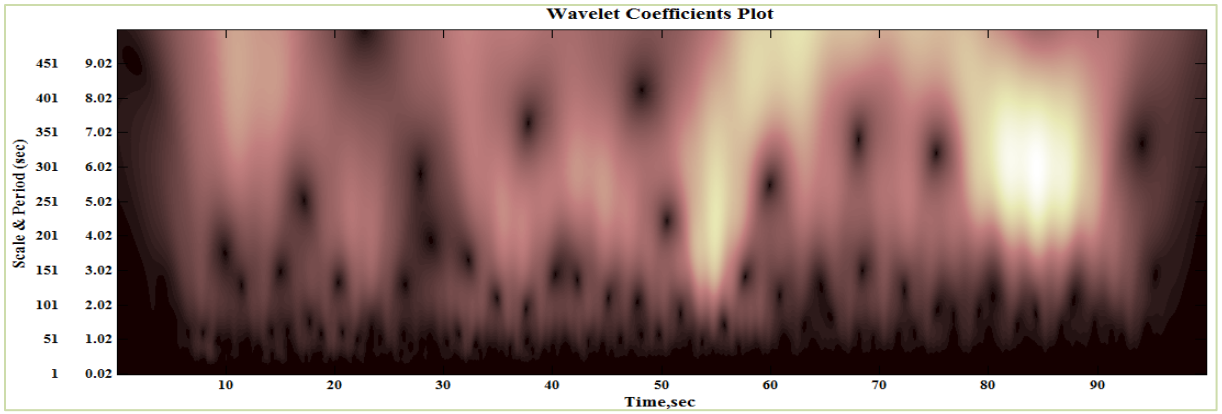

Figure C-20 Wavelet coefficients plot using Complex Guassian wavelet analysis program of order 4

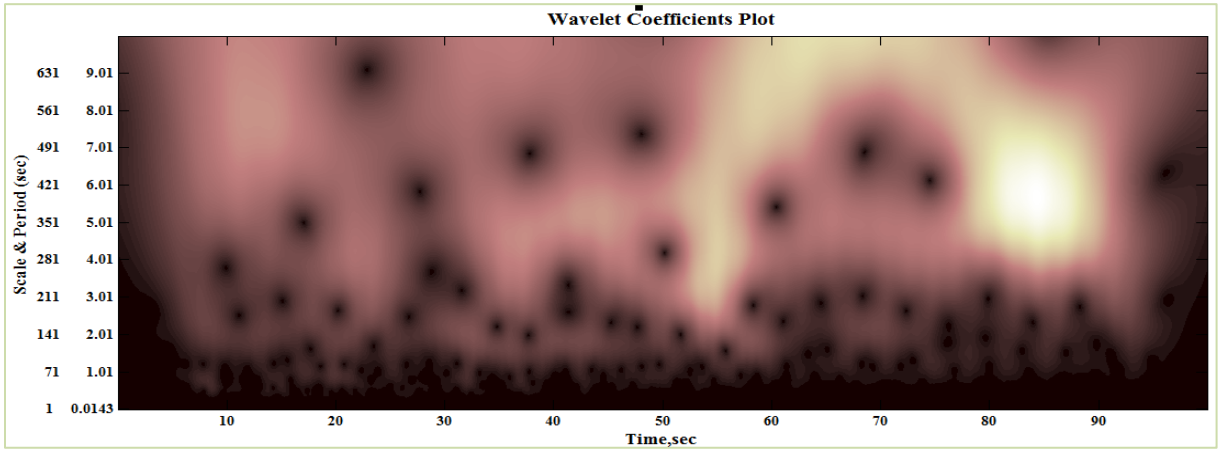

Figure C-21 Wavelet coefficients plot using Complex Guassian wavelet analysis program of order 8

C.4.3 Comparison of 2D and 3D wavelet transform plots

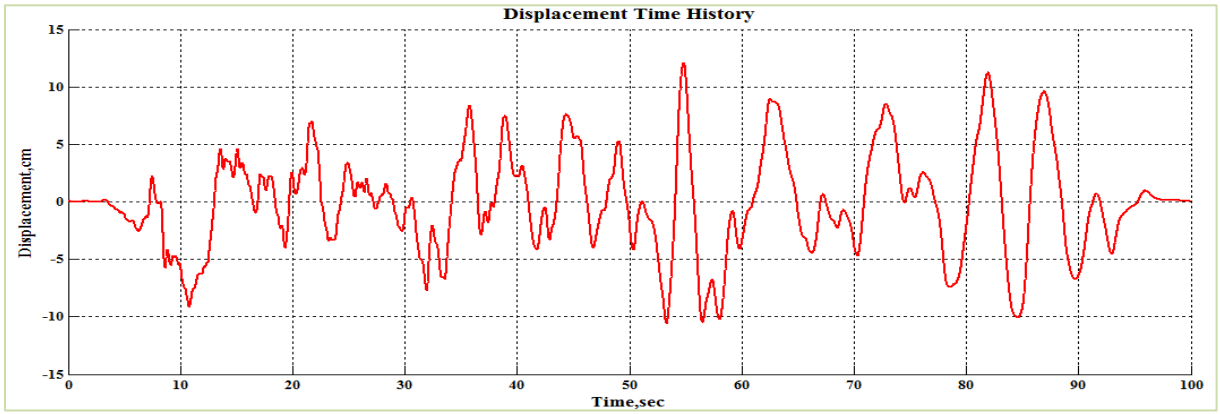

Figure C-22 Displacement Time History of HDLT 262 component of Imperial Valley Earthquake

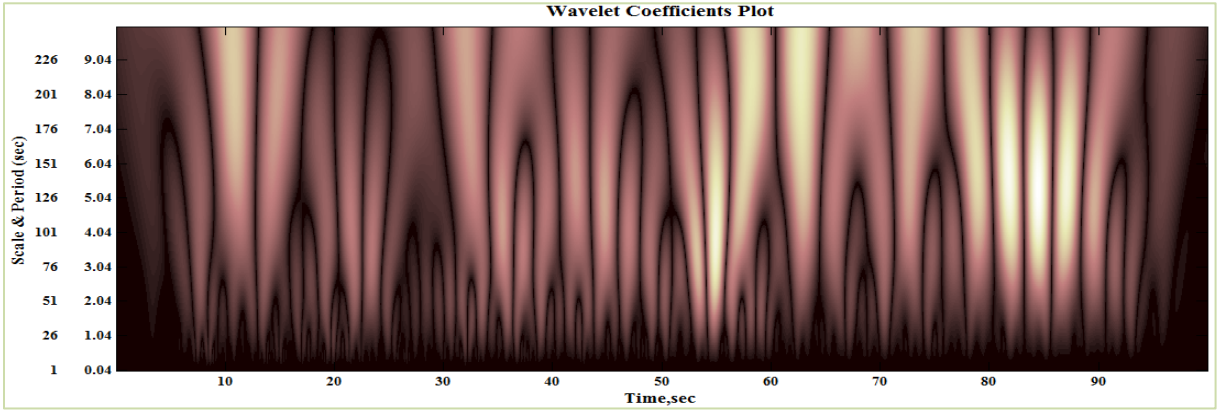

Figure C-23 Wavelet coefficients plot in 2D using Mexican hat wavelet analysis program

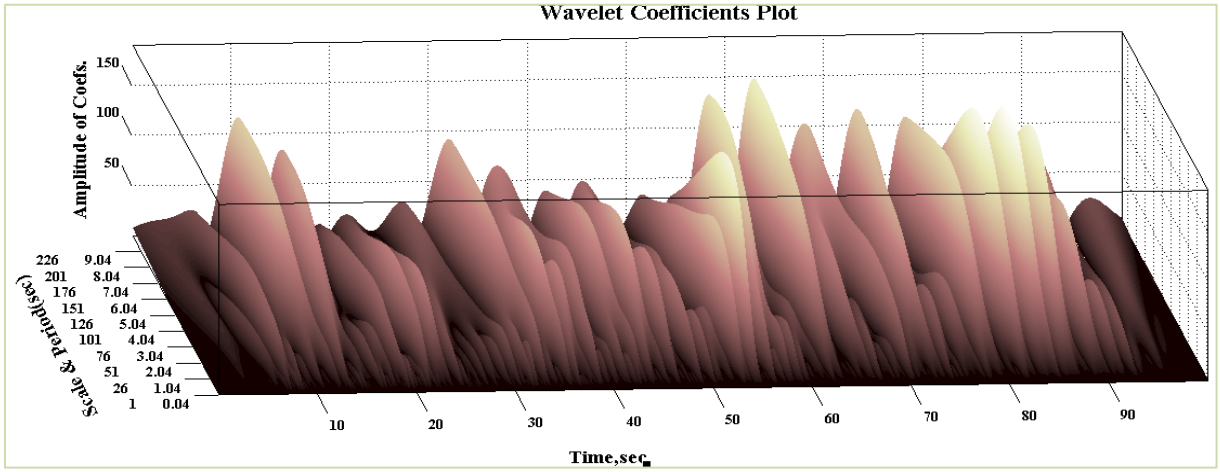

Figure C-24 Wavelet coefficients plot in 3D using Mexican hat wavelet analysis program

C.5 Investigation into Black holes of Frequency Content

C.5.1 Plotting for certain period range near a particular black hole along the whole time series

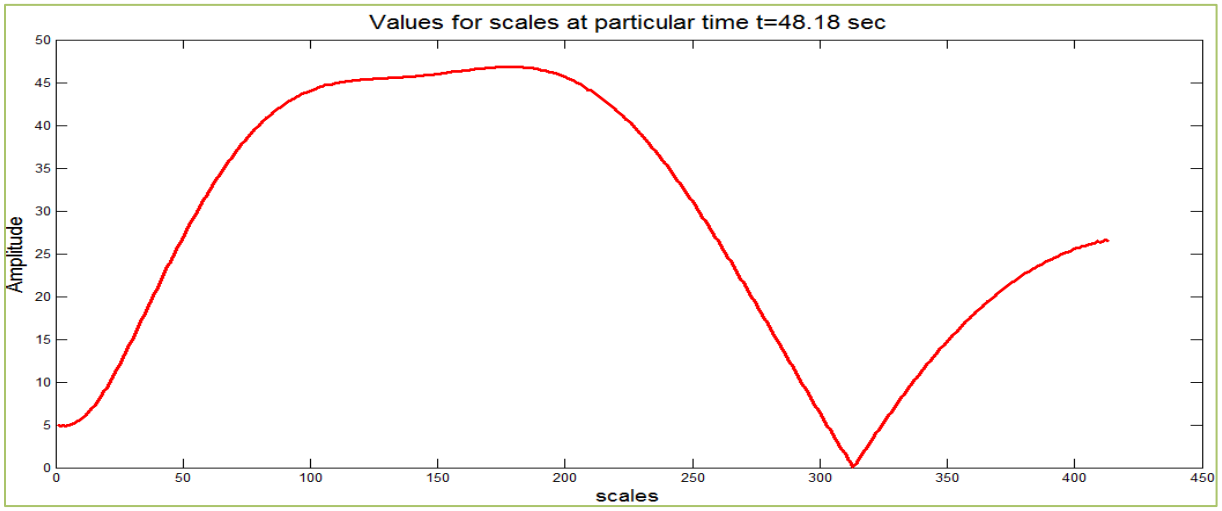

Figure C-25 Plot for DLT262 DTH for periods ranging between 2.00-10.24 sec near black hole region for particular time 48.18 sec for 'cgau4'

Minimum value= 0.401

For period=8.24 sec

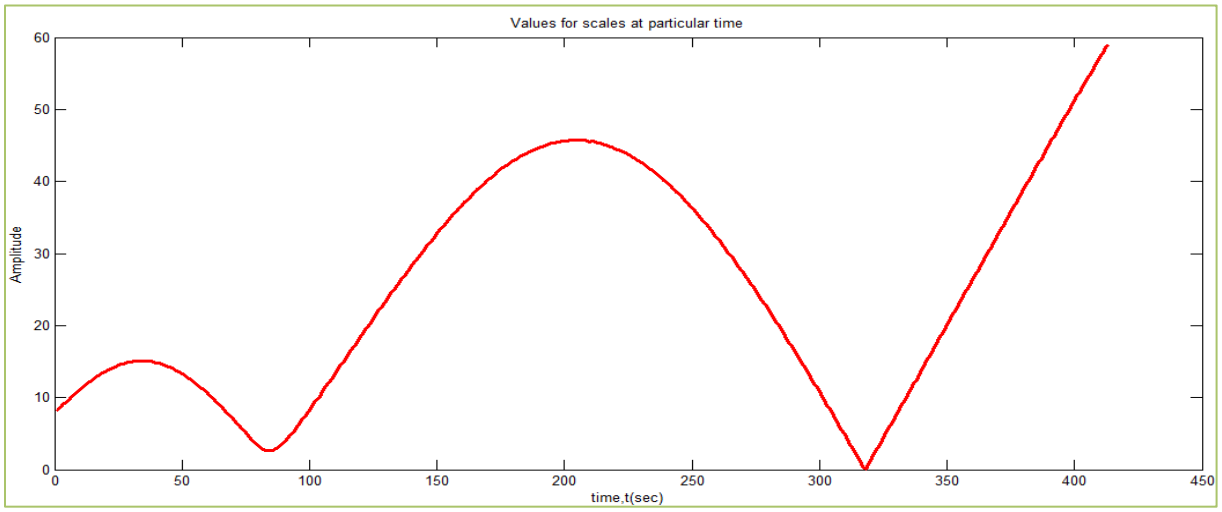

Figure C-26 Plot for DLT262 DTH for periods ranging between 2.00-10.24 sec near black hole region for particular time 68.23 sec for 'cgau6'

Minimum value= 0.123

For period=6.95 sec

C.5.2 plotting for all periods at the time where center of black hole exists

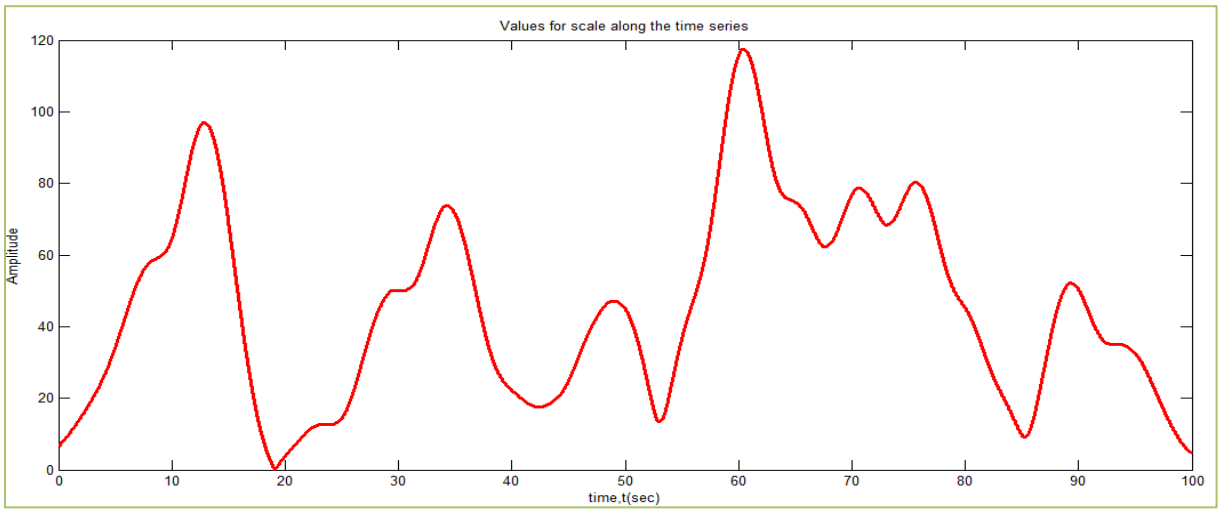

Figure C-27 Plot for DLT262 DTH for period 13.83 sec near black hole region along time series for 'cgau1'

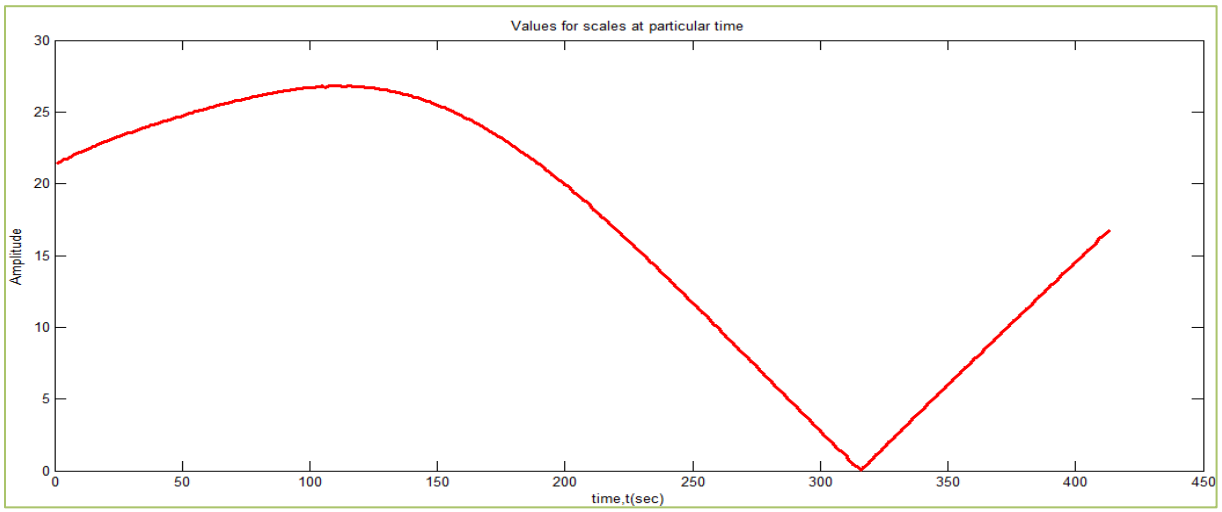

Figure C-28 Plot for DLT262 DTH for periods ranging between 2.00-10.24 sec near black hole region for particular time 19.3 sec for 'cgau1'

Minimum value= 0.019

For period=13.83 sec

C.6. Multiplying portion of signal with wavelet

This section works on determining whether the black hole of frequency content is a property of the signal being analysed, or a product of wavelet transform. From the plots shown in Figure 5-37, it can be seen that near the black hole region, the integral of the signal* real part of wavelet and signal*complex part of wavelet is going to be near zero (approximately same area above the axis as below). The integral of the signal*absolute part of the wavelet is not zero near the black hole region. This clearly tells us that black holes are not part of the signal. This is significant because absolute values of the wavelet (obtained by taking square root of the sum of squares of real and complex part) neglect the sign. This conclusion makes to proceed to approach 2 for further investigation in black holes to completely get rid of them.

C.6.1. Using Gabor (complex Gaussian) of order 4 for Black hole at (48.08, 8.24)

Steps involved in the process:

1. The Delta 262 component of Displacement Time History which is shown in the Figure 5-37.

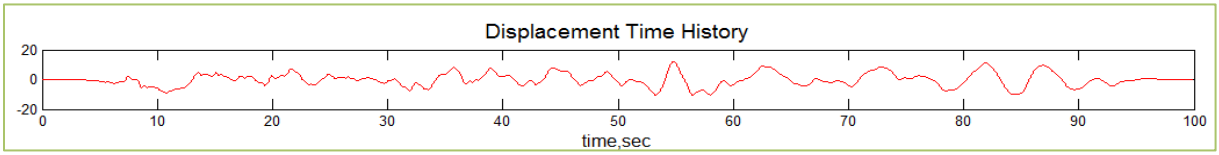

Figure C-29 Displacement Time History of Delta 262 component

2. The black hole whose center located at (48.08, 8.24) sec is chosen. The coordinates are corresponding to time and period.

3. The new signal (which is a part of the above signal but from time 35.72 sec to 60.43 sec) is plotted over time as shown below.

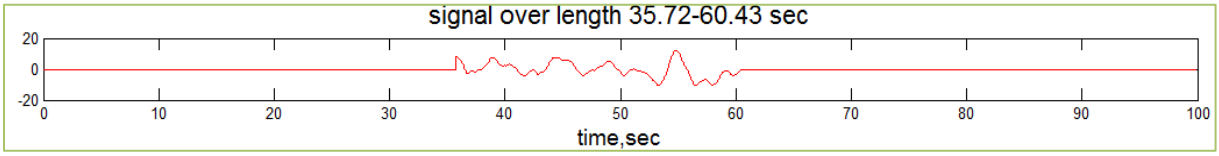

Figure C-30 Part of the Displacement Time History of Delta 262 component

4. The Gabor wavelet of order 4 is plotted for a period of 8.24 sec (the period corresponding to the black hole location) keeping the remaining values as zero as shown in Figures 5-39,5-40,5-41.

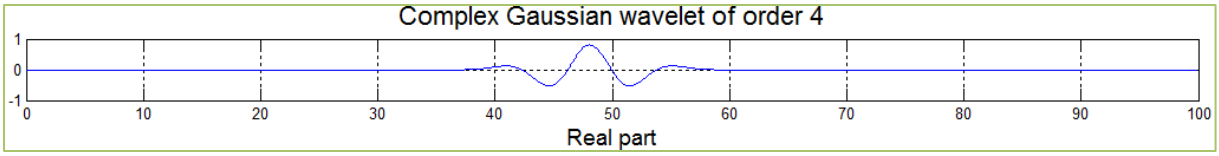

Figure C-31 Real part of Complex Guassian (Gabor) wavelet of order 4

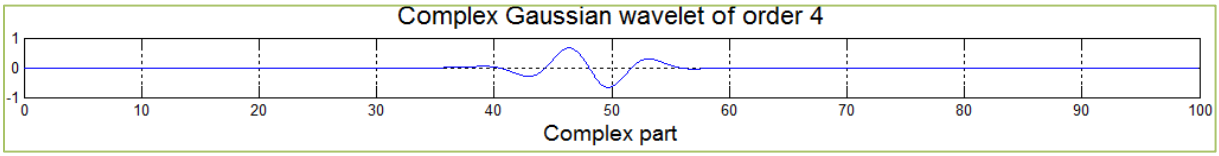

Figure C-32 Complex part of Complex Guassian (Gabor) wavelet of order 4

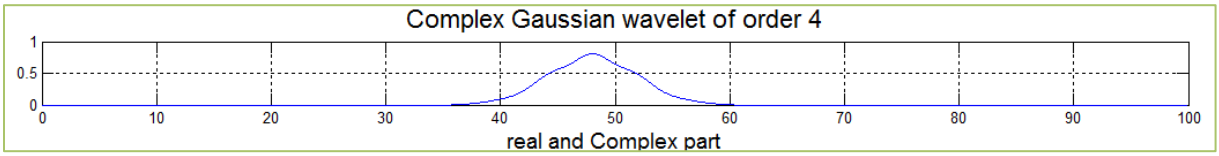

Figure C-33 Real and complex part of Complex Guassian (Gabor) wavelet of order 4

5. Multiplying the signal with the wavelet gives the following Figures 5-42,5-43,5-44.

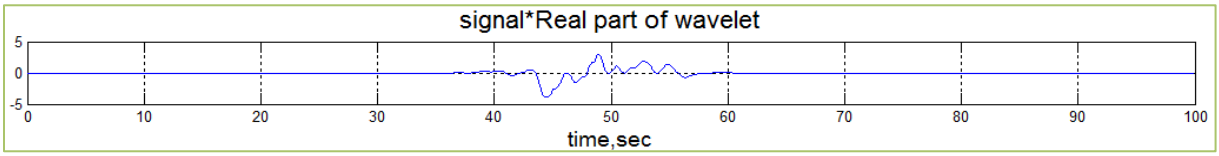

Figure C-34 Multiplying Figure 38 with Figure 39

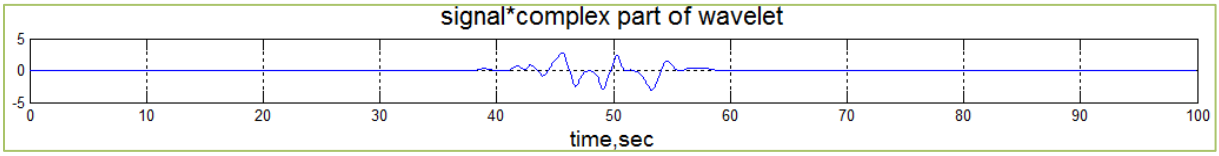

Figure C-35 Multiplying Figure 38 with Figure 40

Figure C-36 Multiplying Figure 38 with Figure 41

6. The above shown plots in single plot are shown below in Figure 5-45

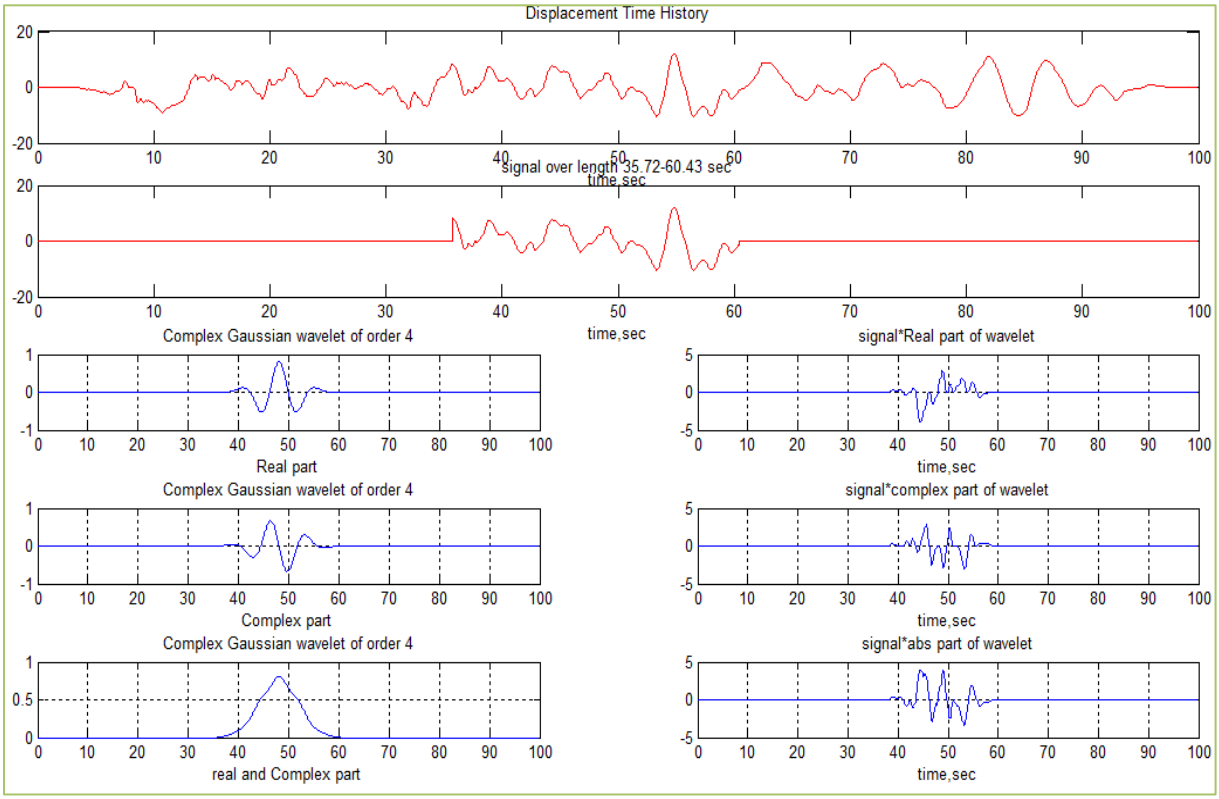

Figure C-37 Multiplying the signal with Complex Guassian wavelet

C.6.2. Using Complex Morlet wavelet (cmor0.5-3.5) for Black hole at (37.76, 7.3)

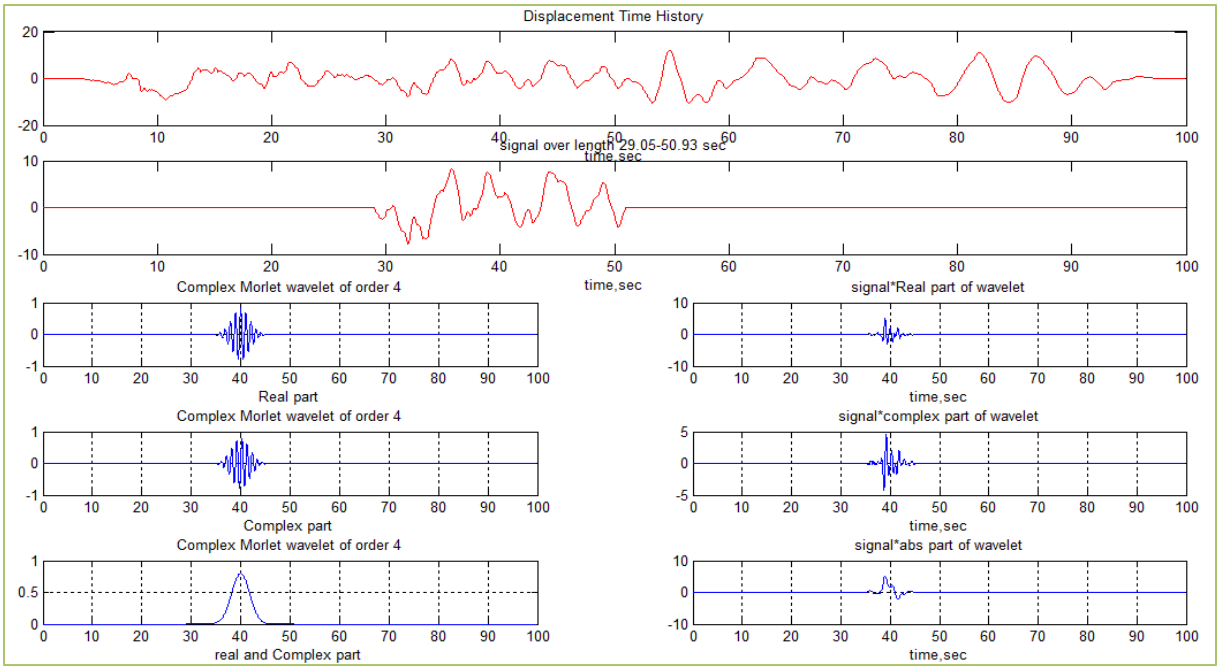

Figure C-38 Multiplying the signal with Complex Morlet wave

C.7. Combination of two wavelets

This section aims at combining wavelet coefficients of two different wavelet transforms. The combination of frequency content of two wavelets is done by taking the maximum absolute values from the two wavelets at the corresponding period. Figure 5-49 shows that the combination of frequency content of two different wavelets which contains regions of low frequency content (black hole) results in the removal of black holes. But the result shown in Figure 5-49 is not as smooth as desired. Since the smoothness of the plot is a resolution problem, which is a 2D plot whose width along the time axes is the width of the wavelet and width along the period axes is the period of the frequency content. Figure 5-50 in section 5.9 shows the resolution plot for Complex Guassian wavelet of order 4 for horizontal component of 262^0 component.

Combining Complex Guassian of order 4 and Complex Morlet of bandwidth 0.5 and frequency 3.5

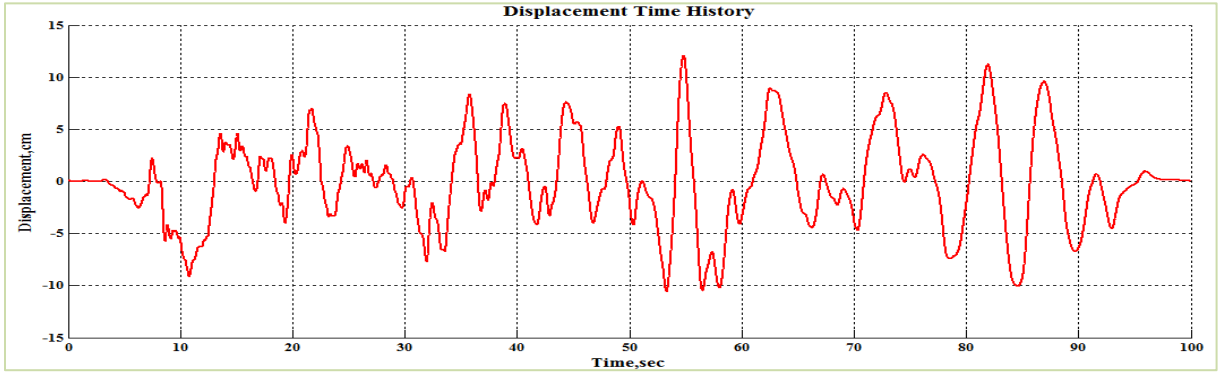

Figure C-39 Displacement Time History of HDLT262 component of Imperial Valley Earthquake

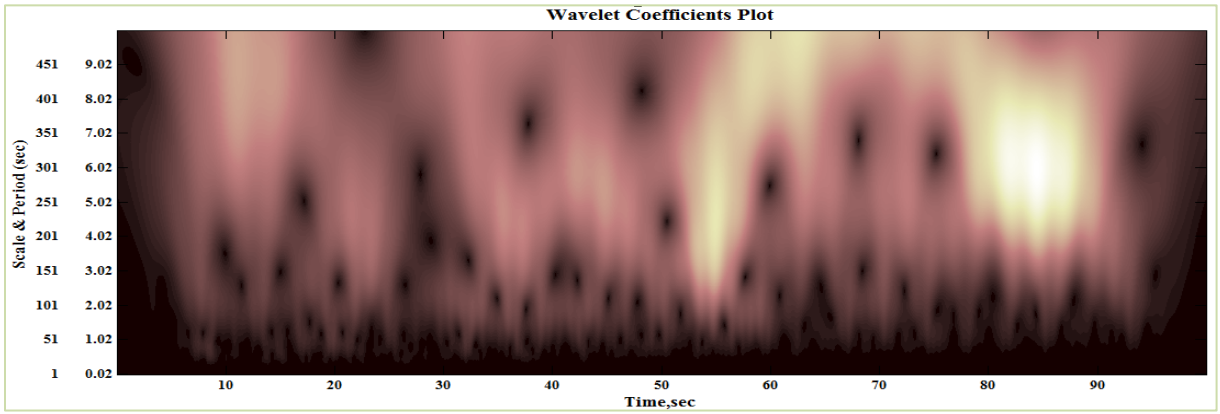

Figure C-40 Wavelet coefficients plot using Complex Guassian wavelet analysis program of order 4

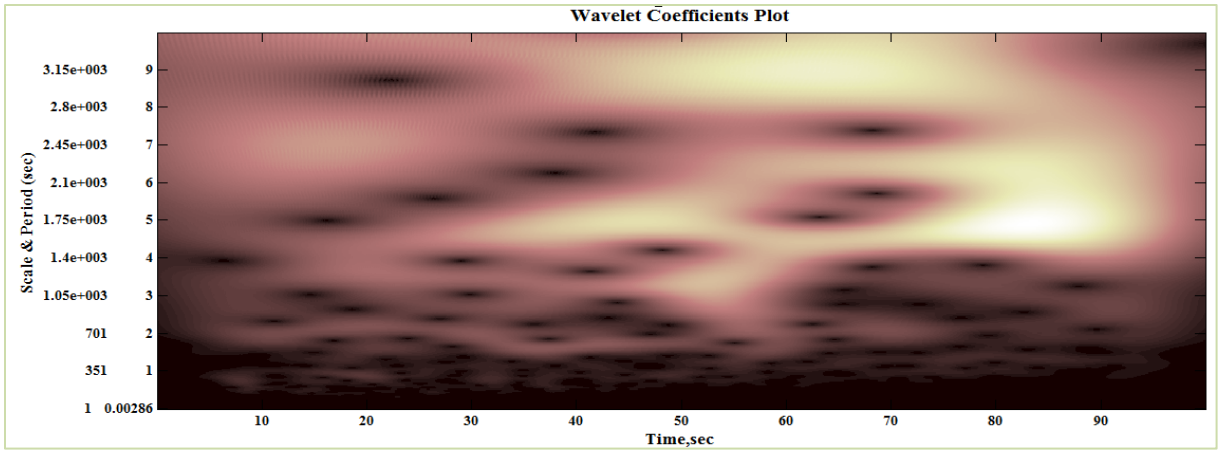

Figure C-41 Wavelet coefficients plot using Complex Morlet wavelet 0.5-3.5

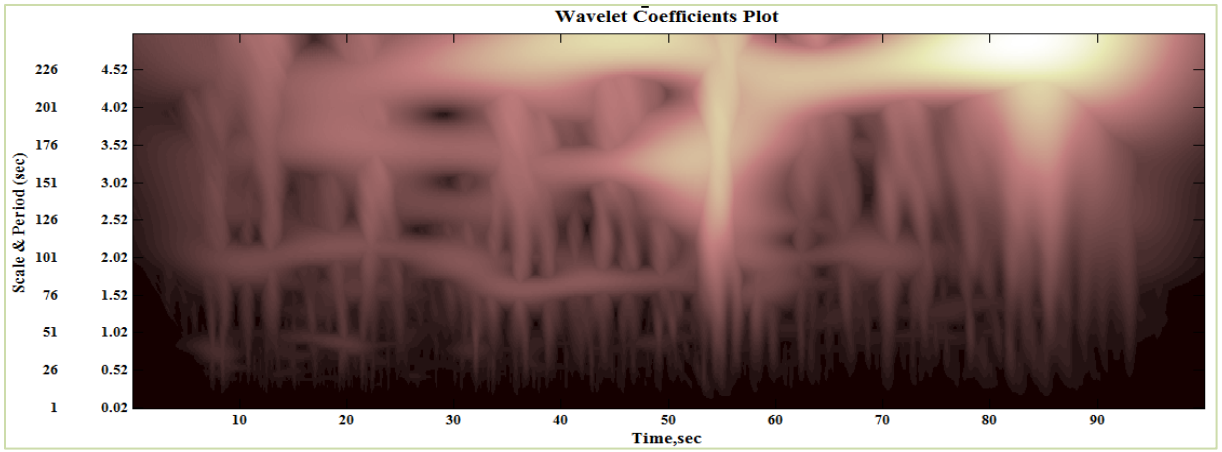

Figure C-42 Combination of Complex Guassian of order 4 and Complex Morlet of bandwidth 0.5 and frequency 3.5

APPENDIX D: CALCULATIONS

As level P corresponds to a frequency band of $[(1/2)^{p+1}\ (1/2)^{p}]$, the maximum frequency for level p is given by Equation D-1.

$$f_a = (1/2)^{p} \quad \textbf{D-1}$$

The scale- frequency relation is given by equation D-2

$$f_a = \frac{f_c}{S*\Delta T} \quad \textbf{D-2}$$

For complex gaussian wavelet of order 1, fc=0.30

Since the sampling period for the signal $=\Delta T = 1$

Substituting in Equation D-2, $f_a=\frac{0.30}{S}$

By using trail and error method,

to know the frequency corresponding to a scale of 150,

$$f_a = \frac{0.30}{150} \quad \textbf{D-3}$$

Equating D-3 and D-1, we get level number (p)=9.

Thus, the frequency content corresponding to level 9 of discrete wavelet is equivalent to a scale of 150 of complex guassian wavelet of order 1.

Similarly, it can be proved that the frequency content corresponding to level 9 of discrete wavelet is equivalent to a scale of 125 of mexican hat wavelet (having center frequency 0.25 and sampling period 1).